Regulation of inflammasome activation: roles for phospholipase C and mitochondria

Dissertation

zur

Erlangung des Doktorgrades (Dr. rer. nat.)

der

Mathematisch-Naturwissenschaftlichen Fakultät

der

Rheinischen Friedrich-Wilhelms-Universität Bonn

vorgelegt von

Tomasz Próchnicki

aus

Kraków (Polen)

Bonn, Oktober 2020

Angefertigt mit Genehmigung der Mathematisch-Naturwissenschaftlichen Fakultät der
Rheinischen Friedrich-Wilhelms-Universität Bonn

1. Gutachter: Prof. Dr. Eicke Latz

2. Gutachterin: Prof. Dr. rer. nat. Irmgard Förster

Tag der Promotion: 19.05.2021

Erscheinungsjahr: 2021

Table of contents

Acknowledgements

I would like to thank Prof. Dr. Eicke Latz for accepting me as a PhD student five years ago and for his trust, patience, and respect all along the way. At this stage of my life, I couldn't have asked for a better supervisor.

I was lucky enough to meet more wonderful mentors during my stay at the Institute of Innate Immunity. Here I would like to especially thank Dr. Matthew S. Mangan, always happy to share reagents and advice, and Prof. Dr. rer. nat. Dagmar Wachten for her involvement in the project.

In the past three years I also got the opportunity to supervise three brilliant students: Jieyan (Jane) He, Lena Standke, and Thomas Bajaj. I hope they were able to learn from me half as much as I learned from them and I thank them for their input to our shared projects and for putting up with my chaotic ways.

The Institute of Innate Immunity has an exceptional team of technical assistants. I would like to thank Fraser G. Duthie for generating multiple plasmids that I used in my Thesis and for constantly enlightening me on the topic of popular culture. Furthermore, I would like to thank Maximilian Rothe for generating bone marrow-derived macrophages, Romina Kaiser for looking out for the cell lines database of our Institute, Rainer Stahl for maintaining the database of plasmids, and Gudrun Engels for generating L929 cell conditioned media, for maneuvering the ordering system of the University, and for the incidental Hörverstehen Übungen.

None of my work would have been possible without the gentle auspices of Dr. Gabor Horvath, who manages the Microscopy Core Facility of the Medical Faculty at the University of Bonn.

I would like to thank Prof. Dr. rer. nat. Thomas Kufer from the University of Hohenheim for providing NLRP10-deficient bone marrows.

I would like to thank the members of the Institute of Innate Immunity whose reagents – cell lines and plasmids – I have used in my work: Dr. Dominic De Nardo, Prof. Dr.

Bernardo S. Franklin, Dr. rer. nat. Damien Bertheloot, Dr. rer. nat. Andrea Stutz, Dr. rer. nat. Karin Pelka, Dr. Christina Budden, Marta Lovotti, and Brian Monks. Brian and I spent many nights in the lab and I've been missing his presence since he moved back to the U.S. in 2019.

Thank you to my office family – in addition to several Institute members mentioned above in particular Olivia van Ray, Dr. Pia Langhoff, Tobias Dierkes, Dr. Yonatan Herzig, Victor Saavedra Yturriagagoitia, Miki Uchima, Ornina Marma, and Dr. rer. nat. Anette Christ – for their endorsement and for providing a gracious backdrop for the occasional drama.

I would like to thank my Thesis Committee: Prof. dr. rer. nat. Irmgard Förster, Prof. Dr. Zeinab Abdullah, and Prof. Dr. Wolfgang Lück for agreeing to evaluate my research project, for their time and consideration.

Lastly, I would like to thank my parents, Maria and Włodzimierz Próchniccy, and my aunt Ada Próchnicka, who, despite our differences, were always supportive of my endeavors.

Summary

Inflammasomes are protein complexes serving as activation platforms for the protease caspase-1, which leads to a pro-inflammatory type of cell death termed pyroptosis and to maturation and release of the cytokines interleukin- (IL)-1β and IL-18. These processes are involved in host protection against pathogens and in the control of commensal microbial communities; however, under pathological conditions, they may contribute to diseases such as Alzheimer's disease, atherosclerosis, gout, or type 2 diabetes. Several receptors and sensors are capable of assembling inflammasomes. For example, absent in melanoma 2 (AIM2) triggers inflammasome formation in the presence of cytosolic double-stranded (ds) DNA, whereas NACHT, LRR, and PYD domains-containing protein 3 (NLRP3) nucleates the inflammasome in response to multiple stimuli, many of which deplete the cytosolic pool of K^+ ions.

The molecular mechanisms governing the NLRP3 inflammasome activation are incompletely understood. Here, I characterized the inflammasome activation by *m*-3M3FBS, a reported phospholipase C (PLC) agonist previously suggested to activate NLRP3. Unexpectedly, I found that the *m*-3M3FBS-induced inflammasome assembly does not require NLRP3. Furthermore, I provided evidence that PLC inhibitors, previously reported to inhibit the NLRP3 inflammasome formation, do so through off-target effects. These observations raised the questions of which sensors/receptors are involved in inflammasome formation in cells treated with *m*-3M3FBS, and how this response is initiated.

Using a combination of forward- and reverse-genetic approaches, I identified two inflammasome-forming proteins activated by *m*-3M3FBS: AIM2 and NLRP10. By employing fluorescence microscopy techniques and pharmacological manipulation of cell signaling, I discovered that the *m*-3M3FBS mechanism of action consists of the induction of mitochondrial (mt) rupture. This damage exposes mtDNA to AIM2, leading to inflammasome formation. In opposition to the previously proposed models of inflammasome activation, NLRP3 was not involved in this response to mtDNA. The activation of the NLRP10 inflammasome was also mtDNA-independent, but likely relying on another factor exposed by the disrupted organelles. In further experiments, I identified three more activators of the AIM2 and NLRP10 inflammasomes (thapsigargin,

SMBA1, and SC-10) and two NLRP10-specific inflammasome activators (*o*-3M3FBS and SC-9).

In my Thesis, I characterize in detail the off-target activity of *m*-3M3FBS as an inducer of mitochondrial damage. I also provide evidence that AIM2 can be activated by endogenous mtDNA. Furthermore, I describe NLRP10 as a novel inflammasome-forming sensor possibly responding to mitochondrial rupture. Finally, my findings indicate that the NLRP3 inflammasome formation is not dependent on PLC and mtDNA, significantly simplifying the current model of NLRP3 activation.

Zusammenfassung

Inflammasomen sind Proteinkomplexe, die die Aktivierung der Protease Caspase-1 ermöglichen. Dieses führt zu einem proinflammatorischen Zelltod, der als Pyroptose bezeichnet wird, sowie zur Spaltung und Sekretion der Zytokine Interleukin- (IL)-1β und IL-18. Diese immunologische Reaktion hilft, den Körper gegen Pathogene zu schützen und spielt eine Rolle bei der Kontrolle von kommensalen Mikroorganismen. Unter pathologischen Bedingungen kann die Inflammasom-Aktivierung jedoch zu Krankheiten wie Alzheimer, Arteriosklerose, Gicht oder Typ-2-Diabetes führen. Verschiedene Rezeptoren und Sensoren können die Bildung von Inflammasomen initiieren. Absent in Melanoma 2 (AIM2) wird in Gegenwart von zytosolischer doppelsträngiger (ds) Deoxyribonukleinsäure (DNA) aktiviert und NACHT-, LRR- und PYD Domains-Containing Protein 3 (NLRP3) bildet das Inflammasom als Reaktion auf mehrere Stimuli, viele von denen den Ausfluss von Kalium-Ionen aus der Zelle verursachen.

Die molekularen Mechanismen der NLRP3-Aktivierung sind noch nicht vollständig verstanden. In meiner Dissertation habe ich die Inflammasom-Aktivierung durch *m*-3M3FBS charakterisiert. *m*-3M3FBS ist ein niedermolekularer Agonist der Phospholipase C (PLC) und wurde als ein Aktivator des NLRP3-Inflammasomes beschrieben. Unerwartet habe ich aber festgestellt, dass die durch *m*-3M3FBS induzierte Inflammasom-Aktivierung von NLRP3 unabhängig ist. Weiterhin habe ich gezeigt, dass PLC-Inhibitoren, die zuvor verwendet wurden, um die Beteiligung von PLC an der Aktivierung des NLRP3-Inflammasomes zu beweisen, durch unspezifische Effekte wirken. Infolge dieser Ergebnisse habe ich die Fragen gestellt, welche Sensoren oder Rezeptoren in *m*-3M3FBS-stimulierten Zellen Inflammasomen bilden können, und welche Signalwege daran beteiligt sind.

Durch genetische Ansätze habe ich zwei Inflammasom-bildende Proteine identifiziert, die auf die Stimulierung mit *m*-3M3FBS reagieren: AIM2 und NLRP10. Durch Fluoreszenzmikroskopie als auch pharmakologische Manipulation der Signalwege habe ich anschließend entdeckt, dass der Wirkmechanismus von *m*-3M3FBS in der Induktion der mitochondrialen Störung besteht. Dieser Zusammenbruch der Mitochondrien setzt die mtDNA frei, was dann zur Aktivierung des AIM2-Inflammasomes führt. Im Gegensatz

zu den vorherigen Modellen ist NLRP3 an der Reaktion auf mtDNA nicht beteiligt. Die Aktivierung des NLRP10-Inflammasomes hängt ebenfalls nicht von mtDNA ab, könnte aber von anderen Faktoren verursacht werden, die die zerstörten Organellen freisetzen. In weiteren Experimenten habe ich noch drei Aktivatoren der AIM2- und NLRP10-Inflammasomen (Thapsigargin, SMBA1 und SC-10) und zwei NLRP10-spezifische Inflammasom-Aktivatoren (*o*-3M3FBS und SC-9) identifiziert.

In meiner Doktorarbeit habe ich den Off-Target-Effekt von *m*-3M3FBS beschrieben, der eine mitochondriale Störung verursacht. Diese führt zur Aktivierung des AIM2-Inflammasomes durch endogene mtDNA. Parallel dazu habe ich den Sensor NLRP10 charakterisiert, der in den Zellen, in den die Mitochondrien geschädigt werden, Inflammasomen bilden kann. Schließlich habe ich gezeigt, dass die Bildung des NLRP3-Inflammasomes von PLC und mtDNA unabhängig ist, was das aktuelle Modell der NLRP3-Aktivierung erheblich vereinfacht.

Abbreviations index

2-APB, 2-Aminoethoxydiphenylborane
8-OH-dG, 8-hydroxy-2'-deoxyguanosine (monomeric)
8-OH-dG, 8-hydroxy-2'-deoxyguanosine (residues within a DNA strand)
8-oxo-dGTP, 8-oxo-2'-deoxyguanosine-5'-triphosphate
AIM2, absent in melanoma 2
ALR, AIM2-like receptor
ANT[1], adenine nucleotide translocator [1] (also known as Slc25a4)
APAF1, apoptotic protease activating factor 1
APLAID, autoinflammation and phospholipase Cγ2-associated antibody deficiency and immune dysregulation
ASC, apoptosis-associated speck like protein containing a CARD
ATP, adenosine-5'-triphosphate
Bad, BCL-2-associated agonist of cell death
Bak, BCL-2 homologous antagonist/killer
Bax, BCL-2-associated X, apoptosis regulator
BCL-2, B-cell lymphoma 2
BCL-W, BCL-2-like protein 2
BCL-XL, B-cell lymphoma-extra large
BCR, B-cell receptor
BFP, blue fluorescent protein
Bid, BH3 interacting-domain death agonist
Bim, BCL-2-interacting mediator of cell death
BMDM, bone marrow-derived macrophage
Bok, BCL-2-related ovarian killer
bp, base pair
cAMP, 3',5'-cyclic adenosine monophosphate
CARD, caspase activation and recruitment domain
CaSR, calcium-sensing receptor
cGAMP, 2',3'-cyclic guanosine monophosphate-adenosine monophosphate
cGAS, 2',3'-cyclic guanosine monophosphate-adenosine monophosphate synthase
CD, cluster of differentiation
cIAP, baculoviral IAP repeat-containing protein
CLR, C-type lectin-like receptor
CRISPR, clustered regularly interspaced short palindromic repeats
CsA, cyclosporin A
CXCL8, chemokine (C-X-C motif) ligand 8
CytD, cytochalasin D
CytoD, cytochalasin D
DAG, diacylglycerol
DAMP, damage-associated molecular pattern
ddC, 2',3'-dideoxycytidine
DDOST, dolichyl-diphosphooligosaccharide-protein glycosyltransferase non-catalytic subunit
DDX3X, DEAD-box helicase 3 X-linked
DMEM, Dulbecco's Modified Eagle's Medium
DMSO, Dimethyl sulfoxide
DNA, Deoxyribonucleic acid
dNTP, deoxynucleoside-5'-triphosphate

DPBS, Dulbecco's phosphate-buffered saline
ds, double-stranded
ER, endoplasmic reticulum
EtBr, ethidium bromide
FADD, Fas-associated protein with death domain
FBS, fetal bovine serum
FIIND, function-to-find domain
FPR, formyl peptide receptor
g, gravitational acceleration
GCN2, general control nonderepressible 2
GPCR, G protein-coupled receptor
Gsdm, gasdermin
h [prefix], human
h, hour
HAMP, homeostasis-altering molecular process
HEK, human embryonic kidney
HIN-200, hematopoietic expression, interferon-inducible nature, and nuclear localization-200
HIV, human immunodeficiency virus
HMGB1, high mobility group box 1 protein
HRI, heme-regulated inhibitor
HSP90, heat shock protein 90
HTRF, homogenous time-resolved fluorescence
IAP, inhibitor of apoptosis protein
IC_{50}, half maximal inhibitory concentration
IFN, interferon
IL, interleukin
iMac, immortalized macrophage
IMM, inner mitochondrial membrane
IMS, intermembrane space
IP_1, inositol monophosphate
IP_3, inositol 1,4,5-trisphosphate
IP_3R, IP_3 receptor
IRE1α, inositol-requiring enzyme 1 α
IRES, internal ribosomal entry site
IRF, interferon regulatory factor
ISR, integrated stress response
LAMP1, lysosomal-associated membrane protein 1
Leu-Leu-O-Me, Leu-Leu methyl ester
LMW, low molecular weight
LPS, lipopolysaccharide
LRR, leucine-rich repeat
m [prefix], murine
M. leprae, *Mycobacterium leprae*
MAVS, mitochondrial antiviral signaling protein
MCD, methylcyclodextrin
MCL-1, myeloid cell leukemia sequence 1 (BCL-2-related)
MCU, mitochondrial Ca^{2+} uniporter
MEM, minimal essential medium
MHC, major histocompatibility complex

min, minute
MLKL, mixed lineage kinase domain-like protein
MOMP, mitochondrial outer membrane permeabilization
mPT, mitochondrial permeability transition
mPTP, mitochondrial permeability transition pore
MSS, minimal salt solution
mt, mitochondrial
MW, molecular weight
NACHT, nucleotide-binding oligomerization domain
NAIP, neuronal apoptosis inhibitory protein/baculoviral inhibitor of apoptosis domain [IAP] repeat-containing protein
NEK7, never in mitosis gene A (NIMA)-related kinase 7
NET, neutrophil extracellular trap
NFAT, nuclear factor of activated T cells
NF-κB, nuclear factor kappa-light-chain-enhancer of activated B cells
NK, natural killer
NLR, NOD-like receptor
NLRC4, NLR family CARD domain-containing protein 4
NLRP, NACHT, LRR, and PYD domains-containing protein
NOD2, Nucleotide-binding oligomerization domain-containing protein 2
Noxa, see: PMAIP1
nuc [prefix], nuclear
OMM, outer mitochondrial membrane
ox[-] [prefix], oxidized
P. aeruginosa, *Pseudomonas aeruginosa*
P_2X_7R, P2X purinoceptor 7
P_2Y_2R, P2Y purinoceptor 2
PAMP, pathogen-associated molecular pattern
PARL, presenilins-associated rhomboid-like protein
PBMC, peripheral blood mononuclear cell
PBS, phosphate-buffered saline
PC, phosphatidylcholine
PCR, polymerase chain reaction
PERK, PKR-like ER kinase
PI, phosphatidylinositol
PI4P, phosphatidylinositol 4-phosphate
PINK1, PTEN-induced kinase 1
PIP_2, phosphatidylinositol 4,5-bisphosphate
PKC, protein kinase C
PKD, protein kinase D
PKR, protein kinase RNA-activated
PLC, phospholipase C
PMA, phorbol-12-myristate-13-acetate
PMAIP1, phorbol-12-myristate-13-acetate-induced protein 1
poly-(dA:dT), poly(deoxyadenylic-deoxythymidylic) acid
PPIA, peptidyl-prolyl cis-trans isomerase A
PPIF, peptidyl-prolyl cis-trans isomerase A
PRR, pattern recognition receptor
PYCARD/*Pycard*, PYD and CARD domain-containing protein (the name of the gene encoding ASC)

PYD, pyrin domain
qPCR, quantitative polymerase chain reaction
RAGE, receptor for advanced glycation end products
RIG-I, retinoic acid-inducible gene-I
RIPK, receptor-interacting serine/threonine-protein kinase
RLR, RIG-I-like receptor
RNA, ribonucleic acid
ROS, reactive oxygen species
rpm, revolutions per minute
RPMI, Roswell Park Memorial Institute [tissue culture medium]
rRNA, ribosomal RNA
RT, room temperature
s, second
SCAP, sterol regulatory element-binding protein cleavage-activating protein
SD, standard deviation
SERCA, sarco/endoplasmic reticulum Ca^{2+}-ATPase
SGK, serum and glucocorticoid-regulated kinase
shRNA, short hairpin RNA
Slc25a4, Solute Carrier Family 25 Member 4 (also known as adenine nucleotide translocator 1)
SLR, sequestosome-1-like receptor
SMAC, second mitochondria-derived activator of caspases
ss, single-stranded
STING, stimulator of interferon genes
tBid, truncated Bid
TCR, T-cell receptor
TGOLN2, Trans-Golgi Network Protein 2
TIM, translocase of the inner [mitochondrial] membrane
TIR, Toll/IL-1 receptor homology [domain]
TLR, Toll-like receptor
TOM, translocase of the outer [mitochondrial] membrane
TOMM20, Mitochondrial import receptor subunit TOM20 homolog
TRIF, TIR-domain-containing adaptor inducing interferon-β
tRNA, transfer RNA
TSPO, translocator protein (also known as peripheral benzodiazepine receptor)
TXNIP, thioredoxin-interacting protein
UPR, unfolded protein response
UPR^{mt}, mitochondrial unfolded protein response
VDAC, voltage-dependent anion channel
WT, wild-type
XIAP, X-linked inhibitor of apoptosis protein
Y. pestis, *Yersinia pestis*
ZBP1, Z-DNA-binding protein 1
$\Delta\Psi$, potential gradient

1. Introduction

1.1. Overview of mammalian immune systems

All animals share their bodies and their environment with other organisms, including viruses, bacteria, and fungi. Most of these microorganisms are neutral or beneficial to their hosts (Dethlefsen et al., 2007) but some of them, if allowed to reproduce and/or spread in an uncontrolled manner, may pose a threat to the host survival (Méthot and Alizon, 2014). The ability to detect microorganisms and mount appropriate responses is an essential component of normal animal physiology. Such responses can lead to spatial containment of the microorganisms, to tolerance, or they may aim at eliminating potential pathogens. Classically, coordination of host interactions with the surrounding microbes is the primary function of the immune system (Pradeu, 2020).

Mechanisms defined as *immune* have been identified in all branches of the tree of life; it has been proposed that possession of an immune system is an inherent feature of all living organisms (Pradeu, 2020). Consequently, the diversity of the described immune systems is immense. In my thesis, I investigated immune pathways active in murine and human cells, so in this Chapter I will present a brief characterization of mammalian immunity. Of note, the principal characteristics of the immune systems of mammals are shared with other vertebrates.

The mammalian immune system can be described in terms of a 'layered' structure consisting of the following levels: (1) physical and chemical barriers, (2) constitutive innate immune responses, (3) induced innate immune responses, and (4) adaptive immune responses (Paludan et al., 2020).

The physical barriers, chiefly the skin and the mucous membranes lining organs such as the lungs and the intestines, enable mechanical separation between the host and the microorganisms. These surfaces are also the site of action of host factors contributing to antimicrobial defenses, such as antimicrobial peptides and lysozyme. Importantly, barrier organs may be inhabited by commensal microbial communities. One of the consequences of this microbial colonization is that the commensal microorganisms

compete with potential pathogens, promoting host protection (Holt et al., 2008; Murphy, 2016; Peterson and Artis, 2014; Spadoni et al., 2017).

The constitutive innate immune responses are permanently active processes that may contribute to antimicrobial defense but frequently also have other functions. Examples of such responses include constitutive phagocytosis, autophagy, proteasomal degradation of proteins, and hydrolysis of nucleic acids by nucleases present in the extracellular fluid, in the lumen of the endolysosomal compartment, and in the cytosol (Bartok and Hartmann, 2020). Of note, some of the constitutive innate immune mechanisms are not only active in professional immune cells but also in multiple other cell types as well as in blood plasma and in interstitial fluids. Many constitutive innate immune responses promote physical separation and hydrolytic degradation of microbes and dead or damaged host cells. As a consequence, the microbial components and host cell debris are being turned over and their buildup is prevented (Paludan et al., 2020).

The induced innate immune responses can be defined as processes that are not active in the absence of microbe- or damaged host cell-derived signals and only initiated under conditions indicative of tissue damage or microbial invasion (Paludan et al., 2020). The nature of the activating signals, frequently interpreted as immunological danger signals, is still a matter of debate. I will discuss the current hypotheses on the mechanisms of initiation of the induced innate immune responses in Section 1.2. Important characteristics of these responses are the relative speed at which they occur, the reliance on germline-encoded sensors and receptors, and the involvement of several specialized immune cell types as well as non-immune cells (Murphy, 2016). Of note, the activity of immune pathways in cell types classically regarded as non-immune is termed *cell-autonomous immunity*. Its consequence is that non-immune cells may detect signs of microbial invasion and either recruit support of professional immune cells, or even attempt to eliminate the threat on their own (Randow et al., 2013).

The mechanisms employed during induced innate immune responses aim at eliminating a potential threat, but also at informing other cells in the body of the host about a potentially dangerous situation and at recruiting some of these cells to fight a microbial invasion (Murphy, 2016). The specific inducible innate immune mechanisms include receptor-mediated phagocytosis, targeted degradation and chemical inactivation of

microbes, production and release of molecular signals that inform other cells about the ongoing immune process, and immunological cell death.

Phagocytosis of an encountered microbe typically leads to its degradation by hydrolases in the lysosomal compartment and by chemical antimicrobial agents such as reactive oxygen species (ROS) (Dupré-Crochet et al., 2013; Gordon, 2016). Microbes found in the cytosol may be targeted by autophagy, which can also lead to elimination of pathogens through fusion of autophagosomes with vesicles of the endolysosomal compartment (Gomes and Dikic, 2014). In addition to the direct antimicrobial effects, foreign material internalized through phagocytosis and autophagy may be processed and transported to organs known as lymph nodes (Blander, 2008; Germic et al., 2019). There, these antigens are used for instruction and activation of the adaptive immune responses (Murphy, 2016).

Under certain conditions, cells may use programmed cell death as an innate immune mechanism. This encompasses two classes of scenarios. First, the death of an immune cell may occur in response to an intracellular infection in an autonomous manner. This eliminates the replication niche of a pathogen and may also lead to the release of danger signals for the neighboring cells (Man et al., 2017). The second scenario involves the immune cell-mediated induction of programmed cell death in infected or otherwise harmful cells (Murphy, 2016).

Apart from direct engagement of antimicrobial mechanisms, innate immune cells also produce a wide range of molecules that inform other cells about the status of a microbial invasion and/or an immune response. These signaling molecules include lipid mediators (arachidonic acid derivatives known as eicosanoids; Soberman and Christmas, 2003) and proteins: chemokines (Griffith et al., 2014), cytokines (Altan-Bonnet and Mukherjee, 2019), and interferons (Ivashkiv and Donlin, 2013). Collectively, these molecules coordinate the actions of immune and non-immune cells (for example, smooth muscles or blood vascular endothelium). Eicosanoids, chemokines, cytokines, and interferons may serve as calls for support from other immune cells, and the intercellular communication that these molecules mediate helps achieve an optimal outcome of the immune response.

The cells of the hematopoietic system responsible for mounting innate immune responses are monocytes, macrophages and dendritic cells, granulocytes (neutrophils, basophils, and eosinophils), mast cells, and natural killer (NK) cells (Murphy, 2016). Monocytes and macrophages are phagocytes patrolling the blood and peripheral tissues. They can both phagocytose and eliminate microbes, and produce lipid mediators, chemokines, cytokines, and interferons to provide information about a potential threat for other cells in the body. Monocytes and macrophages may also process antigens and present them to T cells (Jakubzick et al., 2017), but dendritic cells, another phagocytic cell type, are considered more specialized in this function.

Neutrophils are professional microbicidal phagocytes that can internalize microbes and kill them inside of the phagolysosomal compartment vesicles using hydrolytic enzymes and ROS (Segal, 2005). They may also release their contents to fight bacterial and fungal infections outside of the cell (Amulic et al., 2017; Brinkmann, 2004). Eosinophils and basophils release granules with proteolytic and chemical factors in response to multicellular parasites. Mast cells may also release their granules on the surface of parasitic organisms (Murphy, 2016).

NK cells stand in contrast to the cell types described so far in this section both with respect to their ontogeny (NK cells derive from a common lymphoid progenitor, whereas the other mentioned innate immune cell types are myeloid cells) and to their contribution to the immune defense: NK cells may recognize certain virus-infected or tumor cells, and release factors triggering programmed cell death of these cells in a targeted manner (Murphy, 2016).

***

In contrast to innate immunity, the adaptive immune responses rely on non-germline-encoded antigen recognition system. Adaptive immunity is driven by lymphocytes: B cells and T cells. Their receptors, respectively, are called B-cell and T-cell receptors (BCRs and TCRs) and they are products of somatic recombination and, in the case of BCRs, subsequent mutagenesis. In vertebrates, these processes generate a highly diverse repertoire of antigen-specific immune receptors and also result in the formation of antigen-specific memory. The adaptive immune response is substantially slower than

innate immune responses, as time is needed for clonal expansion of antigen-specific B cells and T cells. Importantly, innate immune cell types and mechanisms are necessary to mount adaptive immunity, and, conversely, the adaptive immune responses direct the behavior of innate immune cells (Jack and Pasquier, 2019; Murphy, 2016).

BCRs and their soluble forms, termed antibodies, bind to antigens in their native form, either on the surface of the microbes or the infected cells, or in bodily fluids. Antibodies, depending on their class and isotype, can mark their targets for opsonization and lysis, phagocytosis by myeloid phagocytes, NK cell-mediated killing, or the release of granulocyte contents, or they can directly neutralize the activity of bacterial toxins or counteract viral entry into host cells (Lu et al., 2017).

TCRs recognize peptide antigens presented on the surfaces of other cells in the context of major histocompatibility complex (MHC)-I or II molecules. These antigens are no longer in their native state, and instead undergo multistep processing. T lymphocytes may be very broadly divided into $CD4^+$ (helper) T cells, which provide signals driving macrophage and B-cell responses, and $CD8^+$ (cytotoxic) T cells, which can directly kill virus-infected or tumor cells (Jack and Pasquier, 2019; Murphy, 2016).

***

Even though immunity had been classically associated with infection biology, it has become clear that the immune system also plays a role in multiple physiological processes not directly related to the host-microbe interactions. These include homeostatic clearance of dead cells and their molecular remnants, as well as developmental and regeneration processes (Pradeu, 2020). Furthermore, immunity is not always targeted at foreign microorganisms; the immune responses can also be mounted against the components of the host, which may lead to autoinflammatory (Dinarello, 2009) and autoimmune pathologies (Rosenblum et al., 2015). Finally, there are instances where infection-related and -unrelated inputs result in the activation of similar host responses; I will provide an example of such a situation in Section 1.2, where the integrated stress response (ISR) will be described as one of cell-autonomous innate immune mechanisms (Pakos Zebrucka et al., 2016).

In my Thesis, I investigated a protein complex known as the inflammasome. The inflammasome activation has initially been described in macrophages and dendritic cells (Martinon et al., 2002), and it is best understood in the context of innate immune responses. Therefore, in the next sections I will focus on the mechanisms by which innate immune cells sense the microbes and sterile (host) damage (Section 1.2). As the inflammasome signaling is the subject of my research, this process will be discussed in particular detail (Sections 1.3 and 1.4).

1.2. Activation mechanisms of induced innate immune responses

Three classes of signals recognized by the innate immune system can be distinguished: pathogen-associated molecular patterns (PAMPs; Janeway, 1989), damage-associated molecular patterns (DAMPs; Gong et al., 2019; Land, 2003), and homeostasis-altering molecular processes (HAMPs; Liston and Masters, 2017).

PAMPs are microbial-derived molecules whose presence or anomalous localization is indicative of infection. Examples of PAMPs include lipopolysaccharide (LPS), a component of the outer membrane of Gram-negative bacteria, bacterial lipoproteins, and flagellin, a building block of bacterial flagella (Kumar et al., 2011; Mogensen, 2009). An important group of PAMPs are also bacterial and viral nucleic acids, which may be distinguished from host nucleic acids based on specific chemical modifications and on atypical localization patterns (Bartok and Hartmann, 2020; Schlee and Hartmann, 2016).

DAMPs were initially defined as host-derived molecules that are normally shielded from innate immune receptors but may be exposed or released by damaged cells. Currently the abbreviation *DAMPs* is also frequently expanded as 'danger-associated molecular patterns', a broader and less well-defined category (Gong et al., 2019). Examples of canonical DAMPs include extracellular adenosine-5'-triphosphate (ATP) (Mariathasan et al., 2006; Pelegrín and Surprenant, 2006), displaced host nucleic acids (Bartok and Hartmann, 2020; Schlee and Hartmann, 2016), N-formylated peptides released from ruptured mitochondria (Dorward et al., 2015), or histones derived from ruptured nuclei (Allam et al., 2013). Collectively, PAMPs and DAMPs are chemically defined molecules or classes of molecules and the mechanisms by which they activate their cognate receptors

– the pattern recognition receptors (PRRs) – can usually be explained in terms of ligand-receptor interactions.

Somewhat in contrast, HAMPs have been proposed as a third category of innate immune responses-activating signals. HAMPs do not fit the definition of molecularly defined ligands and instead are biological processes whose abnormally high or low rate may be indicative of an infection or another type of pathology. It is generally believed that the information about disrupted homeostasis is transmitted to the HAMP sensors through post-translational modifications (Liston and Masters, 2017).

The group of receptors most frequently associated with PAMPs, DAMPs, and HAMPs recognition are the PRRs. Five protein families are classified in this group: Toll-like receptors (TLRs), nucleotide-binding oligomerization domain (NOD)-like receptors (NLRs), retinoic acid-inducible gene-I (RIG-I)-like receptors (RLRs), C-type lectin-like receptors (CLRs), and absent in melanoma 2 (AIM2)-like receptors (ALRs) (Takeuchi and Akira, 2010a). Sometimes the PRR definition is also proposed to include sequestosome-1-like receptors (SLRs), which can initiate autophagic engulfment of cytoplasmic contents (Deretic et al., 2013). PRR families, their agonists, and the effects of their activation (described below) are presented in Scheme 1.1.

TLRs and CLRs are membrane proteins and they sample the extracellular compartment (including the lumina of endosomes) for microbial products (Takeda et al., 2003). Examples of their ligands include bacterial lipoproteins (ligands of TLR1/2/6; Kirschning and Schumann, 2002; Takeda et al., 2002; Takeuchi et al., 2002), LPS (TLR4; Chow et al., 1999; Poltorak, 1998; Qureshi et al., 1999), flagellin (TLR5; Gewirtz et al., 2001; Hayashi et al., 2001), dsRNA (TLR3; Alexopoulou et al., 2001), DNA (TLR9; Hemmi et al., 2000), or the fungal saccharide beta-glucan (the CLR family member Dectin-1; Brown and Gordon, 2001). RLRs, NLRs, ALRs, and SLRs are all cytosolic proteins and they sample the contents of the intracellular compartment. RLR ligands are well-characterized and they include bacterial and viral RNA molecules (Chow et al., 2018; Rehwinkel and Gack, 2020), whereas the ligand for AIM2 is cytosolic dsDNA (Fernandes-Alnemri et al., 2009; Hornung et al., 2009).

The mechanisms of activation of NLRs are less well-defined. While some NLRs have defined direct ligands (for example, NOD2 binds to muramyl dipeptide, a component of bacterial cell walls; Girardin et al., 2003a; 2003b; Inohara et al., 2003) and some recognize their cognate ligands through an adaptor (for example, NLR family caspase activation and recruitment domain [CARD]-containing protein 4 [NLRC4] can be activated by flagellin and by components of bacterial type 3 secretion systems [Zhao et al., 2011b], which bind to adaptors known as baculoviral inhibitor of apoptosis domain [IAP] repeat-containing proteins [NAIPs[1]; Kofoed and Vance, 2011; Lightfield et al., 2008; Molofsky et al., 2006; Rayamajhi et al., 2013; Yang et al., 2013]), other NLRs, such as NACHT, LRR, and PYD domains-containing protein 1 (NLRP1) and NLRP3, have less straightforward activation mechanisms. It is generally considered that HAMPs may play a role in these processes (Liston and Masters, 2017). The existing models of NLRP3 activation will be discussed in Section 1.4.

In a simplified model, three classes of responses can be triggered by PRRs: induction of gene expression (by TLRs, CLRs, RLRs, and some NLRs; Takeuchi and Akira, 2010b), cell death (by several NLRs and the ALR family member AIM2; Man et al., 2017), or autophagy (by SLRs; Deretic et al., 2013; Gomes and Dikic, 2014). TLRs, CLRs, and some NLRs initiate pro-inflammatory gene expression through activation of the transcription factor nuclear factor kappa-light-chain-enhancer of activated B cells (NF-κB). This occurs in a multi-step cascade involving protein-protein interactions and post-translational modifications and leads to production of cell adhesion molecules, chemokines, which attract other immune cells to the site of infection, cytokines, which contribute to directing the course of the immune response as well as of inflammatory lipid mediators and nitric oxide. Additionally, activation of some TLRs may also cause activation of transcription factors termed interferon regulatory factors (IRFs), triggering a process known as type I interferon (IFN) response (Ivashkiv and Donlin, 2013). RLRs also initiate type I IFN response, albeit through a different signaling cascade than TLRs (Rehwinkel and Gack, 2020; Takeuchi and Akira, 2010b). Type I IFNs (IFN-α and -β) are secreted signaling proteins that were initially described as agents that counteract viral replication (Isaacs and Lindemann, 1957; Isaacs et al., 1957), for example, by

[1] The archaic name of this protein – and the source of the *NAIP* abbreviation – was *neuronal apoptosis inhibitory protein*.

suppressing protein translation and cell proliferation. Of note, the production of type I IFNs is not limited to viral infections.

The inflammatory cell death pathway initiated by PRR activation – specifically by the ALR family member AIM2 and the NLR family members NLRP1, NLRP3, NLRC4, and possibly NLRP6, NLRP12, and murine NLRP9B – is known as pyroptosis (Man et al., 2017). NLRP1, -3, -6, -9B, and -12 are paralogs sharing similar domain architecture: an N-terminal pyrin domain (PYD), a central nucleotide-binding oligomerization (NACHT) domain, and a C-terminal domain containing leucine-rich repeats (LRRs). Additionally, NLRP1 contains a function-to-find domain (FIIND) and a CARD, whereas the NLR family member NLRC4 has an N-terminal CARD instead of a PYD (Meunier and Broz, 2017). AIM2 has an N-terminal PYD but instead of NACHT and/or LRR domains, it has a C-terminal hematopoietic expression, interferon-inducible nature, and nuclear localization (HIN)-200 domain (Fernandes-Alnemri et al., 2009; Hornung et al., 2009; Jin et al., 2012). Collectively, these proteins can initiate the process of inflammasome activation.

Inflammasome activation involves the recruitment of an adaptor protein apoptosis-associated speck like protein containing a CARD (ASC) and, subsequently, of pro-caspase-1, a precursor form of the pyroptosis effector protease caspase-1 (Latz et al., 2013). Thus, the inflammasome serves as a caspase-1 activation platform. Caspase-1 activation enables the proteolytic cleavage of the pore-forming protein gasdermin (Gsdm) D, leading to pyroptotic cell death (He et al., 2015; Kayagaki et al., 2015; Shi et al., 2015b). Additionally, caspase-1 catalyzes the maturation of the pro-forms of the pro-inflammatory cytokine interleukin (IL)-1β and the pleiotropic cytokine IL-18 (Black et al., 1989; Ghayur et al., 1997; Kostura et al., 1989). In turn, these cytokines regulate transcriptional programs (IL-1β, IL-18) and proliferation/cell death (IL-1β) of neighboring cells (Garlanda et al., 2013).

Lastly, autophagy, which is an effector mechanism of SLRs, enables engulfment of both host- and microbe-derived material in the cytosol. This process results in the formation of autophagosomes, which can fuse with lysosomes leading to degradative clearance of the engulfed matter (Deretic et al., 2013; Gomes and Dikic, 2014). Unlike NF-κB- and IRFs-mediated transcriptional responses and pyroptosis, autophagy is a mechanism active under both basal and PAMP-, DAMP-, or HAMP-stimulated conditions. Therefore,

it can also be classified as a constitutive innate immune mechanism (Paludan et al., 2020).

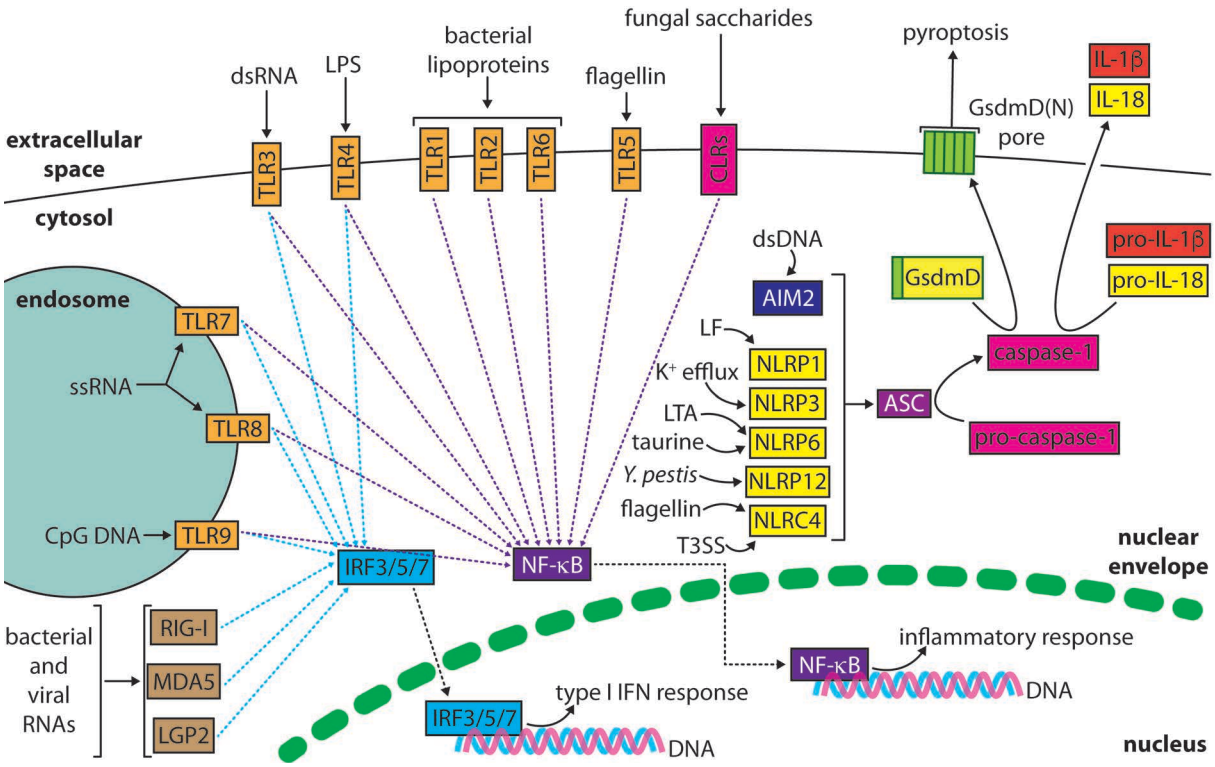

Scheme 1.1. Pattern recognition receptors, their ligands, and their signaling outputs
Toll-like receptors (TLRs) sample the contents of the extracellular space as well as the endosomal lumina for pathogen-associated molecular patterns (PAMPs) and damage-associated molecular patterns (DAMPs). Among the TLR ligands are bacterial lipoproteins and acylated peptides (TLR1/2/6), bacterial nucleic acids (TLR3/7/8/9), lipopolysaccharide (TLR4) and the bacterial protein flagellin (TLR5). In a simplified model, the activation of TLRs leads to the engagement of two groups of transcription factors: nuclear factor kappa-light-chain-enhancer of activated B cells (NF-κB) and interferon (IFN) regulatory factors (IRFs). This induces, respectively, the pro-inflammatory and the type I IFN transcriptional responses. Somewhat similar to TLRs, C-type lectin-like receptors (CLRs) are plasma membrane-resident proteins, whose activation induces an NF-κB-driven pro-inflammatory transcriptional response.
Retinoic acid-inducible gene I (RIG-I)-like receptors (RLRs) RIG-I, MDA5, and LGP2 are sensors of bacterial and viral RNA molecules. Indirectly, these receptors activate the IRF transcription factors, triggering the type I IFN response.
The inflammasome formation can be initiated by the absent in melanoma 2 (AIM2)-like receptor (ALR) AIM2 and by several members of the NOD-like receptor (NLR) family: NACHT, LRR, and PYD domains-containing protein 1 (NLRP1), NLRP3, NLRP6, NLRP12, and NLR family CARD domain-containing protein 4 (NLRC4). These proteins serve as receptors or sensors of molecules or physiological alterations associated with infection and/or tissue damage. Numerous factors and conditions have been described to activate inflammasomes: infection with *Yersinia* (*Y.*) *pestis*, bacterial and viral dsDNA, bacterial proteases (for example, lethal factor [LF] of *Bacillus anthracis*), taurine, lipoteichoic acid (LTA), and the components of bacterial type 3 secretion systems (T3SS). Activation of the inflammasome-forming proteins leads to the recruitment of an adaptor protein apoptosis-associated speck like protein containing a CARD (ASC) and the proteolytic maturation of the inflammasome effector – caspase-1. Caspase-1 cleaves gasdermin (Gsdm) D, and thus released N-terminal domain of GsdmD forms pores in the plasma membrane, resulting in pyroptotic cell death. Caspase-1 also cleaves the pro-forms of the pro-inflammatory cytokine interleukin (IL)-1β and the pleiotropic cytokine IL-18. Mature IL-1β and IL-18 are released through GsdmD pores (not pictured) as well as through other mechanisms.

Importantly, the model presented above provides a simplified version of the biological reality. Crosstalk between the innate immune pathways is a commonly observed phenomenon and, as a consequence, some innate immune response outcomes are difficult to predict (Jack and Pasquier, 2019). The results of PRRs activation are dictated by the doses of PAMPs, DAMPs, or HAMPs, the temporal characteristics of PRR stimulation, and the cell type-specific expression patterns of receptors/sensors, adaptor, and effector molecules (Cheng et al., 2020; Lee and Kim, 2007; Taylor et al., 2020).

In addition to canonical PRRs, several other proteins also fulfill the PRR definition in that they are activated under conditions indicative of infection or damage and they initiate signaling pathways aimed at counteracting a pathogen invasion. Examples of such receptors and sensors include protein kinase RNA-activated (PKR) (García et al., 2007), cyclic GMP/AMP (cGAMP) synthase (cGAS) (Ablasser et al., 2013; Civril et al., 2013; Sun et al., 2013), receptor for advanced glycation end products (RAGE) (Peng et al., 2016; Riehl et al., 2010), pyrin, or formyl peptide receptors (FPRs) (Dorward et al., 2015).

PKR is a cytosol-resident kinase that, upon binding to viral dsRNA molecules, initiates a set of processes known as the ISR (Pakos Zebrucka et al., 2016). The most prominent manifestation of the ISR is a global inhibition of translation. Notably, other signals can also activate the ISR. The unfolded protein response (UPR), or accumulation of unfolded proteins in the endoplasmic reticulum (ER), promotes activation of the ISR through activation of PKR-like ER kinase (PERK) (Harding et al., 1999), amino acid starvation triggers the ISR through activation of general control nonderepressible 2 (GCN2) kinase (Dever et al., 1993; 1992), and iron deficiency may activate heme-regulated inhibitor (HRI) kinase (Chen and London, 1995). Thus, the ISR is an example of a situation where both immune (PKR) and non-immune (PERK, GCN2, and HRI) inputs engage the same effector mechanism.

cGAS is a soluble cytosolic catalytic receptor that produces the cyclic dinucleotide cGAMP upon encountering dsDNA (Ablasser et al., 2013; Civril et al., 2013; Sun et al., 2013). cGAMP is a second messenger and a ligand for stimulator of IFN genes (STING), initiating the type I IFN response. RAGE is a plasma membrane protein acting as a receptor for multiple ligands, including extracellular DNA and RNA (Bertheloot et al.,

2016; Sirois et al., 2013). Ligation of RAGE by these molecules may trigger internalization of the agonist but also a transcriptional response (Peng et al., 2016; Riehl et al., 2010). Pyrin is an inflammasome-nucleating sensor of several bacterial toxins that becomes activated through post-translational modifications (Gao et al., 2016). Lastly, FPRs are plasma membrane-resident G protein-coupled receptors (GPCRs) that enable a chemotactic response of neutrophils. N-formylation is a chemical modification encountered in mitochondrially-encoded and bacterial peptides, serving as a potential PAMP and DAMP (Dorward et al., 2015).

RAGE, cGAS, and pyrin are examples of molecules that can initiate the same types of immune responses as PRRs despite the fact that they do not belong to the five or six canonical PRR families. PKR and FPRs are examples of PAMP and DAMP sensors that trigger responses outside of the typical PRR signaling outputs. Collectively, this demonstrates that PAMP, DAMP, and HAMP detection is not exclusively mediated by TLRs, NLRs, CLRs, ALRs, RLRs, and SLRs, and that the signaling outcomes of PAMP, DAMP, and HAMP recognition are not limited to transcription, cell death, and autophagy.

1.3. Inflammasome assembly and signaling: cell death as an effector mechanism of innate immunity

Inflammasomes are protein complexes minimally composed of a receptor/sensor molecule, the adaptor molecule ASC (recruited upon activation of the inflammasome-forming sensor/receptor), and the protease caspase-1. In molecular terms, inflammasome activation occurs through homotypic interactions between the death domains of the inflammasome components (Latz et al., 2013).

Inflammasome-forming molecules – AIM2 (Fernandes-Alnemri et al., 2009; Hornung et al., 2009), NLRP1 (Martinon et al., 2002), -3 (Hoffman et al., 2001), -6 (Hara et al., 2018; Levy et al., 2015), -9B (Zhu et al., 2017), -12 (Vladimer et al., 2012), and pyrin (Richards et al., 2001) – all have an N-terminal PYD, whereas NLRC4 (Zhao et al., 2011b) has an N-terminal CARD. ASC (encoded by the gene named *PYCARD*) consists of two death domains, an N-terminal PYD and a C-terminal CARD (Srinivasula et al., 2002). Inflammasome activating signals enable the interaction between the PYDs of ASC and the PYDs of an inflammasome-forming receptor/sensor molecule. In turn, the CARD of

ASC serves as a recruitment domain for pro-caspase-1, which also possesses a CARD. The close apposition of pro-caspase-1 molecules recruited to ASC enables caspase-1 autoproteolytic activation[2] (Elliott et al., 2009; Wilson et al., 1994).

Importantly, the PYDs of two ASC molecules can interact with each other, which has important consequences on the biophysical characteristics of the inflammasome complex. The current model proposes that activation of several molecules of the inflammasome sensor component leads to prion-like polymerization of virtually all molecules of ASC in the cell (Cai et al., 2014; Lu et al., 2014). This process results in the formation of one large (~1 μm) complex termed an ASC speck (Richards et al., 2001). Correspondingly, an ASC speck can recruit multiple molecules of pro-caspase-1. An important repercussion of the formation of a large prion-like ASC complex is the relative irreversibility of this process, as an ASC speck persists in, or even outside of, the cell after pyroptotic cell death (Baroja-Mazo et al., 2014; Franklin et al., 2014). A negative feedback in this system is provided by caspase-1 proteolytic self-inactivation (Boucher et al., 2018).

In most elementary terms, the function of inflammasomes is activation of caspase-1 (Martinon et al., 2002). The most well-studied substrates of caspase-1 include GsdmD (whose N-terminal domain released by the caspase-1-catalyzed cleavage forms pores in the plasma membrane) and the pro-forms of the cytokines IL-1β and IL-18 (Black et al., 1989; Ghayur et al., 1997; Kayagaki et al., 2015; Kostura et al., 1989). Insertion of GsdmD into the plasma membrane may lead to the loss of cell integrity, promoting lytic cell death (Kayagaki et al., 2015; Liu et al., 2016; Shi et al., 2015b). However, activation of caspase-1 can trigger cell death also in the absence of GsdmD (Kayagaki et al., 2015). GsmdD pores also serve as a release gate for mature IL-1β and IL-18 (Heilig et al., 2018; Hu et al., 2020), although other secretion routes have also been proposed (Monteleone et al., 2018).

[2] Activation of the NLRP1 and NLRC4 inflammasomes is, to an extent, an exception to this scenario. NLRC4 can directly recruit both ASC and pro-caspase-1 through CARD-CARD interactions, whereas NLRP1, which contains both a PYD and a CARD, can recruit pro-caspase-1 directly as well as through the ASC adaptor (Broz et al., 2010; Jin et al., 2013; Nour et al., 2009; Poyet et al., 2001; Van Opdenbosch et al., 2014; reviewed by Malik and Kanneganti, (2017)).

IL-1β induces a pro-inflammatory response through activation of the NF-κB transcription factor in neighboring cells; it also plays a role in neutrophil recruitment. Systemic release of IL-1β promotes fever and other signs of inflammation such as production of acute phase proteins in the liver. IL-18-triggered signaling also leads to activation of NF-κB and systemically injected IL-18 has pro-inflammatory activity (Dinarello, 2017). However, IL-18 release in the gut is suggested to be constitutive and in some experimental models it promotes the barrier function of the gut epithelium (Elinav et al., 2011; Levy et al., 2015). This evidence of the protective activity of IL-18 suggests that it may be prudent to classify this cytokine as pleiotropic rather than pro-inflammatory.

Pyroptosis, the cell death pathway initiated by the caspase-1-mediated cleavage of GsdmD, can deliver pro-inflammatory signals to the neighboring cells. Additionally, pyroptosis is suggested to function as a mechanism to eliminate the replicative niche of intracellular pathogens (Man et al., 2017), and even trap such microorganisms inside the pyroptotic cell remnants. This may facilitate spatial containment of pathogens and subsequent phagocytosis by neutrophils (Jorgensen et al., 2016).

Inflammasome signaling was initially described in myeloid cells: monocytes, macrophages, and dendritic cells (Martinon et al., 2002), as well as in microglia, the brain-resident macrophages (Heneka et al., 2012). While inflammasome activation is beneficial for certain antiviral (Allen et al., 2009) and antifungal (Hise et al., 2009) defenses, this immune response also gained recognition as a driving force behind the pathogenesis of diseases such as atherosclerosis (Duewell et al., 2010; Rajamäki et al., 2010), gout (Martinon et al., 2006), Alzheimer's disease (Heneka et al., 2012) as well as a range of genetic disorders caused by hypermorphic NLRP3 variants (Hoffman et al., 2001). Pharmacological inhibition of IL-1 signaling is a successful therapeutic strategy in genetic inflammasomopathies (Dinarello et al., 2012), and recent evidence suggests that IL-1β blockade may also lead to beneficial outcomes in cardiovascular diseases (Ridker et al., 2017). Studies in animal models suggest that inflammasome-forming molecules such as NLRP3 could also become drug targets in the future (Mangan et al., 2018).

Accumulating evidence also indicates that the inflammasome signaling is not limited to myeloid cells. In $CD4^+$ T cells, inflammasome activation has been proposed to be

involved both in optimal antiviral responses (Arbore et al., 2016) and in autoimmune pathology (Li et al., 2019). Furthermore, inflammasome signaling may contribute to cell-autonomous immunity in barrier organs such as the skin (Zhong et al., 2016) and the gut (Levy et al., 2015; Mukherjee et al., 2020).

1.4. Mechanisms triggering inflammasome activation

The mechanisms downstream of inflammasome formation – the activation of caspase-1 and GsdmD, the lytic cell death, and the physiological outcomes of IL-1β and IL-18 secretion – are relatively well understood. In contrast, the processes that lead to inflammasome assembly by the inflammasome sensor/receptor components are still being investigated. AIM2 and NLRC4 both have well defined molecular ligands (Fernandes-Alnemri et al., 2009; Hornung et al., 2009; Zhao et al., 2011b). The AIM2 agonist is cytosolic dsDNA, whereas NLRC4 recognizes the bacterial proteins flagellin and components of the type 3 secretion systems through adaptors from the NAIP family.

The activation mechanisms of NLRP1, NLRP3, and pyrin are much more complicated. These proteins are examples of HAMP sensors that are probably regulated by combinations of post-translational modifications (Liston and Masters, 2017). NLRP1 is activated during *Bacillus anthracis* infection; specifically, it is a target of the protease lethal factor produced by this bacterium (Boyden and Dietrich, 2006; Hellmich et al., 2012; Levinsohn et al., 2012). Lethal factor cleaves NLRP1 close to the N-terminus, destabilizing the sensor and leading to its ubiquitination. A partial proteasomal degradation of NLRP1 ensues and a C-terminal portion of NLRP1 is released to trigger ASC speck assembly (Chui et al., 2019; Sandstrom et al., 2019). Of note, other bacterial effectors also enhance NLRP1 ubiquitination and proteasomal degradation (Sandstrom et al., 2019), suggesting that NLRP1 could be an integration hub for several signals indicative of bacterial invasion. The NLRP1 activation model is an example of autoinhibition release mediated by controlled proteolysis.

Pyrin is present in cells in a constitutively phosphorylated form. This pyrin form is sequestered in an inactive conformation by proteins called 14-3-3ε, preventing inflammasome activation. Pyrin-phosphorylating kinases are indirectly inhibited during several bacterial infections, leading to a gradual loss of pyrin phosphorylation,

dissociation of the 14-3-3ε proteins, and a shift toward the active pyrin conformation, which nucleates an ASC speck (Gao et al., 2016). The pyrin activation model is an example of sensor autoinhibition released by gradual erasure of a constitutive post-translational modification. Of note, there are additional signaling inputs impacting on the pyrin inflammasome activation, some of which are likely related to the status of the microtubule cytoskeleton. The tubulin polymerization inhibitor colchicine blocks the pyrin inflammasome assembly (Park et al., 2016).

Among inflammasome-forming receptors and sensors, NLRP3 may be the most relevant for human pathology but its activation mechanism is the most controversial. At present, four sources of inputs that activate the NLRP3 inflammasome are proposed to exist, namely the canonical NLRP3 activation (Mariathasan et al., 2006; Muñoz-Planillo et al., 2013; Perregaux and Gabel, 1994; Petrilli et al., 2007; Walev et al., 1995), the non-canonical NLRP3 activation (Kayagaki et al., 2015; 2011), the alternative NLRP3 activation (Gaidt et al., 2016), and NLRP3 activation by stimuli that directly target glycolytic metabolism and the mitochondria (Groß et al., 2016; Sanman et al., 2016; Wolf et al., 2016), which I will call here 'the metabolic NLRP3 activation mechanism'.

With few exceptions, the NLRP3 inflammasome assembly is a two-step process. The first stage is transcriptional priming, which can be mediated by TLRs as well as other pathways leading to activation of the transcription factor NF-κB. In most cell types, NLRP3 is not expressed under basal conditions, so the most important function of the priming stimulus is the induction of NLRP3 transcription (Bauernfeind et al., 2009). Similarly, pro-IL-1β is usually not present in cells under basal conditions, so the priming stimulus also enables production of this cytokine pro-form. Lastly, the priming stimulus is also proposed to impact on the NLRP3 inflammasome activation through additional mechanisms such as post-translational modifications (López-Castejón et al., 2013; Py et al., 2013; Song et al., 2017). However, several reductionist models indicate that NLRP3 overexpression allows to circumvent the requirement for inflammasome priming (Bauernfeind et al., 2009; Chen and Chen, 2018).

Importantly, under most circumstances, the priming stimulus is not sufficient for the NLRP3 inflammasome activation (Bauernfeind et al., 2009). Instead, NLRP3 synthesized upon TLRs stimulation remains in the cytosol in the inactive conformation until the cells

encounter a second stimulus, termed the triggering stimulus, which will induce the NLRP3 shift to the active conformation and the recruitment of ASC and caspase-1.

The canonical NLRP3 activation is initiated by stimuli that deplete K^+ ions from the cytosol (Mariathasan et al., 2006; Muñoz-Planillo et al., 2013; Perregaux and Gabel, 1994; Petrilli et al., 2007; Walev et al., 1995). Under homeostatic conditions, a gradient of K^+ ions exists across the plasma membrane, with the intracellular K^+ concentration of ~110-140 mM, and the extracellular K^+ concentration of ~5 mM. (This gradient is countered by the corresponding gradient of Na^+ ions, whose extracellular concentration is within the range of ~120-140 mM, and the intracellular concentration is ~10-20 mM.) Treatments such as the electroneutral K^+/H^+ ionophore nigericin (Pressman, 1976), extracellular ATP (an agonist of the purinergic receptor P_2X_7R, a low-selectivity metal cation channel; Mariathasan et al., 2006; Pelegrín and Surprenant, 2006), and lysosomal destabilization and rupture (Duewell et al., 2010; Hornung et al., 2008; Martinon et al., 2006; Rajamäki et al., 2010) have all been demonstrated to act as strong and specific NLRP3 activators in a manner dependent on K^+ efflux (Muñoz-Planillo et al., 2013).

The non-canonical NLRP3 activation is triggered by cytosolic LPS, which is a PAMP potentially indicative of an invasion by intracellular Gram-negative bacteria (Kayagaki et al., 2011; 2015; Shi et al., 2014). This pathway can also be triggered by several host-derived oxidized lipid species, which may be associated with membrane damage (Zanoni et al., 2016). Collectively, these agents are ligands for the human caspases-4 and -5 (their murine ortholog is caspase-11). These proteases catalyze cleavage of GsdmD (Kayagaki et al., 2015), whose N-terminal domain forms pores in the plasma membrane, leading to K^+ efflux and the engagement of – essentially – the canonical mechanism of NLRP3 activation (He et al., 2015; Shi et al., 2015b; for historical reasons, the nomenclature is somewhat misleading). Of note, caspases-4, -5, and -11 cannot catalyze the proteolytic maturation of pro-IL-1β and pro-IL-18, so while the intracellular LPS-induced response does not require the inflammasome for pyroptosis, it does require NLRP3 for the initiation of IL-1 signaling (Kayagaki et al., 2015).

The alternative NLRP3 activation is a less commonly encountered mechanism. It appears to be specific to monocytes from certain species (for example, this pathway is active in human but not murine monocytes) (Gaidt et al., 2016). The alternative NLRP3

activation is initiated by TLR4 binding to extracellular LPS, and over the course of several hours leads to NLRP3- and ASC-dependent caspase-1 activation. The mediators of this response are the TLR signaling adaptor Toll/IL-1 receptor homology (TIR)-domain-containing adaptor inducing interferon-β (TRIF), the kinase receptor-interacting serine/threonine-protein kinase 1 (RIPK1), the scaffold protein Fas-associated protein with death domain (FADD), and caspase-8. The alternative NLRP3 activation differs from the canonical and non-canonical pathways in that it does not rely on K^+ efflux and it is not associated with ASC speck formation. Unlike other instances of NLRP3 activation, in this model the priming signal (LPS) is sufficient for the NLRP3 inflammasome assembly without the need for the additional triggering stimulus (Gaidt et al., 2016). Of note, during influenza infection, a cytosolic viral sensor Z-DNA-binding protein 1 (ZBP1) has also been reported to engage caspase-8 to induce NLRP3 activation, but in this case the identified adaptor was RIPK3 (Kuriakose et al., 2016).

Lastly, I use the term 'metabolic' mechanisms of NLRP3 activation to describe a group of independently reported NLRP3-triggering stimuli that affect the cellular energy metabolism. These include R837 (imiquimod), a low molecular weight (LMW) inhibitor of the mitochondrial electron transport chain complex I (Groß et al., 2016), N-acetylglucosamine, a component of the cell walls of Gram-positive bacteria that acts as an inhibitor of the glycolytic enzyme hexokinase and promotes its dissociation from the voltage-dependent anion channel (VDAC) on the outer mitochondrial membrane (OMM) (Wolf et al., 2016), and two other inhibitors of glycolysis: koningic (heptelidic) acid and ENOblock (Sanman et al., 2016). The pathways currently proposed to engage the NLRP3 inflammasome are summarized in Scheme 1.2.

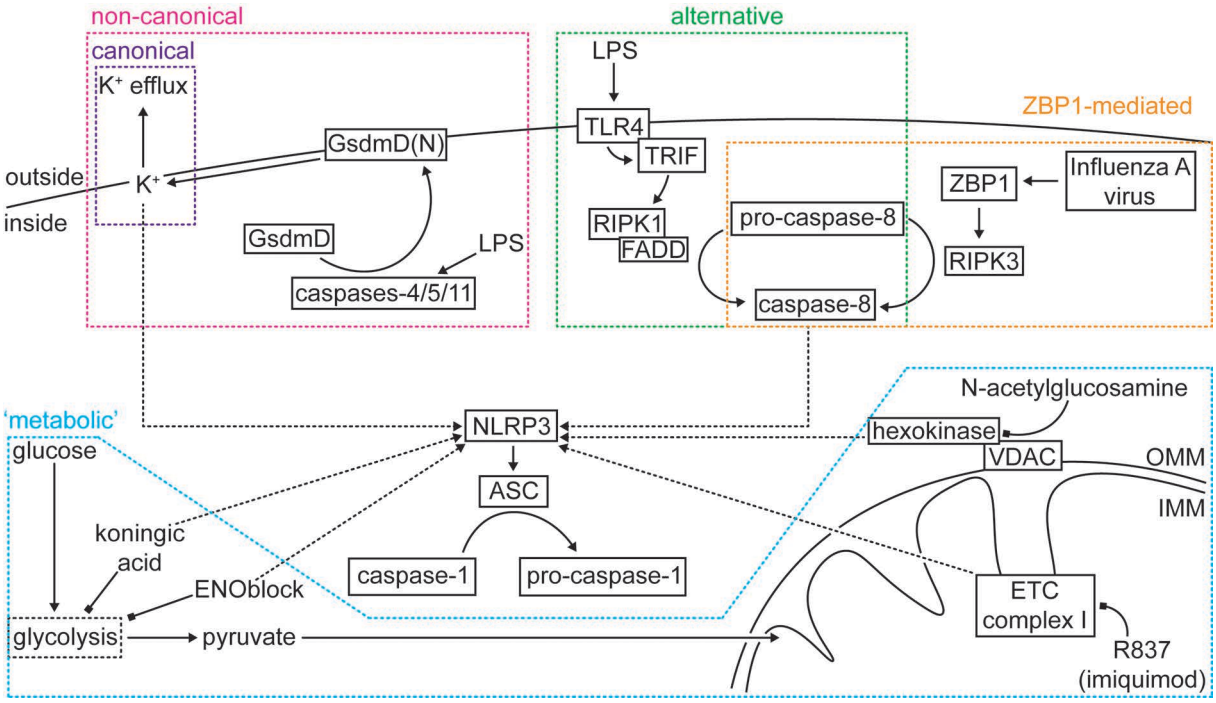

Scheme 1.2. The NLRP3 inflammasome as a hub integrating multiple signals
Multiple input signals have been suggested to activate the NACHT, LRR, and PYD domains-containing protein 3 (NLRP3) inflammasome. The canonical NLRP3 activation (purple) is initiated by stimuli that deplete the cytosolic K^+ pool by enabling K^+ efflux (for example, nigericin, ATP, or phagocytosed crystalline material). How the information about the decrease in the cytosolic K^+ concentration is transmitted to NLRP3 is still a matter of debate.
The non-canonical NLRP3 activation (pink) is triggered by cytosolic LPS, whose presence is detected by human caspases-4 or -5, or by murine caspase-11. These proteases release the N-terminal domain of gasdermin (Gsdm) D, which then translocates to the plasma membrane to form the pyroptotic pores. The GsdmD pores are a route for K^+ ions efflux, leading to the initiation of the canonical NLRP3 activation pathway.
The alternative NLRP3 activation (green) is a mechanism currently only described in human and porcine monocytes. This pathway is triggered by lipopolysaccharide (LPS) binding to Toll-like receptor (TLR) 4 and it leads to the NLRP3 inflammasome activation in a manner dependent on caspase-8. In this scenario, the activation of caspase-8 requires the engagement of a signaling cascade involving Toll/IL-1 receptor homology (TIR)-domain-containing adaptor inducing interferon-β (TRIF), receptor-interacting serine/threonine-protein kinase 1 (RIPK1), and Fas-associated protein with death domain (FADD).
RNA viruses like the influenza A virus may also trigger the NLRP3 inflammasome activation (yellow) in a caspase-8-dependent manner, in a mechanism involving the nucleic acid sensor Z-DNA-binding protein 1 (ZBP1) and RIPK3.
Lastly, several conditions altering the cell's energy metabolism have been reported to activate the NLRP3 inflammasome (blue). Among these stimuli are some inhibitors of glycolysis (N-acetylglucosamine, koningic acid and ENOblock) and R837 (imiquimod), an inhibitor of mitochondrial respiration. N-acetylglucosamine causes dissociation of the glycolytic enzyme hexokinase from the voltage-dependent anion channel (VDAC) on the surface of the mitochondria, whereas one of the activities of R837 is the inhibition of the mitochondrial electron transport chain (ETC) complex I.
OMM, outer mitochondrial membrane; IMM, inner mitochondrial membrane.

Collectively, the 'metabolic' stimuli trigger the NLRP3 inflammasome activation in a manner independent of K^+ efflux. It is currently unknown if R837, N-acetylglucosamine, koningic acid, and ENOblock circumvent the K^+ efflux requirement and directly target a proximal step in the NLRP3 activation cascade, or if they represent a distinct mechanism of NLRP3 activation. Given that the K^+ efflux-inducing NLRP3 activators are on the whole

stronger inflammasome agonists and that they seem to be active in a broader range of cell types than the 'metabolic' activators, the latter option is more likely.

***

A common feature of the NLRP3 activation mechanisms described above is that none of them propose a direct event triggering the NLRP3 shift from the inactive to the active conformation. For the canonical and non-canonical NLRP3 activation pathways, K^+ efflux appears to be the minimal NLRP3-activating stimulus (Muñoz-Planillo et al., 2013) but how the information about the decreased cytosolic K^+ concentration could be transmitted to NLRP3 is currently unknown. Similarly, it is unclear how caspase-8 could trigger the NLRP3 inflammasome assembly during the alternative or ZBP1-mediated activation (Gaidt et al., 2016; Kuriakose et al., 2016). While the impacts of R837, N-acetylglucosamine, koningic acid, and ENOblock on the cellular energy metabolism are well-described (Groß et al., 2016; Sanman et al., 2016; Wolf et al., 2016), it is not known how the information about the changes induced by these molecules is passed on to NLRP3. Consequently, the nature of the direct NLRP3-activating stimulus remains a topic of debate.

Multiple mechanisms have been proposed to be the direct signal-transducing modules that activate the NLRP3 inflammasome but none of them are universal and many have been demonstrated to stem from experimental artifacts. The best-studied group of NLRP3 triggers are K^+ efflux agonists, which elicit the canonical NLRP3 activation pathway (Mariathasan et al., 2006; Perregaux and Gabel, 1994; Petrilli et al., 2007; Walev et al., 1995). It was initially proposed that these stimuli induce the generation of mitochondrial (mt) ROS, and that these agents promote the formation of a complex between thioredoxin-interacting protein (TXNIP) and NLRP3, leading to the NLRP3 inflammasome formation (Zhou et al., 2009; 2010). Around the same time, two other models of the NLRP3 inflammasome activation were suggested. According to one of them, K^+ efflux agonists cause leakage of mtDNA into the cytosol and activation of NLRP3 through binding to oxidized (ox-) mtDNA (Nakahira et al., 2010; Shimada et al., 2012). Another model proposed that K^+ efflux agonists regulate the levels of two cytosolic second messengers: 3',5'-cyclic adenosine monophosphate (cAMP) and inositol 1,4,5-trisphosphate (IP_3) (Lee et al., 2012; Murakami et al., 2012; Rossol et al., 2012).

cAMP was suggested to directly bind to NLRP3 and act as an inhibitor of inflammasome activation (Lee et al., 2012; Sokolowska et al., 2015; Yan et al., 2015). The canonical NLRP3 activators were accordingly proposed to decrease the cytosolic cAMP concentration (Lee et al., 2012), releasing the inhibitory signal. In parallel, NLRP3 activators were also suggested to induce phospholipase C (PLC) through GPCR signaling (Lee et al., 2012; Murakami et al., 2012; Rossol et al., 2012). PLC is an enzyme that hydrolyzes the lipid phosphatidylinositol 4,5-bisphosphate (PIP_2) yielding two second messengers: diacylglycerol (DAG) and IP_3 (Kadamur and Ross, 2013). DAG may then function as an agonist for a class of signaling enzymes known as protein kinases C, whereas IP_3 binds to the IP_3 receptors (IP_3Rs), which are ligand-gated Ca^{2+} channels in the ER membrane. IP_3Rs opening releases Ca^{2+} ions to the cytosol, and this increase in the cytosolic Ca^{2+} concentration was proposed to act as an NLRP3 trigger (Lee et al., 2012; Murakami et al., 2012), although the specific mechanism has not been defined. In support of this model, a reported LMW PLC activator *m*-3M3FBS was shown to cause inflammasome activation (Lee et al., 2012; Muñoz-Planillo et al., 2013)[3]. Importantly, none of the NLRP3 activation mechanisms described in this paragraph are universally accepted; the role of mtROS upstream of the NLRP3 inflammasome formation was contested in a study by Muñoz-Planillo et al. (2013), and multiple studies provided evidence that the apparent link between Ca^{2+} signaling and NLRP3 activation is a product of experimental artifacts (Baldwin et al., 2017; Katsnelson et al., 2016; 2015; Muñoz-Planillo et al., 2013).

In addition to TXNIP, several other protein partners were proposed to form complexes with NLRP3, resulting in inflammasome activation. The kinase never in mitosis gene A (NIMA)-related kinase 7 (NEK7) was identified as an NLRP3 binding partner during the canonical NLRP3 activation (He et al., 2016; Schmid-Burgk et al., 2016; Shi et al., 2015a), and it was proposed that the interaction between NEK7 and NLRP3 is enhanced by mtROS (Shi et al., 2015a), similar to the interaction between NLRP3 and TXNIP. Other proteins reported to be required for the canonical NLRP3 activation are the gatekeeper of cholesterol synthesis sterol regulatory element-binding protein cleavage-activating protein (SCAP), which is a membrane protein in the endoplasmic reticulum (Guo et al.,

[3] The experimental models employed in the studies of the role of Ca^{2+} in NLRP3 activation are discussed in detail in Chapters 4, 5, and 6, whereas the experimental models used for demonstrating the role of ox-mtDNA in the NLRP3 inflammasome activation are discussed in Chapter 8.

2018) and the RNA helicase DEAD-box helicase 3 X-linked (DDX3X), which is involved in stress granule formation but has been proposed to mediate the NLRP3 inflammasome activation through a distinct mechanism (Samir et al., 2019). Furthermore, mitochondrial antiviral signaling protein (MAVS) was proposed to enhance the NLRP3 inflammasome responses (Subramanian et al., 2013), but these results have later been contested (Allam et al., 2014). To my knowledge, no studies have tested whether forced (for example, by synthetic dimerization domains) interactions between NLRP3 and its proposed binding partners are sufficient for inflammasome activation. Furthermore, very few studies addressed the possible biochemical and/or functional relationships between the different reported NLRP3 interaction partners.

In addition to forming complexes with other proteins, NLRP3 has also been proposed to be recruited to organelle membranes through interactions with lipids: the inner mitochondrial membrane (IMM) component cardiolipin (Iyer et al., 2013) and the Golgi apparatus phospholipid phosphatidylinositol 4-phosphate (PI4P) (Chen and Chen, 2018).

Finally, post-translational modifications of NLRP3 have also been proposed to serve as licensing steps during the NLRP3 inflammasome activation. To my knowledge, there is no instance where a post-translational modification is described as *sufficient* for NLRP3 activation, but there are reports of dephosphorylation steps that are *required* for NLRP3 activation (Stutz et al., 2017). Correspondingly, depending on the position of the modified amino acid residue, phosphorylation reactions were reported as both inhibiting NLRP3 (Guo et al., 2016; Mortimer et al., 2016) and required for NLRP3 activation (Zhang et al., 2017). Lastly, NLRP3 deubiquitination has also been proposed as a step required for the NLRP3 inflammasome assembly (Py et al., 2013; Ren et al., 2019).

Collectively, the multiple reports of NLRP3 post-translational modifications indicate that there may exist a phosphorylation/ubiquitination 'code', whereby combinations of post-translational marks shift NLRP3 between the inactive and the active conformations. In contrast, it does not seem plausible that NLRP3 activation could be a simple event of receptor oligomerization on a (multivalent) ligand. Taking at face value the results of the numerous studies on NLRP3 activation, it is very difficult to explain how NLRP3 could

simultaneously form complexes with the membrane components of several cellular compartments (the OMM [MAVS], the IMM [cardiolipin], the ER [SCAP], the Golgi [PI4P]). It is therefore likely that future research will reevaluate, refine, and unify the current models of the NLRP3 inflammasome formation.

Several NLRP family members have functions less clearly defined than NLRP1 and NLRP3. There is evidence that NLRP6 may nucleate an inflammasome in the presence of gut microbes-derived molecules such as taurine or lipoteichoic acid (Hara et al., 2018; Levy et al., 2015). Murine NLRP9B has been proposed to act as an inflammasome-forming dsRNA sensor in a model of viral infection (Zhu et al., 2017). NLRP12 has been proposed to form an inflammasome in response to infection with the bacterium *Yersinia pestis* (Vladimer et al., 2012) but it may also act as a negative regulator of the innate immune responses in an inflammasome-independent manner (Chen et al., 2017). Notably, NLRP10, the only NLRP subfamily member without the LRR domain, has been proposed to act as a negative regulator of inflammasome activation (Imamura et al., 2010; Murphy et al., 2013; Wang et al., 2004); the validity of these claims will be addressed in Chapters 6, 7, and 8 of my Thesis. NLRP10 was also proposed to regulate immune signaling in an inflammasome-independent manner (Clay et al., 2017; Damm et al., 2016; Lautz et al., 2012; Vacca et al., 2017).

The cellular and physiological processes involving NLRP2, -4, -5, -7, -8, -9, -11, -13, and -14 are not well defined and it is unclear whether these proteins can form functional inflammasome complexes. Importantly, the NLRP subfamily members with unknown function typically retain both the domain composition (PYD, NACHT, and LRR) and the conserved ATPase activity-warranting residues in the NACHT domain (MacDonald et al., 2013; Meunier and Broz, 2017), indicating their evolutionary conservation.

1.5. Mitochondria as a signaling hub for inflammasome activation and cell death

Mitochondria are organelles best known for their role in the cellular energy metabolism but currently also gaining attention as signaling hubs for inflammation and cell death. The mitochondrial structure can be divided into four subcompartments, the OMM, the IMM, the intermembrane space (IMS) between the OMM and the IMM, and the mitochondrial matrix, which is enclosed by the IMM. The OMM is permeable to water

and small solutes, whereas the IMM is a tight barrier across which a potential gradient ($\Delta\Psi^{mt}$) is generated by the activity of the respiratory chain. In the mitochondrial matrix resides mtDNA, the genomic material of these organelles encoding mitochondrial rRNAs and tRNAs as well as ~20 proteins. The remaining mitochondrial proteins are imported through a system of translocases in the OMM and the IMM, and further communication between the mitochondria and the cytosol is mediated by a range of solute transporters (Alberts et al., 2017). Mitochondria are a focus of innate immunity research because they are a potential source of DAMPs (mtDNA, mitochondrial RNAs, N-formylated peptides) but also of immunologically relevant metabolites, such as fumarate (Humphries et al., 2020) and itaconate (Hooftman et al., 2020; Mills et al., 2018).

Many studies proposed a role for the mitochondria in activation of the NLRP3 inflammasome. Specifically, NLRP3 has been proposed to bind to mtDNA (Nakahira et al., 2010; Shimada et al., 2012; Zhong et al., 2018)[4] and to MAVS (Subramanian et al., 2013). Furthermore, mtROS generation is proposed to cause, or at least support, NLRP3 activation and promote the interactions between NLRP3 and TXNIP (Zhou et al., 2010) and NLRP3 and NEK7 (Shi et al., 2015a). Two NLRP3 activators have been demonstrated to directly target the mitochondria: R837 (imiquimod) is an inhibitor of the mitochondrial electron transport chain complex I (Groß et al., 2016), and N-acetylglucosamine is an inhibitor of the glycolytic enzyme hexokinase that causes hexokinase dissociation from VDAC on the OMM (Wolf et al., 2016). The IMM lipid cardiolipin has also been proposed to act as a direct agonist of NLRP3 (Iyer et al., 2013). Lastly, NLRP3 translocation to the mitochondria has been observed in cells treated with inflammasome activators and it has been proposed that this step is required for the NLRP3 inflammasome assembly (Misawa et al., 2013). Importantly, some of the proposed mechanisms by which mitochondria-related events impact on the NLRP3 inflammasome activation have been challenged by later studies (for example by Muñoz-Planillo et al. (2013) and implicitly by Dang et al. (2017)). There is also no unified model of how the mitochondrial signals could be coordinated to activate the inflammasome.

[4] Of note, mitochondrial DNA has also been proposed to act as a ligand for the activation of the AIM2 inflammasome (Dang et al., 2017), and it has also been demonstrated to act as an agonist of cGAS (Huang et al., 2020; Maekawa et al., 2019; McArthur et al., 2018; Riley et al., 2018).

Mitochondria are known to be involved in the initiation of apoptotic cell death in a process termed intrinsic apoptosis (Bock and Tait, 2019; Kale et al., 2017). Briefly, the intrinsic apoptosis pathway is initiated by permeabilization of the OMM (MOMP, for mitochondrial outer membrane permeabilization), which results in the release of the protein cytochrome c from the IMS (Kluck, 1997; Yang, 1997). Cytochrome c is a direct ligand of apoptotic protease activating factor 1 (APAF1), a signaling protein that recruits and enables the activation of the protease caspase-9 (Li et al., 1997; Pan et al., 1998; Zou et al., 1997). Caspase-9, in turn, cleaves and thereby activates caspases-3 and -7, known as the executioner caspases[5]. These caspases coordinate a cell death program that involves cleavage of cytoskeletal proteins and of DNA, and cell fragmentation resulting in apoptotic bodies formation. The remnants of apoptotic cells can be cleared by tissue-patrolling phagocytes, typically macrophages. Of note, the enzymatic activity of apoptotic caspases may be blocked by a group of proteins known as inhibitor of apoptosis proteins (IAPs), including baculoviral IAP repeat-containing proteins (cIAPs) 1 and 2, and X-linked inhibitor of apoptosis protein (XIAP) (Deveraux, 1998; Roy, 1997; Takahashi et al., 1998). Until recently, apoptosis was considered to be a non-immunogenic, 'silent' form of programmed cell death, in opposition to pyroptosis and necrosis/necroptosis (not discussed here).

MOMP is a regulated process that involves formation of protein-lined pores by B-cell lymphoma 2 (BCL-2) homologous antagonist/killer (Bak; Chittenden et al., 1995; Kiefer et al., 1995), BCL-2-associated X, apoptosis regulator (Bax; Antonsson, 1997; Manon et al., 1997; Oltval et al., 1993; Wolter et al., 1997), and/or BCL-2-related ovarian killer (Bok; Hsu et al., 1997). Under basal conditions, Bak, Bax, and Bok are cytosolic proteins (Kale et al., 2017), and their cytosolic, inactive state is stabilized by a group of antiapoptotic BCL-2 proteins: BCL-2, BCL-2-like protein 2 (BCL-W), B-cell lymphoma-extra large (BCL-XL), and myeloid cell leukemia sequence 1 (BCL-2-related) (MCL-1) (Chao and Korsmeyer, 1998; Shamas-Din et al., 2013). Under conditions of antiapoptotic BCL-2 proteins depletion or pharmacological inhibition, Bak, Bax, and Bok may translocate to the OMM and form pores that enable the egress of cytochrome c into the cytosol (Bock and Tait, 2019; Kale et al., 2017). Alternatively, Bak/Bax/Bok pore

[5] For the sake of completeness, the extrinsic apoptosis pathway is initiated when a class of receptors in the plasma membrane are ligated by the so-called death ligands. Inside of the cell, death receptors recruit and activate caspase-8 through the adaptor FADD, and caspase-8 activates caspases-3 and -7 leading to the engagement of the programmed cell death effector mechanisms.

formation may be induced by pro-apoptotic members of the BCL-2 family such as the direct activators BCL-2 homology domain 3 (BH3) interacting-domain death agonist (Bid) and BCL-2-interacting mediator of cell death (Bim) or the so-called sensitizers BCL-2-associated agonist of cell death (Bad) and phorbol-12-myristate-13-acetate-induced protein 1 (PMAIP1, also known as Noxa) (Kale et al., 2017; Shamas-Din et al., 2011; Westphal et al., 2011; Zhang et al., 2012). While direct activators form complexes with Bax and shift this protein towards the pore-forming state, sensitizers sequester antiapoptotic BCL-2 family proteins, promoting the apoptotic pore formation through inhibition of the antiapoptotic signaling (Kale et al., 2017).

Bid, Bim, Bad, and Noxa can initiate MOMP through accumulation, prevailing over the anti-apoptotic BCL-2 proteins, but post-translational modifications may also play a role in this process (Kale et al., 2017). For example, the cleavage of Bid catalyzed by caspase-8 produces a truncated form of this apoptotic activator (tBid), which is a strong inducer of Bax pore formation (Gross et al., 1999; Li et al., 1998; Luo et al., 1998). A simplified model of the apoptotic MOMP is presented in Scheme 1.3.

The biophysical characteristics of Bak, Bax, and/or Bok pores and the exact mechanisms by which pore formation is induced are still a matter of debate (Kale et al., 2017). A recent report demonstrated that, in addition to Bak, Bax, and Bok, the N-terminal domain of GsdmE may also permeabilize the OMM to release cytochrome c. Interestingly, this process was described as a secondary event during the extrinsic apoptosis cascade and it was suggested to provide an amplification of the cell death-promoting signals by recruiting the molecular machinery of intrinsic apoptosis (Rogers et al., 2019). Surprisingly, recent reports also indicated that MOMP can trigger the permeabilization of the IMM (McArthur et al., 2018; Riley et al., 2018). Though the mechanism of this process is poorly understood and is currently proposed to involve IMM extrusion through Bak/Bax pores followed by mechanical rupture, the damage inflicted is sufficient to cause translocation of mtDNA to the cytosol, the induction of cGAS/STING signaling, and the type I IFN response (McArthur et al., 2018; Riley et al., 2018; reviewed by Bock and Tait, 2019).

In LPS-primed macrophages, the induction of the intrinsic apoptosis cascade has been demonstrated to cause IL-1β maturation and release. This reaction is suggested to be at

least in part mediated by the NLRP3 inflammasome (Deo et al., 2020; Lawlor et al., 2017; 2015; Vince et al., 2018). These observations rekindle the interest in whether and how mitochondrial stress could trigger the inflammasome activation.

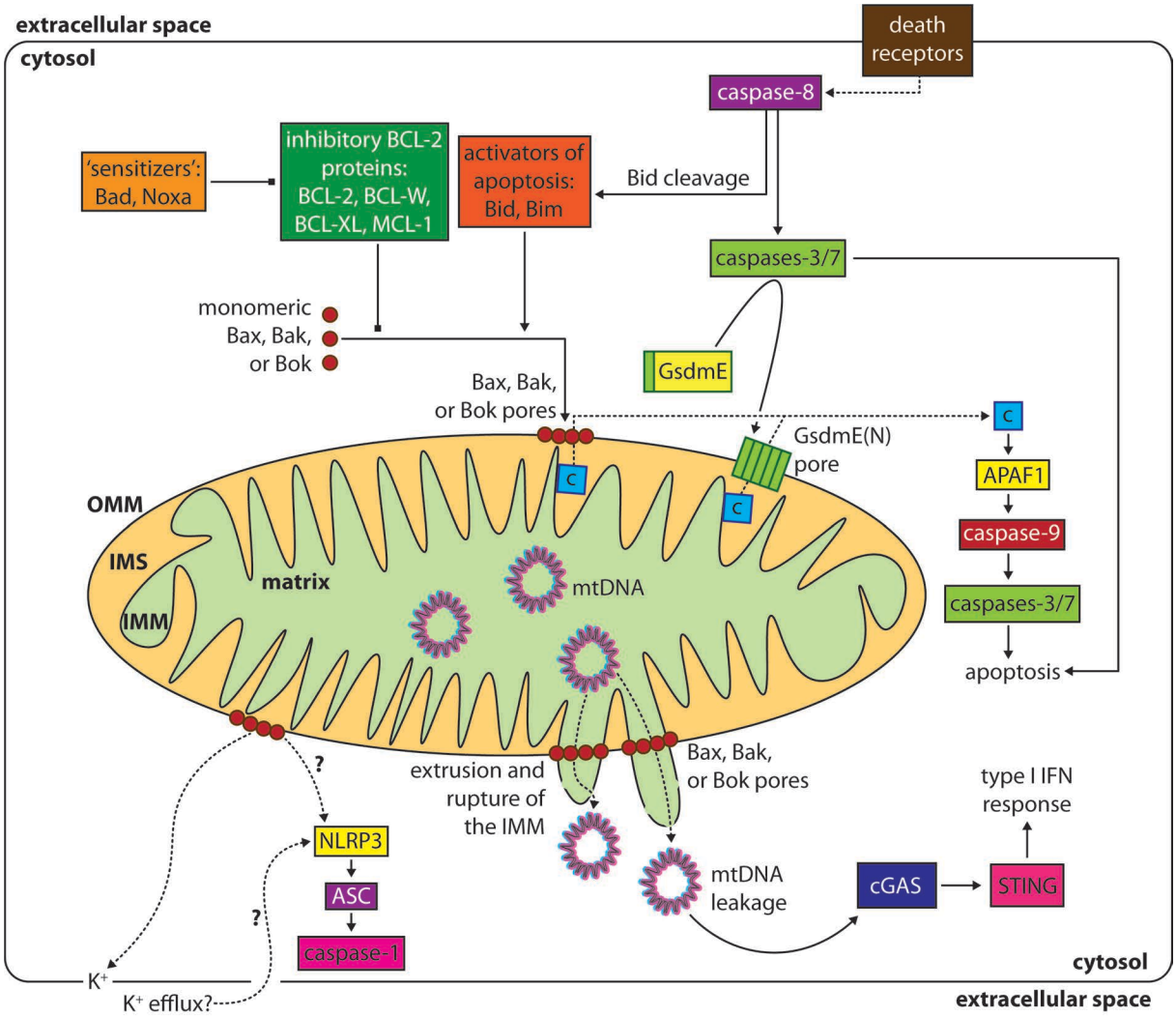

Scheme 1.3. A simplified model of mitochondrial cell death signaling
Apoptotic cell death can be initiated through the intrinsic and the extrinsic pathway. Intrinsic apoptosis beings with the permeabilization of the outer mitochondrial membrane (OMM) by Bax, Bak, and/or Bok. These three proteins are believed to form pores in the OMM. Inhibitors of apoptosis from the BCL-2 family (BCL-2, BCL-W, BCL-XL, MCL-1) prevent the OMM permeabilization, whereas apoptotic sensitizers (Bad, Noxa) and activators (Bid, Bim) promote Bax/Bak pore formation. Cytochrome c (c) released from the intermembrane space (IMS) upon mitochondrial permeabilization acts as a ligand for APAF1, which, when bound to cytochrome c, serves as an activation platform for caspase-9. This protease, in turn, activates the executioner caspases (caspases-3 and -7), causing apoptotic cell death.
The OMM permeabilization has recently been demonstrated to also lead to the permeabilization of the inner mitochondrial membrane (IMM). The molecular details of this process are lacking but it may involve extrusion of the IMM folds through Bax/Bak pores in the OMM. The concomitant permeabilization of both mitochondrial membranes exposes mtDNA to the cytosol, triggering the activation of cyclic GMP/AMP synthase (cGAS)/stimulator of interferon (IFN) genes (STING) signaling and type I IFN response. It has also been reported that permeabilization of the OMM and/or the IMM by pro-apoptotic stimuli may cause the NACHT, LRR, and PYD domains-containing protein 3 (NLRP3) inflammasome activation, possibly through a mechanism linked to K^+ efflux.
The extrinsic apoptosis pathway can be physiologically initiated be a group of proteins known as death ligands, which are agonists of death receptors in the plasma membrane. Ligation of these receptors

induces a signaling cascade leading to the activation of caspase-8, which, similar to caspase-9, activates the executioner caspases-3 and -7. Of note, caspase-8 also cleaves the apoptotic activator protein Bid, yielding a truncated (t) Bid form that is a strong inducer of the OMM permeabilization by Bax. Thus, the caspase-8-catalyzed Bid cleavage provides an amplification loop of the initial pro-apoptotic signal by engaging the intrinsic apoptosis mechanisms.
Recent studies also suggest that proteins other than Bax, Bak, and Bok may form pores in the OMM. One of these proteins is gasdermin (Gsdm) E. GsdmE is cleaved by the executioner caspases and the GsdmE N-terminal domain permeabilizes the OMM leading to the cytochrome c release and an APAF1-mediated secondary amplification of the pro-apoptotic signal.

In this respect, one pathway of mitochondrial damage not related to intrinsic apoptosis may be of interest. In the presence of increased ROS levels or high Ca^{2+} concentrations (Kwong and Molkentin, 2015), the mitochondria have been reported to undergo a process called the mitochondrial permeability transition (mPT). The mPT consists of the opening of the mitochondrial permeability transition pore (mPTP) in the IMM, which is permeable to water and small solutes (up to 1.5 kDa; Halestrap, 2009). This leads to the loss of $\Delta\Psi^{mt}$ and, according to some reports, to the swelling of the mitochondrial matrix and the rupture of the OMM. Neither the molecular composition nor the pharmacological properties of the mPTP are well-defined (I discuss this problem in detail in Section 9.6), so determining whether the mPT is involved in a process of interest is difficult.

The mPT has been proposed to occur during NLRP3 activation (Murakami et al., 2012; Yu et al., 2014), potentially leading to the release of mtDNA to the cytosol (Nakahira et al., 2010). The fact that a single mitochondrial nucleoid is much larger than the 1.5-kDa cutoff of the mPTP puts under question the validity of such a model. The literature is not conclusive on whether the mPT is actually required for the NLRP3 inflammasome activation; likely, at least in part, because of the difficulties in defining the molecular composition and the biophysical characteristics of the mPTP.

The involvement of the mitochondria in the innate immune responses will probably be an important research topic in the next couple of years. As regards the inflammasome signaling, the most important task will be to validate and unify the existing models of how mitochondria could regulate NLRP3 activation. A part of this effort will be to determine how mitochondrial damage could differentially cause the activation of NLRP3 (Nakahira et al., 2010; Shimada et al., 2012; Zhong et al., 2018), AIM2 (Dang et al., 2017), and cGAS (Huang et al., 2020; Maekawa et al., 2019; McArthur et al., 2018; Riley et al., 2018), and to establish which mitochondria-derived DAMPs could have an impact on these responses.

2. Rationale and objectives of the study

NLRP3 is an inflammasome-forming sensor implicated in numerous pathologies but the signaling events upstream of the NLRP3 inflammasome activation are still incompletely understood. Several scenarios have been proposed for how NLRP3 activation is controlled. One of these models posited that NLRP3 agonists induce activation of PLC and, consequently, cytosolic Ca^{2+} fluxes (Lee et al., 2012; Murakami et al., 2012; Rossol et al., 2012). While the involvement of Ca^{2+} ions in the NLRP3 inflammasome assembly has been contested (Baldwin et al., 2017; Katsnelson et al., 2015; 2016; Muñoz-Planillo et al., 2013), the role of PLC in NLRP3 activation has not been conclusively ruled out (Chae et al., 2015; Martín-Nalda et al., 2020).

The initial aim of my Thesis was **to explain if and how PLC activation by the LMW PLC agonist *m*-3M3FBS (Lee et al., 2012) leads to the NLRP3 inflammasome assembly**. However, at an early stage of my work, I found that the *m*-3M3FBS-induced inflammasome activation is NLRP3-independent (Chapter 4). Consequently, the aims of my Dissertation have been adapted to address the following scientific problems:

a) **to determine the mechanism through which PLC inhibitors (Lee et al., 2012; Murakami et al., 2012; Rossol et al., 2012) block the NLRP3 inflammasome activation** (Chapter 5);
b) **to identify the receptors and/or sensors involved in the inflammasome response to *m*-3M3FBS** (Chapter 6);
c) **to characterize the molecular mechanism by which *m*-3M3FBS activates the inflammasome** (chiefly Chapters 6, 8, and 9).

3. Materials and methods

3.1. Laboratory plastics and equipment

Table 3.1 provides a summary of laboratory plastics, equipment, and instrumentation used in my Thesis. Of note, the 96-well plates that were used for microscopy experiments (96-well plates, flat-bottom, tissue culture-treated, μ-clear, black wells [for imaging; Greiner Bio-One] and 96-well plates, flat-bottom, tissue culture-treated, Cell Carrier Ultra, black wells [for imaging; PerkinElmer]) were coated in-house with poly-L-lysine to improve cell adhesion. Briefly, 60-80 μL of ~0.01% aqueous solution of poly-L-lysine was added per well, followed by a 30-60-min incubation at room temperature (RT). This was followed by removal of the poly-L-lysine solution (to ensure that no traces of the coating solution remain in the wells, the plates were centrifuged in an upside-down position for 5 min at 1000 × g, at RT).

Type of product	**Source**
0.1-2 μL pipette	Mettler-Toledo/Rainin
2-20 μL pipette	Mettler-Toledo/Rainin
20-100 μL pipette	Mettler-Toledo/Rainin
100-1000 μL pipette	Mettler-Toledo/Rainin
2-20 μL 12-channel pipette	Mettler-Toledo/Rainin
20-200 μL 12-channel pipette	Mettler-Toledo/Rainin
20 μL pipette tips	Mettler-Toledo/Rainin
250 μL pipette tips	Mettler-Toledo/Rainin
1000 μL pipette tips	Mettler-Toledo/Rainin
20 μL filter tips	Mettler-Toledo/Rainin
200 μL filter tips	Mettler-Toledo/Rainin
1000 μL filter tips	Mettler-Toledo/Rainin
6-well plates, tissue culture-treated	VWR/Sarstedt/Greiner Bio-One
24-well plates, tissue culture-treated	VWR/Sarstedt/Greiner Bio-One
96-well plates, flat-bottom, tissue culture-treated	VWR/Sarstedt/Greiner Bio-One
96-well plates, flat-bottom, tissue culture-treated, μ-clear, black wells (for imaging)	Greiner Bio-One
96-well plates, flat-bottom, tissue culture-treated, Cell Carrier Ultra, black wells (for imaging)	PerkinElmer
96-well plates, V-bottom (for supernatant collection)	Greiner Bio-One
384-well plates, V-bottom (for supernatant collection)	Greiner Bio-One
384-well plates, low-volume, white (for HTRF assays)	Greiner Bio-One
PIPETBOY Acu2 Pipette Controller	Integra
~5-mL serological pipettes	Costar
~10-mL serological pipettes	Costar
~25-mL serological pipettes	Costar
Cell scrapers, small	Sarstedt
Cell scrapers, large	Sarstedt
Syringes (5 mL; for bone flushing)	BD Biosciences
Luer-Lok syringes (10 mL; for retrovirus harvesting)	BD Biosciences

Needles, 20 G (for bone flushing)	B. Braun
Blunt needles, 18 G (for retrovirus harvesting)	B. Braun
0.45 μm filters (for retrovirus purification)	Merck Millipore
25-cm² tissue culture flasks, tissue culture-treated, with filter	Greiner Bio-One
75-cm² tissue culture flasks, tissue culture-treated, with filter	Greiner Bio-One
175-cm² tissue culture flasks, tissue culture-treated, with filter	Greiner Bio-One
10-cm tissue culture dishes, tissue culture-treated	Greiner Bio-One
Cryopreservation vials	Greiner Bio-One
Mr. Frosty freezing containers	Thermo Fisher Scientific
CellCamper freezing containers	neoLab
Vacuum filter bottles, 100 mL	Corning
Vacuum filter bottles, 250 mL	Corning
Vacuum filter bottles, 500 mL	Corning
PCR tubes	Biozym
Eppendorf-type tubes, 1.5-mL	Eppendorf
Eppendorf-type tubes, 2-mL	Sarstedt
Conical tubes (Falcon-type), 15-mL	Greiner Bio-One
Conical tubes (Falcon-type), 50-mL	Greiner Bio-One
Liquid reservoirs, 50 mL	VWR
Liquid reservoirs, 12-channel	Carl Roth
Petri dishes for bacterial culture	Greiner Bio-One
15-mL tubes for small bacterial cultures	BD Falcon
Pasteur pipettes (glass)	Brand
Bunsen burner, Fuego Basic	WLD-TEC
PCR thermocycler, T3000	Biometra
Quant Studio 6 Flex System	Thermo Fisher Scientific
Spectramax i3 multi-mode platform with HTRF cartridge	Molecular Devices
Epoch Microplate Spectrophotometer with Take3 Micro-Volume Plate	BioTek/Agilent
Observer.Z1 fluorescence microscope	Zeiss
SP5 confocal microscope AOBS with SMD	Leica
Inverted phase-contrast microscope, TS100	Nikon
Tabletop fluorescence microscope, EVOS-FL	Thermo Fisher Scientific (Life Technologies)
IKA Vortex 3 mixer	Sigma/Merck
Large centrifuge (for 15-50-mL tubes and plates), 5810R	Eppendorf
Large centrifuge (for 15-50-mL tubes), 4-16KS	Sigma/Merck
Small centrifuge (for 1.5-2-mL tubes), 5425	Eppendorf
Neubauer cell counting chamber (0.1 mm)	Paul Marienfeld GmBH & Co.KG
Balance (~0.01 g accuracy), Entris	Sartorius
Balance (~0.001 g accuracy), Extend	Sartorius
Tissue culture incubator	Sanyo
Small bacterial shaker	Heidolph
Thermoshake incubator shaker	C. Gerhardt Analytical
Bacterial incubator	Thermo Fisher Scientific
AccuBlock thermoblock	Labnet
Thermomixer thermoblock	Eppendorf
4°C fridge	Liebherr
-20°C freezer	Liebherr
-80°C freezer	Thermo Fisher Scientific
-150°C freezer	Sanyo

Table 3.1. List of laboratory plastics and equipment used in my Thesis.

3.2. Molecular cloning

Cloning of all constructs was performed following standard procedures and according to the instructions provided by the manufacturers of all the reagents. The inserts were amplified by polymerase chain reaction (PCR) using the PfuUltra II Hotstart PCR Master Mix (Agilent Technologies). The PCR reactions were performed in 50 μL final volumes, using 0.5 μM forward and reverse primers and ~100-500 ng of DNA per reaction. For site-directed mutagenesis, the overlap-extension PCR protocol was used (Aiyar et al., 1996). Generally, PCR was initiated with a 1-min denaturation step (94°C), followed by 35 or 40 cycles of (1) denaturation (94°C, 30 s), (2) primer annealing (58-65°C, 30 s), and (3) elongation (72°C, 1 min/kb of DNA). At the end of the reaction, a 5- or 10- min final elongation step at 72°C was included. The PCR products were electrophoretically separated in an agarose (Biozym) gel (1-1.5%) with green DNA-RNA dye (PEQ-green, Peqlab/WVR; ~1.5×10^4 dilution) and isolated using PureLink Quick Gel Extraction kit (Invitrogen/Thermo Fisher Scientific). Next, sticky ends were generated by digestion with a pair of restriction enzymes (Thermo Fisher Scientific) according to the manufacturer's instructions in final volumes of 50 μL. Inserts generated in this fashion were re-run in an agarose gel (1-1.5%) and purified.

The backbone vectors were linearized by restriction by restriction digest with the same pair of restriction enzymes as the insert, and then isolated from a 1% agarose gel after electrophoretic digest.

Ligation (20 μL final volume) was performed according to the manufacturer's instructions. Briefly, the insert of interest was mixed with the backbone at the ratio of 3:1-9:1 and kept on ice (~4°C) with T4 DNA ligase (Thermo Fisher Scientific) in the presence of 1 × ligation buffer. After preparation of this reaction mix, the tubes were shifted to 22°C for 20 min. Then the. Then, the reaction mixes were returned to the ice bath. Vectors generated in this manner (1-5 μL) were used for transformation of chemically competent DH5α *Escherichia coli* cells (15 μL). The heat shock transformation protocol was employed; briefly, the cells were incubated with the ligation products on ice (~4°C) for 5 min, followed by 45-s incubation at 42°C, and a 2-min 'regeneration' step on ice (~4°C). Then, the transformed cells were diluted in Luria-

Bertani (LB) broth without antibiotics (~150 µL) and incubated for 30 min at 37°C with shaking (400-600 rpm). After this, the cells were plated in LB-agar (Thermo Fisher Scientific) plates with ampicillin (100 µg/mL, Sigma/Merck) used as selection antibiotic. All of the constructs used in my thesis contained the ampicillin resistance gene. Following an overnight incubation at 37°C, colonies were picked from agar plates. They were then used for inoculation of small bacterial cultures (6 mL, LB broth with 100 µg/mL ampicillin), which were grown for 16-18 h at 37°C with shaking (~360 rpm). After this time, bacterial cells from these cultures were harvested and plasmid DNA was isolated using the PureLink Quick Plasmid Miniprep kit (Invitrogen/Thermo Fisher Scientific), following the manufacturer's instructions. Complete sequences of the inserts from the purified plasmids were obtained by Sanger sequencing performed by GATC or Eurofins Genomics. Of the positive clones, one was selected to prepare a cryopreserved stock (bacterial suspension in LB broth with 100 µg/mL ampicillin supplemented with 25% glycerol [Sigma/Merck]; stored at -80°C). The glycerol stocks were used for inoculation of larger-scale bacterial cultures (120-150 mL grown in LB broth with 100µg/mL ampicillin for 16-18 h at 37°C with shaking [~340 rpm]), from which plasmid DNA was isolated using the PureLink Quick Plasmid Maxiprep kit (Invitrogen/Thermo Fisher Scientific). To ensure that the correct plasmids were amplified, the inserts were once again subjected to Sanger sequencing performed by GATC or Eurofins Genomics. For all subsequent applications, plasmid DNA from those validated Maxiprep preparations was used.

Several constructs that I used in my Thesis were cloned independently of my research project by other scientists at the III (Bonn); these cases are noted in the *Source and references* column in Table 3.2.

ID in the III database	**Insert**	**Applications**	**Source and references**
1051	Human NLRP1-IRES-mCitrine	Overexpression of human NLRP1	This Thesis
1052	Human NLRP2-IRES-mCitrine	Overexpression of human NLRP2	This Thesis
1053	Human NLRP3-IRES-mCitrine	Overexpression of human NLRP3	This Thesis
1054	Human NLRP4-IRES-mCitrine	Overexpression of human NLRP4	This Thesis
1055	Human NLRP5-IRES-mCitrine	Overexpression of human NLRP5	This Thesis

1133	Human NLRP6-IRES-mCitrine	Overexpression of human NLRP6	This Thesis
1134	Human NLRP6-linker-mCitrine	Overexpression of human NLRP6	This Thesis
1056	Human NLRP7-IRES-mCitrine	Overexpression of human NLRP7	This Thesis
1057	Human NLRP9-IRES-mCitrine	Overexpression of human NLRP9	This Thesis
1058	Human NLRP10-IRES-mCitrine	Overexpression of human NLRP10	This Thesis
1059	Human NLRP11-IRES-mCitrine	Overexpression of human NLRP11	This Thesis
1060	Human NLRP12-IRES-mCitrine	Overexpression of human NLRP12	This Thesis
1061	Human NLRP13-IRES-mCitrine	Overexpression of human NLRP13	This Thesis
1062	Human NLRP14-IRES-mCitrine	Overexpression of human NLRP14	This Thesis
1120	Human NLRP10-linker-mCitrine	Overexpression of human NLRP10	This Thesis
1612	Human NLRP10-linker-mCherry	Overexpression of human NLRP10	This Thesis
1121	Murine Nlrp10-linker-mCitrine	Overexpression of murine Nlrp10	This Thesis
1122	Human NLRP10(PYD)-linker-mCitrine	Overexpression of the PYD domain of human NLRP10	This Thesis
1123	Human NLRP10(NACHT)-linker-mCitrine	Overexpression of the NACHT domain of human NLRP10	This Thesis
1124	Murine Nlrp10(PYD)-linker-mCitrine	Overexpression of the PYD domain of murine Nlrp10	This Thesis
1125	Murine Nlrp10(NACHT)-linker-mCitrine	Overexpression of the NACHT domain of murine Nlrp10	This Thesis
1378	Human NLRP10^{K179M}-linker-mCitrine	Overexpression of a Walker A motif mutant of human NLRP10	This Thesis
1447	Human NLRP10^{D249N}-linker-mCitrine	Overexpression of a Walker B motif mutant of human NLRP10	This Thesis
1448	Human NLRP10^{D249A}-linker-mCitrine	Overexpression of a Walker B motif mutant of human NLRP10	This Thesis
1379	Murine Nlrp10^{K175M}-linker-mCitrine	Overexpression of a Walker A motif mutant of murine Nlrp10	This Thesis
1453	Murine Nlrp10^{D245N}-linker-mCitrine	Overexpression of a Walker B motif mutant of murine Nlrp10	This Thesis
1454	Murine Nlrp10^{D245A}-linker-mCitrine	Overexpression of a Walker B motif mutant of murine Nlrp10	This Thesis
241	mCitrine-linker-human AIM2	Overexpression of human AIM2	Generated by Dr. Andrea Stutz (III Bonn)
1044	Human AIM2-linker-TagGFP2	Overexpression of human AIM2	Generated by Brian Monks (III Bonn)
1349	Murine Aim2-IRES-mCherry	Overexpression of murine Aim2	This Thesis
1040	Human pyrin-IRES-mCitrine	Overexpression of human pyrin	Generated by Brian Monks (III Bonn)
799	Human ASC-linker-TagBFP	Overexpression of human ASC as a fusion protein with TagBFP, fluorescent reporter of ASC speck formation	MSc Thesis of Tomasz Prochnicki (III Bonn)
389	Human ASC-linker-mCerulean	Overexpression of human ASC as a fusion protein with mCerulean, fluorescent reporter of ASC speck	Generated by Brian Monks (III Bonn)

		formation	
596	HMGB1-linker-mCitrine	Overexpression of human HMGB1 as a fusion protein with mCitrine; due to the nuclear localization of HMGB1 under basal condition – fluorescent marker of the nuclei	Generated by Dr. Damien Bertheloot (III Bonn)
597	HMGB1-linker-mCherry	Overexpression of human HMGB1 as a fusion protein with mCitrine; due to the nuclear localization of HMGB1 under basal condition – fluorescent marker of the nuclei	Generated by Dr. Damien Bertheloot (III Bonn)
819	mCitrine targeted to the mitochondrial matrix using the COX8A sequence	Fluorescent marker of the mitochondrial matrix	Generated by Rainer Stahl (III Bonn)
820	mCherry targeted to the mitochondrial matrix using the COX8A sequence	Fluorescent marker of the mitochondrial matrix	Generated by Rainer Stahl (III Bonn)
1176	TOMM20-linker-mCitrine	Fluorescent marker of the mitochondria (integral protein of the OMM)	Generated by Marta Lovotti (III Bonn)
1177	MAVS-linker-mCitrine	Fluorescent marker of the mitochondria, peroxisomes, and mitochondria-associated membranes (transmembrane protein)	Generated by Marta Lovotti (III Bonn)
1163	DDOST-linker-mCitrine	Fluorescent marker of the ER	Generated by Marta Lovotti (III Bonn)
1216	TGOLN2-linker-mCitrine	Fluorescent marker of the Golgi apparatus	Generated by Marta Lovotti (III Bonn)
1165	LAMP1-linker-mCitrine	Fluorescent marker of the lysosomal compartment	Generated by Marta Lovotti (III Bonn)
1626	mTurquoise-linker-human PLCγ2 (WT)	Overexpression of human PLCγ2	This Thesis
1627	Human PLCγ2 (WT)-linker-mTurquoise	Overexpression of human PLCγ2	This Thesis
1630	mTurquoise-linker-human PLCγ2^{S707Y}	Overexpression of a reported hypermorphic variant of human PLCγ2	This Thesis
1631	Human PLCγ2^{S707Y}-linker-mTurquoise	Overexpression of a reported hypermorphic variant of human PLCγ2	This Thesis
1137	G_q α (WT)-IRES-mCherry	Overexpression of G_q α protein	This Thesis
1138	G_q α^{Q209L}-IRES-mCherry	Overexpression of a constitutively active variant of G_q α protein (GTPase-null)	This Thesis
1673	TagBFP-T2A- G_q α (WT)	Overexpression of G_q α protein	This Thesis
1674	TagBFP-T2A- G_q α^{Q209L}	Overexpression of a constitutively active variant of G_q α protein (GTPase-null)	This Thesis
849	Human galectin 1-linker-mCitrine	Overexpression of human galectin 1 as a fusion protein with mCitrine; galectin 1 speckle formation may indicate damage of the endolysosomal compartment	Generated by Dr. Matthew Mangan (III Bonn)
850	Human galectin 3-linker-mCitrine	Overexpression of human galectin 3 as a fusion protein with mCitrine; galectin 1 speckle formation may indicate damage of the endolysosomal compartment	Generated by Dr. Matthew Mangan (III Bonn)
851	Human galectin 8-linker-mCitrine	Overexpression of human galectin 8 as a fusion protein with mCitrine; galectin 1	Generated by Dr. Matthew Mangan

		speckle formation may indicate damage of the endolysosomal compartment	(III Bonn)
852	Human galectin 9-linker-mCitrine	Overexpression of human galectin 9 as a fusion protein with mCitrine; galectin 1 speckle formation may indicate damage of the endolysosomal compartment	Generated by Dr. Matthew Mangan (III Bonn)
1462	Human GsdmD^{FL}-IRES-mCherry	Overexpression of full-length human GsdmD (nontoxic)	Generated by Dr. Christina Budden (III Bonn)
1746	Human GsdmD$^{1-275}$-IRES-mCherry	Overexpression of the N-terminal domain of human GsdmD (cytotoxic)	This Thesis
1747	Human GsdmE^{FL}-IRES-mCherry	Overexpression of full-length human GsdmE (nontoxic)	This Thesis
1748	Human GsdmE$^{1-270}$-IRES-mCherry	Overexpression of the N-terminal domain of human GsdmE (cytotoxic)	This Thesis
1749	Human GsdmD^{FL}-linker-mCherry	Overexpression of full-length human GsdmD (nontoxic)	This Thesis
1750	Human GsdmD$^{1-275}$-linker-mCherry	Overexpression of the N-terminal domain of human GsdmD (cytotoxic)	This Thesis
1751	Human GsdmE^{FL}-linker-mCherry	Overexpression of full-length human GsdmE (nontoxic)	This Thesis
1752	Human GsdmE$^{1-270}$-linker-mCherry	Overexpression of the N-terminal domain of human GsdmE (cytotoxic)	This Thesis
288	MCS-IRES-mCitrine	Empty vector control (with fluorescent reporter and puromycin resistance gene)	Generated by Rainer Stahl (III Bonn)
289	MCS-IRES-mCherry	Empty vector control (with fluorescent reporter and puromycin resistance gene)	Generated by Rainer Stahl (III Bonn)
290	MCS-IRES-mTurquoise	Empty vector control (with fluorescent reporter and puromycin resistance gene)	Generated by Rainer Stahl (III Bonn)
1516	TagBFP-T2A-MCS	Empty vector control (with fluorescent reporter and puromycin resistance gene)	Generated by Fraser Duthie (III Bonn)
56	vsv-g	Generation of retroviral particles	Generated by Dr. Gabor Horvath/Dr. Karin Pelka (III Bonn)
57	gag-pol	Generation of retroviral particles	Generated by Dr. Gabor Horvath/Dr. Karin Pelka (III Bonn)
782	B-GECO1	Fluorescent Ca^{2+} sensor; here: template source for generation of oxidized DNA by PCR (Section 3.9)	MSc Thesis of Tomasz Prochnicki (III Bonn)

Table 3.2. List of plasmids used in my Thesis.

3.3. Tissue culture and generation of stable cell lines

The majority of experiments performed in my Thesis was performed in murine immortalized macrophages (iMac cells) and in human embryonic kidney (HEK) 293T cells with various genetic modifications. All stable cell lines used in my Thesis (Table 3.3) were adherent cells and they were cultured in 25-cm^2, 75-cm^2, or 175-cm^2 tissue

culture-treated flasks in Dulbecco's Modified Eagle's Medium (DMEM) with 4.5 g/L glucose, 2 mM L-glutamine, and phenol red supplemented with 10% fetal bovine serum (FBS) and penicillin-streptomycin (100 × dilution). The typical volumes of growth media per flask were 7.5 mL (25-cm^2 flask), 14 mL (75-cm^2 flask), or 32 mL (175-cm^2 flask). Cells were kept in tissue culture incubators at 37°C, in the presence of 5% CO_2 with passive humidification. Cells were split every second or third day. Briefly, the cells in the flask were washed at RT with 5 mL (25-cm^2 flask), 10 mL (75-cm^2 flask) or 12 mL (175-cm^2 flask) Dulbecco's phosphate-buffered saline (DPBS). This was followed by an incubation (1-5 min, RT) with TrypLE Express Enzyme (1 ×) cell dissociation reagent with phenol red (1.5 mL per 25-cm^2 flask, 2 mL per 75-cm^2 flask, or 3 mL per 175-cm^2 flask). The surface attachment of the cells was monitored using a phase-contrast microscope. After the cells detached, the cell dissociation reagent was then neutralized with 10 mL of complete tissue culture medium (RT) and the cells were transferred to a fresh flask at the desired dilution (3 × to 25 ×). The list of tissue culture reagents can be found in Table 3.4.

Cells were not allowed to exceed the confluence threshold of 90% and all experiments were performed on cells between passage 2 and passage 20. All cell lines were screened for mycoplasma contaminations and are deposited in the Institute of Innate Immunity (III) cell lines bank (Table 3.3). For cryopreservation, cells were harvested from 80-90%-confluent 75-cm^2 or 175-cm^2 flasks using the same detachment protocol as during routine passaging. Then, the cells were spun down at 340 × g (RT), resuspended in cryopreservation medium (FBS with the addition of 10% DMSO, RT), and aliquoted into cryopreservation vials. Cells from a 75-cm^2 flask were typically distributed into 3 cryopreservation vials, whereas cells from a 175-cm^2 flask were typically distributed into 4-5 cryopreservation vials. The vials with cell suspensions were then transferred into Mr. Frosty or CellCamper freezing containers, placed in a -80°C freezer for 24 h-1 week, and eventually stored at -150°C for prolonged periods of time. To thaw frozen cells, the vials with cryopreserved cell suspensions were thawed 'in hand'; their contents were then diluted with complete DMEM (~11 mL DMEM supplemented with 10% FBS and 1:100 penicillin-streptomycin per ~1 mL frozen cell suspension), transferred into 15-mL conical tubes, spun down at 340 × g (RT), resuspended in fresh complete DMEM, and transferred to 75-cm^2 tissue culture flasks.

To generate cell lines stably transduced with constructs of interest (Table 3.3), retroviruses were used as a nucleic acid vector. HEK 293T cells were used for production of retroviruses. Briefly, ~5×10^5 HEK 293T cells per well were seeded in 6-well plates in complete DMEM (~3 mL). After an overnight incubation (37°C, 5% CO_2) the cells were transfected with combinations of three vectors: the vector of interest (carrying the insert to be stably integrated into the genome of the target cell line; 2 μg/well), the packaging vector (gag-pol; vector 57 in the III plasmid database; 1 μg/well), and the entry vector (vsv-g; vector 56 in the III plasmid database; 100 ng/well). To prepare transfection mixes, (per one transfection well) GeneJuice transfection reagent (8 μL; approx. 2.6 μL of GeneJuice per 1 μg of DNA) was combined with 100 μL of FBS- and antibiotic-free DMEM, and, in a separate tube, the three plasmids were mixed and filled with FBS- and antibiotic-free DMEM to 20 μL. After 5 min, $GeneJuice_{DMEM}$ and $plasmids_{DMEM}$ were mixed and left for 20 min to allow for the formation of transfection complexes. After this time, transfection complexes were transferred to the HEK cells, followed by a 18-20-h incubation (37°C, 5% CO_2). After this time, the tissue culture media were removed, discarded, and replaced with ~2 mL of DMEM (4.5 g/L glucose, 2 mM L-glutamine) supplemented with 30% FBS and penicillin-streptomycin (100 × dilution). The high-FBS (30%) conditions promote the generation of retroviral particles. After ~24 h of incubation under the high-FBS conditions (37°C, 5% CO_2), the retrovirus-containing tissue culture supernatants were harvested. Briefly, the supernatants were collected in a Luer-Lok syringe using a blunt 18 G needle. Then, the supernatants were filtered through a 0.45 μm membrane filter. Such supernatants were either directly used for stable transgene delivery into target cell lines, or they were cryopreserved at -80°C in cryopreservation vials. For retrovirus-mediated transgene delivery (retroviral transduction), the target cells were plated at ~5×10^4 cells/well (one day before transduction) or ~10^5 cells/well (on the day of transduction) in 24-well plates. Next, the cells were subjected to several doses of retrovirus-containing supernatants (typically 5-500 μL). After 24-48 h of retroviral transduction (37°C, 5% CO_2), the transduction efficiency was assessed using an epifluorescence microscope (if the delivered transgenes contained a constitutively expressed fluorescent protein) and, if necessary, the wells containing populations of positive cells were subjected to antibiotic selection with puromycin (~10 μg/mL; at 37°C and in the presence of 5%

CO_2). All vectors used in my thesis carried the eukaryotic puromycin resistance cassette. After successful transduction, the resulting cell lines were expanded and used for experiments at passages 4-20 following retroviral transduction and/or cryopreserved at -150°C. The cells that underwent retrovirus-mediated transgene delivery were considered to be biosafety level 2 organisms for three passages following retroviral transduction, after which time they were considered to be biosafety level 1 organisms. Unless otherwise indicated, all hands-on steps of the procedure above were performed at RT, under a tissue culture hood appropriate for biosafety level 2 work. The incubations were performed in a tissue culture incubator dedicated to biosafety level 2 work.

ID in the III database	Name in text and figures	Cell type	Genetic modifications	Source and references
CL13	WT iMac	Immortalized murine macrophages	n.a.	Generated by Dr. Dominic DeNardo (III Bonn)
CL170	WT iMac + [h]ASC^{mCerulean}	Immortalized murine macrophages	Stable overexpression of human ASC-linker-mCerulean (vector 389)	This Thesis
CL12	[m]NLRP3/[h]ASC^{mCerulean} [reporter] iMac	Immortalized murine macrophages	Stable overexpression of human ASC-linker-mCerulean (vector 389) and of murine NLRP3	Franklin et al. (2014); Stutz et al. (2013)
CL96	[m]NLRP3/[h]ASC^{mCerulean} [reporter] iMac [+] control [empty] vector	Immortalized murine macrophages	Stable overexpression of human ASC-linker-mCerulean (vector 389), of murine NLRP3, and of an empty construct (vector 288)	This Thesis
CL97	[m]NLRP3/[h]ASC^{mCerulean} [reporter] iMac [+] hNLRP10	Immortalized murine macrophages	Stable overexpression of human ASC-linker-mCerulean (vector 389), of murine NLRP3, and of human NLRP10 (WT; vector 1120)	This Thesis
CL98	[m]NLRP3/[h]ASC^{mCerulean} [reporter] iMac [+] mNlrp10	Immortalized murine macrophages	Stable overexpression of human ASC-linker-mCerulean (vector 389), of murine NLRP3, and of murine Nlrp10 (WT; vector 1121)	This Thesis
CL185	[m]NLRP3/[h]ASC^{mCerulean} [reporter] iMac [+] hNLRP10^{K179M}	Immortalized murine macrophages	Stable overexpression of human ASC-linker-mCerulean (vector 389), of murine NLRP3, and of a Walker A motif of human NLRP10 (vector 1378)	This Thesis
CL186	[m]NLRP3/[h]ASC^{mCerulean} [reporter] iMac [+] hNLRP10^{D249N}	Immortalized murine macrophages	Stable overexpression of human ASC-linker-mCerulean (vector 389), of murine NLRP3, and of a Walker B motif of human NLRP10	This Thesis

			(vector 1447)	
CL187	[m]NLRP3/[h]ASC^{mCerulean} [reporter] iMac [+] hNLRP10^{D249A}	Immortalized murine macrophages	Stable overexpression of human ASC-linker-mCerulean (vector 389), of murine NLRP3, and of a Walker B motif of human NLRP10 (vector 1448)	This Thesis
CL118	[m]NLRP3/[h]ASC^{mCerulean}/ HMGB1^{mCitrine} [reporter] iMac	Immortalized murine macrophages	Stable overexpression of human ASC-linker-mCerulean (vector 389), of murine NLRP3, and of an HMGB1-based fluorescent nuclear marker (vector 596)	This Thesis
CL119	[m]NLRP3/[h]ASC^{mCerulean}/ mito^{mCitrine} [reporter] iMac	Immortalized murine macrophages	Stable overexpression of human ASC-linker-mCerulean (vector 389), of murine NLRP3, and of a fluorescent marker of the mitochondrial matrix (vector 819)	This Thesis
CL14	*Nlrp3*$^{-/-}$ iMac	Immortalized murine macrophages	NLRP3 deficiency	Juliana et al. (2010; 2012)
CL20	*Aim2*^{CRISPR} iMac*	Immortalized murine macrophages	AIM2 deficiency	Generated and validated by Brian Monks (III Bonn)
CL104	*Aim2*^{CRISPR} iMac + empty [control] vector	Immortalized murine macrophages	AIM2-deficient cells stably transduced with an empty construct (vector 288)	This Thesis
CL181	*Aim2*^{CRISPR} iMac + hAIM2 (#1/vector 241)**	Immortalized murine macrophages	AIM2-deficient cells reconstituted with human AIM2 (vector 241)	This Thesis
CL105	*Aim2*^{CRISPR} iMac + hAIM2 (#2/vector 1044)	Immortalized murine macrophages	AIM2-deficient cells reconstituted with human AIM2 (vector 1044)	This Thesis
CL106	*Aim2*^{CRISPR} iMac + mAim2	Immortalized murine macrophages	AIM2-deficient cells reconstituted with murine Aim2 (vector 1349)	This Thesis
CL107	*Aim2*^{CRISPR} iMac + hNLRP10	Immortalized murine macrophages	AIM2-deficient cells stably overexpressing human NLRP10 (WT; vector 1120)	This Thesis
CL108	*Aim2*^{CRISPR} iMac + mNlrp10	Immortalized murine macrophages	AIM2-deficient cells stably overexpressing murine Nlrp10 (WT; vector 1121)	This Thesis
CL182	*Aim2*^{CRISPR} iMac + hNLRP10-PYD	Immortalized murine macrophages	AIM2-deficient cells stably overexpressing the PYD domain of human NLRP10 (vector 1122)	This Thesis
CL183	*Aim2*^{CRISPR} iMac + hNLRP10-NACHT	Immortalized murine macrophages	AIM2-deficient cells stably overexpressing the NACHT domain of human NLRP10 (vector 1123)	This Thesis
CL184	*Aim2*^{CRISPR} iMac + hNLRP10^{K179M}	Immortalized murine macrophages	AIM2-deficient cells stably overexpressing a Walker A mutant of human NLRP10 (vector 1378)	This Thesis
CL260	*Aim2*^{CRISPR} iMac + hNLRP10^{D249N}	Immortalized murine macrophages	AIM2-deficient cells stably overexpressing a Walker B mutant of human NLRP10	This Thesis

			(vector 1447)	
CL261	*Aim2*^{CRISPR} iMac + hNLRP10^{D249A}	Immortalized murine macrophages	AIM2-deficient cells stably overexpressing a Walker B mutant of human NLRP10 (vector 1448)	This Thesis
CL23	HEK [293T]	HEK cells	n.a.	ATCC
CL115/ CL169	[h]ASC^{TagBFP} HEK	HEK cells	HEK cells stably overexpressing human ASC as a fusion protein with TagBFP (vector 799), may serve as a fluorescent reporter of ASC speck formation	This Thesis
CL172	[h]ASC^{mCerulean} HEK	HEK cells	HEK cells stably overexpressing human ASC as a fusion protein with mCerulean (vector 389), may serve as a fluorescent reporter of ASC speck formation	This Thesis
CL168	mCitrine/[h]ASC^{TagBFP} HEK	HEK cells	HEK cells stably overexpressing mCitrine (vector 288) and human ASC as a fusion protein with TagBFP (vector 799), may serve as a fluorescent reporter of ASC speck formation	This Thesis
CL100	[h]NLRP10^{mCitrine}/ [h]ASC^{TagBFP} HEK	HEK cells	HEK cells stably overexpressing human NLRP10 (vector 1120) and human ASC as a fusion protein with TagBFP (vector 799), may serve as a fluorescent reporter of ASC speck formation in response to NLRP10 inflammasome activators	This Thesis
CL163	[h]NLRP10^{mCherry}/ [h]ASC^{mCerulean} HEK	HEK cells	HEK cells stably overexpressing human NLRP10 (vector 1612) and human ASC as a fusion protein with mCerulean (vector 389), may serve as a fluorescent reporter of ASC speck formation in response to NLRP10 inflammasome activators	This Thesis
CL165	[h]NLRP10^{mCitrine} HEK	HEK cells	HEK cells stably overexpressing human NLRP10 as a fusion protein with mCitrine (vector 1120), may serve as a fluorescent reporter of NLRP10 subcellular localization	This Thesis
CL236	[h]NLRP10^{mCherry} HEK	HEK cells	HEK cells stably overexpressing human NLRP10 as a fusion protein with mCherry (vector 1612), may serve as a fluorescent reporter of NLRP10 subcellular localization	This Thesis
CL262	[m]Nlrp10^{mCitrine} HEK	HEK cells	HEK cells stably	This Thesis

			overexpressing murine Nlrp10 as a fusion protein with mCitrine (vector 1121), may serve as a fluorescent reporter of Nlrp10 subcellular localization	
CL101	[m]Nlrp10^{mCitrine}/ [h]ASC^{TagBFP} HEK	HEK cells	HEK cells stably overexpressing murine Nlrp10 (vector 1121) and human ASC as a fusion protein with TagBFP (vector 799), may serve as a fluorescent reporter of ASC speck formation in response to Nlrp10 inflammasome activators	This Thesis
CL166	[h]NLRP10-IRES-mCitrine HEK	HEK cells	HEK cells stably overexpressing human NLRP10 and mCitrine as two separate polypeptides (vector 1058), serves as a control cell line for the cell lines in which NLRP10 localization was monitored using NLRP10-mCitrine fusion constructs	This Thesis
CL116	[h]NLRP10^{mCitrine}/ [h]ASC^{TagBFP}/ [h]HMGB1^{mCherry} HEK	HEK cells	HEK cells stably overexpressing human NLRP10 as a fusion protein with mCitrine (vector 1120), human ASC as a fusion protein with TagBFP (vector 799), and an HMGB1-based fluorescent nuclear marker (vector 597)	This Thesis
CL117	[h]NLRP10^{mCitrine}/ [h]ASC^{TagBFP}/mito^{mCherry} HEK	HEK cells	HEK cells stably overexpressing human NLRP10 as a fusion protein with mCitrine (vector 1120), human ASC as a fusion protein with TagBFP (vector 799), and a fluorescent marker of the mitochondrial matrix (vector 820)	This Thesis
CL258	mito^{mCitrine} [reporter] HEK	HEK cells	HEK cells stably overexpressing a fluorescent marker of the mitochondrial matrix (vector 819)	This Thesis
CL277	[h]NLRP10^{mCherry}/ TOMM20^{mCitrine} HEK	HEK cells	HEK cells stably overexpressing human NLRP10 as a fusion protein with mCherry (vector 1612) and the mitochondrial marker TOMM20 as a fusion protein with mCitrine (vector 1176)	This Thesis

Table 3.3. List of stable cell lines used in my Thesis.
*Here only used as a parental cell line to generate other cell lines. The AIM2-deficient cells used in experiments throughout my Thesis is CL20 stably transduced with the empty vector (vector 288 in the III database), that is, CL104.
**Only used in the experiment in Figure 7.7.

Reagent	**Source**
Dulbecco's Modified Eagle's Medium (DMEM), 4.5 g/L glucose, 2 mM L-glutamine, with phenol red	Thermo Fisher Scientific
DMEM without glucose, without phenol red	Thermo Fisher Scientific
DMEM without glucose, without amino acids, with phenol red	Genaxxon
Roswell Park Memorial Institute (RPMI) tissue culture medium	Thermo Fisher Scientific
Minimal Essential Medium (MEM)	Thermo Fisher Scientific
OptiMEM	Thermo Fisher Scientific
Dulbecco's phosphate-buffered saline (DPBS)	Thermo Fisher Scientific
TrypLE Express (1 ×) Enzyme	Gibco (Thermo Fisher Scientific)
Fetal bovine serum (FBS)	Gibco (Thermo Fisher Scientific)
L929 cell conditioned medium	Generated by Gudrun Engels (III Bonn)
Penicillin-streptomycin (10,000 U/mL)	Thermo Fisher Scientific
Puromycin (10 mg/mL)	Gibco (Thermo Fisher Scientific)
Ampicillin (100 mg/mL)	Sigma/Merck
Sodium pyruvate (100 mM)	Life Technologies (Thermo Fisher Scientific)
poly-L-lysine (0.1% aqueous solution)	Sigma
Ethidium bromide (10 mg/mL)	Sigma (Merck)
2',3'-dideoxycytidine	abcam
Water (water-for-injection grade)	Fresenius
Nuclease-free water	Thermo Fisher Scientific
Sodium chloride (5 M aqueous solution)	Sigma (Merck)
Potassium chloride (75 mM aqueous solution)	Sigma (Merck)
Calcium chloride (1 M aqueous solution)	Sigma (Merck)
Magnesium chloride (1 M aqueous solution)	Sigma (Merck)
Lithium chloride (8 M aqueous solution)	Sigma (Merck)
Sodium hydroxide (1 N aqueous solution)	Sigma (Merck)
Glucose (10%, or ~555 mM, aqueous solution)	Sigma (Merck)
HEPES pH 7.4 (1 M aqueous solution)	Sigma (Merck)
Lipofectamine 2000	Thermo Fisher Scientific
Lipofectamine 3000 and P3000 reagent	Thermo Fisher Scientific
GeneJuice Transfection Reagent	Merck Millipore
DMSO (tissue culture grade)	PanReac AppliChem
Ethanol absolute (molecular biology grade)	PanReac AppliChem
Lipopolysaccharide (LPS) from *Escherichia coli* 0111:B4	Invivogen
Nigericin	Thermo Fisher Scientific
Silica	US Silica (MIN-U5/MIN-U15)
poly-(dA:dT)	Sigma (Merck)
m-3M3FBS	Sigma (Merck), Cayman Chemical
o-3M3FBS	Tocris
Thapsigargin	Enzo Life Sciences
SMBA1	Tocris
SC-9	Tocris
SC-10	abcam
DRAQ5 nuclear stain (5 mM)	Invitrogen (Thermo Fisher Scientific)
PhosSTOP phosphatase inhibitor tablets	Roche/Sigma (Merck)
Formaldehyde (16% aqueous solution, methanol-free)	Thermo Fisher Scientific
Triton X-100	Carl Roth
Isopropanol (technical grade)	PanReac AppliChem

Table 3.4. List of tissue culture reagents, chemicals, and inflammatory stimuli.

3.4. DNA transfection (for protein overexpression)

Of the cell lines used in my Thesis, only HEK cells could be subjected to transient transfection with plasmid DNA to enable transient protein overexpression. iMac cells express a range of endogenous innate immune DNA sensors (most prominently AIM2 and cGAS), so cytosolic DNA delivery may lead to drastic off-target effects including cell death. Therefore, all genetic modifications in iMac cells were performed by stable transgene delivery using retroviral vectors (Section 3.3).

For transient protein overexpression, GeneJuice transfection reagent was used for DNA delivery into the cell. Typically, the transfection reagent was combined with plasmid DNA at the ratio of 2.3-2.8 μL of GeneJuice per 1 μg of plasmid DNA. Briefly, GeneJuice was first mixed with serum- and antibiotic-free OptiMEM, and, in a separate tube, the plasmid of interest was mixed with the same volume of serum- and antibiotic-free OptiMEM. After a 5-10-min incubation at RT, the contents of both tubes were combined, and the resulting mixture was incubated at RT for 15-20 min to allow for the formation of transfection complexes. Thus formed transfection complexes were transferred to HEK cells plated 6-24 h in advance in complete DMEM medium (with 4.5 g/L glucose and 2 mM L-glutamine, with the 10% FBS and penicillin-streptomycin [100 × dilution] supplementation[1]) in either uncoated 6-well tissue culture-treated plates, or in poly-L-lysine-coated 96-well tissue culture-treated microscopy-adapted plates. The typical plating densities were between 5×10^3-2.2×10^4 cells/well (or 1.6×10^4-6.9×10^4 cells/cm^2) in 96-well plates, or ~5×10^5 cells/well (or ~5.3×10^4 cells/cm^2) in 6-well plates. The final volume of the transfection mix was generally kept under 100 μL/well for cells transfected in 96-well plates, or under 200 μL/well for cells transfected in 6-well plates so as to avoid an excessive dilution of the growth medium. Addition of DNA transfection complexes was followed by a centrifugation step (340 × g, 5 min at RT). All prolonged (> 15 min) incubations of cells were performed at 37°C in the presence of 5% CO_2.

For the transfections performed in 96-well plates, the cells were imaged after 24-48 h (depending on the experiment), either after direct fixation (4% formaldehyde with the nuclear counterstain [5 μM DRAQ5]) or following a treatment with inflammasome

[1] Instances where any additional substances were included in the media during transfection experiments are detailed in figure legends.

activators (Section 3.10) and subsequent fixation. For the transfections performed in 6-well plates, the cells were incubated with the transfection complexes for 24 h (37°C, 5% CO_2). Next, the cells were detached from the growth surface (Section 3.3) and replated in poly-L-lysine-coated tissue culture-treated microscopy-adapted 96-well plates. After a 24-h 'resting' period (37°C, 5% CO_2), these cells were treated with inflammasome activators (Section 3.10), fixed (4% formaldehyde with the nuclear counterstain [5 μM DRAQ5]) and inspected by fluorescence microscopy. Specific details of each experimental setup (the ratio of transfection reagent to DNA, the initial cell plating density, the experimental timeline, and the incorporation of a re-plating step) are provided in figure legends.

3.5. DNase I protein transfection

Protein transfection with DNase I was performed using the PULSin protein transfection reagent (Polyplus Transfection) following the manufacturer's instructions, as described by (Jabir et al., 2014). Briefly, the cells were loaded with DNase I (from bovine pancreas [Sigma/Merck]; 0, 60, 300, or 500 ng per well in a 96-well plate) using the PULSin protein transfection reagent (at the ratio of 4 μL of PULSin per 1 μg of protein). The loading step (5 h, 37°C, 5% CO_2) was performed in OptiMEM without FBS or penicillin-streptomycin supplementation. After the DNase I delivery, the cells were shifted for 90 min to DMEM (4.5 g/L glucose, 2 mM L-glutamine) supplemented with 10% FBS and penicillin-streptomycin (100 × dilution), at 37°C in the presence of 5% CO_2. This was followed by treatment with inflammasome agonists (Section 3.10).

3.6. Bone marrow extraction and generation of bone marrow-derived macrophages (BMDMs)

Femurs and tibias were typically obtained from 6-24-week-old mice with the following genotypes: C57BL/6 ('wild-type' [WT]), *Pycard*$^{-/-}$ (ASC-deficient), *Aim2*$^{-/-}$ (AIM2-deficient), *Nlrp3*$^{-/-}$ (NLRP3-deficient), *Nlrp10*$^{-/-}$ (NLRP10-deficient), and *Nlrp10*$^{flox/flox}$ (WT-equivalent control for NLRP10-deficient experiments). *Nlrp10*$^{-/-}$ and *Nlrp10*$^{flox/flox}$ bones were a gift from Prof. Thomas Kufer (University of Hohenheim).

After isolation, the bones were briefly washed in DPBS in a tissue-culture dish, followed by a 30-s incubation in 70% $ethanol_{aq}$. Then, the bones were transferred to DPBS in a fresh tissue-culture dish and kept there until the bone marrow extraction step (< 30 min). The bones were opened using scissors and flushed (using a syringe) with FBS- and antibiotic-free DMEM (4.5 g/L glucose, 2 mM L-glutamine; bones from one mouse were flushed ~10 mL of medium) in a fresh tissue-culture dish. The bone marrow suspensions in DMEM were centrifuged (340 × g, 5 min) and either cryopreserved at -150°C (as described in Section 3.3; in FBS supplemented with 10% DMSO; bone marrow from one mouse was distributed into two cryopreservation vials) or resuspended in DMEM (4.5 g/L glucose, 2 mM L-glutamine) supplemented with 10% FBS, penicillin-streptomycin (100 × dilution) and 15-30% L929 cell conditioned medium, which contains the factors necessary for BMDM differentiation. Bone marrow from one mouse was resuspended in ~40 mL of such medium. All steps of this procedure were performed at RT.

BMDM differentiation was conducted over the period of 7 days in a tissue culture incubator (37°C, 5% CO_2). Bone marrow from one mouse was typically distributed into two 175-cm^2 flasks or three to four 75-cm^2 flasks. On the last day of differentiation, the L929 cell conditioned media-containing differentiation media were discarded and the cells were washed with DPBS (~10 mL per flask for both the 75-cm^2 and the 175-cm^2 flasks). DPBS from this wash was collected and replaced with fresh DPBS (~12 mL per flask for both the 75-cm^2 and the 175-cm^2 flasks), in which the cells were detached using a cell scraper. The BMDM suspensions in DPBS were collected and the flasks were washed one last time with DPBS (~10 mL per flask for both the 75-cm^2 and the 175-cm^2 flasks), which was also collected. Finally, the cell suspensions were spun down (340 × g, 8 min), the DPBS supernatants were discarded, and BMDMs were resuspended in DMEM (4.5 g/L glucose, 2 mM L-glutamine) supplemented with 10% FBS, penicillin-streptomycin (100 × dilution) and 1-5% L929 cell conditioned medium (bone marrow from one mouse was resuspended in ~12 mL of this medium). Then, the cells were counted and the volumes of cell suspensions were adjusted to reach the final concentration of $\sim 5 \times 10^5$ cells/mL. For further experimentation, BMDMs were plated in 96-well plates at the density of 5×10^4 cells/well (or $\sim 1.56 \times 10^5$ cells/cm^2). All steps of this procedure were performed at RT. Experiments using BMDMs were performed after

a 16-18-h resting period in a tissue culture incubator (37°C, 5% CO_2) following cell plating.

3.7. Generation of mtDNA-depleted cells

mtDNA depletion experiments were all performed in 96-well plates. Initial populations of NLRP3/ASC^{mCerulean} reporter iMac cells (2.5×10^3 cells per well in a 96-well plate, or $\sim 7.8 \times 10^3$ cells/cm^2), WT iMac cells (2.5×10^3 cells per well in a 96-well plate, or $\sim 7.8 \times 10^3$ cells/cm^2), or NLRP10^{mCitrine}/ASC^{TagBFP} HEK cells (2.5×10^3 cells per well in a 96-well plate, or $\sim 7.8 \times 10^3$ cells/cm^2; or 5×10^3 cells per well in a 96-well plate, or $\sim 1.56 \times 10^4$ cells/cm^2) were grown for 72-96 h in DMEM (4.5 g/L glucose, 2 mM L-glutamine) supplemented with 10% FBS, penicillin-streptomycin (100 × dilution), 1 mM sodium pyruvate and either ethidium bromide (EtBr; 50 or 75 ng/mL) or 2',3'-dideoxycytidine (ddC; 40 or 80 μg/mL) under standard conditions (37°C, 5% CO_2). Control cells were grown in DMEM (4.5 g/L glucose, 2 mM L-glutamine) supplemented with 10% FBS, penicillin-streptomycin (100 × dilution), and 1 mM sodium pyruvate. After the cells reached 80-90% confluence, the experiments (Sections 3.8 and 3.10) were performed in the same wells in which the cells had been plated.

3.8. Measurement of the cellular mtDNA content

Total cell DNA from mtDNA-depleted and control cells (Section 3.7) was isolated using QIAmp DNA micro kit (Qiagen), following the manufacturer's instructions. Per condition, material from nine wells of a 96-well plate was collected.

The total cellular mtDNA content was analyzed by quantitative PCR (qPCR) using sequences from nuclear DNA as a reference ('housekeeping') whose level is not strongly affected by addition of the mtDNA-depleting agents. The sequences of [q]PCR primers can be found in Table 3.5.

Primer name	Primer sequence (5'-3')	Source
Leu-tRNA for (h-mtDNA)	GATGGCAGAGCCCGGTAATCGC	Hashiguchi and Zhang-Akiyama, 2009
Leu-tRNA rev (h-mtDNA)	TAAGCATTAGGAATGCCATTGCG	Hashiguchi and Zhang-Akiyama, 2009
pol-gamma for (h-nucDNA)	AGCGACGGGCAGCGGCGGCGGCA	Hashiguchi and Zhang-Akiyama, 2009
pol-gamma rev (h-nucDNA)	CCCTCCGAGGATAGCACTTGCGGC	Hashiguchi and Zhang-Akiyama, 2009

D-loop for (m-mtDNA)	AATCTACCATCCTCCGTGAAACC	West et al., 2015
D-loop rev (m-mtDNA)	TCAGTTTAGCTACCCCCAAGTTTAA	West et al., 2015
Tert for (m-nucDNA)	CTAGCTCATGTGTCAAGACCCTCTT	West et al., 2015
Tert rev (m-nucDNA)	GCCAGCACGTTTCTCTCGTT	West et al., 2015

Table 3.5. Primer sequences used for the qPCR assessment of mtDNA depletion efficiency.

For the qPCR reaction mixes (20 μL), 100 ng DNA per sample was analyzed. The primers were used at the final concentrations of 500 nM per primer. The qPCR master mix (Maxima SYBR Green/ROX 2 × qPCR Master Mix [Thermo Fisher Scientific]) was based on SYBR Green DNA detection and it was supplied as a 2 × concentrated working solution. 10 μL of qPCR master mix were used per reaction, and nuclease-free water was added to the final volume of 20 μL.

qPCR was run in technical duplicates according to the standard two-step cycling protocol. Briefly, the DNA samples were denatured for 10 min at 95°C, followed by 40 cycles of (1) denaturation (95°C, 15 s) and (2) annealing and elongation (60°C, 1 min). The fluorescence signal was acquired during the annealing and elongation step, following the manufacturer's instruction. The fold changes in the mtDNA content values were calculated using the $2^{-\Delta\Delta Ct}$ method (Livak and Schmittgen, 2001).

3.9. Generation of oxidized DNA (oxDNA) fragments by PCR

To generate double-stranded (ds) oxDNA fragments, a PCR reaction was performed on vector 782 in the III database (encoding the blue fluorescent Ca^{2+} sensor B-GECO1 [Zhao et al., 2011a]; the choice of vector was dictated by the size of the amplicon and the availability of plasmid DNA and primers) using the following primers (5'-3'): forward TTTTTTGGCGCGCCACCATGGTCGACTCACCACGTC, and reverse AAAAAAGCGGCCGCCTACTTCGCTGTCATCATTTGTAC. The PCR reaction (50 μL) was run on 100 ng DNA using 500 nM concentration of each of the primers. The PCR master mix (PfuUltra II Hotstart PCR Master Mix [Agilent Technologies]) was supplied as 2 × working solution and 25 μL of master mix per reaction were added. To introduce oxidative DNA modifications into the PCR products, 8-oxo-dGTP (0, 0.1, 0.2, or 0.5 mM; Jena Bioscience) was added to the PCR reaction (typically, the concentrations of dNTPs in PCR reactions are ~0.2 mM). The cycling protocol consisted of a 1-min denaturation step at 94°C, followed by 40 cycles of (1) denaturation (94°C, 30 s), (2) annealing (60°C,

30 s), and (3) elongation (72°C, 2 min), and concluded by a final elongation step of 10 min (72°C). Next, the PCR products were electrophoretically separated from the unoxidized template DNA in an agarose gel (1%) and isolated using PureLink Quick Gel Extraction kit (Invitrogen/Thermo Fisher Scientific). DNA fragments purified in this way served as ligands in inflammasome activation experiments (Section 3.10). Incorporation of ox-guanosine residues was confirmed by antibody staining (Section 3.15).

Single-stranded (ss) (ox)DNA fragments were generated as described above with several important modifications. The reverse primer used in the PCR reaction (AAAAAAGCGGCCGCCTACTTCGCTGTCATCATTTGTAC) was phosphorylated at the 5'-end (the forward primer did not contain any modifications). Additionally, only the 8-oxo-dGTP-free ('0 mM') and 0.5 mM 8-oxo-dGTP conditions were selected. Following the PCR reaction, the products were subjected to digest with Lambda exonuclease (Thermo Fisher Scientific). Lambda exonuclease is a highly processive enzyme that degrades the 5'-phosphorylated but not the 5'-unphosphorylated strands in dsDNA molecules, yielding ssDNA fragments. The reaction (400 μL) was performed in the presence of Lambda exonuclease buffer supplied by the manufacturer and using 16 μL of the enzyme (10 U/μL) for 60 min at 37°C. This was followed by an enzyme inactivation step (10 min at 80°C). ssDNA generated in this manner was electrophoretically separated from leftover dsDNA substrate (1% agarose gel) and then purified from the gel (PureLink Quick Gel Extraction kit, Invitrogen/Thermo Fisher Scientific) and used in inflammasome activation assays (Section 3.10).

3.10. Activation of the inflammasome

One day before the experiment, the cells were detached from growth surface (as described in Section 3.3) and plated in 96-well plates in DMEM (4.5 g/L glucose, 2 mM L-glutamine) supplemented with 10% FBS and penicillin-streptomycin (100 × dilution). The plating densities were typically 6×10^4 cells per well (~1.88×10^5 cells/cm^2) for WT iMac cells and cell lines derived from these cells, *Nlrp3*$^{-/-}$ iMac cells, and *Aim2*^{CRISPR} iMac cells and cell lines derived from these cells, 5×10^4 cells per well (~1.56×10^5 cells/cm^2) for NLRP3/ASC^{mCerulean} reporter iMac cells, and 3.5-3.8$\times10^4$ cells per well (~1.1×10^5-

1.19×10^5 cells/cm^2) for HEK 293T cells and cell lines derived from these cells. The cells were kept in a tissue culture incubator (37°C, 5% CO_2) overnight (16-18 h).

On the day of the experiment, the cells were primed with LPS (200 ng/mL, 2 h at 37°C, 5% CO_2) in DMEM (4.5 g/L glucose, 2 mM L-glutamine) supplemented with 10% FBS and penicillin-streptomycin (100 × dilution), or they were left unprimed. Of note, NLRP3/ASC^{mCerulean} reporter iMac cells do not require the priming step for the NLRP3 inflammasome activation due to the constitutive overexpression of NLRP3. For the experiments where the IL-1β secretion from these cells was to be measured, the priming step (200 ng/mL, 2 h at 37°C, 5% CO_2) was included. Any deviations from the standard priming protocol described here are indicated in figure legends.

For inflammasome activation, the cells were shifted to the standard extracellular buffer/minimal salt solution consisting of (in mM) 123 NaCl, 5 KCl, 2 $MgCl_2$, 1 $CaCl_2$, 10 glucose, 10 HEPES, pH 7.4. For some experiments this list of buffer ingredients was modified; the compositions of all extracellular buffers used in my Thesis is summarized in Table 3.6. The details on extracellular milieu compositions are also provided in figure legends. Typically, at this point 90 μL per well of the extracellular buffer were added. Next, the cells were stimulated with the following inflammasome activators: nigericin (final concentration 10 μM), thapsigargin (final concentration ~20 μM), *m*-3M3FBS (final concentration ~85 μM), *o*-3M3FBS (final concentration ~85 μM), or poly-(dA:dT) (model dsDNA transfection complexes, administered at 200 ng/well [2]). The inflammasome activators (typically 10 μL per well) were administered as 10 × concentrated working solutions, so, for example, 10 μL of 100 μM nigericin were added to 90 μL of the extracellular medium to produce the final concentration of 10 μM nigericin. The addition of inflammasome agonists was followed by gently flicking the

[2] Poly-(dA:dT) transfection complexes were prepared by mixing (per well) 0.5 μL of Lipofectamine 2000 with 5 μL OptiMEM and, in a separate tube, 200 ng of poly-(dA:dT) with 5 μL OptiMEM. After a 5-min incubation at RT, the contents of both tubes were mixed and incubated for further 10-15 min to allow for the formation of transfection complexes. Then, 10 μL per well of transfection complexes were transferred to the cells, with 90 μL of the extracellular buffer already present in the medium. These amounts correspond to the final concentration of 2 μg/mL poly-(dA:dT) dsDNA complexed with 5 μL of Lipofectamine 2000. Of note, for a set of specific experiments (Sections 8.9 and 8.10), Lipofectamine 3000 with the P3000 reagent were used as transfection reagents to deliver DNA to the cytosol for inflammasome activation. Those instances, as well as the ratios of DNA to Lipofectamine 3000 to the P3000 reagents are indicated in the respective figure legends.

plate with a finger, a centrifugation step[3] (340 × g, 5 min, at RT), and a 30-60-min incubation (37°C, 5% CO_2). After this time, tissue culture supernatants were collected, and/or the cells were fixed (4% formaldehyde) and counterstained with a nuclear dye (5 μM DRAQ5).

There were two reasons why I used minimal salt solutions as extracellular media for inflammasome activation in my Thesis. First, several experiments involved testing of the influence of increased concentrations of certain ions (K^+, Ca^{2+}) on inflammasome activation, or of the impact of certain ions' depletion (K^+, Ca^{2+}, Mg^{2+}, Cl^-). There are no commercially available media to easily examine such conditions, so using buffers prepare in-house was a sensible alternative. Secondly, the inflammasome responses to *m*-3M3FBS and thapsigargin were much more efficient in the standard extracellular buffer than they were in DMEM (4.5 g/L glucose, 2 mM L-glutamine) supplemented with 10% FBS and penicillin-streptomycin (100 × dilution) (Supplementary Methods Figure SM1). In an attempt to determine whether the decrease in inflammasome activation could be attributed to the presence of FBS or bovine serum albumin (BSA; the major protein component of serum), I tested whether addition of FBS (0.1-10%) or BSA (0.05-5 mg/mL) to the standard extracellular buffer would block the inflammasome responses to *m*-3M3FBS and thapsigargin (Supplementary Methods Figure SM2). However, the inhibitory effect of FBS and BSA (Supplementary Methods Figure SM2) was less evident than the inhibitory effect of DMEM (4.5 g/L glucose, 2 mM L-glutamine) supplemented with 10% FBS and penicillin-streptomycin (100 × dilution) (Supplementary Methods Figure SM1). To determine whether DMEM (4.5 g/L glucose, 2 mM L-glutamine) itself contained ingredients that acted as inhibitors of the inflammasome responses to *m*-3M3FBS and thapsigargin, I inspected the strength of the inflammasome activation by these stimuli in WT iMac cells, NLRP3/$ASC^{mCerulean}$ reporter iMac cells (Supplementary Methods Figure SM3), and $NLRP10^{mCitrine}$/ASC^{TagBFP} HEK cells (Supplementary Methods Figure SM4) in the presence of various serum-free extracellular media: the minimal salt solution, DPBS, DMEM (4.5 g/L glucose, 2 mM L-glutamine), DMEM (glucose-free and without phenol red), DMEM (glucose- and amino acid-free, with phenol red), RPMI, OptiMEM, and MEM. Overall, there was no indication that any of the tested media may contain a complete inhibitor of the *m*-3M3FBS-/thapsigargin-induced inflammasome

[3] Centrifugation of the cells was essential for an efficient inflammasome activation by thapsigargin and poly-(dA:dT).

activation but because of the reliably high levels of inflammasome activation in the minimal salt solution and because of the easiness with which the composition of this extracellular buffer can be manipulated, I performed the majority of the experiments in my Thesis in an extracellular buffer consisting of (in mM) 123 NaCl, 5 KCl, 2 $MgCl_2$, 1 $CaCl_2$, 10 glucose, 10 HEPES, pH 7.4.

A certain deviation from the protocol for activation of the inflammasome with nigericin, *m*-3M3FBS, *o*-3M3FBS, thapsigargin, and poly-(dA:dT) was the stimulation of the AIM2 and NLRP10 inflammasomes with SC-9, SC-10, and SMBA1. For the three latter stimulations, the cells were shifted to 50 μL per well of the standard extracellular buffer, followed by addition of 50 μL per well of the inflammasome stimuli in the form of 2 × concentrated working solutions (SMBA1: typically 100 μM working solution, 50 μM final concentration; SC-9: typically 200 μM working solution, 100 μM final concentration; SC-10: typically 200 μM working solution, 100 μM final concentration). Similar to other inflammasome activation protocols, the addition of inflammasome agonists was followed by gently flicking the plate with a finger, a centrifugation step (340 × g, 5 min, at RT), and a 30-60-min incubation (37°C, 5% CO_2). After this time, tissue culture supernatants were collected, or the cells were fixed (4% formaldehyde) and counterstained with a nuclear dye (5 μM DRAQ5).

The exception to this general protocol was the NLRP3 inflammasome activation with silica crystals. This stimulation was performed in the presence of DMEM (4.5 g/L glucose, 2 mM L-glutamine) supplemented with 10% FBS and penicillin-streptomycin (100 × dilution). Briefly, silica crystal suspension (500 μg/mL) was added to the cells, followed by gently flicking the plate with a finger, a centrifugation step (340 × g, 5 min, at RT), and a 6-h incubation (37°C, 5% CO_2). After this time, tissue culture supernatants were collected, or the cells were fixed (4% formaldehyde) and counterstained with a nuclear dye (5 μM DRAQ5).

Name of buffer	**Composition**
Minimal salt solution (standard)	123 mM NaCl, 5 mM KCl, 2 mM $MgCl_2$, 1 mM $CaCl_2$, 10 mM glucose, 10 mM HEPES, pH 7.4. Adjust the pH to 7.4 with 1 N $NaOH_{aq}$ (~500 μL of 1 N $NaOH_{aq}$ per 500 mL of buffer).
Minimal salt solution (high potassium)	125 mM KCl, 2 mM $MgCl_2$, 1 mM $CaCl_2$, 10 mM glucose, 10 mM HEPES, pH 7.4. Adjust the pH to 7.4 with 1 N $NaOH_{aq}$ (~500 μL of 1 N $NaOH_{aq}$ per 500 mL of buffer).

Minimal salt solution (potassium-free)	123 mM NaCl, 2 mM $MgCl_2$, 1 mM $CaCl_2$, 10 mM glucose, 10 mM HEPES, pH 7.4. Adjust the pH to 7.4 with 1 N $NaOH_{aq}$ (~500 μL of 1 N $NaOH_{aq}$ per 500 mL of buffer).
Minimal salt solution (calcium-free)	123 mM NaCl, 5 mM KCl, 2 mM $MgCl_2$, 10 mM glucose, 10 mM HEPES, pH 7.4. Adjust the pH to 7.4 with 1 N $NaOH_{aq}$ (~500 μL of 1 N $NaOH_{aq}$ per 500 mL of buffer).
Minimal salt solution (calcium and magnesium free)	131 mM NaCl, 5 mM KCl, 10 mM glucose, 10 mM HEPES, pH 7.4. Adjust the pH to 7.4 with 1 N $NaOH_{aq}$ (~500 μL of 1 N $NaOH_{aq}$ per 500 mL of buffer).
Minimal salt solution (chloride-free; acetate-based)	131 mM sodium acetate, 5 mM potassium acetate, 10 mM glucose, 10 mM HEPES, pH 7.4. Adjust the pH to 7.4 with 1 N $NaOH_{aq}$ (~500 μL of 1 N $NaOH_{aq}$ per 500 mL of buffer).
Minimal salt solution (chloride-free, gluconate-based)	131 mM sodium gluconate, 5 mM potassium gluconate, 10 mM glucose, 10 mM HEPES pH 7.4. Adjust the pH to 7.4 with 1 N $NaOH_{aq}$ (~500 μL of 1 N $NaOH_{aq}$ per 500 mL of buffer).
Minimal salt solution (with lithium chloride, high osmolarity)	125 mM NaCl, 50 mM LiCl, 5 mM KCl, 2 mM $MgCl_2$, 1 mM $CaCl_2$, 10 mM glucose, 10 mM HEPES, pH 7.4. Adjust the pH to 7.4 with 1 N $NaOH_{aq}$ (~500 μL of 1 N $NaOH_{aq}$ per 500 mL of buffer).
Minimal salt solution (with lithium chloride, osmolarity-compensated)	75 mM NaCl, 50 mM LiCl, 5 mM KCl, 2 mM $MgCl_2$, 1 mM $CaCl_2$, 10 mM glucose, 10 mM HEPES, pH 7.4. Adjust the pH to 7.4 with 1 N $NaOH_{aq}$ (~500 μL of 1 N $NaOH_{aq}$ per 500 mL of buffer).
Minimal salt solution (high osmolarity)	175 mM NaCl, 50 mM LiCl, 5 mM KCl, 2 mM $MgCl_2$, 1 mM $CaCl_2$, 10 mM glucose, 10 mM HEPES, pH 7.4. Adjust the pH to 7.4 with 1 N $NaOH_{aq}$ (~500 μL of 1 N $NaOH_{aq}$ per 500 mL of buffer).

Table 3.6. Compositions of the minimal media/extracellular buffers for inflammasome activation. All buffers were prepared using water-for-injection grade water.

3.11. Testing of LMW inhibitors

Multiple experiments throughout my thesis were performed using LMW inhibitors of signaling enzymes, or blockers of channels and transporters. The comprehensive list of all tested treatments, together with their commercial sources and reported mechanisms of action, is provided in Table 3.7. These assays were performed in 96-well plates and the cells were prepared for the experiment as described in Section 3.10.

The basic setup of the inhibition experiments was as follows: for experiments in which the readout was the measurement of IL-1β concentration in tissue culture supernatants, the cells were primed with LPS (200 ng/mL, 2 h in DMEM [4.5 g/L glucose, 2 mM L-glutamine] supplemented with 10% FBS and penicillin-streptomycin [100 × dilution], at 37°C, 5% CO_2). For experiments in which the readout was imaging of ASC specks, the cells were generally left unprimed. Next, the cells were shifted to an extracellular medium consisting of (in mM) 123 NaCl, 5 KCl, 2 $MgCl_2$, 1 $CaCl_2$, 10 glucose, 10 HEPES, pH 7.4, with the addition of LMW inhibitors/blockers, or vehicle [solvent] controls (90 μL/well when the next step was inflammasome activation with nigericin, *m*-3M3FBS, *o*-3M3FBS, thapsigargin, poly-[dA:dT], or silica, or 50 μL when the next step was

inflammasome activation with SMBA1, SC-9, or SC-10). The tested concentrations inhibitor/blocker concentrations are indicated in figure legends. Inhibitor addition was followed by ~10-min incubation at 37°C, 5% CO_2. Then, the cells were stimulated with inflammasome activators (typically 10 or 50 μL/well), as described in Section 3.10. The addition of inflammasome agonists was followed by gently flicking the plate with a finger, a centrifugation step (340 × g, 5 min, at RT), and a 30-60-min incubation (37°C, 5% CO_2). After this time, tissue culture supernatants were collected, or the cells were fixed (4% formaldehyde) and counterstained with a nuclear dye (5 μM DRAQ5). Any deviations from this general protocol are specified in figure legends.

Name	**Source**	**Solvent (vehicle)**	**Reported mechanism of action**
2-APB	Sigma (Merck)	DMSO	Inhibitor of IP_3 receptors in the endoplasmic reticulum membrane
3-methyladenine	Sigma (Merck)	Ethanol	Inhibitor of autophagy
4-phenylbutyric acid	Sigma (Merck)	Water	Chemical chaperone – expected to counteract proteotoxic stress
8-hydroxy-2'-deoxyguanosine	Sigma (Merck)	DMSO	Reported inhibitor of NLRP3
A-92	Axon Medchem	DMSO	GCN2 kinase inhibitor
ABT263 (navitoclax)	Selleckchem	DMSO	BCL-2/XL/W inhibitor
ABT737	Selleckchem	DMSO	BCL-2/XL/W inhibitor
Actinomycin D	Sigma (Merck)	DMSO	Inhibitor of eukaryotic mRNA transcription
Alisporivir (Debio025)	MedChem Express	DMSO	Non-immunosuppressive analog of cyclosporin A (blocks mitochondrial damage)
AMG PERK 44	Tocris	DMSO	PERK kinase inhibitor
Amprenavir	Sigma (Merck)	DMSO	Inhibitor of HIV protease
Apoptosis activator 2	Tocris	DMSO	Inducer of intrinsic apoptosis
Artemisinin	Tocris	DMSO	Reported inhibitor of sarco/endoplasmic reticulum Ca^{2+} ATPase
Ascomycin	Biomol/Cayman Chemical	DMSO	Inhibitor of calcineurin/nuclear factor of activated T cells signaling
AT406	Cayman Chemical	DMSO	SMAC mimetic (pro-apoptotic)
Atazanavir	Sigma (Merck)	DMSO	Inhibitor of HIV protease
Auranofin	Sigma (Merck)	DMSO	Cytotoxic agent reported to induce mtROS generation
Bafilomycin A1	Adipogen	DMSO	Inhibitor of vacuolar H^+-ATPase
Barium chloride ($BaCl_2$)	Sigma (Merck)	Water	Reported inhibitor of mitochondrial permeability transition pore
BAM7	Tocris	DMSO	Agonist of Bax
BAPTA-AM	Enzo Life Sciences	DMSO	Intracellular Ca^{2+} chelator
Benzenesulfonamide	Sigma (Merck)	DMSO	Chemical scaffold of *m*-3M3FBS and related molecules
Betulinic acid	Sigma (Merck)	DMSO	Activator of intrinsic apoptosis
BHQ	Tocris	DMSO	Inhibitor of sarco/endoplasmic reticulum Ca^{2+} ATPase
BI-6C9	Santa Cruz	DMSO	Inhibitor of tBid-mediated apoptosis
Bisindolylmaleimide II	Tocris	DMSO	Inhibitor of protein kinase C

Birinapant	Biomol/Cayman Chemical	DMSO	SMAC mimetic
Bongkrekic acid	Sigma (Merck)	TBS	Inhibitor of Slc25a4, reported to inhibit mPT
Bortezomib	Selleckchem	DMSO	Proteasome inhibitor
Bovine serum albumin (BSA)	Sigma/Merck	Water	Major serum protein component
Brefeldin A	Sigma/Merck	DMSO	Inhibitor of protein transport from the ER to the Golgi apparatus
Bryostatin 1	Enzo Life Sciences	DMSO	Activator of protein kinase C
BTSA1	Selleckchem	DMSO	Agonist of Bax
C-1	Tocris	DMSO	Inhibitor of protein kinases A, C, and G
C16	Tocris	DMSO	PKR kinase inhibitor
Calcium chloride ($CaCl_2$)	Sigma/Merck	Water	Source for extracellular Ca^{2+} ions
Carboxyatractyloside	Biomol/Cayman Chemical	DMSO	Inhibitor of Slc25a4, reported to activate mPT
CCCP	Tocris	DMSO	Mitochondrial uncoupler
CDDO	Cayman Chemical	DMSO	Inducer of mitochondrial unfolded protein response
CDDO-Me	Tocris	DMSO	Inducer of mitochondrial unfolded protein response
Chelerythrine chloride	Calbiochem	DMSO	Inhibitor of protein kinase C
Chloramphenicol	Sigma/Merck	Ethanol	Antibacterial antibiotic with reported mitochondria-damaging activity
CkI7	Santa Cruz	DMSO	SGK kinases inhibitor
Cobalt(II) chloride ($CoCl_2$)	Sigma/Merck	Water	Chemical inducer of hypoxia-like cellular state
Colchicine	Sigma/Merck	DMSO	Inhibitor of microtubule polymerization
Concanavalin A (type IV)	Sigma/Merck	PBS	Lectin used for induction of neutrophil extracellular trap formation
Concanavalin A (type VI)	Sigma/Merck	PBS	Lectin used for induction of neutrophil extracellular trap formation
CRID3	Pfizer	Ethanol	Inhibitor of NLRP3
CRT0066101	abcam	DMSO	Inhibitor of protein kinase D
Cyclopiazonic acid	Tocris	DMSO	Inhibitor of sarco/endoplasmic reticulum Ca^{2+} ATPase
Cyclosporin A	Sigma/Merck	DMSO	Inhibitor of mitochondrial damage as well as calcineurin/nuclear factor of activated T cells signaling
Cytochalasin D	Sigma/Merck	DMSO	Phagocytosis inhibitor (through actin polymerization inhibition)
D609	Tocris	DMSO	Phosphatidylcholine (PC)-phospholipase C inhibitor
Debio025 (alisporivir)	MedChem Express	DMSO	Non-immunosuppressive analog of cyclosporin A (blocks mitochondrial damage)
Dexpramipexole dihydrochloride	Sigma/Merck	DMSO	Mitoprotective agent, possibly through mPT inhibition
Diazoxide	Tocris	DMSO	K^+ channel blocker
DIDS	Tocris	DMSO	Inhibitor of Cl^- channels
Doxorubicine	Biomol/Cayman Chemical	DMSO	Antitumor agent triggering DNA damage, intercalating agent inhibiting topoisomerase II
DS16570511	Aobious	DMSO	Mitochondrial Ca^{2+} uniporter inhibitor

DS44170716	Sigma/Merck	DMSO	Mitoprotective agent, possibly through mPT inhibition
Edelfosine	Enzo Life Sciences	Ethanol	Phosphatidylinositol (PI)-phospholipase C inhibitor
Emricasan	Sigma/Merck	DMSO	Pan-caspase inhibitor
Eperezolid	AdooQ Bioscience	DMSO	Antibacterial antibiotic with reported mitochondria-damaging activity
ER000444793	MedChem Express	DMSO	Mitoprotective agent, possibly through inhibition of mPT
FCCP	Tocris	DMSO	Mitochondrial uncoupler
FK506	Tocris	DMSO	Inhibitor of calcineurin/nuclear factor of activated T cells signaling
Gadolinium chloride ($GdCl_3$)	Sigma/Merck	Water	Reported inhibitor of mitochondrial permeability transition pore
Gambogic acid	Tocris	DMSO	Inducer of intrinsic apoptosis
GF109203X	Tocris	DMSO	Inhibitor of protein kinase C
Glycine	Sigma/Merck	PBS	Inhibitor of lytic cell death
Gö6983	Tocris	DMSO	Inhibitor of protein kinase C
GSK650394	Tocris	DMSO	Inhibitor of SGK kinases
GSK2606414	Tocris	DMSO	PERK kinase inhibitor
GTPP	MedChem Express	DMSO	Inducer of mitochondrial unfolded protein response
HA14-1	Tocris	DMSO	Inducer of intrinsic apoptosis
IAA-94	Sigma/Merck	DMSO	Cl^- channel blocker
ICH-1	Sigma/Merck	DMSO	Caspase-2 inhibitor
Idebenone	Sigma/Merck	DMSO	Synthetic analog of coenzyme Q in the IMM
iMAC2	Tocris	DMSO	Inhibitor of intrinsic apoptosis
Importazole	Sigma/Merck	DMSO	Inhibitor of nuclear protein import
Ionomycin	Enzo Life Sciences	DMSO	Ca^{2+} ionophore
Ivermectin	Tocris	DMSO	Reported inhibitor of nuclear protein import
K252c	Enzo Life Sciences	DMSO	Inhibitor of protein kinase C
KB-R7943 mesylate	Cayman Chemical	DMSO	Inhibitor of mitochondrial Ca^{2+} uniporter and of Na^+/Ca^{2+} exchanger
KPT-185	Selleckchem	DMSO	Inhibitor of nuclear export
KPT-330 (Selinexor)	Biomol/Cayman Chemical	DMSO	Inhibitor of nuclear export
LCL161	Cayman Chemical	DMSO	SMAC mimetic
Leptomycin B	Sigma/Merck	Methanol: water (7:3)	Inhibitor of nuclear export
Leu-Leu-O-Me	Chem-Impex International	DMSO	Activator of NLRP3 through the lysosomal damage pathway
Linezolid	Tocris	DMSO	Antibacterial antibiotic with reported mitochondria-damaging activity
Lithium chloride (LiCl)	Sigma/Merck	Water	GSK3 kinase inhibitor; used here as an inhibitor of inositol monophosphate dephosphorylation
Lonidamine	Sigma/Merck	DMSO	Inhibitor of hexokinase with reported mitochondrial activity
Lopinavir	Sigma/Merck	DMSO	Inhibitor of HIV protease
Maleimide	Sigma/Merck	DMSO	Chemical scaffold of U73122 and related molecules
MCD-cholesterol	Sigma/Merck	PBS	Water-soluble form of cholesterol
Mdivi-1	Tocris	DMSO	Inhibitor of mitochondrial fission
Metformin	Tocris	DMSO	Likely acts on multiple targets; some reports suggest mitoprotective activity
Minocycline	Enzo Life Sciences	DMSO	Antibacterial antibiotic with reported

			mitochondria-damaging activity
Mirin	Enzo Life Sciences	DMSO	Inhibitor of DNA repair, suggested to also disrupt mtDNA
MitoBloCK-6	Focus Biomolecules/tebu-bio	DMSO	Inhibitor of mitochondrial protein import
MitoBloCK-12	tebu-bio	DMSO	Inhibitor of mitochondrial protein import
N-ethylmaleimide	Sigma/Merck	DMSO	Chemical scaffold of U73122 and related molecules
N-ethyltoluene-4-sulfonamide	Sigma/Merck	DMSO	Chemical scaffold of *m*-3M3FBS and related molecules
N-methyl-*p*-toluenesulfonamide	Sigma/Merck	DMSO	Chemical scaffold of *m*-3M3FBS and related molecules
Navitoclax (ABT263)	Selleckchem	DMSO	BCL-2/XL/W inhibitor
Necrostatin-1	Tocris	DMSO	Inhibitor of necroptosis
Necrosulfonamide	Merck	DMSO	Inhibitor of necroptosis
Nelfinavir	Sigma/Merck	DMSO	Inhibitor of HIV protease
Nifedipine	Tocris	DMSO	Ca^{2+} channel blocker
NIM811	MedChem Express	DMSO	Non-immunosuppressive analog of cyclosporin A (blocks mitochondrial damage)
NSC668394	EMD Millipore/ Calbiochem	DMSO	Inhibitor of ezrin
Oligomycin A	Selleckchem	Ethanol	Inhibitor of ATP synthase (mitochondrial)
p-toluenesulfonamide	Sigma/Merck	DMSO	Chemical scaffold of *m*-3M3FBS and related molecules
PF-543	Tocris	DMSO	Sphingosine kinase inhibitor with reported mitoprotective activity
Pitstop 2	Sigma/Merck	DMSO	Clathrin inhibitor demonstrated to cause a breach in the nuclear permeability barrier
PMA	Sigma/Merck	DMSO	Activator of protein kinase C
Potassium chloride (KCl)	Sigma/Merck	Water	Major salt inside of the cell
Q-Vd-OPh	Cayman Chemical	DMSO	Pan-caspase inhibitor
R-(+)-N-(1-phenylethyl)maleimide	Sigma/Merck	DMSO	Chemical scaffold of U73122 and related molecules
R837	Invivogen	PBS	Activator of NLRP3 through inhibition of the mitochondrial electron transport chain complex I
Ritonavir	Tocris	DMSO	Inhibitor of HIV protease
RO32-0432	Tocris	DMSO	Inhibitor of protein kinase C
Rotenone	Sigma/Merck	DMSO	Inhibitor of the mitochondrial electron transport chain complex I
S63845	Cayman Chemical	DMSO	Inhibitor of the BCL-2 family protein MCL-1
SC79	Selleckchem/Biozol	DMSO	Activator of protein kinase B (Akt)
Selinexor (KPT-330)	Biomol/Cayman Chemical	DMSO	Inhibitor of nuclear export
Sodium acetate	Sigma/Merck	Water	Replacement of NaCl in Cl^- depletion experiments
Sodium azide (NaN_3)	Sigma/Merck	Water	Inhibitor of the mitochondrial electron transport chain complex IV
Sodium chloride (NaCl)	Sigma/Merck	Water	Major salt in extracellular fluids
Sodium gluconate	Sigma/Merck	Water	Replacement of NaCl in Cl^- depletion experiments
Succinimide	Sigma/Merck	DMSO	Chemical scaffold of U73343 and related molecules

Staurosporine	Enzo Life Sciences	DMSO	Pan-kinase inhibitor
Tetracycline	Sigma/Merck	Ethanol	Antibacterial antibiotic with reported mitochondria-damaging activity
TRO19622	Tocris	DMSO	Mitoprotective agent, possibly through inhibition of mPT
Tunicamycin	Tocris	DMSO	Inhibits protein glycosylation in the ER, leading to ER stress
TW37	Cayman Chemical	DMSO	Inducer of intrinsic apoptosis
U73122	Sigma/Merck	DMSO	Phosphatidylinositol (PI)-phospholipase C inhibitor
U73343	Tocris	DMSO	Inactive analog of U73122
Valinomycin	Sigma/Merck	DMSO	Electrogenic K^+ ionophore
VBIT-4	Aobious	DMSO	Inhibitor of voltage-dependent anion channel
VX-765	Selleckchem	DMSO	Inhibitor of caspase-1
Z-IETD-FMK	R&D Systems	DMSO	Inhibitor of caspase-8

Table 3.7. List of low molecular weight enzyme inhibitors, channel/transporter blockers, and other treatments aimed at perturbing cellular processes.
PBS, phosphate-buffered saline; TBS, TRIS-buffered saline.

3.12. U73122, maleimide, and CRID3 inhibitor washout experiment

Unprimed NLRP3/ASC^{mCerulean} reporter iMac cells or LPS-primed (200 ng/mL, 2 h) WT iMac cells were shifted to an extracellular medium consisting of (in mM) 123 NaCl, 5 KCl, 2 $MgCl_2$, 1 $CaCl_2$, 10 glucose, 10 HEPES, pH 7.4 and pre-treated for 10 min with CRID3 (5 μM) or two doses of U 73122 or maleimide (10 or 20 μM) at 37°C in the presence of 5% CO_2. This was followed by 0, 1, or 2 washes with the extracellular medium (RT) and addition of nigericin (10 μM) in the extracellular medium consisting of (in mM) 123 NaCl, 5 KCl, 2 $MgCl_2$, 1 $CaCl_2$, 10 glucose, 10 HEPES, pH 7.4. The negative controls were subjected to medium alone. Immediately after addition of nigericin, the plates were centrifuged at 340 × g for 5 min (RT) and then transferred to a tissue culture incubator (37°C, 5% CO_2) to allow for inflammasome activation. After 60 min, the supernatants were collected and IL-1β concentrations were measured, or the cells were fixed with 4% formaldehyde, counterstained for the nuclei with 5 μM DRAQ5 and imaged using a fluorescence microscope.

3.13. Induction of intrinsic apoptosis

Intrinsic apoptosis was induced by treatments described by Vince et al. (2018), McArthur et al. (2018), and Riley et al. (2018). Briefly, LPS-primed (100 ng/mL, 1 h; 37°C , 5% CO_2; LPS was kept in the stimulation media for the entire duration of the experiments) or unprimed cells were subjected to the transcription inhibitor

actinomycin D (2 μM) or the MCL-1 inhibitor S63845 (5 μM), or they were left untreated (-) in the presence or absence of the pan-caspase inhibitors Q-Vd-OPh (20 μM) or emricasan (20 μM), or the caspase-1 inhibitor VX-765 (20 μM). Immediately after administration of these treatments, the cells were stimulated with the BCL-2 family inhibitors ABT263 (0, 10, 25, or 50 μM) or ABT737 (0, 10, 25, or 50 μM). All stimulations were performed in DMEM (4.5 g/L glucose, 2 mM L-glutamine) supplemented with 5% FBS and penicillin-streptomycin (100 × dilution). Immediately after addition of inflammasome activators, the plates were centrifuged at 340 × g for 5 min (RT). After a 24-h incubation at 37°C in the presence of 5% CO_2, the supernatants were collected for IL-1β concentrations measurement, or the cells were fixed with 4% formaldehyde and counterstained with the nuclear dye DRAQ5 (5 μM).

Any modifications to this general protocol (for example, introduction of pre-incubation steps with LMW inhibitors of various signaling molecules or addition of increased KCl concentration to the stimulation medium) are specified in figure legends.

Other long-term (≥ 6 h) stimulations were performed using a similar setup (in DMEM [4.5 g/L glucose, 2 mM L-glutamine] supplemented with 5-10% FBS and penicillin-streptomycin [100 × dilution], with a decreased concentration of 'priming' LPS [100 ng/mL], and with LPS present in the stimulation medium for the entire duration of the experiment); all the deviations from this general protocol are noted in figure legends.

3.14. Chemical-induced hypoxia and ischemia *in vitro* models

For the $CoCl_2$-induced *in vitro* hypoxia model, cells plated in wells of 96-well plates (as described in Section 3.10) were treated overnight (~16 h) with $CoCl_2$ (0, 100, or 250 μM) in DMEM (4.5 g/L glucose, 2 mM L-glutamine) supplemented with 10% FBS and penicillin-streptomycin (100 × dilution; 37°C, 5% CO_2). On the next day, the cells were shifted to $CoCl_2$-free media and primed with LPS or left unprimed; or they were kept in $CoCl_2$ (0, 100, or 250 μM)-containing media and LPS-primed or left unprimed (all incubations were performed at 37°C in the presence of 5% CO_2). Next, the cells were shifted to an extracellular medium consisting of (in mM) 123 NaCl, 5 KCl, 2 MgCl2, 1 CaCl2, 10 glucose, 10 HEPES pH 7.4 without or with $CoCl_2$ (0, 100, or 250 μM) and

stimulated with the inflammasome activators *m*-3M3FBS (85 μM), thapsigargin (20 μM), nigericin (10 μM) or poly-(dA:dT) (2 μg/mL complexed with 5 μL Lipofectamine 2000). Immediately after addition of inflammasome activators, the plates were centrifuged at 340 × g for 5 min (RT). After 30-60 min (37°C, 5% CO_2), tissue culture supernatants were collected for IL-1β concentration measurement, or the cells were fixed with 4% formaldehyde and counterstained with the nuclear dye DRAQ5 (5 μM).

For the NaN_3-induced *in vitro* ischemia model, LPS-primed (200 ng/mL, 2 h; 37°C, 5% CO_2) WT iMac cells, NLRP3/$ASC^{mCerulean}$ reporter iMac cells, and $NLRP10^{mCitrine}$/ASC^{TagBFP} HEK cells were shifted to an extracellular medium consisting of (in mM) 123 NaCl, 5 KCl, 2 $MgCl_2$, 1 $CaCl_2$, 10 glucose, 10 HEPES pH 7.4, without or with NaN_3 (0.5, 1, 2.5, 5, 10, or 20 mM). The cells were incubated under these conditions for 30 min or for 90 min (controls) at 37°C in the presence of 5% CO_2. After 30 min, NaN_3 was washed away, and the cells were incubated for further 60 min (37°C, 5% CO_2) in the experimental medium without NaN_3 (during this time, the cells from the 90-min NaN_3 condition were further incubated with NaN_3). At this point, the positive (*m*-3M3FBS) control cells were stimulated with 85 μM *m*-3M3FBS. At the completion of the experiment, the tissue culture supernatants were collected for IL-1β concentrations assessment, or the cells were fixed with 4% formaldehyde and counterstained with the nuclear dye DRAQ5 (5 μM).

3.15. Antibody staining

An antibody staining was performed to assess the efficiency of oxidized guanosine residues incorporation into PCR reaction products generated in the presence of 8-oxo-dGTP (Section 3.9). Briefly, NLRP3/$ASC^{mCerulean}$ reporter iMac cells in wells of a 96-well plate were stimulated (37°C, 5% CO_2) with PCR reaction products-Lipofectamine 2000 complexes at 1 μg/mL DNA complexed with 2.5 μL Lipofectamine 2000 (corresponding to 100 ng DNA and 0.25 μL Lipofectamine 2000 per well). Immediately after addition of DNA transfection complexes, the plates were centrifuged at 340 × g for 5 min (RT). After 60 min (37°C, 5% CO_2), the cells were fixed with 4% formaldehyde (37°C, 60 min). Next, formaldehyde was discarded, and its residues were 'quenched' by and overnight incubation with 150 mM NH_4Cl_{DPBS} (at 4°C). Subsequently, the samples were

permeabilized and blocked in 0.3% Triton-X100 in DPBS with 3% BSA (blocking buffer; RT, 60 min). Then, the blocking buffer was removed, and the primary antibody was added (mouse anti-8-oxo-dG monoclonal antibody, Trevigen; supplied as a 0.5-mg/mL solution and used here at a 100 × dilution in blocking buffer) for 2 h, at RT. Next, the samples were washed three times with DPBS, followed by incubation with the secondary antibody (goat anti-mouse IgG $F(ab')_2$ fragments conjugated with Alexa Fluor 568, Invitrogen/Thermo Fisher Scientific; supplied as a 2-mg/mL solution and used here at a 500 × dilution in blocking buffer) for 1 h, at RT in the dark. Next, the samples were washed three times with DPBS in the dark and counterstained for the nuclei with DRAQ5 (final concentration: 5 μM in DPBS). Samples prepared in this manner were subjected to widefield fluorescence imaging (Section 3.16).

3.16. Widefield fluorescence imaging of fixed samples

Formaldehyde-fixed cell samples were analyzed by fluorescence microscopy no later than one week after completion of the experiment. Until that time, the samples were stored at 4°C.

Samples were imaged at the Microscopy Core Facility (Medical Faculty, University of Bonn) using the Observer.Z1 fluorescence microscope (Zeiss) with a dry 20 × LD Plan Neo Fluor objective (numerical aperture 0.4) or a dry 20 × Plan Apochromat objective (numerical aperture 0.8). Scale bars (typically 50 μm) are included in the overlay microscopy images presented in my Thesis. The microscope was operated using Zen 2.3 Pro software (Zeiss). Image acquisition was performed at RT.

All imaging assays were performed in 96-well plates. For most experiments, six images per well were acquired[4]. Automated acquisition was set up in the microscope software; as all fixed samples were counterstained with the nuclear dye DRAQ5, the DRAQ5 channel was used as the reference channel for software autofocus.

Generally, a phase-contrast micrograph was acquired for every condition, with the DAPI filter set (Zeiss filter set #49) in the light path. For the fluorescent proteins and dyes

[4] For example, a result of three independent experiments performed in technical duplicate is pooled from 36 images (6 images/well × 2 wells/repeat of experiment × 3 independent experiments).

used in my Thesis, the following filter sets were used: TagBFP, Zeiss filter set #49 (DAPI); mCerulean, Zeiss filter set #47 HE (CFP); mCitrine, Zeiss filter set #46 HE (YFP); mCherry, Zeiss filter set #43 HE (DsRed); Alexa Fluor 568, Zeiss filter set #43 HE (DsRed); DRAQ5, Zeiss filter set #50 (Cy5).

After acquisition, where applicable, sample images were exported as TIFF files using Zen Lite software (Zeiss). Only linear adjustments were applied to the images (adjustments to the lower and upper boundaries of the lookup table), and these adjustments were uniformly applied to all sample images within one experiment. No non-linear adjustments were applied. TIFF files exported from Zen Lite software were directly imported into figures, which were prepared using Ai Illustrator software (Adobe Creative Cloud). In Ai Illustrator, the images were cropped and, when necessary, the image dimensions were adjusted to the layout of the figure.

For image quantification (Section 3.22), raw imaging data were imported into Cell Profiler 3.1.8 or 3.1.9 software (Carpenter et al., 2006; Kamentsky et al., 2011; McQuin et al., 2018).

3.17. Time-lapse (live) widefield fluorescence imaging

Samples were imaged at the Microscopy Core Facility (Medical Faculty, University of Bonn) using the Observer.Z1 fluorescence microscope (Zeiss) with a dry 20 × LD Plan Neo Fluor objective (numerical aperture 0.4) or a dry 20 × Plan Apochromat objective (numerical aperture 0.8) and the 37°C incubation chamber. Scale bars (typically 50 μm) are included in the overlay microscopy images presented in my Thesis. The microscope was operated using Zen 2.3 Pro software (Zeiss). The cells were stimulated with inflammasome activators as detailed in Section 3.10. The stimuli were added either directly to cells in the microscope incubation chamber just after the onset of imaging (< 1 min), or, when a centrifugation step was necessary, they were added outside of the incubation chamber just before the onset of imaging (< 2 min).

All imaging assays were performed in 96-well plates. For most experiments, 1-2 images per well were acquired. Automated acquisition with time-lapse recording was set up in the microscope software; the phase contrast was typically used as the reference channel

for software autofocus, or the definite focus option was used. The time interval between consecutive acquisitions of a given imaging field was 1 min or 4 min, depending on the activator (the time intervals for each treatment are specified in figure legends).

Generally, a phase-contrast micrograph was acquired for every condition, with the DAPI filter set (Zeiss filter set #49) in the light path. For the fluorescent proteins and dyes used in my Thesis, the following filter sets were used: TagBFP, Zeiss filter set #49 (DAPI); mCerulean, Zeiss filter set #47 HE (CFP); mCitrine, Zeiss filter set #46 HE (YFP); mCherry, Zeiss filter set #43 HE (DsRed).

After acquisition, where applicable, sample images were exported as TIFF files using Zen Lite software (Zeiss). Only linear adjustments were applied to the images (adjustments to the lower and upper boundaries of the lookup table). No non-linear adjustments were applied. TIFF files exported from Zen Lite software were directly imported into figures, which were prepared using Ai Illustrator software (Adobe Creative Cloud). In Ai Illustrator, the images were cropped and, when necessary, the image dimensions were adjusted to the layout of the figure.

3.18. Confocal laser scanning microscopy

All imaging assays were performed in 96-well plates. Formaldehyde-fixed cell samples were analyzed by confocal laser scanning microscopy no later than one week after completion of the experiment. Until that time, the samples were stored at 4°C.

Samples were imaged at the Microscopy Core Facility (Medical Faculty, University of Bonn) using the SP5 AOBS with SMD confocal microscope (Leica) with a water immersion 63 × HCX PL APO objective (numerical aperture 1.2). The images were acquired at a 1024×1024 resolution with the line averaging of 8. Scale bars (typically 5 μm) are included in the overlay microscopy images presented in my Thesis. The microscope was operated using LAS AF 2.7.3 software (Leica). Image acquisition was performed at RT.

Generally, a transmitted light micrograph was acquired for every condition. For the fluorescent proteins and dyes used in my Thesis, the following lasers were used:

mCerulean, argon laser (the 458 nm line); mCitrine, argon laser (the 514 nm line); mCherry, DPSS laser (561 nm); DRAQ5, HeNe laser (633 nm).

After acquisition, where applicable, sample images were exported as TIFF files using LAS X Lite software (Leica). Only linear adjustments were applied to the images (adjustments to the lower and upper boundaries of the lookup table). No non-linear adjustments were applied. TIFF files exported from LAS X Lite software were directly imported into figures, which were prepared using Ai Illustrator software. In Ai Illustrator, when necessary, the image dimensions were adjusted to the layout of the figure.

3.19. Assessment of inflammasome activation by measurement of IL-1β concentrations in tissue culture supernatants

IL-1β concentrations in tissue culture supernatants were assessed by a homogenous time-resolved fluorescence (HTRF) 'sandwich' antibody-based assay (Cisbio), following the manufacturer's instructions. The supernatants were analyzed either directly upon completion of the experiment, or they were stored at 4°C for up to 24 h.

Briefly, the anti-murine IL-1β antibody solutions (the antibody pair consisted of a fluorescence donor- [cryptate]-conjugated antibody and a fluorescence acceptor- [d2]-conjugated antibody) were mixed at a 1:1 ratio. 4 μL/well of this mixture were distributed in white low-volume medium-binding HTRF-adapted 384-well assay plates. This was followed by addition of the samples (tissue culture supernatants; 16 μL/well). The plates were centrifuged at RT, 1000 × g for 5 min, followed by a 2-6-h incubation at RT, or a 16-18-h incubation at 4°C. After this time, the fluorescence signals were measured using Spectramax i3 (Molecular Devices) with HTRF cartridge. In parallel with the analysis of experimental samples, IL-1β standard curve was prepared in duplicate, according to the manufacturer's instructions. It was against the fluorescence values obtained for the standard curve that the values of IL-1β concentrations in the experimental samples were estimated.

3.20. Assessment of the interference between S63845 fluorescence and the HTRF signal

S63845 was diluted in PBS (to the final concentrations of 1, 5, or 10 μM) and the fluorescence signal of these solutions was measured and compared to an IL-1β standard curve prepared according to the manufacturer's instructions (66-4200 pg/mL), as described in Section 3.19. Tissue culture supernatants were not added to any of these samples.

3.21. Assessment of PLC activity by measurement of inositol monophosphate (IP_1) concentrations in tissue culture supernatants

Inositol monophosphate (IP_1) concentrations in tissue culture lysates were assessed by an HTRF competitive antibody- and labelled ligand-based assay (IPONE G_q HTRF kit, Cisbio), following the manufacturer's instructions. The lysates were analyzed directly upon completion of the experiment.

Briefly, the cells were lysed with 0.5% Triton-X100 in a medium consisting of (in mM) 75 or 125 NaCl, 50 LiCl, 5 KCl, 2 $MgCl_2$, 1 $CaCl_2$, 10 glucose, 10 HEPES, pH 7.4, with the addition of the PhosSTOP phosphatase inhibitor cocktail (diluted as per the manufacturer's instructions). Next, the d2- (fluorescence acceptor)-labelled IP_1 solution (3 μL/well) was distributed in white low-volume medium-binding HTRF-adapted 384-well assay plates[5]. The experimental samples (14 μL/well) were added to the d2-conjugated IP_1, followed by a brief centrifugation (RT, 1000 × g for 1 min). Next, the cryptate- (fluorescence acceptor)-conjugated anti-IP_1 antibody solution was added (3 μL/well), and the plates were centrifuged at RT, 1000 × g for 5 min. Following a 2-h incubation at RT, the fluorescence signals were measured using Spectramax i3 (Molecular Devices) with HTRF cartridge. In parallel with the analysis of experimental samples, IP_1 standard curve was prepared in duplicate, according to the manufacturer's instructions. It was against the fluorescence values obtained for the standard curve that the values of IP_1 concentrations in the experimental samples were estimated.

[5] The use of low-volume assay plates for the IPONE HTRF assay is crucial, high-volume wells produce experimental artifacts.

3.22. ASC specks and nuclei counting (image quantification)

For image quantification (obtaining nuclear and ASC specks counts from images acquired on the Zeiss Observer.Z1 widefield fluorescence microscope), raw imaging data were imported into Cell Profiler 3.1.8 or 3.1.9 software (Carpenter et al., 2006; Kamentsky et al., 2011; McQuin et al., 2018). To each image, an analysis pipeline was applied consisting of the following steps: first, the DNA (DRAQ5) and ASC (TagBFP or mCerulean) channels were extracted. Then, the illumination correction was calculated for each channel (using the background method with block size of 60, with rescaling of the illumination function, and using the fit polynomial smoothing method), and the illumination correction was applied. In these corrected images, the primary objects (nuclei and ASC specks) were identified and counted. For identification of the nuclei, typical diameter of 10-80 pixels was used (this parameter could be adjusted between image sets), and objects outside this diameter range were discarded. Objects touching the border of the image were retained. The thresholding strategy was global, and the thresholding method was robust background. The lower and upper outlier fractions were set to 0.02. The averaging method was mode, and the variance method was standard deviation. The number of deviations was set to 0, threshold smoothing scale to 1.3488, threshold correction factor to 1.86, and the lower and upper bounds on threshold were set between ~0.001-~1 (this parameter could be adjusted between image sets, depending on the brightness of the nuclear signal). The methods to distinguish between clumped objects and to draw dividing lines between clumped objects were both set to intensity. The size of smoothing filter for declumping and the minimum allowed distance between local maxima were both automatically calculated. Lower-resolution images were used to find local maxima. Holes in identified objects were filled after both thresholding and declumping.

For identification of ASC specks, the background illumination-corrected image was first enhanced using feature type ‘speckles’, feature size 14, and slow speed and accuracy. ASC specks were identified in these enhanced images by setting the typical diameter of objects to ~2-~19 pixels (this parameter could be adjusted between image sets), and objects outside this diameter range were discarded. Objects touching the border of the image were retained. The thresholding strategy was global, and the thresholding method was robust background. The lower and upper outlier fractions were set to 0.02.

The averaging method was mode, and the variance method was standard deviation. The number of deviations was set to 0, threshold smoothing scale to 1.3488, threshold correction factor to 1.97, and the lower and upper bounds on threshold were set between ~0-~0.05 for HEK cells and ~0.01-~1 for macrophages (this parameter could be adjusted between image sets, depending on the brightness of the ASC signal). The method to distinguish between clumped objects was shape, and the method to draw dividing lines between clumped objects was intensity. The size of smoothing filter for declumping and the minimum allowed distance between local maxima were both automatically calculated. Lower-resolution images were used to find local maxima. Holes in identified objects were filled after both thresholding and declumping.

After performing nuclear and ASC specks counts, Cell Profiler generated a 'report' file, containing the numbers of ASC specks and nuclei in each image. This file was then imported into Microsoft Excel, where the ratio of ASC specks to nuclei in each well was calculated.

3.23. Assessment of mitochondrial granularity (image quantification)

Raw imaging data from time-lapse recordings of cells overexpressing fluorescent protein-based markers targeted to the mitochondrial matrix were imported into Cell Profiler 3.1.9 software (Carpenter et al., 2006; Kamentsky et al., 2011; McQuin et al., 2018). The granularity of the mitochondrial fluorescence signal was assessed in unprocessed images. The module used was 'MeasureGranularity', with the following parameter settings: measurement within objects was disabled, the subsampling factor for granularity measurements was 0.25, the subsampling factor for background reduction was 0.25, the radius of structuring element was 3, and the range of the granular spectrum was 1. To facilitate the comparisons between multiple recordings, the image granularity in the first frame of the recording was set to 100% and the values obtained from subsequently recorded frames were normalized to this initial value.

3.24. Further data analysis and software

The list of software used in my Thesis, together with the sources and applications, is provided in Table 3.8.

Name of software	Version, source	Applications
Geneious	R9-Prime 2020	Molecular cloning manager software, storage of plasmid DNA sequencing data
LAS AF	2.7.3, Leica	Operating the Leica SP5 AOBS with SMD confocal laser scanning microscope
LAS X Lite	Leica	Export of images acquired on the Leica SP5 AOBS with SMD confocal laser scanning microscope
Zen Pro	2.3, Zeiss	Operating the Zeiss Observer.Z1 widefield fluorescence microscope
Zen Lite	Zeiss	Export of images acquired on the Zeiss Observer.Z1 widefield fluorescence microscope
Cell Profiler	3.1.8, 3.1.9; Carpenter et al. (2006), Kamentsky et al. (2011), and McQuin et al. (2018)	Image quantification (obtaining nuclear and ASC specks counts from images acquired on the Zeiss Observer.Z1 widefield fluorescence microscope)
Gen5 Image+	3.03, BioTek/Agilent	Operating the Epoch Microplate Spectrophotometer with Take3 Micro-Volume Plate for DNA concentration measurements, calculating DNA concentrations
SoftMax Pro	6.3, Molecular Devices	Operating the Spectramax i3 multi-mode platform, acquiring and exporting data from HTRF assays
QuantStudio Software	1.7.1, Thermo Fisher Scientific	Operating the Quant Studio Flex 6 System qPCR cycler, export of Ct data from the qPCR assay
Clustal W	Sievers et al. (2011)	Comparison of protein sequences
Microsoft Excel	16, Microsoft	Import and processing of numerical data
Prism	6, 7, 8, GraphPad	Preparation of plots
Ai Illustrator	CC 2018 (22.1.0), 2020 (24.1), Adobe Creative Cloud	Preparation of figures

Table 3.8. List of software used for data acquisition and analysis.

4. *m*-3M3FBS activates the inflammasome in a manner independent of NLRP3

Despite the enormous body of research on the NLRP3 inflammasome, there is still no unified model explaining the activation mechanism of this sensor. Among the molecular events proposed to occur upstream of the NLRP3 inflammasome assembly is PLC activation (Chae et al., 2015; Lee et al., 2012; Murakami et al., 2012; Rossol et al., 2012). These early studies demonstrated that the NLRP3 inflammasome responses are sensitive to PLC inhibition and suggested that cytosolic Ca^{2+} fluxes are the link between PLC signaling and NLRP3 activation. Later, the role of Ca^{2+} in this process has been contested (Katsnelson et al., 2015; Muñoz-Planillo et al., 2013), but this criticism did not aim at the involvement of PLC. Here I will focus on the inflammasome activation by *m*-3M3FBS, a low molecular weight agonist of PLC. Initially reported as an inflammasome-triggering compound (Lee et al., 2012), this molecule has not received as much attention as PLC inhibitors in the follow-up studies. Hoping to establish whether and, if yes, how PLC regulates the NLRP3 inflammasome, I began my project by characterizing *m*-3M3FBS as an inflammasome activator.

4.1. *m*-3M3FBS activates the inflammasome in immortalized murine macrophages

I first tested whether *m*-3M3FBS can activate the inflammasome in NLRP3/$ASC^{mCerulean}$ reporter iMac and LPS-primed WT iMac cells, two immortalized murine macrophage cell lines that I use throughout my thesis. Importantly, NLRP3/$ASC^{mCerulean}$ reporter iMac cells constitutively overexpress NLRP3, which allows to circumvent the requirement for the NLRP3 priming stimulus in assays relying on fluorescent ASC specks imaging. (For assays relying on the measurement of IL-1β concentrations in tissue culture supernatants, NLRP3/$ASC^{mCerulean}$ reporter iMac cells still have to be primed with LPS.) To determine the potential of *m*-3M3FBS to activate the inflammasome, I challenged NLRP3/$ASC^{mCerulean}$ reporter iMac and LPS-primed WT iMac cells with increasing concentrations of *m*-3M3FBS, or of its PLC-inactive isomer *o*-3M3FBS (Figure 4.1). I assessed the degree of inflammasome activation by measurement of the secreted IL-1β concentrations (Figure 4.1 A) and imaging of ASC specks (Figure 4.1 B). The NLRP3 activator nigericin and the AIM2 agonist poly-(dA:dT) served as positive controls. Consistent with earlier reports (Chae et al., 2015; Lee et al., 2012; Muñoz-Planillo et al., 2013), *m*-3M3FBS triggered robust inflammasome responses at all tested

concentrations. In contrast, the stimulation with the inactive isomer *o*-3M3FBS did not lead to IL-1β secretion or ASC speck formation.

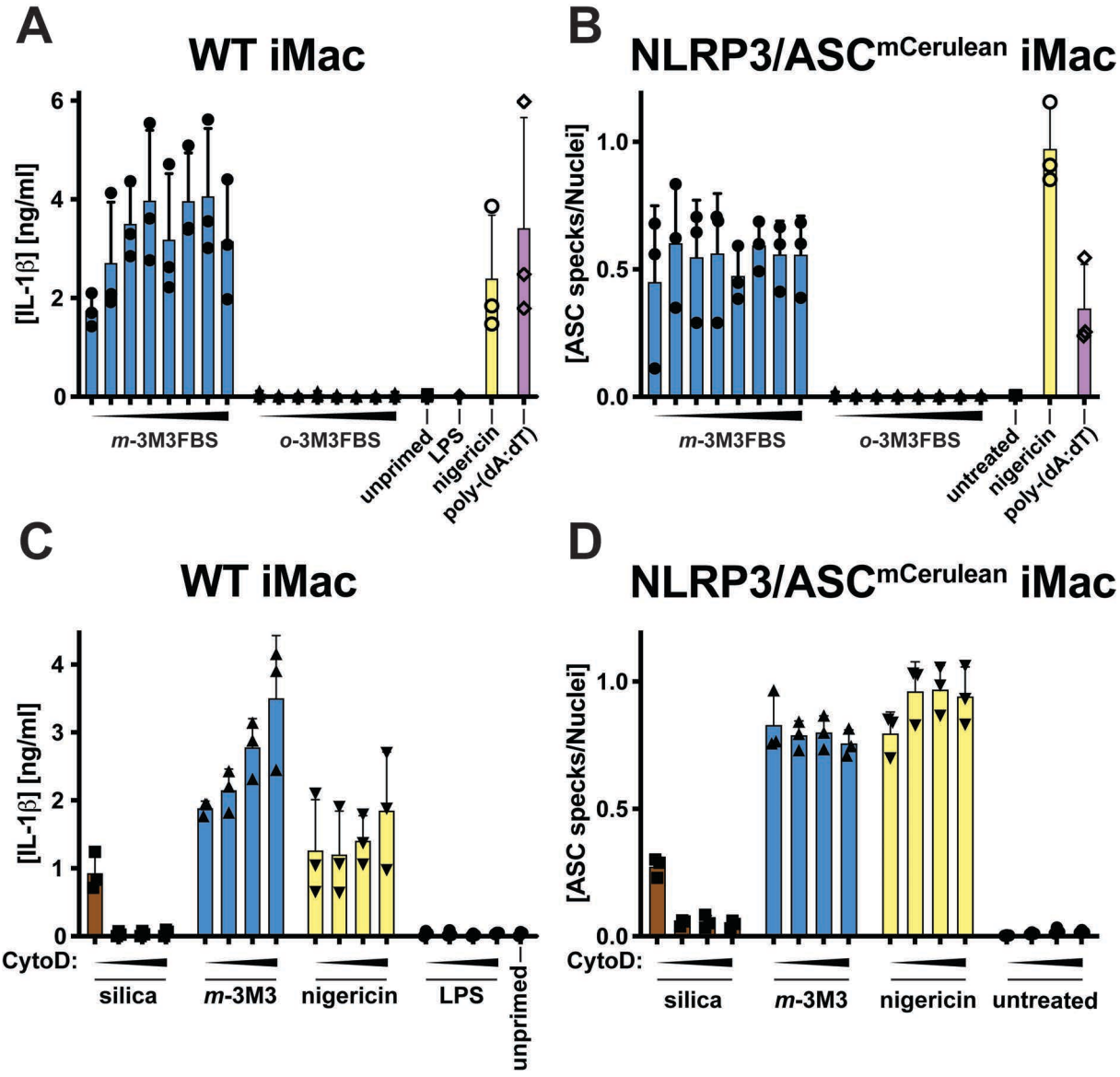

Figure 4.1. *m*-3M3FBS activates the inflammasome in WT iMac and NLRP3/ASC^{mCerulean} reporter iMac cells in a manner independent of crystal formation

A, B: LPS-primed (200 ng/mL, 2 h) WT iMac cells (A) or unprimed NLRP3/ASC^{mCerulean} reporter iMac cells (B) were stimulated with *m*-3M3FBS, *o*-3M3FBS (both at 30, 40, 50, 60, 70, 80, 90, or 100 μM), nigericin (10 μM), or poly-(dA:dT) (2 μg/mL complexed with 5 μL Lipofectamine 2000) in an extracellular medium consisting of (in mM) 123 NaCl, 5 KCl, 2 $MgCl_2$, 1 $CaCl_2$, 10 glucose, 10 HEPES, pH 7.4. The unprimed and LPS controls were subjected to medium alone. Immediately after addition of inflammasome activators, the plates were centrifuged at 340 × g for 5 min (RT). After 60 min, the supernatants were collected and IL-1β concentrations were measured by HTRF (A), or the cells were fixed, counterstained for the nuclei and imaged using a fluorescence microscope (B).

C, D: For the assessment of the sensitivity of the inflammasome activation to cytochalasin D (CytoD; phagocytosis inhibitor), LPS-primed (200 ng/mL, 2 h) WT iMac cells (C) or unprimed NLRP3/ASC^{mCerulean} reporter iMac cells (D) were pre-treated with CytoD (0 [DMSO control], 10, 25, or 50 μM) for 10 min, and then stimulated with silica crystals (0.5 mg/mL, 6 h), *m*-3M3FBS (*m*-3M3; 85 μM, 60 min), or nigericin (10 μM, 60 min). The silica stimulations as well as the unprimed and LPS control stimulations (6 h) were performed in DMEM supplemented with 10% FBS. The *m*-3M3FBS and nigericin stimulations were performed in an extracellular medium consisting of (in mM) 123 NaCl, 5 KCl, 2 $MgCl_2$, 1 $CaCl_2$, 10 glucose,

10 HEPES, pH 7.4. Immediately after addition of inflammasome activators, the plates were centrifuged at 340 × g for 5 min (RT). After the stimulations were completed, the supernatants were collected and IL-1β concentrations were measured by HTRF (C), or the cells were fixed, counterstained for the nuclei and imaged using a fluorescence microscope (D).
The results are plotted as means from 3 independent experiments performed in technical triplicate. Error bars represent SD. Individual data points represent means of the technical triplicate values from each of the independent experiments.

m-3M3FBS has a relatively low solubility in aqueous media. Because precipitates and crystals are known to activate NLPR3 through the lysosomal damage pathway (Duewell et al., 2010; Franchi and Núñez, 2008; Hornung et al., 2008; Rajamäki et al., 2010), I proceeded to verify whether the observed inflammasome activation could be a result of *m*-3M3FBS precipitation. To this end, I challenged NLRP3/ASC^{mCerulean} reporter iMac cells and LPS-primed WT iMac cells with *m*-3M3FBS in the presence or absence of the phagocytosis inhibitor cytochalasin D. Cytochalasin D prevents internalization of crystals by macrophages (Hornung et al., 2008), so if the *m*-3M3FBS-driven inflammasome activation was mediated by agonist precipitation, cytochalasin D would inhibit this response. I assessed the level of inflammasome activation by measuring the secreted IL-1β concentrations and imaging of ASC specks (Figure 4.1 C, D). Nigericin served as a phagocytosis-independent control, whereas the silica crystals were a cytochalasin D-sensitive control activator.

While the NLRP3 inflammasome activation with silica crystals was blocked by all tested concentrations of cytochalasin D, the *m*-3M3FBS-induced inflammasome activation was not sensitive to (Figure 4.1 D) or even slightly increased by (Figure 4.1 C) this inhibitor, indicating that *m*-3M3FBS does not activate the inflammasome through crystal formation and lysosomal destabilization.

4.2. Inflammasome activation by *m*-3M3FBS is dependent on ASC and caspase-1

To confirm that the *m*-3M3FBS-driven response exhibits the typical characteristics of inflammasome activation, I examined whether the *m*-3M3FBS-elicited IL-1β secretion is dependent on the inflammasome adaptor ASC (the murine gene encoding ASC is called *Pycard*), and on the effector protease caspase-1. For this purpose, I challenged LPS-primed WT and ASC-deficient (*Pycard*$^{-/-}$) BMDMs (Figure 4.2 A), and LPS primed, vehicle- or VX-765- (caspase-1 inhibitor)-pre-treated WT BMDMs (Figure 4.2 B) with increasing doses of *m*-3M3FBS. I assessed the extent of the inflammasome response by

measurement of secreted IL-1β. The inflammasome activators nigericin and poly-(dA:dT) served as control stimuli whose dependence on ASC and caspase-1 is well-established.

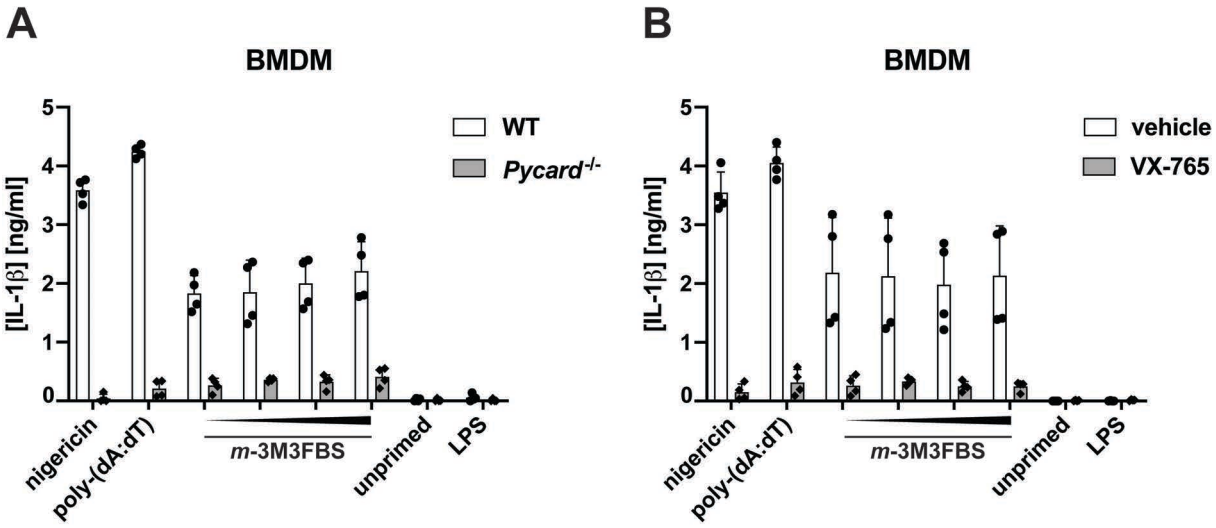

Figure 4.2. The *m*-3M3FBS-driven inflammasome response relies on ASC and caspase-1
A: To determine whether the *m*-3M3FBS-induced inflammasome activation is dependent on ASC, BMDMs generated from WT and ASC-deficient (*Pycard*$^{-/-}$) bone marrows were primed with LPS (200 ng/mL, 2 h) and then stimulated with *m*-3M3FBS, (at 55, 65, 75, or 85 μM), nigericin (10 μM), or poly-(dA:dT) (2 μg/mL complexed with 5 μL Lipofectamine 2000) in an extracellular medium consisting of (in mM) 123 NaCl, 5 KCl, 2 $MgCl_2$, 1 $CaCl_2$, 10 glucose, 10 HEPES, pH 7.4. The unprimed and LPS controls were subjected to medium alone. Immediately after addition of inflammasome activators, the plates were centrifuged at 340 × g for 5 min (RT). After 60 min, the supernatants were collected and IL-1β concentrations were measured by HTRF.
B: To determine whether the *m*-3M3FBS-induced inflammasome activation is dependent on caspase-1, BMDMs generated from WT bone marrows were primed with LPS (200 ng/mL, 2 h), pre-treated with the caspase-1 inhibitor VX-765 (40 μM, 10 min) or vehicle (DMSO), and then stimulated as in (A). After 60 min, the supernatants were collected and IL-1β concentrations were measured by HTRF.
The results are plotted as means from 4 independent experiments performed in technical triplicate. Error bars represent SD. Individual data points represent means of the technical triplicate values from each of the independent experiments.

IL-1β secretion by *m*-3M3FBS-stimulated BMDMs was dependent on ASC (Figure 4.2 A) and caspase-1 (Figure 4.2 B), consistent with the typical course of the inflammasome activation cascade.

4.3. Inflammasome responses to *m*-3M3FBS, nigericin, and poly-(dA:dT) are all comparably sensitive to PLC inhibitors

m-3M3FBS has previously been employed to demonstrate that PLC activation can trigger the NLRP3 inflammasome assembly (Chae et al., 2015; Lee et al., 2012). However, there are no published reports addressing whether PLC inhibitors can block

the inflammasome response to *m*-3M3FBS. Only two phosphatidylinositol- (PI)-PLC inhibitors are commercially available, U 73122 and edelfosine. To test how these compounds impact on the inflammasome activation, I pre-treated NLRP3/ASC^{mCerulean} reporter iMac cells and LPS-primed WT iMac cells with increasing doses of U 73122 or edelfosine and challenged them with nigericin, poly-(dA:dT), or *m*-3M3FBS. The degree of the inflammasome responses was assessed by measurement of IL-1β concentrations in the supernatants (Figure 4.3 A, C) and imaging of ASC specks (Figure 4.3 B, D).

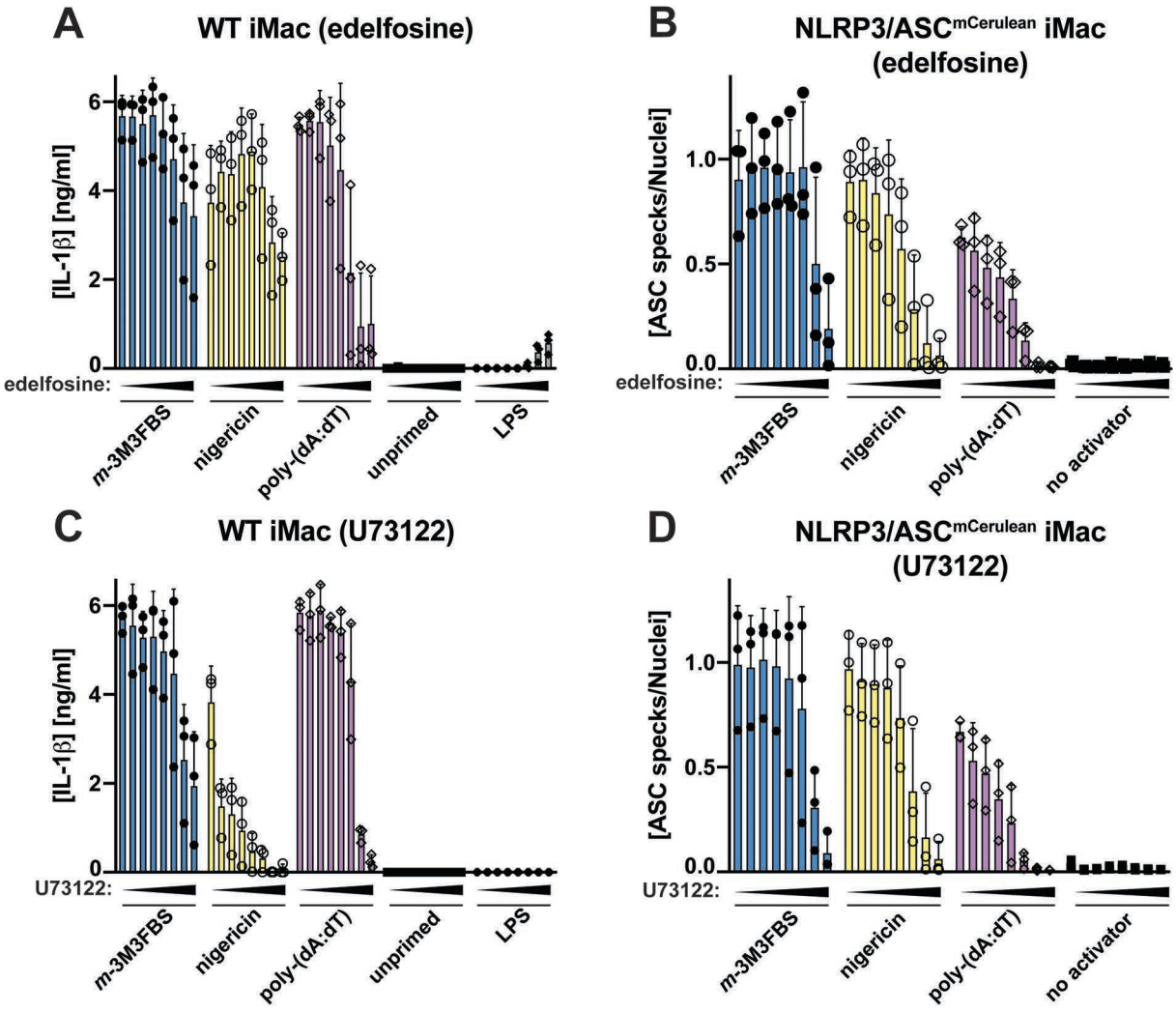

Figure 4.3. The PLC inhibitors edelfosine and U 73122 non-selectively inhibit multiple inflammasome responses

A-D: To determine whether the inflammasome responses to *m*-3M3FBS, nigericin, and poly-(dA:dT) are sensitive to edelfosine and U 73122, LPS-primed (200 ng/mL, 2 h) WT iMac cells (A, C) or unprimed NLRP3/ASC^{mCerulean} reporter iMac cells (B, D) were pre-treated with edelfosine (A, B; 0 [ethanol], 1, 2.5, 5, 10, 25, 50, or 75 μM; 10 min) or U 73122 (C, D; 0 [DMSO], 0.5, 1, 2.5, 5, 10, 25, or 50 μM; 10 min) and then stimulated with *m*-3M3FBS (85 μM), nigericin (10 μM), or poly-(dA:dT) (2 μg/mL complexed with 5 μL Lipofectamine 2000) in an extracellular medium consisting of (in mM) 123 NaCl, 5 KCl, 2 $MgCl_2$, 1 $CaCl_2$, 10 glucose, 10 HEPES, pH 7.4. The unprimed and LPS controls were subjected to medium alone. Immediately after addition of inflammasome activators, the plates were centrifuged at 340 × g for 5 min (RT). After 60 min, the supernatants were collected and IL-1β concentrations were measured by HTRF (A,

C), or the cells were fixed, counterstained for the nuclei and imaged using a fluorescence microscope (B, D).
The results are plotted as means from 3 independent experiments performed in technical duplicate. Error bars represent SD. Individual data points represent means of the technical duplicate values from each of the independent experiments.

Strikingly, the inflammasome activation with the PLC agonist *m*-3M3FBS was not particularly sensitive to the PLC inhibitors. Edelfosine inhibited the inflammasome responses to nigericin and poly-(dA:dT) more strongly than it inhibited the inflammasome activation with *m*-3M3FBS (Figure 4.3 A, B). U 73122 inhibited all tested inflammasome activations with similar potency on the ASC specking level (Figure 4.3 D), whereas it was a very strong inhibitor of the nigericin-induced IL-1β secretion (Figure 4.3 C). Neither of the tested PLC inhibitors provided an indication that the *m*-3M3FBS-induced inflammasome activation could be specifically mediated by PLC[1]. This observation was the first hint that *m*-3M3FBS might be activating the inflammasome through a PLC-unrelated off-target effect. I will elaborate on this topic in Chapters 5 and 6.

4.4. *m*-3M3FBS does not exhibit the typical characteristics of an NLRP3 agonist

In the previous section, I demonstrated that the *m*-3M3FBS-induced inflammasome activation is not sensitive to PLC inhibition. Another issue not sufficiently explored in the literature is whether *m*-3M3FBS has pharmacological and cell biological properties similar to other NLRP3 agonists.

The NLRP3 signaling cascade consists of two steps, priming, chiefly involving the induction of NLRP3 expression (Bauernfeind et al., 2009), and activation. For a number of NLRP3 agonists, the activation step is mediated by K^+ efflux from the cytosol into the extracellular fluid (Muñoz-Planillo et al., 2013; Petrilli et al., 2007). Therefore, the NLRP3 activation by many, though not all (Groß et al., 2016; Sanman et al., 2016; Wolf et al., 2016), stimuli can be blocked by bathing the cells in media containing high KCl concentrations. Finally, there is a specific, high-affinity inhibitor of NLRP3 known as CRID3, MCC950, or CP-456773 (Coll et al., 2019; Tapia-Abellán et al., 2019; Vande Walle

[1] Of note, U 73122 and edelfosine are not structurally related. These molecules are also not similar to *m*-3M3FBS. For that reason, it is unlikely that *m*-3M3FBS and edelfosine or *m*-3M3FBS and U 73122 could compete for the same binding pocket of PLC enzymes.

et al., 2019). CRID3 blocks the NLRP3 inflammasome through direct binding to the NLRP3 protein, leading to global inhibition of the NLRP3 responses.

To determine to what extent the inflammasome activation by *m*-3M3FBS conforms to the characteristics outlined above, I addressed the following questions:

1. Does the inflammasome activation by *m*-3M3FBS require the priming stimulus, such as LPS?
2. Is the inflammasome activation by *m*-3M3FBS blocked by high extracellular KCl concentrations?
3. Is the inflammasome activation by *m*-3M3FBS inhibited by CRID3?

The first question has not been answered by the literature to date. To my knowledge, the second and, indirectly, the third questions were only addressed in a single study (Muñoz-Planillo et al., 2013)[2], which suggested that *m*-3M3FBS activates the NLRP3 inflammasome through K^+ efflux. I set out to verify these observations.

To test whether the *m*-3M3FBS-driven inflammasome activation requires the priming step, I challenged unprimed and LPS-primed $ASC^{mCerulean}$ reporter WT iMac cells with *m*-3M3FBS, nigericin (a model priming-dependent NLRP3 inflammasome activator), or poly-(dA:dT) (a model priming-independent AIM2 inflammasome agonist). The degree of inflammasome activation was then evaluated by imaging of ASC specks (Figure 4.4 A).

[2] The relevant data can be found in the Supplementary Figure S2 L in the cited article.

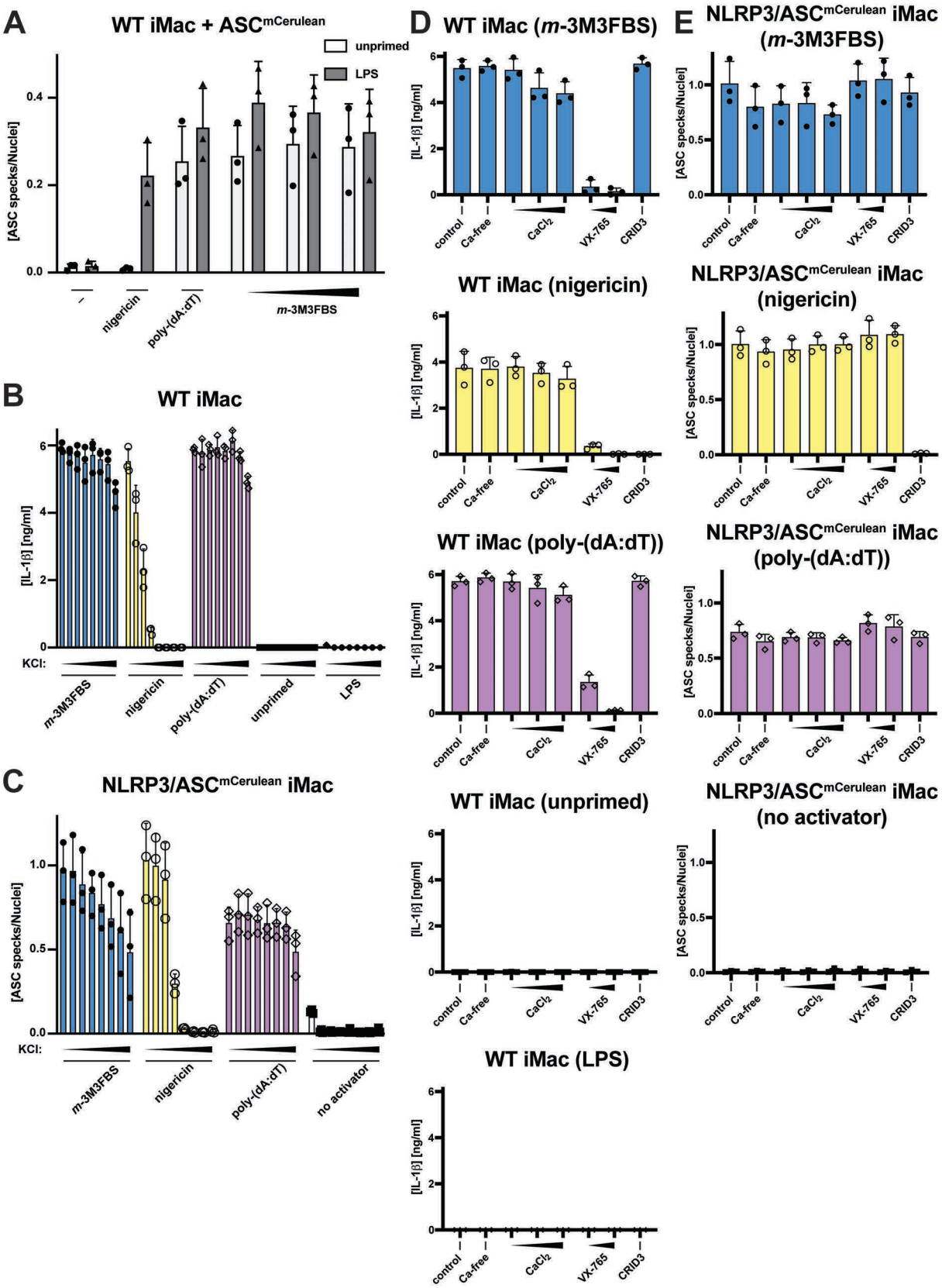

Figure 4.4. The *m*-3M3FBS-induced inflammasome activation is independent of LPS priming, not relying on K^+ efflux, and not sensitive to CRID3

A: To determine whether the *m*-3M3FBS-induced inflammasome activation requires the priming step, $ASC^{mCerulean}$-overexpressing WT iMac cells were primed with LPS (200 ng/mL, 2 h) or left unprimed, and then stimulated with *m*-3M3FBS (65, 75, or 85 μM), nigericin (10 μM), or poly-(dA:dT) (2 μg/mL complexed with 5 μL Lipofectamine 2000) in an extracellular medium consisting of (in mM) 123 NaCl, 5

KCl, 2 $MgCl_2$, 1 $CaCl_2$, 10 glucose, 10 HEPES, pH 7.4. The negative controls were subjected to medium alone. Immediately after addition of inflammasome activators, the plates were centrifuged at 340 × g for 5 min (RT). After 60 min, the cells were fixed, counterstained for the nuclei and imaged using a fluorescence microscope.
B, C: To determine whether the *m*-3M3FBS-induced inflammasome activation requires K^+ efflux, LPS-primed (200 ng/mL, 2 h) WT iMac cells (B) or unprimed NLRP3/$ASC^{mCerulean}$ reporter iMac cells (C) were shifted to media with non-physiological concentrations of KCl (0, 5, 10, 25, 50, 75, 100, or 125 mM; for the KCl concentrations above 5 mM, the NaCl concentrations were accordingly decreased so as to maintain a constant osmolarity) and then stimulated with *m*-3M3FBS (85 μM), nigericin (10 μM), or poly-(dA:dT) (2 μg/mL complexed with 5 μL Lipofectamine 2000). Apart from NaCl (123-0 mM) and KCl (0-125 mM), the extracellular media consisted of (in mM) 2 $MgCl_2$, 1 $CaCl_2$, 10 glucose, 10 HEPES, pH 7.4. The negative controls were subjected to medium alone. Immediately after addition of inflammasome activators, the plates were centrifuged at 340 × g for 5 min (RT). After 60 min, the supernatants were collected and IL-1β concentrations were measured by HTRF (B) or the cells were fixed, counterstained for the nuclei (5 μM DRAQ5) and imaged using a fluorescence microscope (C).
D, E: To determine whether the *m*-3M3FBS-induced inflammasome activation is modulated by the extracellular Ca^{2+} concentrations, the caspase-1 inhibitor VX-765, or the NLRP3 inhibitor CRID3 LPS-primed (200 ng/mL, 2 h) WT iMac cells (D) or unprimed NLRP3/$ASC^{mCerulean}$ reporter iMac cells (E) were pre-treated for 10 min with a range of $CaCl_2$ concentrations (0, 1 [control], 2.5, 5, or 10 mM), VX-765 (10 or 25 μM), or CRID3 (5 μM), and then stimulated with *m*-3M3FBS (85 μM), nigericin (10 μM), or poly-(dA:dT) (2 μg/mL complexed with 5 μL Lipofectamine 2000) in an extracellular medium consisting of (in mM) 123 NaCl, 5 KCl, 2 $MgCl_2$, 1 $CaCl_2$ (except for the Ca^{2+}-free and the increased [$CaCl_2$] conditions), 10 glucose, 10 HEPES, pH 7.4. The negative controls were subjected to medium alone. Immediately after addition of inflammasome activators, the plates were centrifuged at 340 × g for 5 min (RT). After 60 min, the supernatants were collected and IL-1β concentrations were measured by HTRF (D) or the cells were fixed, counterstained for the nuclei (5 μM DRAQ5) and imaged using a fluorescence microscope (E).
The results are plotted as means from 3 independent experiments performed in technical triplicate (A) or duplicate (B-E). Error bars represent SD. Individual data points represent means of the technical triplicate (A) or duplicate (B-E) values from each of the independent experiments.

While the nigericin-induced ASC speck formation was fully dependent on the priming stimulus, both poly-(dA:dT) and *m*-3M3FBS produced an ASC specking signal in the absence of LPS priming (Figure 4.4 A). Even though the LPS treatment was associated with a modest increase in ASC speck formation upon *m*-3M3FBS and poly-(dA:dT) stimulations, unprimed macrophages still showed considerable responses to these inflammasome activators.

I next assessed the reliance of the *m*-3M3FBS-triggered inflammasome activation on K^+ efflux by shifting NLRP3/$ASC^{mCerulean}$ reporter iMac cells and LPS-primed WT iMac cells to extracellular buffers containing a range (0-125 mM) of KCl concentrations. This was followed by stimulation with *m*-3M3FBS, nigericin (a model K^+ efflux-dependent NLRP3 inflammasome activator), or poly-(dA:dT) (a model K^+ efflux-independent AIM2 inflammasome ligand). The levels of the inflammasome responses were evaluated by measurement of IL-1β concentrations in the cell culture supernatants (Figure 4.4 B), and by imaging of ASC specks (Figure 4.4 C). Whereas the nigericin-driven NLRP3 activation was abolished by KCl concentrations above 25 mM (Figure 4.4 B, C), the *m*-3M3FBS-

elicited inflammasome activation was fully independent of K^+ efflux, similar to poly-(dA:dT).

Finally I examined the sensitivity of the *m*-3M3FBS-induced inflammasome activation to the NLRP3 inhibitor CRID3. Briefly, I pre-treated NLRP3/ASC^{mCerulean} reporter iMac or LPS-primed WT iMac cells with CRID3 and stimulated them with *m*-3M3FBS, nigericin (a CRID3-sensitive NLRP3 activator), or poly-(dA:dT) (a CRID3-insensitive AIM2 agonist). I assessed the degree of inflammasome activation by measurement of secreted IL-1β concentrations (Figure 4.4 D) and imaging of ASC specks (Figure 4.4 E). The caspase-1 inhibitor VX-765 was employed here as a control compound expected to inhibit all tested inflammasome responses at the IL-1β secretion level, but none at the ASC specking level. Calcium-free or high-$CaCl_2$ media were used additionally to address the question of the inflammasome activation dependence on extracellular Ca^{2+} (Horng, 2014; Katsnelson et al., 2015; Lee et al., 2012; Muñoz-Planillo et al., 2013; Murakami et al., 2012; Rossol et al., 2012).

Whereas IL-1β secretion in response to all tested stimuli was blocked by the caspase-1 inhibitor VX-765, only the nigericin-triggered NLRP3 inflammasome activation was inhibited by CRID3. *m*-3M3FBS activated the inflammasome in a manner not sensitive to CRID3. Neither the extracellular Ca^{2+} depletion, nor the increased (up to 10 mM) extracellular $CaCl_2$ concentrations affected the inflammasome activation by any of the tested stimuli (Figure 4.4 D).

On the level of ASC speck formation, VX-765 did not interfere with inflammasome activation. Consistent with the results of the IL-1β assay, the ASC specking response to nigericin was completely abolished by CRID3, but the response to *m*-3M3FBS was not affected by the NLRP3 inhibitor. The extracellular Ca^{2+} depletion and the high extracellular $CaCl_2$ concentrations had no impact on the inflammasome activation (Figure 4.4 E).

Collectively, the results presented in Figure 4.4 indicate that *m*-3M3FBS activates the inflammasome independently of the priming stimulus and of K^+ efflux, and in a manner not inhibitable by CRID3. Two alternative scenarios could explain these findings. The first one is that *m*-3M3FBS triggers a signaling event very close upstream of the NLRP3

inflammasome formation, possibly even acting as a direct NLRP3 binding partner. The second option is that this compound activates the inflammasome in an NLRP3-independent manner.

4.5. NLRP3 is dispensable for the *m*-3M3FBS-induced inflammasome activation in murine macrophages

Out of the two scenarios proposed at the end of the last section, the second one was much easier to address experimentally. To test whether the inflammasome activation by *m*-3M3FBS requires NLRP3, I stimulated LPS-primed WT or NLRP3-deficient (*Nlrp3*$^{-/-}$) BMDMs with increasing doses of *m*-3M3FBS and measured the concentrations of IL-1β secreted by these cells. Nigericin served as an NLRP3-dependent control, whereas the AIM2 ligand poly-(dA:dT) was a model NLRP3-independent inflammasome agonist (Figure 4.5).

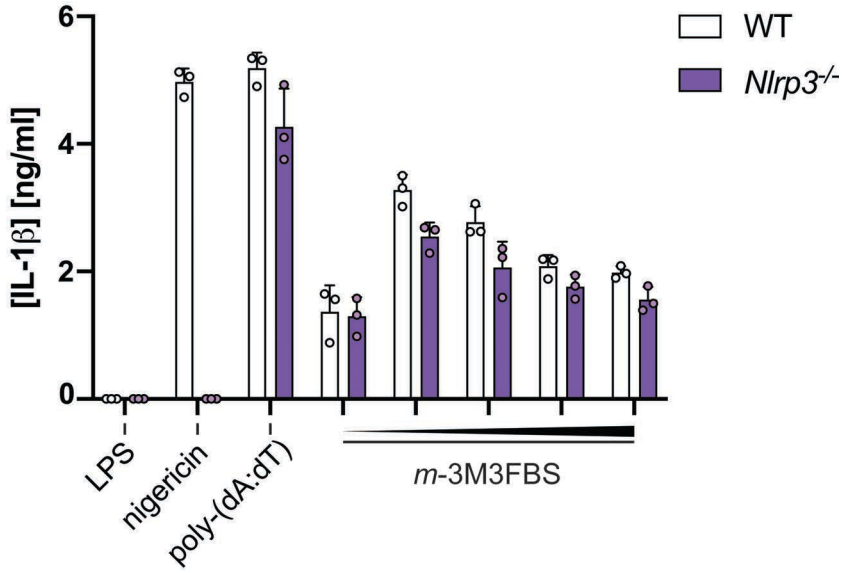

Figure 4.5. NLRP3-deficient BMDMs activate the inflammasome in response to *m*-3M3FBS
To determine whether the *m*-3M3FBS-induced inflammasome activation is dependent on NLRP3, BMDMs generated from WT and NLRP3-deficient (*Nlrp3*$^{-/-}$) bone marrows were primed with LPS (200 ng/mL, 2 h) and then stimulated with *m*-3M3FBS, (at 18, 36, 54, 72, or 85 μM), nigericin (10 μM), or poly-(dA:dT) (2 μg/mL complexed with 5 μL Lipofectamine 2000) in an extracellular medium consisting of (in mM) 123 NaCl, 5 KCl, 2 $MgCl_2$, 1 $CaCl_2$, 10 glucose, 10 HEPES, pH 7.4. The LPS control was subjected to medium alone. Immediately after addition of inflammasome activators, the plates were centrifuged at 340 × g for 5 min (RT). After 60 min, the supernatants were collected and IL-1β concentrations were measured by HTRF.
The results are plotted as means from 3 independent experiments performed in technical duplicate. Error bars represent SD. Individual data points represent means of the technical duplicate values from each of the independent experiments.

In contrast to nigericin, which triggered IL-1β secretion in a manner fully dependent on NLRP3, *m*-3M3FBS elicited robust secretion of IL-1β from NLRP3-deficient cells (Figure 4.5). This observation indicates that in murine macrophages *m*-3M3FBS is an NLRP3-independent inflammasome activator.

Based on the results presented in this chapter, some revisions may be required to our understanding of the NLRP3 inflammasome activation. I confirmed the previously reported observation that the PLC agonist *m*-3M3FBS can activate the inflammasome (Chae et al., 2015; Lee et al., 2012; Muñoz-Planillo et al., 2013). I further established that this process is dependent on ASC and caspase-1. However, I was unable to reproduce the results indicating that NLRP3 is the inflammasome sensor molecule engaged during the stimulation with *m*-3M3FBS (Muñoz-Planillo et al., 2013). Instead, my data hint that there may be another inflammasome sensor responding to this treatment. Furthermore, I did not observe considerable sensitivity of the *m*-3M3FBS-driven inflammasome activation to the PLC inhibitors edelfosine and U 73122. This result, combined with the observed low selectivity of the PLC inhibitors, suggests that off-target effects may be at play. In the following chapters I will examine the mechanisms of these off-target effects (Chapters 5 and 6). I will also determine which inflammasome sensor molecules are activated by *m*-3M3FBS and attempt to propose how this activation could occur (Chapters 6 and 8).

5. PLC is not involved in the NLRP3 inflammasome activation

PLC has been suggested to act as a positive upstream regulator of the NLRP3 inflammasome based on three lines of evidence. First, the PLC inhibitor U 73122 and several Ca^{2+} signaling-targeting molecules block the inflammasome responses (Lee et al., 2012; Murakami et al., 2012; Rossol et al., 2012). Secondly, the PLC activator *m*-3M3FBS was observed to activate the inflammasome (Lee et al., 2012), and there was some evidence that this process may be NLRP3-dependent (Muñoz-Planillo et al., 2013). Finally, people with hypermorphic mutations in the gene encoding PLCγ2, one of the PLC isoforms, suffer from an autoinflammatory disease. Peripheral blood mononuclear cells (PBMCs) isolated from these patients exhibit elevated spontaneous inflammasome activation compared to healthy controls (Chae et al., 2015; Martín-Nalda et al., 2020). This evidence was critically evaluated in several studies (primarily Baldwin et al., 2017; Katsnelson et al., 2016; 2015; Muñoz-Planillo et al., 2013) and it was suggested that at least some of the results interpreted as a proof of PLC/Ca^{2+} involvement in the NLRP3 activation could be due to off-target effects. Despite these reservations, treatments such as U 73122 have been used in a number of studies to demonstrate the involvement of the PLC-NLRP3 'signaling axis' in various biological processes (a non-exhaustive list includes the studies by Zhou et al., 2015; Deng et al., 2019; Gutiérrez-López et al., 2018; Freeman et al., 2017; Negash et al., 2019; Irmscher et al., 2019; and Martín-Nalda et al., 2020).

In Chapter 4 I have demonstrated that the reported PLC agonist *m*-3M3FBS activates the inflammasome in an NLRP3-independent manner. I have also suggested that it might activate the inflammasome in a manner independent of PLC. Here, I would like to experimentally reassess the evidence on the PLC involvement in the NLRP3 inflammasome activation.

5.1. U 73122 may inhibit the NLRP3 inflammasome through a cysteine alkylation-related off-target effect

By far the most frequently invoked piece of evidence that PLC is required for the NLRP3 activation is the observation that the NLRP3 inflammasome responses are suppressed by the PLC inhibitor U 73122 (originally reported by Lee et al., 2012; Murakami et al.,

2012; Rossol et al., 2012). Notably, edelfosine, the only other commercially available PI-PLC inhibitor, has been included in inflammasome studies much less frequently. To my knowledge, the only reports addressing the sensitivity of the NLRP3 activation to edelfosine are the articles by Lee et al. (2012)[1], where 100 μM (*sic*) edelfosine is shown to fully inhibit the NLRP3 activation with ATP, and Robblee et al. (2016)[2], where 25 μM edelfosine partially inhibits the inflammasome activation with ATP and several ER stress-inducing stimuli. Importantly, in my experiments, 25 μM was a threshold edelfosine concentration that inhibited both the NLRP3 activation with nigericin and the AIM2 activation with poly-(dA:dT) (Figure 4.3 A, B). Based on this observation, and with no other accounts of edelfosine-mediated inflammasome inhibition, it is likely that this molecule blocks the inflammasome responses in a non-selective manner. Because of this, edelfosine is not a suitable tool for establishing the links between PLC activity and the inflammasome formation.

As regards the observation that the PLC inhibitor U 73122 blocks the NLRP3 inflammasome activation, interpretation of the experimental results obtained with this compound is difficult because of its numerous off-target effects. Most importantly, U 73122 is a cysteine-alkylating agent (Horowitz et al., 2005), as it contains a maleimide moiety (Figure 5.1 A). This part of the U 73122 molecule includes a β-unsaturated carbonyl group, which can act as a Michael reaction acceptor (Maucher et al., 2017; Nair et al., 2013). The other substrate is provided by the thiol groups of protein cysteinyl residues, which can act as Michael donors. The reaction between these substrates may lead to the formation of covalent protein-U 73122 adducts and broadly affect multiple exposed cysteinyl residues in the cell's proteome.

A PLC non-targeting analog of U 73122 is commercially available and marketed as U 73343 (Figure 5.1 A, B). To their credit, Lee et al. (2012) tested whether U 73343 could inhibit the NLRP3 inflammasome responses and observed no influence of this compound on the inflammasome activation. However, the difference between the U 73122 and U 73343 molecules is precisely the presence of the double bond that can react with the thiol groups in protein cysteinyl residues (Figure 5.1 A, B). This means that U 73343 is not a suitable control for the protein-alkylating activity of U 73122.

[1] The relevant data can be found in the Supplementary Figure S5 A in the cited article.
[2] The relevant data can be found in Figure 7 B in the cited article.

Importantly, multiple instances of NLRP3 inhibition by cysteine-reactive compounds have been described (Cocco et al., 2014; 2016; 2017; He et al., 2014; Juliana et al., 2010). Taking these reports into account, I tested whether maleimide alone could inhibit the inflammasome activation with nigericin (NLRP3), poly-(dA:dT) (AIM2), or *m*-3M3FBS. To this end, I pre-treated NLRP3/ASC^{mCerulean} reporter iMac and LPS-primed WT iMac cells with U 73122, maleimide, U 73343, or succinimide (a maleimide analog without the cysteine-targeting double bond), followed by the challenge with inflammasome activators. The strength of the inflammasome responses was assessed by measurement of secreted IL-1β concentrations and imaging of ASC specks (Figure 5.1 C, D).

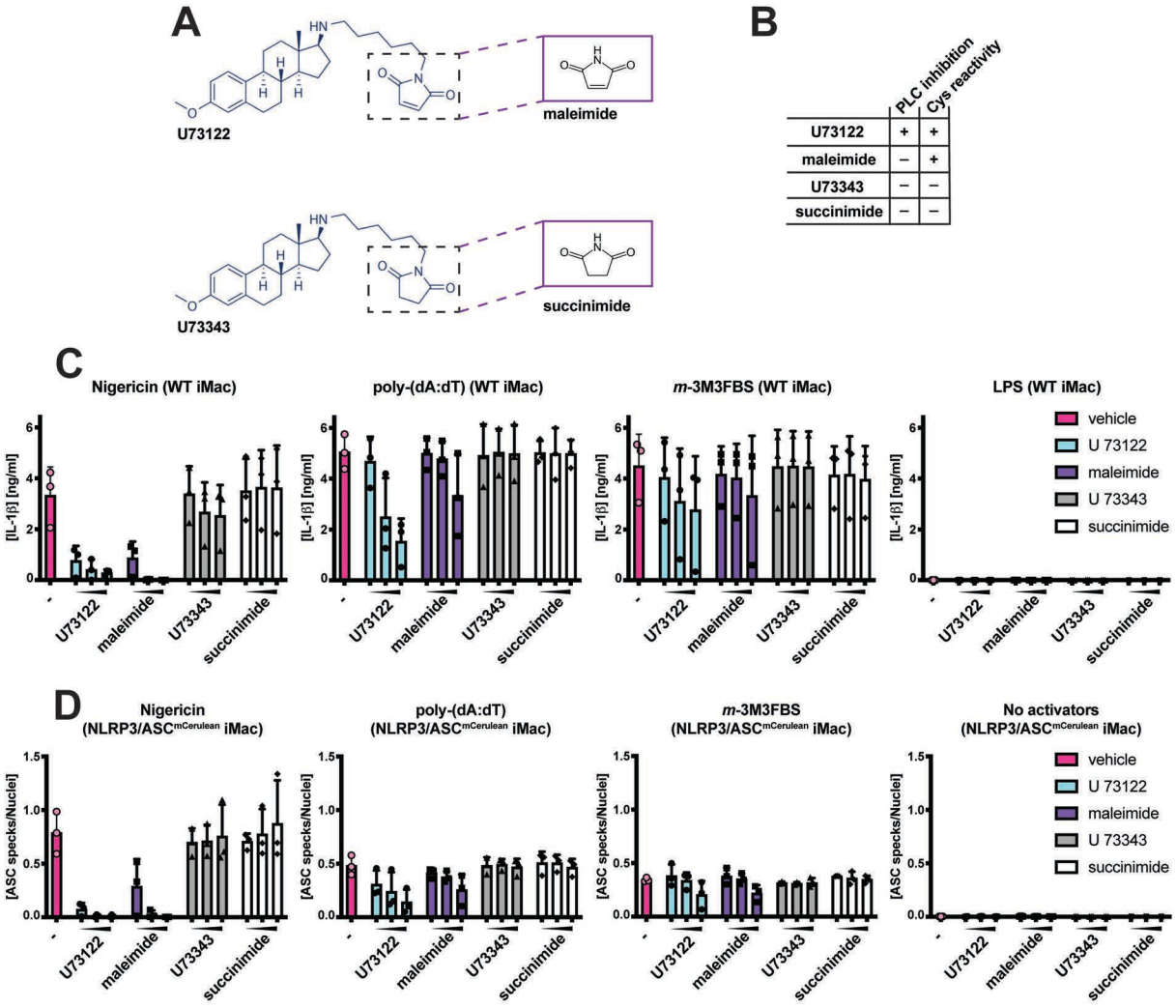

Figure 5.1. Influence of U 73122, maleimide, U 73343, and succinimide on the inflammasome responses to nigericin, poly-(dA:dT), and *m*-3M3FBS
A: Structural formulas of U 73122, maleimide, U 73343, and succinimide.
B: Comparison of cell biological (ability to inhibit PLC) and biochemical (ability to react with protein cysteinyl residues) properties of U 73122, maleimide, U 73343, and succinimide.
C, D: To determine how U 73122, maleimide, U 73343, and succinimide impact on inflammasome activation, LPS-primed (200 ng/mL, 2 h) WT iMac cells (C) or unprimed NLRP3/ASC^{mCerulean} reporter iMac cells (D) were pre-treated for 10 min with increasing doses of U 73122, maleimide, U 73343, or

succinimide (5, 10, or 20 μM). The vehicle for these compounds was DMSO. Then the cells were stimulated with *m*-3M3FBS (85 μM), nigericin (10 μM), or poly-(dA:dT) (2 μg/mL complexed with 5 μL Lipofectamine 2000) in an extracellular medium consisting of (in mM) 123 NaCl, 5 KCl, 2 $MgCl_2$, 1 $CaCl_2$, 10 glucose, 10 HEPES, pH 7.4. The negative controls were subjected to medium alone. Immediately after addition of inflammasome activators, the plates were centrifuged at 340 × g for 5 min (RT). After 60 min, the supernatants were collected and IL-1β concentrations were measured by HTRF (C) or the cells were fixed, counterstained for the nuclei and imaged using a fluorescence microscope (D).
The results are plotted as means from 3 independent experiments performed in technical duplicate. Error bars represent SD. Individual data points represent means of the technical duplicate values from each of the independent experiments.

Two principal conclusions can be drawn from the results of this experiment. First, U 73122 and maleimide both inhibited the nigericin-driven NLRP3 activation with similar potencies, reaching full inhibition at the concentration of 10 μM (Figure 5.1 C, D). This observation suggests that U 73122 may inhibit NLRP3 through cysteinyl residues alkylation rather than because of its effect on PLC. In line with the report by Lee et al. (2012), U 73343 did not inhibit the inflammasome activation, and neither did succinimide (Figure 5.1 C, D). Secondly, in agreement with my previous observations (Figure 4.3 C, D), the NLRP3 activation with nigericin was much more sensitive to the inhibition with U 73122/maleimide than the inflammasome activations with *m*-3M3FBS and poly-(dA:dT) (Figure 5.1 C, D). Of note, the poly-(dA:dT)-induced AIM2 activation was more strongly inhibited by U 73122 than was the inflammasome activation with *m*-3M3FBS. Together these observations indicate that U 73122 targets multiple inflammasome responses in a non-selective manner, likely because of cysteinyl residues alkylation.

5.2. N-substituted maleimide derivatives have an NLRP3-inhibitory activity

To gain more insight into the relative impacts of maleimide-containing molecules on the inflammasome activations with nigericin, *m*-3M3FBS, and poly-(dA:dT), I determined the half maximal inhibitory concentration (IC_{50}) values for U 73122, maleimide, N-ethylmaleimide, and R-(+)-N-(1-phenylethyl)maleimide in an ASC speck formation assay. Briefly, I pre-treated NLRP3/$ASC^{mCerulean}$ reporter iMac cells with 0-80 μM concentrations of these cysteine-alkylating agents, followed by stimulation with inflammasome activators (Figure 5.2).

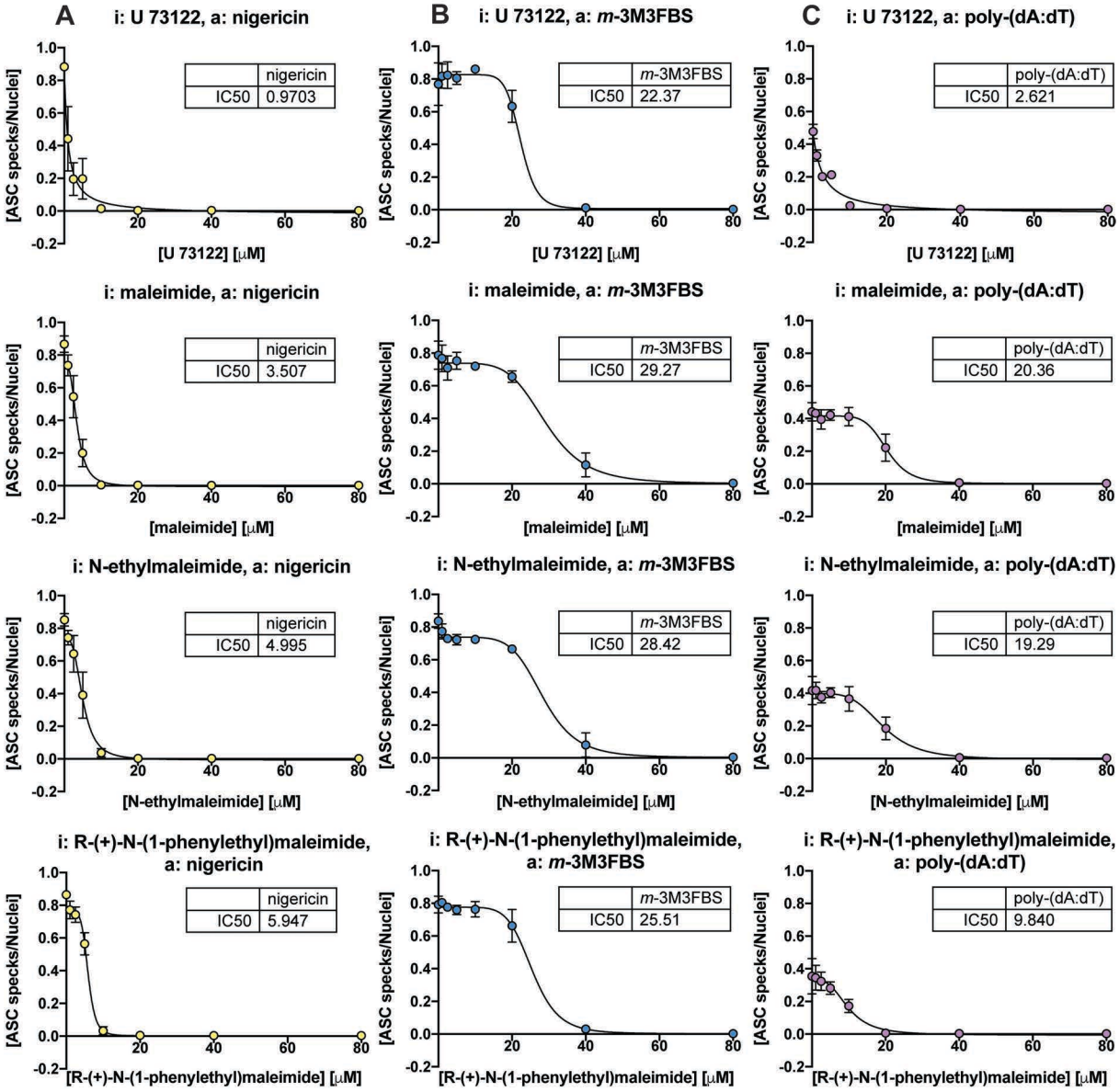

Figure 5.2. Influence of N-substituted maleimide derivatives on the inflammasome responses to nigericin, *m*-3M3FBS, and poly-(dA:dT)

A-C: To determine the relative potencies with which maleimide and its derivatives (U 73122, N-ethylmaleimide, and R-(+)-N-(1-phenylethyl)maleimide) inhibit the inflammasome responses to nigericin, *m*-3M3FBS, and poly-(dA:dT), unprimed NLRP3/ASC^{mCerulean} reporter iMac cells were pre-treated for 10 min with increasing doses of U 73122, maleimide, N-ethylmaleimide, or R-(+)-N-(1-phenylethyl)maleimide (0 [DMSO], 1, 2.5, 5, 10, 20, 40 or 80 μM). Then the cells were stimulated with nigericin (10 μM; A) *m*-3M3FBS (85 μM; B), or poly-(dA:dT) (2 μg/mL complexed with 5 μL Lipofectamine 2000; C) in an extracellular medium consisting of (in mM) 123 NaCl, 5 KCl, 2 $MgCl_2$, 1 $CaCl_2$, 10 glucose, 10 HEPES, pH 7.4. Immediately after addition of inflammasome activators, the plates were centrifuged at 340 × g for 5 min (RT). After 60 min, the cells were fixed, counterstained for the nuclei and imaged using a fluorescence microscope.

The results are plotted as means from 3 independent experiments performed in monoplicate. Error bars represent SD.

The estimated IC_{50} values revealed that the nigericin-mediated NLRP3 activation is similarly sensitive to maleimide, U 73122, and the two other tested N-substituted maleimide derivatives (IC_{50} ranging from approximately 1 to 5 μM; Figure 5.2 A). The *m*-

3M3FBS-induced ASC speck formation was less sensitive to the cysteine-alkylating agents (all IC_{50} values between 20 and 30 μM; Figure 5.2 B). The IC_{50} values for the inhibition of the poly-(dA:dT)-induced activation of AIM2 lay between the values obtained for nigericin and *m*-3M3FBS, indicating intermediate sensitivity (Figure 5.2 C). This is consistent with my previous observation that the nigericin-induced inflammasome activation was the most sensitive to U 73122, and the *m*-3M3FBS-induced inflammasome activation – the least sensitive (Figure 4.3 C, D), although presently I registered a slightly higher potency of U 73122.

5.3. U 73122 behavior in a washout assay suggests that it could be acting through a covalent cysteine modification

To test whether U 73122 and maleimide behave like covalent inhibitors in the context of the NLRP3 activation, I performed a washout experiment. Such experimental setup allows establishing to which extent a molecule is 'trapped' inside of the cell after a period of pre-incubation followed by removal of the compound from the extracellular milieu (the 'washing steps'; Figure 5.3 A). I tested whether washing away U 73122 and maleimide could restore the NLRP3 inflammasome response to nigericin in NLRP3/$ASC^{mCerulean}$ reporter iMac and LPS-primed WT iMac cells. IL-1β concentration measurement and imaging of ASC specks served as readouts of inflammasome activation (Figure 5.3 B-D). The non-covalent NLRP3 inhibitor CRID3 was used for the purpose of comparison.

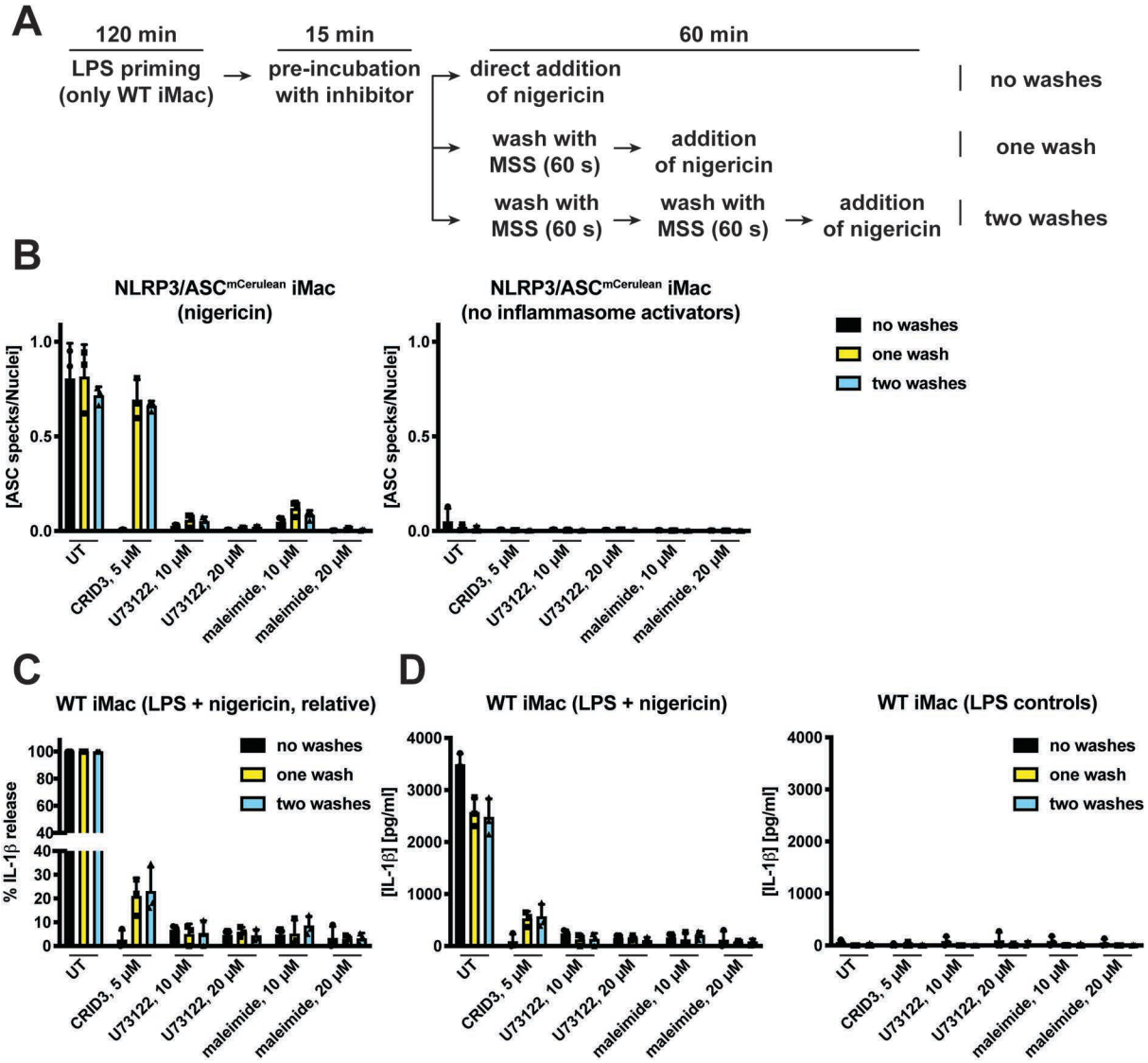

Figure 5.3. Characteristics of U 73122 and maleimide as NLRP3 inhibitors in a washout experiment
A: Scheme of the experimental setup.
B-D: To determine whether the inhibitory impact of U 73122 and maleimide on the nigericin-induced NLRP3 activation could be alleviated by washing away the inhibitors, unprimed NLRP3/ASC^{mCerulean} reporter iMac cells (B) or LPS-primed (200 ng/mL, 2 h) WT iMac cells (C, D) were pre-treated for 10 min with CRID3 (5 µM) or two doses of U 73122 or maleimide (10 or 20 µM), followed by the indicated number of washes and addition of nigericin (10 µM) in an extracellular medium consisting of (in mM) 123 NaCl, 5 KCl, 2 $MgCl_2$, 1 $CaCl_2$, 10 glucose, 10 HEPES, pH 7.4. The negative controls were subjected to medium alone. Immediately after addition of nigericin, the plates were centrifuged at 340 × g for 5 min (RT). After 60 min, the supernatants were collected and IL-1β concentrations were measured by HTRF (C, D) or the cells were fixed, counterstained for the nuclei and imaged using a fluorescence microscope (B). The values in (C) are normalized to the conditions of optimal NLRP3 activation (without CRID3, U 73122, or maleimide); the values in (D) are absolute concentrations of IL-1β detected in cell culture supernatants. The results are plotted as means from 3 independent experiments performed in technical duplicate. Error bars represent SD. Individual data points represent means of the technical duplicate values from each of the independent experiments.

On the level of ASC speck formation in NLRP3/ASC^{mCerulean} reporter iMac cells, washing away of U 73122/maleimide led to a minimal (at 10 µM inhibitor concentration) or no (at 20 µM) recovery of the NLRP3 activation with nigericin. In contrast, washing away of

CRID3 (5 μM) resulted in an almost complete recovery of the NLRP3 inflammasome response (Figure 5.3 B). On the level of IL-1β secretion by LPS-primed WT iMac cells, washing away of U 73122/maleimide did not restore the NLRP3 inflammasome activation, while removal of CRID3 led to a partial recovery of the inflammasome activity (Figure 5.3 C, D). As the washes alone produced a slight but noticeable decrease in the inflammasome activation level (Figure 5.3 D), I also provide the normalized IL-1β secretion values (Figure 5.3 C). In this normalization, the 100% values were the concentrations of IL-1β detected in the samples without inhibitors after the indicated number of washes.

U 73122 and maleimide exhibited similar behavior in the washout assay. This observation is compatible with the scenario whereby the maleimide derivatives inhibit NLRP3 by covalent modification of protein cysteinyl residues. Importantly, though, it is not a proof that the covalent modification is the cause of NLRP3 inhibition. For example, non-covalent inhibitors that bind to the inactive conformations of their targets with high affinity would be expected to produce similar results. Furthermore, compounds that are 'trapped' inside of the cell by certain enzymatic modifications could also behave in the same way. Finally, as maleimide and U 73122 (Horowitz et al., 2005) are both promiscuous cysteine-alkylating agents, it is impossible to conclude whether they inhibit the inflammasome activation through direct alkylation of NLRP3, through specific alkylation of another target, or through a general toxicity resulting from multiple covalent modifications at the proteome scale.

Regardless of the mechanistic details of the U 73122-mediated NLRP3 inhibition, the data presented in Sections 4.3 and 5.1-5.3 indicate that the commercially available PLC inhibitors block the inflammasome responses in a non-selective manner, with numerous off-target effects. Therefore, it is impossible to state that PLC is involved in the NLRP3 activation based on the results obtained using these inhibitors.

5.4. Direct assessment of PLC activity under conditions of inflammasome activation

Can a definitive conclusion regarding the role of PLC in the NLRP3 inflammasome activation be reached? Inhibitor-based perturbation experiments are uninterpretable

because of the lack of selectivity of edelfosine (Section 4.3) and the broad off-target effects of U 73122 (Sections 5.1-5.3). Genetic approaches to tackle the same question are difficult because there are 13 PLC isoenzymes encoded by the human genome, with partial redundancy with respect to the stimuli that activate them and full redundancy regarding the reaction that they catalyze (Kadamur and Ross, 2013). Ca^{2+} signaling, a downstream effector of PLC activation, may be approached experimentally but this only addresses one 'arm' of the PLC-elicited signal. Furthermore, Ca^{2+} is not exclusively mobilized by PLC, and the role of Ca^{2+} ions upstream of the NLRP3 inflammasome activation has been contested (Baldwin et al., 2017; Katsnelson et al., 2015; 2016; Muñoz-Planillo et al., 2013).

Taking these issues into consideration, I set to determine whether the inflammasome-activating stimuli also trigger PLC activation using the inositol monophosphate (IP_1) concentration measurement assay (IP_1 HTRF). This method allows for a relatively direct estimation of PLC activity. It relies on the measurement of the IP_1 concentrations in cell lysates. In the presence of Li^+ ions, IP_1 is the final breakdown product of the PLC product IP_3 so the IP_1 concentrations may serve as surrogate values for the IP_3 concentrations (Zhang et al., 2010).

To my knowledge, there is only one instance where a similar assay has been applied to demonstrate the involvement of PLC in the NLRP3 inflammasome activation (Lee et al., 2012)[3]. In this study, the authors showed that the IP_1 concentrations were increased in macrophages treated with the inflammasome activators ATP and $CaCl_2$, compared to untreated controls[4]. A critical evaluation of these results points to several ambiguities:

1. The PLC activity assay was performed in NLRP3-proficient cells, but there were no control experiments to ensure that the observed increase in IP_1 is not occurring downstream of the NLRP3 inflammasome activation.

2. The choice of the tested inflammasome activators (ATP and $CaCl_2$/calcium phosphate crystals) was peculiar. ATP activates the NLRP3 inflammasome in a

[3] The relevant data can be found in Figure 2 C of the cited paper.
[4] It was later demonstrated that under the conditions applied in the study by Lee et al. (2012), the Ca^{2+} ions precipitate with inorganic phosphate, forming crystals that activate NLRP3 through the lysosomal damage pathway (Muñoz-Planillo et al., 2013).

manner fully dependent on P_2X_7R (Mariathasan et al., 2006; Solle et al., 2001; Sutterwala et al., 2006), an ion channel enabling K^+ efflux upon binding to extracellular ATP. P_2X_7R activation has not been linked to PLC activation. However, ATP may still act on another receptor, the P_2Y_2 receptor (P_2Y_2R; del Rey et al., 2006; Elliott et al., 2009). P_2Y_2R is a G_q-coupled GPCR and its activation may stimulate PLC in a manner not relevant for the NLRP3 activation. Consequently, detecting an increase in the IP_1 concentration in ATP-stimulated cells does not prove a causal link to the NLRP3 activation pathway. As for $CaCl_2$, it was initially suggested to activate PLC and the NLRP3 inflammasome through CaSR, a G_q-coupled GPCR family member. Later studies contested the existence of such signaling axis (Katsnelson et al., 2015; Muñoz-Planillo et al., 2013). To date, there have been no further reports indicating if other NLRP3 stimuli could induce PLC activation.

3. The IP_1 assay was developed for screening of G_q-coupled GPCR agonists and antagonists, and it is well suited for this purpose. In this relatively linear sequence of events (ligand – GPCR – G_q – PLCβ – IP_3 – IP_1), IP_1 is solely derived as a breakdown product of IP_3, and further dephosphorylation of IP_1 is prevented by the addition of a high (50 mM) concentration of LiCl.

Activation of the NLRP3 inflammasome is likely not such a simple process. Consequently, at least two concerns need to be addressed. First, the addition of 50 mM LiCl to the tissue culture medium may not be completely neutral for the macrophage behavior, and it might interfere with some of the processes involved in the inflammasome activation. Li^+ ions have known cellular effects (Raghavendra et al., 2013), and the addition of 50 mM LiCl requires either a significant change in the osmolarity of the extracellular milieu (100 mOsm on top of the typical tissue culture medium osmolarity of approximately 300 mOsm) or a reduction in the NaCl concentration to keep the osmolarity constant (from the typical 110-140 mM NaCl concentration to 60-90 mM). Secondly, the IP_1 concentration may increase in the cell independent of the PLC-IP_3 axis. To confidently establish that an increase in the IP_1 concentration is caused by PLC, it needs to be inhibitable by PLC blockers, unspecific as they are. These concerns have not been considered in the literature.

The first issue I addressed was testing the compatibility of the inflammasome activation with the IP_1 assay conditions. To this end, I challenged NLRP3/ASC^{mCerulean} reporter iMac and LPS-primed WT iMac cells with the inflammasome activators nigericin, poly-(dA:dT), and *m*-3M3FBS in the presence of standard MSS, MSS with 50 mM LiCl and the normal NaCl concentration (125 mM), MSS with 175 mM NaCl (high osmolarity control), or MSS with 50 mM LiCl and the NaCl concentration decreased to 75 mM to keep the osmolarity constant. For WT iMac cells, the LPS priming step was performed under Li^+-free conditions (DMEM supplemented with 10% FBS). The degree of inflammasome activation was assessed by IL-1β concentration measurement (Figure 5.4 A) and imaging of ASC specks (Figure 5.4 B).

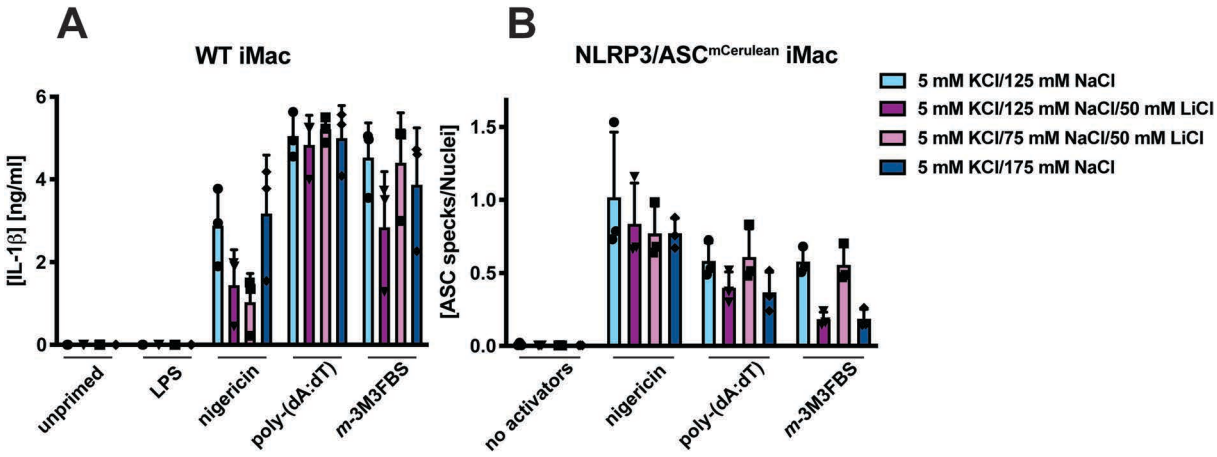

Figure 5.4. Influence of 50 mM LiCl on the inflammasome responses to nigericin, poly-(dA:dT), and *m*-3M3FBS

A, B: To determine whether high-LiCl conditions are optimal for inflammasome activation, LPS-primed (200 ng/mL, 2 h) WT iMac cells (A) or unprimed NLRP3/ASC^{mCerulean} reporter iMac cells (B) were shifted to extracellular media consisting of (in mM): 125 NaCl, 5 KCl, 2 $MgCl_2$, 1 $CaCl_2$, 10 glucose, 10 HEPES, pH 7.4 (5 mM KCl/125 mM NaCl), 50 LiCl 125 NaCl, 5 KCl, 2 $MgCl_2$, 1 $CaCl_2$, 10 glucose, 10 HEPES, pH 7.4 (5 mM KCl/125 mM NaCl/50 mM LiCl), 50 LiCl, 75 NaCl, 5 KCl, 2 $MgCl_2$, 1 $CaCl_2$, 10 glucose, 10 HEPES, pH 7.4 (5 mM KCl/75 mM NaCl/50 mM LiCl), or 175 NaCl, 5 KCl, 2 $MgCl_2$, 1 $CaCl_2$, 10 glucose, 10 HEPES, pH 7.4 (5 mM KCl/175 mM NaCl) and then stimulated with *m*-3M3FBS (85 μM), nigericin (10 μM), or poly-(dA:dT) (2 μg/mL complexed with 5 μL Lipofectamine 2000). The negative controls were subjected to media alone. Immediately after addition of inflammasome activators, the plates were centrifuged at 340 × g for 5 min (RT). After 60 min, the supernatants were collected and IL-1β concentrations were measured by HTRF (A) or the cells were fixed, counterstained for the nuclei and imaged using a fluorescence microscope (B).
The results are plotted as means from 3 independent experiments performed in technical triplicate. Error bars represent SD. Individual data points represent means of the technical triplicate values from each of the independent experiments.

In WT iMac cells, both the high osmolarity and the osmolarity-compensated LiCl-containing media slightly inhibited the NLRP3 activation with nigericin, while the high osmolarity LiCl medium also affected the inflammasome activation with *m*-3M3FBS.

None of the conditions interfered with the AIM2 inflammasome activation with poly-(dA:dT) (Figure 5.4 A). On the ASC specking level, neither of the LiCl-containing media inhibited the NLRP3 activation with nigericin but the high osmolarity media appeared to interfere with the *m*-3M3FBS-induced inflammasome activation and with the AIM2 activation by poly-(dA:dT) (Figure 5.4 B). These results indicate that whereas the inflammasome activation in the LiCl-containing media may be suboptimal, it is in principle possible. With that in mind, I proceeded to evaluate how the IP_1 levels change in cells challenged with inflammasome activators.

5.5. The K^+ efflux-triggering NLRP3 agonist nigericin is neither a strong nor a specific inducer of PLC in immortalized murine macrophages

For a comprehensive overview of the IP_1 levels under the conditions of inflammasome activation, I challenged unprimed or LPS-primed WT iMac cells with nigericin, poly-(dA:dT), *m*-3M3FBS, or *o*-3M3FBS (the PLC-inactive isomer of *m*-3M3FBS), followed by lysis and measurement of the IP_1 concentrations in the cell lysates. To gain better insight into the links between PLC activation and the inflammasome assembly, I tested the impact of the following pre-treatments: U 73122, edelfosine (PLC inhibitors), maleimide (the active moiety of U 73122 without the specific PLC-targeting properties), CRID3 (NLRP3 inhibitor), and VX-765 (caspase-1 inhibitor). Furthermore, to partially address the risk of artifacts from the high-LiCl buffers, I performed the assay in parallel in 50 mM LiCl/75 mM NaCl and 50 mM LiCl/125 mM NaCl media. As the conclusions from both of these setups were the same, I present the results obtained in the 50 mM LiCl/75 mM NaCl medium below (Figure 5.5), while the results from the 50 mM LiCl/125 mM NaCl medium can be inspected in the Supplementary Figure S1.

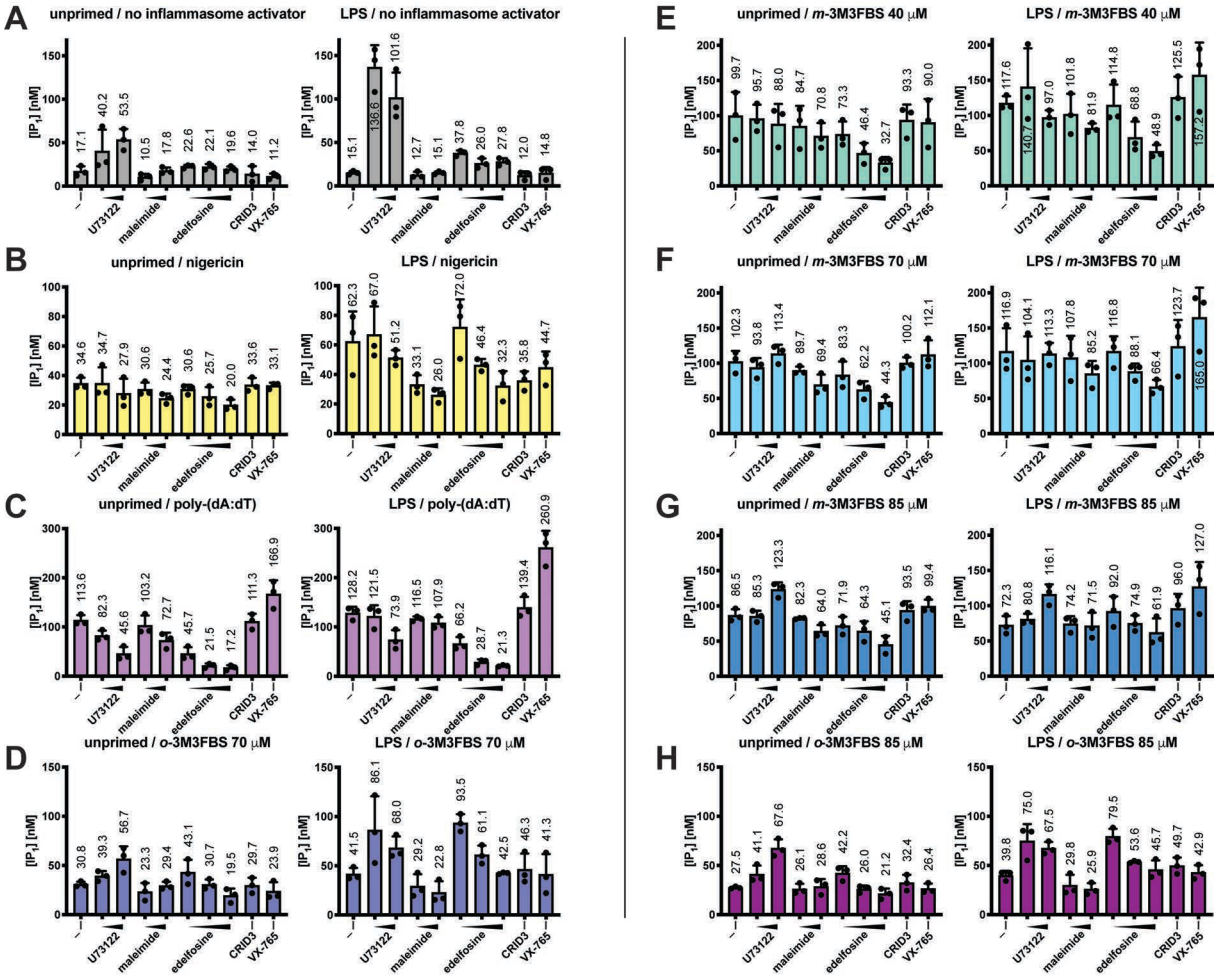

Figure 5.5. IP_1 levels in unprimed or LPS-primed WT iMac cells treated with inflammasome activators in a minimal salt solution containing 50 mM LiCl and 75 mM NaCl

A-H: To determine whether the inflammasome activators nigericin, poly-(dA:dT), and *m*-3M3FBS are capable of eliciting PLC activation, unprimed or LPS-primed (200 ng/mL, 2 h) WT iMac cells were shifted to an extracellular medium consisting of (in mM): 50 LiCl, 75 NaCl, 5 KCl, 2 $MgCl_2$, 1 $CaCl_2$, 10 glucose, 10 HEPES, pH 7.4. Then the cells were left untreated or pre-treated for 10 min with U 73122 (5 or 25 μM), maleimide (5 or 25 μM), edelfosine (10, 25, or 50 μM), CRID3 (5 μM), or VX-765 (40 μM). This pre-incubation was followed by administration of the inflammasome activators: 10 μM nigericin (B), 2 μg/mL poly-(dA:dT) complexed with 5 μL lipofectamine (C), 40-85 μM *m*-3M3FBS (E-G), or 70-85 μM *o*-3M3FBS (D, H; PLC-inactive isomer of *m*-3M3FBS). The negative controls (A) were subjected to the medium alone. Immediately after addition of inflammasome activators, the plates were centrifuged at 340 × g for 5 min (RT). After 45 min of stimulation, the cells were lysed by addition of Triton X-100 (final concentration 0.5%) and the concentrations of IP_1 in the supernatants were assessed by HTRF.

Because the tested treatments led to a relatively wide range of detected IP_1 concentrations, the scales on the y-axes differ between panels A-H. To enable easier comparisons, absolute mean values are specified above each bar or within the bars.

The results are plotted as means from 3 independent experiments performed in technical duplicate. Error bars represent SD. Individual data points represent means of the technical duplicate values from each of the independent experiments.

To consider an inflammasome-triggering stimulus as a PLC activator, it has to fulfill the following criteria:

1. It produces a marked increase in the cytosolic concentration of IP_1;

2. This increase is inhibitable by edelfosine and/or U 73122, but not by maleimide;
3. The increase in IP_1 is not blocked by CRID3 or VX-765. Sensitivity to the latter two treatments would suggest that the IP_1 increase occurs downstream of the inflammasome activation.

Unexpectedly, the inflammasome activator that best fit to these characteristics was the AIM2 agonist poly-(dA:dT), which produced a strong, U 73122-/edelfosine-sensitive increase in the IP_1 level (Figure 5.5 C and Supplementary Figure S1 C). The observation that the caspase-1 inhibitor VX-765 enhanced the poly-(dA:dT)-induced increase in the IP_1 concentration suggests that blocking pyroptosis may allow the cells to maintain the production of IP_3.

The NLRP3 activator nigericin triggered a much lower increase in the IP_1 levels, which was not sensitive to U 73122/edelfosine, but was partially blocked by CRID3 under the LPS-primed conditions (Figure 5.5 B and Supplementary Figure S1 B).

Treatments with the PLC activator *m*-3M3FBS resulted in IP_1 levels higher than in untreated cells or in cells treated with the inactive isomer *o*-3M3FBS (Figure 5.5 A, D-H and Supplementary Figure S1 A, D-H). Notably, the *m*-3M3FBS-induced activation of PLC was partially sensitive to edelfosine, but not sensitive to U 73122 (Figure 5.5 E-G and Supplementary Figure S1 E-G).

Finally, the treatment with U 73122 alone led to a marked increase in the detected IP_1 concentrations (Figure 5.5 A and Supplementary Figure S1 A). Though confusing, this result was consistent with a report that demonstrated that one of the off-target effects of U 73122 is in fact direct PLC activation (Klein et al., 2011).

Interpreted together with my earlier results (Sections 4.3, 5.1-5.3) as well as observations from other studies (Horowitz et al., 2005; Klein et al., 2011), the data presented in Figure 5.5 and Supplementary Figure S1 point to two conclusions:

1. PLC is not required for activation of the NLRP3 inflammasome;
2. Global PLC activation does not trigger the activation of NLRP3.

I believe these statements are warranted in particular by the observation that murine macrophage transfection with the AIM2 agonist poly-(dA:dT) results in an increase in PLC activity. Poly-(dA:dT) is a well characterized AIM2 ligand and has been broadly validated as a specific trigger of the AIM2-mediated inflammasome formation in murine macrophages (Fernandes-Alnemri et al., 2009; Hornung et al., 2009; Jin et al., 2012; Rathinam et al., 2010). The AIM2 deficiency fully abolishes the inflammasome response to poly-(dA:dT), while the NLRP3 deficiency does not affect it. Given that poly-(dA:dT) does not activate NLRP3, but it appears to induce PLC, it can be inferred that PLC activation alone does not lead to the NLRP3 inflammasome assembly. This conclusion is in agreement with the previous studies that provided arguments against the model proposing that PLC/Ca^{2+} signaling triggers the NLRP3 inflammasome activation (Katsnelson et al., 2015; Muñoz-Planillo et al., 2013).

5.6. NLRP3 activation does not stimulate PLC in BMDMs

To test whether the key observations on PLC activity in the inflammasome activator-treated WT iMac cells also hold true in BMDMs, I measured the IP_1 levels in WT, ASC-deficient (*Pycard*$^{-/-}$), and VX-765 (caspase-1 inhibitor)-pre-treated WT BMDMs challenged with a range of inflammasome stimuli (Figure 5.6). I assessed the IP_1 concentrations under both unprimed (Figure 5.6 A) and LPS-primed (Figure 5.6 B) conditions. Consistent with the results obtained in WT iMac cells (Figure 5.5 and Supplementary Figure S1), the strongest inducer of PLC in BMDMs was poly-(dA:dT) (Figure 5.6). Importantly, the increase in the IP_1 concentration detected upon poly-(dA:dT) transfection was further enhanced by the ASC deficiency and by caspase-1 inhibition, indicating that it was not a downstream effect of the AIM2 inflammasome assembly. Nigericin did not cause an increase in the IP_1 concentration under any of the tested conditions. The increase in the IP_1 level elicited by *m*-3M3FBS was noticeable but lower than the increase triggered by poly-(dA:dT). Finally, the PLC-inactive isomer *o*-3M3FBS also produced a moderate IP_1 increase, especially in LPS-primed cells.

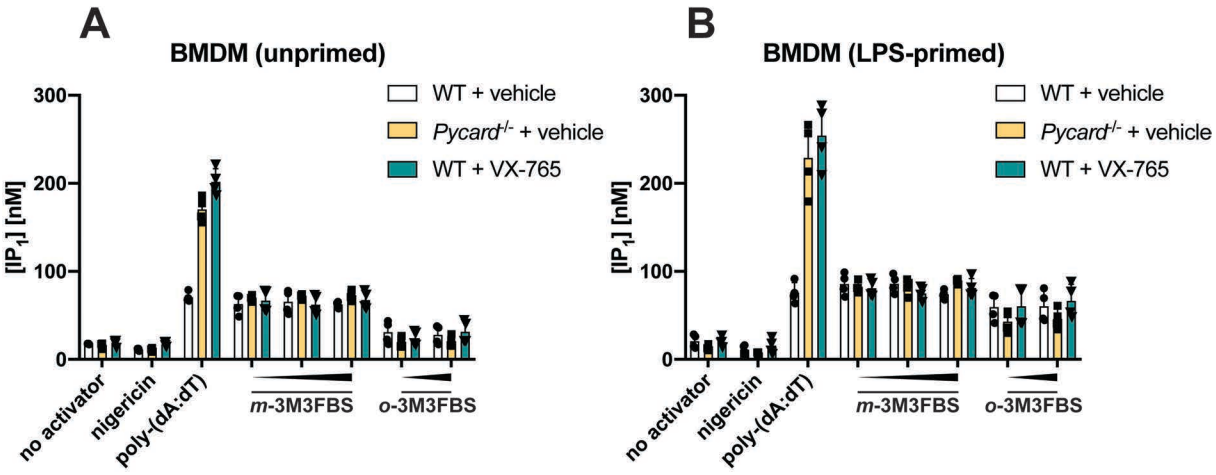

Figure 5.6. IP_1 levels in WT, ASC-deficient (*Pycard*$^{-/-}$), and VX-765- (caspase-1 inhibitor)-pre-treated BMDMs stimulated with inflammasome activators in the minimal salt solution containing 50 mM LiCl and 75 mM NaCl

A, B: To determine whether the inflammasome activators nigericin, poly-(dA:dT), and *m*-3M3FBS are capable of eliciting PLC activation in BMDMs, unprimed (A) or LPS-primed (200 ng/mL, 2 h; B) WT or ASC-deficient (*Pycard*$^{-/-}$) BMDMs were shifted to an extracellular medium consisting of (in mM): 50 LiCl, 75 NaCl, 5 KCl, 2 $MgCl_2$, 1 $CaCl_2$, 10 glucose, 10 HEPES, pH 7.4. Then the cells were pre-treated with the caspase-1 inhibitor VX-765 (40 μM) or vehicle (DMSO) for 10 min. This pre-incubation was followed by administration of the inflammasome activators: 10 μM nigericin, 2 μg/mL poly-(dA:dT) complexed with 5 μL lipofectamine, 50, 75, or 85 μM *m*-3M3FBS, or 75 or 85 μM *o*-3M3FBS (PLC-inactive isomer of *m*-3M3FBS). The negative controls were subjected to the medium alone. Immediately after addition of inflammasome activators, the plates were centrifuged at 340 × g for 5 min (RT). After 45 min of stimulation, the cells were lysed by addition of Triton X-100 (final concentration 0.5%) and the concentrations of IP_1 in the supernatants were assessed by HTRF.
The results are plotted as means from 4 independent experiments performed in technical quadruplicate. Error bars represent SD. Individual data points represent means of the technical quadruplicate values from each of the independent experiments.

Next, I tested the IP_1 responses to the inflammasome activators in NLRP3-deficient (*Nlrp3*$^{-/-}$) and AIM2-deficient (*Aim2*$^{-/-}$) BMDMs (Figure 5.7). Despite the higher background PLC activity in this assay, I observed strong PLC induction with poly-(dA:dT) but no increase in the IP_1 levels upon stimulation with nigericin (Figure 5.7), consistent with my previous results (Figure 5.6). Here, both the *m*-3M3FBS and *o*-3M3FBS treatments resulted in elevated IP_1 concentrations (Figure 5.7).

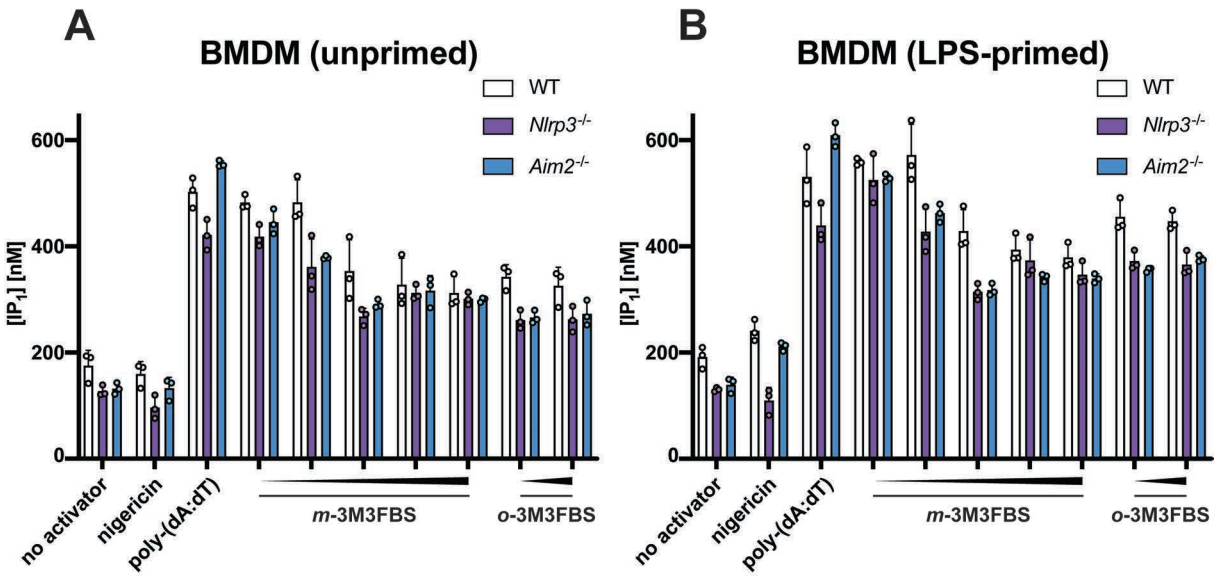

Figure 5.7. IP_1 levels in WT, NLRP3-deficient (*Nlrp3*$^{-/-}$), and AIM2-deficient (*Aim2*$^{-/-}$) BMDMs stimulated with inflammasome activators in the minimal salt solution containing 50 mM LiCl and 75 mM NaCl

A, B: To determine whether the inflammasome activators nigericin, poly-(dA:dT), and *m*-3M3FBS are capable of eliciting PLC activation in BMDMs, unprimed (A) or LPS-primed (200 ng/mL, 2 h; B) WT, NLRP3-deficient (*Nlrp3*$^{-/-}$), or AIM2-deficient (*Aim2*$^{-/-}$) BMDMs were shifted to an extracellular medium consisting of (in mM): 50 LiCl, 75 NaCl, 5 KCl, 2 $MgCl_2$, 1 $CaCl_2$, 10 glucose, 10 HEPES, pH 7.4. Then the cells were stimulated with the inflammasome activators: 10 μM nigericin, 2 μg/mL poly-(dA:dT) complexed with 5 μL lipofectamine, 18, 36, 54, 72, or 85 μM *m*-3M3FBS, or 72 or 85 μM *o*-3M3FBS (PLC-inactive isomer of *m*-3M3FBS). The negative controls were subjected to the medium alone. Immediately after addition of inflammasome activators, the plates were centrifuged at 340 × g for 5 min (RT). After 45 min of stimulation, the cells were lysed by addition of Triton X-100 (final concentration 0.5%) and the concentrations of IP_1 in the supernatants were assessed by HTRF.
The results are plotted as means from 3 independent experiments performed in technical triplicate. Error bars represent SD. Individual data points represent means of the technical triplicate values from each of the independent experiments.

The evidence presented in the present Chapter and in Sections 4.3 and 4.5 indicates that PLC is likely not involved in the NLRP3 inflammasome activation. First, *m*-3M3FBS activates the inflammasome in a manner independent of NLRP3 and not sensitive to the PLC inhibitors U 73122 and edelfosine. Secondly, U 73122 appears to inhibit the canonical NLRP3 activation through an off-target effect linked to covalent modifications of protein cysteinyl residues. Furthermore, edelfosine is not a selective NLRP3 inhibitor as it inhibits the AIM2 inflammasome activation by poly-(dA:dT) with similar potency. Thirdly, the NLRP3 activator nigericin does not produce a major increase in the cellular IP_1 concentration, whereas transfection with poly-(dA:dT) strongly increases the IP_1 level[5].

[5] Of note, it is unlikely that the PLC induction by poly-(dA:dT) is linked to the AIM2 inflammasome activation. A more plausible explanation is that the increased IP_1 levels result from activation of other DNA- or DNA/Lipofectamine 2000 complex-sensing mechanisms.

What evidence remains in favor of the model whereby PLC activation occurs upstream of the NLRP3 inflammasome assembly? There are two reports of an autoinflammatory disease termed autoinflammation and phospholipase Cγ2-associated antibody deficiency and immune dysregulation (APLAID) (Chae et al., 2015; Martín-Nalda et al., 2020). This condition is proposed to be caused by hypermorphic mutations in PLCγ2 (characterized in detail by Walliser et al., (2018) and Martín-Nalda et al., (2020)). Monocytes from patients suffering from APLAID manifest with spontaneous inflammasome activation upon LPS treatment, which is considered as evidence that increased PLC activity triggers the NLRP3 inflammasome. Importantly, neither Chae et al. (2015) nor Martín-Nalda et al. (2020) addressed the NLRP3 dependency of the observed phenotype (for example by using CRID3 or NLRP3-targeting siRNAs). Moreover, the involvement of PLC/Ca^{2+} signaling has been inferred from experiments employing BAPTA-AM (shown to act through an off-target effect by Katsnelson et al. (2015)), 2-APB (shown to act through an off-target effect by Katsnelson et al. (2015) and Baldwin et al. (2017)), and U 73122 (shown to act through an off-target effect in my thesis). Taking all of this under consideration, it would probably be prudent to re-evaluate both the mechanism of inflammasome activation in APLAID patients and the inflammasome sensor molecule engaged in the excessive inflammatory response. However, as there is no APLAID patient cohort available in Bonn, this topic will not be further investigated in my thesis.

In the following Chapters, I will identify the inflammasome sensor molecules engaged during the *m*-3M3FBS stimulation and examine the mechanisms by which *m*-3M3FBS activates the inflammasome.

6. *m*-3M3FBS disrupts the mitochondrial compartment and activates the NLRP10 and AIM2 inflammasomes

In Chapters 4 and 5, I have demonstrated that PLC is not involved in the NLRP3 inflammasome activation, that *m*-3M3FBS activates the inflammasome independently of NLRP3, and that this molecule likely acts through a mechanism not relying on PLC (Scheme 6.1). These conclusions prompt two questions: which inflammasome sensor components are activated by *m*-3M3FBS, and how this process occurs.

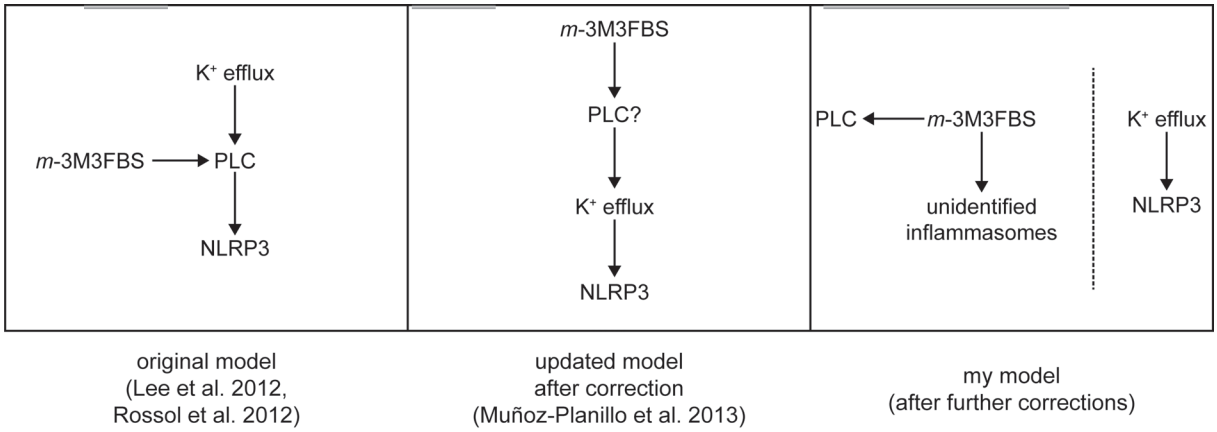

Scheme 6.1. Comparison of the existing models of the phospholipase C involvement in the NLRP3 inflammasome activation
Left: The model implicitly suggested by studies by Lee et al. (2012) and Rossol et al. (2012). K^+ efflux agonists activating NLRP3 were proposed to trigger PLC activation, which was considered to be necessary for the inflammasome activation. *m*-3M3FBS was proposed to act directly at the level of PLC.
Center: The model emerging from the revision by Muñoz-Planillo et al. (2013). In this study, *m*-3M3FBS was proposed to activate the inflammasome in a K^+ efflux-dependent manner, potentially placing PLC activation upstream of K^+ efflux, which is in contrast to the studies by Lee et al. (2012) and Rossol et al. (2012).
Right: The model proposed in my thesis based on the results presented in Chapters 4 and 5. Here, *m*-3M3FBS activates the inflammasome in a manner independent of K^+ efflux, of NLRP3, and of PLC. The model K^+ efflux agonist nigericin did not trigger PLC activation. Collectively, my observations point to a model in which the *m*-3M3FBS-induced inflammasome activation, the *m*-3M3FBS-induced PLC activation, and the NLRP3 activation by K+ efflux agonists are all unconnected events.

6.1. An overexpression screen in ASC^{TagBFP} HEK cells identifies NLRP10 as a prospective inflammasome-forming sensor responding to *m*-3M3FBS

In order to determine which sensor could initiate the inflammasome assembly upon stimulation with *m*-3M3FBS, I transiently overexpressed several PYD-containing proteins in ASC^{TagBFP} HEK cells. I then treated these cells with *m*-3M3FBS or nigericin (as a control) and assessed their ASC specking responses by fluorescence microscopy (Figures 6.1-6.3). Transient transfections with the different PYD-containing proteins led

to variable levels of background ASC specking under the unstimulated conditions. Consequently, I decided to present the results here as normalized to the unstimulated control. The graphs with the non-normalized values obtained in this screen can be found in the Supplementary Figures S2-S4.

Importantly, this screening approach was feasible because ASC^{TagBFP} HEK cells and ASC^{TagBFP} HEK cells transfected with the empty (control) vector did not have increased levels of ASC speck formation when exposed to *m*-3M3FBS (Figures 6.1 A, B, 6.2 A, B, and 6.3 A, B). The disadvantage of this method was the high likelihood of obtaining false negative results, especially for the PYD-containing proteins that produced high background ASC specking levels (Supplementary Figures S2-S4).

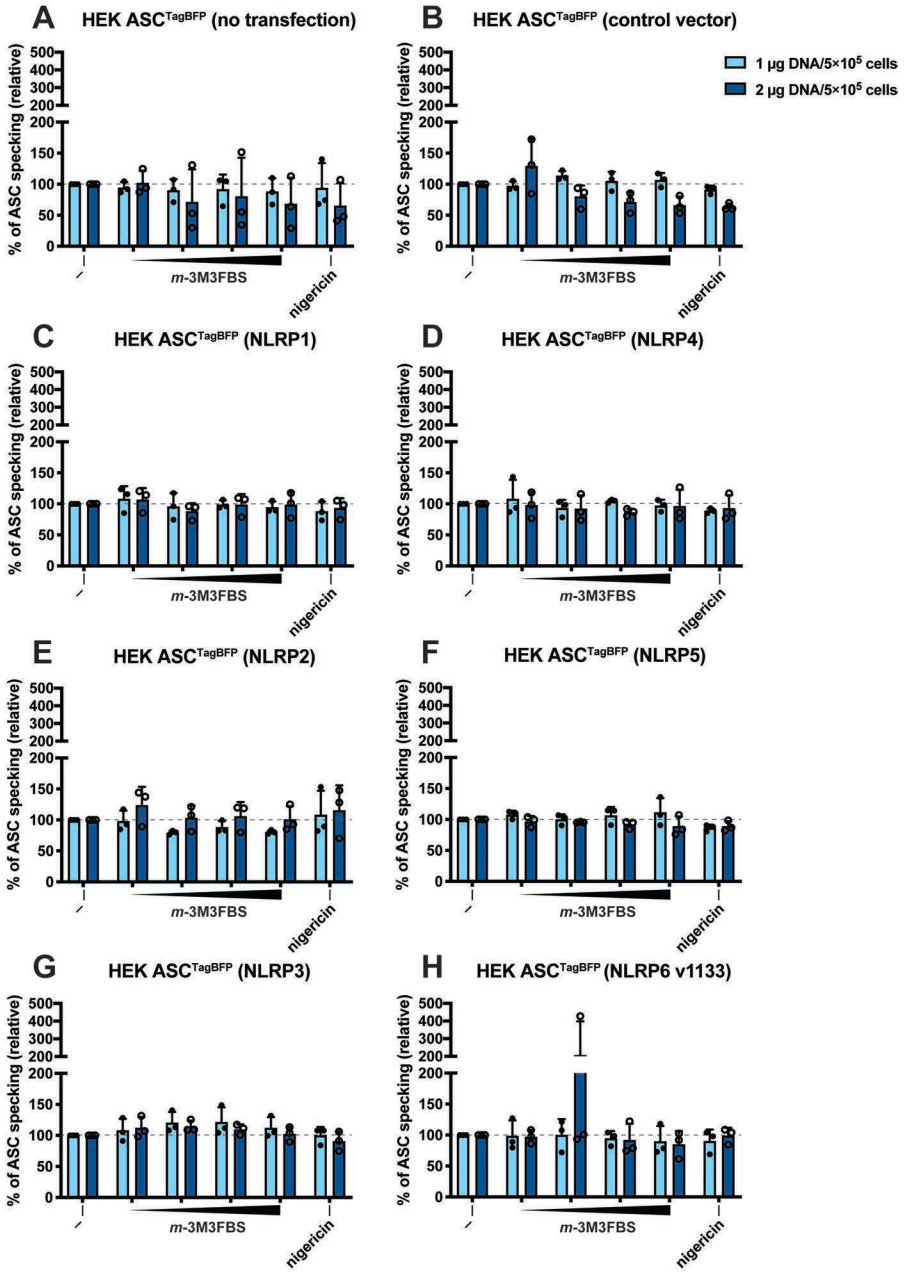

Figure 6.1. ASC specking responses to *m*-3M3FBS in ASC^{TagBFP} HEK cells transiently overexpressing human NLRP1, human NLRP2, human NLRP3, human NLRP4, human NLRP5, or human NLRP6

A-H: ASC^{TagBFP} HEK cells were left untransfected (A) or were transiently transfected in wells of a 6-well plate with the empty vector (B) or with vectors encoding human (h) NLRP1 (C), hNLRP2 (E), hNLRP3 (G), hNLRP4 (D), hNLRP5 (F), or hNLRP6 (H; plasmid ID in the Institute of Innate Immunity database was 1133). The transfected DNA amount was 1 µg per 5 × 10^5 cells (light blue bars; the number of cells refers to the initial cell population) or 2 µg per 5 × 10^5 cells (dark blue bars; the number of cells refers to the initial cell population). The transfection reagent was Gene Juice and it was combined with DNA at the ratio of 2.3 µL of Gene Juice per 1 µg of DNA. After 24 h of transfection, the cells were replated into 96-well plates, and after additional 24 h they were shifted to an extracellular medium consisting of (in mM) 123 NaCl, 5 KCl, 2 $MgCl_2$, 1 $CaCl_2$, 10 glucose, 10 HEPES pH 7.4. Then, the cells were left untreated (-), or they were stimulated with *m*-3M3FBS (40, 55, 70, or 85 µM) or with nigericin (10 µM). Immediately after addition of inflammasome activators, the plates were centrifuged at 340 × g for 5 min (RT). After 30 min, the cells were fixed with 4% formaldehyde, counterstained with the nuclear dye DRAQ5 (5 µM) and imaged using a widefield fluorescence microscope.

The results are plotted as mean normalized values (the untreated [-] control within each of the panels was taken as 100%) from 3 independent experiments performed in technical duplicate. Error bars represent SD. Individual data points represent means of the technical duplicate values from each of the independent experiments.

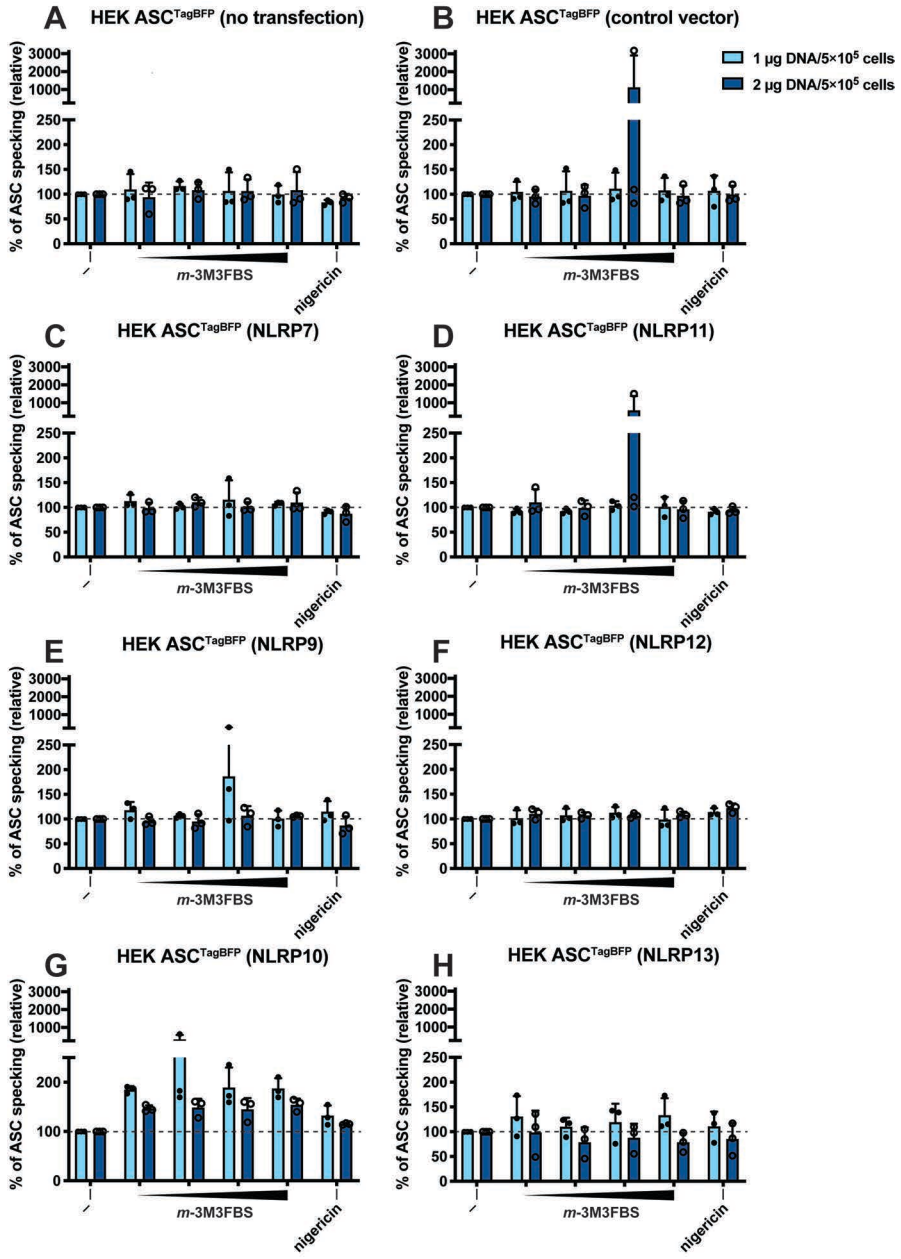

Figure 6.2. ASC specking responses to *m*-3M3FBS in ASC^{TagBFP} HEK cells transiently overexpressing human NLRP7, human NLRP9, human NLRP10, human NLRP11, human NLRP12, or human NLRP13
A-H: ASC^{TagBFP} HEK cells were left untransfected (A) or were transiently transfected in wells of a 6-well plate with the empty vector (B) or with vectors encoding human (h) NLRP7 (C), hNLRP9 (E), hNLRP10 (G), hNLRP11 (D), hNLRP12 (F), or hNLRP13 (H). The transfected DNA amount was 1 µg per 5×10^5 cells (light blue bars; the number of cells refers to the initial cell population) or 2 µg per 5×10^5 cells (dark blue bars; the number of cells refers to the initial cell population). The transfection reagent was Gene Juice and it was combined with DNA at the ratio of 2.3 µL of Gene Juice per 1 µg of DNA. After 24 h of transfection, the cells were replated into 96-well plates, and after additional 24 h they were shifted to an extracellular medium consisting of (in mM) 123 NaCl, 5 KCl, 2 $MgCl_2$, 1 $CaCl_2$, 10 glucose, 10 HEPES pH 7.4. Then, the cells were left untreated (-), or they were stimulated with *m*-3M3FBS (40, 55, 70, or 85 µM) or with nigericin (10 µM). Immediately after addition of inflammasome activators, the plates were centrifuged at $340 \times g$ for 5 min (RT). After 30 min, the cells were fixed with 4% formaldehyde, counterstained with the nuclear dye DRAQ5 (5 µM) and imaged using a widefield fluorescence microscope.
The results are plotted as mean normalized values (the untreated [-] control within each of the panels was taken as 100%) from 3 independent experiments performed in technical duplicate. Error bars represent SD. Individual data points represent means of the technical duplicate values from each of the independent experiments.

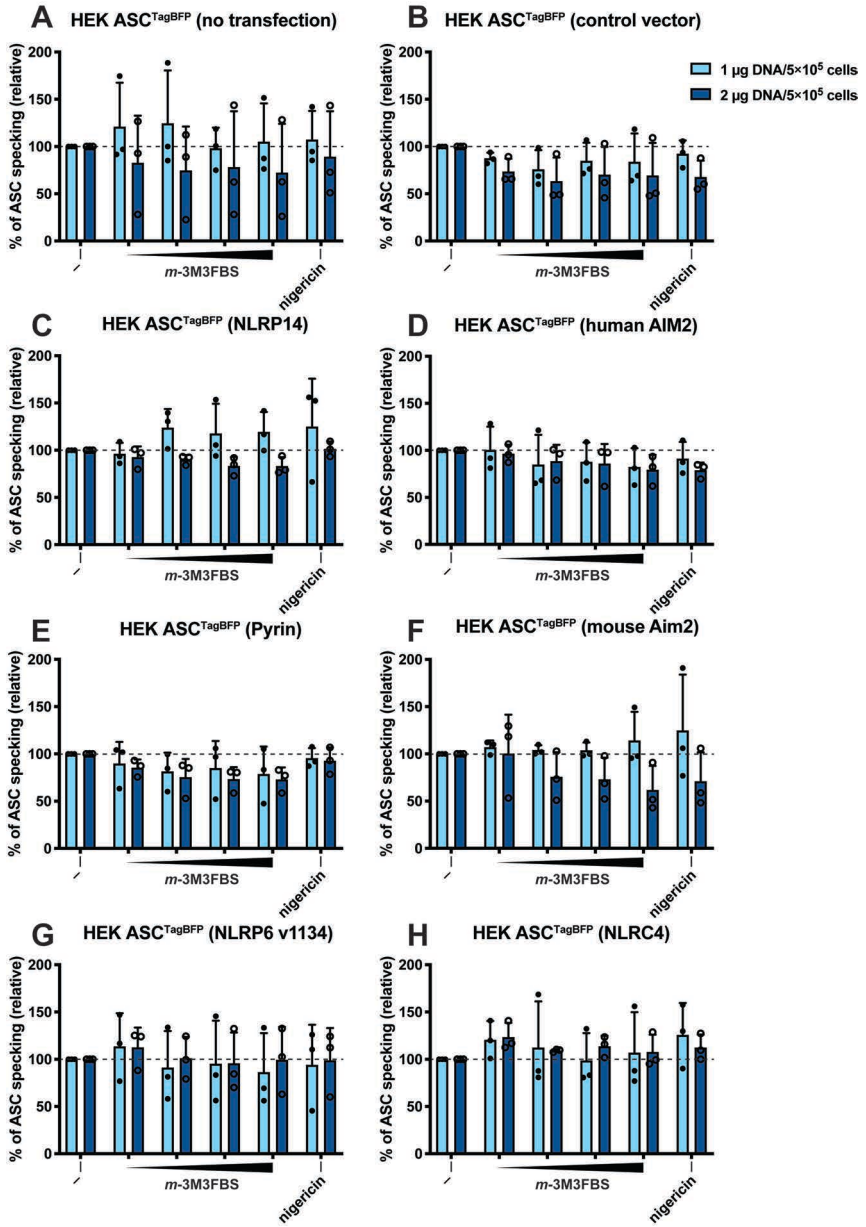

Figure 6.3. ASC specking responses to *m*-3M3FBS in ASC^{TagBFP} HEK cells transiently overexpressing human NLRP14, human pyrin, human AIM2, murine AIM2, human NLRP6, or human NLRC4

A-H: ASC^{TagBFP} HEK cells were left untransfected (A) or were transiently transfected in wells of a 6-well plate with the empty vector (B) or with vectors encoding human (h) NLRP14 (C), hPyrin (E), hNLRP6 (G; the vector ID in the Institute of Innate Immunity database was 1134), hAIM2 (D), murine Aim2 (F), or hNLRC4 (H). The transfected DNA amount was 1 µg per 5×10^5 cells (light blue bars; the number of cells refers to the initial cell population) or 2 µg per 5×10^5 cells (dark blue bars; the number of cells refers to the initial cell population). The transfection reagent was Gene Juice and it was combined with DNA at the ratio of 2.3 µL of Gene Juice per 1 µg of DNA. After 24 h of transfection, the cells were replated into 96-well plates, and after additional 24 h they were shifted to an extracellular medium consisting of (in mM) 123 NaCl, 5 KCl, 2 $MgCl_2$, 1 $CaCl_2$, 10 glucose, 10 HEPES pH 7.4. Then, the cells were left untreated (-), or they were stimulated with *m*-3M3FBS (40, 55, 70, or 85 µM) or with nigericin (10 µM). Immediately after addition of inflammasome activators, the plates were centrifuged at 340 × g for 5 min (RT). After 30 min, the cells were fixed with 4% formaldehyde, counterstained with the nuclear dye DRAQ5 (5 µM) and imaged using a widefield fluorescence microscope.

The results are plotted as mean normalized values (the untreated [-] control within each of the panels was taken as 100%) from 3 independent experiments performed in technical duplicate. Error bars represent SD. Individual data points represent means of the technical duplicate values from each of the independent experiments.

Out of the prospective inflammasome-forming sensors tested, the only one whose overexpression consistently led to a noticeable increase in ASC specking upon stimulation with *m*-3M3FBS was NLRP10 (Figure 6.2 G). This result was unexpected for several reasons. First, NLRP10 is a unique member of the NLRP subfamily in that it lacks the LRR domain (MacDonald et al., 2013). Based on this fact, several previous reports proposed that NLRP10 may have an inhibitory impact on the inflammasome formation (Imamura et al., 2010; Murphy et al., 2013; Wang et al., 2004), though these studies can in no way be considered conclusive (I address this issue in more detail in Sections 7.5, 8.4, and 10.5). Finally, NLRP10 is not highly expressed in the hematopoietic system (Lautz et al., 2012; Nakajima et al., 2018; Vacca et al., 2017) so it is unlikely that it could be the sensor responding to *m*-3M3FBS in murine macrophages (Chapter 4; murine macrophage responses to *m*-3M3FBS were also previously reported by Deng et al. (2019); Lee et al. (2012); Muñoz-Planillo et al. (2013); Rossol et al. (2012)).

6.2. NLRP10 stably overexpressed in ASC^{TagBFP} HEK cells enables ASC specking responses to both *m*-3M3FBS and *o*-3M3FBS

To validate the finding that NLRP10 may be an inflammasome-forming sensor activated by *m*-3M3FBS (Figure 6.2 G), I generated ASC^{TagBFP} HEK cells stably transduced with the empty vector, human (h) NLRP10^{mCitrine}, or murine (m) NLRP10^{mCitrine}. I stimulated these cells with *m*-3M3FBS, *o*-3M3FBS (the *m*-3M3FBS isomer without PLC-inducing activity), nigericin, or poly-(dA:dT) and assessed the levels of ASC speck formation by fluorescence microscopy (Figure 6.4 A-C). NLRP3/ASC^{mCerulean} reporter iMac cells served as a control (Figure 6.4 D).

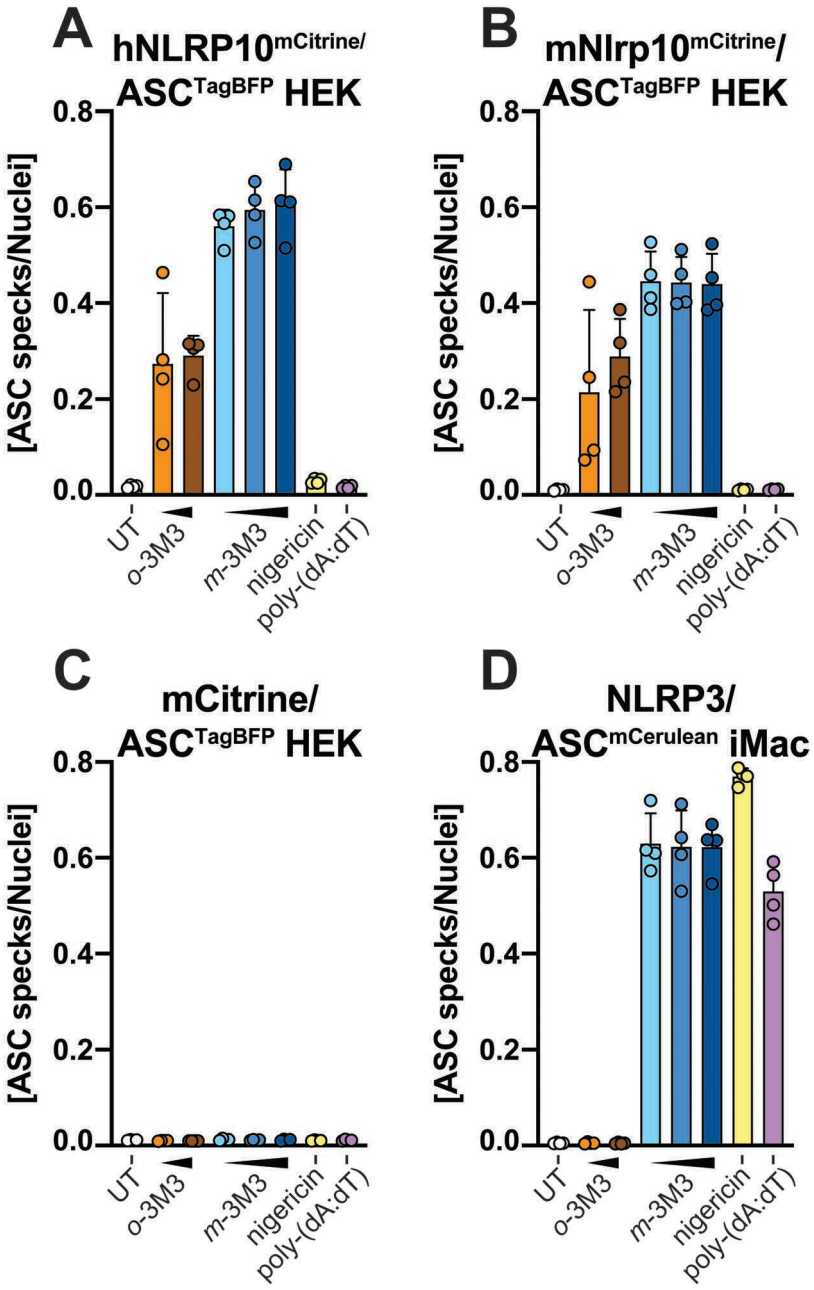

Figure 6.4. ASC specking responses to *m*-3M3FBS and *o*-3M3FBS in ASC^{TagBFP} HEK cells stably transduced with the empty vector, human NLRP10^{mCitrine}, or murine NLRP10^{mCitrine}, and in NLRP3/ASC^{mCerulean} reporter iMac cells

A-D: Human (h) NLRP10^{mCitrine}/ASC^{TagBFP} HEK cells (A), murine (m) Nlrp10^{mCitrine}/ASC^{TagBFP} HEK cells (B), mCitrine/ASC^{TagBFP} HEK cells (C), and NLRP3/ASC^{mCerulean} reporter iMac cells (D) were shifted to an extracellular medium consisting of (in mM) 123 NaCl, 5 KCl, 2 $MgCl_2$, 1 $CaCl_2$, 10 glucose, 10 HEPES pH 7.4. Then the cells were left untreated (UT), or they were stimulated with *m*-3M3FBS (*m*-3M3; 65, 75, or 85 μM), *o*-3M3FBS (*o*-3M3; 75 or 85 μM), nigericin (10 μM), or poly-(dA:dT) (2 μg/mL complexed with 5 μL Lipofectamine 2000). Immediately after addition of inflammasome activators, the plates were centrifuged at 340 × g for 5 min (RT). After 30 min (A-C) or 60 min (D), the cells were fixed with 4% formaldehyde, counterstained with the nuclear dye DRAQ5 (5 μM) and imaged using a widefield fluorescence microscope.

The results are plotted as means from 4 independent experiments performed in technical triplicate. Error bars represent SD. Individual data points represent means of the technical triplicate values from each of the independent experiments.

Consistent with my previous observation (Figure 4.1), *m*-3M3FBS elicited a strong ASC specking response in NLRP3/ASC^{mCerulean} reporter iMac cells, while *o*-3M3FBS did not have inflammasome-stimulating activity in these cells (Figure 6.4 D). In contrast, in hNLRP10^{mCitrine}/ASC^{TagBFP} and mNLRP10^{mCitrine}/ASC^{TagBFP} HEK cells, both the *m*-3M3FBS and *o*-3M3FBS treatments resulted in ASC speck formation (Figure 6.4 A, B), though *m*-3M3FBS was a stronger NLRP10 activator. ASC^{TagBFP} HEK cells transduced with the empty vector did not respond to *m*-/*o*-3M3FBS (Figure 6.4 C). Importantly, the NLRP3 activator nigericin and the AIM2 ligand poly-(dA:dT) did not cause NLRP10-driven ASC speck formation (Figure 6.4 A-C), whereas they produced robust inflammasome responses in NLRP3/ASC^{mCerulean} reporter iMac cells (Figure 6.4 D).

This experiment confirmed that both the human and murine NLRP10 proteins, when overexpressed in HEK cells, can initiate ASC speck formation upon exposure to *m*-3M3FBS. Surprisingly, a weaker, HEK cell-specific ASC specking response was also observed in *o*-3M3FBS-treated cells. The responsiveness to *o*-3M3FBS is difficult to interpret. This compound is considered to be a PLC-inactive isomer of *m*-3M3FBS (Bae et al., 2003). However, I have earlier determined that *m*-3M3FBS likely activates the inflammasome in a manner not linked to PLC activation (Figures 4.3, 5.1, and 5.2). Theoretically, a common off-target effect of both isomers could exist and it could be involved in the NLRP10 activation. As *m*-3M3FBS activates the inflammasome in both murine macrophages and HEK cells overexpressing NLRP10, whereas *o*-3M3FBS only appears to be active in HEK cells, in the following sections, I will focus on the inflammasome activation with *m*-3M3FBS.

6.3. Cell biological characteristics of the *m*-3M3FBS-induced NLRP10 activation in HEK cells resemble the characteristics of the *m*-3M3FBS-driven inflammasome response in murine macrophages

To test whether the *m*-3M3FBS-driven NLRP10 activation in HEK cells shows signs of dependence on PLC, I pre-treated NLRP10^{mCitrine}/ASC^{TagBFP} HEK cells with increasing doses of edelfosine (Figure 6.5 A), or U 73122 (Figure 6.5 B), followed by a challenge with *m*-3M3FBS. I assessed the degree of the inflammasome response by ASC speck imaging.

Similar to the observations from immortalized macrophages (Figure 4.3), only the highest, non-selective doses of the PLC inhibitors blocked the NLRP10 activation with *m*-3M3FBS, indicating that this process likely does not rely on PLC (Figure 6.5). Notably, transient overexpression of the hyperactive PLCγ2 variant (p.S707Y; described by Chae et al. (2015) and Walliser et al. (2018)) or of the constitutively active G_q α protein mutant (Q209L) in NLRP10/ASC fluorescent reporter HEK cells did not lead to ASC speck formation (Supplementary Figure S5). These observations further suggest that activation of PLC does not promote the NLRP10 inflammasome assembly.

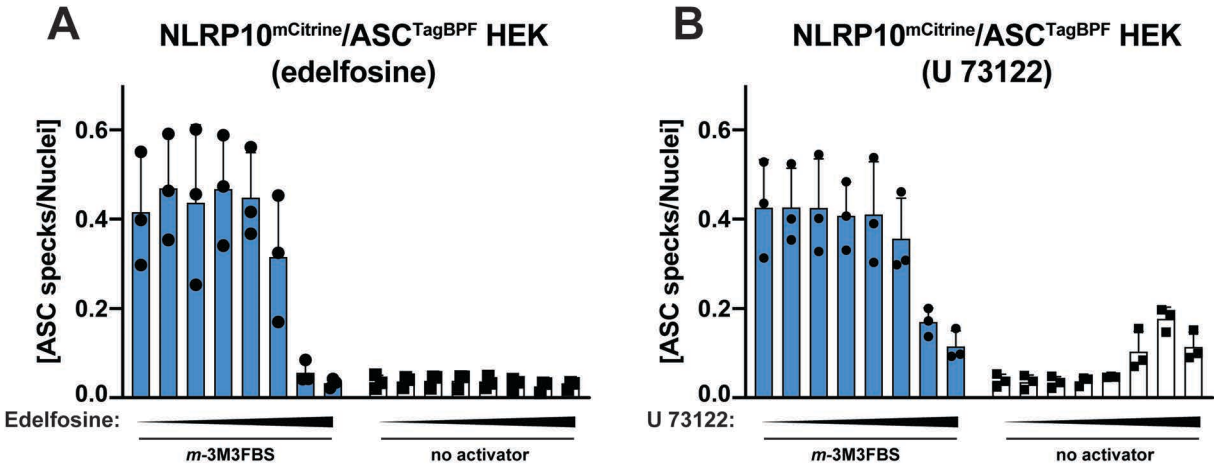

Figure 6.5. Influence of the PLC inhibitors edelfosine and U 73122 on the *m*-3M3FBS-induced ASC speck formation in NLRP10^{mCitrine}/ASC^{TagBFP} HEK cells

A-B: To determine whether the NLRP10 inflammasome response to *m*-3M3FBS is sensitive to edelfosine and U 73122, human (h) NLRP10^{mCitrine}/ASC^{TagBFP} HEK cells were pre-treated with edelfosine (A; 0 [ethanol], 1, 2.5, 5, 10, 25, 50, or 75 μM; 10 min) or U 73122 (B; 0 [DMSO], 0.5, 1, 2.5, 5, 10, 25, or 50 μM; 10 min) and then stimulated with *m*-3M3FBS (85 μM) or left untreated (no activator) in an extracellular medium consisting of (in mM) 123 NaCl, 5 KCl, 2 $MgCl_2$, 1 $CaCl_2$, 10 glucose, 10 HEPES, pH 7.4. Immediately after addition of inflammasome activators, the plates were centrifuged at 340 × g for 5 min (RT). After 30 min, the cells were fixed, counterstained for the nuclei and imaged using a fluorescence microscope.
The results are plotted as means from 3 independent experiments performed in technical triplicate. Error bars represent SD. Individual data points represent means of the technical triplicate values from each of the independent experiments.

I went on to examine whether the NLRP3-inhibiting KCl concentrations could have an impact on the NLRP10 activation with *m*-3M3FBS (Figure 6.6 A). This process was not inhibited by any of the tested KCl concentrations (0-125 mM), indicating that it is not dependent on K^+ efflux.

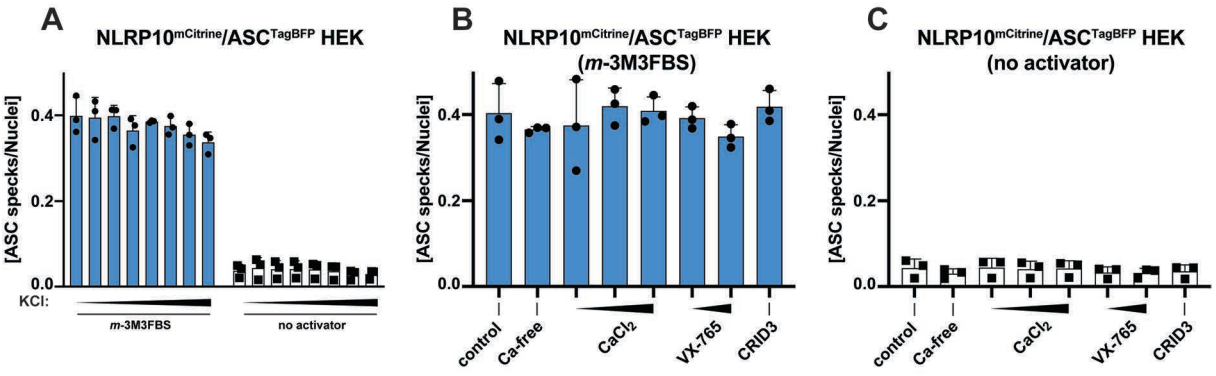

Figure 6.6. The *m*-3M3FBS-induced ASC speck formation in NLRP10^{mCitrine}/ASC^{TagBFP} reporter HEK cells is not blocked by the NLRP3 inflammasome inhibitors

A: To determine whether the *m*-3M3FBS-induced inflammasome activation requires K^+ efflux, human (h) NLRP10^{mCitrine}/ASC^{TagBFP} HEK cells were shifted to media with non-physiological concentrations of KCl (0, 5, 10, 25, 50, 75, 100, or 125 mM; for the KCl concentrations above 5 mM, the NaCl concentrations were accordingly decreased so as to maintain a constant osmolarity) and then stimulated with *m*-3M3FBS (85 μM) or left untreated (no activator). Apart from NaCl (123-0 mM) and KCl (0-125 mM), the extracellular media consisted of (in mM) 2 $MgCl_2$, 1 $CaCl_2$, 10 glucose, 10 HEPES, pH 7.4. Immediately after addition of inflammasome activators, the plates were centrifuged at 340 × g for 5 min (RT). After 30 min, the cells were fixed, counterstained for the nuclei (5 μM DRAQ5) and imaged using a fluorescence microscope.

B, C: To determine whether the *m*-3M3FBS-induced inflammasome activation is modulated by the extracellular Ca^{2+} concentrations, the caspase-1 inhibitor VX-765, or the NLRP3 inhibitor CRID3 hNLRP10^{mCitrine}/ASC^{TagBFP} HEK cells were pre-treated for 10 min with a range of $CaCl_2$ concentrations (0, 1 [control], 2.5, 5, or 10 mM), VX-765 (10 or 25 μM), or CRID3 (5 μM), and then stimulated with *m*-3M3FBS (85 μM; B) or left untreated (no activator; C) in an extracellular medium consisting of (in mM) 123 NaCl, 5 KCl, 2 $MgCl_2$, 1 $CaCl_2$ (except for the Ca^{2+}-free and the increased [$CaCl_2$] conditions), 10 glucose, 10 HEPES, pH 7.4. Immediately after addition of inflammasome activators, the plates were centrifuged at 340 × g for 5 min (RT). After 30 min, the cells were fixed, counterstained for the nuclei (5 μM DRAQ5) and imaged using a fluorescence microscope.

The results are plotted as means from 3 independent experiments performed in technical triplicate. Error bars represent SD. Individual data points represent means of the technical triplicate values from each of the independent experiments.

Finally, I assessed the sensitivity of the *m*-3M3FBS-elicited NLRP10-driven ASC speck formation to the NLRP3 inhibitor CRID3, the caspase-1 inhibitor VX-765, as well as to Ca^{2+}-free and high-$CaCl_2$ media. None of these treatments blocked (Figure 6.6 B) or activated (Figure 6.6 C) NLRP10. Overall, the general characteristics of the *m*-3M3FBS-induced NLRP10 activation in HEK cells were similar to the *m*-3M3FBS-driven inflammasome response in murine macrophages (Figure 4.4).

6.4. NLRP10 is dispensable for the *m*-3M3FBS-induced inflammasome activation in BMDMs

NLRP10 is not expressed in myeloid cells (Lautz et al., 2012; Nakajima et al., 2018; Vacca et al., 2017), so it is unlikely to be the mediator of inflammasome formation in BMDMs (Figures 4.2 and 4.5). Nevertheless, considering the results presented in Sections 6.1-

6.3, I proceeded to determine whether the macrophage inflammasome response to *m*-3M3FBS is dependent on NLRP10. To this end, I challenged LPS-primed *Nlrp10*$^{flox/flox}$ and *Nlrp10*$^{-/-}$ BMDMs (a kind gift from Prof. Thomas Kufer, University of Hohenheim, Germany) with increasing doses of *m*-3M3FBS and measured the concentrations of secreted IL-1β to assess the strength of the inflammasome responses (Figure 6.7). Nigericin and poly-(dA:dT) served as NLRP10-independent controls.

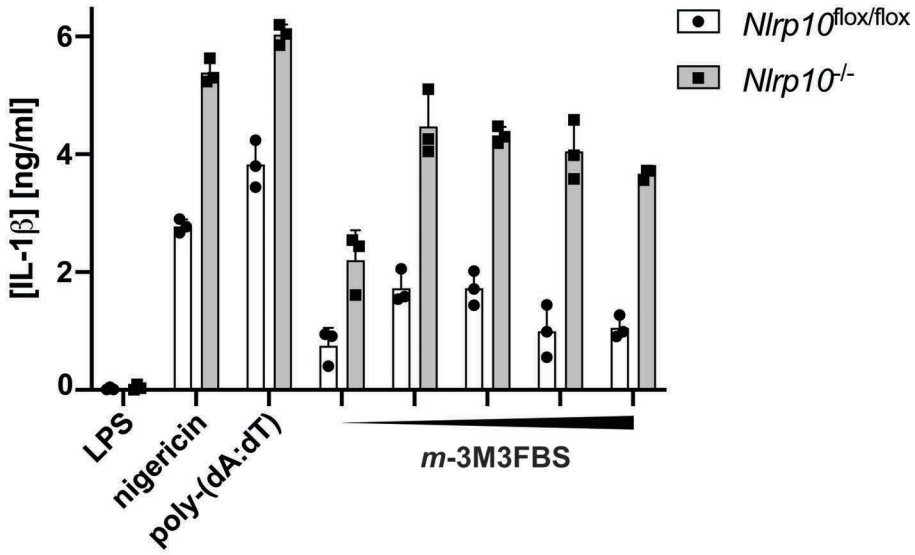

Figure 6.7. NLRP10-deficient (*Nlrp10*$^{-/-}$) BMDMs do not exhibit a defective inflammasome response to *m*-3M3FBS
LPS-primed (200 ng/mL, 2 h) BMDMs from NLRP10-proficient (*Nlrp10*$^{flox/flox}$; white bars) or NLRP10-deficient (*Nlrp10*$^{-/-}$; grey bars) mice were shifted to an extracellular medium consisting of (in mM) 123 NaCl, 5 KCl, 2 $MgCl_2$, 1 $CaCl_2$, 10 glucose, 10 HEPES pH 7.4 and stimulated with nigericin (10 μM), poly-(dA:dT) (2 μg/mL complexed with 5 μL Lipofectamine 2000), or *m*-3M3FBS (18, 36, 54, 72, or 85 μM). The LPS controls were subjected to medium alone. Immediately after addition of inflammasome activators, the plates were centrifuged at 340 × g for 5 min (RT). After 60 min, the supernatants were collected and IL-1β concentrations were measured by HTRF.
The results are plotted as means from 3 independent experiments performed in technical duplicate. Error bars represent SD. Individual data points represent means of the technical duplicate values from each of the independent experiments.

NLRP10-deficient BMDMs did not have a decreased IL-1β response to *m*-3M3FBS. In fact, all tested inflammasome responses were elevated in NLRP10-deficient cells, compared to WT controls (Figure 6.7).

It is difficult to comment on this apparent global increase in the inflammasome responses upon NLRP10 deficiency. A safe conclusion from the data presented in Figure 6.7 is that NLRP10 is not required for the *m*-3M3FBS-induced inflammasome activation in macrophages. A less obvious question is whether the increased inflammasome responses in NLRP10-deficient cells should be interpreted as an indication that NLRP10

is an inflammasome inhibitor. Several groups reported normal levels of inflammasome activation in NLRP10-deficient myeloid cells compared to WT controls (Krishnaswamy et al., 2015; Nakajima et al., 2018; Vacca et al., 2017). Based on these studies and on my own observations (Sections 7.5 and 8.4), I will argue that it is unlikely that NLRP10 acts as a broad inhibitor of inflammasome activation. Instead, it is possible that the increased inflammasome responses recorded in Figure 6.7 are a result of mouse breeding strategies or other confounding factors.

6.5. NLRP10 is a soluble cytosolic protein that changes its localization pattern on stimulation with *m*-3M3FBS

So far, my attempts to determine how *m*-3M3FBS activates the inflammasome have raised more questions than they have answered. In macrophages, *m*-3M3FBS activates the inflammasome independently of NLRP3, and likely in a manner not related to PLC. Overexpression experiments in HEK cells suggest that NLRP10 could act as a sensor responding to *m*-3M3FBS, but this protein is not expressed in macrophages and not required for the macrophage response to *m*-3M3FBS. Hoping to gain a better understanding of the cellular events elicited by *m*-3M3FBS, I performed confocal imaging of h/m NLRP10$^{\text{mCitrine}}$ under basal and *m*-3M3FBS-stimulated conditions (Figure 6.8).

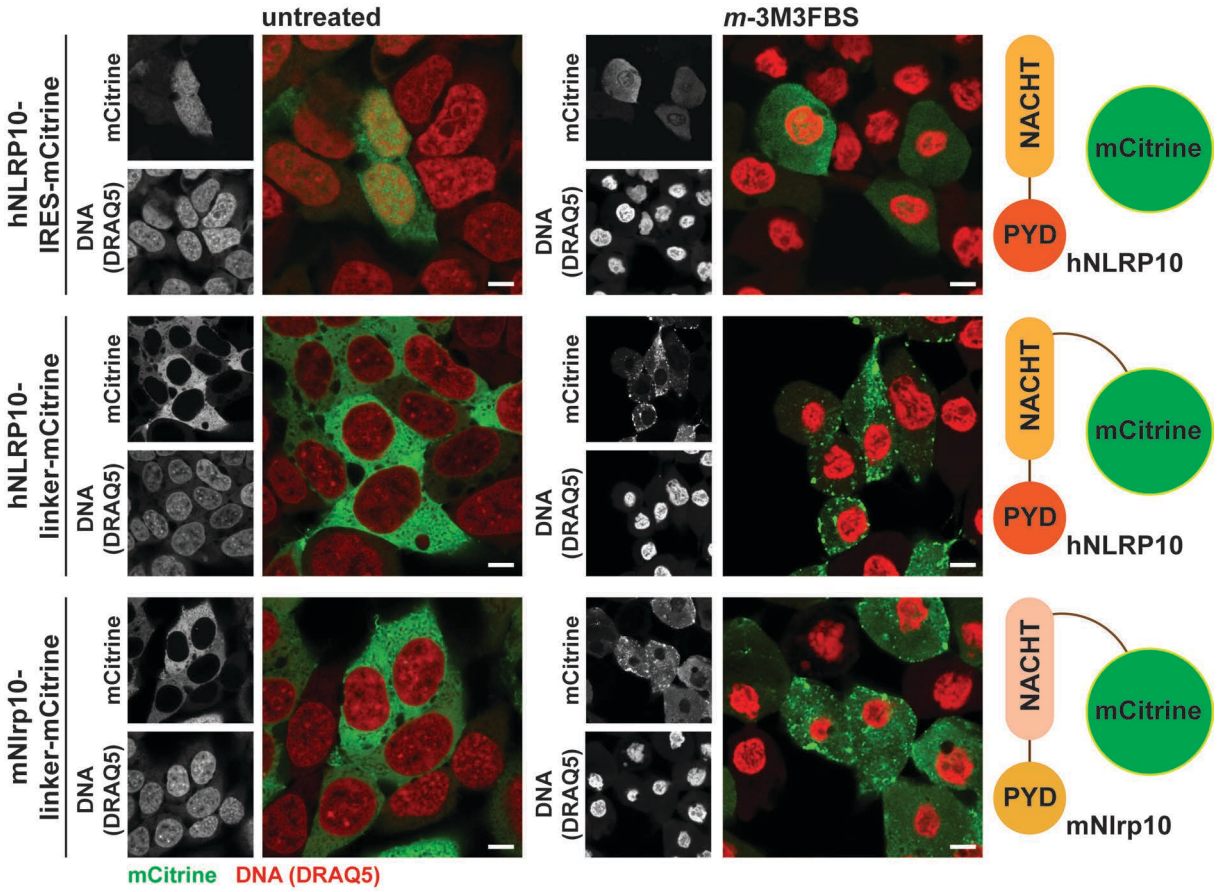

Figure 6.8. Localization of human and murine NLRP10 in HEK cells under basal and *m*-3M3FBS-stimulated conditions
HEK cells stably overexpressing human (h) NLRP10-IRES-mCitrine (two separate polypeptides), hNLRP10-linker-mCitrine (a single polypeptide), or murine (m) Nlrp10-linker-mCitrine (a single polypeptide) were shifted to an extracellular medium consisting of (in mM) 123 NaCl, 5 KCl, 2 $MgCl_2$, 1 $CaCl_2$, 10 glucose, 10 HEPES pH 7.4 and left untreated or stimulated with *m*-3M3FBS (85 μM). After 30 min, the cells were fixed with 4% formaldehyde, counterstained with the nuclear dye DRAQ5 (5 μM) and imaged using a confocal microscope.
Images are representative of 4 independent experiments. Scale bars correspond to 5 μm.

I examined NLRP10 localization in HEK cells stably overexpressing h/m NLRP10^{mCitrine} fusion proteins. Of note, these cells did not overexpress ASC to exclude the risk that the observed localization changes could result from ASC speck formation downstream of NLRP10 activation. To ensure that the localization changes are driven by NLRP10, and not by mCitrine, I also recorded the localization of mCitrine without a fusion partner in HEK cells overexpressing NLRP10 and mCitrine as two separate polypeptide chains (divided by an IRES sequence). A schematic of the overexpressed constructs is presented in the right column of Figure 6.8.

HEK cells overexpressing h/m NLRP10^{mCitrine} or hNLRP10-IRES-mCitrine were treated with *m*-3M3FBS (30 min), followed by fixation, nuclear counterstaining, and confocal

microscopy (Figure 6.8). Under basal conditions, NLRP10 was a soluble cytosolic protein strongly excluded from the nuclei. Upon stimulation with *m*-3M3FBS, the NLRP10 subcellular localization underwent a shift toward a punctate distribution pattern. This was observed for both human and murine NLRP10. mCitrine overexpressed as a separate polypeptide was a soluble protein uniformly distributed in the entire nucleocytosolic compartment. It did not change its localization patter upon stimulation with *m*-3M3FBS, indicating that the puncta formation is driven by NLRP10 and not by mCitrine. Importantly, the cells stimulated with *m*-3M3FBS underwent noticeable morphological changes, of which the best visible here is chromatin condensation (Figure 6.8; DRAQ5/nuclei channel).

6.6. Organelle marker proteins do not exhibit evident localization changes upon *m*-3M3FBS stimulation

The localization pattern of NLRP10 upon stimulation with *m*-3M3FBS suggested that this protein could translocate to one of the organelles. To examine whether any evident changes could be observed in organelle structures in cells stimulated with *m*-3M3FBS, I transiently overexpressed fluorescently labeled organelle markers in HEK cells and performed confocal imaging of fixed and nuclei-counterstained untreated, or *m*-3M3FBS-treated and nigericin-treated cells (Figure 6.9). I focused on the following compartments: the ER (DDOST), the endolysosomal compartment (LAMP1), the mitochondria (TOMM20, MAVS), and the Golgi (TGOLN2).

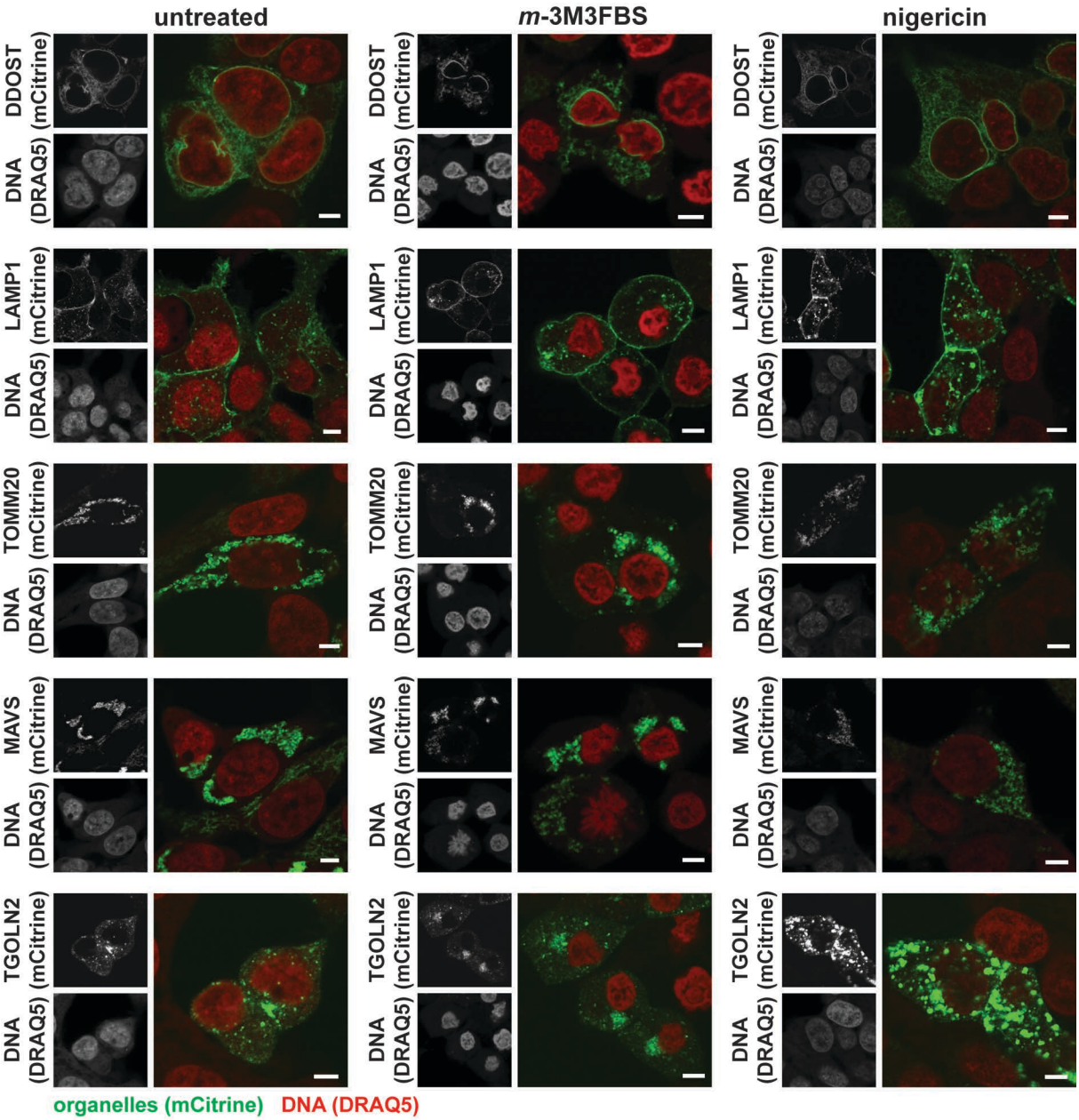

Figure 6.9. Organelle morphologies in HEK cells under basal and *m*-3M3FBS- or nigericin-stimulated conditions

HEK cells were transiently transfected (200 ng of DNA per well of a 96-well plate combined with 0.5 µL of Gene Juice [transfection reagent], or 2 µg/mL of DNA combined with 5 µL of Gene Juice) with vectors encoding the following organelle markers expressed as fusion proteins with mCitrine: DDOST (the endoplasmic reticulum), LAMP1 (the endolysosomal system), TOMM20 (the mitochondria), MAVS (the mitochondria), or TGOLN2 (the Golgi apparatus). After 24 h of transfection, the cells were shifted to an extracellular medium consisting of (in mM) 123 NaCl, 5 KCl, 2 $MgCl_2$, 1 $CaCl_2$, 10 glucose, 10 HEPES pH 7.4 and left untreated, or were stimulated with *m*-3M3FBS (85 µM) or nigericin (10 µM). After 30 min, the cells were fixed with 4% formaldehyde, counterstained with the nuclear dye DRAQ5 (5 µM) and imaged using a confocal microscope.

Images are representative of 4 independent experiments. Scale bars correspond to 5 µm.

Upon challenge with *m*-3M3FBS, no obvious morphological changes were detected in the endolysosomal compartment, the mitochondria, and the Golgi. The ER structure also remained unaltered, but the nuclear envelope, which also stains positive for DDOST,

appeared to be disrupted by *m*-3M3FBS. A leakage of the nuclear contents to the cytosol was noticeable. This nuclear envelope rupture was not observed in nigericin-treated cells. In contrast, nigericin treatment appeared to result in an expansion of the Golgi apparatus compared to the untreated control. Collectively, with the exception of the nuclear envelope, the observation of organelle morphologies in HEK cells treated with *m*-3M3FBS revealed no drastic changes compared to the untreated controls.

6.7. NLRP10 localizes to TOMM20-positive mitochondria in HEK cells treated with *m*-3M3FBS

For most of the examined organelles, I did not observe an altered morphology upon *m*-3M3FBS treatment, but this does not exclude the possibility of significant changes occurring at the subcellular level. To see whether the translocation of NLRP10 could point me in the direction of the compartment affected by *m*-3M3FBS, I transiently overexpressed mCitrine-labeled organelle markers for the ER, the endolysosomal system, the mitochondria, and the Golgi in NLRP10^{mCherry} HEK cells. I then challenged these cells with *m*-3M3FBS or nigericin and performed confocal microscopy on fixed, nuclei-counterstained samples (Figure 6.10).

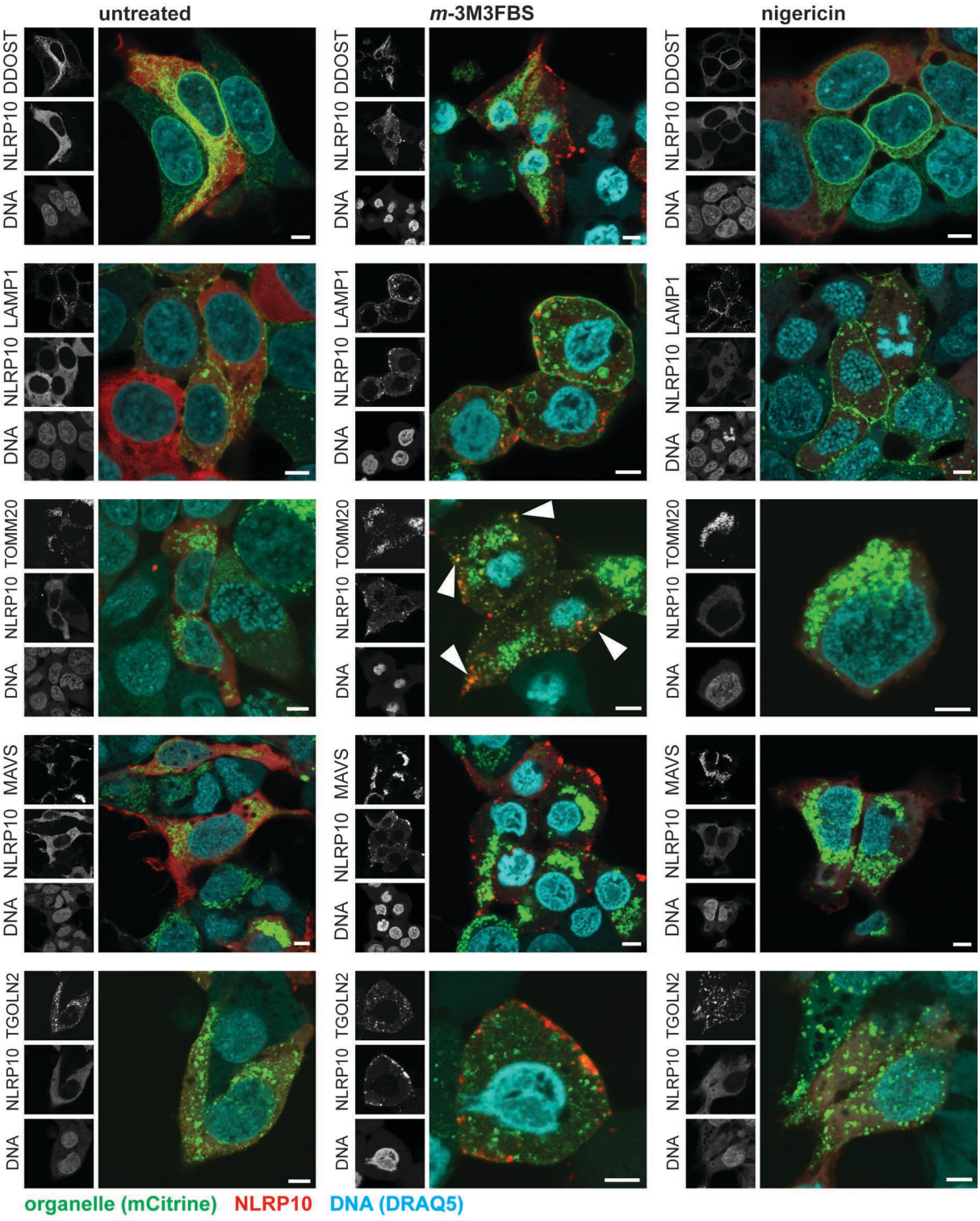

Figure 6.10. Localization of NLRP10^{mCherry} under basal and *m*-3M3FBS- or nigericin-stimulated conditions in HEK cells transiently overexpressing mCitrine-labeled organelle markers

Human NLRP10^{mCherry} HEK cells were transiently transfected (200 ng of DNA per well of a 96-well plate combined with 0.5 µL of Gene Juice [transfection reagent], or 2 µg/mL of DNA combined with 5 µL of Gene Juice) with vectors encoding the following organelle markers expressed as fusion proteins with mCitrine: DDOST (the endoplasmic reticulum), LAMP1 (the endolysosomal system), TOMM20 (the mitochondria), MAVS (the mitochondria), or TGOLN2 (the Golgi apparatus). After 24 h of transfection, the cells were shifted to an extracellular medium consisting of (in mM) 123 NaCl, 5 KCl, 2 $MgCl_2$, 1 $CaCl_2$, 10 glucose, 10 HEPES pH 7.4 and left untreated, or were stimulated with *m*-3M3FBS (85 µM) or nigericin (10 µM). After 30 min, the cells were fixed with 4% formaldehyde, counterstained with the nuclear dye DRAQ5 (5 µM) and imaged using a confocal microscope.

Images are representative of 4 independent experiments. Scale bars correspond to 5 µm.

Stimulation with nigericin did not affect the localization pattern of NLRP10 compared to the untreated controls, whereas the treatment with *m*-3M3FBS resulted in NLRP10 puncta formation (Figure 6.10), consistent with my previous observation (Figure 6.8). On the organelle level, *m*-3M3FBS caused prominent disruption of the nuclear envelope (marked by DDOST), but NLRP10 did not colocalize with the ER/nuclear envelope membranes (Figure 6.10). NLRP10 was also not detected on the vesicles of the endolysosomal compartment (LAMP1), on the MAVS-positive mitochondrial membranes, or on the Golgi (TGOLN2). Instead, under *m*-3M3FBS-stimulated conditions, a large proportion of the NLRP10 puncta appeared to colocalize with the TOMM20-positive compartment, suggesting translocation to the mitochondria. White arrowheads point to several examples of TOMM20-NLRP10 colocalization in *m*-3M3FBS-treated cells (Figure 6.10, column 2, row 3).

6.8. *m*-3M3FBS is an activator of the AIM2 inflammasome in murine macrophages

My results suggested that *m*-3M3FBS may affect two organelles, the nucleus (through the disruption of the nuclear envelope) and the mitochondria (based on the observed mitochondrial translocation of NLRP10). Both of these compartments contain DNA, as they respectively host the nuclear and the mitochondrial genomes. Could AIM2, the inflammasome sensor component activated by dsDNA, be involved in the inflammasome response to *m*-3M3FBS in macrophages? To answer this question, I stimulated WT, NLRP3-deficient (*Nlrp3*$^{-/-}$; a control), and AIM2-deficient (*Aim2*$^{-/-}$) BMDMs with increasing doses of *m*-3M3FBS and measured the concentrations of secreted IL-1β to assess the degree of the inflammasome activation (Figure 6.11). Nigericin and poly-(dA:dT) served as NLRP3- and AIM2-dependent controls, respectively.

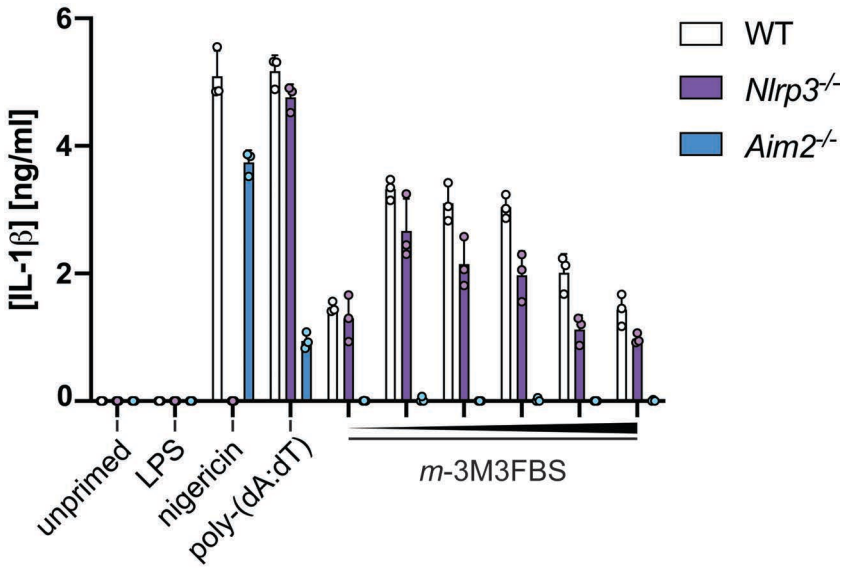

Figure 6.11. IL-1β secretion from WT, NLRP3-deficient (*Nlrp3*$^{-/-}$), and AIM2-deficient (*Aim2*$^{-/-}$) BMDMs stimulated with *m*-3M3FBS

BMDMs from WT (white bars), NLRP3-deficient (*Nlrp3*$^{-/-}$; purple bars), or AIM2-deficient (*Aim2*$^{-/-}$; blue bars) mice were primed with LPS (200 ng/mL, 2 h) or left unprimed, and then shifted to an extracellular medium consisting of (in mM) 123 NaCl, 5 KCl, 2 $MgCl_2$, 1 $CaCl_2$, 10 glucose, 10 HEPES pH 7.4 and stimulated with nigericin (10 μM), poly-(dA:dT) (2 μg/mL complexed with 5 μL Lipofectamine 2000), or *m*-3M3FBS (18, 36, 54, 72, 85, or 100 μM). The unprimed and LPS controls were subjected to medium alone. Immediately after addition of inflammasome activators, the plates were centrifuged at 340 × g for 5 min (RT). After 60 min, the supernatants were collected and IL-1β concentrations were measured by HTRF.

The results are plotted as means from 3 independent experiments performed in technical triplicate. Error bars represent SD. Individual data points represent means of the technical triplicate values from each of the independent experiments.

In agreement with my earlier observation (Figure 4.5), both WT and NLRP3-deficient BMDMs secreted high amounts of IL-1β when treated with *m*-3M3FBS (Figure 6.11). In contrast, the inflammasome response to *m*-3M3FBS was completely abolished in AIM2-deficient BMDMs, indicating that in murine macrophages, the inflammasome activation by *m*-3M3FBS is non-redundantly dependent on AIM2 (Figure 6.11). Of note, I did not observe the AIM2 activation by *m*-3M3FBS in the overexpression screen performed in ASC^{TagBFP} HEK cells (Figure 6.3 D, F). This was likely a false negative result due to the very high background ASC specking signal associated with the transient overexpression of AIM2 (Supplementary Figure S4 D, F).

6.9. Thapsigargin, another compound with mitochondria-damaging properties, is an activator of AIM2 and NLRP10

As *m*-3M3FBS appeared to have a mitochondria-related activity and was an agonist of the AIM2 and NLRP10 inflammasomes, I went on to test whether thapsigargin could

cause a response similar to *m*-3M3FBS. Thapsigargin, commonly known as an inhibitor of the sarco/endoplasmic reticulum Ca^{2+}-ATPase (SERCA), has an infamous record in inflammasome research. On different occasions it has been reported to be an NLRP3 activator (Bronner et al., 2015; Lerner et al., 2012; Menu et al., 2012; Rada et al., 2014; Robblee et al., 2016), inhibitor (Murakami et al., 2012), or to have no effect on NLRP3 activation (Katsnelson et al., 2015). Thapsigargin can be expected to share some of its downstream effects with *m*-3M3FBS. Both of these compounds trigger cytosolic Ca^{2+} fluxes, albeit by different mechanisms. In addition, thapsigargin is known to disrupt the mitochondria, which is believed to rely on the induction of the mPT (Korge and Weiss, 1999).

To test whether I could reproduce the results demonstrating inflammasome activation by thapsigargin, I treated LPS-primed WT or ASC-deficient (*Pycard*$^{-/-}$) BMDMs with increasing doses of this compound in the presence or absence of the caspase-1 inhibitor VX-765. To assess the degree of inflammasome activation, I measured the concentrations of secreted IL-1β (Figure 6.12).

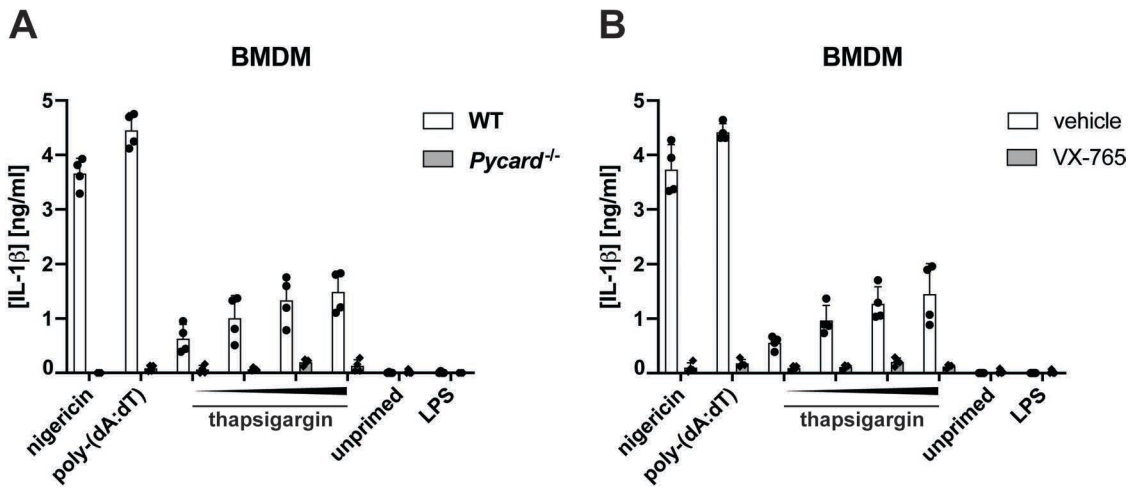

Figure 6.12. High doses of thapsigargin activate the inflammasome in BMDMs
A: BMDMs generated from WT (white bars) and ASC-deficient (*Pycard*$^{-/-}$; grey bars) bone marrows were left unprimed or were primed with LPS (200 ng/mL, 2 h) and then stimulated with thapsigargin (at 10, 15, 20, or 25 μM), nigericin (10 μM), or poly-(dA:dT) (2 μg/mL complexed with 5 μL Lipofectamine 2000) in an extracellular medium consisting of (in mM) 123 NaCl, 5 KCl, 2 $MgCl_2$, 1 $CaCl_2$, 10 glucose, 10 HEPES, pH 7.4. The unprimed and LPS controls were subjected to medium alone. Immediately after addition of inflammasome activators, the plates were centrifuged at 340 × g for 5 min (RT). After 60 min, the supernatants were collected and IL-1β concentrations were measured by HTRF.
B: BMDMs generated from WT bone marrows were left unprimed or were primed with LPS (200 ng/mL, 2 h), pre-treated with the caspase-1 inhibitor VX-765 (40 μM, 10 min; grey bars) or vehicle (DMSO; white bars), and then stimulated as in (A). After 60 min, the supernatants were collected and IL-1β concentrations were measured by HTRF.
The results are plotted as means from 4 independent experiments performed in technical triplicate. Error bars represent SD. Individual data points represent means of the technical triplicate values from each of the independent experiments.

High concentrations of thapsigargin triggered a dose-dependent IL-1β release from BMDMs. This IL-1β response was lower than the responses to nigericin or poly-(dA:dT), but it was completely abolished in ASC-deficient cells (Figure 6.12 A) and in WT cells pre-treated with the caspase-1 inhibitor VX-765 (Figure 6.12 B), consistent with the typical characteristics of inflammasome activation.

To determine which inflammasome forming sensor is activated by thapsigargin, I stimulated LPS-primed WT, NLRP3-deficient (*Nlrp3*$^{-/-}$), and AIM2-deficient (*Aim2*$^{-/-}$) BMDMs with increasing doses of this molecule and evaluated the degree of the inflammasome response by measuring the concentrations of secreted IL-1β (Figure 6.13).

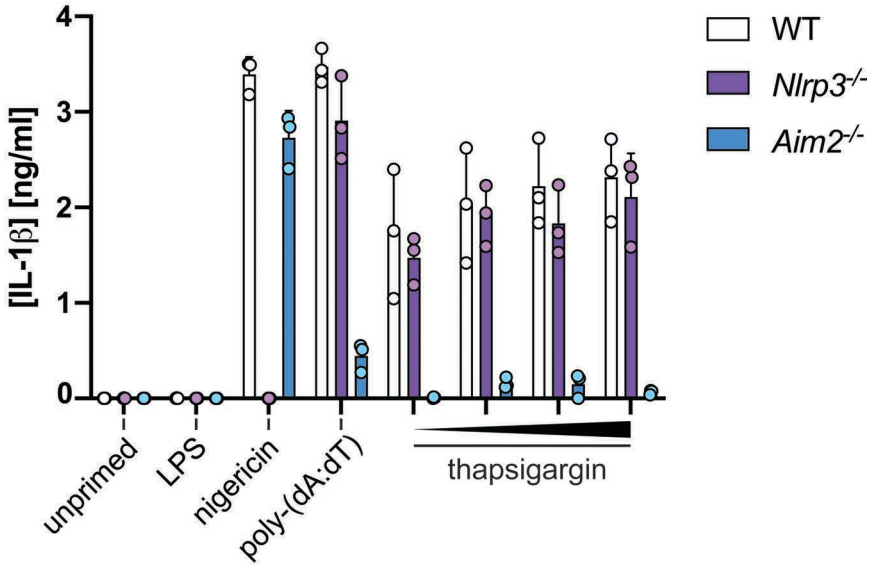

Figure 6.13. In BMDMs, the inflammasome activation by thapsigargin is dependent on AIM2, but independent of NLRP3
BMDMs from WT (white bars), NLRP3-deficient (*Nlrp3*$^{-/-}$; purple bars), or AIM2-deficient (*Aim2*$^{-/-}$; blue bars) mice were primed with LPS (200 ng/mL, 2 h) or left unprimed, and then shifted to an extracellular medium consisting of (in mM) 123 NaCl, 5 KCl, 2 $MgCl_2$, 1 $CaCl_2$, 10 glucose, 10 HEPES pH 7.4 and stimulated with nigericin (10 μM), poly-(dA:dT) (2 μg/mL complexed with 5 μL Lipofectamine 2000), or thapsigargin (10, 15, 20, or 25 μM). The unprimed and LPS controls were subjected to medium alone. Immediately after addition of inflammasome activators, the plates were centrifuged at 340 × g for 5 min (RT). After 60 min, the supernatants were collected and IL-1β concentrations were measured by HTRF.
The results are plotted as means from 3 independent experiments performed in technical triplicate. Error bars represent SD. Individual data points represent means of the technical triplicate values from each of the independent experiments.

As evidenced above (Figure 6.13), NLRP3-deficient BMDMs were as capable as WT cells at eliciting the inflammasome response to thapsigargin, whereas this response was completely abolished in AIM2-deficient BMDMs. This result indicates that in this

experimental model, AIM2 was the inflammasome-forming sensor non-redundantly mediating the IL-1β response to thapsigargin.

My observations (Figures 6.12 and 6.13) confirm the previous reports that thapsigargin may have inflammasome-activating properties (Bronner et al., 2015; Lerner et al., 2012; Menu et al., 2012; Rada et al., 2014; Robblee et al., 2016). An important difference compared to earlier studies is that I identified AIM2, not NLRP3, as the inflammasome-forming sensor involved in the response to thapsigargin. The biological significance and potential sources of this observed discrepancy will be discussed in Section 10.2.

I next examined whether thapsigargin could to elicit the NLRP10-driven ASC specking response in NLRP10-overexpressing ASC^{TagBFP} HEK cells, similar to *m*-3M3FBS. To this end, I stimulated h/m $NLRP10^{mCitrine}/ASC^{TagBFP}$ HEK cells or empty vector-transduced controls with increasing concentrations of thapsigargin and imaged the ASC specks after fixation and nuclear counterstaining (Figure 6.14 A-C). In parallel, I tested whether the IL-1β secretion observed in BMDMs stimulated with thapsigargin would be reflected by ASC speck formation in NLRP3/$ASC^{mCerulean}$ reporter iMac cells (Figure 6.14 D).

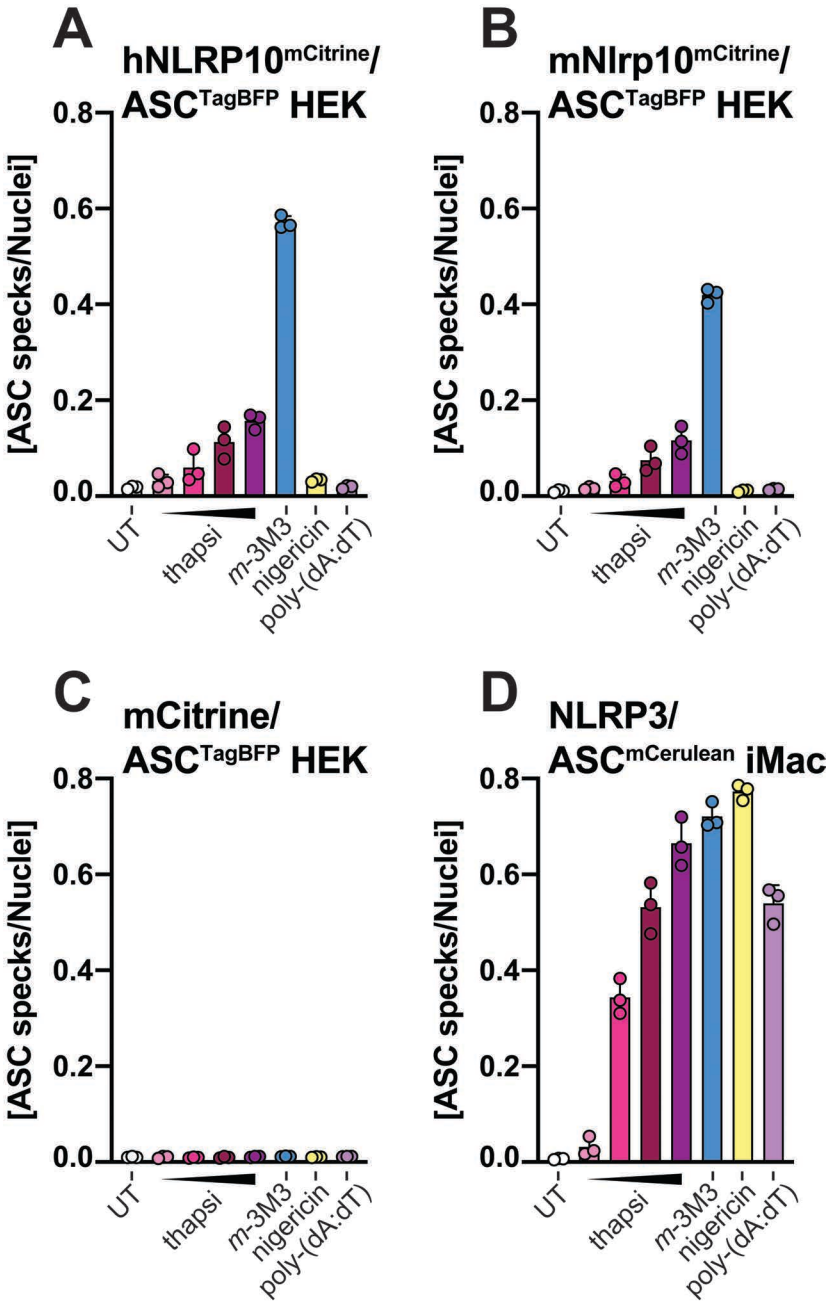

Figure 6.14. Thapsigargin triggers ASC speck formation in human/mouse NLRP10^{mCitrine}/ASC^{TagBFP} HEK cells and in NLRP3/ASC^{mCerulean} reporter iMac cells

A-D: Human (h) NLRP10^{mCitrine}/ASC^{TagBFP} HEK cells (A), murine (m) Nlrp10^{mCitrine}/ASC^{TagBFP} HEK cells (B), mCitrine/ASC^{TagBFP} HEK cells (C), and NLRP3/ASC^{mCerulean} reporter iMac cells (D) were shifted to an extracellular medium consisting of (in mM) 123 NaCl, 5 KCl, 2 $MgCl_2$, 1 $CaCl_2$, 10 glucose, 10 HEPES pH 7.4. Then the cells were left untreated (UT), or they were stimulated with thapsigargin (thapsi; 5, 10, 15, or 20 μM), *m*-3M3FBS (*m*-3M3; 85 μM), nigericin (10 μM), or poly-(dA:dT) (2 μg/mL complexed with 5 μL Lipofectamine 2000). Immediately after addition of inflammasome activators, the plates were centrifuged at 340 × g for 5 min (RT). After 30 min (A-C) or 60 min (D), the cells were fixed with 4% formaldehyde, counterstained with the nuclear dye DRAQ5 (5 μM) and imaged using a widefield fluorescence microscope.

The results are plotted as means from 3 independent experiments performed in technical triplicate. Error bars represent SD. Individual data points represent means of the technical triplicate values from each of the independent experiments.

In h/m NLRP10^{mCitrine}/ASC^{TagBFP} HEK cells, stimulation with thapsigargin led to a dose-dependent increase in ASC speck formation (Figure 6.14 A, B). This ASC specking signal was not as strong as in cells treated with *m*-3M3FBS, but fully attributable to the NLRP10 overexpression, as ASC speck formation was not observed in ASC^{TagBFP} HEK cells transduced with the empty vector (Figure 6.14 C). In NLRP3/ASC^{mCerulean} reporter iMac cells, thapsigargin elicited a dose-dependent ASC speck formation at a level similar to other inflammasome activators (Figure 6.14 D).

The results presented in this Section indicate that thapsigargin, similar to *m*-3M3FBS, activates the AIM2 and NLRP10 inflammasomes. I went on to determine whether the principal cell biological and pharmacological characteristics are shared between the thapsigargin- and the *m*-3M3FBS-driven inflammasome responses. Similar to *m*-3M3FBS, the inflammasome activation by thapsigargin was independent of phagocytosis (Supplementary Figure S6 A, B), as no sensitivity to cytochalasin D was detected. Similar to other AIM2 activators, the thapsigargin-elicited inflammasome response did not require LPS priming (Supplementary Figure S6 C). The NLRP3 inhibitor CRID3 did not block the thapsigargin-induced ASC speck formation and IL-1β secretion (Supplementary Figure S7), whereas the caspase-1 inhibitor VX-765 blocked the thapsigargin-induced IL-1β secretion (Supplementary Figure S8 A), but not ASC specking (Supplementary Figure S8 B, C). Collectively, these observations are consistent with the results of analogous experiments performed with *m*-3M3FBS (Figures 4.1, 4.2, 4.4, 4.5, and 6.6).

6.10. NLRP10 translocates to TOMM20-positive mitochondria in HEK cells stimulated with thapsigargin

To test whether thapsigargin affects the NLRP10 localization in a manner similar to *m*-3M3FBS, I performed confocal microscopy on NLRP10^{mCherry} HEK cells overexpressing the TOMM20^{mCitrine} mitochondrial marker. The cells were stimulated with thapsigargin, *m*-3M3FBS (positive control), or nigericin (negative control), fixed, nuclei-counterstained, and imaged (Figure 6.15).

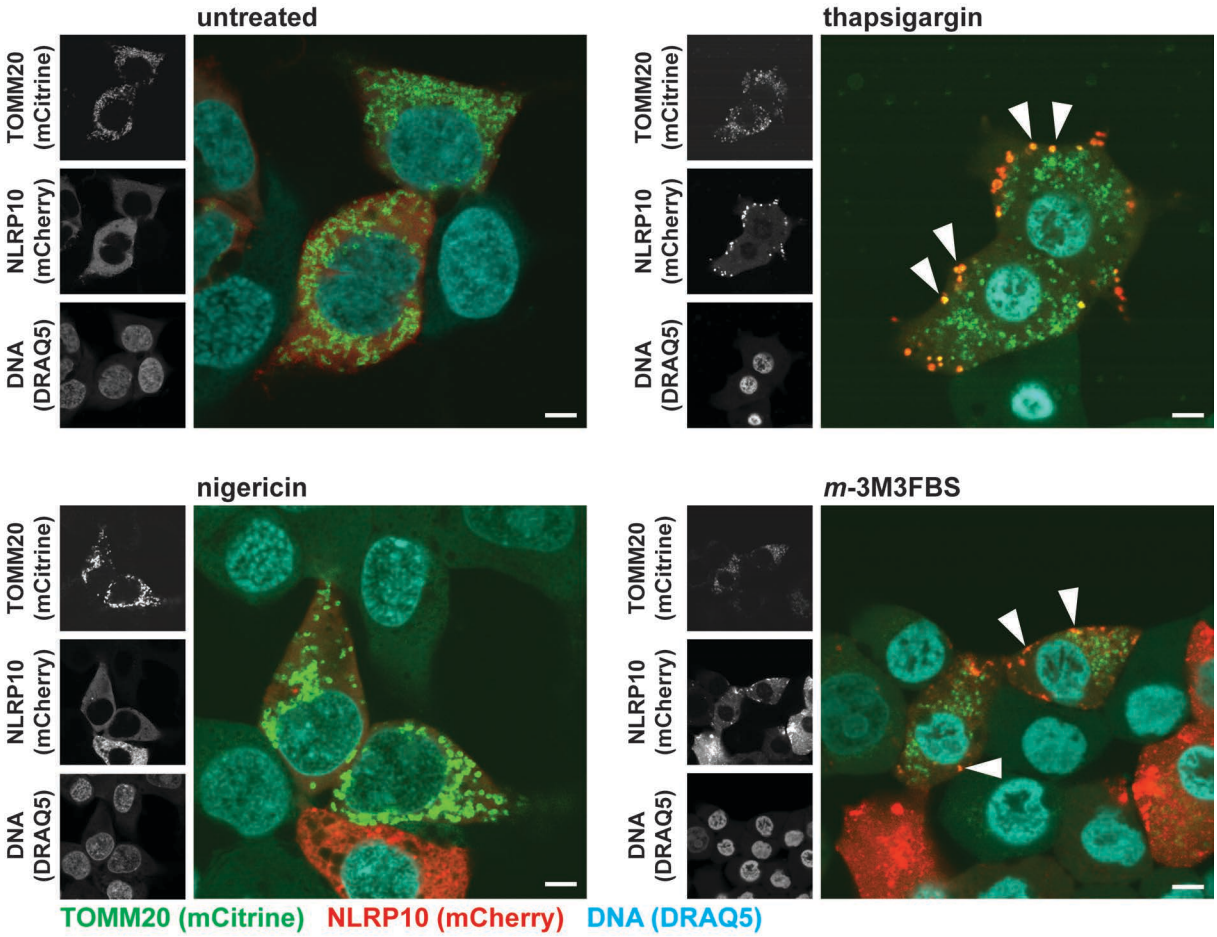

Figure 6.15. Thapsigargin and *m*-3M3FBS induce NLRP10 translocation to the mitochondria
Human NLRP10^{mCherry} HEK cells were transiently transfected (200 ng of DNA per well of a 96-well plate combined with 0.5 µL of Gene Juice [transfection reagent], or 2 µg/mL of DNA combined with 5 µL of Gene Juice) with a vector encoding the mitochondrial marker TOMM20 expressed as a fusion protein with mCitrine. After 24 h of transfection, the cells were shifted to an extracellular medium consisting of (in mM) 123 NaCl, 5 KCl, 2 $MgCl_2$, 1 $CaCl_2$, 10 glucose, 10 HEPES pH 7.4 and left untreated, or were stimulated with thapsigargin (20 µM), *m*-3M3FBS (85 µM) or nigericin (10 µM). After 30 min, the cells were fixed with 4% formaldehyde, counterstained with the nuclear dye DRAQ5 (5 µM) and imaged using a confocal microscope.
Images are representative of 3 independent experiments. Scale bars correspond to 5 µm.

Thapsigargin induced a shift in the NLRP10 localization from cytosolic to granular/vesicular. The thapsigargin-elicited NLRP10 puncta colocalized with TOMM20-positive mitochondria (Figure 6.15).

Because thapsigargin is known to cause ER stress, I also tested whether this compound could trigger morphological changes of the ER and whether NLRP10 translocation to the ER membranes could be observed (Supplementary Figure S9). Although thapsigargin stimulation did change the ER architecture compared to the untreated conditions, I did not detect the NLRP10 puncta colocalization with the ER marker DDOST. Of note, the nuclear envelope rupture that could be observed upon treatment with *m*-3M3FBS

(Figures 6.9, 6.10, Supplementary Figure S9) was not detected in thapsigargin-treated cells (Supplementary Figure S9).

Thapsigargin and *m*-3M3FBS both activate the AIM2 and NLRP10 inflammasomes. Stimulations with these compounds induce NLRP10 colocalization with the mitochondria. Taking these similarities into consideration, it is likely that there is some overlap in the intracellular signals initiated by *m*-3M3FBS and thapsigargin. In the following sections, I will try to pinpoint which of these signals could be relevant for the inflammasome activation.

6.11. No evidence that Ca^{2+} signaling acts downstream of *m*-3M3FBS/thapsigargin to activate the AIM2 and NLRP10 inflammasomes

Both *m*-3M3FBS and thapsigargin mobilize cellular Ca^{2+} stores. Thapsigargin causes Ca^{2+} fluxes chiefly through inhibition of the SERCA Ca^{2+} pump, whereas *m*-3M3FBS triggers the IP_3R-mediated ER Ca^{2+} release downstream of PLC activation (Bae et al., 2003) as well as ER-independent Ca^{2+} fluxes (Krjukova et al., 2004). To determine whether Ca^{2+} ions could transmit the inflammasome-activating signals from *m*-3M3FBS and thapsigargin, I applied two approaches to interfere with Ca^{2+} signaling: chelation of intracellular Ca^{2+} ions with the plasma membrane-permeant Ca^{2+} chelator BAPTA-AM (Figure 6.16) and blocking of the IP_3R ER Ca^{2+} channels with 2-aminoethoxydiphenylborane (2-APB, an IP_3R antagonist) (Figure 6.17). In addition, I tested how the Ca^{2+} ionophore ionomycin impacts on the inflammasome activation (Figure 6.18). For comparison purposes, all of the experiments were performed in parallel in media containing 1 mM $CaCl_2$ and in Ca^{2+}-free media. Briefly, NLRP3/$ASC^{mCerulean}$ reporter iMac cells, (h) $NLRP10^{mCitrine}$/ASC^{TagBFP} HEK cells, and LPS-primed WT iMac cells were pre-incubated for 15 min with BAPTA-AM, 2-APB, or ionomycin in 1 mM $CaCl_2$ or Ca^{2+}-free media, followed by challenge with *m*-3M3FBS, thapsigargin, nigericin, or poly-(dA:dT). The degree of inflammasome activation was assessed by IL-1β HTRF (WT iMac cells; Figures 6.16 A, B, 6.17 A, B, and 6.18 A, B) and ASC speck imaging (NLRP3/$ASC^{mCerulean}$ reporter iMac cells and (h) $NLRP10^{mCitrine}$/ASC^{TagBFP} HEK cells; Figures 6.16 C-F, 6.17 C-F, and 6.18 C-F).

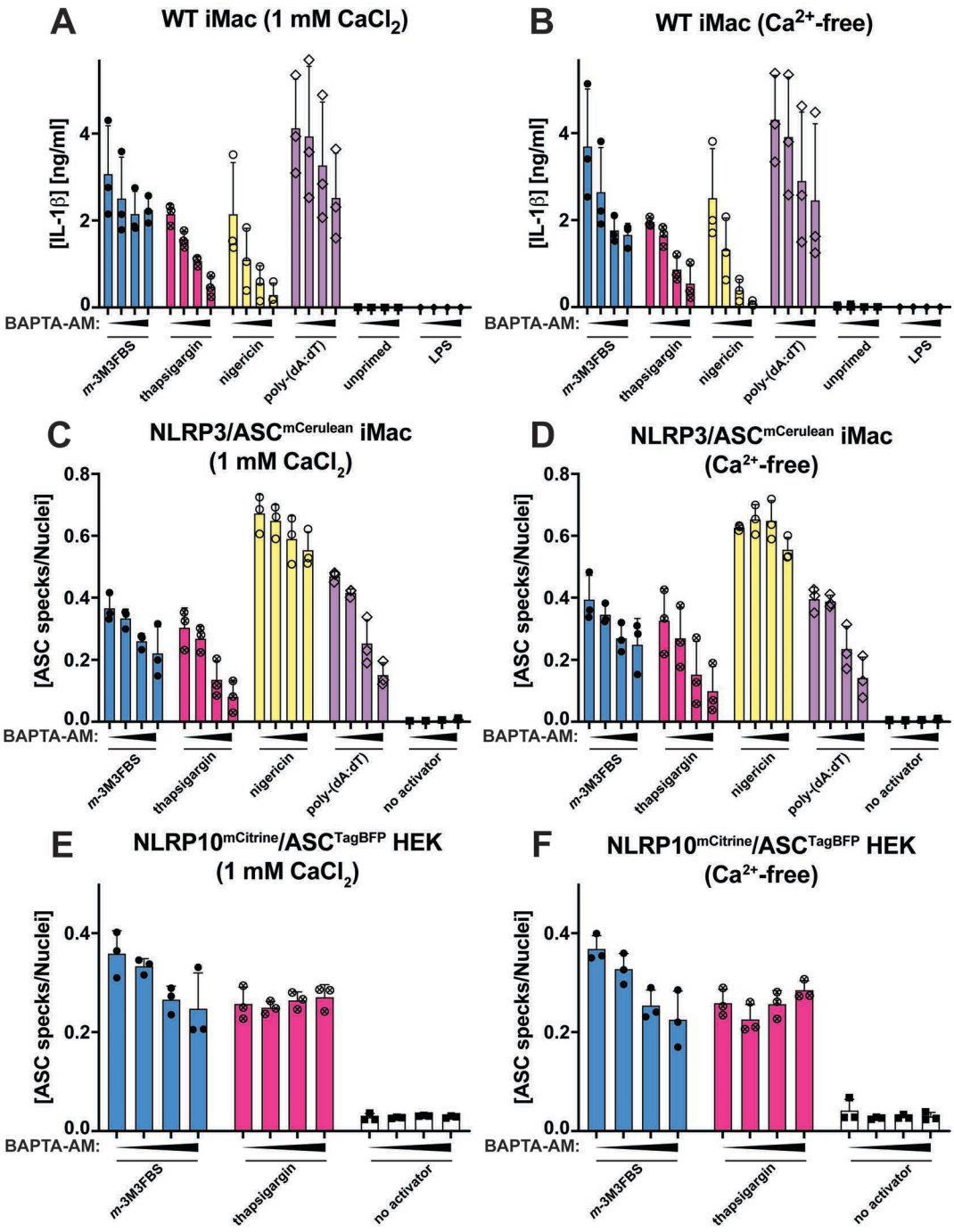

Figure 6.16. Influence of the Ca^{2+} chelator BAPTA-AM on the inflammasome responses to *m*-3M3FBS, thapsigargin, nigericin, and poly-(dA:dT)

A-F: LPS-primed (200 ng/mL, 2 h) WT iMac cells (A, B), NLRP3/$ASC^{mCerulean}$ reporter iMac cells (C, D), and $NLRP10^{mCitrine}/ASC^{TagBFP}$ HEK cells (E, F) were treated for 10 min with BAPTA-AM (0, 10, 25, or 50 μM) in the presence (A, C, E) or absence (B, D, F) of extracellular Ca^{2+} and then subjected to the inflammasome activators *m*-3M3FBS (85 μM), thapsigargin (20 μM), nigericin (10 μM) or poly-(dA:dT) (2 μg/mL complexed with 5 μL Lipofectamine 2000) in an extracellular medium consisting of (in mM) 123 NaCl, 5 KCl, 2 $MgCl_2$, 0 or 1 $CaCl_2$, 10 glucose, 10 HEPES, pH 7.4. The LPS (A, B) and unprimed (A-F) controls were subjected to medium alone. Immediately after addition of inflammasome activators, the plates were centrifuged at 340 × g for 5 min (RT). After 30 min (E, F) or 60 min (A-D), the supernatants were collected and IL-1β concentrations were measured by HTRF (A, B) or the cells were fixed with 4% formaldehyde, counterstained with the nuclear dye DRAQ5 (5 μM) and imaged using a widefield fluorescence microscope (C-F).

The results are plotted as means from 3 independent experiments performed in technical duplicate. Error bars represent SD. Individual data points represent means of the technical duplicate values from each of the independent experiments.

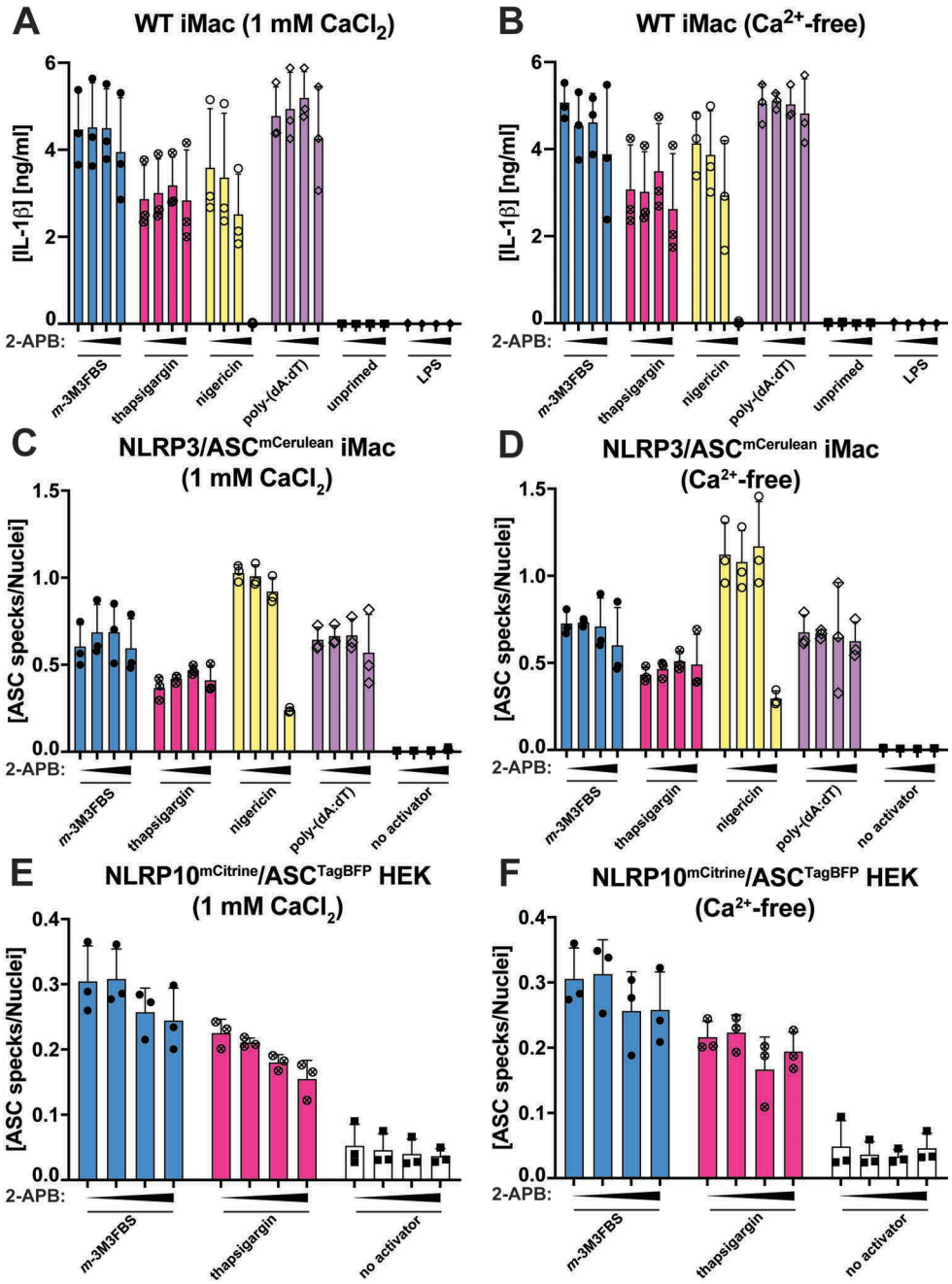

Figure 6.17. Influence of the IP$_3$R blocker 2-APB on the inflammasome responses to *m*-3M3FBS, thapsigargin, nigericin, and poly-(dA:dT)

A-F: LPS-primed (200 ng/mL, 2 h) WT iMac cells (A, B), NLRP3/ASC^{mCerulean} reporter iMac cells (C, D), and NLRP10^{mCitrine}/ASC^{TagBFP} HEK cells (E, F) were treated for 10 min with 2-APB (0, 5, 10, or 50 μM) in the presence (A, C, E) or absence (B, D, F) of extracellular Ca^{2+} and then subjected to the inflammasome activators *m*-3M3FBS (85 μM), thapsigargin (20 μM), nigericin (10 μM) or poly-(dA:dT) (2 μg/mL complexed with 5 μL Lipofectamine 2000) in an extracellular medium consisting of (in mM) 123 NaCl, 5 KCl, 2 $MgCl_2$, 0 or 1 $CaCl_2$, 10 glucose, 10 HEPES, pH 7.4. The LPS (A, B) and unprimed (A-F) controls were subjected to medium alone. Immediately after addition of inflammasome activators, the plates were centrifuged at 340 × g for 5 min (RT). After 30 min (E, F) or 60 min (A-D), the supernatants were collected and IL-1β concentrations were measured by HTRF (A, B) or the cells were fixed with 4% formaldehyde, counterstained with the nuclear dye DRAQ5 (5 μM) and imaged using a widefield fluorescence microscope (C-F).

The results are plotted as means from 3 independent experiments performed in technical duplicate. Error bars represent SD. Individual data points represent means of the technical duplicate values from each of the independent experiments.

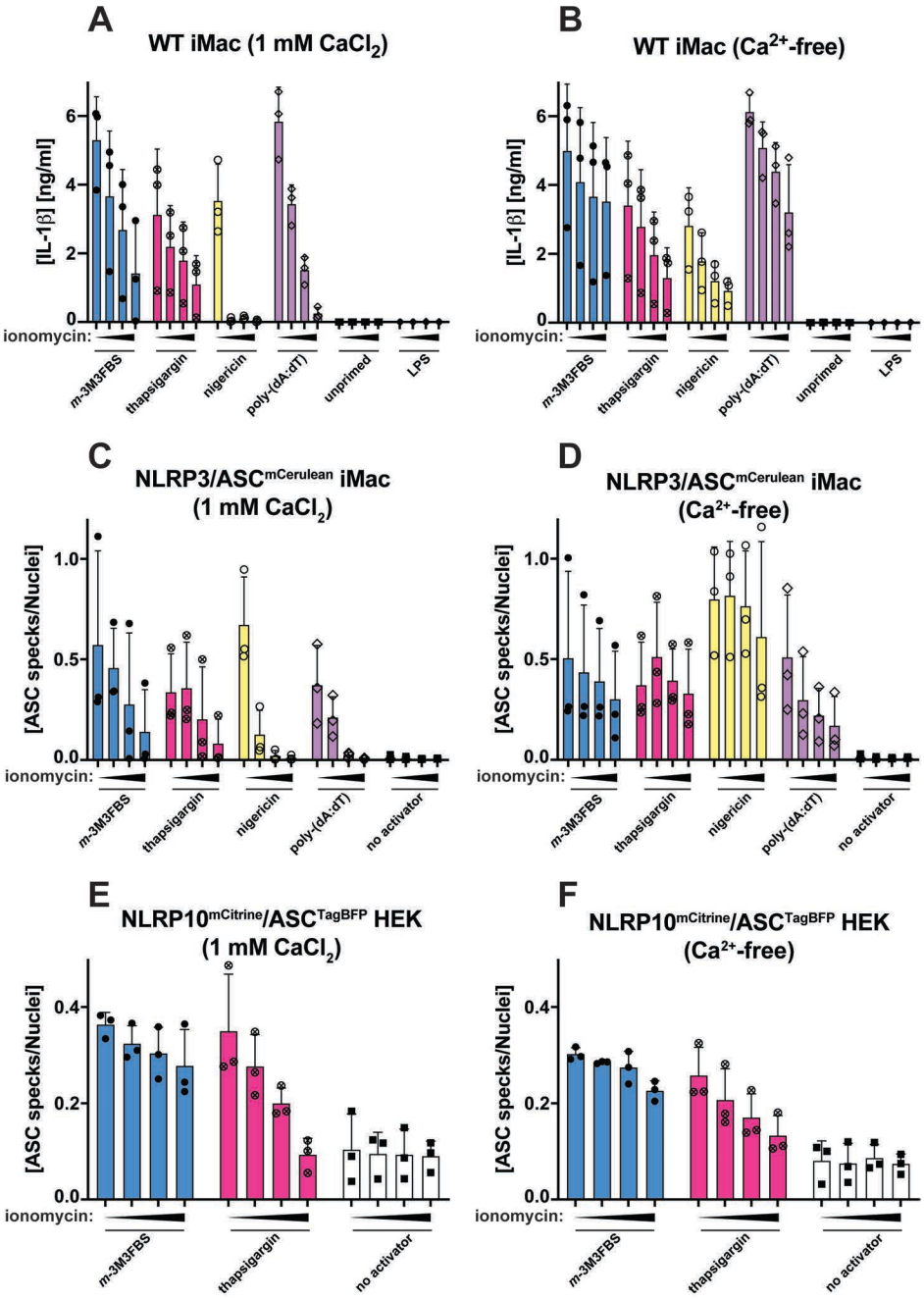

Figure 6.18. Influence of the Ca^{2+} ionophore ionomycin on the inflammasome responses to *m*-3M3FBS, thapsigargin, nigericin, and poly-(dA:dT)

A-F: LPS-primed (200 ng/mL, 2 h) WT iMac cells (A, B), NLRP3/$ASC^{mCerulean}$ reporter iMac cells (C, D), and $NLRP10^{mCitrine}$/ASC^{TagBFP} HEK cells (E, F) were treated for 10 min with ionomycin (0, 5, 10, or 15 μM) in the presence (A, C, E) or absence (B, D, F) of extracellular Ca^{2+} and then subjected to the inflammasome activators *m*-3M3FBS (85 μM), thapsigargin (20 μM), nigericin (10 μM) or poly-(dA:dT) (2 μg/mL complexed with 5 μL Lipofectamine 2000) in an extracellular medium consisting of (in mM) 123 NaCl, 5 KCl, 2 $MgCl_2$, 0 or 1 $CaCl_2$, 10 glucose, 10 HEPES, pH 7.4. The LPS (A, B) and unprimed (A-F) controls were subjected to medium alone. Immediately after addition of inflammasome activators, the plates were centrifuged at 340 × g for 5 min (RT). After 30 min (E, F) or 60 min (A-D), the supernatants were collected and IL-1β concentrations were measured by HTRF (A, B) or the cells were fixed with 4% formaldehyde, counterstained with the nuclear dye DRAQ5 (5 μM) and imaged using a widefield fluorescence microscope (C-F).

The results are plotted as means from 3 independent experiments performed in technical duplicate. Error bars represent SD. Individual data points represent means of the technical duplicate values from each of the independent experiments.

Of the tested treatments, 2-APB had no influence on the AIM2 and NLRP10 activations (Figure 6.17) and only blocked the NLRP3 activation by nigericin at the highest tested concentration (50 μM; Figure 6.17 A-D). The 2-APB-mediated NLRP3 inhibition is known to rely on a Ca^{2+}-independent activity of 2-APB (Baldwin et al., 2017; Katsnelson et al., 2015). Chelation of intracellular Ca^{2+} ions with BAPTA-AM inhibited the inflammasome activation with thapsigargin and nigericin with similar potencies at the level of IL-1β release (Figure 6.16 A, B). At the level of ASC speck formation, the thapsigargin- and poly-(dA:dT)-induced inflammasome activations were similarly sensitive to the BAPTA-AM pre-treatment (Figure 6.16 C, D). BAPTA-AM had no impact on the NLRP10 activation in HEK cells (Figure 6.16 E, F). The lack of BAPTA-AM selectivity (Figure 6.16 A-D) and the fact that only very high (25 and 50 μM) concentrations of BAPTA-AM inhibit the inflammasome responses suggest that the observed effect may be due to toxicity rather than because of the interference with Ca^{2+} signaling. Of note, Katsnelson et al. (2015) demonstrated that the BAPTA-AM-mediated NLRP3 inhibition is caused by an off-target effect.

Ionomycin at the lower concentrations (5-10 μM) had a selective inhibitory effect on the NLRP3 activation with nigericin that was dependent on extracellular Ca^{2+} (Figure 6.18 A-D). This suggests that overloading the cytosol with Ca^{2+} ions negatively interferes with the NLRP3 inflammasome assembly, consistent with a previous report (Katsnelson et al., 2016). The higher concentrations of ionomycin non-selectively inhibited the inflammasome responses to all tested stimuli in macrophages (Figure 6.18 A-D) but was a much less potent inhibitor of the NLRP10 inflammasome in HEK cells (Figure 6.18 E-F). Of note, the ionomycin-mediated cytosolic delivery of Ca^{2+} ions alone was not a sufficient stimulus for the inflammasome activation in any of the tested models. This will be discussed in more detail in Section 6.14.

Because four previous reports linked *m*-3M3FBS and Ca^{2+} signaling to cell death and suggested that the Ca^{2+} channel blocker nifedipine could inhibit this reaction (Chen, 2014; Fang et al., 2009; Liu, 2013; Tsai, 2010), I also tested the impact of nifedipine on the inflammasome responses to *m*-3M3FBS, thapsigargin, nigericin, and poly-(dA:dT) (Supplementary Figure S10). I detected no inflammasome-inhibiting activity of nifedipine under any of the tested conditions. Importantly, the cited studies proposing

that nifedipine could counteract the effects of *m*-3M3FBS bear uncanny resemblance, putting into question the validity of the reported findings.

As the effects of thapsigargin and *m*-3M3FBS appeared to be independent of Ca^{2+} signaling, I tested whether artemisinin (Riganti et al., 2009), BHQ (Jayasinghe et al., 2016), or cyclopiazonic acid (Seidler et al., 1989) (SERCA inhibitors structurally unrelated to thapsigargin) could trigger inflammasome activation (Supplementary Figures S11 and S12). While thapsigargin elicited the AIM2 (Supplementary Figure S11) and NLRP10 (Supplementary Figure S12) inflammasome responses within 60 min of administration, artemisinin, BHQ, and cyclopiazonic acid did not cause inflammasome activation. At the 6-h time point, BHQ and cyclopiazonic acid elicited an ASC specking response in macrophages (Supplementary Figure S11 D) but no IL-1β was detected in the supernatants (Supplementary Figure S11 B), and no NLRP10 activation was observed (Supplementary Figure S12 B). These results suggest that thapsigargin probably activates AIM2 and NLRP10 through a mechanism unrelated to its activity on the SERCA Ca^{2+} pump. This conclusion is also supported by the observation that very high doses of thapsigargin are required for the inflammasome activation (> 10 μM), whereas SERCA inhibition already occurs at thapsigargin concentrations below 1 μM.

6.12. No evidence that protein kinase C is involved in the inflammasome activation with *m*-3M3FBS/thapsigargin

Protein kinase C (PKC) is one of the downstream effectors of PLC. Even though my earlier observations indicated that *m*-3M3FBS likely activates the AIM2 and NLRP10 inflammasomes through a PLC-unrelated off-target effect, I went on to determine whether PKC could be a mediator of the inflammasome activation by *m*-3M3FBS/thapsigargin. First, I tested whether a short (15 min) pre-incubation with the pan-kinase inhibitor staurosporine could block the *m*-3M3FBS- or thapsigargin-induced inflammasome activation in NLRP10/ASC fluorescent reporter HEK cells, NLRP3/$ASC^{mCerulean}$ reporter iMac cells, or LPS-primed WT iMac cells (Figure 6.19).

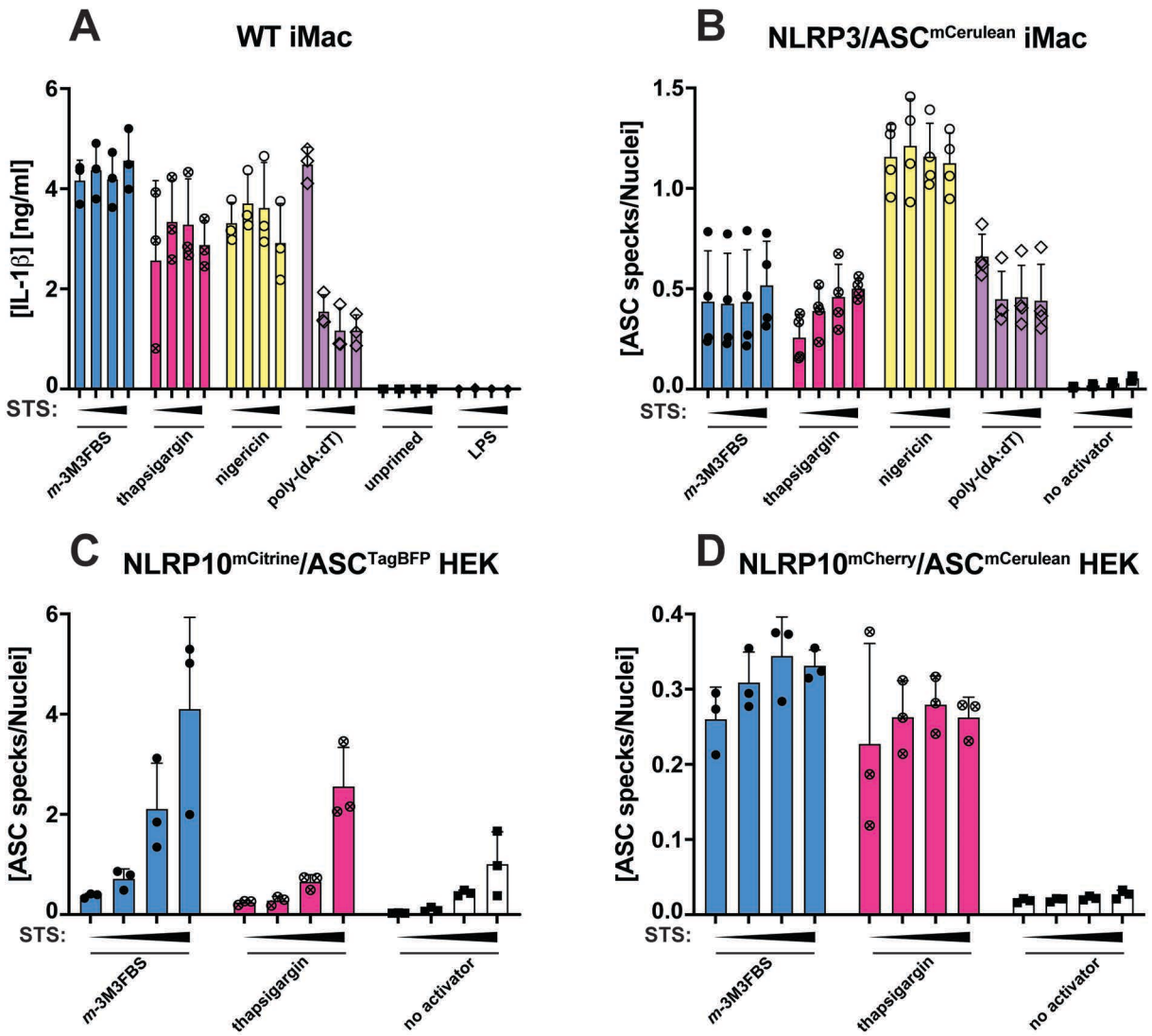

Figure 6.19. Influence of the pan-kinase inhibitor staurosporine on the inflammasome responses to *m*-3M3FBS, thapsigargin, nigericin, and poly-(dA:dT)

A-D: LPS-primed (200 ng/mL, 2 h) WT iMac cells (A), NLRP3/ASC^{mCerulean} reporter iMac cells (B), NLRP10^{mCitrine}/ASC^{TagBFP} HEK cells (C), and NLRP10^{mCherry}/ASC^{mCerulean} HEK cells (D) were treated for 10 min with staurosporine (STS; 0, 1, 5, or 10 μM in panels A-C; 0, 1.25, 2.5, or 5 μM in panel D) and then subjected to the inflammasome activators *m*-3M3FBS (85 μM), thapsigargin (20 μM), nigericin (10 μM) or poly-(dA:dT) (2 μg/mL complexed with 5 μL Lipofectamine 2000) in an extracellular medium consisting of (in mM) 123 NaCl, 5 KCl, 2 $MgCl_2$, 1 $CaCl_2$, 10 glucose, 10 HEPES, pH 7.4. The LPS (A) and unprimed (A-D) controls were subjected to medium alone. Immediately after addition of inflammasome activators, the plates were centrifuged at 340 × g for 5 min (RT). After 30 min (C, D) or 60 min (A, B), the supernatants were collected and IL-1β concentrations were measured by HTRF (A) or the cells were fixed with 4% formaldehyde, counterstained with the nuclear dye DRAQ5 (5 μM) and imaged using a widefield fluorescence microscope (B-D).

The results are plotted as means from 3 (A, C, D) or 4 (B) independent experiments performed in technical duplicate. Error bars represent SD. Individual data points represent means of the technical duplicate values from each of the independent experiments.

In macrophages, staurosporine did not block the inflammasome responses to *m*-3M3FBS, thapsigargin, and nigericin, and only partially blocked the response to poly-(dA:dT), which might be indicative of the toxicity of the kinase inhibitor (Figure 6.19 A, B). In NLRP10^{mCitrine}/ASC^{TagBFP} HEK cells, the influence of staurosporine on the NLRP10

activation could not be assessed as the compound exhibited strong autofluorescence in the BFP channel, producing a false-positive signal (artifactually high ASC specks-to-nuclei ratios) (Figure 6.19 C). To overcome this problem, I generated NLRP10^{mCherry}/ASC^{mCerulean} HEK cells and tested the influence of staurosporine on the NLRP10 activation by *m*-3M3FBS/thapsigargin in this model (Figure 6.19 D). No inhibition of ASC speck formation was observed, indicating that kinase activity is not required for the inflammasome activation with *m*-3M3FBS and thapsigargin.

To validate this result, I screened the AIM2, NLRP3, and NLRP10 inflammasome responses against several more specific PKC inhibitors: bisindolylmaleimide II, C-1, chelerythrine chloride (Figure 6.20), GF109203X, Gö6983 (Figure 6.21), K252c, and RO32-0432 (Figure 6.22). The only instance of consistent inhibition of the inflammasome formation was observed in cells pre-treated with chelerythrine chloride (Figure 6.20 I-L). This compound exhibited features of a pan-inflammasome inhibitor. The other tested PKC inhibitors either had no influence on the inflammasome activation or were only blocking it at the highest concentrations tested (typically at least 5-fold higher than the commercially reported IC_{50}). These results indicate that PKC is not required for the inflammasome activation. Of note, among the tested PKC inhibitors, K252c (an analog of staurosporine) exhibited strong autofluorescence in the BFP channel, resulting in artifactually high ASC speck counts in NLRP10^{mCitrine}/ASC^{TagBFP} reporter HEK cells (Figure 6.22 C). All of the tested compounds were compatible with ASC speck detection in the mCerulean channel, so the results obtained in NLRP3/ASC^{mCerulean} reporter iMac cells and NLRP10^{mCherry}/ASC^{mCerulean} HEK cells could be interpreted.

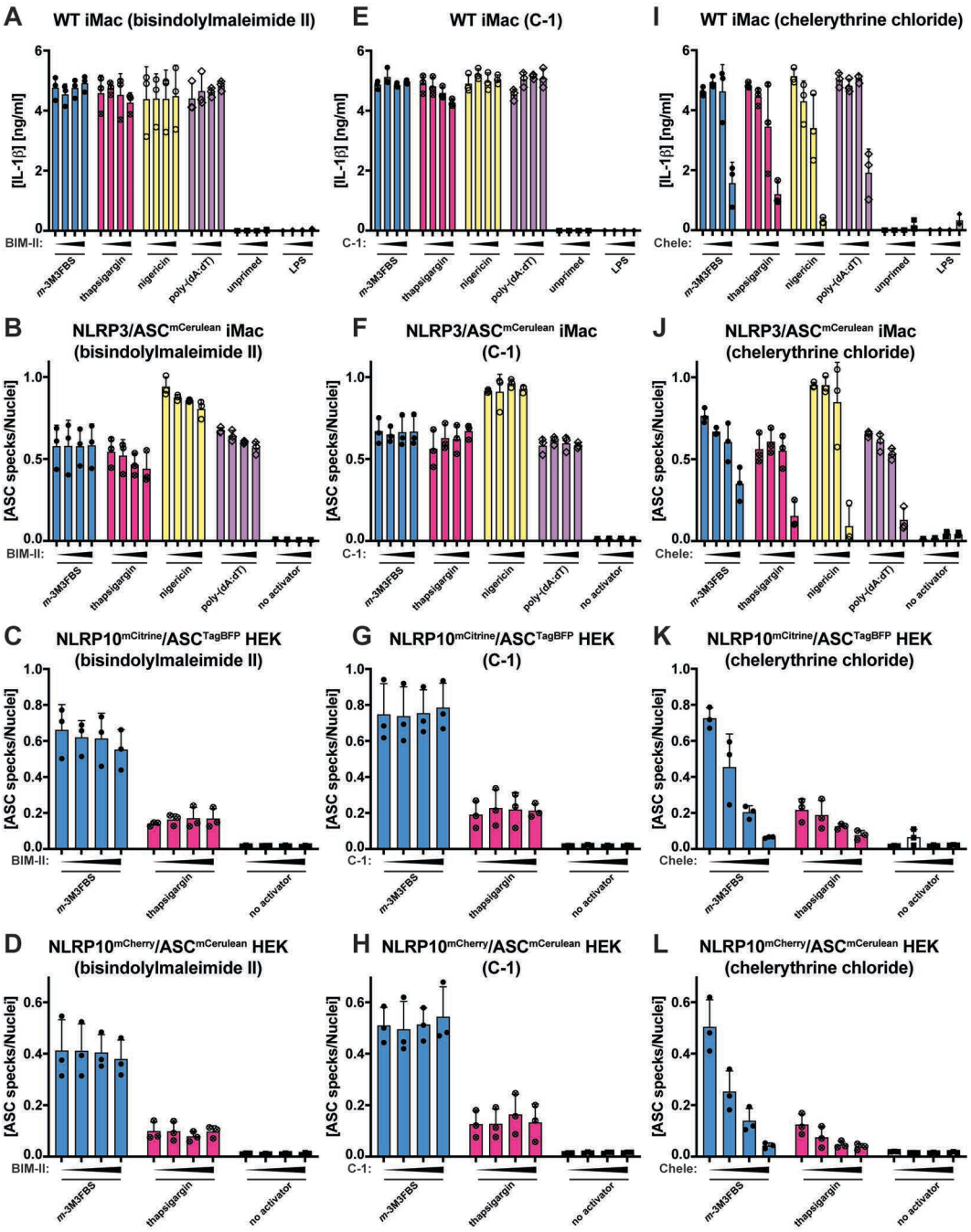

Figure 6.20. Influence of the PKC inhibitors bisindolylmaleimide II, C-1, and chelerythrine chloride on the inflammasome responses to *m*-3M3FBS, thapsigargin, nigericin, and poly-(dA:dT)

A-L: LPS-primed (200 ng/mL, 2 h) WT iMac cells (A, E, I), NLRP3/ASC^{mCerulean} reporter iMac cells (B, F, J), NLRP10^{mCitrine}/ASC^{TagBFP} HEK cells (C, G, K), and NLRP10^{mCherry}/ASC^{mCerulean} HEK cells (D, H, L) were treated for 10 min with bisindolylmaleimide-II (BIM-II; 0, 5, 10, or 20 μM; A-D), C-1 (0, 25, 50, or 100 μM; E-H), or chelerythrine chloride (Chele; 0, 5, 10, or 25 μM; I-L) and then subjected to the inflammasome activators *m*-3M3FBS (85 μM), thapsigargin (20 μM), nigericin (10 μM) or poly-(dA:dT) (2 μg/mL complexed with 5 μL Lipofectamine 2000) in an extracellular medium consisting of (in mM) 123 NaCl, 5 KCl, 2 $MgCl_2$, 1 $CaCl_2$, 10 glucose, 10 HEPES, pH 7.4. The LPS (A, E, I) and unprimed (A-L) controls were subjected to medium alone. Immediately after addition of inflammasome activators, the plates were centrifuged at 340 × g for 5 min (RT). After 30 min (C, D, G, H, K, L) or 60 min (A, B, E, F, I, J), the supernatants were collected and IL-1β concentrations were measured by HTRF (A, E, I) or the cells were fixed with 4% formaldehyde, counterstained with the nuclear dye DRAQ5 (5 μM) and imaged using a widefield fluorescence microscope (B-D, F-H, J-L).

The results are plotted as means from 3 independent experiments performed in technical duplicate. Error bars represent SD. Individual data points represent means of the technical duplicate values from each of the independent experiments.

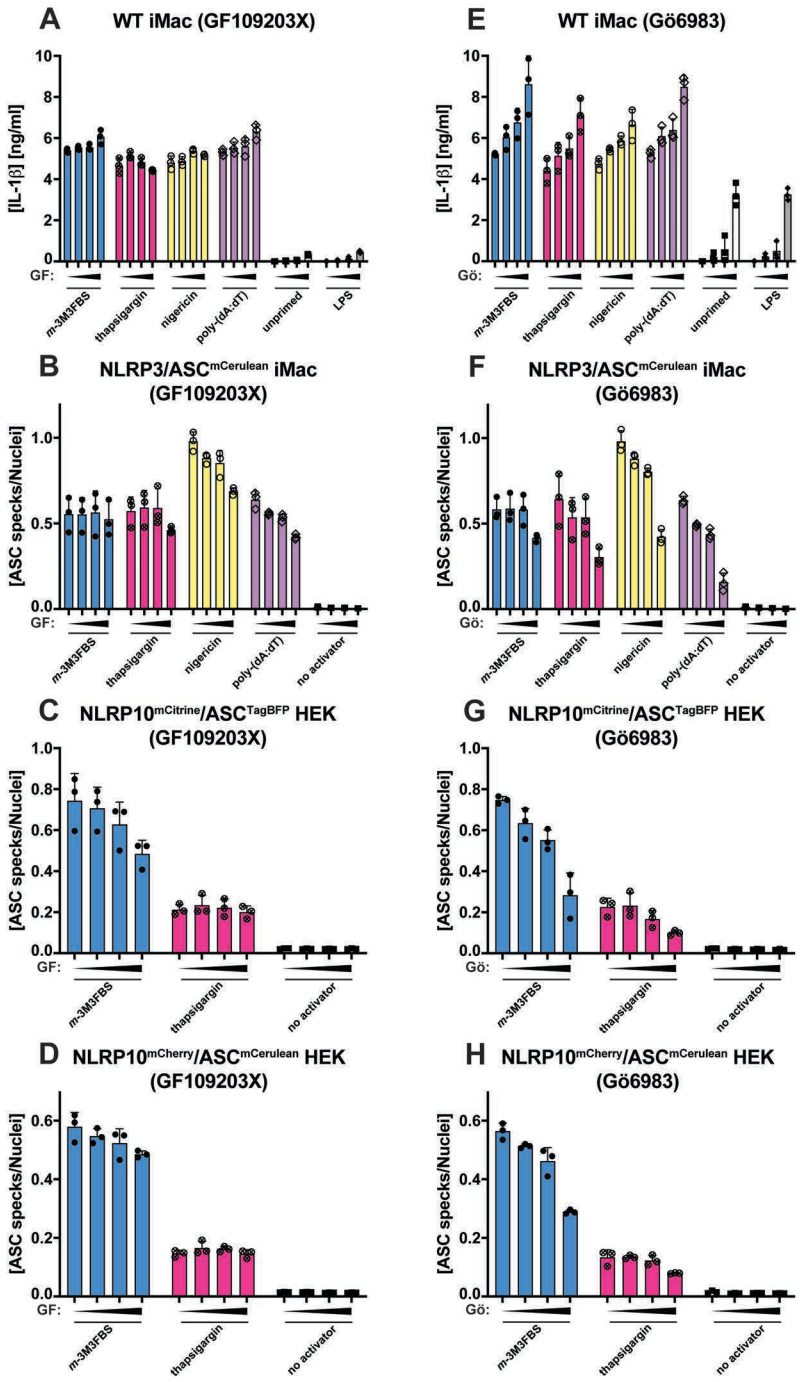

Figure 6.21. Influence of the PKC inhibitors GF109203X and Gö6983 on the inflammasome responses to *m*-3M3FBS, thapsigargin, nigericin, and poly-(dA:dT)

A-H: LPS-primed (200 ng/mL, 2 h) WT iMac cells (A, E), NLRP3/ASC^{mCerulean} reporter iMac cells (B, F), NLRP10^{mCitrine}/ASC^{TagBFP} HEK cells (C, G), and NLRP10^{mCherry}/ASC^{mCerulean} HEK cells (D, H) were treated for 10 min with GF109203X (GF; 0, 5, 10, or 50 μM; A-D) or Gö6983 (Gö; 0, 5, 10, or 50 μM; E-H) and then subjected to the inflammasome activators *m*-3M3FBS (85 μM), thapsigargin (20 μM), nigericin (10 μM) or poly-(dA:dT) (2 μg/mL complexed with 5 μL Lipofectamine 2000) in an extracellular medium consisting of (in mM) 123 NaCl, 5 KCl, 2 $MgCl_2$, 1 $CaCl_2$, 10 glucose, 10 HEPES, pH 7.4. The LPS (A, E) and unprimed (A-H) controls were subjected to medium alone. Immediately after addition of inflammasome activators, the plates were centrifuged at 340 × g for 5 min (RT). After 30 min (C, D, G, H) or 60 min (A, B, E, F), the supernatants were collected and IL-1β concentrations were measured by HTRF (A, E) or the cells were fixed with 4% formaldehyde, counterstained with the nuclear dye DRAQ5 (5 μM) and imaged using a widefield fluorescence microscope (B-D, F-H).

The results are plotted as means from 3 independent experiments performed in technical duplicate. Error bars represent SD. Individual data points represent means of the technical duplicate values from each of the independent experiments.

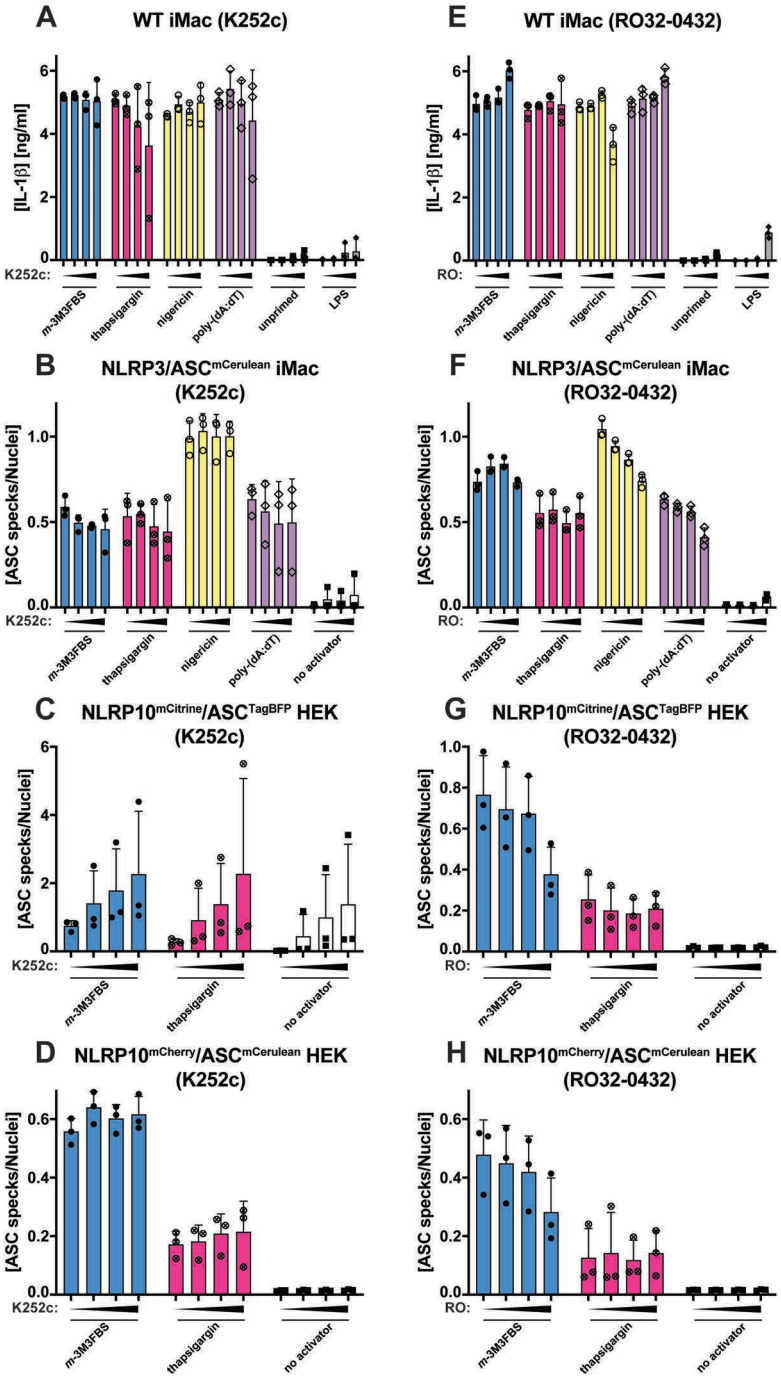

Figure 6.22. Influence of the PKC inhibitors K252c and RO32-0432 on the inflammasome responses to *m*-3M3FBS, thapsigargin, nigericin, and poly-(dA:dT)

A-H: LPS-primed (200 ng/mL, 2 h) WT iMac cells (A, E), NLRP3/ASC^{mCerulean} reporter iMac cells (B, F), NLRP10^{mCitrine}/ASC^{TagBFP} HEK cells (C, G), and NLRP10^{mCherry}/ASC^{mCerulean} HEK cells (D, H) were treated for 10 min with K252c (0, 10, 25, or 50 μM; A-D) or RO32-0432 (RO; 0, 5, 10, or 25 μM; E-H) and then subjected to the inflammasome activators *m*-3M3FBS (85 μM), thapsigargin (20 μM), nigericin (10 μM) or poly-(dA:dT) (2 μg/mL complexed with 5 μL Lipofectamine 2000) in an extracellular medium consisting of (in mM) 123 NaCl, 5 KCl, 2 $MgCl_2$, 1 $CaCl_2$, 10 glucose, 10 HEPES, pH 7.4. The LPS (A, E) and unprimed (A-H) controls were subjected to medium alone. Immediately after addition of inflammasome activators, the plates were centrifuged at 340 × g for 5 min (RT). After 30 min (C, D, G, H) or 60 min (A, B, E, F), the supernatants were collected and IL-1β concentrations were measured by HTRF (A, E) or the cells were fixed with 4% formaldehyde, counterstained with the nuclear dye DRAQ5 (5 μM) and imaged using a widefield fluorescence microscope (B-D, F-H).

The results are plotted as means from 3 independent experiments performed in technical duplicate. Error bars represent SD. Individual data points represent means of the technical duplicate values from each of the independent experiments.

I further tested how several commercially available PKC activators impact on the inflammasome responses to *m*-3M3FBS, thapsigargin, poly-(dA:dT), and nigericin in ASC fluorescent reporter HEK cells with or without the NLRP10 overexpression cassettes, NLRP3/ASC^{mCerulean} reporter iMac cells, and LPS-primed WT iMac cells. I focused on the following molecules: PMA, bryostatin 1 (Figure 6.23), SC-9, and SC-10 (Figure 6.24).

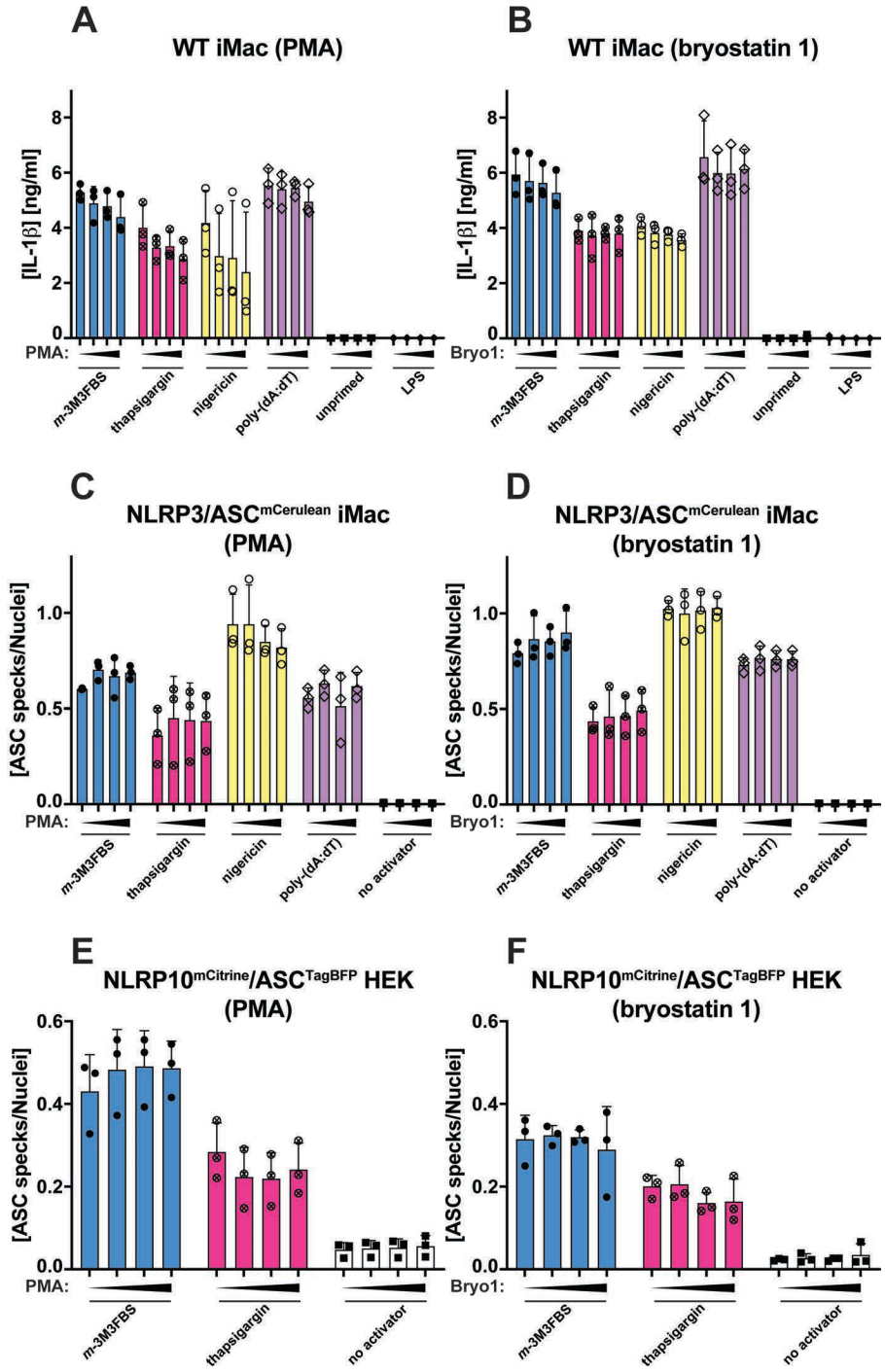

Figure 6.23. Influence of the PKC agonists PMA and bryostatin 1 on the inflammasome responses to *m*-3M3FBS, thapsigargin, nigericin, and poly-(dA:dT)

A-F: LPS-primed (200 ng/mL, 2 h) WT iMac cells (A, B), NLRP3/ASC^{mCerulean} reporter iMac cells (C, D), and NLRP10^{mCitrine}/ASC^{TagBFP} HEK cells (E, F) were treated for 10 min with PMA (0, 0.5, 1, or 5 μM; A-C) or bryostatin 1 (Bryo1; 0, 10, 100, or 500 nM; D-F) and then subjected to the inflammasome activators *m*-3M3FBS (85 μM), thapsigargin (20 μM), nigericin (10 μM) or poly-(dA:dT) (2 μg/mL complexed with 5 μL Lipofectamine 2000) in an extracellular medium consisting of (in mM) 123 NaCl, 5 KCl, 2 $MgCl_2$, 1 $CaCl_2$, 10 glucose, 10 HEPES, pH 7.4. The LPS (A, B) and unprimed (A-F) controls were subjected to medium alone. Immediately after addition of inflammasome activators, the plates were centrifuged at 340 × g for 5 min (RT). After 30 min (E, F) or 60 min (A-D), the supernatants were collected and IL-1β concentrations were measured by HTRF (A, B) or the cells were fixed with 4% formaldehyde, counterstained with the nuclear dye DRAQ5 (5 μM) and imaged using a widefield fluorescence microscope (C-F).

The results are plotted as means from 3 independent experiments performed in technical duplicate. Error bars represent SD. Individual data points represent means of the technical duplicate values from each of the independent experiments.

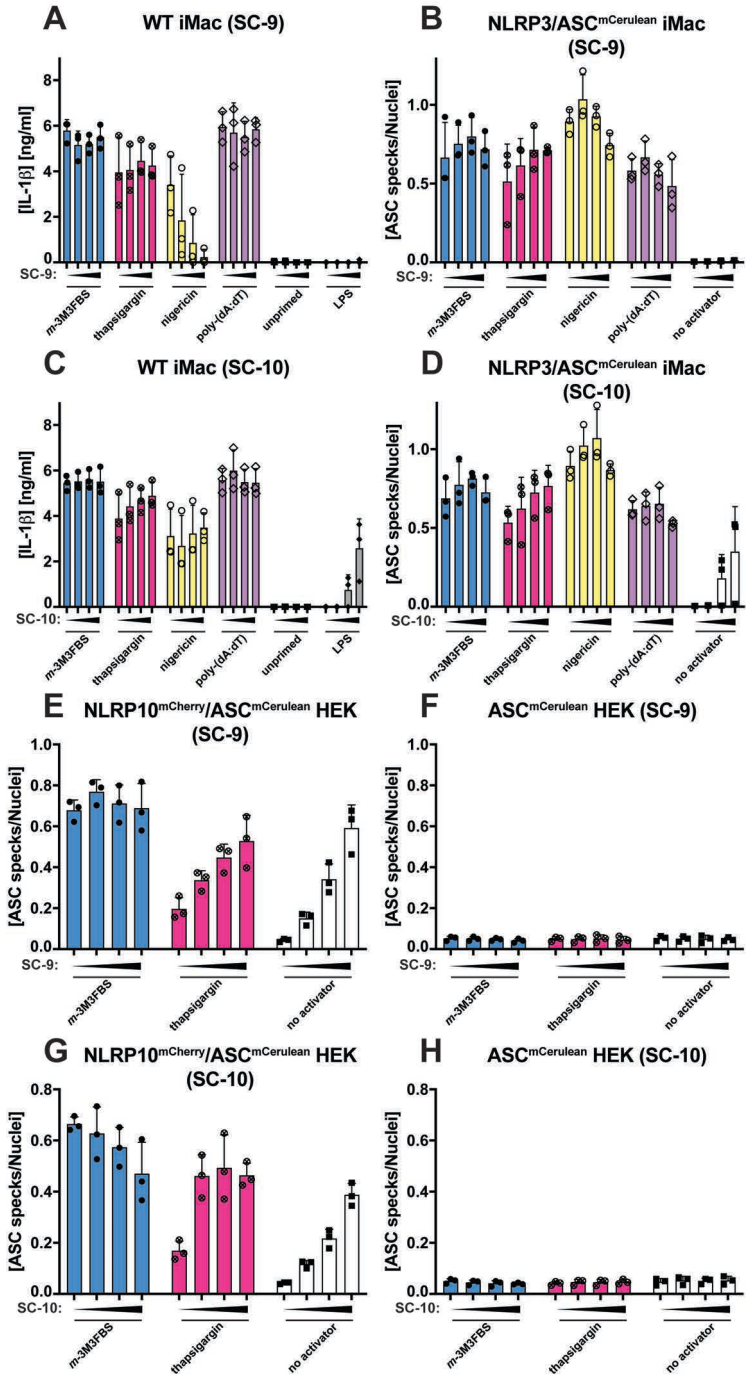

Figure 6.24. Influence of the PKC agonists SC-9 and SC-10 on the inflammasome responses to *m*-3M3FBS, thapsigargin, nigericin, and poly-(dA:dT)

A-H: LPS-primed (200 ng/mL, 2 h) WT iMac cells (A, C), NLRP3/ASC^{mCerulean} reporter iMac cells (B, D), NLRP10^{mCherry}/ASC^{mCerulean} HEK cells (E, G), and ASC^{mCerulean} HEK cells (NLRP10-negative control; F, H) were treated for 10 min with SC-9 (0, 25, 50, or 100 μM; A, B, E, F) or SC-10 (0, 25, 50, or 100 μM; C, D, G, H) and then subjected to the inflammasome activators *m*-3M3FBS (85 μM), thapsigargin (20 μM), nigericin (10 μM) or poly-(dA:dT) (2 μg/mL complexed with 5 μL Lipofectamine 2000) in an extracellular medium consisting of (in mM) 123 NaCl, 5 KCl, 2 $MgCl_2$, 1 $CaCl_2$, 10 glucose, 10 HEPES, pH 7.4. The LPS (A, C) and unprimed (A-H) controls were subjected to medium alone. Immediately after addition of inflammasome activators, the plates were centrifuged at 340 × g for 5 min (RT). After 30 min (E-H) or 60 min (A-D), the supernatants were collected and IL-1β concentrations were measured by HTRF (A, C) or the cells were fixed with 4% formaldehyde, counterstained with the nuclear dye DRAQ5 (5 μM) and imaged using a widefield fluorescence microscope (B, D-H).

The results are plotted as means from 3 independent experiments performed in technical duplicate. Error bars represent SD. Individual data points represent means of the technical duplicate values from each of the independent experiments.

PMA and bryostatin 1 did not inhibit any of the tested inflammasome responses. These compounds also did not have inflammasome-activating properties (Figure 6.23). Unexpectedly, SC-10, but not SC-9, robustly induced inflammasome activation in macrophages (Figure 6.24 A-D). The SC-10-induced IL-1β release relied on caspase-1, as it was sensitive to the caspase-1 inhibitor VX-765, but the inflammasome activation by SC-10 was independent of phagocytosis and of NLRP3 because it was not inhibited by cytochalasin D and by CRID3 (Supplementary Figure S13).

Somewhat perplexingly, both SC-9 and SC-10 stimulated the ASC speck formation in NLRP10^{mCherry}/ASC^{mCerulean} HEK cells (Figure 6.24 E, G). This was fully attributable to the NLRP10 overexpression, as HEK cells overexpressing ASC^{mCerulean} alone did not respond to SC-9 and to SC-10 (Figure 6.24 F, H). Of note, experiments using SC-9 and SC-10 required particular attention to the compound autofluorescence interfering with the experimental readouts, as both molecules were strongly fluorescent in the BFP channel (Supplementary Figure S14). SC-9 and SC-10 did not interfere with the mCerulean channel so reporter cell lines overexpressing ASC^{mCerulean} could be used to generate interpretable results, as evidenced in Figure 6.24 E-H.

Taking the data presented in this Section at face value, it is impossible to provide a coherent interpretation of the discrepant observations. On the one hand, pan-kinase as well as more specific PKC inhibitors did not block the AIM2/NLRP10 responses to *m*-3M3FBS and thapsigargin. Correspondingly, the relatively well-characterized PKC activators PMA and bryostatin 1 were not inflammasome activators. However, it cannot be ignored that the reported PKC activators SC-9 and SC-10 (Ito et al., 1986) were capable of eliciting an NLRP10-driven ASC speck formation, and SC-10 activated the inflammasome in an NLRP3-independent manner in murine macrophages.

Upon closer inspection, I noticed that SC-9 and SC-10 are structurally similar to *m*-3M3FBS and *o*-3M3FBS. All these molecules are sulfonamides with the sulfur atom connected to a bulky aromatic group (chloronaphthalene in the case of SC-9/SC-10 and trimethylbenzene in the case of *m*-/*o*-3M3FBS; Supplementary Figure S15). Of note, the sulfonamide functional group is relatively well exposed in the 'double' macrophage/HEK activators *m*-3M3FBS and SC-10. In contrast, this group is partially masked in the 'HEK-only' activators *o*-3M3FBS and SC-9, either by the substitution pattern of the

trifluorotolyl group connected to the nitrogen atom (*o*-3M3FBS) or by the attachment of the phenyl ring to the alkyl chain connected to the nitrogen atom (SC-9).

I tested whether several commercially available benzenesulfonamide derivatives with structures broadly similar to *m*-/*o*-3M3FBS and SC-9/SC-10 could also activate the inflammasome (Supplementary Figure S16). None of the compounds I examined elicited ASC speck formation in NLRP3/ASC^{mCerulean} reporter iMac cells or in ASC fluorescent reporter HEK cells with or without the NLRP10 overexpression cassette. This observation indicates that the molecules I selected likely did not recapitulate the minimal chemical structure responsible for the biological effects of *m*-3M3FBS, *o*-3M3FBS, SC-9, and SC-10. Despite that, the most plausible explanation for the inflammasome-triggering activities of SC-9 and SC-10 is that they act through a PKC-independent off-target effect shared with *m*-3M3FBS and/or *o*-3M3FBS. Collectively, my results provide no indication that PKC is necessary or sufficient for the AIM2 and NLRP10 responses to *m*-3M3FBS and thapsigargin.

6.13. Mitochondrial and nuclear dynamics in cells treated with *m*-3M3FBS and thapsigargin

All my evidence suggests that *m*-3M3FBS, *o*-3M3FBS, SC-9, SC-10, and thapsigargin activate the AIM2 and NLRP10 inflammasomes in a manner that does not rely on their main reported targets. My previous observations pointed toward two organelles that are likely affected by *m*-3M3FBS and thapsigargin, the nuclei and the mitochondria (Sections 6.7 and 6.9). To gain insight into the dynamic changes inflicted by *m*-3M3FBS and thapsigargin on these compartments, I performed live cell imaging of NLRP3/ASC^{mCerulean} reporter iMac cells and NLRP10^{mCitrine}/ASC^{TagBFP} HEK cells overexpressing mitochondrial or nuclear markers (mCitrine or mCherry targeted to the mitochondrial matrix, or fusion proteins between the nuclear protein HMGB1 and mCitrine/mCherry, respectively). Briefly, I stimulated cells with the inflammasome activators *m*-3M3FBS, thapsigargin, nigericin, and poly-(dA:dT) directly in the widefield fluorescence microscope incubation chamber after the onset of imaging (*m*-3M3FBS and nigericin), or just before the onset of imaging (thapsigargin and poly-[dA:dT][1]). The nuclear (HMGB1) recordings are shown in Figures 6.25 (HEK cells) and 6.26 (macrophages), whereas the mitochondrial recordings are shown in Figures 6.27 (HEK cells) and 6.28 (macrophages).

[1] For these two activators, a brief centrifugation (30 s at 340 × g, RT) was necessary, so direct stimulation in the microscope incubation chamber was not possible.

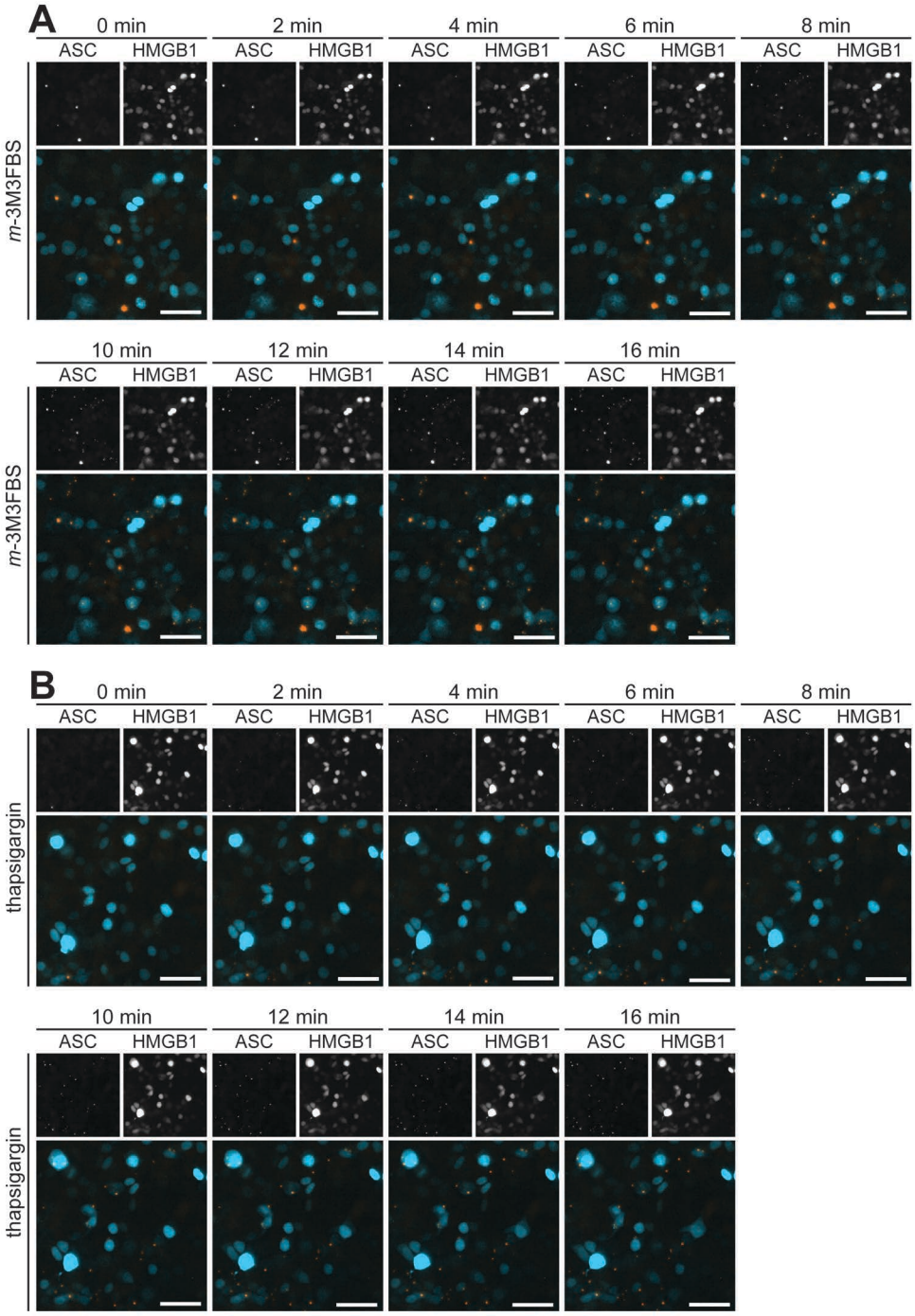
A
0 min
2 min
4 min
6 min
8 min
ASC
HMGB1
m-3M3FBS
10 min
12 min
14 min
16 min
B
thapsigargin

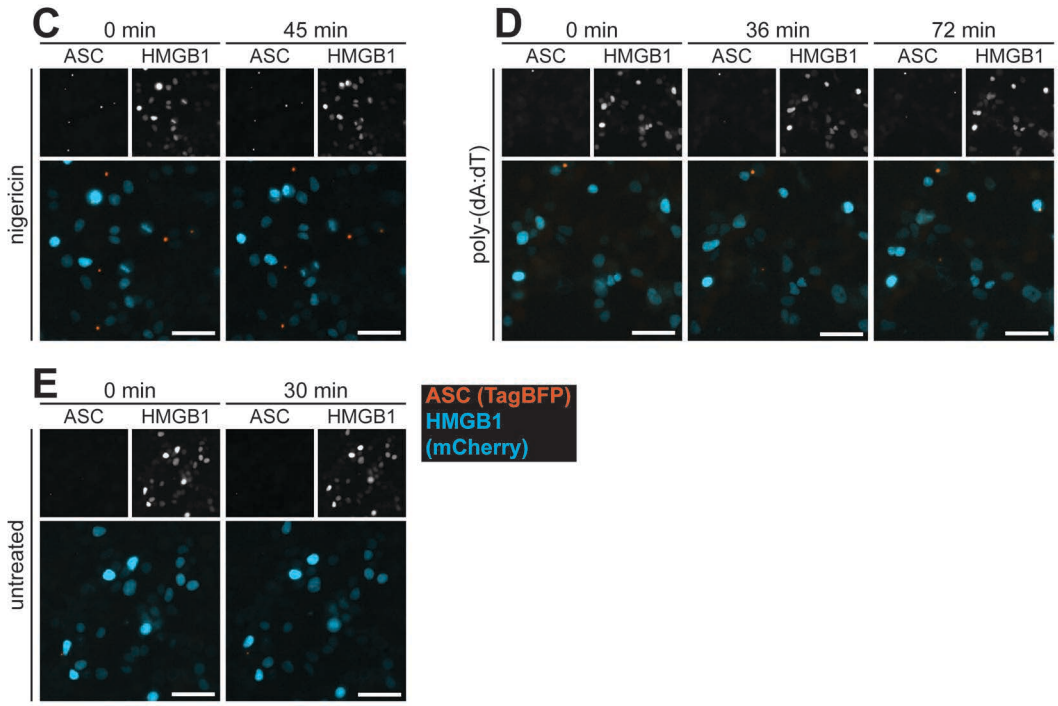

Figure 6.25 (this and previous page). Nuclear dynamics monitored by HMGB1 localization in NLRP10^{mCitrine}/ASC^{TagBFP}/HMGB1^{mCherry} HEK cells stimulated with *m*-3M3FBS, thapsigargin, nigericin, or poly-(dA:dT)

A-E: HEK cells stably overexpressing human NLRP10^{mCitrine}, ASC^{TagBFP}, and the nuclear marker HMGB1^{mCherry} were shifted to an extracellular medium consisting of (in mM) 123 NaCl, 5 KCl, 2 $MgCl_2$, 1 $CaCl_2$, 10 glucose, 10 HEPES, pH 7.4. Next, the cells were left untreated (E), or were stimulated with *m*-3M3FBS (85 μM; A), thapsigargin (20 μM; B), nigericin (10 μM; C), or poly-(dA:dT) (2 μg/mL complexed with 5 μL Lipofectamine 2000; D), and live imaging was performed using a widefield fluorescence microscope to capture the nuclear dynamics. The time interval between the acquired images was approximately 1 min (A-C, E) or 4 min (D). For the duration of the experiment, the cells were kept at 37°C in the microscope incubation chamber, but they were **not** perfused with CO_2 (CO_2-based buffers do not require CO_2 perfusion to maintain constant pH). The stimuli were added to the cells either directly in the microscope incubation chamber immediately after the onset of imaging (*m*-3M3FBS [A] and nigericin [C]), or they were added to the cells **outside** of the microscope incubation chamber (thapsigargin [B] and poly-(dA:dT) [D]), followed by a brief centrifugation (340 × g at RT for 30 s), after which the imaging was started.

Images are representative of 3 independent experiments. In each of the panels (A-E), the same field (that is, approximately the same population of cells) is followed over time. Scale bars correspond to 50 μm.

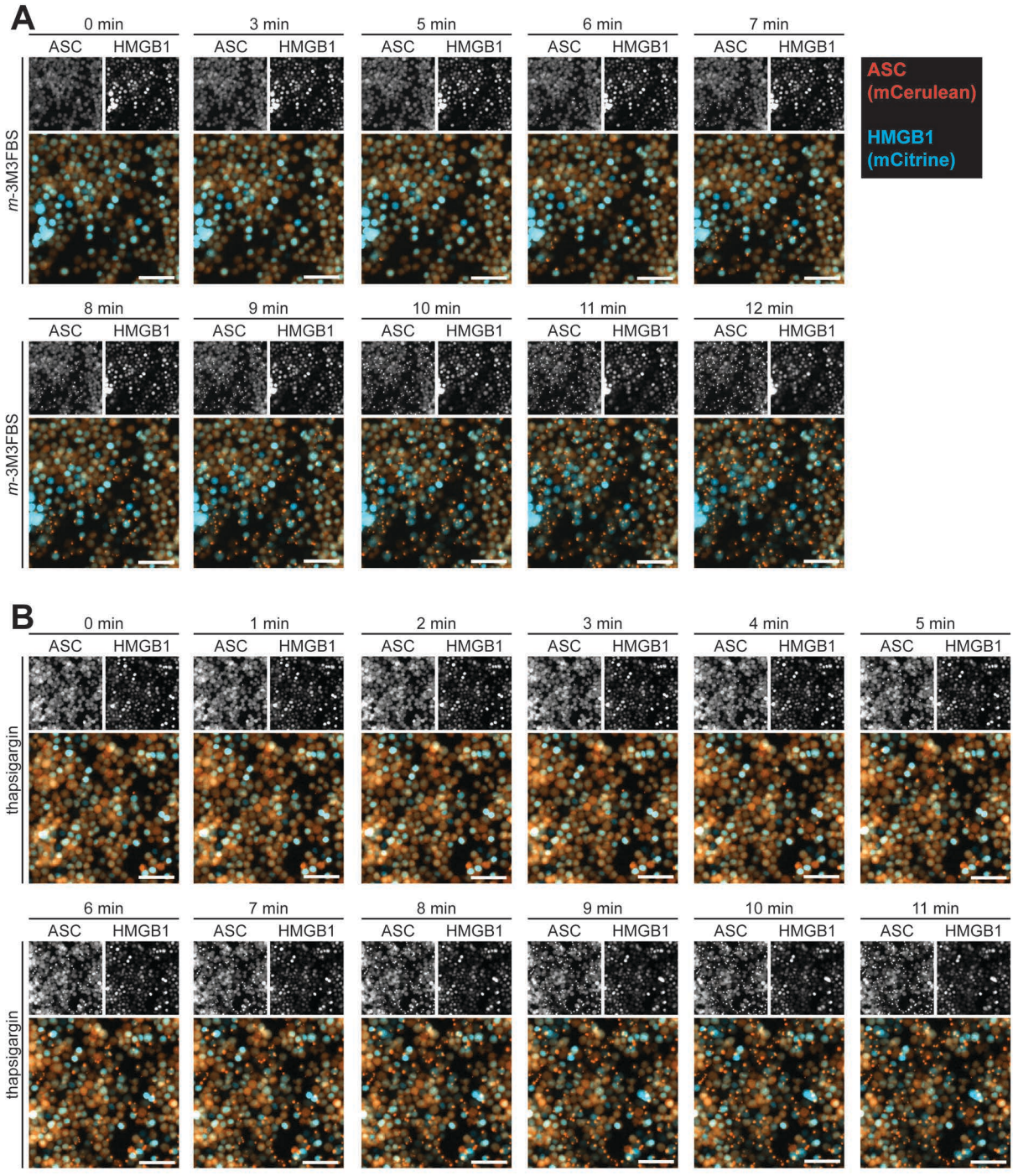
A
0 min
3 min
5 min
6 min
7 min
8 min
9 min
10 min
11 min
12 min
ASC
HMGB1
m-3M3FBS
ASC (mCerulean)
HMGB1 (mCitrine)
B
0 min
1 min
2 min
3 min
4 min
5 min
6 min
7 min
8 min
9 min
10 min
11 min
thapsigargin

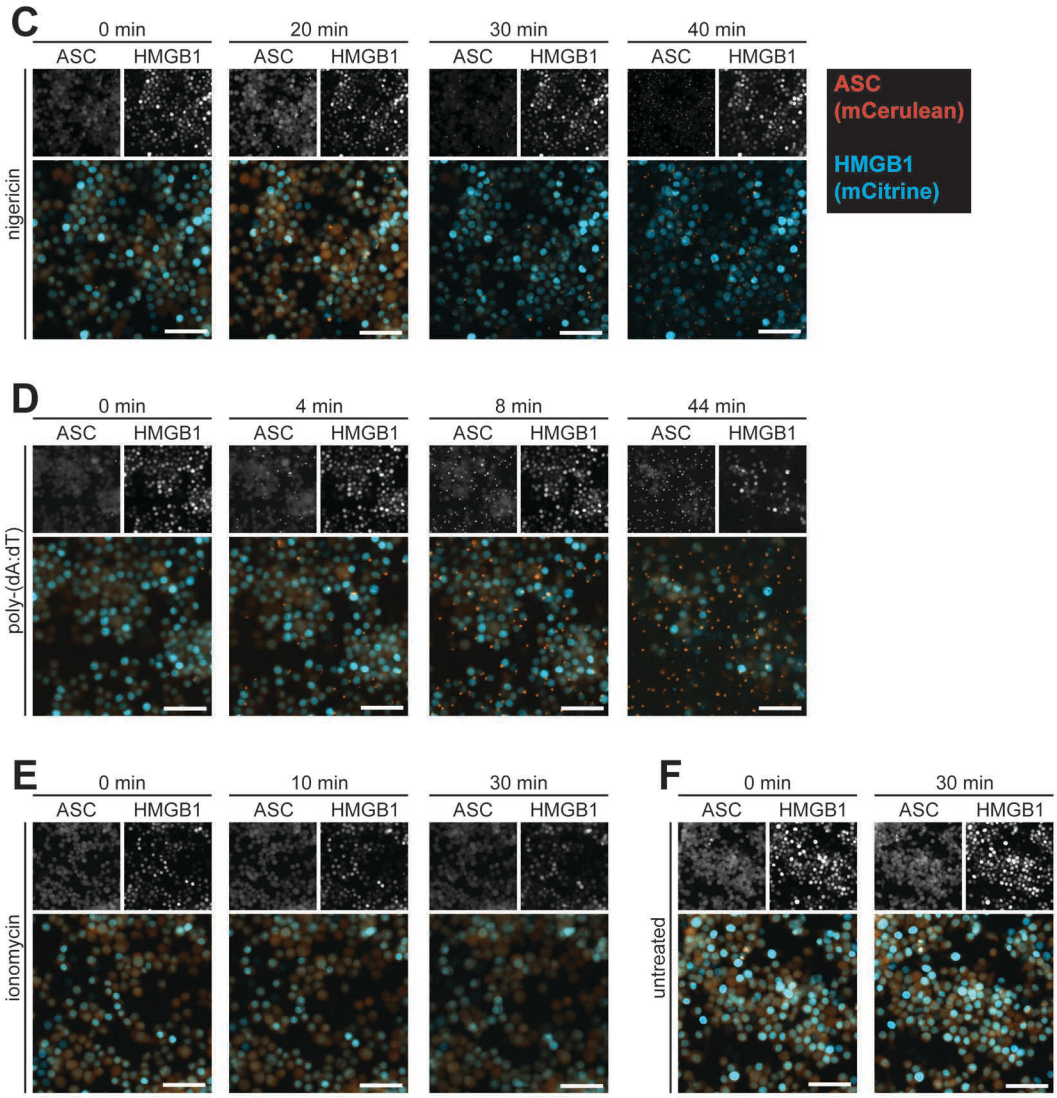

Figure 6.26 (this and previous page). Nuclear dynamics monitored by HMGB1 localization in NLRP3/ASC^{mCerulean}/HMGB1^{mCitrine} reporter iMac cells stimulated with *m*-3M3FBS, thapsigargin, nigericin, poly-(dA:dT), or ionomycin

A-F: NLRP3/ASC^{mCerulean} reporter iMac cells stably overexpressing the nuclear marker HMGB1^{mCitrine} were shifted to an extracellular medium consisting of (in mM) 123 NaCl, 5 KCl, 2 $MgCl_2$, 1 $CaCl_2$, 10 glucose, 10 HEPES, pH 7.4. Next, the cells were left untreated (F), or were stimulated with *m*-3M3FBS (85 μM; A), thapsigargin (20 μM; B), nigericin (10 μM; C), poly-(dA:dT) (2 μg/mL complexed with 5 μL Lipofectamine 2000; D), or ionomycin (10 μM; E), and live imaging was performed using a widefield fluorescence microscope to capture the nuclear dynamics. The time interval between the acquired images was approximately 1 min (A-C, E, F) or 4 min (D). For the duration of the experiment, the cells were kept at 37°C in the microscope incubation chamber, but they were **not** perfused with CO_2 (HEPES-based buffers do not require CO_2 perfusion to maintain constant pH). The stimuli were added to the cells either directly in the microscope incubation chamber immediately after the onset of imaging (*m*-3M3FBS [A], nigericin [C], and ionomycin [E]), or they were added to the cells **outside** of the microscope incubation chamber (thapsigargin [B] and poly-(dA:dT) [D]), followed by a brief centrifugation (340 × g at RT for 30 s), after which the imaging was started.

Images are representative of 3 independent experiments. In each of the panels (A-F), the same field (that is, approximately the same population of cells) is followed over time. Scale bars correspond to 50 μm.

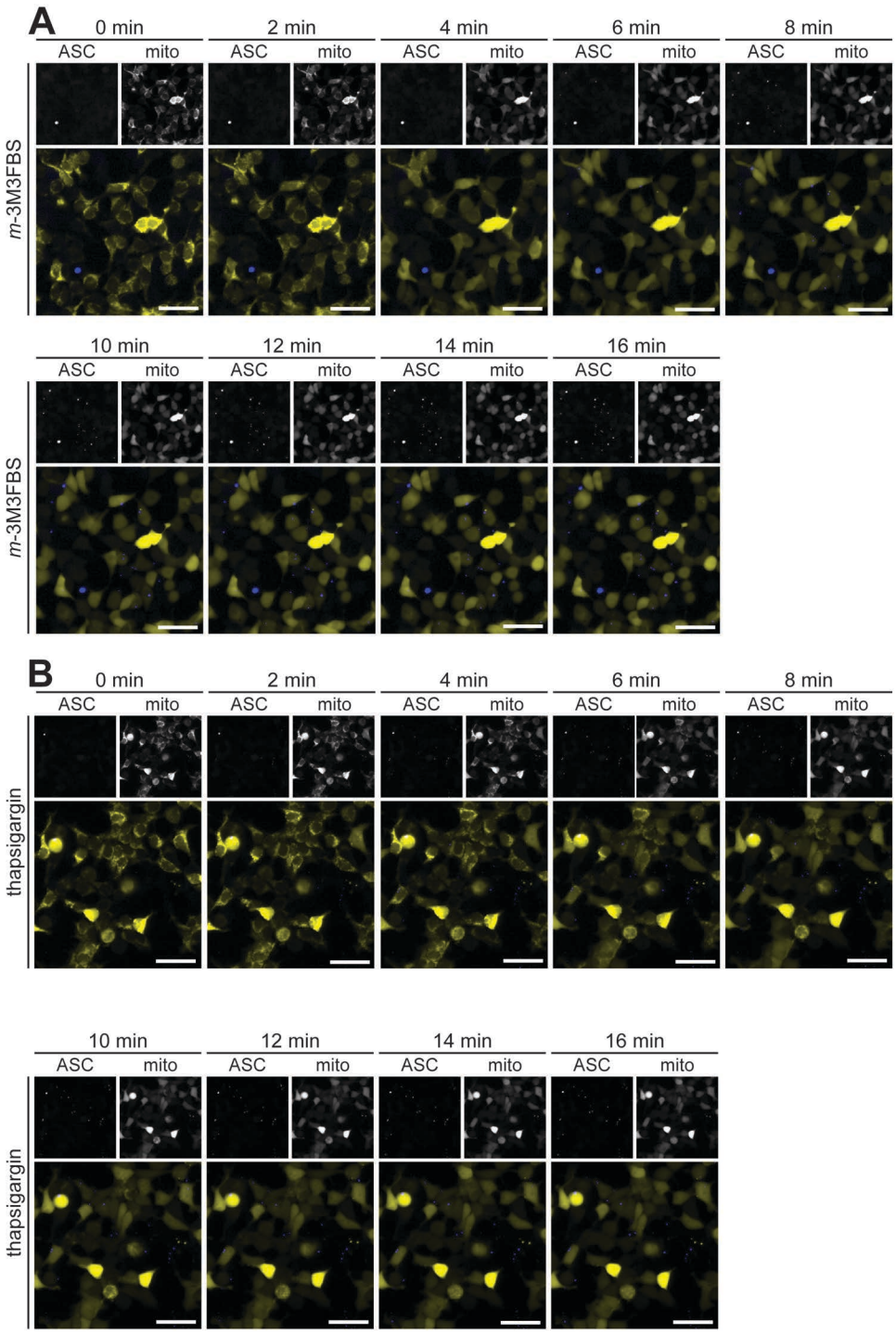
A
0 min
2 min
4 min
6 min
8 min
ASC
mito
m-3M3FBS
10 min
12 min
14 min
16 min
B
thapsigargin

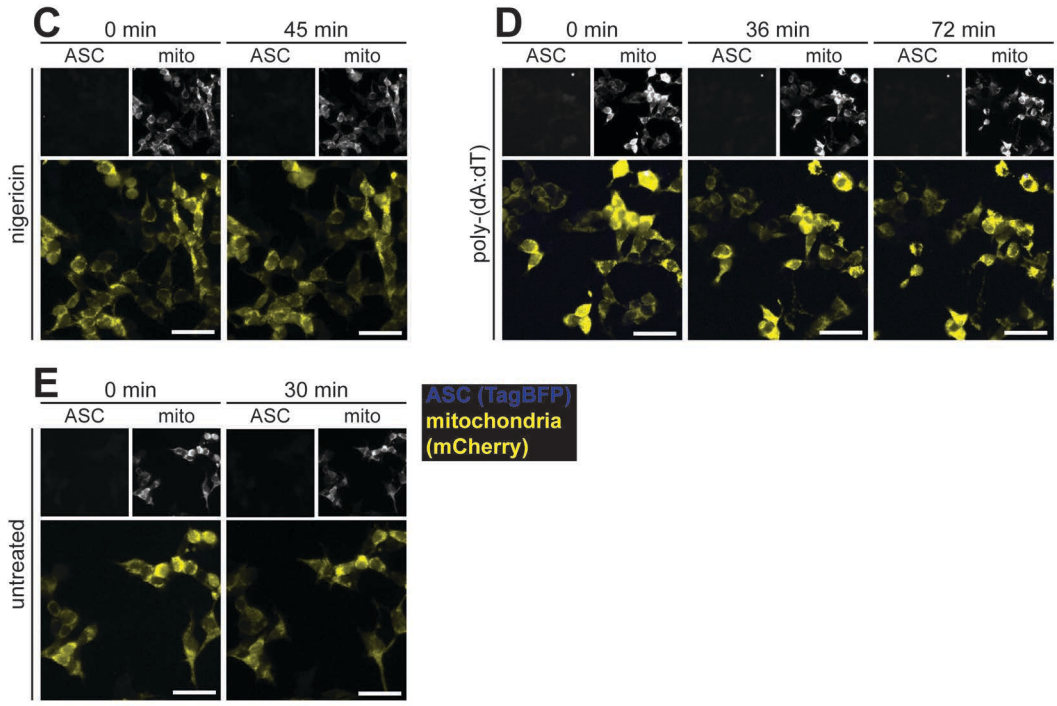

Figure 6.27 (this and previous page). Mitochondrial dynamics monitored by mitochondrial matrix-targeted mCherry localization in NLRP10^{mCitrine}/ASC^{TagBFP}/mito^{mCherry} HEK cells stimulated with *m*-3M3FBS, thapsigargin, nigericin, or poly-(dA:dT)

A-E: HEK cells stably overexpressing human NLRP10^{mCitrine}, ASC^{TagBFP}, and the mitochondrial marker mito^{mCherry} were shifted to an extracellular medium consisting of (in mM) 123 NaCl, 5 KCl, 2 $MgCl_2$, 1 $CaCl_2$, 10 glucose, 10 HEPES, pH 7.4. Next, the cells were left untreated (E), or were stimulated with *m*-3M3FBS (85 μM; A), thapsigargin (20 μM; B), nigericin (10 μM; C), or poly-(dA:dT) (2 μg/mL complexed with 5 μL Lipofectamine 2000; D), and live imaging was performed using a widefield fluorescence microscope to capture the mitochondrial dynamics. The time interval between the acquired images was approximately 1 min (A-C, E) or 4 min (D). For the duration of the experiment, the cells were kept at 37°C in the microscope incubation chamber, but they were **not** perfused with CO_2 (HEPES-based buffers do not require CO_2 perfusion to maintain constant pH). The stimuli were added to the cells either directly in the microscope incubation chamber immediately after the onset of imaging (*m*-3M3FBS [A] and nigericin [C]), or they were added to the cells **outside** of the microscope incubation chamber (thapsigargin [B] and poly-(dA:dT) [D]), followed by a brief centrifugation (340 × g at RT for 30 s), after which the imaging was started.

Images are representative of 3 independent experiments. In each of the panels (A-E), the same field (that is, approximately the same population of cells) is followed over time. Scale bars correspond to 50 μm.

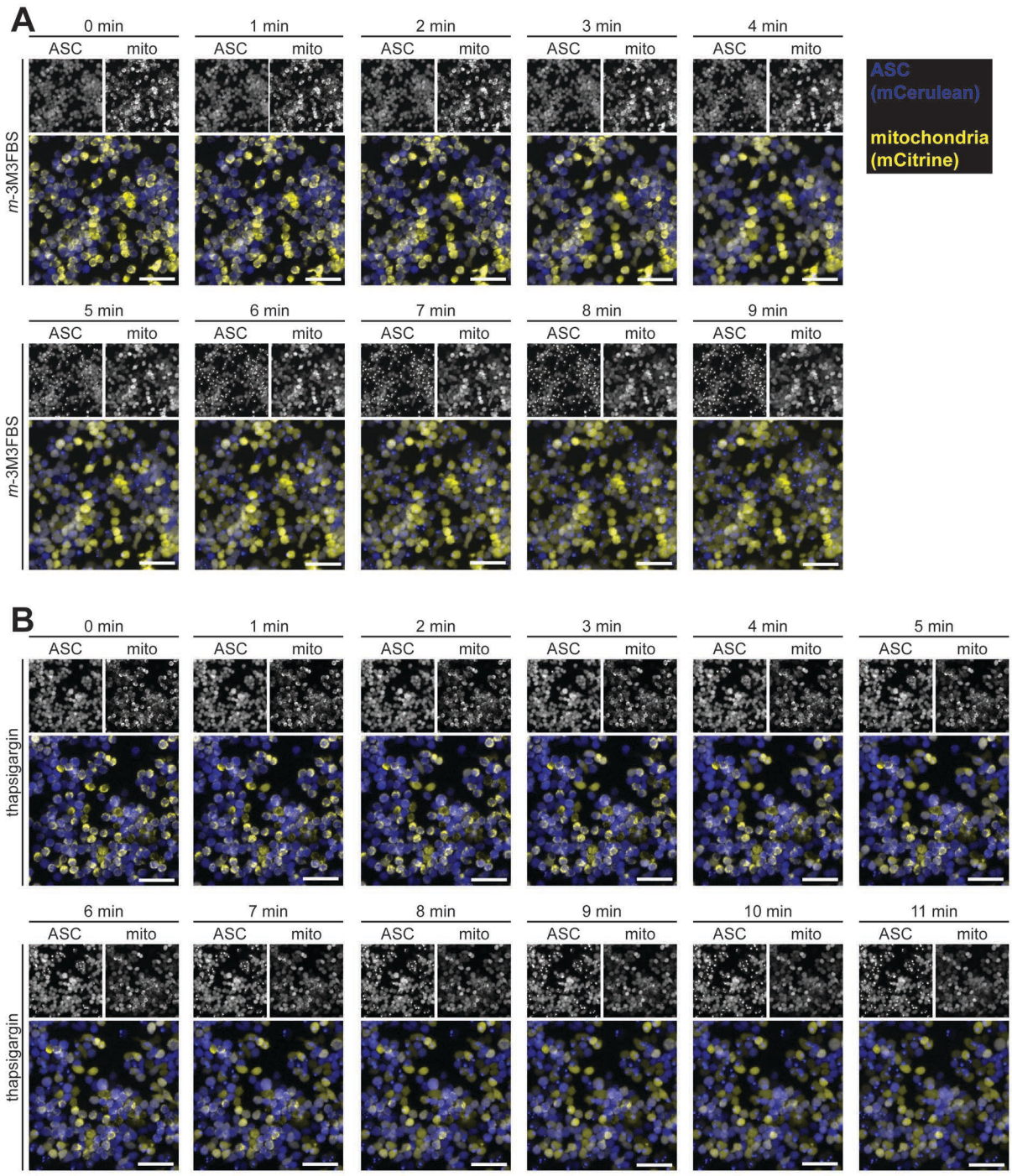
A
0 min
1 min
2 min
3 min
4 min
ASC
mito
m-3M3FBS
5 min
6 min
7 min
8 min
9 min
ASC (mCerulean)
mitochondria (mCitrine)
B
thapsigargin
10 min
11 min

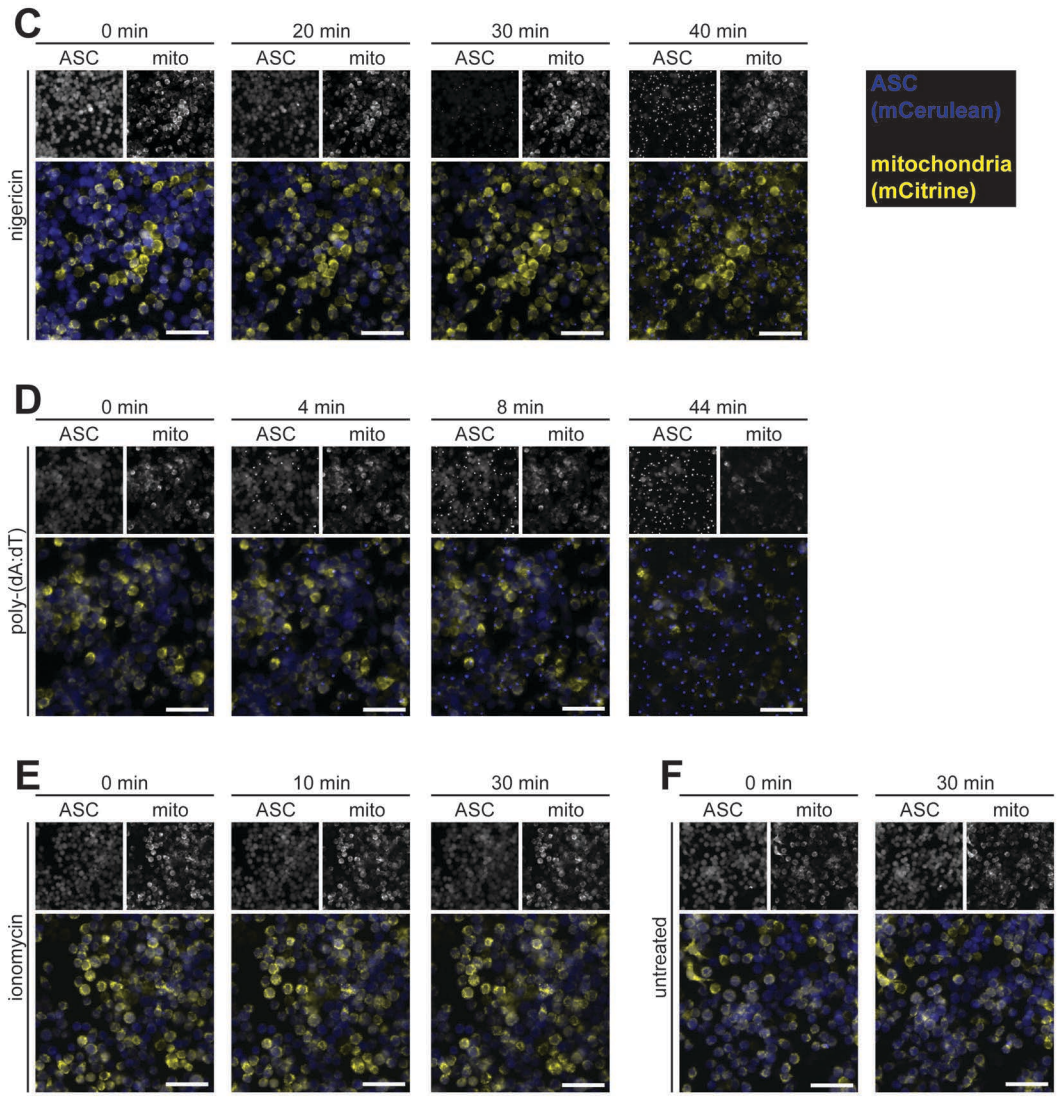

Figure 6.28 (this and previous page). Mitochondrial dynamics monitored by mitochondrial matrix-targeted mCitrine localization in NLRP3/ASC^{mCerulean}/mito^{mCitrine} reporter iMac cells stimulated with *m*-3M3FBS, thapsigargin, nigericin, poly-(dA:dT), or ionomycin

A-F: NLRP3/ASC^{mCerulean} reporter iMac cells stably overexpressing the mitochondrial marker mito^{mCitrine} were shifted to an extracellular medium consisting of (in mM) 123 NaCl, 5 KCl, 2 $MgCl_2$, 1 $CaCl_2$, 10 glucose, 10 HEPES, pH 7.4. Next, the cells were left untreated (F), or were stimulated with *m*-3M3FBS (85 μM; A), thapsigargin (20 μM; B), nigericin (10 μM; C), poly-(dA:dT) (2 μg/mL complexed with 5 μL Lipofectamine 2000; D), or ionomycin (10 μM; E), and live imaging was performed using a widefield fluorescence microscope to capture the mitochondrial dynamics. The time interval between the acquired images was approximately 1 min (A-C, E, F) or 4 min (D). For the duration of the experiment, the cells were kept at 37°C in the microscope incubation chamber, but they were **not** perfused with CO_2 (HEPES-based buffers do not require CO_2 perfusion to maintain constant pH). The stimuli were added to the cells either directly in the microscope incubation chamber immediately after the onset of imaging (*m*-3M3FBS [A], nigericin [C], and ionomycin [E]), or they were added to the cells **outside** of the microscope incubation chamber (thapsigargin [B] and poly-(dA:dT) [D]), followed by a brief centrifugation (340 × g at RT for 30 s), after which the imaging was started.

Images are representative of 3 independent experiments. In each of the panels (A-F), the same field (that is, approximately the same population of cells) is followed over time. Scale bars correspond to 50 μm.

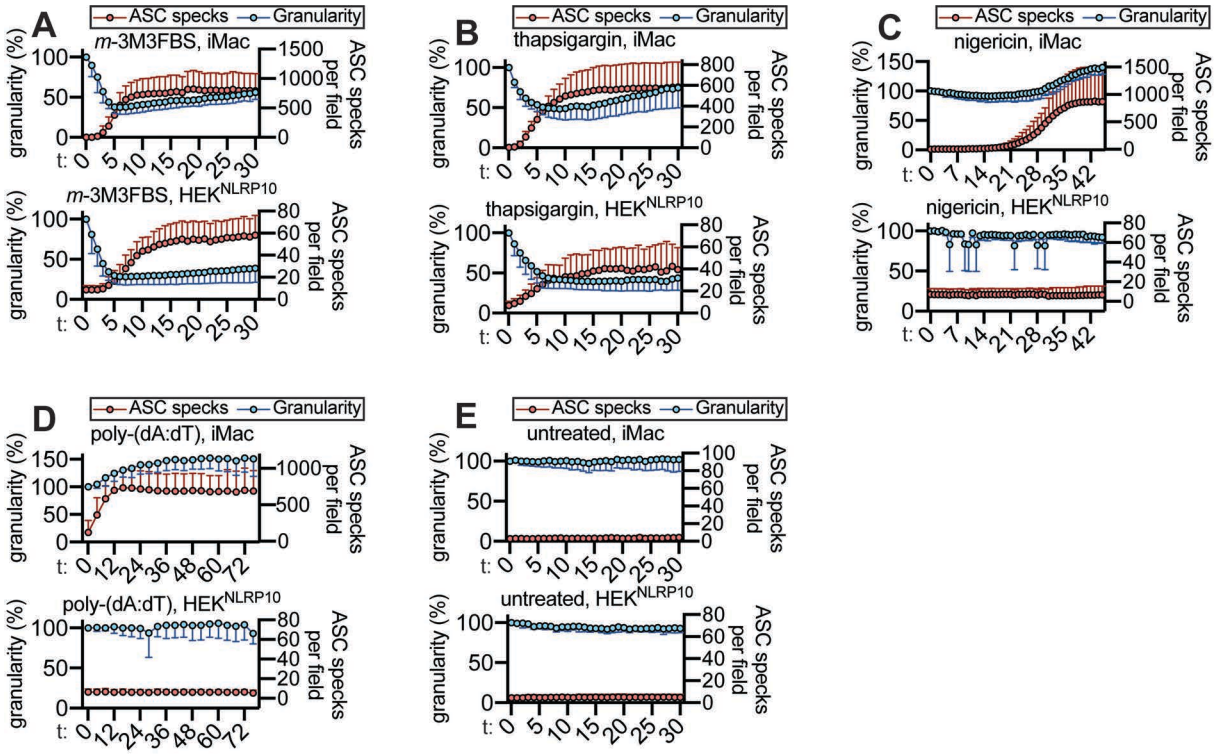

Figure 6.27/28Q. Quantifications of the granularity of the mitochondrial signal in Figures 6.27 ('HEK^{NLRP10}') and 6.28 A-D, F ('iMac')

A-E: Granularity of the mitochondrial fluorescence signal in NLRP10^{mCitrine}/ASC^{TagBFP}/mito^{mCherry} HEK cells ('HEK^{NLRP10}') and in NLRP3/ASC^{mCerulean}/mito^{mCitrine} reporter iMac cells ('iMac') treated with *m*-3M3FBS (A), thapsigargin (B), nigericin (C) or poly-(dA:dT) (D), or left untreated (E). The granularity of the mitochondrial matrix-targeted fluorescent protein signal was calculated as a proxy for the mitochondrial integrity. High granularity values correlate with the intact status of the mitochondria, while a decrease in granularity correlates with the cytosolic dissipation of the mitochondrial fluorescence signal. The initial granularity value was taken as 100% for the purpose of signal normalization. The numbers of ASC specks per imaging field were treated as absolute values and no normalization has been performed. The data points are means from 6-8 time-lapse recordings per condition per cell line, collected over 3 independent experiments. The error bars represent SD. The time (t) unit is minute (x-axis).

Under untreated conditions, HMGB1 was contained within the nuclei (Figures 6.25 E and 6.26 F) and the mitochondrially targeted fluorescent proteins had a granular distribution pattern consistent with enclosure in the mitochondrial matrix (Figures 6.27 E and 6.28 F). Strikingly, both *m*-3M3FBS and thapsigargin caused a rapid (within less than 15 min) leakage of the nuclear HMGB1 into the cytosol (Figures 6.25 A, B and 6.26 A, B) and a loss of the granular localization pattern of mitochondrially targeted mCitrine/mCherry (Figures 6.27 A, B and 6.28 A, B). The quantifications of the granularity of the mitochondrial signal and the ASC speck counts in cells treated with inflammasome activators (Figures 6.27 and 6.28 A-D, F) are presented in Figure 6.27/28Q. The onset of the mitochondrial changes occurred slightly before the onset of ASC speck formation, while the onset of the nuclear leakage coincided with or closely followed the onset of ASC speck formation. The strength of the mitochondrial effect was

comparable between *m*-3M3FBS and thapsigargin, whereas the nuclear effect of *m*-3M3FBS appeared to be stronger than that of thapsigargin.

The cytosolic translocation of mitochondrial matrix contents upon challenge with *m*-3M3FBS/thapsigargin likely indicates major damage occurring at the level of the IMM and the OMM. This disruption enables leakage of biomolecules as large as folded fluorescent proteins (slightly above 25 kDa)[2]. Importantly, the NLRP3 activator nigericin and the AIM2 ligand poly-(dA:dT) did not induce the nuclear and mitochondrial changes that had been observed in cells treated with *m*-3M3FBS and thapsigargin, even at relatively late time points (Figures 6.25 C, D, 6.26 C, D, 6.27 C, D, and 6.28 C, D). This indicates that the observed cellular alterations are not a common step in the inflammasome signaling and also likely not an effect of caspase-1 activation. Instead, they may represent specific cellular events triggered by *m*-3M3FBS and thapsigargin, with possible relevance for the AIM2 and NLRP10 activations. Of note, nigericin has been proposed to elicit mitochondrial damage in a fashion relevant for the NLRP3 inflammasome activation (Misawa et al., 2013; Subramanian et al., 2013; Zhou et al., 2010). Based on my observations, *m*-3M3FBS and thapsigargin affect the mitochondria in different manner than nigericin.

As *m*-3M3FBS and thapsigargin both increase the cytosolic Ca^{2+} concentration, I tested whether the ionomycin-mediated Ca^{2+} delivery could also trigger changes in the nuclei or the mitochondria (Figures 6.26 E, 6.28 E, 6.29, and 6.30). Ionomycin treatment led to a leakage of HMGB1 from the nuclei in a manner dependent on extracellular Ca^{2+} (Figures 6.26 E, 6.29), albeit with slower kinetics than *m*-3M3FBS and thapsigargin. In contrast to *m*-3M3FBS and thapsigargin, ionomycin did not alter the mitochondrial matrix localization of $mito^{mCitrine}$/$mito^{mCherry}$ (Figures 6.28 E, 6.30). It also did not cause ASC speck formation, consistent with my earlier observation (Figure 6.18). These results suggest that while the nuclear damage in *m*-3M3FBS- and thapsigargin-treated cells may be Ca^{2+}-mediated, the mitochondrial disruption is probably not caused by the Ca^{2+} fluxes. As the ionomycin-induced nuclear permeabilization alone is not sufficient for the activations of AIM2 and NLRP10, the mitochondria are more likely than the nuclei to be

[2] An alternative interpretation of this observation would be that the mitochondrial import mechanisms are blocked upon treatment with *m*-3M3FBS/thapsigargin. While this could also be true, the extremely fast rate (minutes) at which the delocalization of the mitochondrial contents occurs is a strong argument in favor of the unspecific rupture/leakage scenario.

involved in the assembly of these inflammasomes. I will discuss this issue in more detail in Sections 6.14 and 6.15.

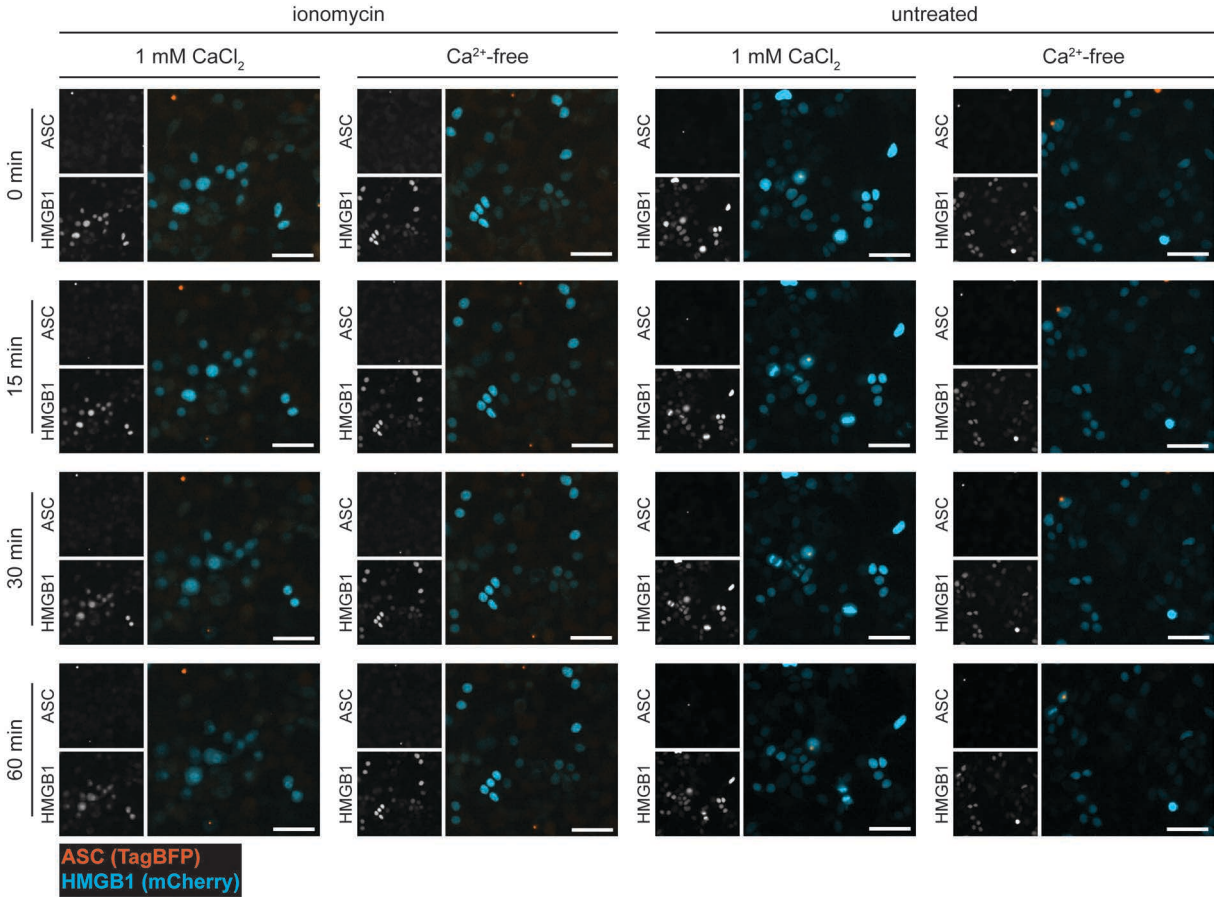

Figure 6.29. Nuclear dynamics monitored by HMGB1 localization in NLRP10^{mCitrine}/ASC^{TagBFP}/HMGB1^{mCherry} HEK cells treated with ionomycin in the presence of 1 mM $CaCl_2$ or in Ca^{2+}-deficient medium

HEK cells stably overexpressing human NLRP10^{mCitrine}, ASC^{TagBFP}, and the nuclear marker HMGB1^{mCherry} were shifted to an extracellular medium consisting of (in mM) 123 NaCl, 5 KCl, 2 $MgCl_2$, 0 or 1 $CaCl_2$, 10 glucose, 10 HEPES, pH 7.4. Next, the cells were left untreated, or were stimulated with ionomycin (10 μM), and live imaging was performed using a widefield fluorescence microscope to capture the nuclear dynamics. The time interval between the acquired images was approximately 1 min. For the duration of the experiment, the cells were kept at 37°C in the microscope incubation chamber, but they were **not** perfused with CO_2 (HEPES-based buffers do not require CO_2 perfusion to maintain constant pH). Ionomycin was added to the cells either directly in the microscope incubation chamber immediately after the onset of imaging. Scale bars correspond to 50 μm.

Images are representative of 3 independent experiments. In each of the columns, the same field (that is, approximately the same population of cells) is followed over time.

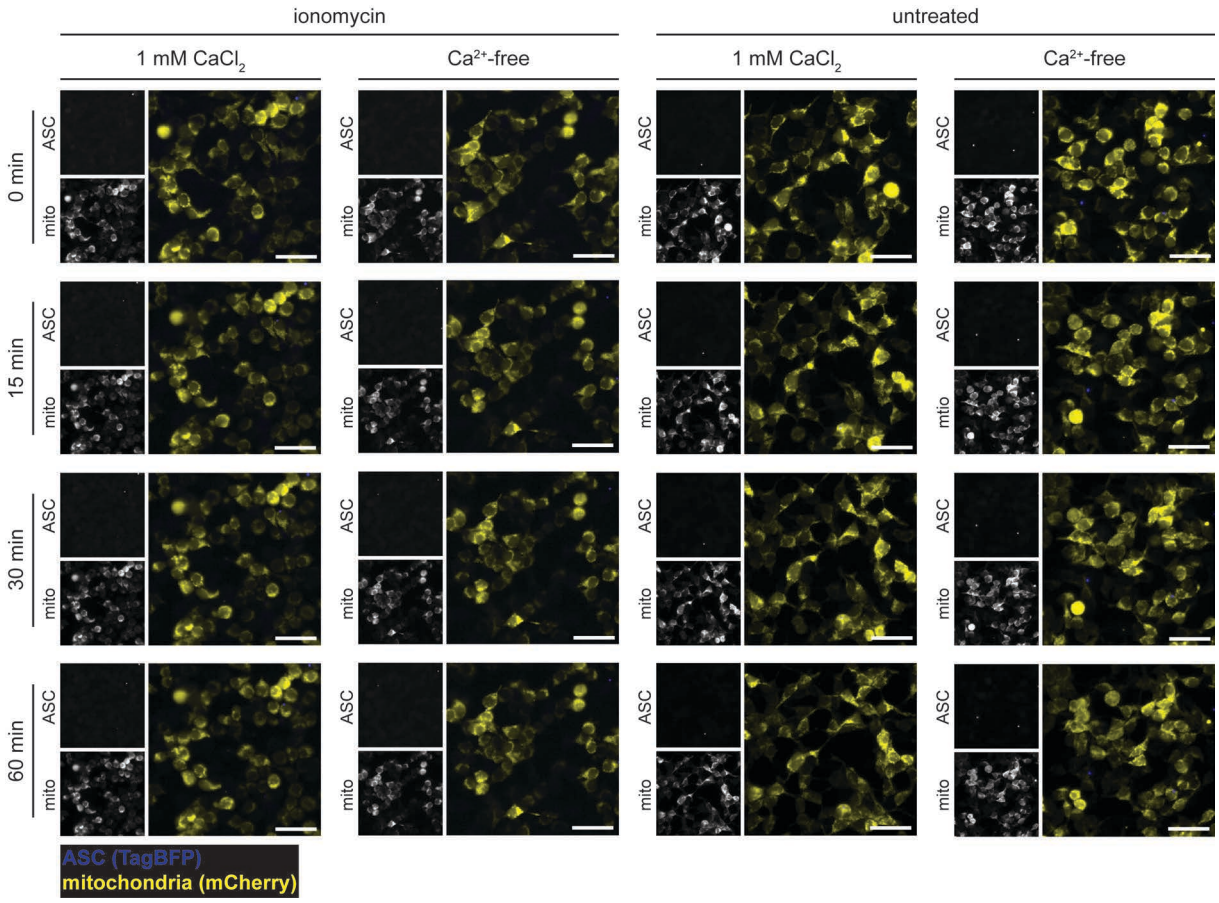

Figure 6.30. Mitochondrial dynamics monitored by mitochondrial matrix-targeted mCherry localization in NLRP10^{mCitrine}/ASC^{TagBFP}/mito^{mCherry} HEK cells treated with ionomycin in the presence of 1 mM $CaCl_2$ or in Ca^{2+}-deficient medium

HEK cells stably overexpressing human NLRP10^{mCitrine}, ASC^{TagBFP}, and the mitochondrial marker mito^{mCherry} were shifted to an extracellular medium consisting of (in mM) 123 NaCl, 5 KCl, 2 $MgCl_2$, 0 or 1 $CaCl_2$, 10 glucose, 10 HEPES, pH 7.4. Next, the cells were left untreated, or were stimulated with ionomycin (10 μM), and live imaging was performed using a widefield fluorescence microscope to capture the mitochondrial dynamics. The time interval between the acquired images was approximately 1 min. For the duration of the experiment, the cells were kept at 37°C in the microscope incubation chamber, but they were **not** perfused with CO_2 (HEPES-based buffers do not require CO_2 perfusion to maintain constant pH). Ionomycin was added to the cells either directly in the microscope incubation chamber immediately after the onset of imaging.
Images are representative of 3 independent experiments. In each of the columns, the same field (that is, approximately the same population of cells) is followed over time. Scale bars correspond to 50 μm.

The leakage of the nuclear and mitochondrial contents was not observed in cells stimulated with nigericin and with poly-(dA:dT). Therefore, the involvement caspase-1 downstream of the inflammasome responses to *m*-3M3FBS and thapsigargin was unlikely to be the mediator of the mitonuclear damage. Nevertheless, I went on to ensure that the observed effects of the *m*-3M3FBS and thapsigargin treatments were not caspase-1-dependent. To this end, I performed live imaging of NLRP3/ASC^{mCerulean} reporter iMac cells[3] overexpressing HMGB1^{mCitrine} (Figure 6.31) or mito^{mCitrine} (Figure

[3] HEK cells do not express caspase-1, so they were not tested in this experiment.

6.32) and stimulated with *m*-3M3FBS, thapsigargin, nigericin, or poly-(dA:dT) in the presence or absence of the caspase-1 inhibitor VX-765.

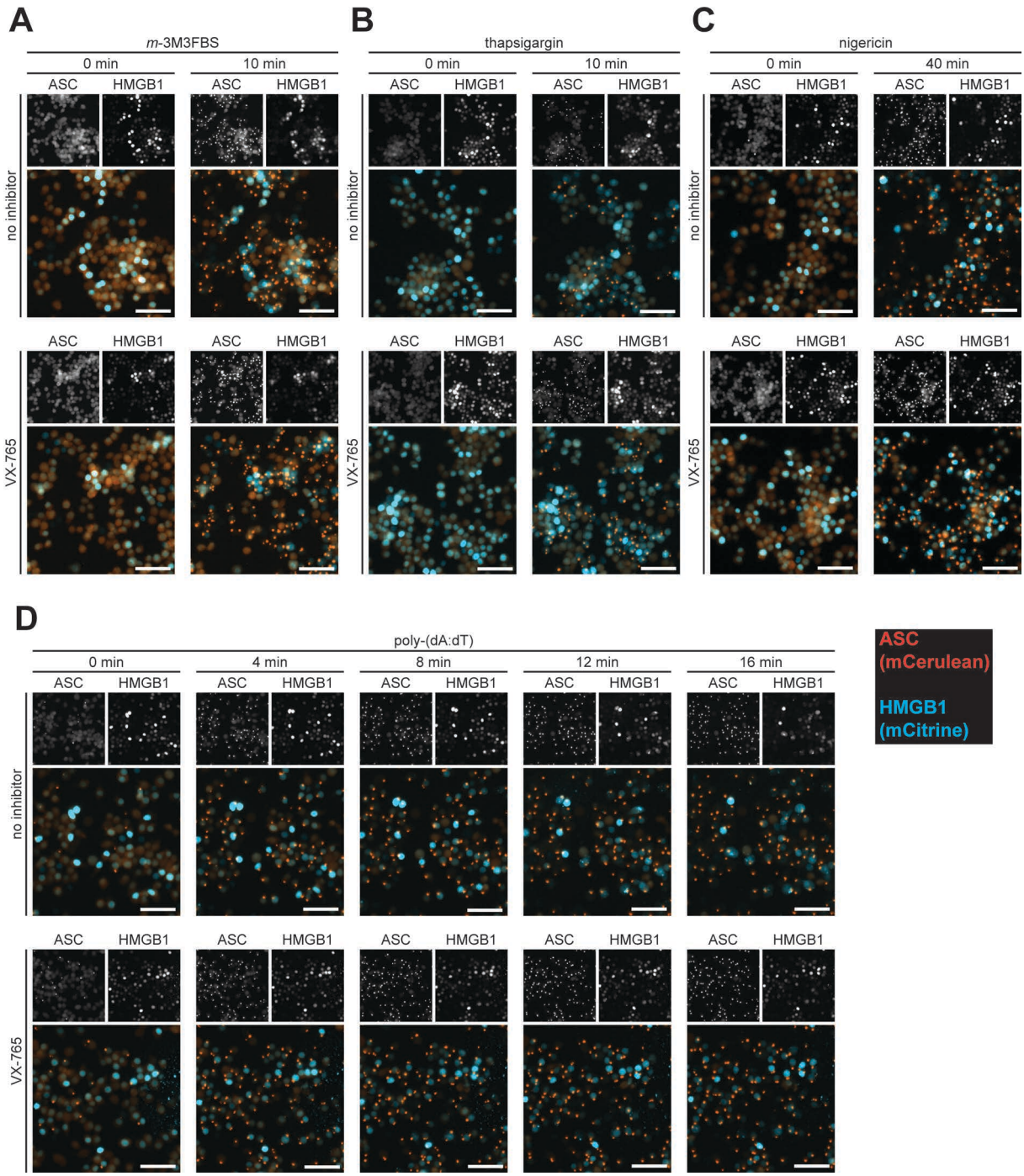

Figure 6.31. Nuclear dynamics monitored by HMGB1 localization in NLRP3/ASC^{mCerulean}/HMGB1^{mCitrine} reporter iMac cells treated with *m*-3M3FBS, thapsigargin, nigericin, or poly-(dA:dT) in the presence or absence of the caspase-1 inhibitor VX-765

A-D: NLRP3/ASC^{mCerulean} reporter iMac cells stably overexpressing the nuclear marker HMGB1^{mCitrine} were shifted to an extracellular medium consisting of (in mM) 123 NaCl, 5 KCl, 2 $MgCl_2$, 1 $CaCl_2$, 10 glucose, 10 HEPES, pH 7.4 in the absence ('no inhibitor') or presence of the caspase-1 inhibitor VX-765 (50 μM). Next, the cells were stimulated with *m*-3M3FBS (85 μM; A), thapsigargin (20 μM; B), nigericin (10 μM; C), or poly-(dA:dT) (2 μg/mL complexed with 5 μL Lipofectamine 2000; D), and live imaging was performed using a widefield fluorescence microscope to capture the nuclear dynamics. The time interval between the acquired images was approximately 1 min (A-C) or 4 min (D). For the duration of the experiment, the cells

were kept at 37°C in the microscope incubation chamber, but they were **not** perfused with CO_2 (HEPES-based buffers do not require CO_2 perfusion to maintain constant pH). The stimuli were added to the cells either directly in the microscope incubation chamber immediately after the onset of imaging (*m*-3M3FBS [A] and nigericin [C]), or they were added to the cells **outside** of the microscope incubation chamber (thapsigargin [B] and poly-(dA:dT) [D]), followed by a brief centrifugation (340 × g at RT for 30 s), after which the imaging was started.
Images are representative of 3 independent experiments. In each of the panels (A-D), the same field (that is, approximately the same population of cells) is followed over time. Scale bars correspond to 50 μm.

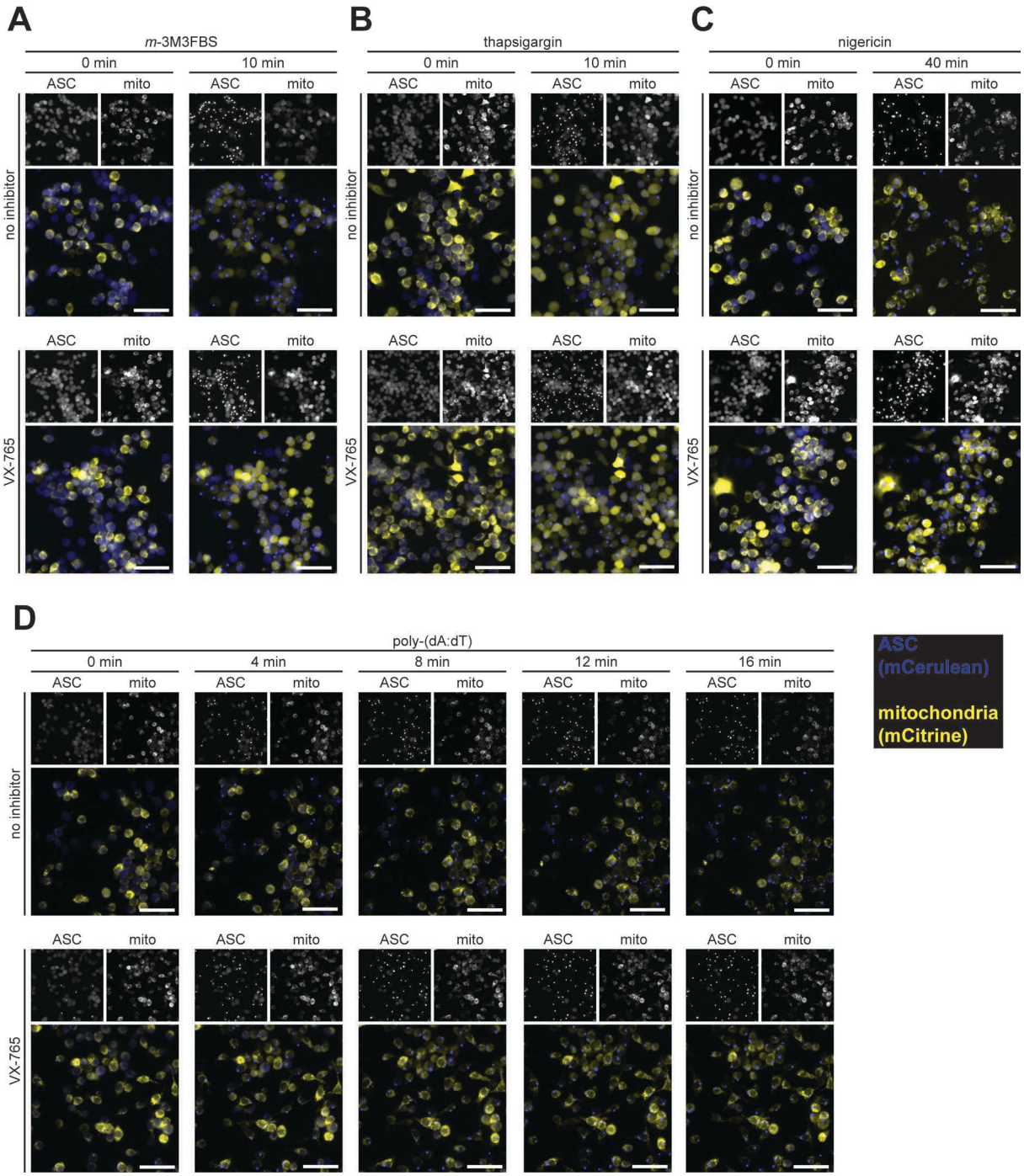

Figure 6.32. Mitochondrial dynamics monitored by localization of mitochondrial matrix-targeted mCitrine in NLRP3/ASC^{mCerulean}/mito^{mCitrine} reporter iMac cells treated with *m*-3M3FBS, thapsigargin, nigericin, or poly-(dA:dT) in the presence or absence of the caspase-1 inhibitor VX-765

◂ **A-D:** NLRP3/ASC^{mCerulean} reporter iMac cells stably overexpressing the mitochondrial marker mito^{mCitrine} were shifted to an extracellular medium consisting of (in mM) 123 NaCl, 5 KCl, 2 $MgCl_2$, 1 $CaCl_2$, 10 glucose, 10 HEPES, pH 7.4 in the absence ('no inhibitor') or presence of the caspase-1 inhibitor VX-765 (50 μM). Next, the cells were stimulated with *m*-3M3FBS (85 μM; A), thapsigargin (20 μM; B), nigericin (10 μM; C), or poly-(dA:dT) (2 μg/mL complexed with 5 μL Lipofectamine 2000; D), and live imaging was performed using a widefield fluorescence microscope to capture the mitochondrial dynamics. The time interval between the acquired images was approximately 1 min (A-C) or 4 min (D). For the duration of the experiment, the cells were kept at 37°C in the microscope incubation chamber, but they were **not** perfused with CO_2 (HEPES-based buffers do not require CO_2 perfusion to maintain constant pH). The stimuli were added to the cells either directly in the microscope incubation chamber immediately after the onset of imaging (*m*-3M3FBS [A] and nigericin [C]), or they were added to the cells **outside** of the microscope incubation chamber (thapsigargin [B] and poly-(dA:dT) [D]), followed by a brief centrifugation (340 × g at RT for 30 s), after which the imaging was started.
Images are representative of 3 independent experiments. In each of the panels (A-D), the same field (that is, approximately the same population of cells) is followed over time. Scale bars correspond to 50 μm.

Consistent with my previous observations, *m*-3M3FBS and thapsigargin caused a rapid HMGB1 leakage to the cytosol (Figure 6.31 A, B) and a loss of mitochondrial localization of the mito^{mCitrine} protein (Figure 6.32 A, B). The nigericin and poly-(dA:dT) stimulations did not lead to these effects (Figures 6.31 C, D and 6.32 C, D). VX-765 did not suppress the *m*-3M3FBS- and thapsigargin-induced mitonuclear damage, indicating that it is not mediated by caspase-1.

The changes observed in the mitochondrial and nuclear compartments in *m*-3M3FBS- and thapsigargin-treated cells could not be attributed to PKC activation (downstream of the *m*-3M3FBS-PLC axis). The PKC activators PMA and bryostatin 1 did not cause a cytosolic leakage of the mitochondrial or nuclear contents in HEK cells (Supplementary Figure S17) and in macrophages (Supplementary Figure S18) overexpressing the mitochondrial or nuclear reporter constructs (mito$^{mCitrine/mCherry}$ and HMGB1$^{mCitrine/mCherry}$).

6.14. No evidence that the nuclear disruption is a mediator in the AIM2 and NLRP10 activation by *m*-3M3FBS/thapsigargin

Two arguments support the notion that the mitochondrial damage rather than the nuclear contents egress is the cause of the inflammasome activation by *m*-3M3FBS and thapsigargin. First, NLRP10 translocates to the mitochondria, not to the nucleus, in *m*-3M3FBS- and thapsigargin-treated cells. Secondly, triggering the nuclear contents leakage by ionomycin does not activate the AIM2 and NLRP10 inflammasomes.

However compelling these observations may be, they do not provide sufficient evidence to fully exclude the role of the nuclei in AIM2 and NLRP10 activations. Below I will present further experimental evidence suggesting that the nuclear damage is not involved in the inflammasome responses under investigation[4]. To examine the significance of the nuclear damage for the inflammasome responses to *m*-3M3FBS and thapsigargin I applied two approaches: pharmacological perturbation of the nucleocytosolic transport in the presence or absence of the AIM2/NLRP10 activators, and pharmacological perturbation of the nuclear barrier.

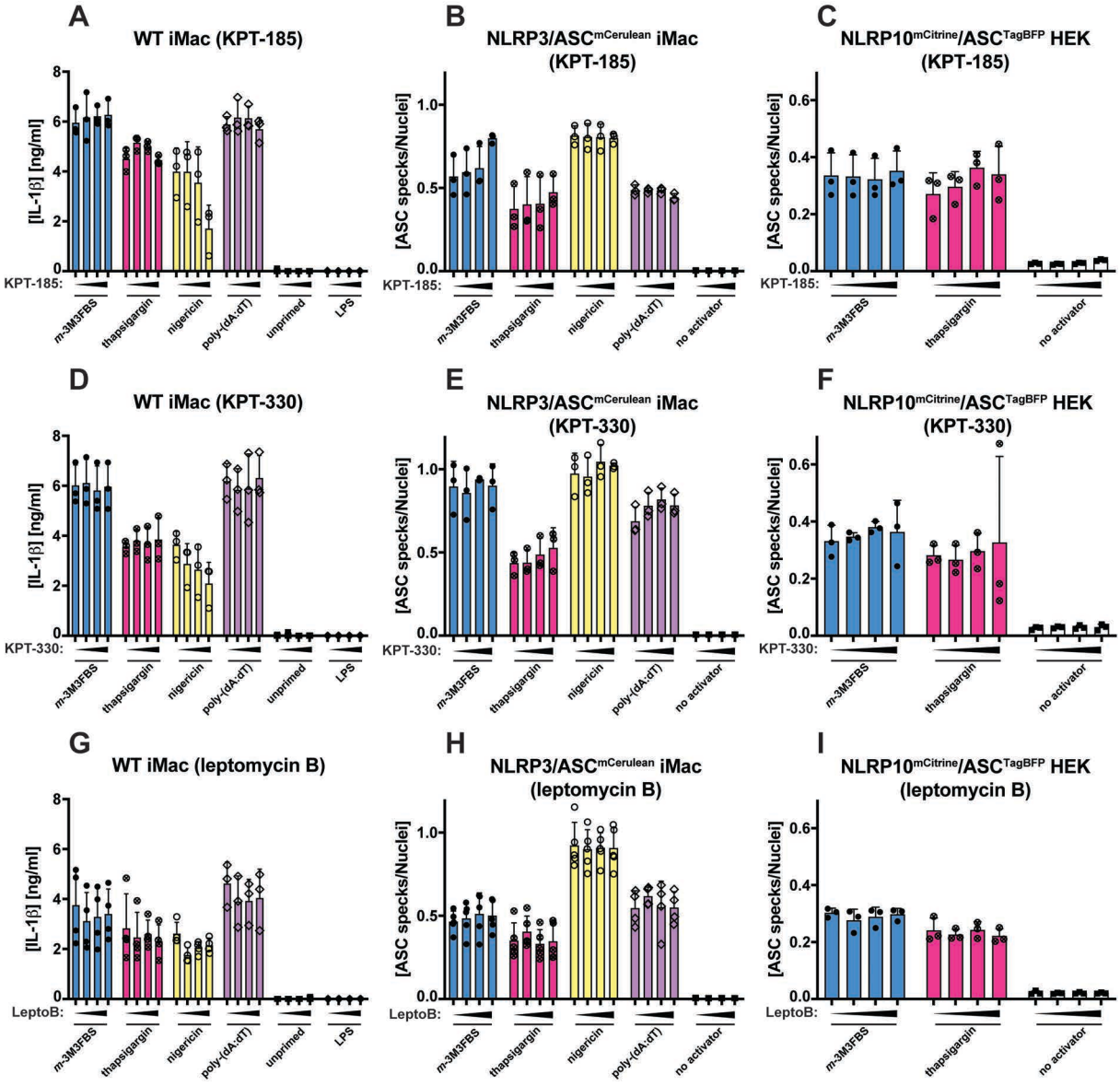

Figure 6.33. Influence of the nuclear export inhibitors KPT-185, KPT-330 (selinexor), and leptomycin B on the inflammasome responses to *m*-3M3FBS, thapsigargin, nigericin, and poly-(dA:dT)

[4] The formal proof that the mitochondria are responsible for the AIM2 activation by *m*-3M3FBS and thapsigargin will be the topic of Chapter 8 of my Thesis.

◂ **A-I:** LPS-primed (200 ng/mL, 2 h) WT iMac cells (A, D, G), NLRP3/ASC^{mCerulean} reporter iMac cells (B, E, H), and NLRP10^{mCitrine}/ASC^{TagBFP} HEK cells (C, F, I) were treated for 10 min with KPT-185 (0, 5, 10, or 50 μM; A-C), KPT-330/selinexor (0, 5, 10, or 50 μM; D-F), or leptomycin B (LeptoB; 0, 10, 20, or 40 ng/mL; G-I) and then subjected to the inflammasome activators *m*-3M3FBS (85 μM), thapsigargin (20 μM), nigericin (10 μM) or poly-(dA:dT) (2 μg/mL complexed with 5 μL Lipofectamine 2000) in an extracellular medium consisting of (in mM) 123 NaCl, 5 KCl, 2 $MgCl_2$, 1 $CaCl_2$, 10 glucose, 10 HEPES, pH 7.4. The LPS (A, D, G) and unprimed (A-I) controls were subjected to medium alone. Immediately after addition of inflammasome activators, the plates were centrifuged at 340 × g for 5 min (RT). After 30 min (C, F, I) or 60 min (A, B, D, E, G, H), the supernatants were collected and IL-1β concentrations were measured by HTRF (A, D, G) or the cells were fixed with 4% formaldehyde, counterstained with the nuclear dye DRAQ5 (5 μM) and imaged using a widefield fluorescence microscope (B, C, E, F, H, I).
The results are plotted as means from 3 (A-F, I, and poly-(dA:dT) in panel G) or 4 (G [except the stimulation with poly-(dA:dT)] and H) independent experiments performed in technical duplicate. Error bars represent SD. Individual data points represent means of the technical duplicate values from each of the independent experiments.

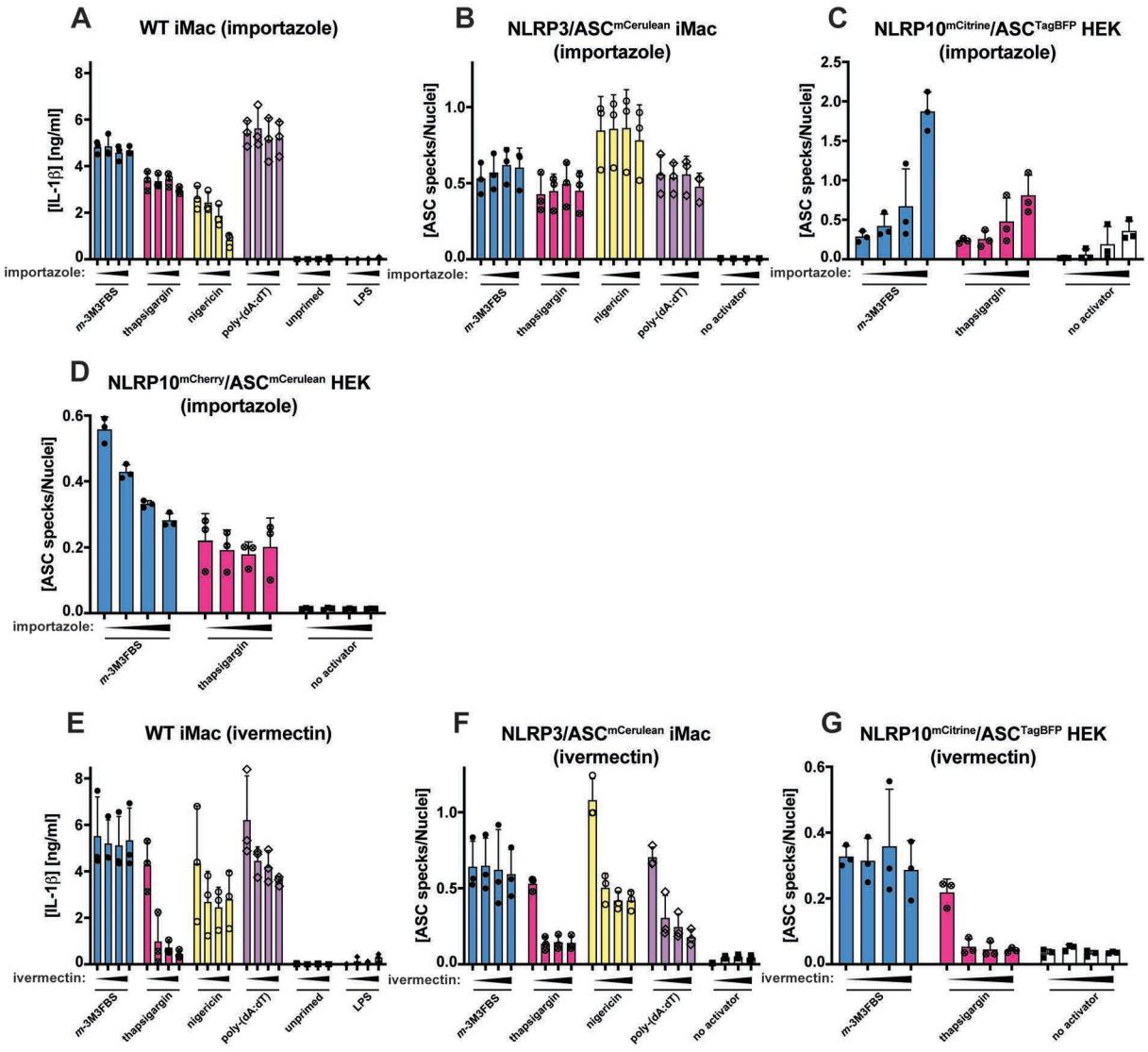

Figure 6.34. Influence of the nuclear import inhibitors importazole and ivermectin on the inflammasome responses to *m*-3M3FBS, thapsigargin, nigericin, and poly-(dA:dT)
A-G: LPS-primed (200 ng/mL, 2 h) WT iMac cells (A, E), NLRP3/ASC^{mCerulean} reporter iMac cells (B, F), NLRP10^{mCitrine}/ASC^{TagBFP} HEK cells (C, G), and NLRP10^{mCherry}/ASC^{mCerulean} HEK cells (D) were treated for 10 min with importazole (0, 10, 25, or 50 μM; A-D) or ivermectin (0, 25, 50, or 100 μM; E-G) and then subjected to the inflammasome activators *m*-3M3FBS (85 μM), thapsigargin (20 μM), nigericin (10 μM) or poly-(dA:dT) (2 μg/mL complexed with 5 μL Lipofectamine 2000) in an extracellular medium consisting

of (in mM) 123 NaCl, 5 KCl, 2 $MgCl_2$, 1 $CaCl_2$, 10 glucose, 10 HEPES, pH 7.4. The LPS (A, E) and unprimed (A-G) controls were subjected to medium alone. Immediately after addition of inflammasome activators, the plates were centrifuged at 340 × g for 5 min (RT). After 30 min (C, D, G) or 60 min (A, B, E, F), the supernatants were collected and IL-1β concentrations were measured by HTRF (A, E) or the cells were fixed with 4% formaldehyde, counterstained with the nuclear dye DRAQ5 (5 μM) and imaged using a widefield fluorescence microscope (B-D, F, G).
The results are plotted as means from 3 independent experiments performed in technical duplicate. Error bars represent SD. Individual data points represent means of the technical duplicate values from each of the independent experiments.

I tested whether three inhibitors of nuclear export (KPT-185, KPT-330, and leptomycin B; Figure 6.33 and Supplementary Figure S19) and two – of nuclear import (importazole and ivermectin; Figure 6.34) could trigger the inflammasome activation or block the AIM2/NLRP10 responses to *m*-3M3FBS/thapsigargin. The nuclear export inhibitors were not inflammasome activators by themselves and had essentially no impact on the inflammasome responses to any of the tested stimuli (Figure 6.33 and Supplementary Figure S19). Among the nuclear import inhibitors, importazole had a slight inhibitory effect on the NLRP3 activation with nigericin on the level of IL-1β secretion (Figure 6.34 A) but not ASC speck formation (Figure 6.34 B), and it was a weak inhibitor of the *m*-3M3FBS-driven NLRP10 activation in NLRP10^{mCherry}/ASC^{mCerulean} reporter HEK cells (Figure 6.34 D). Importazole also exhibited strong autofluorescence in the BFP channel (Figure 6.34 C), so its effect could only be assessed in NLRP3/ASC^{mCerulean} reporter iMac cells and NLRP10^{mCherry}/ASC^{mCerulean} HEK cells.

Ivermectin was a strong inhibitor of the thapsigargin-induced AIM2/NLRP10 activation and it also partially inhibited the nigericin- and poly-(dA:dT)-induced inflammasome responses (Figure 6.34 E-G). Because of the multiple reported targets of ivermectin, it is difficult to draw conclusions from these observations in the absence of clear effects of the other tested nuclear transport inhibitors. Collectively, my results indicate that 'canonical' nuclear export is not required for the AIM2 and NLRP10 activations by *m*-3M3FBS and thapsigargin, but they do not provide a definitive answer as to the involvement of the nuclear import in this process.

To examine the potential role of the nuclear barrier breach in the inflammasome activation, I exploited the fact that ionomycin in the presence of extracellular Ca^{2+} was capable of eliciting the nuclear contents leakage. I bathed NLRP10^{mCitrine}/ASC^{TagBFP} HEK cells, NLRP3/ASC^{mCerulean} reporter iMac cells, and LPS-primed WT iMac cells in buffers containing a range of $CaCl_2$ concentrations (0-1 mM) in the presence or absence of

ionomycin or *m*-3M3FBS. While *m*-3M3FBS triggered AIM2 (Figure 6.35 A, B) and NLRP10 (Figure 6.35 C) responses at all tested extracellular Ca^{2+} concentrations, ionomycin was fully incapable of inducing inflammasome activation, consistent with my earlier results (Figure 6.18). Importantly, both *m*-3M3FBS and ionomycin treatments abolished the nuclear exclusion of NLRP10 (Supplementary Figure S20): *m*-3M3FBS at all tested extracellular $CaCl_2$ concentrations and ionomycin at extracellular $CaCl_2$ concentrations above 500 μM. This observation indicates that conditions permissive for nuclear content leakage and NLRP10 nuclear influx are not sufficient for inflammasome activation. Such conclusion provides an argument against the involvement of the nuclei in the AIM2 and NLRP10 responses to *m*-3M3FBS and thapsigargin.

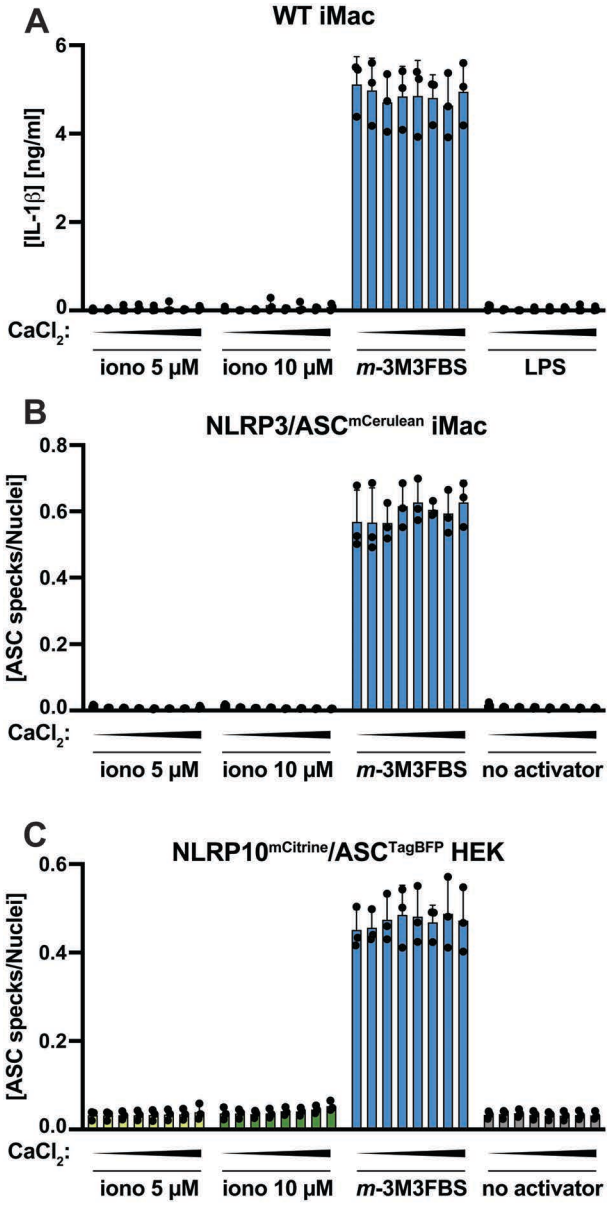

Figure 6.35. Ionomycin-mediated Ca^{2+} delivery does not trigger inflammasome responses, regardless of the extracellular Ca^{2+} concentration

◂ **A-C:** LPS-primed (200 ng/mL, 2 h) WT iMac cells (A), NLRP3/ASC^{mCerulean} reporter iMac cells (B), and NLRP10^{mCitrine}/ASC^{TagBFP} HEK cells (C) were shifted to extracellular media consisting of (in mM) 123 NaCl, 5 KCl, 2 $MgCl_2$, 10 glucose, 10 HEPES pH 7.4 with the addition of 0, 62.5, 125, 250, 500, 600, 750, or 1000 μM $CaCl_2$. Then the cells were stimulated with ionomycin (iono; 5 or 10 μM) or m-3M3FBS (85 μM). The LPS (A) and untreated (B, C) controls were subjected to media alone. Immediately after addition of the stimuli, the plates were centrifuged at 340 × g for 5 min (RT). After 60 min, the supernatants were collected and IL-1β concentrations were measured by HTRF (A) or the cells were fixed with 4% formaldehyde, counterstained with the nuclear dye DRAQ5 (5 μM) and imaged using a widefield fluorescence microscope (B, C).
The results are plotted as means from 3 independent experiments performed in technical triplicate. Error bars represent SD. Individual data points represent means of the technical triplicate values from each of the independent experiments.

A recent study on the neutrophil extracellular trap (NET) formation suggested that the generation of these structures relies on the molecular network involved in mitosis in proliferating cells (Amulic et al., 2017). Of particular relevance to my observations was the reported disassembly of the nuclear envelope. To test whether conditions promoting NET formation could trigger the AIM2 or NLRP10 inflammasome responses in NLRP10^{mCitrine}/ASC^{TagBFP} HEK cells, NLRP3/ASC^{mCerulean} reporter iMac cells, or LPS-primed WT iMac cells, I subjected these cells to combinations of stimuli known to trigger NET formation in the presence or absence of the NLRP3 inhibitor CRID3 and measured IL-1β (Figure 6.36 A, B) or imaged ASC specks (Figure 6.36 C-F) to assess the degree of the inflammasome response. None of the tested NET-inducing treatments led to inflammasome activation in the examined cell lines, providing a further argument against the involvement of the nuclei in the AIM2 and NLRP10 activations.

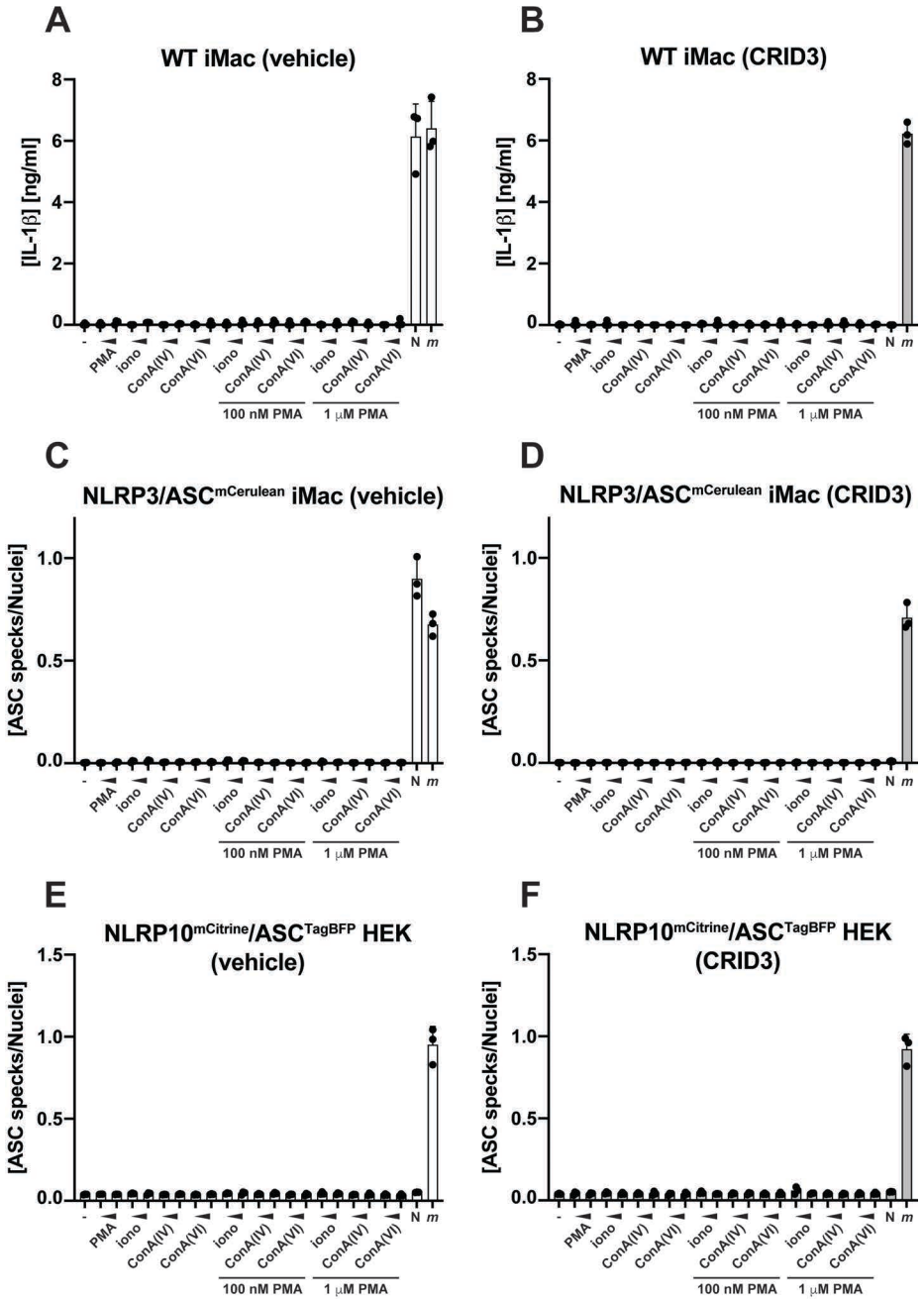

Figure 6.36. Neutrophil extracellular trap (NET) formation-inducing combinations of stimuli are not inflammasome activators

A-F: LPS-primed (200 ng/mL, 2 h) WT iMac cells (A, B), NLRP3/ASC^{mCerulean} reporter iMac cells (C, D), and NLRP10^{mCitrine}/ASC^{TagBFP} HEK cells (E, F) were shifted to OptiMEM supplemented with 1% FBS and 5 μM CRID3 (B, D, F) or vehicle (ethanol; A, C, E). Then the cells were treated for 4 h with stimuli or combinations of stimuli proposed to trigger NET formation in neutrophils: PMA (100 nM or 1 μM), ionomycin (iono; 5 or 10 μM), concanavalin A type IV (ConA(IV); 50 or 100 μg/mL), concanavalin A type VI (ConA(VI); 50 or 100 μg/mL), or combinations of PMA (100 nM or 1 μM) with the indicated stimuli. 60 min before the completion of the experiment, the nigericin (N; 10 μM) and *m*-3M3FBS (*m*; 85 μM) control cells were shifted to an extracellular medium consisting of (in mM) 123 NaCl, 5 KCl, 2 $MgCl_2$, 1 $CaCl_2$, 10 glucose, 10 HEPES pH 7.4 with (B, D, F) or without (vehicle – ethanol; A, C, E) 5 μM CRID3 and they were stimulated with nigericin or *m*-3M3FBS. The untreated (-) were subjected to OptiMEM with 1% FBS. At the completion of the experiment, the supernatants were collected and IL-1β concentrations were measured by HTRF (A, B) or the cells were fixed with 4% formaldehyde, counterstained with the nuclear dye DRAQ5 (5 μM) and imaged using a widefield fluorescence microscope (C-F).

The results are plotted as means from 3 independent experiments performed in technical duplicate. Error bars represent SD. Individual data points represent means of the technical duplicate values from each of the independent experiments.

Finally, a study by Di Micco et al. (2016) demonstrated that several human immunodeficiency virus (HIV) protease inhibitors, chiefly nelfinavir, ritonavir and lopinavir, disrupt the nuclear envelope leading to activation of the AIM2 inflammasome[5]. This was suggested to rely on the nuclear DNA sensing by AIM2. I tested whether the AIM2-triggering HIV protease inhibitors as well as doxorubicin, a nuclei-disrupting antitumor drug (Sardão et al., 2008), could cause inflammasome activation (IL-1β secretion and ASC speck formation) in ASC fluorescent reporter HEK cells with or without the NLRP10 overexpression cassette, NLRP3/ASC^{mCerulean} reporter iMac cells, and LPS-primed immortalized macrophages (Supplementary Figures S21 and S22).

Among the tested treatments, only doxorubicin led to a robust IL-1β secretion (Supplementary Figure S21) and ASC speck formation (Supplementary Figure S22 A) in macrophages. Importantly, this effect was observed regardless of the genotype of the tested cells, suggesting that there may be several redundant pathways through which inflammasomes could sense the doxorubicin-induced damage. Neither the HIV protease inhibitors, nor doxorubicin could elicit ASC speck formation in HEK cells in a manner attributable to NLRP10 (Supplementary Figure S22 B-D), further suggesting that nuclear damage is probably not involved in the AIM2/NLRP10 responses to *m*-3M3FBS and thapsigargin. Pitstop-2, another compound reported to disrupt the nuclear permeability barrier (Liashkovich et al., 2015), was also not an inflammasome activator in murine macrophages (Supplementary Figure S11)[6]. Together, these data suggest that the *m*-3M3FBS- and thapsigargin-induced nuclear permeability barrier disruption is not involved in the AIM2 and NLRP10 inflammasome responses.

[5] Conversely, this effect was not observed for the HIV protease inhibitors amprenavir and atazanavir (Di Micco et al., 2016).

[6] Pitstop-2 autofluorescence in the BFP channel did not allow for obtaining interpretable results in NLRP10^{mCitrine}/ASC^{TagBFP} reporter HEK cells (Supplementary Figure S12) and I did not proceed to test this treatment in other fluorescent reporter cells.

6.15. Cyclosporin A and non-immunosuppressive CsA analogs alisporivir/Debio025 and NIM811 selectively inhibit the thapsigargin-induced AIM2 and NLRP10 inflammasome responses

As I found no compelling evidence that the disruption of the nuclear permeability barrier could activate the AIM2 and NLRP10 inflammasomes, I proceeded to examine whether the observed mitochondrial damage could explain the inflammasome activation by *m*-3M3FBS and thapsigargin. The latter of these two compounds is by far better characterized[7]. Thapsigargin is suggested to trigger mitochondrial damage in a manner sensitive to CsA (Korge and Weiss, 1999). CsA is a prolyl isomerase inhibitor known for suppression of two pathways, the activation of the phosphatase calcineurin and the transcription factor nuclear factor of activated T cells (NFAT) through the inhibition of cyclophilin A (PPIA) (Crabtree and Olson, 2002; Emmel et al., 1989; Flanagan et al., 1991; Handschumacher et al., 1984; Rao et al., 1997), and the mPT through the inhibition of mitochondrial cyclophilin (termed cyclophilin F/PPIF or, archaically, cyclophilin D) (Baines et al., 2005; Basso et al., 2005; Nakagawa et al., 2005; Schinzel et al., 2005). I tested whether the inflammasome responses to *m*-3M3FBS, thapsigargin, nigericin, and poly-(dA:dT) are inhibited by CsA (Figure 6.37 A-C), as well as two specific inhibitors of the calcineurin/NFAT pathway that do not target cyclophilin F (Marton et al., 2015): FK506 (Figure 6.37 D-F) and ascomycin (Figure 6.37 G-H). Briefly, I pre-treated (10 min) LPS-primed WT iMac cells, NLRP3/ASC^{mCerulean} reporter iMac cells, and NLRP10^{mCitrine}/ASC^{TagBFP} HEK cells with increasing doses of the cyclophilin inhibitors, followed by stimulation with inflammasome agonists and assessment of the degree of inflammasome activation by measurement of secreted IL-1β concentrations and imaging of ASC specks.

[7] Apart from the four possibly plagiarized studies (Chen, 2014; Fang et al., 2009; Liu, 2013; Tsai, 2010), there are – until now – no serious reports linking *m*-3M3FBS stimulation to mitochondrial stress.

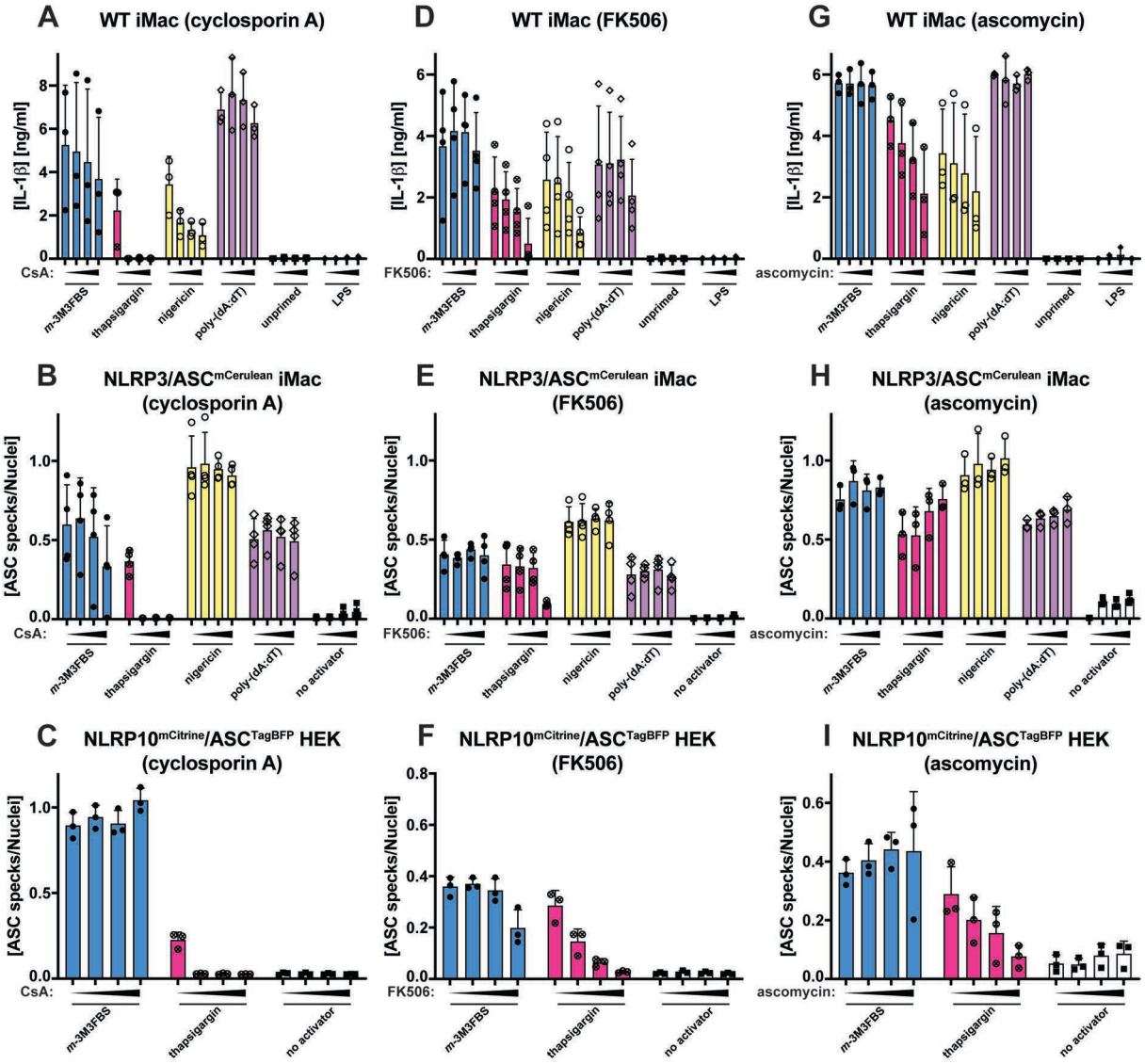

Figure 6.37. Influence of the cyclophilin (prolyl isomerase) inhibitors cyclosporin A, FK506, and ascomycin on the inflammasome responses to *m*-3M3FBS, thapsigargin, nigericin, and poly-(dA:dT)

A-I: LPS-primed (200 ng/mL, 2 h) WT iMac cells (A, D, G), NLRP3/ASC^{mCerulean} reporter iMac cells (B, E, H), and NLRP10^{mCitrine}/ASC^{TagBFP} HEK cells (C, F, I) were treated for 10 min with cyclosporin A (CsA; 0, 10, 15, or 20 μM; A-C), FK506 (0, 10, 25, or 50 μM; D-F), or ascomycin (0, 10, 25, or 50 μM; G-I) and then subjected to the inflammasome activators *m*-3M3FBS (85 μM), thapsigargin (20 μM), nigericin (10 μM) or poly-(dA:dT) (2 μg/mL complexed with 5 μL Lipofectamine 2000) in an extracellular medium consisting of (in mM) 123 NaCl, 5 KCl, 2 $MgCl_2$, 1 $CaCl_2$, 10 glucose, 10 HEPES, pH 7.4. The LPS (A, D, G) and unprimed (A-I) controls were subjected to medium alone. Immediately after addition of inflammasome activators, the plates were centrifuged at 340 × g for 5 min (RT). After 30 min (C, F, I) or 60 min (A, B, D, E, G, H), the supernatants were collected and IL-1β concentrations were measured by HTRF (A, D, G) or the cells were fixed with 4% formaldehyde, counterstained with the nuclear dye DRAQ5 (5 μM) and imaged using a widefield fluorescence microscope (B, C, E, F, H, I).
The results are plotted as means from 3 (A, C, F-I) or 4 (B, D, E) independent experiments performed in technical duplicate. Error bars represent SD. Individual data points represent means of the technical duplicate values from each of the independent experiments.

The *m*-3M3FBS-induced AIM2 and NLRP10 responses were not sensitive to CsA, FK506, and ascomycin (Figure 6.37). In contrast, the thapsigargin-induced AIM2/NLRP10 activations were completely blocked by all tested CsA concentrations (10-20 μM; Figure

6.37 A-C). FK506 and ascomycin (tested here at 10-50 μM; Figure 6.37 D-I) were much less potent inhibitors of the thapsigargin-mediated AIM2/NLRP10 activation, suggesting that the CsA effect is specific. The CsA sensitivity of the thapsigargin-induced NLRP10 activation was confirmed in NLRP10^{mCherry}/ASC^{mCerulean} reporter HEK cells (Supplementary Figure S23). Collectively, these results indicate that CsA selectively blocks the thapsigargin-, but not *m*-3M3FBS-induced AIM2/NLRP10 responses, and that this effect is likely mediated by the mitochondrial disruption and not by the calcineurin/NFAT pathway.

To validate the finding that CsA inhibits the thapsigargin-induced AIM2/NLRP10 activation through targets linked to the mitochondria and not the calcineurin/NFAT pathway, I tested whether two non-immunosuppressive CsA analogs that do not inhibit the calcineurin/NFAT pathway could block the thapsigargin-induced inflammasome responses. These molecules are NIM811 (Billich et al., 1995) and alisporivir/Debio025 (Paeshuyse et al., 2006), and they were tested here at 5, 10, and 20 μM (Figure 6.38) in LPS-primed WT iMac cells, NLRP3/ASC^{mCerulean} reporter iMac cells, NLRP10^{mCitrine}/ASC^{TagBFP} HEK cells, and NLRP10^{mCherry}/ASC^{mCerulean} HEK cells. Alisporivir/Debio025 led to complete inhibition of the thapsigargin-induced AIM2/NLRP10 activation at concentrations above 10 μM, without affecting the inflammasome activation by other tested stimuli (Figure 6.38 A-D). NIM811 was an even more potent inhibitor of the thapsigargin-elicited response, as it fully inhibited the thapsigargin-induced inflammasome activation at all tested concentrations (Figure 6.38 E-H). Similar to alisporivir/Debio025, NIM811 pre-treatment did not have an impact on the other inflammasome activation pathways tested.

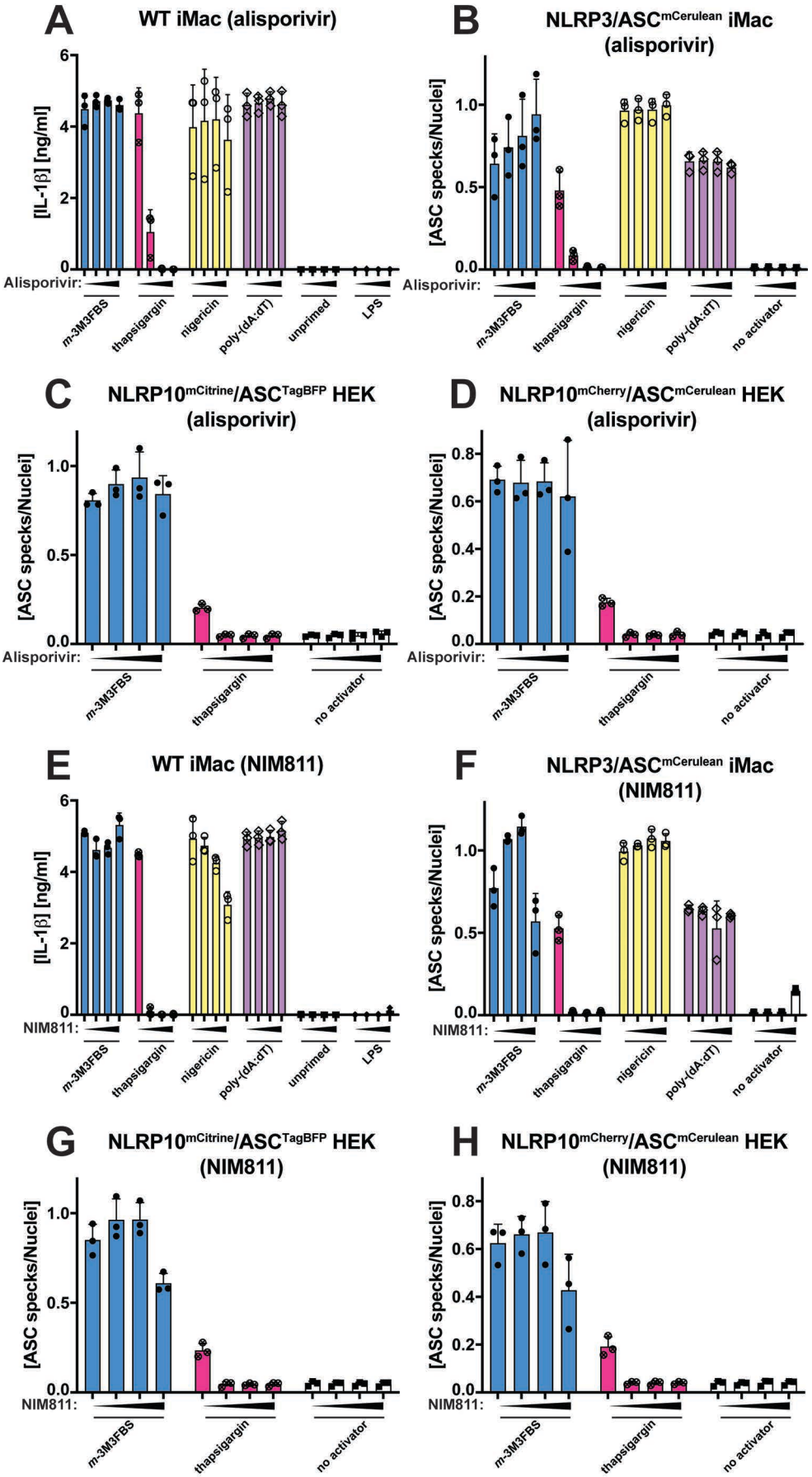

Figure 6.38. Influence of the cyclosporin A non-immunosuppressive analogs alisporivir/Debio025 and NIM811 on the inflammasome responses to *m*-3M3FBS, thapsigargin, nigericin, and poly-(dA:dT)

◂ **A-H:** LPS-primed (200 ng/mL, 2 h) WT iMac cells (A, E), NLRP3/ASC^{mCerulean} reporter iMac cells (B, F), NLRP10^{mCitrine}/ASC^{TagBFP} HEK cells (C, G), and NLRP10^{mCherry}/ASC^{mCerulean} HEK cells (D, H) were treated for 10 min with alisporivir/Debio025 (0, 5, 10, or 20 μM; A-D) or NIM811 (0, 5, 10, or 20 μM; E-H) and then subjected to the inflammasome activators *m*-3M3FBS (85 μM), thapsigargin (20 μM), nigericin (10 μM) or poly-(dA:dT) (2 μg/mL complexed with 5 μL Lipofectamine 2000) in an extracellular medium consisting of (in mM) 123 NaCl, 5 KCl, 2 $MgCl_2$, 1 $CaCl_2$, 10 glucose, 10 HEPES, pH 7.4. The LPS (A, E) and unprimed (A-H) controls were subjected to medium alone. Immediately after addition of inflammasome activators, the plates were centrifuged at 340 × g for 5 min (RT). After 30 min (C, D, G, H) or 60 min (A, B, E, F), the supernatants were collected and IL-1β concentrations were measured by HTRF (A, E) or the cells were fixed with 4% formaldehyde, counterstained with the nuclear dye DRAQ5 (5 μM) and imaged using a widefield fluorescence microscope (B-D, F-H).
The results are plotted as means from 3 independent experiments performed in technical duplicate. Error bars represent SD. Individual data points represent means of the technical duplicate values from each of the independent experiments.

These observations indicate that targeting the thapsigargin-induced mitochondrial disruption can effectively block the AIM2 and NLRP10 inflammasome responses to this molecule. Importantly, the *m*-3M3FBS-driven AIM2/NLRP10 activation was not affected by CsA, NIM811, and alisporivir/Debio025. This suggests that the mechanisms by which *m*-3M3FBS and thapsigargin elicit mitochondrial damage may be distinct, at least at the pharmacological level.

I next examined whether the CsA-mediated inhibition of the thapsigargin-induced inflammasome activation coincides with an observable mitoprotective effect at the level of the mitochondrial matrix-targeted fluorescent protein leakage. In addition, I tested whether CsA could prevent the nuclear contents leakage in thapsigargin-treated cells. To this end, I performed live imaging of inflammasome activator-stimulated NLRP10^{mCitrine}/ASC^{TagBFP}/mito^{mCherry} reporter HEK cells (Figure 6.39), NLRP3/ASC^{mCerulean}/mito^{mCitrine} reporter iMac cells (Figure 6.40), NLRP10^{mCitrine}/ASC^{TagBFP}/HMGB1^{mCherry} reporter HEK cells (Figure 6.41), and NLRP3/ASC^{mCerulean}/HMGB1^{mCitrine} reporter iMac cells (Figure 6.42) in the presence or absence of CsA.

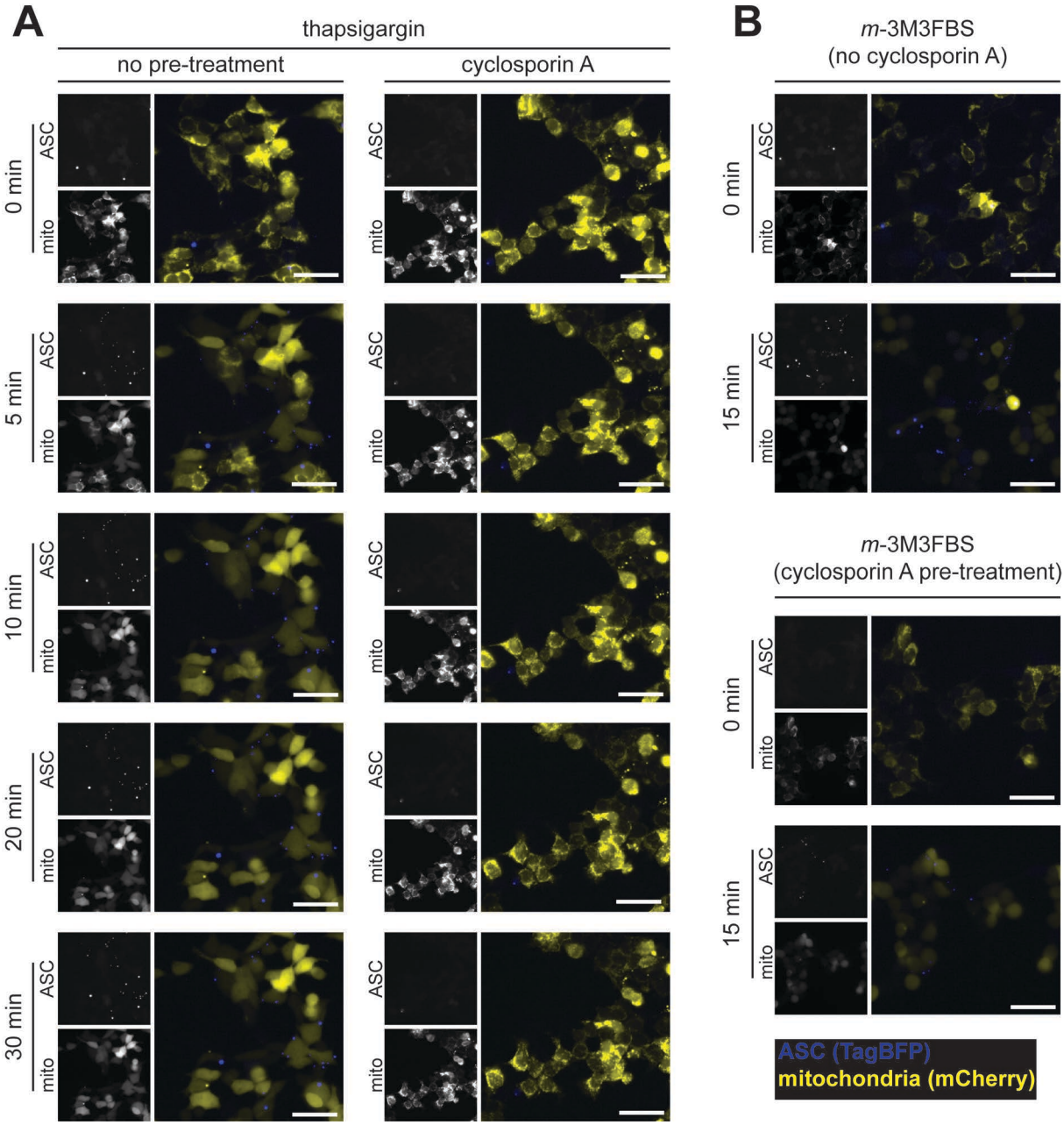

Figure 6.39. Impact of cyclosporin A on the *m*-3M3FBS- and thapsigargin-elicited mitochondrial damage and ASC speck formation in NLRP10^{mCitrine}/ASC^{TagBFP}/mito^{mCherry} reporter HEK cells

A-B: HEK cells stably overexpressing human NLRP10^{mCitrine}, ASC^{TagBFP}, and the mitochondrial marker mito^{mCherry} were shifted to an extracellular medium consisting of (in mM) 123 NaCl, 5 KCl, 2 $MgCl_2$, 1 $CaCl_2$, 10 glucose, 10 HEPES, pH 7.4, with or without cyclosporin A (15 μM). Next, the cells were stimulated with thapsigargin (20 μM; A) or *m*-3M3FBS (85 μM; B), and live imaging was performed using a widefield fluorescence microscope to capture the mitochondrial dynamics. The time interval between the acquired images was approximately 1 min. For the duration of the experiment, the cells were kept at 37°C in the microscope incubation chamber, but they were **not** perfused with CO_2 (HEPES-based buffers do not require CO_2 perfusion to maintain constant pH). The stimuli were added to the cells either directly in the microscope incubation chamber immediately after the onset of imaging (*m*-3M3FBS [B]), or they were added to the cells **outside** of the microscope incubation chamber (thapsigargin [A]), followed by a brief centrifugation (340 × g at RT for 30 s), after which the imaging was started.

Images are representative of 3 independent experiments. In each of the panels (A, B), the same field (that is, approximately the same population of cells) is followed over time. Scale bars correspond to 50 μm.

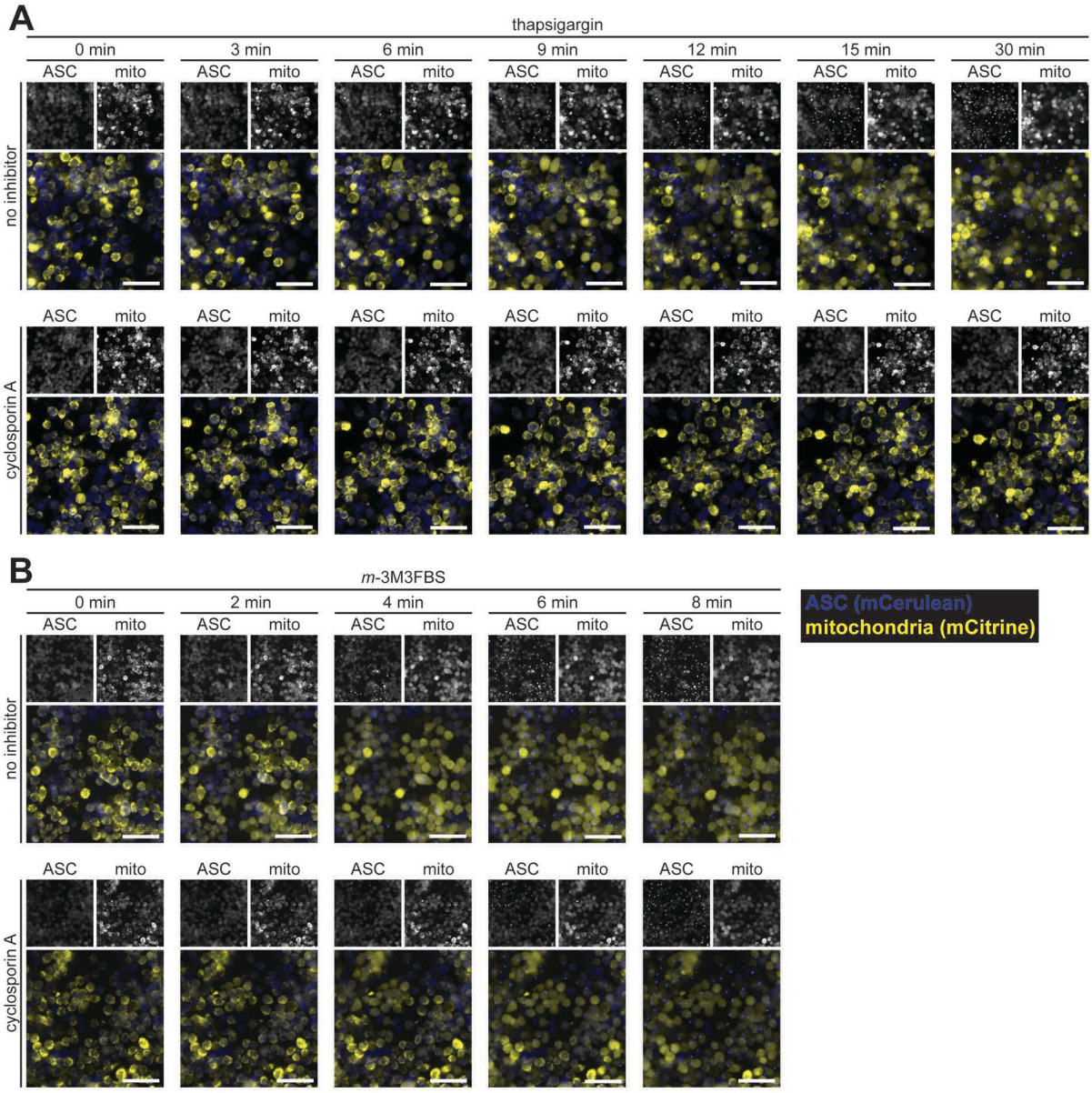
A
thapsigargin
0 min
3 min
6 min
9 min
12 min
15 min
30 min
ASC
mito
no inhibitor
cyclosporin A
B
m-3M3FBS
2 min
4 min
6 min
8 min
ASC (mCerulean)
mitochondria (mCitrine)

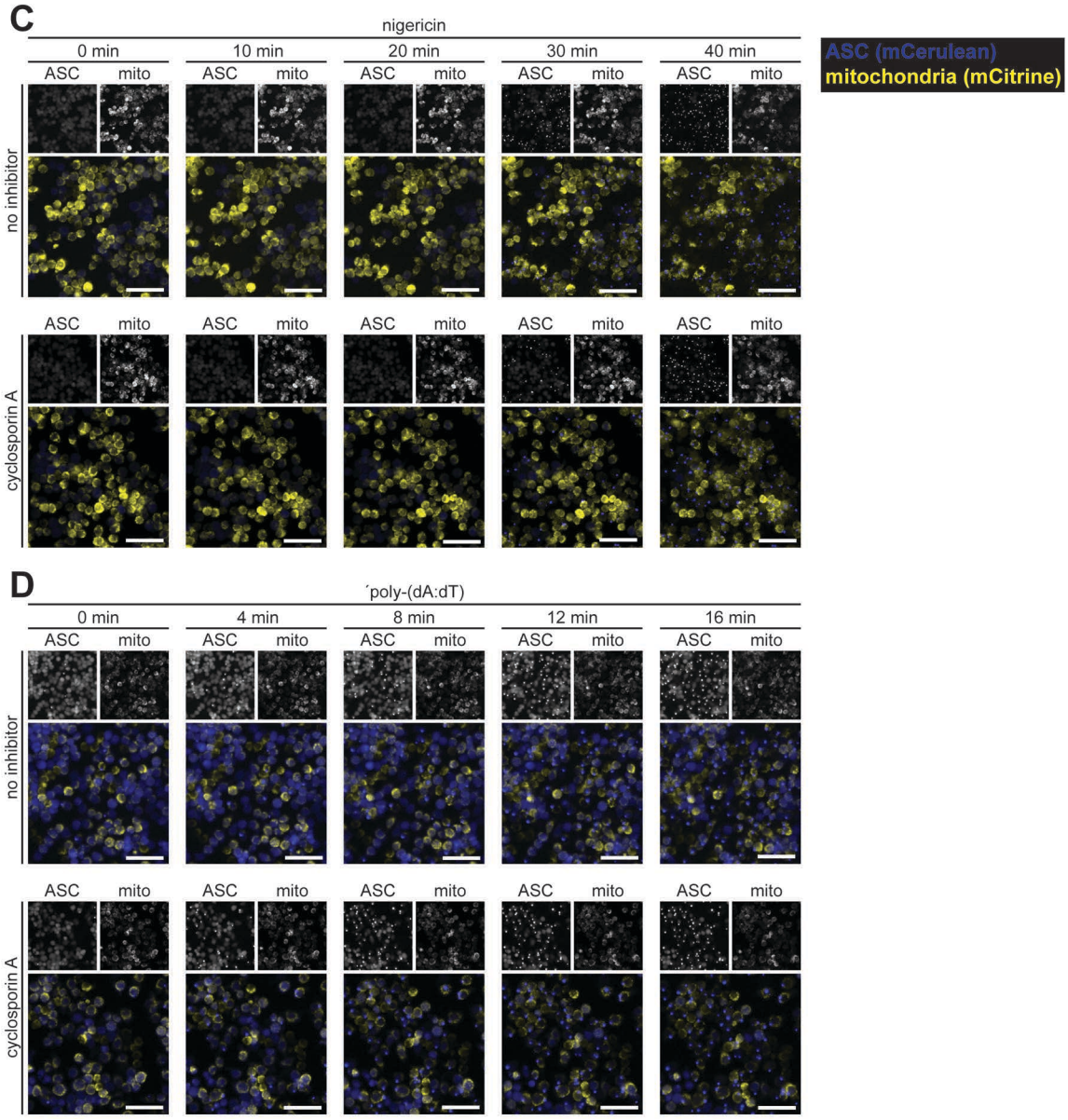

Figure 6.40 (this and previous page). Impact of cyclosporin A on the *m*-3M3FBS- and thapsigargin-elicited mitochondrial damage and ASC speck formation in NLRP3/ASC^{mCerulean}/mito^{mCitrine} reporter iMac cells

A-D: NLRP3/ASC^{mCerulean} reporter iMac cells stably overexpressing the mitochondrial marker mito^{mCitrine} were shifted to an extracellular medium consisting of (in mM) 123 NaCl, 5 KCl, 2 $MgCl_2$, 1 $CaCl_2$, 10 glucose, 10 HEPES, pH 7.4 with or without cyclosporin A (15 μM). Next, the cells were stimulated with thapsigargin (20 μM; A), *m*-3M3FBS (85 μM; B), nigericin (10 μM; C), or poly-(dA:dT) (2 μg/mL complexed with 5 μL Lipofectamine 2000; D), and live imaging was performed using a widefield fluorescence microscope to capture the mitochondrial dynamics. The time interval between the acquired images was approximately 1 min (A-C) or 4 min (D). For the duration of the experiment, the cells were kept at 37°C in the microscope incubation chamber, but they were **not** perfused with CO_2 (HEPES-based buffers do not require CO_2 perfusion to maintain constant pH). The stimuli were added to the cells either directly in the microscope incubation chamber immediately after the onset of imaging (*m*-3M3FBS [B] and nigericin [C]), or they were added to the cells **outside** of the microscope incubation chamber (thapsigargin [A] and poly-(dA:dT) [D]), followed by a brief centrifugation (340 × g at RT for 30 s), after which the imaging was started.
Images are representative of 3 independent experiments. In each of the panels (A-D), the same field (that is, approximately the same population of cells) is followed over time. Scale bars correspond to 50 μm.

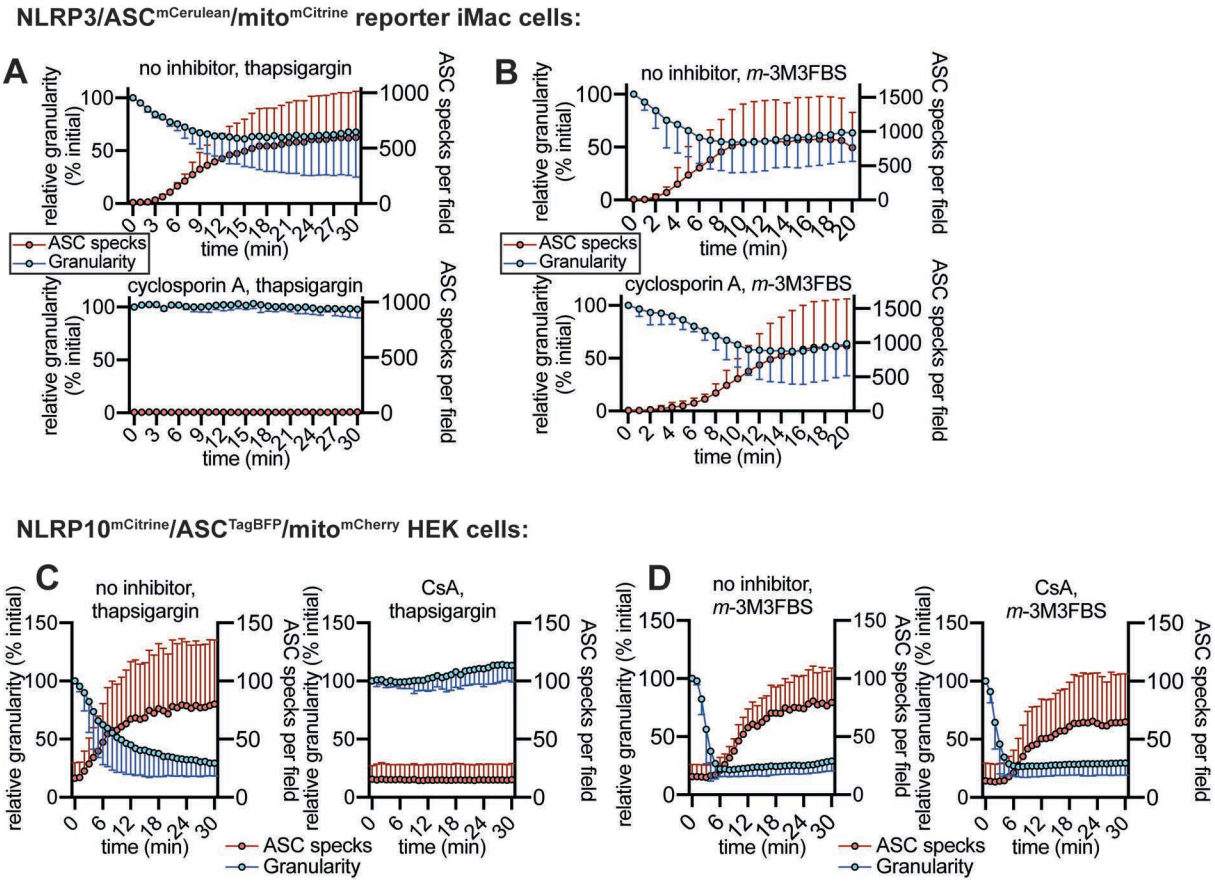

Figure 6.39/40Q. Quantifications of the granularity of the mitochondrial signal in Figures 6.39 and 6.40 A, B

A, B: Quantifications of the signals presented in Figure 40, panels A and B. Granularity of the mitochondrial matrix-targeted fluorescent protein signal was calculated as a proxy for the mitochondrial integrity. High granularity values correlate with the intact status of the mitochondria, while a decrease in granularity correlates with the cytosolic dissipation of the mitochondrial fluorescence signal. The initial granularity value was taken as 100% for the purpose of signal normalization. The numbers of ASC specks per imaging field were treated as absolute values and no normalization has been performed. The data points are means from 3-6 time-lapse recordings per condition, collected over 3 independent experiments. The error bars represent SD.

C, D: Quantifications of the signals presented in Figure 6.39. Granularity of the mitochondrial matrix-targeted fluorescent protein signal was calculated as a proxy for the mitochondrial integrity. High granularity values correlate with the intact status of the mitochondria, while a decrease in granularity correlates with the cytosolic dissipation of the mitochondrial fluorescence signal. The initial granularity value was taken as 100% for the purpose of signal normalization. The numbers of ASC specks per imaging field were treated as absolute values and no normalization has been performed. The data points are means from 3-6 time-lapse recordings per condition, collected over 3 independent experiments. The error bars represent SD.

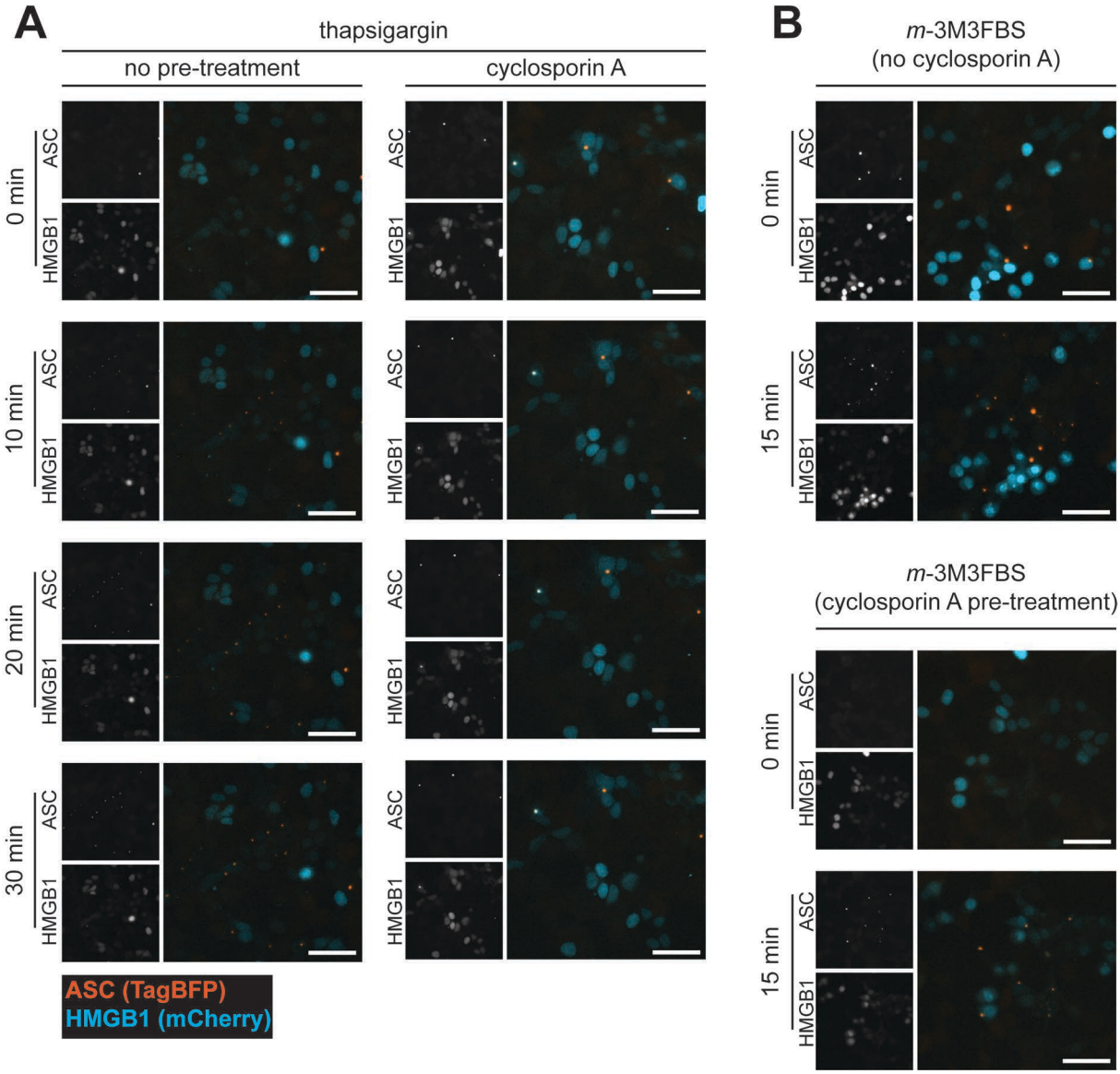

Figure 6.41. Impact of cyclosporin A on the *m*-3M3FBS- and thapsigargin-elicited nuclear damage and ASC speck formation in NLRP10^{mCitrine}/ASC^{TagBFP}/HMGB1^{mCherry} reporter HEK cells

A-B: HEK cells stably overexpressing human NLRP10^{mCitrine}, ASC^{TagBFP}, and the nuclear marker HMGB1^{mCherry} were shifted to an extracellular medium consisting of (in mM) 123 NaCl, 5 KCl, 2 $MgCl_2$, 1 $CaCl_2$, 10 glucose, 10 HEPES, pH 7.4, with or without cyclosporin A (15 μM). Next, the cells were stimulated with thapsigargin (20 μM; A) or *m*-3M3FBS (85 μM; B), and live imaging was performed using a widefield fluorescence microscope to capture the nuclear dynamics. The time interval between the acquired images was approximately 1 min. For the duration of the experiment, the cells were kept at 37°C in the microscope incubation chamber, but they were **not** perfused with CO_2 (HEPES-based buffers do not require CO_2 perfusion to maintain constant pH). The stimuli were added to the cells either directly in the microscope incubation chamber immediately after the onset of imaging (*m*-3M3FBS [B]), or they were added to the cells **outside** of the microscope incubation chamber (thapsigargin [A]), followed by a brief centrifugation (340 × g at RT for 30 s), after which the imaging was started.
Images are representative of 3 independent experiments. In each of the panels (A, B), the same field (that is, approximately the same population of cells) is followed over time. Scale bars correspond to 50 μm.

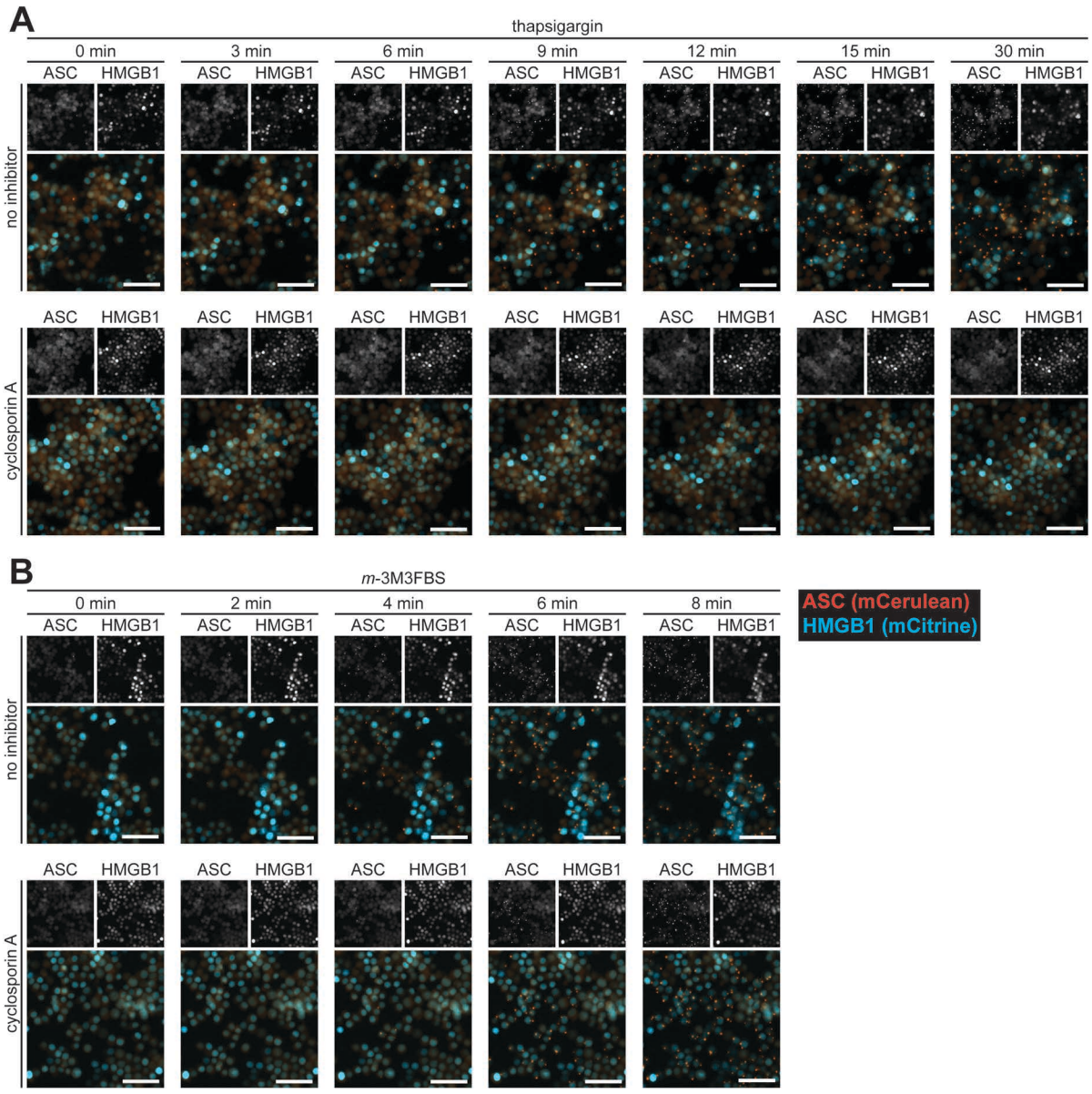
A
thapsigargin
0 min
3 min
6 min
9 min
12 min
15 min
30 min
ASC
HMGB1
no inhibitor
cyclosporin A
B
m-3M3FBS
0 min
2 min
4 min
6 min
8 min
ASC (mCerulean)
HMGB1 (mCitrine)

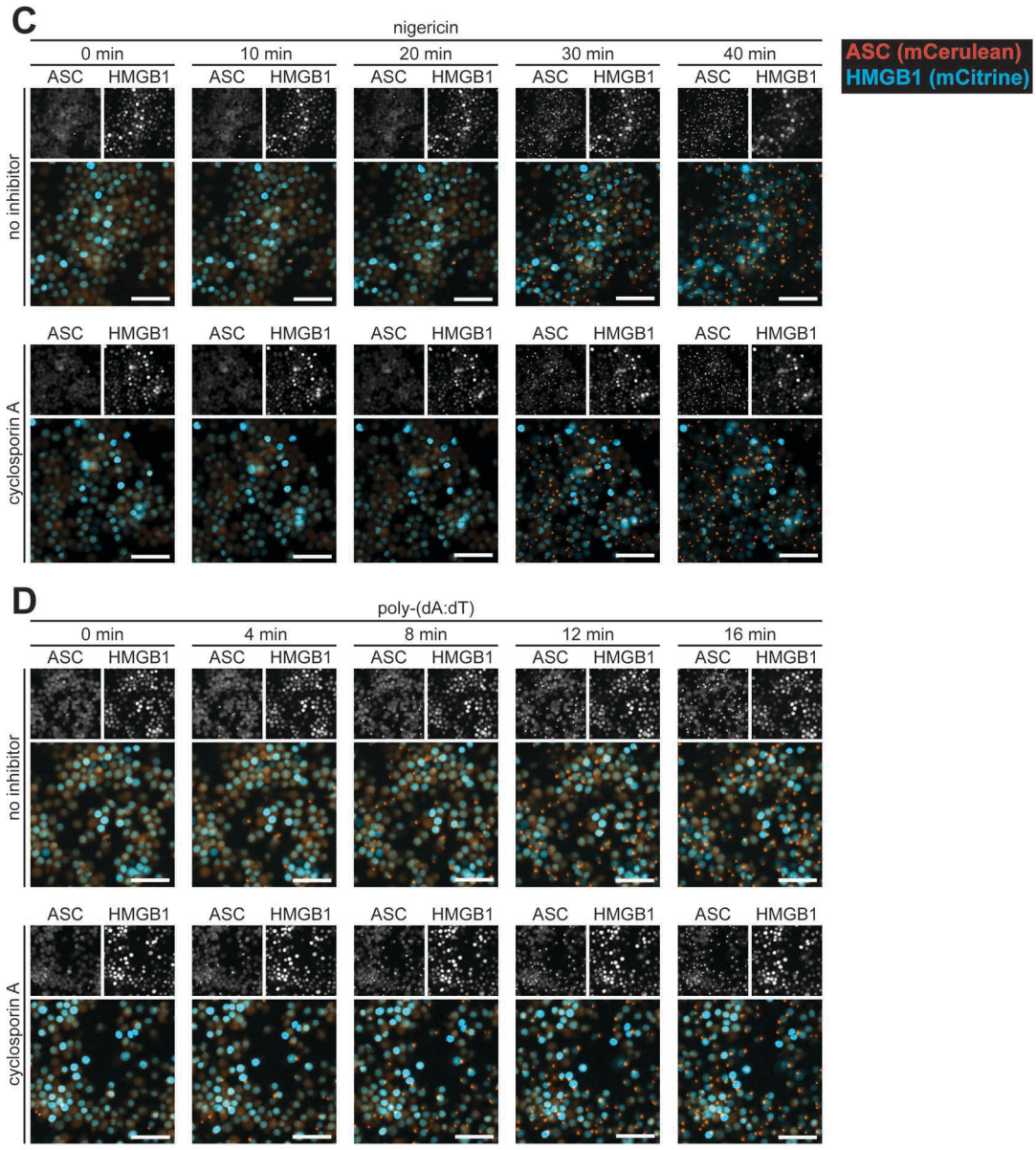

Figure 6.42 (this and previous page). Impact of cyclosporin A on the *m*-3M3FBS- and thapsigargin-elicited nuclear damage and ASC speck formation in NLRP3/ASC^{mCerulean}/HMGB1^{mCitrine} reporter iMac cells

A-D: NLRP3/ASC^{mCerulean} reporter iMac cells stably overexpressing the nuclear marker HMGB1^{mCitrine} were shifted to an extracellular medium consisting of (in mM) 123 NaCl, 5 KCl, 2 $MgCl_2$, 1 $CaCl_2$, 10 glucose, 10 HEPES, pH 7.4 with or without cyclosporin A (15 μM). Next, the cells were stimulated with thapsigargin (20 μM; A), *m*-3M3FBS (85 μM; B), nigericin (10 μM; C), or poly-(dA:dT) (2 μg/mL complexed with 5 μL Lipofectamine 2000; D), and live imaging was performed using a widefield fluorescence microscope to capture the nuclear dynamics. The time interval between the acquired images was approximately 1 min (A-C) or 4 min (D). For the duration of the experiment, the cells were kept at 37°C in the microscope incubation chamber, but they were **not** perfused with CO_2 (HEPES-based buffers do not require CO_2 perfusion to maintain constant pH). The stimuli were added to the cells either directly in the microscope incubation chamber immediately after the onset of imaging (*m*-3M3FBS [B] and nigericin [C]), or they were added to the cells **outside** of the microscope incubation chamber (thapsigargin [A] and poly-(dA:dT) [D]), followed by a brief centrifugation (340 × g at RT for 30 s), after which the imaging was started.
Images are representative of 3 independent experiments. In each of the panels (A-D), the same field (that is, approximately the same population of cells) is followed over time. Scale bars correspond to 50 μm.

In macrophages, consistent with my earlier observations (Section 6.13), nigericin and poly-(dA:dT) did not induce the mitochondrial or nuclear contents leakage (Figures 6.40 C, D, 6.42 C, D). This situation was, predictably, not altered by the pre-treatment with CsA. Thapsigargin stimulation induced leakage of mito^{mCitrine} from the mitochondria (Figure 6.40 A) and of HMGB1^{mCitrine} from the nuclei (Figure 6.42 A). Both of these events were fully inhibited by CsA. Notably, the inhibition of the mitonuclear damage correlated with the inhibition of ASC speck formation. Consistent with the results presented in Figure 6.38, the *m*-3M3FBS-induced mitonuclear damage and ASC speck formation were not affected by CsA pre-treatment (Figures 6.40 B and 6.42 B). The granularity of the mitochondrial signal could be quantified (Figure 6.39/40Q A, B), and these quantifications demonstrate that CsA pre-treatment completely rescued the mitochondrial integrity in thapsigargin-stimulated cells. This rescue correlated with a complete inhibition of ASC speck formation in thapsigargin-stimulated cells.

In HEK cells, the mitoprotective effect of CsA on the thapsigargin-induced mitochondrial damage mirrored the observations from macrophages (Figure 6.39 A). Furthermore, the *m*-3M3FBS-induced mitochondrial content leakage was not sensitive to CsA (Figure 6.39 B). Similar to the situation recorded in macrophages (Figure 6.39/40Q A, B), the CsA-mediated rescue of mitochondrial integrity in thapsigargin-treated HEK cells could be confirmed by the quantification of the mitochondrial granularity (Figure 6.39/40Q C, D). Here, the mitoprotective effect of CsA also correlated with a complete inhibition of ASC speck formation in response to thapsigargin.

The *m*-3M3FBS-elicited HMGB1^{mCherry} leakage from the nuclei was also detected in HEK cells and it was not inhibited by CsA (Figure 6.41 B), consistent with the observations from macrophages (Figure 6.42 C, D). In contrast to my previous result (Figure 6.25 B), in the present experiment, the HMGB1^{mCherry} leakage from the nuclei upon thapsigargin treatment was not detected (Figure 6.41 A), so the influence of CsA on the thapsigargin-induced HEK cell nuclear damage could not be assessed. Importantly, even in the absence of detectable HMGB1^{mCherry} egress, the thapsigargin stimulation triggered ASC speck formation (Figure 6.41 A, left column), which was completely inhibited by CsA (Figure 6.41 A, right column). This suggests that the nuclear damage may not be consistently triggered by thapsigargin, supporting the notion that it may not be the main mediator of the thapsigargin-induced inflammasome activation.

Collectively, my observations suggest that the mitochondria are more likely to be the source of AIM2 and NLRP10 agonists than are the nuclei. Of note, the mitochondrial Ca^{2+} fluxes do not appear to be involved in the *m*-3M3FBS-/thapsigargin-induced AIM2 and NLRP10 activations, as the mitochondrial Ca^{2+} uniporter (MCU) inhibitor KB-R7943 did not inhibit the AIM2/NLRP10 activation (Supplementary Figure S24). The MCU inhibitor DS16570511 (Supplementary Figure S25 E-J) and the mitoprotective compound DS44170716 (Supplementary Figure S25 A-D) acted as weak inflammasome inhibitors, typically only at very high concentrations (50-100 μM for DS16570511 and 25-50 μM for DS44170716). At these doses, DS16570511 and DS44170716 also inhibited the nigericin-induced NLRP3 activation and the poly-(dA:dT)-driven AIM2 response (Supplementary Figure S25). These results are consistent with the observations that the SERCA-Ca^{2+} axis of thapsigargin activity and the PLC-IP_3-IP_3R-Ca^{2+} pathway triggered by *m*-3M3FBS do not appear to be involved in the inflammasome activation.

6.16. Mitochondrial disruption is triggered by multiple AIM2/NLRP10 activators

To further explore the link between mitochondrial damage and the AIM2/NLRP10 responses, I tested the impact of two reported Bax agonists, SMBA1 and BAM7, on the inflammasome activation in NLRP10/ASC fluorescent reporter HEK cells, NLRP3/$ASC^{mCerulean}$ reporter iMac cells, and LPS-primed WT iMac cells (Figure 6.43). Bax is a protein that forms pores in the OMM (Bock and Tait, 2019), best known for their role in the initiation of the intrinsic apoptosis pathway. I reasoned that activation of Bax could trigger cellular events similar to those caused by *m*-3M3FBS and thapsigargin.

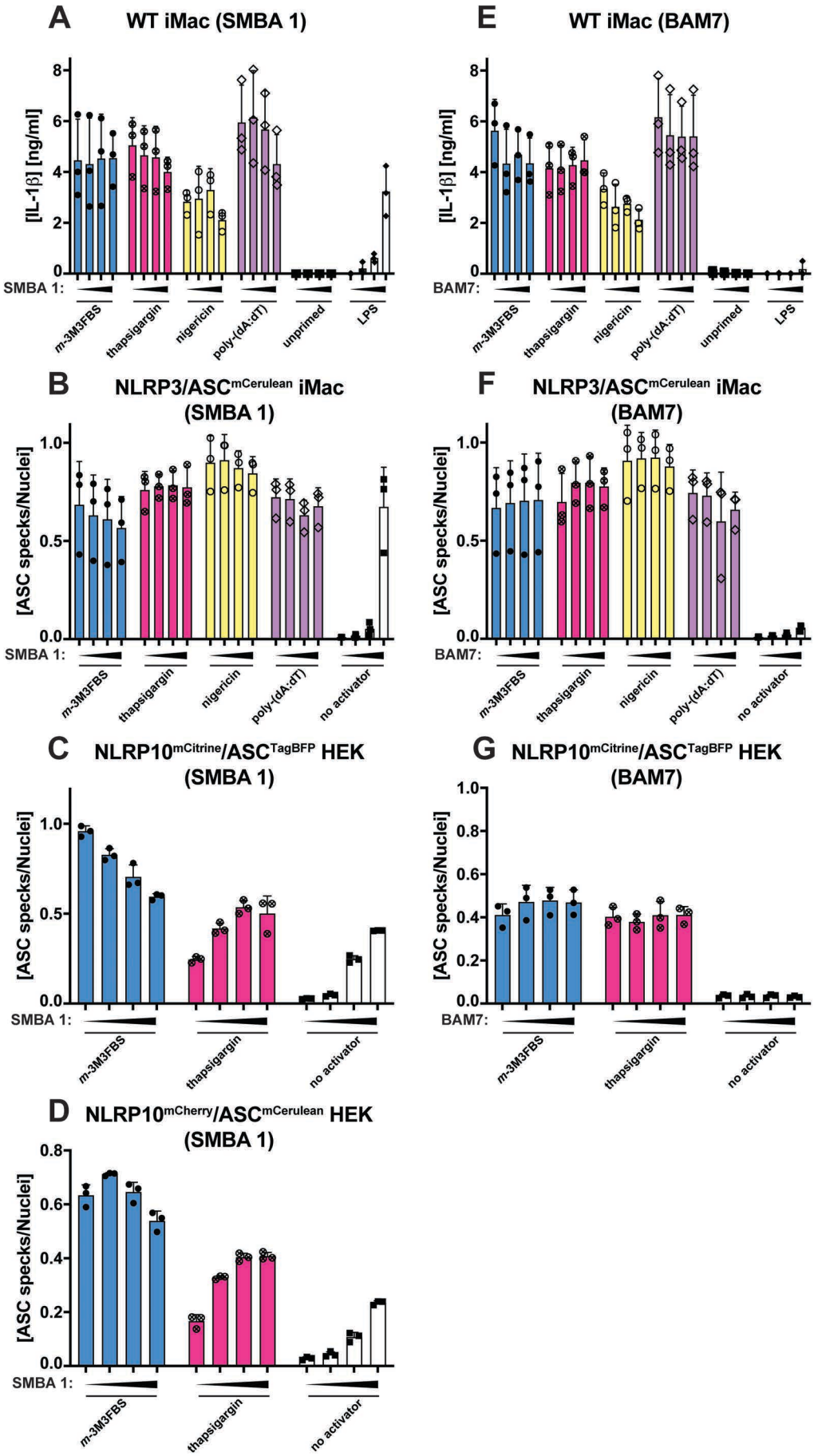

Figure 6.43. Influence of the Bax activators SMBA1 and BAM7 on the inflammasome responses to *m*-3M3FBS, thapsigargin, nigericin, and poly-(dA:dT)

◂ **A-G:** LPS-primed (200 ng/mL, 2 h) WT iMac cells (A, E), NLRP3/ASC^{mCerulean} reporter iMac cells (B, F), NLRP10^{mCitrine}/ASC^{TagBFP} HEK cells (C, G), and NLRP10^{mCherry}/ASC^{mCerulean} HEK cells (D) were treated for 10 min with SMBA1 (0, 5, 10, or 50 μM; A-D) or BAM7 (0, 5, 10, or 50 μM; E-G) and then subjected to the inflammasome activators *m*-3M3FBS (85 μM), thapsigargin (20 μM), nigericin (10 μM) or poly-(dA:dT) (2 μg/mL complexed with 5 μL Lipofectamine 2000) in an extracellular medium consisting of (in mM) 123 NaCl, 5 KCl, 2 $MgCl_2$, 1 $CaCl_2$, 10 glucose, 10 HEPES, pH 7.4. The LPS (A, E) and unprimed (A-G) controls were subjected to medium alone. Immediately after addition of inflammasome activators, the plates were centrifuged at 340 × g for 5 min (RT). After 30 min (C, D, G) or 60 min (A, B, E, F), the supernatants were collected and IL-1β concentrations were measured by HTRF (A, E) or the cells were fixed with 4% formaldehyde, counterstained with the nuclear dye DRAQ5 (5 μM) and imaged using a widefield fluorescence microscope (B-D, F, G).
The results are plotted as means from 3 independent experiments performed in technical duplicate. Error bars represent SD. Individual data points represent means of the technical duplicate values from each of the independent experiments.

While BAM7 was neither an inflammasome activator, nor an inhibitor of inflammasome formation (Figure 6.43 E-G), SMBA1 at high doses (around 50 μM) triggered strong inflammasome responses in macrophages and in NLRP10-overexpressing HEK cells (Figure 6.43 A-D). The fact that these two molecules with similar reported activities produced different outcomes was puzzling. Overall, my observations suggest that the type of mitochondrial damage elicited by *m*-3M3FBS and thapsigargin does not exhibit the typical characteristics of intrinsic apoptosis. The leakage of the mitochondrial contents in *m*-3M3FBS-/thapsigargin-treated cells occurs almost immediately after the stimulus administration, whereas typical apoptotic stimuli act over the course of hours (Gelles and Chipuk, 2016; McArthur et al., 2018; Riley et al., 2018). In addition, the cytosolic translocation of mitochondrial intermembrane space proteins such as cytochrome c is a standard feature of intrinsic apoptosis (Goldstein et al., 2000; Kluck, 1997; Liu et al., 1996), but the leakage of the mitochondrial matrix proteins (Section 6.13) is not commonly reported.

The differences between intrinsic apoptosis and the *m*-3M3FBS-/thapsigargin-induced mitochondrial damage will be the topic of Chapter 9 of my Thesis. Presently, I would like to briefly comment on the possible source of the difference between the observed activities of BAM7 and SMBA1. Both of these molecules were characterized as direct Bax ligands on the biochemical level (Gavathiotis et al., 2012; Xin et al., 2014). Therefore, it is unlikely that they target different steps of the apoptotic cascade, although theoretically it remains possible that SMBA1 has an 'additional' mitochondria-damaging off-target effect not shared with BAM7. A possibly important difference between BAM7 and SMBA1 is the Bax binding interface (SMBA1 binds to Bax in the proximity of the S184 residue, while the BAM7 binding site is proposed to be close to the K21 residue). Based

on the available knowledge, it is impossible to conclude whether the different Bax binding interfaces could explain the difference in the activities of SMBA1 and BAM7.

Because high doses of SMBA1 were required for inflammasome activation, I ensured that this compound is not an NLRP3 agonist acting through the crystal formation/lysosomal damage pathway (Supplementary Figure S26). The SMBA1-induced macrophage inflammasome response was not sensitive to the phagocytosis inhibitor cytochalasin D and to the NLRP3 inhibitor CRID3, whereas the SMBA1-induced IL-1β release was completely blocked by the caspase-1 inhibitor VX-765 (Supplementary Figure S26 A), in contrast to the SMBA1-induced ASC speck formation (Supplementary Figure S26 B). These observations indicate that the SMBA1-induced inflammasome recruits caspase-1, but that this enzyme is not required upstream of ASC speck formation. The SMBA1-triggered inflammasome activation is not dependent on phagocytosis and on NLRP3.

To test whether the macrophage inflammasome responses to SMBA1 and SC-10 (described in Section 6.12) are dependent on AIM2, I stimulated LPS-primed WT, AIM2-deficient (*Aim2*$^{-/-}$), and NLRP3-deficient (*Nlrp3*$^{-/-}$) BMDMs with these compounds and measured the concentrations of secreted IL-1β (Figure 6.44).

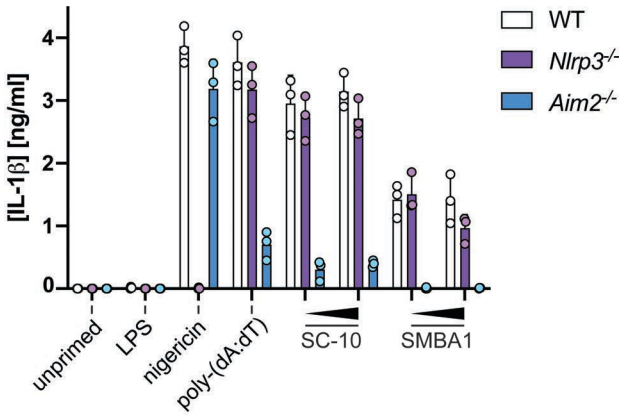

Figure 6.44. In BMDMs, the inflammasome responses to SC-10 and SMBA1 are dependent on AIM2 but independent of NLRP3 in BMDMs
BMDMs from WT (white bars), NLRP3-deficient (*Nlrp3*$^{-/-}$; purple bars), or AIM2-deficient (*Aim2*$^{-/-}$; blue bars) mice were primed with LPS (200 ng/mL, 2 h) or left unprimed, and then shifted to an extracellular medium consisting of (in mM) 123 NaCl, 5 KCl, 2 $MgCl_2$, 1 $CaCl_2$, 10 glucose, 10 HEPES pH 7.4 and stimulated with nigericin (10 μM), poly-(dA:dT) (2 μg/mL complexed with 5 μL Lipofectamine 2000), SC-10 (75 or 100 μM), or SMBA1 (50 or 75 μM). The unprimed and LPS controls were subjected to medium alone. Immediately after addition of inflammasome activators, the plates were centrifuged at 340 × g for 5 min (RT). After 60 min, the supernatants were collected and IL-1β concentrations were measured by HTRF.
The results are plotted as means from 3 independent experiments performed in technical triplicate. Error bars represent SD. Individual data points represent means of the technical triplicate values from each of the independent experiments.

While NLRP3-deficient BMDMs stimulated with SC-10 and SMBA1 secreted the amounts of IL-1β similar to their WT counterparts, the IL-1β secretion from SC-10- and SMBA1-stimulated AIM2-deficient BMDMs was completely abolished. This indicates that in murine macrophages, the inflammasome responses to SC-10 and SMBA1 are non-redundantly dependent on AIM2.

I next tested whether the SC-10-/SMBA1-induced AIM2 responses in macrophages and the SC-9-/SC-10-/SMBA1-induced NLRP10 responses in NLRP10^{mCherry}/ASC^{mCerulean} HEK cells are sensitive to the mitoprotective agent CsA and to the pan-kinase inhibitor staurosporine. Briefly, I pre-treated NLPR3/ASC^{mCerulean} reporter iMac or LPS primed WT iMac cells (Figure 6.45), or NLRP10^{mCherry}/ASC^{mCerulean} HEK cells (Figure 6.46) with CsA or staurosporine (10 min), followed by challenge with inflammasome activators.

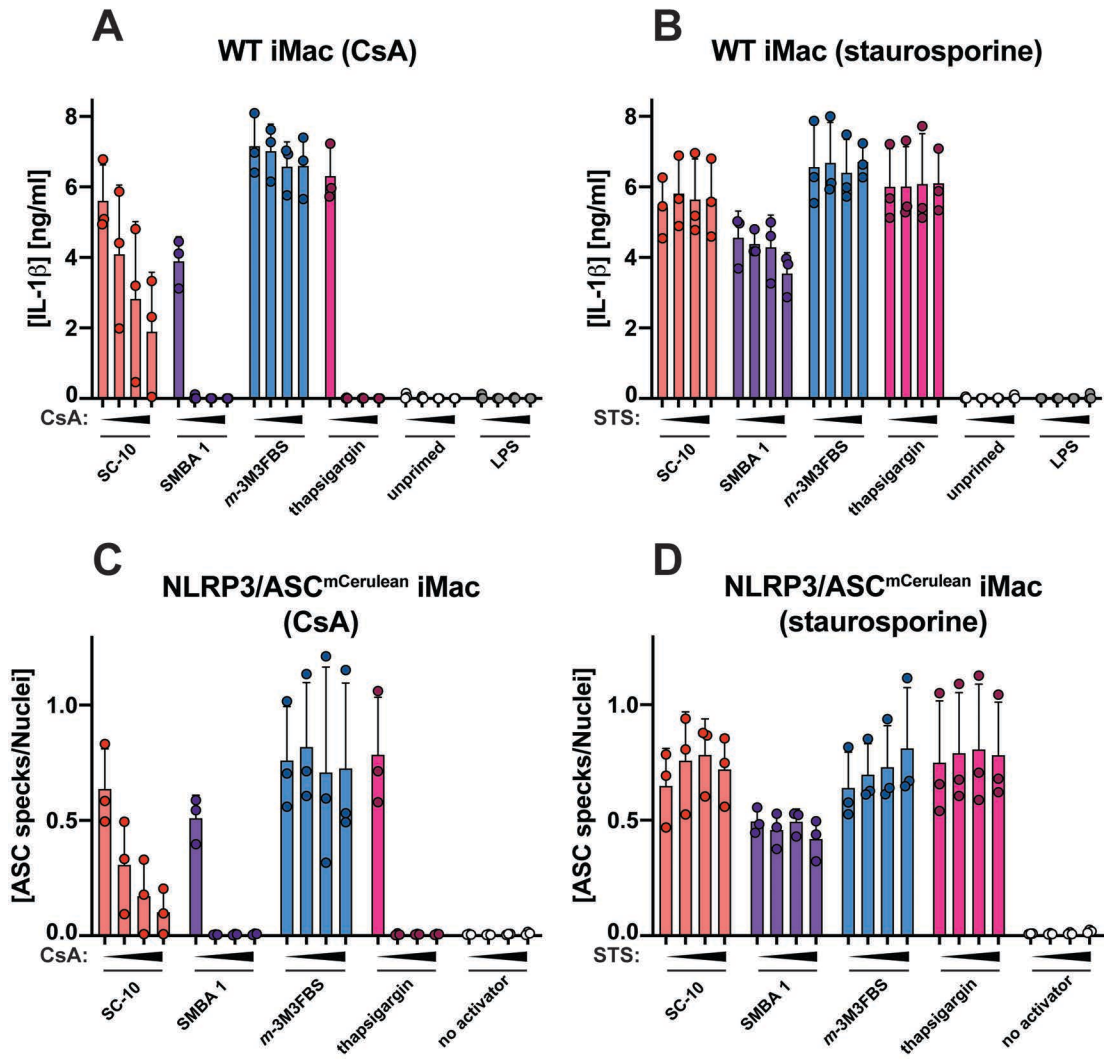

Figure 6.45. Influence of the mitoprotective agent cyclosporin A and the pan-kinase inhibitor staurosporine on the AIM2 inflammasome responses to SC-10, SMBA1, *m*-3M3FBS, and thapsigargin

◂ **A-D:** LPS-primed (200 ng/mL, 2 h) WT iMac cells (A, B) and NLRP3/ASC^{mCerulean} reporter iMac cells (C, D) were treated for 10 min with cyclosporin A (CsA; 0, 10, 15, or 20 μM; A, C) or staurosporine (STS; 0, 1.25, 2.5, or 5 μM; B, D) and then subjected to the inflammasome activators *m*-3M3FBS (85 μM), thapsigargin (20 μM), SC-10 (100 μM), or SMBA1 (50 μM) in an extracellular medium consisting of (in mM) 123 NaCl, 5 KCl, 2 $MgCl_2$, 1 $CaCl_2$, 10 glucose, 10 HEPES, pH 7.4. The LPS (A, B) and unprimed (A-D) controls were subjected to medium alone. Immediately after addition of inflammasome activators, the plates were centrifuged at 340 × g for 5 min (RT). After 60 min, the supernatants were collected and IL-1β concentrations were measured by HTRF (A, B) or the cells were fixed with 4% formaldehyde, counterstained with the nuclear dye DRAQ5 (5 μM) and imaged using a widefield fluorescence microscope (C, D).
The results are plotted as means from 3 independent experiments performed in technical duplicate. Error bars represent SD. Individual data points represent means of the technical duplicate values from each of the independent experiments.

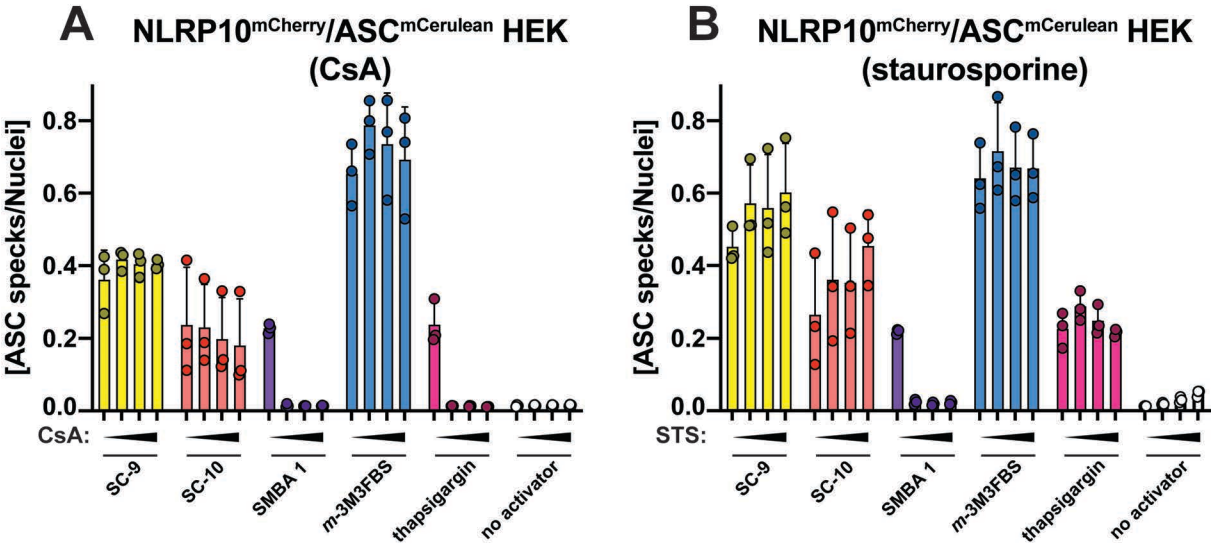

Figure 6.46. Influence of the mitoprotective agent cyclosporin A and the pan-kinase inhibitor staurosporine on the NLRP10 inflammasome responses to SC-9, SC-10, SMBA1, *m*-3M3FBS, and thapsigargin
A-B: NLRP10^{mCherry}/ASC^{mCerulean} HEK cells were treated for 10 min with cyclosporin A (CsA; 0, 10, 15, or 20 μM; A) or staurosporine (STS; 0, 1.25, 2.5, or 5 μM; B) and then subjected to the inflammasome activators *m*-3M3FBS (85 μM), thapsigargin (20 μM), SC-9 (100 μM), SC-10 (100 μM), or SMBA1 (50 μM) in an extracellular medium consisting of (in mM) 123 NaCl, 5 KCl, 2 $MgCl_2$, 1 $CaCl_2$, 10 glucose, 10 HEPES, pH 7.4. The untreated ('no activator') controls were subjected to medium alone. Immediately after addition of inflammasome activators, the plates were centrifuged at 340 × g for 5 min (RT). After 30 min, the cells were fixed with 4% formaldehyde, counterstained with the nuclear dye DRAQ5 (5 μM) and imaged using a widefield fluorescence microscope.
The results are plotted as means from 3 independent experiments performed in technical duplicate. Error bars represent SD. Individual data points represent means of the technical duplicate values from each of the independent experiments.

In macrophages, the SMBA1-induced AIM2 activation was completely inhibited by CsA (Figure 6.45 A, C), but not affected by the staurosporine pre-treatment (Figure 6.45 B, D), similar to the inflammasome responses to thapsigargin. The inflammasome responses to SC-9 (in HEK cells) and SC-10 (in all tested cell types) were not affected by CsA or staurosporine (Figures 6.45 and 6.46), similar to *m*-3M3FBS. These observations are consistent with, but not a proof of, the scenario in which *m*-3M3FBS, *o*-3M3FBS, SC-

9, and SC-10 share a common target relevant for NLRP10 activation, and *m*-3M3FBS and SC-10 additionally share the AIM2-stimulating activity. Notably, the observation that staurosporine does not block the inflammasome responses to SC-9/SC-10 is an argument against the involvement of PKC in this process.

The SMBA1-induced NLRP10 activation in NLRP10^{mCherry}/ASC^{mCerulean} HEK cells was blocked by CsA, similar to thapsigargin, but unexpectedly it was also sensitive to staurosporine (Figure 6.46). SMBA1 likely triggers the mitochondrial damage through Bax (Xin et al., 2014) so the differential sensitivity to staurosporine between SMBA1 and thapsigargin is difficult to interpret. I did not experimentally pursue this issue.

I further examined whether the inflammasome responses to SC-9 (in HEK cells; Figure 6.48), SC-10, and SMBA1 (in macrophages and in HEK cells; Figures 6.47 and 6.48, respectively) are inhibited by FK506 and ascomycin.

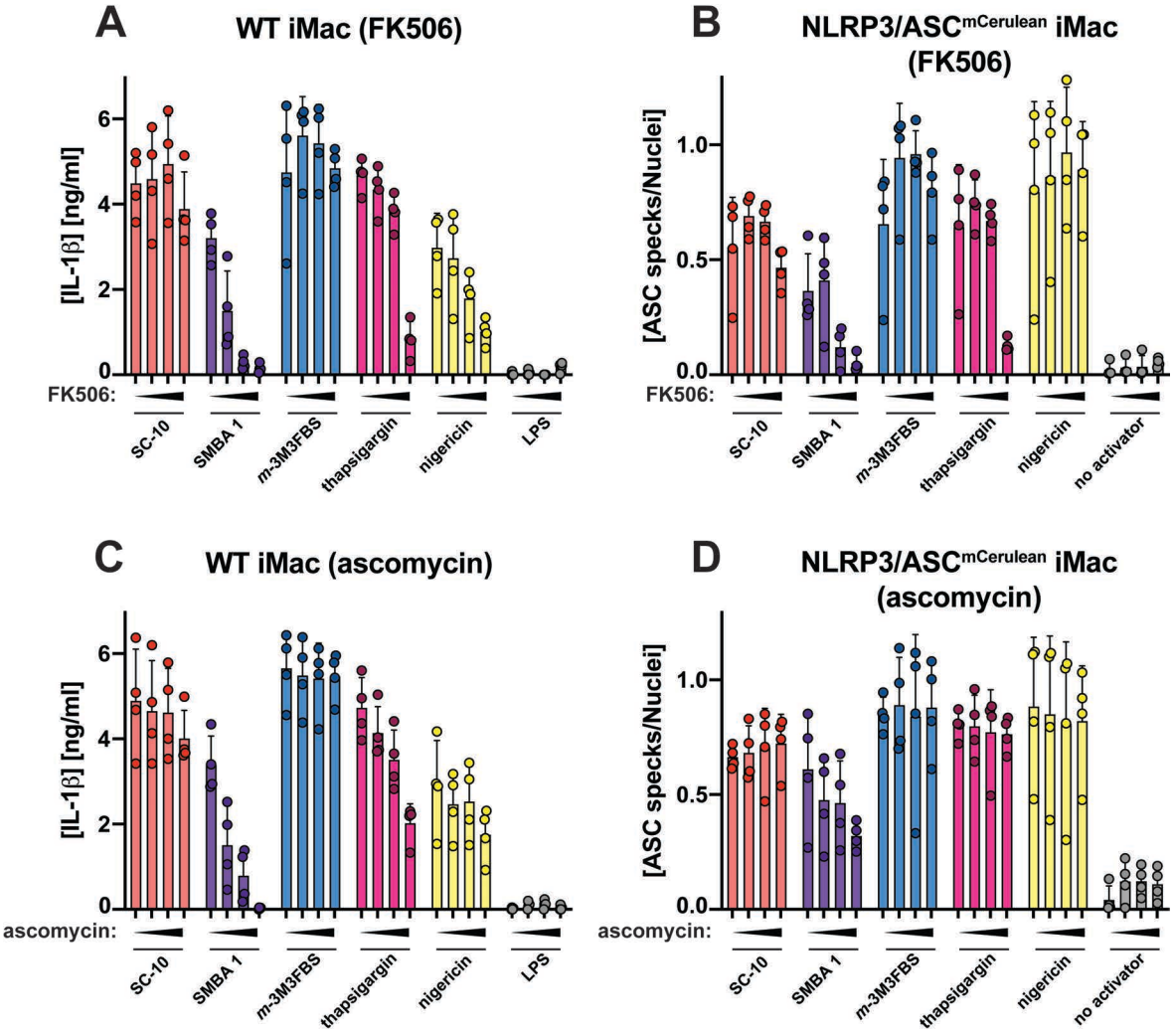

Figure 6.47. Influence of the prolyl isomerase inhibitors FK506 and ascomycin on the inflammasome responses to SC-10, SMBA1, *m*-3M3FBS, thapsigargin, and nigericin

◂ **A-D:** LPS-primed (200 ng/mL, 2 h) WT iMac cells (A, C) and NLRP3/ASC^{mCerulean} reporter iMac cells (B, D) were treated for 10 min with FK506 (0, 10, 25, or 50 μM; A, B) or ascomycin (0, 10, 25, or 50 μM; C, D) and then subjected to the inflammasome activators *m*-3M3FBS (85 μM), thapsigargin (20 μM), SC-10 (100 μM), or SMBA1 (50 μM) in an extracellular medium consisting of (in mM) 123 NaCl, 5 KCl, 2 $MgCl_2$, 1 $CaCl_2$, 10 glucose, 10 HEPES, pH 7.4. The LPS (A, C) and unprimed (A-D) controls were subjected to medium alone. Immediately after addition of inflammasome activators, the plates were centrifuged at 340 × g for 5 min (RT). After 60 min, the supernatants were collected and IL-1β concentrations were measured by HTRF (A, C) or the cells were fixed with 4% formaldehyde, counterstained with the nuclear dye DRAQ5 (5 μM) and imaged using a widefield fluorescence microscope (B, D).
The results are plotted as means from 4 independent experiments performed in technical duplicate. Error bars represent SD. Individual data points represent means of the technical duplicate values from each of the independent experiments.

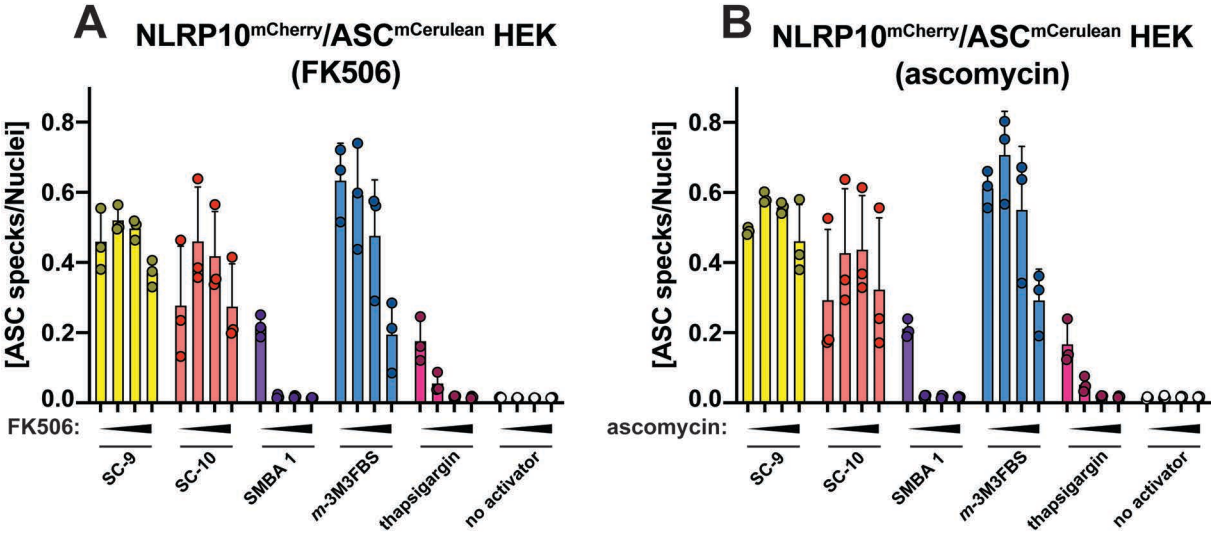

Figure 6.48. Influence of the prolyl isomerase inhibitors FK506 and ascomycin on the NLRP10 inflammasome responses to SC-9, SC-10, SMBA1, *m*-3M3FBS, and thapsigargin
A-B: NLRP10^{mCherry}/ASC^{mCerulean} HEK cells were treated for 10 min with FK506 (0, 10, 25, or 50 μM; A) or ascomycin (0, 10, 25, or 50 μM; B) and then subjected to the inflammasome activators *m*-3M3FBS (85 μM), thapsigargin (20 μM), SC-9 (100 μM), SC-10 (100 μM), or SMBA1 (50 μM) in an extracellular medium consisting of (in mM) 123 NaCl, 5 KCl, 2 $MgCl_2$, 1 $CaCl_2$, 10 glucose, 10 HEPES, pH 7.4. The untreated ('no activator') controls were subjected to medium alone. Immediately after addition of inflammasome activators, the plates were centrifuged at 340 × g for 5 min (RT). After 30 min, the cells were fixed with 4% formaldehyde, counterstained with the nuclear dye DRAQ5 (5 μM) and imaged using a widefield fluorescence microscope.
The results are plotted as means from 3 independent experiments performed in technical duplicate. Error bars represent SD. Individual data points represent means of the technical duplicate values from each of the independent experiments.

In NLRP3/ASC^{mCerulean} iMac cells and LPS-primed WT iMac cells, the SMBA1-induced inflammasome activation was more sensitive to FK506 and ascomycin than was the inflammasome activation with thapsigargin, but full inhibition still required very high concentrations of the prolyl isomerase inhibitors (25-50 μM). The AIM2 activation with SC-10 was completely insensitive to FK506 and ascomycin (Figure 6.47). In NLRP10^{mCherry}/ASC^{mCerulean} HEK cells, the SMBA1-induced NLRP10 activation was fully blocked with FK506 and ascomycin, while the thapsigargin-induced activation was only partially inhibited by these treatments (Figure 6.48). The NLRP10 activation by SC-9 and

SC-10 was not blocked by FK506 and ascomycin, similar to the *m*-3M3FBS-induced NLRP10 activation.

To test whether the stimulations with SC-9, SC-10, and SMBA1 lead to the cytosolic leakage of the mitochondrial contents, I performed end-point imaging of mito^{mCitrine} reporter HEK cells (Figure 6.49) and NLRP3/ASC^{mCerulean}/mito^{mCitrine} reporter iMac cells (Figure 6.50) challenged with a range of inflammasome activators. To gain better insight into the cellular responses to these agents, I also tested the influence of CsA, the pan-caspase inhibitor emricasan, and the caspase-1 inhibitor VX-765 on the mitochondrial phenotype. The CsA pre-treatment was employed to determine whether the CsA-mediated inhibition of the SMBA1-induced inflammasome activation coincides with an observable level of mitoprotection. VX-765 was administered to ensure that none of the observed effects occur downstream of the inflammasome activation. Finally, emricasan was included to account for the possible interference of non-pyroptotic cell death mechanisms with the observed cellular events.

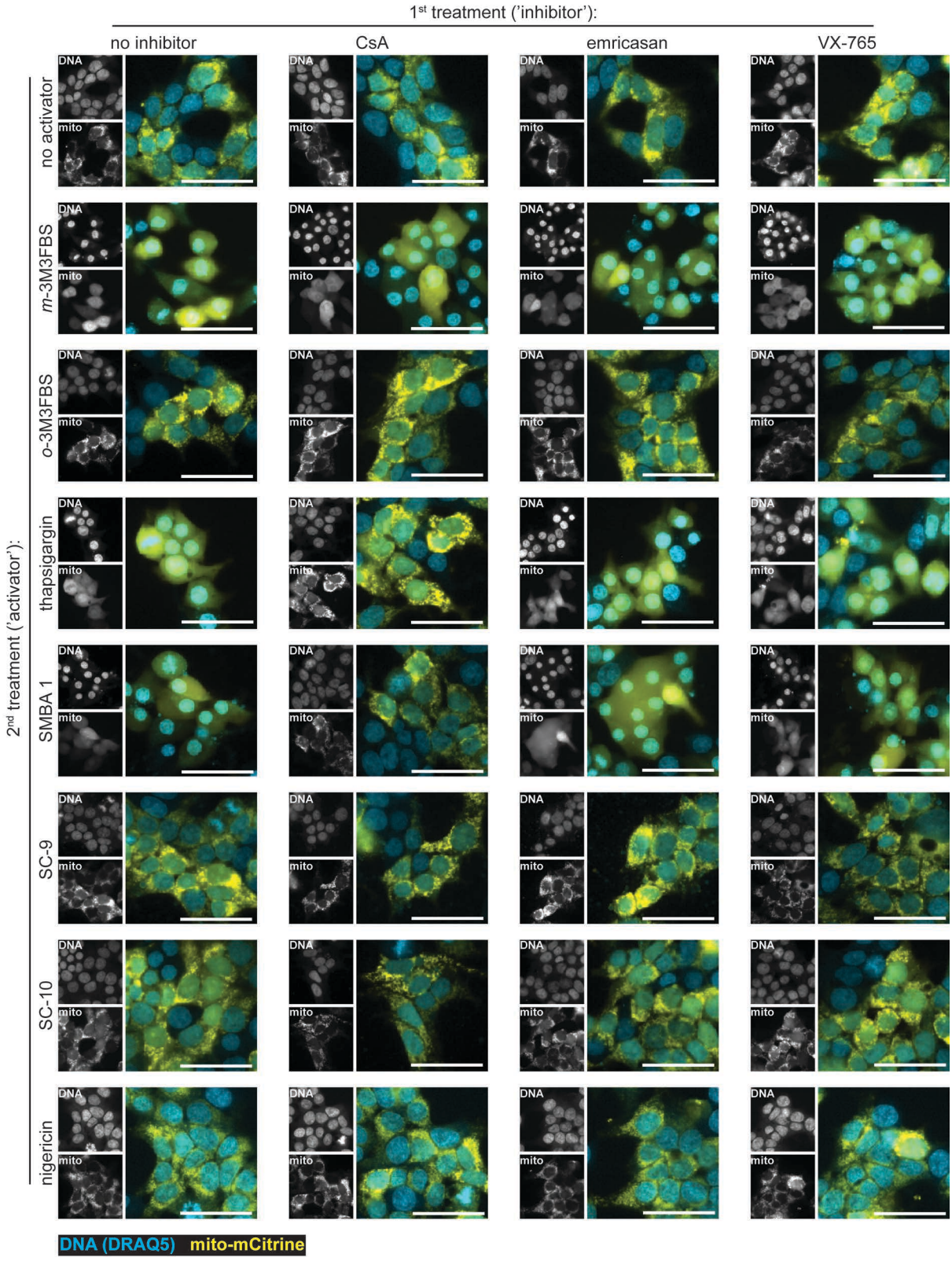

Figure 6.49. Mitochondrial integrity monitored by mito^{mCitrine} localization in mito^{mCitrine} reporter HEK cells stimulated with *m*-3M3FBS, *o*-3M3FBS, thapsigargin, SMBA1, SC-9, SC-10, or nigericin in the presence of the mitoprotective agent cyclosporin A, the pan-caspase inhibitor emricasan, or the caspase-1 inhibitor VX-765

◂ HEK cells stably overexpressing the mitochondrial marker mito^{mCitrine} were shifted to an extracellular medium consisting of (in mM) 123 NaCl, 5 KCl, 2 $MgCl_2$, 1 $CaCl_2$, 10 glucose, 10 HEPES pH 7.4 and left untreated ('no inhibitor') or pre-treated for 10 min with cyclosporin A (CsA; 10 μM), emricasan (20 μM), or VX-765 (20 μM). Then, the cells were stimulated with *m*-3M3FBS (85 μM), *o*-3M3FBS (85 μM), thapsigargin (20 μM), SMBA1 (50 μM), SC-9 (100 μM), SC-10 (100 μM), or nigericin (10 μM). The untreated ('no activator') controls were subjected to medium alone. Immediately after addition of inflammasome activators, the plates were centrifuged at 340 × g for 5 min (RT). After 30 min, the cells were fixed with 4% formaldehyde, counterstained with the nuclear dye DRAQ5 (5 μM) and imaged using a widefield fluorescence microscope.
The images are representative of 3 independent experiments. Scale bars correspond to 50 μm.

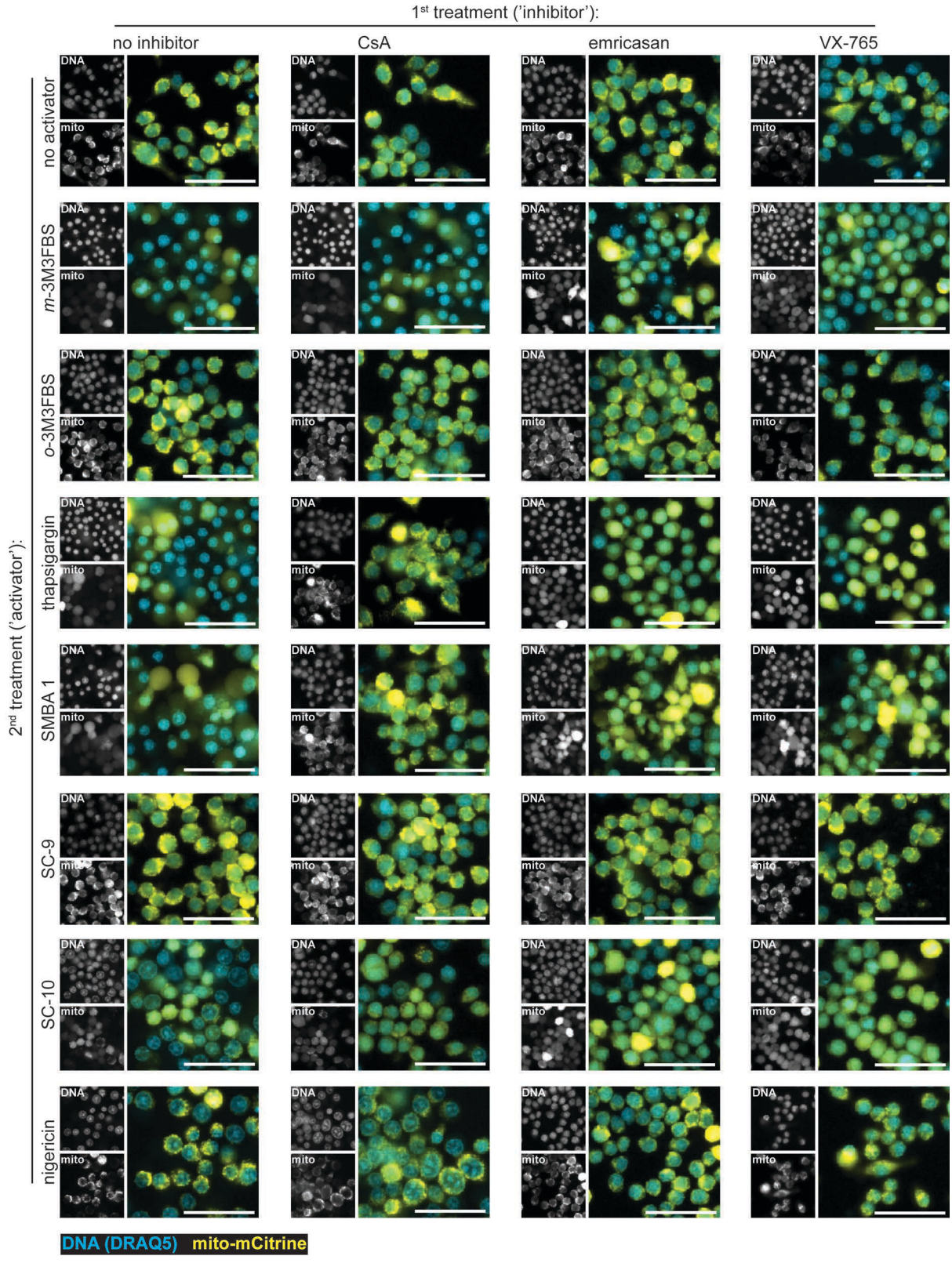

Figure 6.50. Mitochondrial integrity monitored by mito^{mCitrine} localization in NLRP3/ASC^{mCerulean}/mito^{mCitrine} reporter iMac cells stimulated with *m*-3M3FBS, *o*-3M3FBS, thapsigargin, SMBA1, SC-9, SC-10, or nigericin in the presence of the mitoprotective agent cyclosporin A, the pan-caspase inhibitor emricasan, or the caspase-1 inhibitor VX-765

◂ NLRP3/ASC^{mCerulean} reporter iMac cells stably overexpressing the mitochondrial marker mito^{mCitrine} were shifted to an extracellular medium consisting of (in mM) 123 NaCl, 5 KCl, 2 $MgCl_2$, 1 $CaCl_2$, 10 glucose, 10 HEPES pH 7.4 and left untreated ('no inhibitor') or pre-treated for 10 min with cyclosporin A (CsA; 10 μM), emricasan (20 μM), or VX-765 (20 μM). Then, the cells were stimulated with *m*-3M3FBS (85 μM), *o*-3M3FBS (85 μM), thapsigargin (20 μM), SMBA1 (50 μM), SC-9 (100 μM), SC-10 (100 μM), or nigericin (10 μM). The untreated ('no activator') controls were subjected to medium alone. Immediately after addition of inflammasome activators, the plates were centrifuged at 340 × g for 5 min (RT). After 30 min, the cells were fixed with 4% formaldehyde, counterstained with the nuclear dye DRAQ5 (5 μM) and imaged using a widefield fluorescence microscope.
The images are representative of 3 independent experiments. Scale bars correspond to 50 μm.

In NLRP3/ASC^{mCerulean}/mito^{mCitrine} reporter iMac cells (Figure 6.50), the observed mitochondrial contents leakage perfectly correlated with the capacity for the AIM2 inflammasome activation. The AIM2 activators *m*-3M3FBS, thapsigargin, SMBA1 and SC-10 induced mito^{mCitrine} cytosolic egress, whereas *o*-3M3FBS, SC-9, and the NLRP3 activator nigericin did not cause observable leakage of the mitochondrial contents. CsA inhibited the mitochondrial disruption in cells stimulated with thapsigargin and with SMBA1, but not with *m*-3M3FBS and with SC-10, consistent with the IL-1β secretion and ASC speck formation patterns (Figure 6.45). Neither emricasan nor VX-765 blocked the observed mitochondrial damage, indicating that this process was not caspase-dependent.

In mito^{mCitrine} reporter HEK cells (Figure 6.49), the situation was more complicated. In my Thesis I identified six NLRP10 activators: *m*-3M3FBS, *o*-3M3FBS, thapsigargin, SC-9, SC-10, and SMBA1. Among these molecules, *m*-3M3FBS, thapsigargin, and SMBA1 triggered the cytosolic leakage of the mitochondrial matrix contents in HEK cells, whereas *o*-3M3FBS, SC-9, and SC-10 did not have that effect. The mitochondrial disruption induced by SMBA1 and by thapsigargin was inhibited by CsA, consistent with the CsA-mediated inhibition of ASC speck formation (Figure 6.46). In further agreement with the ASC speck formation results (Figure 6.46), the mitochondrial damage caused by *m*-3M3FBS was not blocked by CsA (Figure 6.49). Similar to what was observed in macrophages, caspase activation was not responsible for the observed mitochondrial phenotypes, as no sensitivity to emricasan or VX-765 was detected.

At present, it is impossible to provide an integrative interpretation of the observations made in HEK cells. The direct mechanisms of action of the identified NLRP10 activators are unknown, and so are the NLRP10 cellular ligands. To gain more direct insight into the cellular events involving NLRP10, I performed confocal imaging of cells treated with

mitochondrially inactive NLRP10 stimuli. First, I tested whether the *o*-3M3FBS stimulation could trigger NLRP10 clustering in punctate structures, similar to *m*-3M3FBS (Figure 6.51). In untreated cells, NLRP10 was a uniformly distributed cytosolic protein. After administration of *o*-3M3FBS, NLRP10 formed speckles with kinetics similar to the *m*-3M3FBS-induced aggregation (5 min were sufficient to observe the effect). The morphological characteristics of *o*-3M3FBS-stimulated cells were different compared to *m*-3M3FBS-treated cells (best visible in Figure 6.51 is the fact that *m*-3M3FBS induces chromatin condensation but *o*-3M3FBS does not).

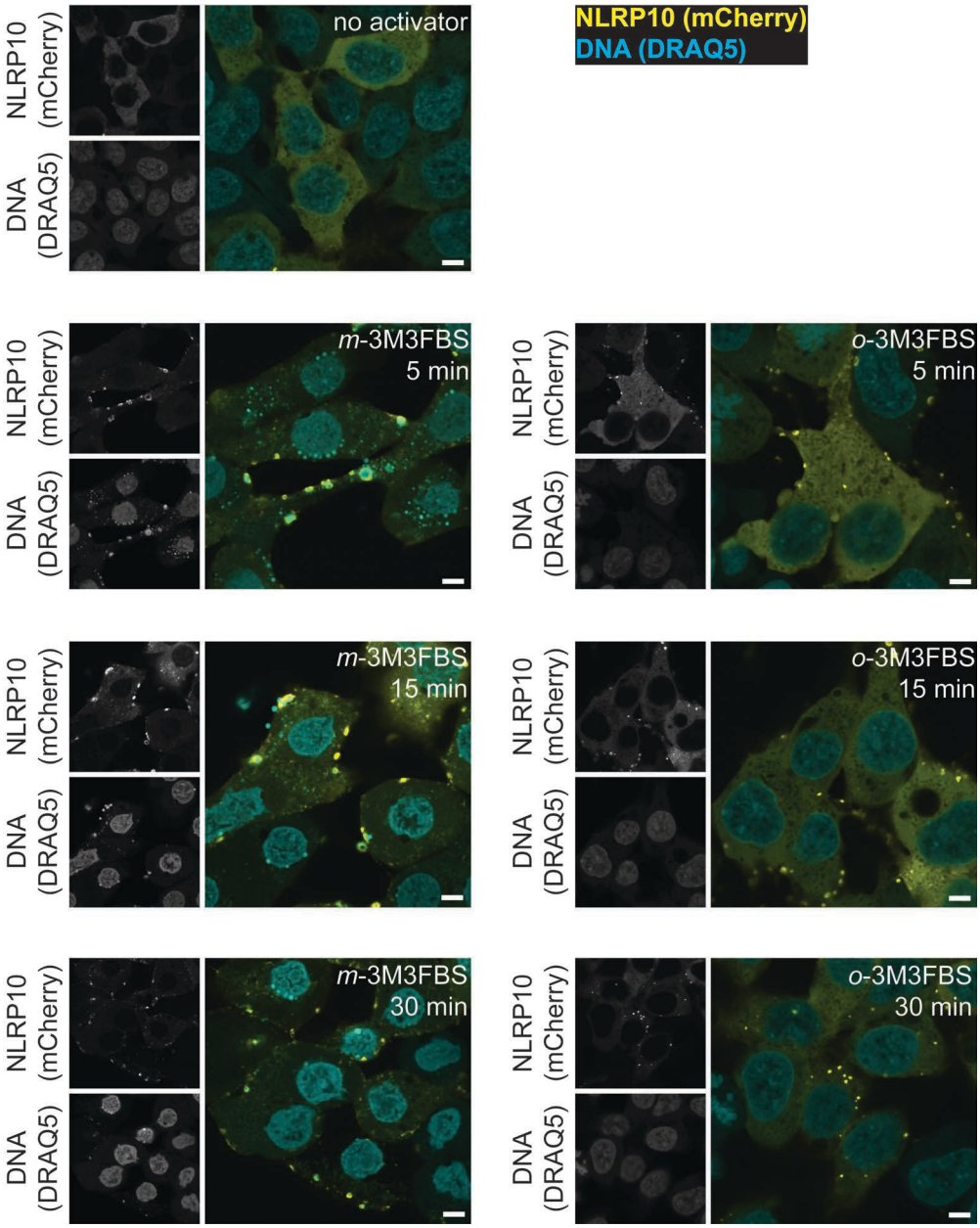

Figure 6.51. Comparison of the *m*-3M3FBS- and *o*-3M3FBS-induced NLRP10 subcellular distribution changes in NLRP10^{mCherry} HEK cells

◂ NLRP10^{mCherry} HEK cells were shifted to an extracellular medium consisting of (in mM) 123 NaCl, 5 KCl, 2 $MgCl_2$, 1 $CaCl_2$, 10 glucose, 10 HEPES pH 7.4 and then subjected to *m*-3M3FBS (85 μM) or *o*-3M3FBS (85 μM) and fixed after the indicated periods of time (5, 15, or 30 min) with 4% formaldehyde, followed by counterstaining with the nuclear dye DRAQ5 (5 μM). The untreated ('no activator') control was subjected to 30 min of medium alone. Immediately after addition of inflammasome activators, the plates were centrifuged at 340 × g for 5 min (RT). After the completion of the experiment, all samples were imaged using a confocal microscope.
The images are representative of 4 independent experiments. Scale bars correspond to 5 μm.

In contrast to the *m*-3M3FBS-induced NLRP10 clusters, the *o*-3M3FBS-induced NLRP10 puncta did not colocalize with TOMM20-positive mitochondria (Figure 6.52). The *o*-3M3FBS-induced NLRP10 aggregates also did not colocalize with the ER marker DDOST (Figure 6.53). Of note, the treatment with *o*-3M3FBS did not result in the disruption of the nuclear envelope, in contrast to *m*-3M3FBS stimulation (Figure 6.53).

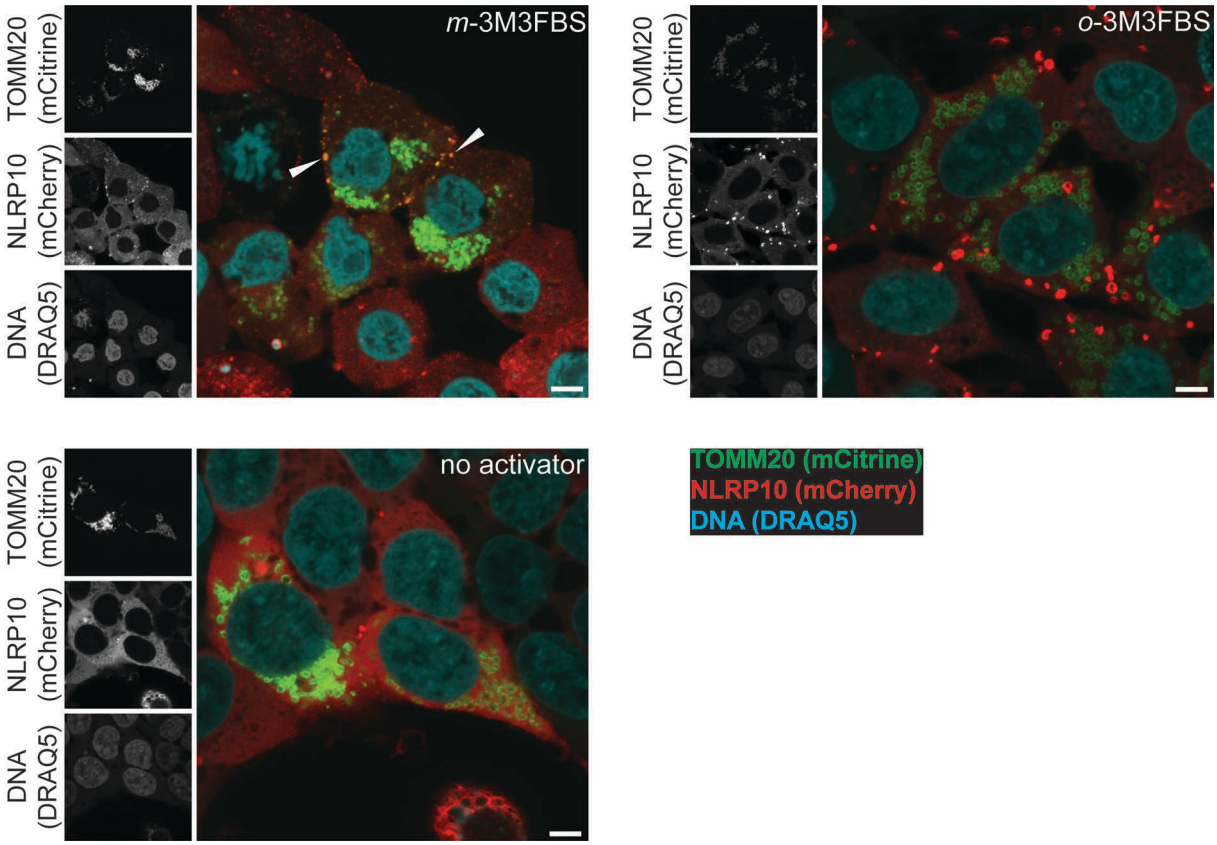

Figure 6.52. NLRP10 localization relative to TOMM20-positive mitochondria in NLRP10^{mCherry}/TOMM20^{mCitrine} HEK cells stimulated with *m*-3M3FBS or *o*-3M3FBS
Human NLRP10^{mCherry} HEK cells stably overexpressing the mitochondrial marker TOMM20 as a fusion protein with mCitrine were shifted to an extracellular medium consisting of (in mM) 123 NaCl, 5 KCl, 2 $MgCl_2$, 1 $CaCl_2$, 10 glucose, 10 HEPES pH 7.4 and were left untreated ('no activator'), or were stimulated with *m*-3M3FBS (85 μM) or *o*-3M3FBS (85 μM). After 30 min, the cells were fixed with 4% formaldehyde, counterstained with the nuclear dye DRAQ5 (5 μM) and imaged using a confocal microscope.
Images are representative of 4 independent experiments. Scale bars correspond to 5 μm.

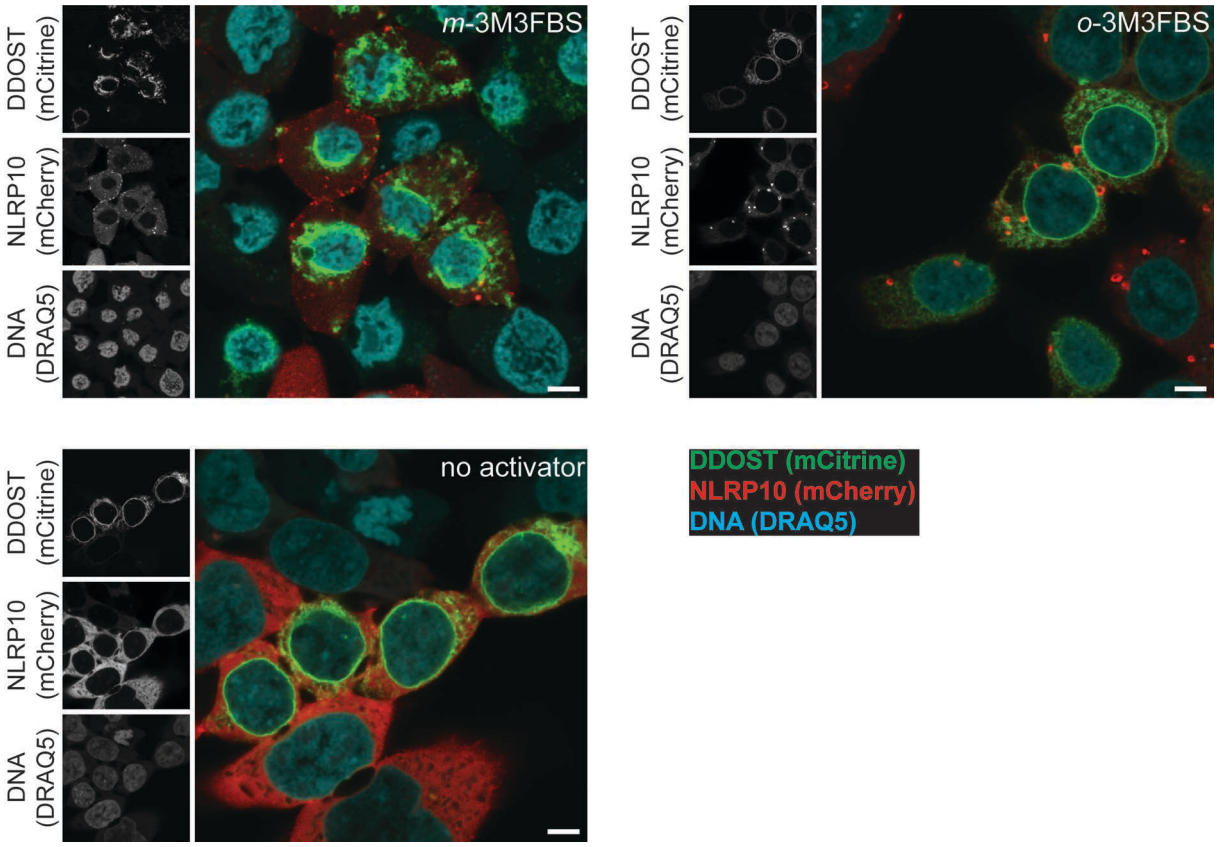

Figure 6.53 NLRP10 localization relative to the ER (DDOST-positive) membranes in NLRP10^{mCherry} HEK cells transiently overexpressing DDOST^{mCitrine} and stimulated with *m*-3M3FBS or *o*-3M3FBS
Human NLRP10^{mCherry} HEK cells were transiently transfected (200 ng of DNA per well of a 96-well plate combined with 0.5 µL of Gene Juice [transfection reagent], or 2 µg/mL of DNA combined with 5 µL of Gene Juice) with a vectors encoding the ER marker DDOST expressed as a fusion protein with mCitrine. After 24 h of transfection, the cells were shifted to an extracellular medium consisting of (in mM) 123 NaCl, 5 KCl, 2 $MgCl_2$, 1 $CaCl_2$, 10 glucose, 10 HEPES pH 7.4 and left untreated ('no activator'), or were stimulated with *m*-3M3FBS (85 µM) or *o*-3M3FBS (85 µM). After 30 min, the cells were fixed with 4% formaldehyde, counterstained with the nuclear dye DRAQ5 (5 µM) and imaged using a confocal microscope.
Images are representative of 4 independent experiments. Scale bars correspond to 5 µm.

Finally, I tested whether the *o*-3M3FBS findings can be extrapolated to the NLRP10 behavior in cells treated with other NLRP10 activators: SC-9, SC-10, and SMBA1 (Figure 6.54). All of these stimulations caused NLRP10 aggregation in puncta, but the appearances of these structures differed both morphologically and with respect to the localization pattern inside of the cell.

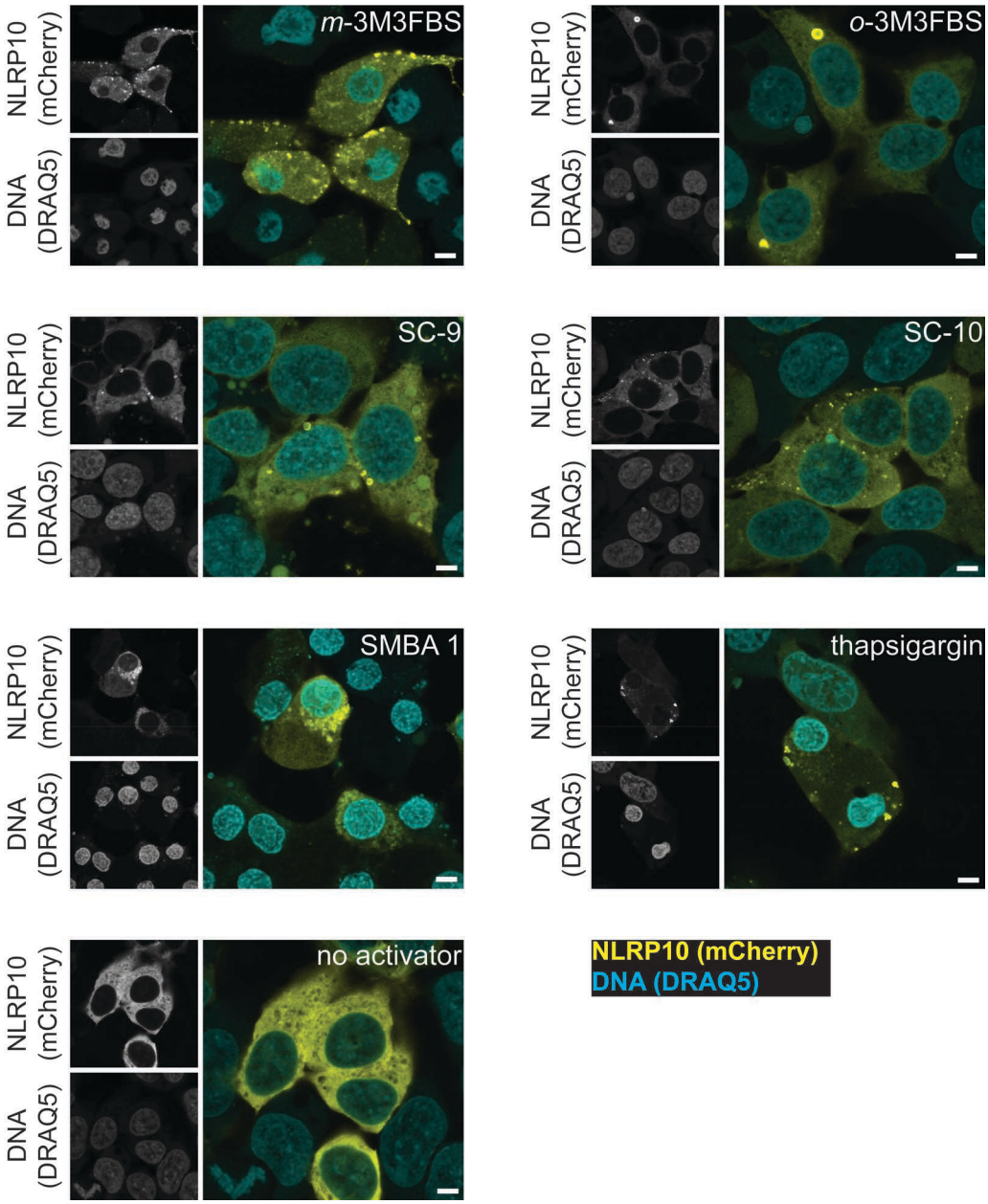

Figure 6.54. NLRP10 localization patterns in NLRP10^{mCherry} HEK cells stimulated with *m*-3M3FBS, *o*-3M3FBS, SC-9, SC-10, SMBA1, or thapsigargin
NLRP10^{mCherry} HEK cells were shifted to an extracellular medium consisting of (in mM) 123 NaCl, 5 KCl, 2 $MgCl_2$, 1 $CaCl_2$, 10 glucose, 10 HEPES pH 7.4 and then subjected to the following NLRP10 activators: *m*-3M3FBS (85 μM), *o*-3M3FBS (85 μM), thapsigargin (20 μM), SMBA1 (50 μM), SC-9 (100 μM), and SC-10 (100 μM). The untreated ('no activator') control was subjected to medium alone. Immediately after addition of inflammasome activators, the plates were centrifuged at 340 × g for 5 min (RT). After 30 min, the cells were fixed with 4% formaldehyde, counterstained with the nuclear dye DRAQ5 (5 μM) and imaged using a confocal microscope.
The images are representative of 2 independent experiments. Scale bars correspond to 5 μm.

To establish whether any of the NLRP10 activators apart from *m*-3M3FBS and thapsigargin could induce NLRP10 colocalization with TOMM20-positive mitochondria, I treated TOMM20^{mCitrine}/NLRP10^{mCherry} HEK cells with *m*-3M3FBS, *o*-3M3FBS, SC-9, SC-10, thapsigargin, and SMBA1 and examined the localizations of NLRP10 and of the

mitochondria by confocal microscopy (Figure 6.55). Among the identified NLRP10 activators, SMBA1, *m*-3M3FBS and thapsigargin induced NLRP10/TOMM20 colocalization, consistent with the capacity to trigger the mitochondrial contents leakage. In contrast, the *o*-3M3FBS-, SC-9-, and SC-10-elicited NLRP10 puncta did not colocalize with TOMM20 (Figure 6.55). Of note, whereas the thapsigargin- and *m*-3M3FBS-elicited NLRP10 speckles were usually observed at the edge of the cell and away from the nucleus, the SMBA1-elicited NLRP10 aggregates were localized in the perinuclear area (Figures 6.54 and 6.55).

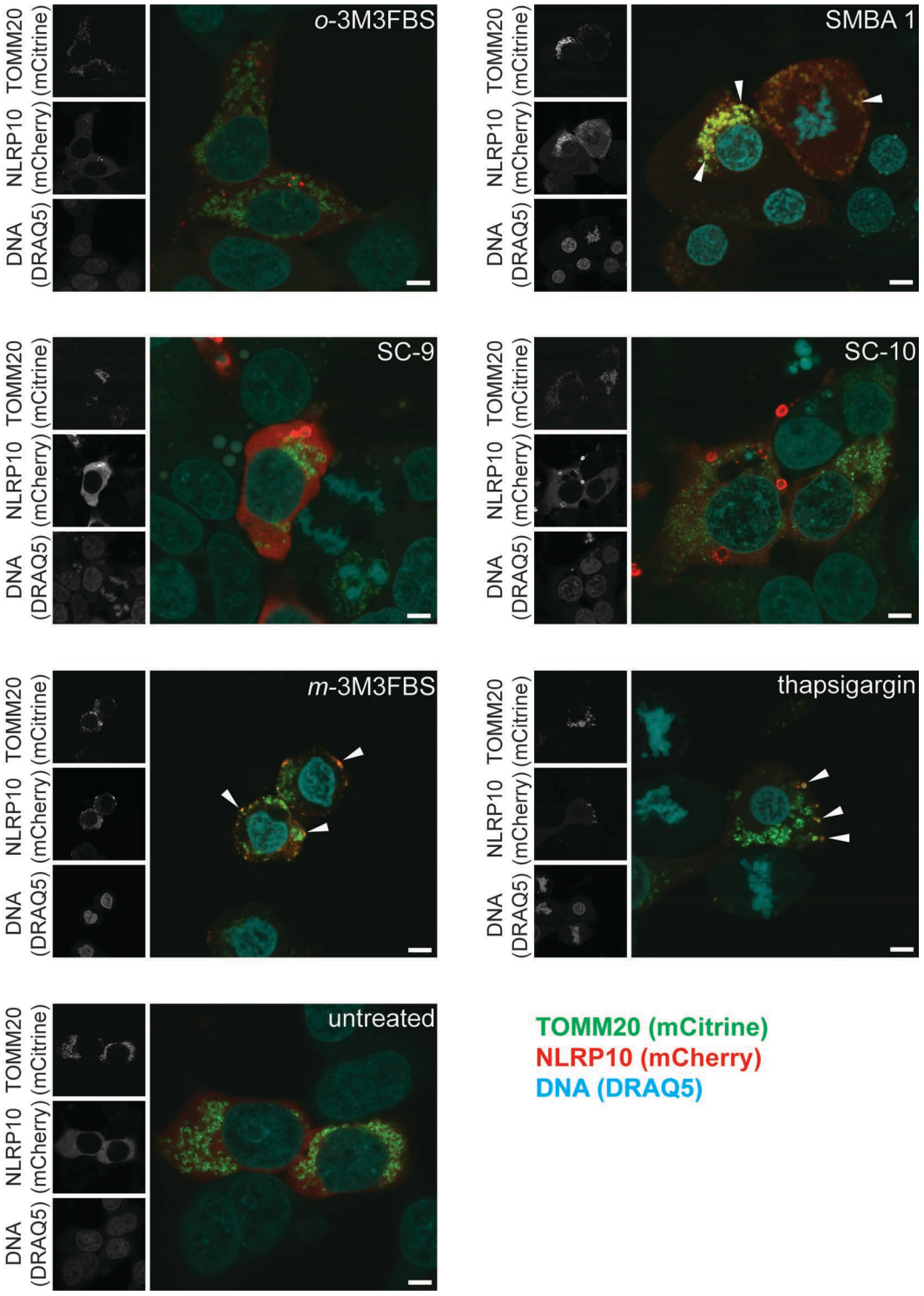

Figure 6.55. NLRP10 localization relative to TOMM20-positive mitochondria in NLRP10^{mCherry}/TOMM20^{mCitrine} HEK cells stimulated with *m*-3M3FBS, *o*-3M3FBS, SC-9, SC-10, SMBA1, or thapsigargin

Human NLRP10^{mCherry} HEK cells stably overexpressing the mitochondrial marker TOMM20 as a fusion protein with mCitrine were shifted to an extracellular medium consisting of (in mM) 123 NaCl, 5 KCl, 2 $MgCl_2$, 1 $CaCl_2$, 10 glucose, 10 HEPES pH 7.4 and then subjected to the following NLRP10 activators: *m*-3M3FBS (85 μM), *o*-3M3FBS (85 μM), thapsigargin (20 μM), SMBA1 (50 μM), SC-9 (100 μM), and SC-10 (100 μM). The untreated control was subjected to medium alone. Immediately after addition of inflammasome activators, the plates were centrifuged at 340 × g for 5 min (RT). After 30 min, the cells were fixed with 4% formaldehyde, counterstained with the nuclear dye DRAQ5 (5 μM) and imaged using a confocal microscope.

The images are representative of 2 independent experiments. Scale bars correspond to 5 μm.

These results indicate that the non-specific leakage of the mitochondrial contents and the permeabilization of the mitochondrial membranes are not required for NLRP10 activation, and that NLRP10 activation can also occur at subcellular locations other than the mitochondria. Conversely, the observations that the CsA-mediated inhibition of the mitochondrial rupture also inhibits the NLRP10 inflammasome activation (Figures 6.46 and 6.49) and that NLRP10 translocates to the mitochondria under conditions of mitochondrial damage (Figure 6.55) provide arguments that disrupted mitochondria may serve as a nucleation platform for the NLRP10 inflammasome.

The final perplexing observation was that SC-10 could trigger mitochondrial rupture in macrophages but not in HEK cells but was able to activate both the AIM2 (macrophages) and the NLRP10 (NLRP10-overexpressing HEK cells) inflammasomes. It is possible that SC-9, *o*-3M3FBS, and (in HEK cells) SC-10 directly initiate a response that in *m*-3M3FBS-, thapsigargin-, and SMBA1-stimulated cells is only activated downstream of the mitochondrial damage (that is, indirectly; Scheme 6.2). In macrophages, the treatment with SC-10 leads to the mitochondrial contents leakage, but this does not exclude the possibility that SC-10 could share other targets with SC-9 and *o*-3M3FBS. Without more knowledge on the binding targets of the AIM2/NLRP10 activators, it is impossible to provide a more detailed overview of the events occurring in cells stimulated with these molecules.

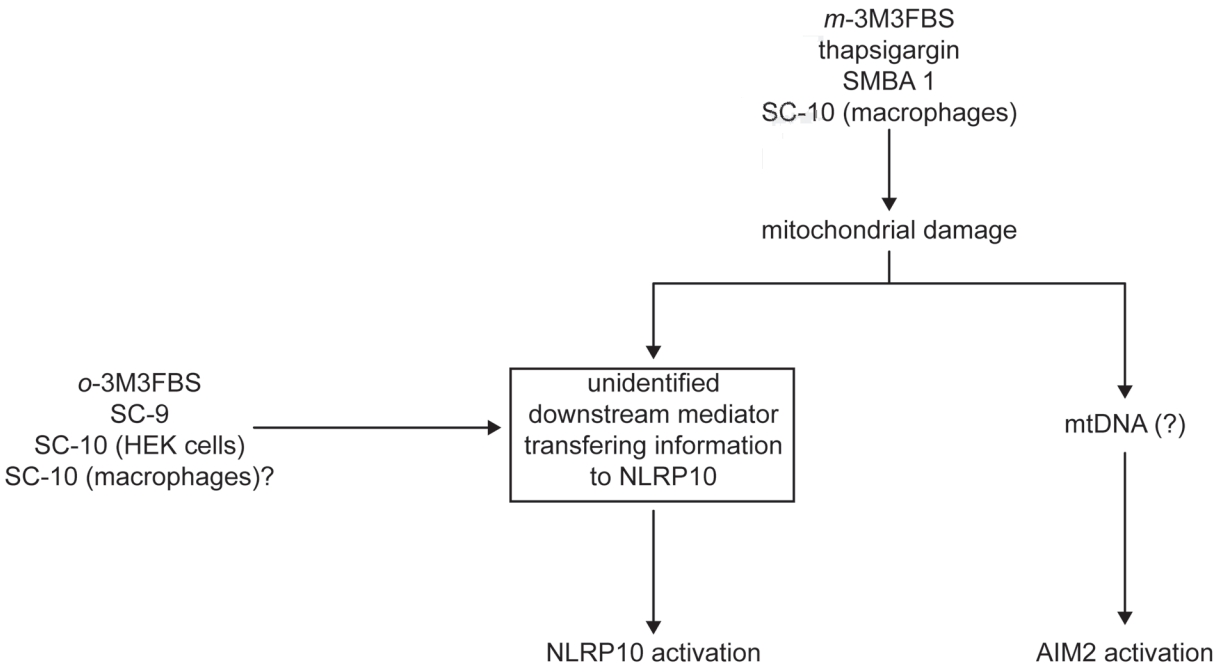

Scheme 6.2. Possible sequences of the molecular events relevant for the inflammasome responses to *m*-3M3FBS, *o*-3M3FBS, thapsigargin, SC-9, SC-10, and SMBA1

A preliminary model of the inflammasome activation by *m*-3M3FBS, *o*-3M3FBS, SC-9, SC-10, thapsigargin, and SMBA1 based on the results presented in Chapters 4-6 of my Thesis.

In macrophages, which express AIM2 but not NLRP10, *m*-3M3FBS, SC-10, thapsigargin, and SMBA1 all trigger mitochondrial damage which coincides with AIM2-dependent inflammasome activation. These events appear to be connected and the involvement of mtDNA as the link between mitochondrial damage and the AIM2 inflammasome activation will be discussed in Chapter 8.

In HEK cells overexpressing NLRP10 and fluorescently labeled ASC (a reporter for ASC speck formation), *m*-3M3FBS, *o*-3M3FBS, SC-9, SC-10, thapsigargin, and SMBA1 all activate the NLRP10 inflammasome, but only *m*-3M3FBS, thapsigargin, and SMBA1 are capable of eliciting mitochondrial rupture. Mitochondrial rupture appears to be linked to the NLRP10 inflammasome activation but is not absolutely required. It is possible that *o*-3M3FBS, SC-9, SC-10 activate cellular events that would otherwise be activated as a result of mitochondrial damage, but more information about the targets of the identified NLRP10 agonists is necessary to provide a comprehensive model of the NLRP10 inflammasome activation.

7. NLRP10 activation by *m*-3M3FBS, thapsigargin, and related molecules exhibits the principal features of inflammasome activation

NLRP10 has not been proposed to serve as an inflammasome-forming sensor in the literature. Consequently, I set forth to characterize the essential cell biological aspects of the NLRP10-driven ASC speck formation to determine how it compares to known inflammasomes.

7.1. *m*-3M3FBS and thapsigargin induce NLRP10-ASC colocalization in a speck-like structure

In Sections 6.1, 6.2, and 6.9 I demonstrated that overexpression of human or murine NLRP10 in ASC^{TagBFP} HEK cells enables ASC specking responses to *m*-3M3FBS and thapsigargin. To determine whether direct recruitment of ASC to NLRP10 could be observed, I performed confocal microscopy on fixed samples of $NLRP10^{mCherry}/ASC^{mCerulean}$ HEK cells challenged with *m*-3M3FBS and thapsigargin (Figure 7.1).

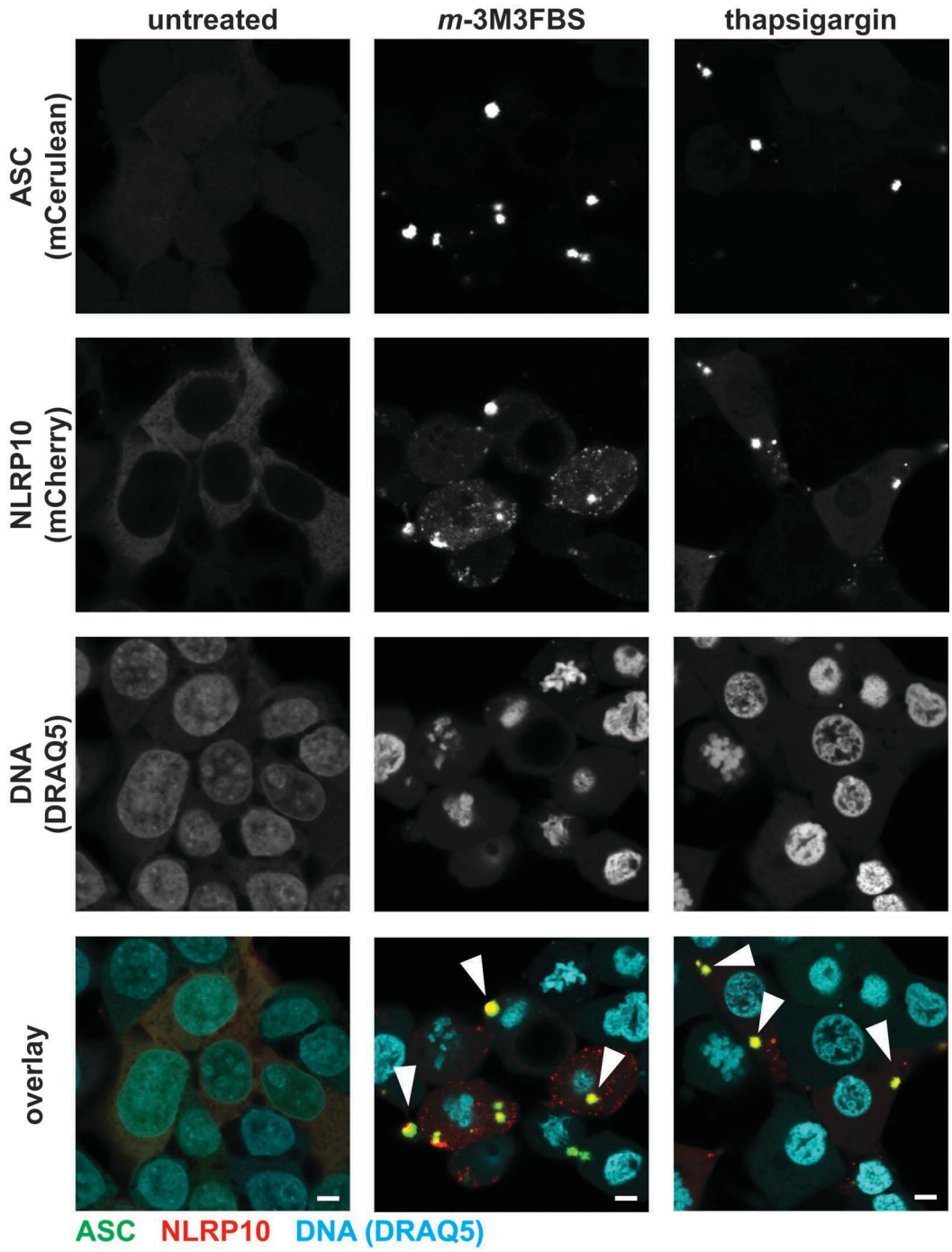

Figure 7.1. Colocalization of ASC^{mCerulean} and NLRP10^{mCherry} in NLRP10^{mCherry}/ASC^{mCerulean} HEK cells stimulated with *m*-3M3FBS and thapsigargin

NLRP10^{mCherry}/ASC^{mCerulean} HEK cells were treated with *m*-3M3FBS (85 μM) or thapsigargin (20 μM) in an extracellular medium consisting of (in mM) 123 NaCl, 5 KCl, 2 $MgCl_2$, 1 $CaCl_2$, 10 glucose, 10 HEPES, pH 7.4. Directly after administration of inflammasome activators, the cells were centrifuged at RT, 340 × g for 5 min. The untreated controls were subjected to medium alone. After 30 min of stimulation, the cells were fixed with 4% formaldehyde, counterstained with the nuclear dye DRAQ5 (5 μM) and imaged using a confocal microscope.

Images are representative of 3 independent experiments. Scale bars correspond to 5 μm.

Under untreated conditions, ASC exhibited a uniform nucleocytosolic localization pattern, whereas NLRP10, consistent with previous observations (Figures 6.8, 6.10, and 6.15), was a cytosolic protein excluded from the nucleus. *m*-3M3FBS and thapsigargin

stimulations led to the formation of NLRP10 clusters and ASC specks (Figure 7.1; examples of the NLRP10-ASC colocalization sites are marked with white arrowheads in the overlay images). Importantly, all of the detected ASC specks were NLRP10-positive, but not all NLRP10 clusters contained ASC, suggesting that the scenario where NLRP10 recruits ASC is more likely than the opposite sequence of events. *o*-3M3FBS and other identified NLRP10 activators (SC-9, SC-10, SMBA1) were similarly able to trigger the NLRP10-ASC colocalization in speck-like structures (Supplementary Figures S27 and S28). These results hint at the possibility that NLRP10 may serve as a nucleation center for ASC speck formation, similar to other inflammasome-forming sensors (Cai et al., 2014; Lu et al., 2014).

7.2. Full-length NLRP10 expressed as a continuous polypeptide chain is required for ASC speck formation

I went on to establish whether the full-length NLRP10 protein is required for ASC speck formation in *m*-3M3FBS-treated HEK cells, or if the NLRP10 PYD or NACHT domains alone could mediate this effect. For this purpose, I transiently transfected ASC^{TagBFP} HEK cells with full-length human or murine NLRP10, the NLRP10 PYD domains alone, the NLRP10 NACHT domains alone, or the PYD and NACHT domains combined as separate polypeptide chains. Next, I imaged the ASC specks formed after the challenge with *m*-3M3FBS (Figure 7.2).

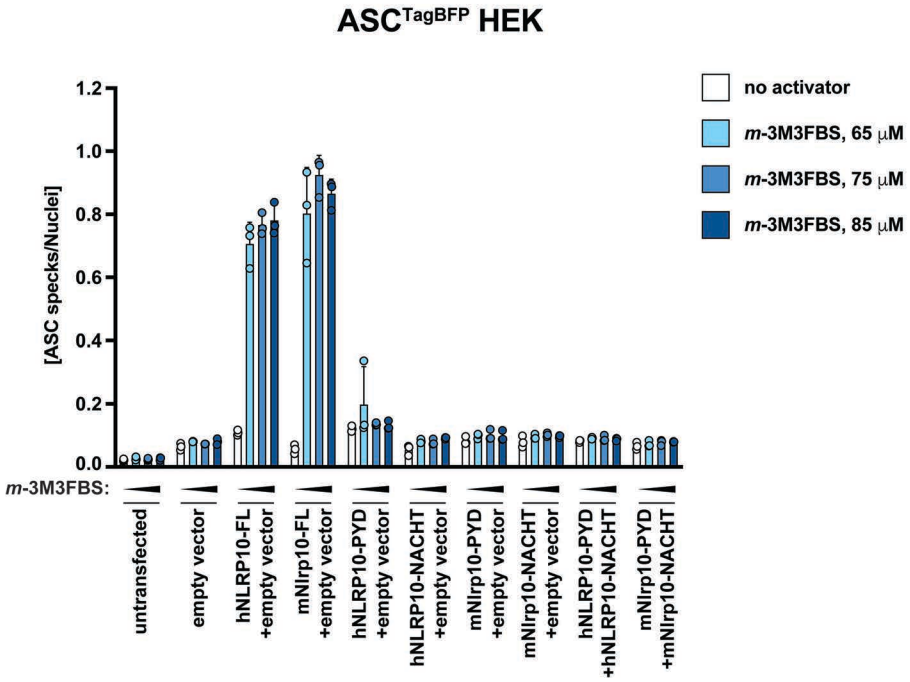

Figure 7.2. Full-length NLRP10 is required to elicit the ASC specking response to *m*-3M3FBS

◂ ASC^{TagBFP} HEK cells were transfected with the following vectors or combinations of vectors in wells of a 96-well plate: empty vector (200 ng), human (h) NLRP10 (full length; 100 ng) plus empty vector (100 ng), murine (m) Nlrp10 (full length, 100 ng) plus empty vector (100 ng), hNLRP10-PYD (100 ng) plus empty vector (100 ng), hNLRP10-NACHT (100 ng) plus empty vector (100 ng), mNlrp10-NACHT (100 ng) plus empty vector (100 ng), hNLRP10-PYD (100 ng) plus hNLRP10-NACHT (100 ng), or mNlrp10-PYD (100 ng) plus mNlrp10-NACHT (100 ng). The transfection reagent was Gene Juice and it was combined with DNA at the ration of 2.7 μL of GeneJuice per 1 μg of DNA. After 48 h of transfection, the cells were shifted to the experimental medium (in mM: 123 NaCl, 5 KCl, 2 $MgCl_2$, 1 $CaCl_2$, 10 glucose, 10 HEPES, pH 7.4) and stimulated with *m*-3M3FBS (0, 65, 75, or 85 μM). The untreated controls were subjected to medium alone. After addition of *m*-3M3FBS, cells were centrifuged at RT, 340 × g for 5 min. After 30 min of stimulation, cells were fixed with 4% formaldehyde, counterstained with the nuclear dye DRAQ5 (5 μM) and imaged using a widefield fluorescence microscope.
The results are plotted as means from 3 independent experiments performed in technical duplicate. Error bars represent SD. Individual data points represent means of the technical duplicate values from each of the independent experiments.

The overexpression of full-length NLRP10 enabled ASC speck formation in cells stimulated with *m*-3M3FBS. The PYD and NACHT domains alone were not sufficient for this response to occur, and co-expression of the two domains as separate polypeptide chains also did not allow for ASC speck formation. Of note, the background ASC specking signal in the untreated samples was not majorly increased by any of the transfected constructs.

7.3. NLRP10 activation is disrupted by mutations in the NACHT domain Walker A and B motifs

The NACHT domains of the NLRP subfamily members have ATPase activity that relies on two conserved functional motifs. These sequences, termed Walker A and B motifs (MacDonald et al., 2013), are involved in ATP binding and hydrolysis (Miller and Enemark, 2016). Clustal Omega (Goujon et al., 2010; McWilliam et al., 2013; Sievers et al., 2011) comparison of the NLRP10 sequences from several mammals (Figure 7.3 A) revealed complete conservation of the essential lysine residue in the Walker A motif and of the aspartic acid residue in the Walker B motif.

Mutations in the NLRP3 Walker A motif abolish the NLRP3 inflammasome activation (Duncan et al., 2007), so I proceeded to test whether the NLRP10 Walker A and B motifs would similarly be required for the NLRP10 activation. To answer this question, I transiently overexpressed several NLRP10 variants in ASC^{TagBFP} HEK cells and examined the ASC specking responses to *m*-3M3FBS and thapsigargin. The tested NLRP10 variants were WT human NLRP10, human NLRP10 Walker A mutant (K179M), two human

NLRP10 Walker B mutants (D249A and D249N) as well as WT murine NLRP10, murine NLRP10 Walker A mutant (K175M), and two murine NLRP10 Walker B mutants (D245A and D245N) (Figure 7.3 B-D).

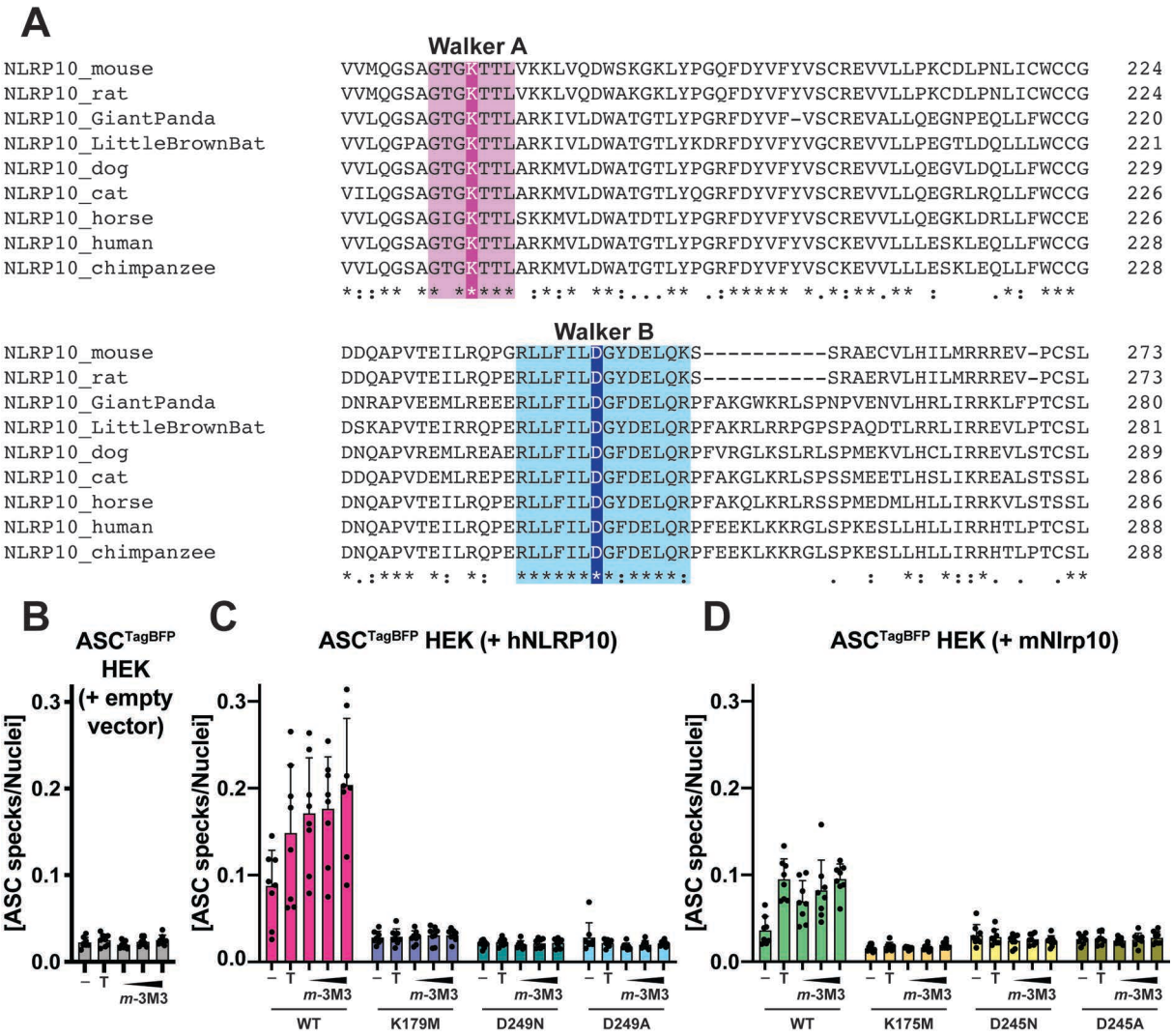

Figure 7.3. ASC specking responses to *m*-3M3FBS and thapsigargin in ASC^{TagBFP} HEK cells overexpressing the Walker A/B mutants of human or murine NLRP10

A: Comparison of the amino acid Walker A/B motif-proximal sequences of NLRP10 from the following species: mouse, rat, giant panda, little brown bat, dog, cat, horse, human, chimpanzee. The amino acid sequences were retrieved from the UniProt database and the sequence alignment was performed using the Clustal Omega software. Walker A motif is highlighted in pink and Walker B motif is highlighted in blue. The catalytically important lysine (K) and aspartic acid (D) residues are marked by more vivid shades of the respective colors.

B-D: ASC^{TagBFP} HEK cells were transfected with the following vectors in wells of a 6-well plate:

B: empty vector (2 μg; B);

C: human (h) WT NLRP10 (2 μg), hNLRP10^{K179M} (Walker A mutant; 2 μg), hNLRP10^{D249N} (Walker B mutant; 2 μg), or hNLRP10^{D249A} (Walker B mutant; 2 μg);

D: murine (m) WT Nlrp10 (2 μg), mNlrp10^{K175M} (Walker A mutant; 2 μg), mNlrp10^{D245N} (Walker B mutant; 2 μg), or mNlrp10^{D245A} (Walker B mutant; 2 μg).

The transfection reagent was Gene Juice and it was combined with DNA at the ration of 2.7 μL of GeneJuice per 1 μg of DNA. After 24 h of transfection, the cells were re-plated into 96-well plates, and after another 24 h they were shifted to the experimental medium (in mM: 123 NaCl, 5 KCl, 2 $MgCl_2$, 1 $CaCl_2$, 10 glucose, 10 HEPES, pH 7.4) and stimulated with *m*-3M3FBS (*m*-3M3; 65, 75, or 85 μM) or thapsigargin (T; 20 μM).

The untreated controls were subjected to medium alone. After addition of the NLRP10 activators, cells were centrifuged at RT, 340 × g for 5 min. After 30 min of stimulation, cells were fixed with 4% formaldehyde, counterstained with the nuclear dye DRAQ5 (5 μM) and imaged using a widefield fluorescence microscope.
The results are plotted as means from 8 independent experiments performed in technical duplicate. Error bars represent SD. Individual data points represent means of the technical duplicate values from each of the independent experiments.

While overexpression of the WT variants of human/murine NLRP10 enabled ASC speck formation upon stimulations with *m*-3M3FBS and thapsigargin (Figure 7.3 C, D), ASC^{TagBFP} HEK cells transfected with the Walker A/B NLRP10 mutants behaved in the same way as cells transfected with the empty vector (Figure 7.3 B-D). This observation indicates that intact Walker A/B motifs are required for the NLRP10-driven ASC speck formation.

7.4. Truncated variants and the Walker A/B mutants of NLRP10 do not have a dominant negative effect on the NLRP10 activation

The NLRP10 NACHT domain alone and the full-length NLRP10 Walker A/B mutants did not enable ASC speck formation upon stimulations with *m*-3M3FBS and thapsigargin. There is very little known about the biophysical and structural properties of NLRP10 (Su et al., 2013), so I proceeded to determine whether the overexpression of either of those inactive NLRP10 variants on top of the full-length WT NLRP10 could have an impact on ASC speck formation. I transiently transfected $NLRP10^{mCitrine}/ASC^{TagBFP}$ HEK cells with increasing amounts of vectors encoding the NLRP10 PYD domain, the NLRP10 NACHT domain, the NLRP10 Walker A/B mutants, or full-length WT NLRP10. Then, I evaluated the levels of ASC specking after the challenge with *m*-3M3FBS (Figure 7.4).

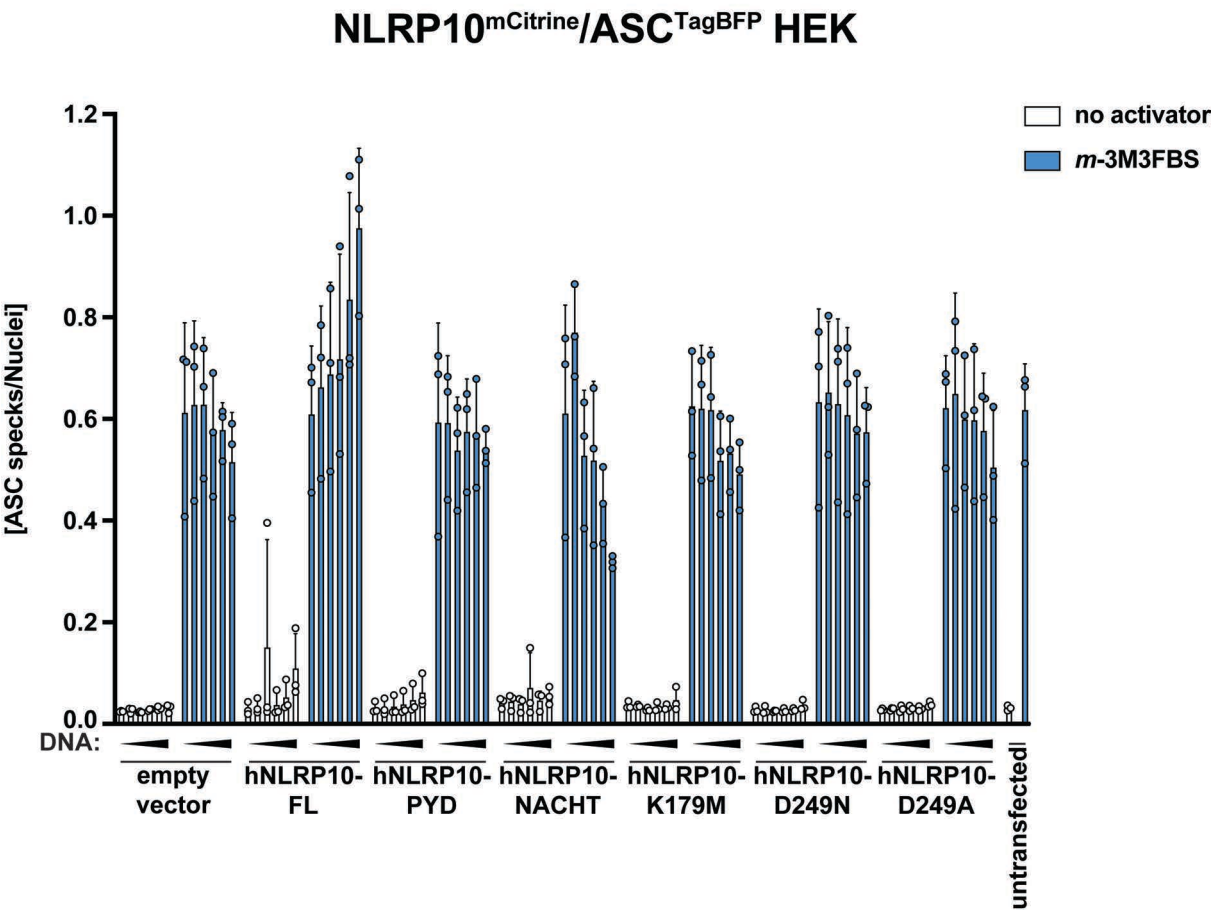

Figure 7.4. The impact of truncated or Walker A/B mutant NLRP10 overexpression on ASC speck formation in NLRP10^{mCitrine}/ASC^{TagBFP} HEK cells
NLRP10^{mCitrine}/ASC^{TagBFP} HEK cells were transfected with the following vectors (6.25 ng, 12.5 ng, 25 ng, 50 ng, 100 ng, or 200 ng per well) in wells of a 96-well plate: empty vector, human (h) WT NLRP10 (full length), hNLRP10-PYD, hNLRP10-NACHT, hNLRP10^{K179M} (Walker A mutant), hNLRP10^{D249N} (Walker B mutant), or hNLRP10^{D249A} (Walker B mutant). The transfection reagent was Gene Juice and it was combined with DNA at the ration of 2.7 μL of GeneJuice per 1 μg of DNA. After 48 h of transfection, the cells were shifted to the experimental medium (in mM: 123 NaCl, 5 KCl, 2 $MgCl_2$, 1 $CaCl_2$, 10 glucose, 10 HEPES, pH 7.4) and stimulated with *m*-3M3FBS (85 μM; blue bars). The untreated controls (white bars) were subjected to medium alone. After addition of *m*-3M3FBS, cells were centrifuged at RT, 340 × g for 5 min. After 30 min of stimulation, cells were fixed with 4% formaldehyde, counterstained with the nuclear dye DRAQ5 (5 μM) and imaged using a widefield fluorescence microscope.
The results are plotted as means from 3 independent experiments performed in technical duplicate. Error bars represent SD. Individual data points represent means of the technical duplicate values from each of the independent experiments.

Overexpression of the Walker A (K179M) and B (D249A, D249N) NLRP10 mutants as well as of the NLRP10 PYD domain did not affect the WT NLRP10 responsiveness to *m*-3M3FBS. Overexpression of extra full-length WT NLRP10 further increased the ASC specking levels upon the *m*-3M3FBS stimulation, whereas overexpression of the NLRP10 NACHT domain had a modest inhibitory effect, suggesting possible competition between the full-length NLRP10 and the NLRP10 NACHT domain (Figure 7.4). However, none of the tested variants exhibited the typical characteristics of a dominant negative mutant.

I next attempted to determine the reason why the NLRP10 Walker A/B mutants are defective in the process of ASC speck nucleation. To this end, I assessed the localization patterns of the truncated and Walker A/B NLRP10 mutants upon the *m*-3M3FBS challenge using confocal microscopy (Figure 7.5).

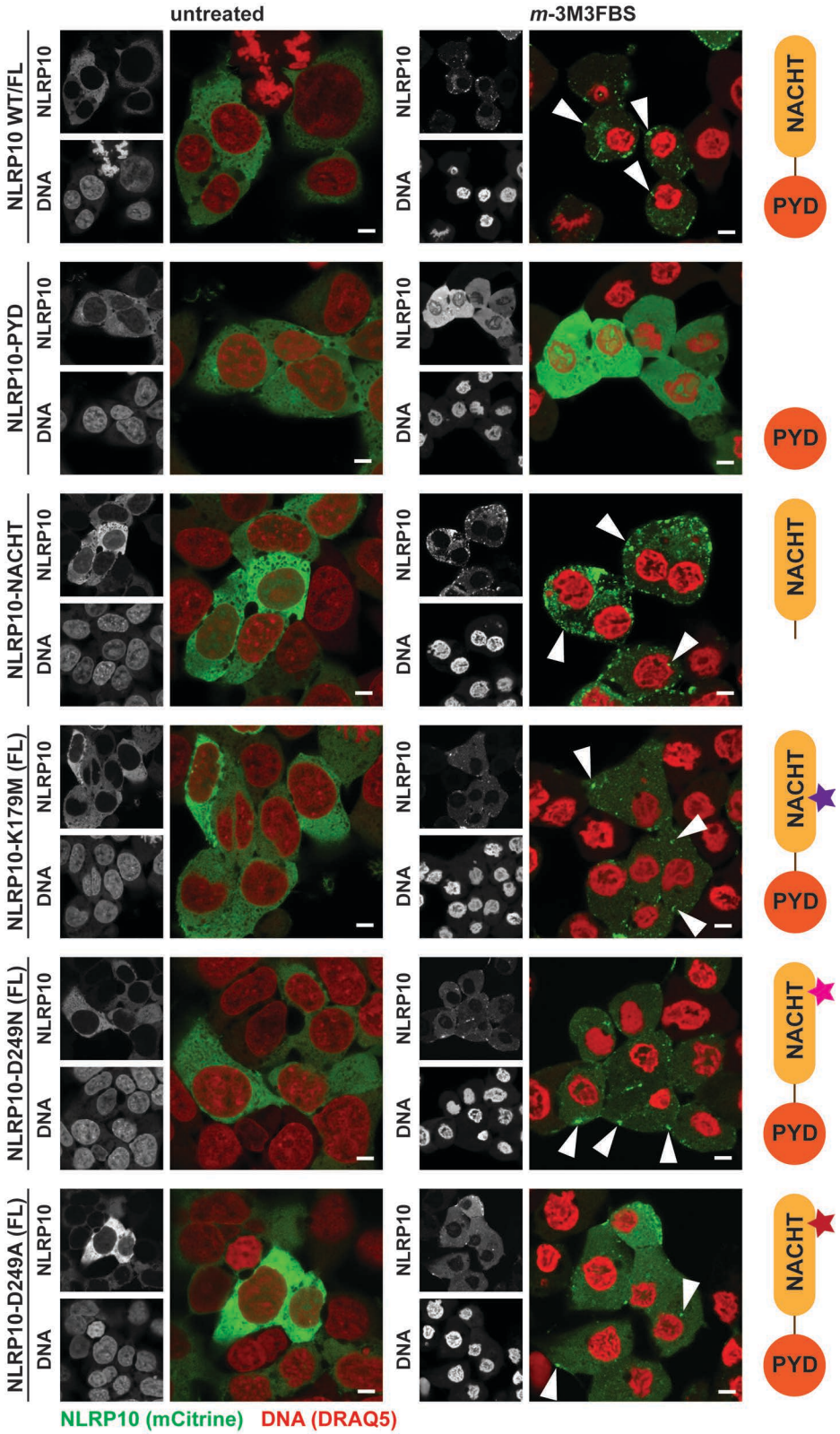

Figure 7.5. Localization of the NLRP10 PYD and NACHT domains and the NLRP10 Walker A/B mutants in untreated and *m*-3M3FBS-stimulated HEK cells

◂ HEK cells were transfected with the following vectors in wells of a 96-well plate (200 ng of DNA per well, all NLRP10 variants were expressed as fusion proteins with mCitrine): human (h) WT NLRP10 (full length), hNLRP10-PYD, hNLRP10-NACHT, hNLRP10^{K179M} (Walker A mutant), hNLRP10^{D249N} (Walker B mutant), or hNLRP10^{D249A} (Walker B mutant). The transfection reagent was Gene Juice and it was combined with DNA at the ration of 2.7 μL of GeneJuice per 1 μg of DNA. After 48 h of transfection, the cells were shifted to the experimental medium (in mM: 123 NaCl, 5 KCl, 2 $MgCl_2$, 1 $CaCl_2$, 10 glucose, 10 HEPES, pH 7.4) and stimulated with *m*-3M3FBS (85 μM). The untreated controls were subjected to medium alone. After addition of *m*-3M3FBS, cells were centrifuged at RT, 340 × g for 5 min. After 30 min of stimulation, cells were fixed with 4% formaldehyde, counterstained with the nuclear dye DRAQ5 (5 μM) and imaged using a confocal microscope.
Images are representative of 4 independent experiments. Scale bars correspond to 5 μm.

Two principal conclusions could be made based on these observations. First, the NLRP10 NACHT domain is a cytosolic protein in unstimulated cells but localizes in puncta upon challenge with *m*-3M3FBS (white arrowheads in the overlay images Figure 7.5 point to the examples of NLRP10 puncta). Such behavior was not observed for the NLRP10 PYD domain, suggesting that the molecular apparatus responsible for sensing of the *m*-3M3FBS-elicited changes and for the NLRP10 translocation resides in the NACHT domain. Secondly, the *m*-3M3FBS-induced puncta formation was not completely abolished by the NLRP10 Walker A/B mutations, even though the localization shift of the Walker A/B mutants was less conspicuous than that of the full-length WT protein. This suggests that the Walker A/B motifs disruption at most confers a partial defect in the NLRP10 translocation. There is relatively little known about the mechanisms linking the NACHT domains' ATPase activity with the inflammasome formation by the NLRP subfamily members, so this observation is difficult to interpret. Based on the research on other AAA+ ATPases, it could be suspected that the mutations in the NLRP10 Walker A/B motifs impede the NLRP10 oligomerization (Proell et al., 2008).

To ensure that the observed changes in the NLRP10 Walker A/B mutant translocation were quantitative (different degree of translocation) rather than qualitative (translocation to a different subcellular compartment), I transiently overexpressed the truncated and Walker A/B NLRP10 mutants fused to mCitrine in HEK cells stably overexpressing full-length WT NLRP10^{mCherry} (NLRP10^{mCherry} HEK cells). I then performed confocal microscopy on untreated and *m*-3M3FBS-stimulated samples and examined the colocalization between the mutant (mCitrine) and WT (mCherry) NLRP10 variants (Figure 7.6).

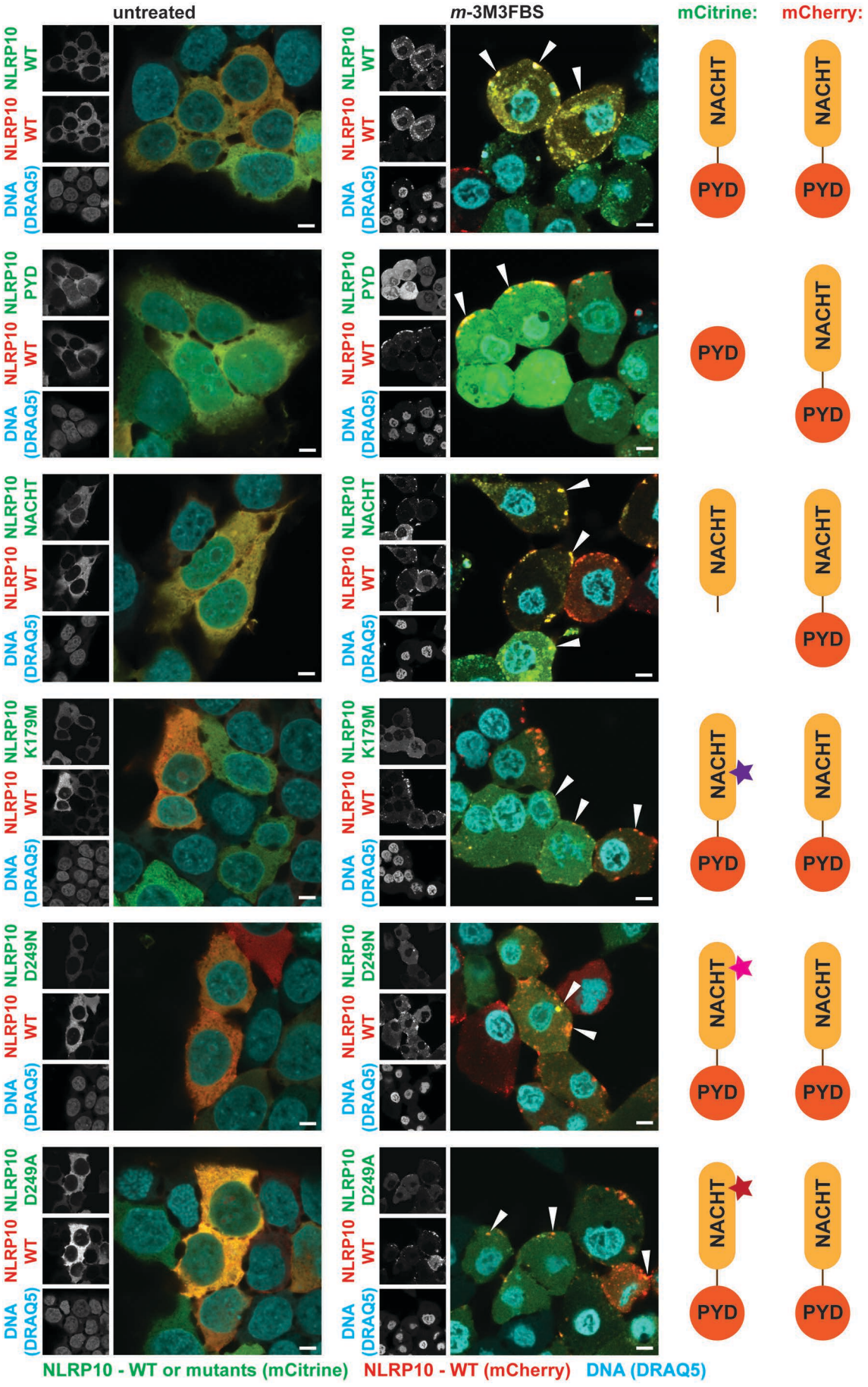

Figure 7.6. Colocalization of full-length WT NLRP10 with the NLRP10 PYD and NACHT domains, and the NLRP10 Walker A/B mutants in untreated and *m*-3M3FBS-stimulated HEK cells

◂ NLRP10^{mCherry} HEK cells were transfected with the following vectors in wells of a 96-well plate (200 ng of DNA per well, all NLRP10 variants were expressed as fusion proteins with mCitrine): human (h) WT NLRP10 (full length), hNLRP10-PYD, hNLRP10-NACHT, hNLRP10^{K179M} (Walker A mutant), hNLRP10^{D249N} (Walker B mutant), or hNLRP10^{D249A} (Walker B mutant). The transfection reagent was Gene Juice and it was combined with DNA at the ration of 2.7 μL of GeneJuice per 1 μg of DNA. After 48 h of transfection, the cells were shifted to the experimental medium (in mM: 123 NaCl, 5 KCl, 2 $MgCl_2$, 1 $CaCl_2$, 10 glucose, 10 HEPES, pH 7.4) and stimulated with *m*-3M3FBS (85 μM). The untreated controls were subjected to medium alone. After addition of *m*-3M3FBS, cells were centrifuged at RT, 340 × g for 5 min. After 30 min of stimulation, cells were fixed with 4% formaldehyde, counterstained with the nuclear dye DRAQ5 (5 μM) and imaged using a confocal microscope.
Images are representative of 4 independent experiments. Scale bars correspond to 5 μm.

Upon challenge with *m*-3M3FBS, the NLRP10 NACHT domain colocalized with full-length NLRP10 almost perfectly, indicating that these proteins follow the same translocation pathway (white arrowheads in Figure 7.6 point to the examples of colocalization between full-length WT NLRP10 and the NLRP10 mutants). In contrast, there was only a low level of recruitment of the NLRP10 PYD domain to the full-length NLRP10 puncta (Figure 7.6), with most of the NLRP10 PYD remaining in the cytosol. This observation is generally consistent with the localization pattern observed for the NLRP10 PYD domain in the absence of full-length NLRP10 (Figure 7.5). Furthermore, it suggests that the NLRP10 PYD domain does not have the intrinsic propensity to form elongated filaments that was reported for the ASC PYD domain (Lu et al., 2014) and the NLRP3 PYD domain (Stutz et al., 2017).

The NLRP10 Walker A and B mutants also colocalized with the WT protein upon the challenge with *m*-3M3FBS (Figure 7.6). Of note, in *m*-3M3FBS-treated cells the distribution of WT NLRP10 was overall more granular than that of the NLRP10 Walker A/B mutants. The WT protein also had a less pronounced residual cytosolic signal upon the *m*-3M3FBS challenge, compared to the mutant variants. This result is consistent with, but does not prove, the possible defect in the NLRP10 oligomerization when the Walker A/B motifs are disrupted.

Taken together, the targeted mutagenesis results demonstrate that the NLRP10 NACHT domain enables the NLRP10 translocation upon the challenge with *m*-3M3FBS. The PYD domain is likely involved in the subsequent recruitment of ASC. The NLRP10 mutations that abolish its ATPase activity do not completely block the NLRP10 translocation, possibly acting at or downstream of the oligomerization step. Although the truncated

and Walker A/B NLRP10 mutants do not have the capacity to seed ASC specks, they do not exhibit dominant negative characteristics.

7.5. NLRP10 overexpression restores the inflammasome responses to *m*-3M3FBS, *o*-3M3FBS, SC-9, SC-10, thapsigargin, and SMBA1 in AIM2-deficient murine macrophages

So far, I have demonstrated that NLRP10 can recruit ASC to speck-like structures in cells challenged with *m*-3M3FBS, *o*-3M3FBS, thapsigargin, SC-9, SC-10, and SMBA1 (Figure 7.1, Supplementary Figures S27 and S28). I have not shown that these ASC specks have the capacity to further engage pro-caspase-1, leading to the productive initiation of the inflammasome signaling. To address this issue, I overexpressed human or murine full-length WT NLRP10 or the NLRP10 truncated or Walker A/B mutants in AIM2-deficient immortalized murine macrophages (*Aim2*^{CRISPR} iMac cells)[1]. I primed these cells with LPS to induce pro-IL-1β expression and challenged them with *m*-3M3FBS or thapsigargin, followed by measurement of IL-1β concentrations in the supernatants (Figure 7.7 A, B, F-L). As controls, I used *Aim2*^{CRISPR} iMac cells reconstituted with two different human AIM2-encoding constructs or with murine AIM2 (Figure 7.7 C-E). As all tested cell lines were NLRP3-proficient, nigericin served as a control to evaluate the general ability to activate the inflammasome. Poly-(dA:dT) stimulation was used to confirm the successful reconstitution of AIM2 in *Aim2*^{CRISPR} iMac cells.

[1] The inflammasome responses to *m*-3M3FBS, thapsigargin, SC-10, and SMBA1 are fully dependent on AIM2 in murine macrophages (Sections 6.8, 6.9, and 6.16), and these cells do not express NLRP10 (Lautz et al., 2012; Nakajima et al., 2018; Vacca et al., 2017).

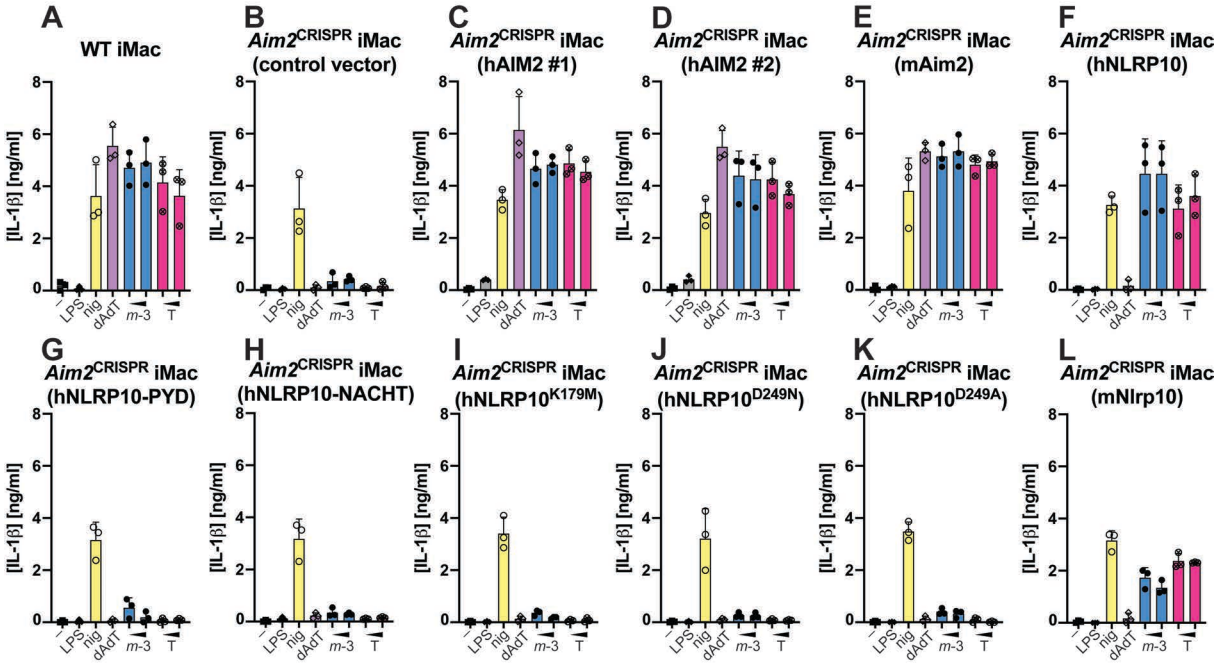

Figure 7.7. IL-1β secretion from AIM2-deficient immortalized murine macrophages (*Aim2*^{CRISPR} iMac cells) overexpressing human or murine AIM2, human or murine full-length WT NLRP10, or human NLRP10 truncation or Walker A/B mutants

A-L: WT iMac cells (A), or *Aim2*^{CRISPR} iMac cells stably transduced with the control vector (B), human (h) AIM2 (vector 241 in the Institute of Innate Immunity database; C), hAIM2 (vector 1044 in the Institute of Innate Immunity database; D), murine (m) Aim2 (E), WT hNLRP10 (F), hNLRP10-PYD domain (G), hNLRP10-NACHT domain (H), hNLRP10^{K179M} (Walker A mutant; I), hNLRP10^{D249N} (Walker B mutant; J), hNLRP10^{D249A} (Walker B mutant; K), or WT mNlrp10 (L) were left unprimed or stimulated with LPS (200 ng/mL, 2 h) to induce pro-IL-1β synthesis. The LPS-primed cells were then left untreated or were further stimulated with *m*-3M3FBS, (*m*-3; 70 or 85 μM), thapsigargin (T; 20 or 25 μM), nigericin (nig; 10 μM), or poly-(dA:dT) (dAdT; 2 μg/mL complexed with 5 μL Lipofectamine 2000) in an extracellular medium consisting of (in mM) 123 NaCl, 5 KCl, 2 $MgCl_2$, 1 $CaCl_2$, 10 glucose, 10 HEPES, pH 7.4. The unprimed (-) and LPS controls were subjected to medium alone. Immediately after addition of inflammasome activators, the plates were centrifuged at 340 × g for 5 min (RT). After 60 min, the supernatants were collected and IL-1β concentrations were measured by HTRF.
The results are plotted as means from 3 independent experiments performed in technical duplicate. Error bars represent SD. Individual data points represent means of the technical duplicate values from each of the independent experiments.

Whereas WT iMac cells responded to all tested inflammasome activators, *Aim2*^{CRISPR} iMac cells transduced with the empty vector only secreted IL-1β in response to nigericin, but not poly-(dA:dT), *m*-3M3FBS, and thapsigargin (Figure 7.7 A, B). Reconstitution with human or murine AIM2 restored the inflammasome responses to poly-(dA:dT), *m*-3M3FBS, and thapsigargin at a level similar to WT iMac cells (Figure 7.7 A, C-E). Reconstitutions with human (Figure 7.7 F) and murine (Figure 7.7 L) full-length WT NLRP10 allowed for IL-1β secretion upon the challenge with *m*-3M3FBS and thapsigargin, but not with poly-(dA:dT). As expected, these responses required the full-length NLRP10 protein with intact Walker A and B motifs (Figure 7.7 G-K).

These observations indicate that NLRP10 is fully capable of eliciting an inflammasome response resulting in IL-1β secretion. Of note, the NLRP10 overexpression in AIM2-deficient cells did not enable the inflammasome response to poly-(dA:dT), suggesting that dsDNA is not a ligand for NLRP10. It is likely that, even though *m*-3M3FBS and thapsigargin activate AIM2 and NLRP10 through similar types of damage, the direct agonists of these sensors are not the same.

Importantly, overexpression of full-length WT NLRP10 as well as all the NLRP10 mutants did not result in the inhibition of the NLRP3 inflammasome activation with nigericin. This observation indicates that NLRP10, contrary to previous reports (Imamura et al., 2010; Wang et al., 2004), may not have a direct inhibitory impact on the inflammasome activation. It also suggests that the elevated inflammasome responses that I observed in NLRP10-deficient BMDMs (Figure 6.7) were not causally linked to the lack of NLRP10 but more likely due to the genetic background differences or other confounding factors. Such interpretation is supported by the fact that NLRP10 is not expressed in macrophages (Lautz et al., 2012; Nakajima et al., 2018; Vacca et al., 2017) and by several studies reporting normal levels of inflammasome activation in NLRP10-deficient cells (Krishnaswamy et al., 2015; Nakajima et al., 2018; Vacca et al., 2017). Overall, the results presented here indicate that NLRP10 is an NLRP family member capable of nucleating a functional inflammasome *in vitro*, and that it is not an inflammasome inhibitory factor.

To establish whether the NLRP10-driven IL-1β release is dependent on caspase-1, I pre-treated LPS-primed NLRP10-overexpressing *Aim2*$^{\text{CRISPR}}$ iMac cells with the caspase-1 inhibitor VX-765, followed by stimulation with the inflammasome activators and measurement of IL-1β concentrations in the supernatants (Figure 7.8). AIM2-deficient cells reconstituted with human or murine AIM2 served as a control. In addition, I tested whether the principal findings on the pharmacology of the *m*-3M3FBS-/thapsigargin-triggered inflammasome responses (Figures 6.6, 6.37, Supplementary Figure S7) could be reproduced in this experimental system. To this end, I tested the sensitivities of the NLRP10 inflammasome responses to the NLRP3 inhibitor CRID3 and to the mitoprotective agent CsA (Figure 7.8).

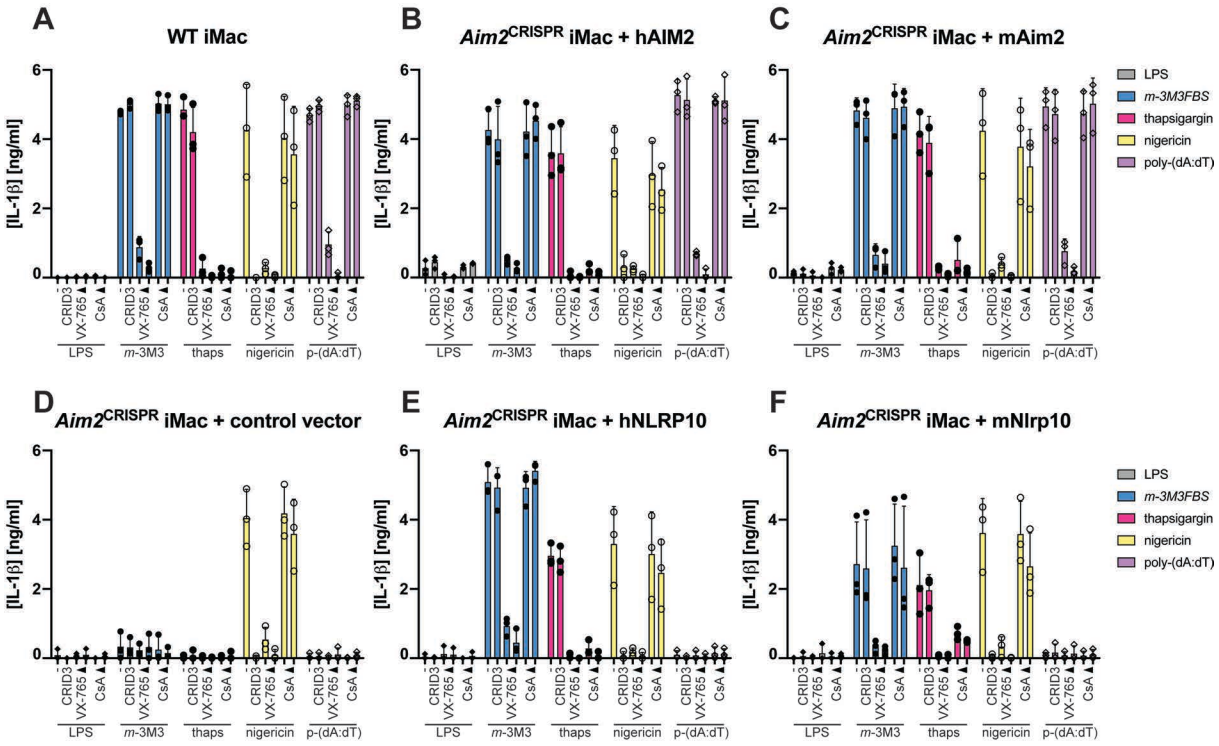

Figure 7.8. The impact of the caspase-1 inhibitor VX-765, the NLRP3 inhibitor CRID3, and the mitoprotective agent cyclosporin A on the AIM2- and NLRP10-driven IL-1β responses
A-F: WT iMac cells (A), or *Aim2*^{CRISPR} iMac cells stably transduced with the control vector (D), human (h) AIM2 (vector 1044 in the Institute of Innate Immunity database; B), murine (m) Aim2 (C), WT hNLRP10 (E), or WT mNlrp10 (F) were stimulated with LPS (200 ng/mL, 2 h) to induce pro-IL-1β synthesis. Next, the cells were shifted to an extracellular medium consisting of (in mM) 123 NaCl, 5 KCl, 2 $MgCl_2$, 1 $CaCl_2$, 10 glucose, 10 HEPES, pH 7.4 and treated for 10 min with the NLRP3 inhibitor CRID3 (5 μM), the caspase-1 inhibitor VX-765 (10 or 25 μM), or the mitoprotective agent cyclosporin A (CsA; 5 or 10 μM), or they were left untreated. Then the cells were further stimulated with *m*-3M3FBS, (*m*-3M3; 85 μM), thapsigargin (thaps; 20 μM), nigericin (10 μM), or poly-(dA:dT) (p-(dA:dT); 2 μg/mL complexed with 5 μL Lipofectamine 2000). The LPS controls were subjected to medium alone. Immediately after addition of inflammasome activators, the plates were centrifuged at 340 × g for 5 min (RT). After 60 min, the supernatants were collected and IL-1β concentrations were measured by HTRF.
The results are plotted as means from 3 independent experiments performed in technical duplicate. Error bars represent SD. Individual data points represent means of the technical duplicate values from each of the independent experiments.

The AIM2 (Figure 7.8 A-C) and NLRP10 (Figure 7.8 E, F) IL-1β responses to *m*-3M3FBS and thapsigargin were abolished by VX-765, indicating the dependence on caspase-1. Consistent with my earlier results (Figure 6.6 and Supplementary Figure S7), these responses were not sensitive to CRID3, whereas the NLRP3 inhibitor fully blocked the nigericin-induced IL-1β secretion (Figure 7.8). In further agreement with my earlier observations (Figure 6.37), CsA blocked the AIM2 and NLRP10 responses to thapsigargin but had no impact on the *m*-3M3FBS-elicited IL-1β secretion (Figure 7.8 A-C, E, F). These results indicate that the NLRP10 overexpression in macrophages enables AIM2- and NLRP3-independent IL-1β responses to *m*-3M3FBS and thapsigargin, and that these responses are mediated by caspase-1.

In my previous experiments, I identified SC-10 and SMBA1 as 'double' AIM2/NLRP10 activators (Figures 6.24, 6.43, and 6.44). Furthermore, two molecules, *o*-3M3FBS and SC-9, elicited the NLRP10-driven ASC speck formation but did not activate the AIM2 inflammasome (Figures 6.4 and 6.24). In the final set of experiments on the inflammasome-forming properties of NLRP10, I tested whether *o*-3M3FBS and SC-9, SC-10, and SMBA1 could induce IL-1β secretion from AIM2-deficient macrophages overexpressing NLRP10 (Figure 7.9 E, F). AIM2-deficient macrophages reconstituted with human or murine AIM2 served as controls (Figure 7.9 B, C).

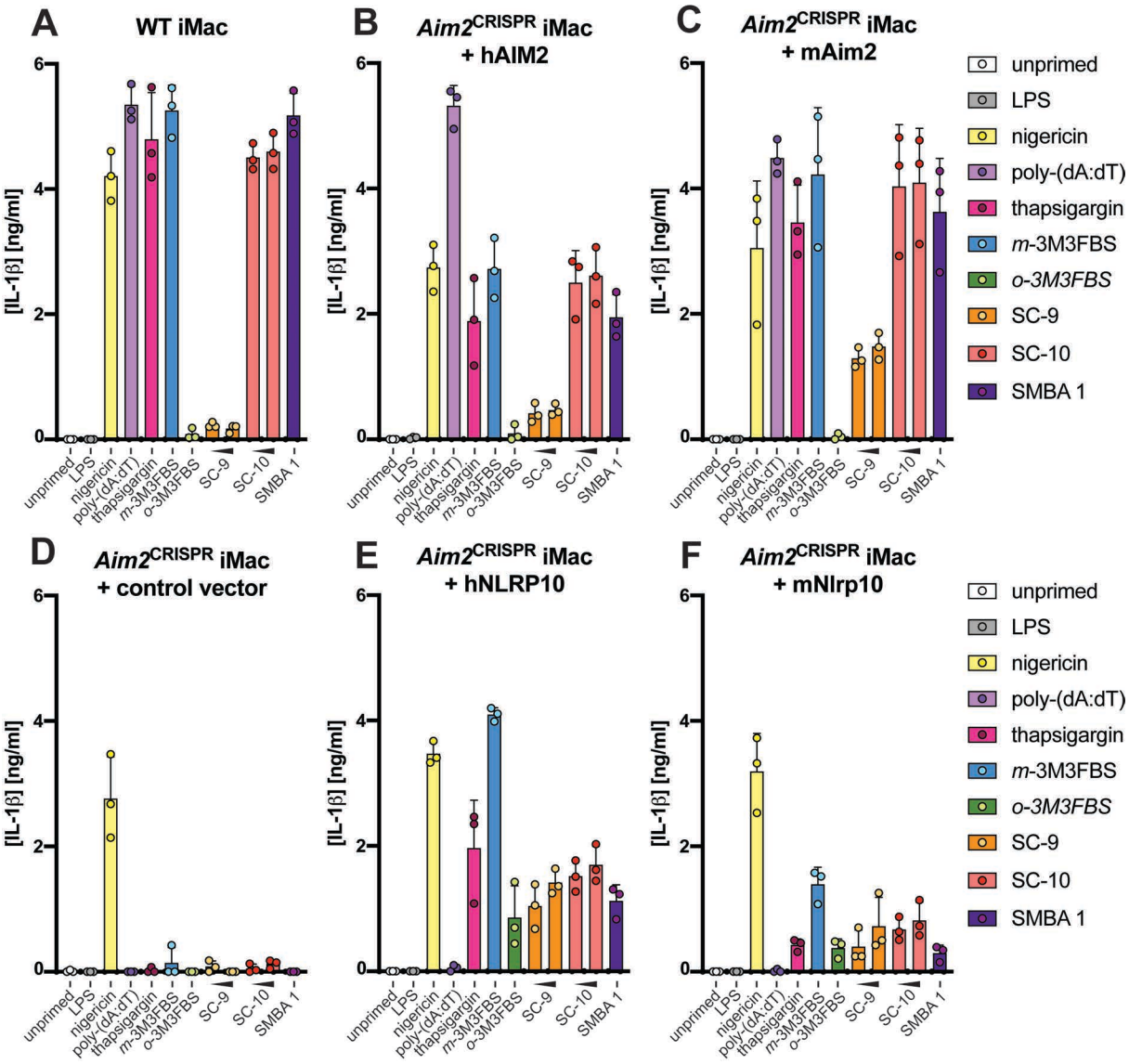

Figure 7.9. The IL-1β responses to *o*-3M3FBS, SC-9, SC-10, and SMBA1 in AIM2-deficient immortalized murine macrophages (*Aim2*^{CRISPR} iMac cells) reconstituted with human or murine NLRP10 or AIM2

A-F: WT iMac cells (A), or *Aim2*^{CRISPR} iMac cells stably transduced with the control vector (D), human (h) AIM2 (vector 1044 in the Institute of Innate Immunity database; B), murine (m) Aim2 (C), WT hNLRP10 (E), or WT mNlrp10 (F) were left unprimed or stimulated with LPS (200 ng/mL, 2 h) to induce pro-IL-1β synthesis. The LPS-primed cells were then left untreated or were further stimulated with *m*-3M3FBS, (85

μM), *o*-3M3FBS (85 μM), thapsigargin (20 μM), SC-9 (75 or 100 μM), SC-10 (75 or 100 μM), SMBA1 (50 μM), nigericin (10 μM), or poly-(dA:dT) (2 μg/mL complexed with 5 μL Lipofectamine 2000) in an extracellular medium consisting of (in mM) 123 NaCl, 5 KCl, 2 $MgCl_2$, 1 $CaCl_2$, 10 glucose, 10 HEPES, pH 7.4. The unprimed and LPS controls were subjected to medium alone. Immediately after addition of inflammasome activators, the plates were centrifuged at 340 × g for 5 min (RT). After 60 min, the supernatants were collected and IL-1β concentrations were measured by HTRF.
The results are plotted as means from 3 independent experiments performed in technical duplicate. Error bars represent SD. Individual data points represent means of the technical duplicate values from each of the independent experiments.

All NLRP10 agonists identified in the ASC specking assays in NLRP10/ASC fluorescent reporter HEK cells also elicited IL-1β secretion from AIM2-deficient macrophages overexpressing NLRP10 (Figure 7.9 E, F). Notably, *m*-3M3FBS, thapsigargin, SC-10, and SMBA1 were overall more potent inflammasome activators than *o*-3M3FBS and SC-9, and reconstitution with human NLRP10 was associated with stronger IL-1β responses than murine NLRP10. The results of the AIM2 reconstitution (Figure 7.9 B, C) in AIM2-deficient cells (Figure 7.9 D) confirmed that the macrophage inflammasome responses to SC-10 and SMBA1 are mediated by AIM2. Intriguingly, SC-9 did not trigger IL-1β secretion from LPS-primed WT iMac cells (Figure 7.9 A), but it elicited a weak/intermediate IL-1β release from AIM2-overexpressing macrophages (Figure 7.9 B, C). This suggests that SC-9 might induce a low level of mitochondrial damage that is not detectable in imaging experiments (Figure 6.50) and cannot trigger the inflammasome response when endogenous amounts of AIM2 are present in the cell, but could potentially be sensed by AIM2 when its expression is driven by a strong exogenous promoter.

The results presented in this Chapter indicate that, contrary to previous reports, NLRP10 is an inflammasome-forming sensor. While the AIM2 and NLRP10 activation pathways described in my thesis show many similarities, several discrepant observations suggest that there are also points of divergence between these processes. In the next Chapter, I will focus on the exact mechanism by which AIM2 senses the mitochondrial damage induced by *m*-3M3FBS, SC-10, thapsigargin, and SMBA1.

8. mtDNA is the agonist of AIM2 in macrophages challenged with *m*-3M3FBS, thapsigargin, SC-10, and SMBA1

Earlier in my thesis, I have demonstrated that the murine macrophage inflammasome responses to *m*-3M3FBS, thapsigargin, SC-10, and SMBA1 are non-redundantly dependent on AIM2 (Sections 6.8, 6.9, and 6.16). The cellular event shared between these treatments is a severe disruption of the mitochondrial integrity, manifesting in the cytosolic leakage of fluorescent proteins targeted to the mitochondrial matrix (Sections 6.13, 6.15, and 6.16). For two of these stimuli, thapsigargin and SMBA1, the mitochondrial damage can be blocked by pre-treatment with CsA (Sections 6.15, 6.16), which correlates with the inhibition of the inflammasome responses. Given that AIM2 is known to be activated by binding to dsDNA (Fernandes-Alnemri et al., 2009; Hornung et al., 2009; Jin et al., 2012), these observations suggest an obvious candidate for the endogenous AIM2 agonist: the mitochondrial nucleoids. However, mtDNA has also been implicated in the activation of other innate immune sensors, in particular the NLRP3 inflammasome (Zhong et al., 2019). In this Chapter, I will first comment on the studies proposing the NLRP3 activation model whereby (ox-)mtDNA acts as an NLRP3 agonist. Then, I will present evidence in favor of an opposite model, suggesting that mtDNA exposed by the stimulations with *m*-3M3FBS and related compounds triggers the AIM2 inflammasome assembly.

Several early studies proposed a role for the mitochondria in the NLRP3 inflammasome activation (Menu et al., 2012; Zhou et al., 2010) but the report that directly linked mtDNA exposure to the NLRP3 activation was published by Nakahira et al. (2010). The authors of this study proposed that mtDNA is required for this response based on two lines of evidence. First, depletion of mtDNA in J774A.1 macrophages (through prolonged culturing in the presence of ethidium bromide [EtBr] or through protein transfection of DNaseI) abolished the NLRP3 response to extracellular ATP. Secondly, stimulation with ATP led to an increase in the cytosolic mtDNA content (up to four- to fivefold in WT cells). Notably, this release of mtDNA appeared to be dependent on NLRP3 and ASC, putting into question the cause/effect direction of the observed phenomenon[1].

[1] An elegant hypothetical explanation was provided by Holley and Schroder (2020): It is possible that NLRP3 agonists cause a release of a very small amount of mtDNA, which then leads to NLRP3 activation and a secondary amplification of mitochondrial damage downstream of the inflammasome assembly.

Importantly, this pioneering study into the role of mtDNA in the NLRP3 activation employed 'priming' controls, demonstrating that EtBr does not block synthesis of pro-IL-1β, but did not test the impact of the prolonged EtBr treatments on the activation of other inflammasomes. This is understandable as the paper under consideration was published less than two years after the discovery of AIM2 as the inflammasome-forming dsDNA receptor (Fernandes-Alnemri et al., 2009; Hornung et al., 2009) and almost a year before the activation of NLRC4 by flagellin and bacterial type III secretion system components was reported (Zhao et al., 2011). Consequently, the study by Nakahira et al. (2010) also did not address the question whether non-NLRP3 inflammasome agonists could trigger mtDNA release to the cytosol.

A further indication that NLRP3 might be activated by (ox-)mtDNA was provided by the observation that NLRP3 overexpressed in HEK 293T cells colocalized with transfected mtDNA, regardless of the oxidation status of the latter (Shimada et al., 2012). Correspondingly, NLRP3 co-immunoprecipitated with mtDNA upon stimulation with ATP, and to a lesser extent with nigericin[2]. LPS-primed AIM2-deficient BMDMs subjected to oxDNA transfection secreted IL-1β, albeit at a very low level (~100 pg/mL, compared to ~500 pg/mL upon stimulation with ATP), whereas NLRP3-deficient BMDMs had a slightly reduced response to oxDNA transfection compared to unoxidized DNA (in WT BMDMs this trend was reversed). In further support of the notion that NLRP3 is activated by ox-mtDNA, Shimada et al. (2012) demonstrated that the NLRP3 agonists cause oxidative damage of mtDNA, manifesting as an increase in the 8-hydroxy-2'-deoxyguanosine (8-OH-dG) content. Exposing cells to high concentrations of monomeric 8-OH-dG nucleosides blocked the NLRP3 inflammasome responses.

A later study proposed that synthesis of mtDNA is an integral part of the priming step in the NLRP3 activation cascade (Zhong et al., 2018). This was demonstrated to rely on the IRF1-driven upregulation of the mitochondrial CMP-UMP kinase 2, an enzyme catalyzing the rate-limiting step providing nucleotides for mtDNA replication. The mtDNA molecules are then believed to activate the NLRP3 inflammasome upon treatment with the NLRP3 triggering stimuli (signal 2). Zhong et al. (2018) reported a dramatic

[2] Of note, all results of NLRP3-mtDNA co-immunoprecipitation experiments published to date were obtained in ASC- and caspase-1-proficient cells, so there remains a possibility that the reported NLRP3-mtDNA interaction could be a downstream effect of ASC speck formation.

decrease in the inflammasome response to oxDNA fragments upon NLRP3 depletion with shRNA, without the need for concomitant AIM2 silencing. This observation was in contrast to the previous report, where NLRP3-deficient BMDMs still secreted relatively high amounts IL-1β when exposed to oxDNA (Shimada et al., 2012). Importantly, although Zhong et al. (2018) reported that IRF1-deficient BMDMs have defective canonical NLRP3 responses, another group did not observe such a dependence and instead detected normal levels of canonical NLRP3 activation in IRF1-deficient cells (Kuriakose et al., 2018; Man et al., 2015).

To add to the confusion, NLRP3 is not the only inflammasome suggested to be activated by (ox-)mtDNA. One study demonstrated that overloading of murine macrophages with cholesterol by treatment with methylcyclodextrin (MCD)-cholesterol complexes could trigger mtDNA release to the cytosol and activation of the AIM2 inflammasome (Dang et al., 2017). Importantly, two models of mtDNA depletion were employed in this paper, the EtBr treatment as well as treatment with 2',3'-dideoxycytidine (ddC), another inhibitor of mtDNA replication. In contrast to the previous reports (Nakahira et al., 2010; Shimada et al., 2012), neither of these treatments inhibited the NLRP3 inflammasome response to extracellular ATP, whereas they abolished the AIM2 activation by mtDNA upon cholesterol delivery. The authors did not comment on this discrepancy. One further study suggested that, in $CD4^+$ T cells, both NLRP3 and AIM2 could be involved in inflammasome formation upon mtDNA release caused by dysfunction of the double-strand break repair protein MRE11A (Li et al., 2019).

Finally, NLRC4 has also been reported to be activated by (ox-)mtDNA in an in vitro *Pseudomonas* (*P.*) *aeruginosa* infection model (Jabir et al., 2014). The authors of this study proposed that *P. aeruginosa* infection results in mtROS-dependent release of mtDNA to the cytosol, and that this mtDNA acts as an NLRC4 agonist. Surprisingly, but in support of this scenario, NLRC4-deficient BMDMs had attenuated responses to transfected unoxidized or oxidized ox-mtDNA. Furthermore, mtDNA depletion (either by EtBr treatment or protein transfection of DNase I) resulted in a decreased NLRC4 inflammasome response to *P. aeruginosa* infection.

Three review articles alerted the scientific community about the discrepancies in the findings linking mtDNA release to the NLRP3 inflammasome activation (Holley and

Schroder, 2020; Lawlor and Vince, 2014; Yabal et al., 2018). Based on these commentaries as well as on my own reflection, the major points of criticism towards the concept that (ox-)mtDNA activates the NLRP3 inflammasome are the following:

1. Zhong et al. (2018) propose that replication of mtDNA occurs during the (LPS) priming step, generating the ligand necessary for the NLRP3 activation. This model is not compatible with the observation that the priming step in the NLRP3 activation can be circumvented by NLRP3 overexpression driven by a constitutive promoter (Bauernfeind et al., 2009). It also does not explain why ectopic NLRP3 overexpression in non-immune cell lines such as HEK 293 enables inflammasome activation (for example Compan et al. (2012); Shi et al. (2016)). Furthermore, the activation of NLRP3 in certain cell types, such as human monocytes, has been reported to occur without the requirement for the priming stimulus (Gritsenko et al.). The question of whether monocytes have high baseline levels of ox-mtDNA has, to my knowledge, not been addressed.
2. If NLRP3 activators triggered the cytosolic release of ox-mtDNA, they would also be expected to activate AIM2, unless a mechanism exists to 'switch off' AIM2 during the NLRP3 activation, or when oxDNA is present in the cytosol. Such mechanism has not been identified so far, and the possibility of its existence has not been explored in the studies proposing that ox-mtDNA is an activator of NLRP3.

In addition, whereas the AIM2/NLRP10 activators *m*-3M3FBS, thapsigargin, SC-10, and SMBA1 all caused leakage of the mitochondrial matrix contents into the cytosol in murine macrophages (Sections 6.13 and 6.16), I did not observe such an event in cells treated with the NLRP3 agonist nigericin. If nigericin is not able to permeabilize the IMM to fluorescent proteins (MW of approximately 25 kDa), it is difficult to conceive of the idea that it could permeabilize the mitochondrial membranes to DNA molecules (the MW of a single mitochondrial nucleoid is approx. 10 MDa, and dsDNA fragments as small as 40 bp already reach the MW of a typical fluorescent protein). Theoretically, nigericin could activate a specific mechanism of mtDNA export into the cytosol, but to my knowledge such a mechanism does not exist[3].

[3] In contrast, nucleic acid *import* into the mitochondria is a phenomenon observed for some tRNA and rRNA molecules, as reviewed by Schneider (2011).

8.1. Culturing of stable cell lines in the presence of ddC or EtBr depletes mtDNA within days

In order to determine whether the AIM2, NLRP3 and NLRP10 activations depend on mtDNA, I first established a model of mtDNA depletion *in vitro*. To that end, most inflammasome studies to date have relied on inhibitors of mtDNA replication, EtBr and ddC. These molecules can be used as a long-time (weeks-months) treatment to generate the so-called ρ^0 cells (Hashiguchi and Zhang-Akiyama, 2009; Schubert et al., 2015). Such cells do not contain any mtDNA but are difficult to maintain and may significantly differ from their parental cell lines because of (oligo)clonal selection and accumulation of mutations over time.

Here, after a failed attempt to acutely deplete cytosolic DNA by DNase I protein transfection (Supplementary Figure S29; Jabir et al., 2014; Nakahira et al., 2010), I opted for a short (72-96 h) EtBr/ddC treatment, based on the protocol developed by Dang et al. (2017). Briefly, I seeded proliferating cells (WT iMac cells, NLRP3/ASC^{mCerulean} reporter iMac cells, and NLRP10^{mCitrine}/ASC^{TagBFP} HEK cells) at a very low density and allowed them to reach confluence in the presence of EtBr or ddC. The rationale behind this procedure was that when a small population of cells undergoes several divisions in the presence of an mtDNA replication inhibitor, the mtDNA content of the resulting expanded population should be strongly reduced (Figure 8.1 A).

I indeed observed a reduction in the mtDNA content in all tested cell lines cultured for 72-96 h with EtBr or ddC (Figure 8.1 B, C). In immortalized macrophages, all tested doses of EtBr and ddC resulted in a final mtDNA content that was below 1% of the mtDNA amount in the population expanded in the absence of EtBr/ddC (Figure 8.1 B). In HEK cells, the decrease in the mtDNA content was less pronounced (Figure 8.1 C). Nevertheless, the higher doses of EtBr and ddC generally resulted in an mtDNA loss of more than 90% compared to the untreated controls, which I considered to be sufficient for further experimentation.

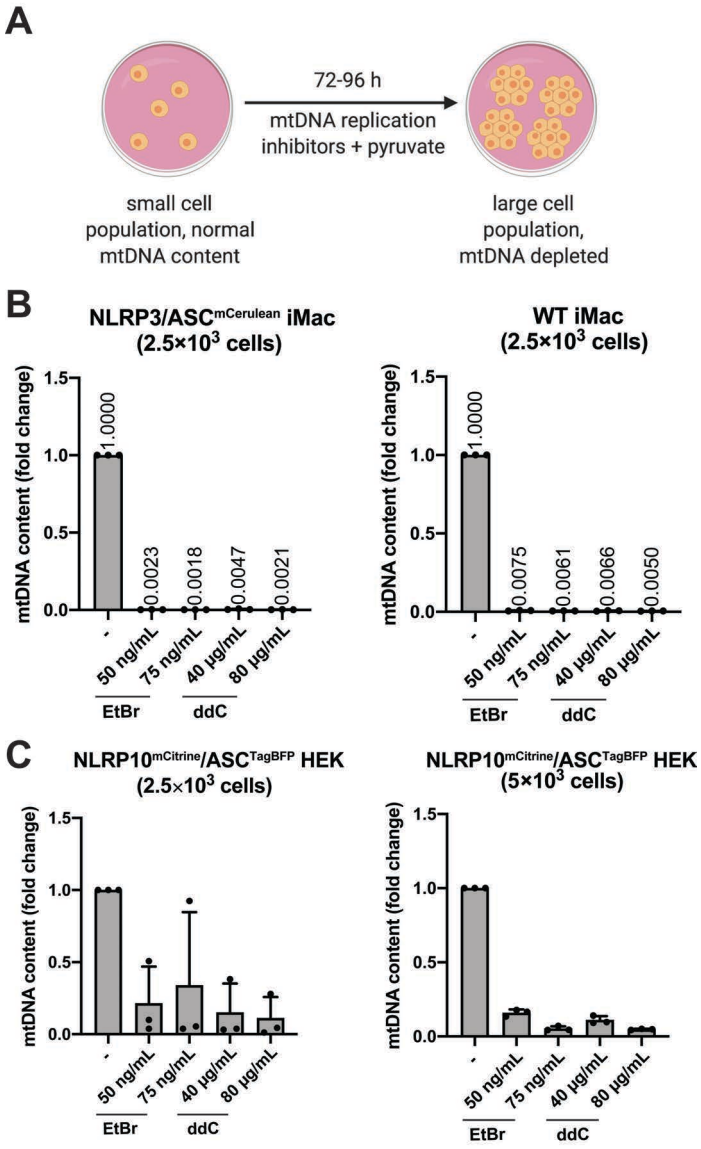

Figure 8.1. The efficiency of mtDNA depletion protocols using ethidium bromide (EtBr) and 2',3'-dideoxycytidine (ddC) in WT iMac cells, NLRP3/ASC^{mCerulean} reporter iMac cells, and NLRP10^{mCitrine}/ASC^{TagBFP} HEK cells

A: Schematic of the rationale behind the applied protocol of mtDNA depletion.

B-C: Initial populations of NLRP3/ASC^{mCerulean} reporter iMac cells (2.5×10^3 cells per well in a 96-well plate, or ~7.8×10^3 cells/cm^2; B, left), WT iMac cells (2.5×10^3 cells per well in a 96-well plate, or ~7.8×10^3 cells/cm^2; B, right), or NLRP10^{mCitrine}/ASC^{TagBFP} HEK cells (C, left panel: 2.5×10^3 cells per well in a 96-well plate, or ~7.8×10^3 cells/cm^2; right panel: 5×10^3 cells per well in a 96-well plate, or ~1.56×10^4 cells/cm^2) were grown for 72-96 h in DMEM supplemented with 10% FBS, penicillin, streptomycin, 1 mM sodium pyruvate and, where indicated, EtBr (50 or 75 ng/mL) or ddC (40 or 80 µg/mL). After this time, the cells were lysed, total DNA was isolated, and the amounts of mtDNA were assessed by quantitative PCR relative to controls grown in the absence of EtBr and ddC, and using sequences from nuclear DNA as reference analytes.

B: In macrophages, the treatments with EtBr and ddC led to a mtDNA loss of more than 99% compared to untreated controls, so the values indicating the fractional mtDNA amounts relative to untreated controls were additionally graphed above the bars.

The results are plotted as means from 3 independent experiments performed in monoplicate. Error bars represent SD. Individual datapoints represent the values obtained in each of the independent experiments.

There are two important advantages to this fast mtDNA depletion approach. The first is the speed of the procedure and the potential to easily adopt it in a range of cell lines similar to the ones in which the method had been established. Secondly, in contrast to ρ^0 cells, the short-term mtDNA-depleted cells are generated anew for each experiment. This decreases the risk of clonal or oligoclonal selection artifacts, which could occur during prolonged periods of culture in EtBr- or ddC-containing media. The drawback of this technique is that the mtDNA depletion is not complete.

8.2. mtDNA is required for the AIM2 inflammasome activation with *m*-3M3FBS and thapsigargin

To test whether mtDNA depletion affects the inflammasome activation in immortalized murine macrophages, I generated mtDNA-deficient WT iMac and NLRP3/ASC^{mCerulean} reporter iMac cells by culturing them with EtBr or ddC for 72-96 h. Control cells were grown in media without the mtDNA replication inhibitors. On the day of the experiment, the cells were either directly activated (NLRP3/ASC^{mCerulean} reporter iMac), or primed with LPS and then activated (WT iMac) with *m*-3M3FBS, thapsigargin, poly-(dA:dT), or nigericin, followed by IL-1β concentration measurement (Figure 8.2 A) and ASC speck imaging (Figure 8.2 B) to assess the degree of inflammasome activation.

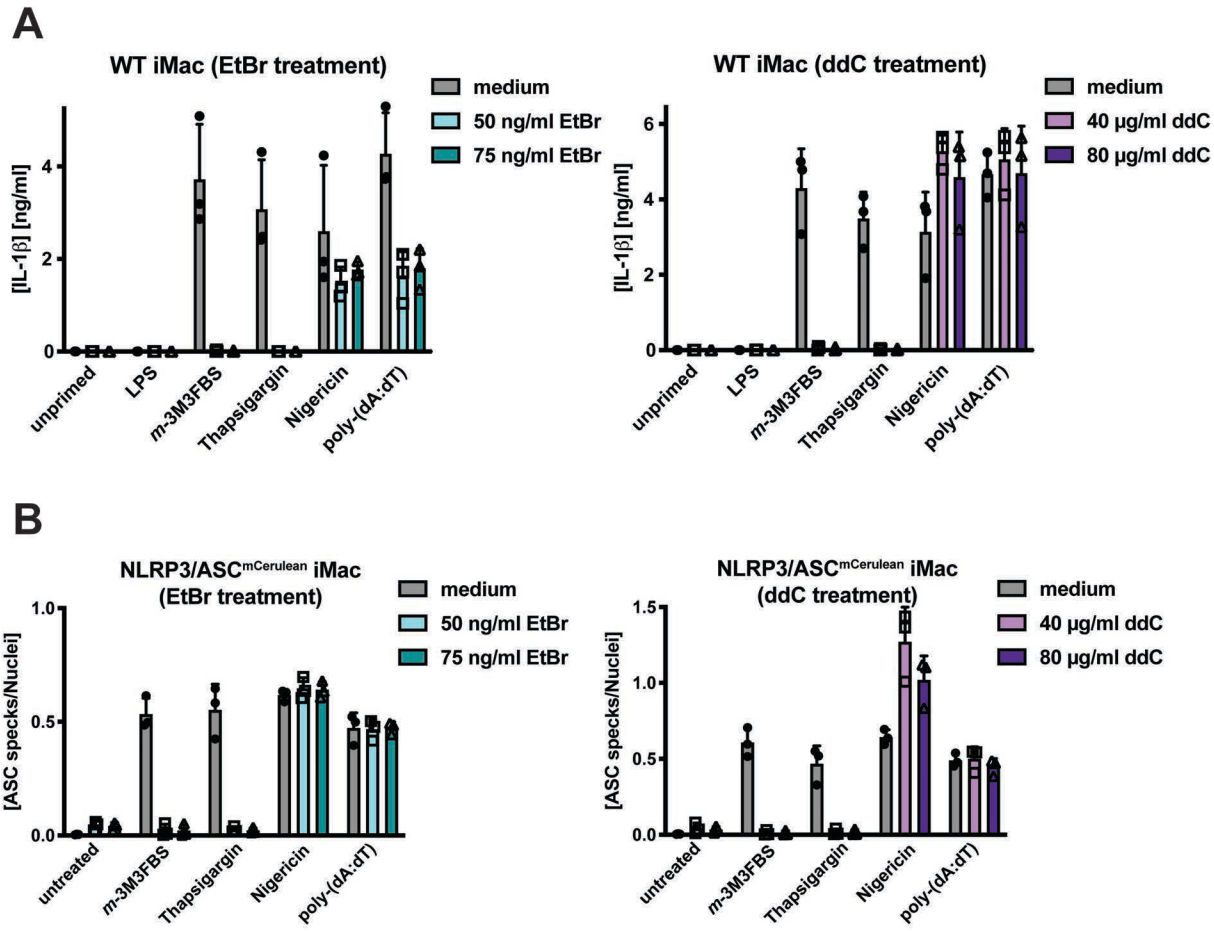

Figure 8.2. The inflammasome responses to *m*-3M3FBS, thapsigargin, poly-(dA:dT), and nigericin in WT iMac cells and NLRP3/ASC^{mCerulean} reporter iMac cells after EtBr- or ddC-mediated mtDNA depletion

A-B: WT iMac cells (A) or NLRP3/ASC^{mCerulean} reporter iMac cells (B) were plated in 96-well plates at 2.5 × 10^3 cells per well, or ~7.8 × 10^3 cells/cm^2 and grown for 72-96 h in DMEM supplemented with 10% FBS, penicillin, streptomycin, 1 mM sodium pyruvate and, where indicated, EtBr (50 or 75 ng/mL; A, B, left panels) or ddC (40 or 80 µg/mL; A, B, right panels). After reaching confluence, the cells were LPS-primed (200 ng/mL, 2 h) and stimulated with inflammasome activators (A), or directly stimulated with inflammasome activators (B) in an extracellular medium consisting of (in mM) 123 NaCl, 5 KCl, 2 $MgCl_2$, 1 $CaCl_2$, 10 glucose, 10 HEPES, pH 7.4. The tested inflammasome activators were *m*-3M3FBS (85 µM), thapsigargin (20 µM), nigericin (10 µM), and poly-(dA:dT) (2 µg/mL complexed with 5 µL Lipofectamine 2000). The LPS (A) and unprimed (A, B) controls were subjected to medium alone. Immediately after addition of inflammasome activators, the plates were centrifuged at 340 × g for 5 min (RT). After 60 min, the supernatants were collected and IL-1β concentrations were measured by HTRF (A) or the cells were fixed with 4% formaldehyde, counterstained with the nuclear dye DRAQ5 (5 µM) and imaged using a widefield fluorescence microscope (B).
The results are plotted as means from 3 independent experiments performed in technical triplicate. Error bars represent SD. Individual data points represent means of the technical triplicate values from each of the independent experiments.

The AIM2 activation with *m*-3M3FBS and thapsigargin was completely abolished in mtDNA-depleted macrophages, both at the level of IL-1β secretion and ASC speck formation. In contrast, mtDNA-depleted macrophages remained responsive to the NLRP3 agonist nigericin and to the AIM2 ligand poly-(dA:dT) (Figure 8.2). Whereas the EtBr treatment did not affect ASC speck formation in cells stimulated with poly-(dA:dT)

and with nigericin (Figure 8.2 B, left panel), it led to decreased levels of secreted IL-1β upon these stimulations (Figure 8.2 A, left panel). This decrease was not observed in cells cultured with ddC (Figure 8.2, right column), suggesting that EtBr may partly interfere with pro-IL-1β production, but not in a manner related to mtDNA depletion.

Two conclusions can be made based on these results. First, mtDNA likely serves as the ligand for AIM2 in *m*-3M3FBS- and thapsigargin-stimulated cells. Secondly, NLRP3 activation with nigericin is not affected by loss of mtDNA, and in some instances is even slightly increased (Figure 8.2 A, B, right panels). This observation suggests that mtDNA might not be the ligand of NLRP3 and might not even be required for activation of this inflammasome. This is in contrast to several previously reported NLRP3 activation models (Nakahira et al., 2010; Shimada et al., 2012; Zhong et al., 2018), which I will explore in more detail in Sections 8.6-8.10.

8.3. mtDNA is not required for the NLRP10 activation with *m*-3M3FBS and thapsigargin

To test whether mtDNA depletion affects the NLRP10 inflammasome activation, I generated mtDNA-deficient NLRP10^{mCitrine}/ASC^{TagBFP} HEK cells by culturing them with EtBr or ddC for 72-96 h. Control cells were grown in media without the mtDNA replication inhibitors. On the day of the experiment, the cells were challenged with *m*-3M3FBS or thapsigargin, and the degree of inflammasome activation was assessed by imaging of ASC specks (Figure 8.3).

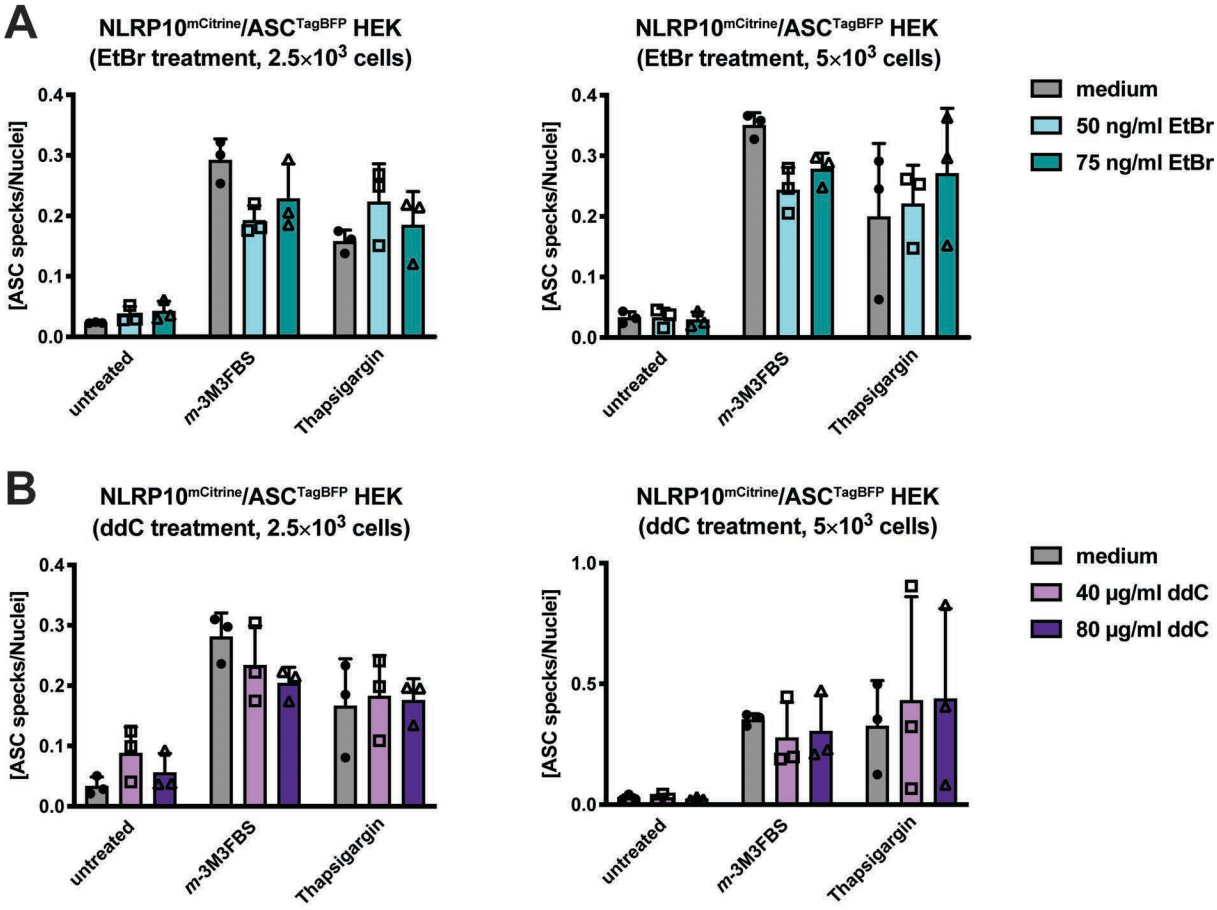

Figure 8.3. NLRP10 activation with *m*-3M3FBS and thapsigargin in mtDNA-depleted NLRP10^{mCitrine}/ASC^{TagBFP} HEK cells

A-B: NLRP10^{mCitrine}/ASC^{TagBFP} HEK cells were plated in 96-well plates at 2.5 × 10^3 cells per well, or ~7.8 × 10^3 cells/cm^2 (A, B, left panels) or at 5 × 10^3 cells per well in a 96-well plate, or ~1.56 × 10^4 cells/cm^2 (A, B, right panels) and grown for 72-96 h in DMEM supplemented with 10% FBS, penicillin, streptomycin, 1 mM sodium pyruvate and, where indicated, EtBr (50 or 75 ng/mL; A) or ddC (40 or 80 µg/mL; B). After reaching confluence, the cells were directly stimulated with inflammasome activators in an extracellular medium consisting of (in mM) 123 NaCl, 5 KCl, 2 $MgCl_2$, 1 $CaCl_2$, 10 glucose, 10 HEPES, pH 7.4. The tested inflammasome activators were *m*-3M3FBS (85 µM) and thapsigargin (20 µM). The untreated controls were subjected to medium alone. Immediately after addition of inflammasome activators, the plates were centrifuged at 340 × g for 5 min (RT). After 30 min, the cells were fixed with 4% formaldehyde,

counterstained with the nuclear dye DRAQ5 (5 μM) and imaged using a widefield fluorescence microscope.
The results are plotted as means from 3 independent experiments performed in technical triplicate. Error bars represent SD. Individual data points represent means of the technical triplicate values from each of the independent experiments.

Regardless of the agent used for mtDNA depletion or the size of the initial cell population, the loss of mtDNA did not result in considerable changes in the NLRP10 activation level (Figure 8.3). On average, the level of the *m*-3M3FBS-elicited ASC specking appeared slightly lower in mtDNA-deficient cells compared to mtDNA-proficient controls, whereas for the thapsigargin-driven NLRP10 activation this trend was reversed. This demonstrates that HEK cells overexpressing NLRP10 remain responsive to *m*-3M3FBS and thapsigargin after mtDNA depletion.

This result indicates that mtDNA is not required for the NLRP10 inflammasome formation. A direct interpretation is that mtDNA is probably not a ligand of NLRP10. Furthermore, it can also be anticipated that the molecules whose synthesis depends on mtDNA are dispensable for the NLRP10 activation. These molecules include mitochondrial rRNAs, mitochondrially encoded tRNAs, as well as several mitochondrial electron transport chain subunits. The knowledge that the NLRP10 activation is not affected by mtDNA deficiency may narrow down the future attempts to identify the cellular agonists of NLRP10.

8.4. Overexpression of NLRP10 restores the inflammasome responses to *m*-3M3FBS and related activators in macrophages depleted of mtDNA

NLRP10 is capable of nucleating a functional inflammasome (Chapter 7). This process is not affected by mtDNA depletion with EtBr/ddC (Figure 8.3). Consequently, it can be expected that the NLRP10 overexpression would rescue the inflammasome responses to *m*-3M3FBS and thapsigargin in mtDNA-deficient macrophages, in which the AIM2 activation by endogenous mtDNA is no longer possible.

To test this hypothesis, I depleted mtDNA in NLRP3/ASC^{mCerulean} reporter iMac cells stably overexpressing WT human or murine NLRP10, Walker A (K179M) or B (D249N, D249A) motif mutants of human NLRP10, or the empty vector. After mtDNA depletion, the cells were primed with LPS and challenged with *m*-3M3FBS, thapsigargin, nigericin,

or poly-(dA:dT), and the level of inflammasome activation was assessed by measurement of the IL-1β concentrations and imaging of ASC specks (Figures 8.4 and 8.5).

In NLRP3/ASC^{mCerulean} reporter iMac cells with mtDNA depleted using ddC, the overexpression of human or murine WT NLRP10 provided full or partial rescue of the inflammasome responses to *m*-3M3FBS and thapsigargin, compared to the empty vector control (Figure 8.4 A-C). The NLRP3 response to nigericin and the AIM2 response to poly-(dA:dT) were both unaffected by mtDNA depletion, consistent with previous results (Figure 8.2). Of note, overexpression of NLRP10 did not inhibit the NLRP3 and AIM2 activations, which is in agreement with the results presented in Figures 7.7-7.9. This confirms that NLRP10 is not an inflammasome-inhibitory molecule. Overexpression of Walker A/B mutants of human NLRP10 did not rescue the inflammasome responses to *m*-3M3FBS and thapsigargin in mtDNA-depleted cells (Figure 8.4 D-F). This observation is in agreement with the results described in Sections 7.3 and 7.5. It confirms that the NLRP10-driven inflammasome formation relies on intact Walker A/B sequences.

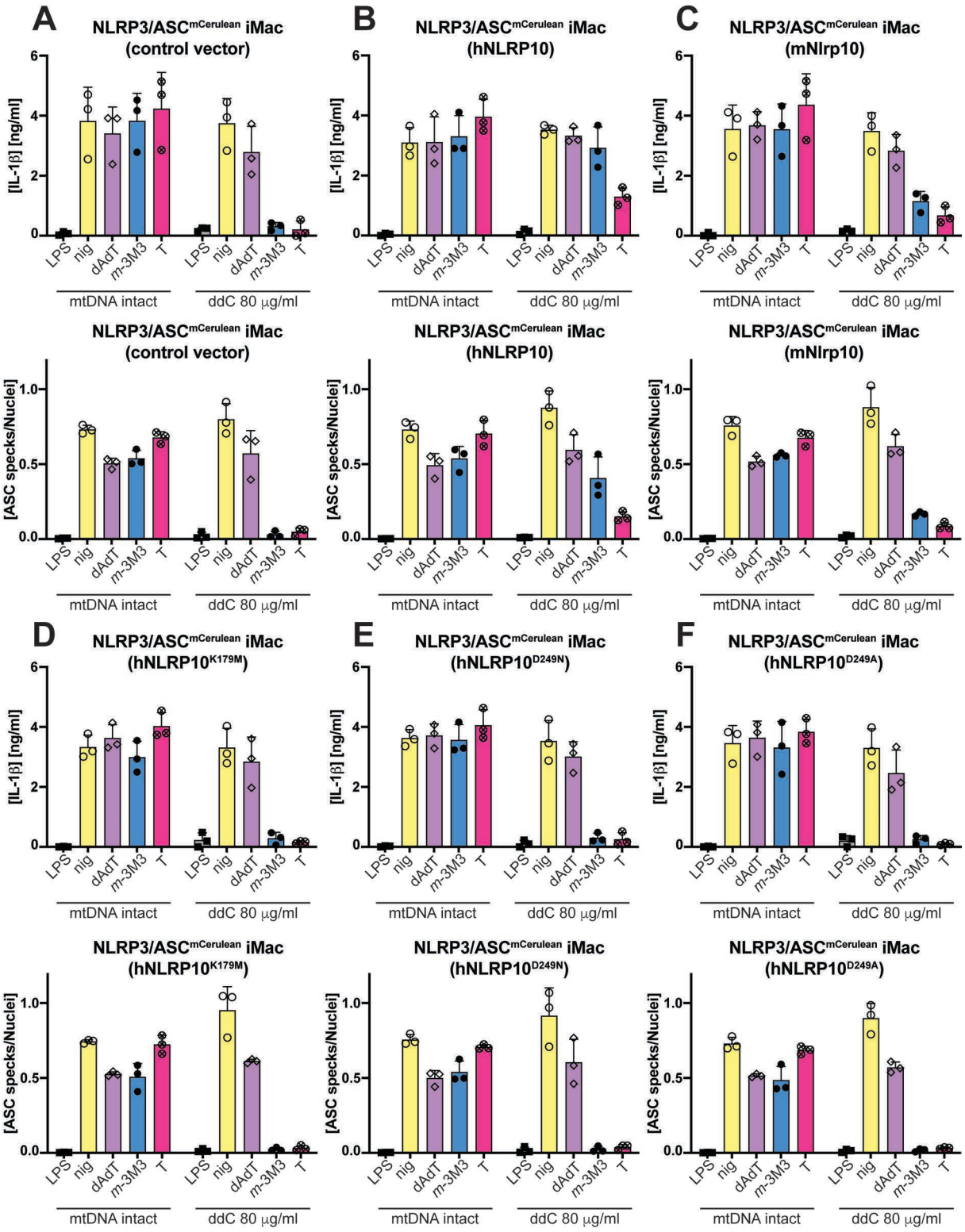

Figure 8.4. NLRP10 overexpression restores the inflammasome responses to *m*-3M3FBS and thapsigargin in macrophages after mtDNA depletion with ddC

A-F: NLRP3/ASC^{mCerulean} reporter iMac cells stably transduced with the control vector (A) or WT human (h) NLRP10 (B), WT murine (m) NLRP10 (C), hNLRP10^{K179M} (Walker A mutant; D), hNLRP10^{D249N} (Walker B mutant; E), or hNLRP10^{D249A} (Walker B mutant; F) were plated in 96-well plates at 2.5 × 10^3 cells per well, or ~7.8 × 10^3 cells/cm^2 and grown for 72-96 h in DMEM supplemented with 10% FBS, penicillin, streptomycin, 1 mM sodium pyruvate and, where indicated, ddC (80 μg/mL). After reaching confluence, the cells were LPS-primed (200 ng/mL, 2 h) and stimulated with inflammasome activators in an extracellular medium consisting of (in mM) 123 NaCl, 5 KCl, 2 $MgCl_2$, 1 $CaCl_2$, 10 glucose, 10 HEPES, pH 7.4. The tested inflammasome activators were *m*-3M3FBS (*m*-3M3; 85 μM), thapsigargin (T; 20 μM),

nigericin (nig; 10 μM), and poly-(dA:dT) (dAdT; 2 μg/mL complexed with 5 μL Lipofectamine 2000). The LPS controls were subjected to medium alone. Immediately after addition of inflammasome activators, the plates were centrifuged at 340 × g for 5 min (RT). After 60 min, the supernatants were collected and IL-1β concentrations were measured by HTRF (A-F, top panels) or the cells were fixed with 4% formaldehyde, counterstained with the nuclear dye DRAQ5 (5 μM) and imaged using a widefield fluorescence microscope (A-F, bottom panels).
The results are plotted as means from 3 independent experiments performed in technical duplicate. Error bars represent SD. Individual data points represent means of the technical duplicate values from each of the independent experiments.

When mtDNA was depleted using EtBr, overexpression of WT human or murine NLRP10 provided full or partial rescue in the responses to *m*-3M3FBS and thapsigargin only at the level of ASC speck formation (Figure 8.5 A-C). Under those conditions, none of the inflammasome stimuli tested were able to trigger the release of IL-1β from mtDNA-depleted cells, suggesting that the EtBr treatment may have resulted in pro-IL-1β synthesis defect, or, less likely, a global defect at the level of pro-IL-1β processing/secretion. Overexpression of Walker A/B mutants of human NLRP10 did not rescue the inflammasome responses to *m*-3M3FBS/thapsigargin (Figure 8.5 D-F). Collectively, these results are consistent with my previous observation that the NLRP10 activation is not inhibited by the loss of mtDNA (Section 8.3). They demonstrate that NLRP10 overexpression can rescue the inflammasome activation with *m*-3M3FBS and thapsigargin in mtDNA-deficient macrophages.

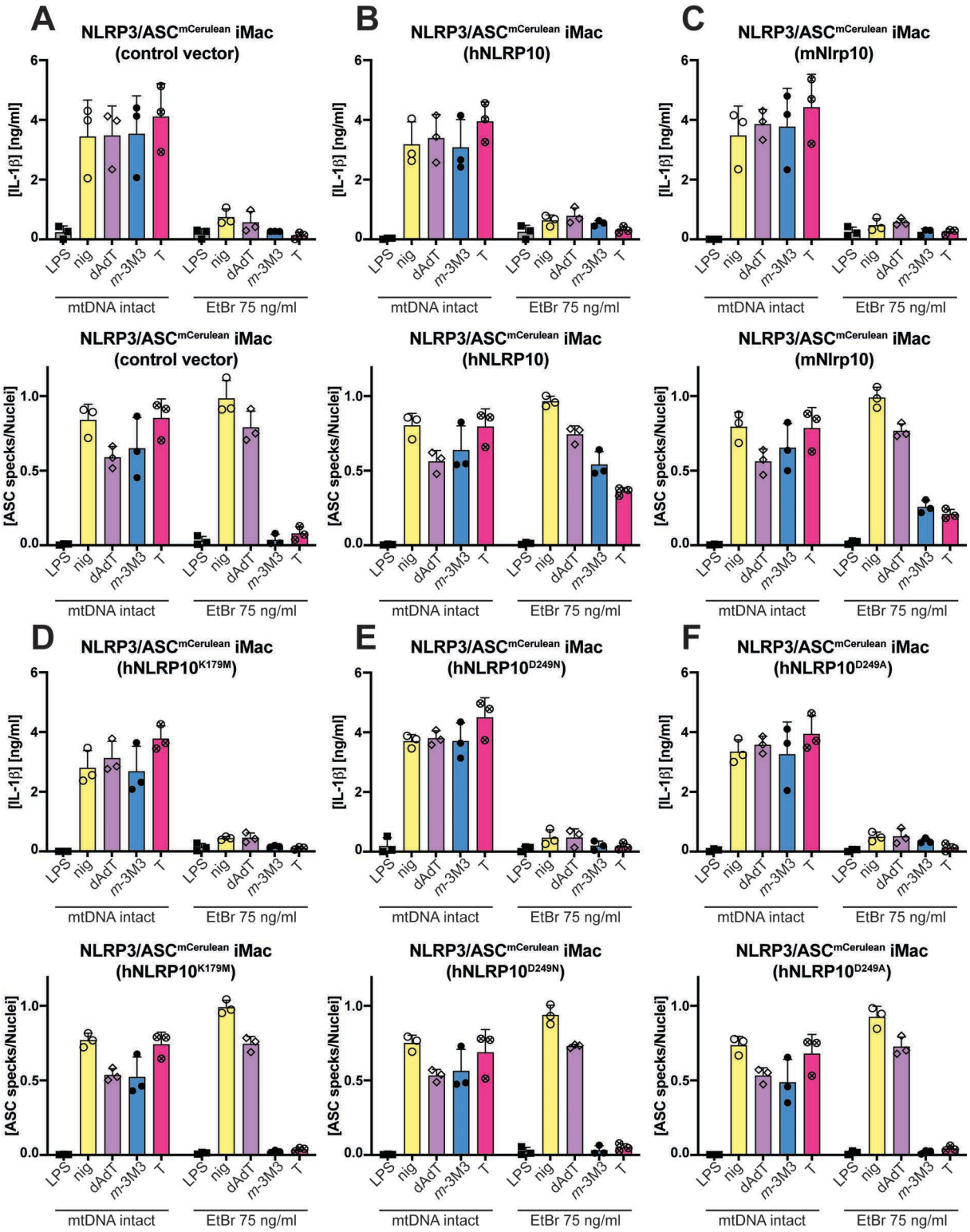

Figure 8.5. NLRP10 overexpression partially restores the inflammasome responses to *m*-3M3FBS and thapsigargin in macrophages after mtDNA depletion with EtBr

A-F: NLRP3/ASC^{mCerulean} reporter iMac cells stably transduced with the control vector (A) or WT human (h) NLRP10 (B), WT murine (m) NLRP10 (C), hNLRP10^{K179M} (Walker A mutant; D), hNLRP10^{D249N} (Walker B mutant; E), or hNLRP10^{D249A} (Walker B mutant; F) were plated in 96-well plates at 2.5×10^3 cells per well, or ~7.8×10^3 cells/cm^2 and grown for 72-96 h in DMEM supplemented with 10% FBS, penicillin, streptomycin, 1 mM sodium pyruvate and, where indicated, EtBr (75 ng/mL). After reaching confluence, the cells were LPS-primed (200 ng/mL, 2 h) and stimulated with inflammasome activators in an extracellular medium consisting of (in mM) 123 NaCl, 5 KCl, 2 $MgCl_2$, 1 $CaCl_2$, 10 glucose, 10 HEPES, pH 7.4. The tested inflammasome activators were *m*-3M3FBS (*m*-3M3; 85 μM), thapsigargin (T; 20 μM),

nigericin (nig; 10 μM), and poly-(dA:dT) (dAdT; 2 μg/mL complexed with 5 μL Lipofectamine 2000). The LPS controls were subjected to medium alone. Immediately after addition of inflammasome activators, the plates were centrifuged at 340 × g for 5 min (RT). After 60 min, the supernatants were collected and IL-1β concentrations were measured by HTRF (A-F, top panels) or the cells were fixed with 4% formaldehyde, counterstained with the nuclear dye DRAQ5 (5 μM) and imaged using a widefield fluorescence microscope (A-F, bottom panels).
The results are plotted as means from 3 independent experiments performed in technical duplicate. Error bars represent SD. Individual data points represent means of the technical duplicate values from each of the independent experiments.

To validate the data from the NLRP10 overexpression experiments performed in NLRP3/ASC^{mCerulean} reporter iMac cells (which are AIM2-proficient), I also tested whether NLRP10 overexpression enables IL-1β secretion in response to NLRP10 agonists from mtDNA-depleted AIM2-deficient macrophages. I depleted mtDNA (EtBr/ddC) in WT iMac cells and in *Aim2*^{CRISPR} iMac cells transduced with the empty vector, human or murine NLRP10, or human or murine AIM2. Then, the cells were primed with LPS and challenged with nigericin, poly-(dA:dT), *m*-3M3FBS, *o*-3M3FBS, SC-9, SC-10, thapsigargin, and SMBA1. The degree of inflammasome activation was assessed by measurement of the IL-1β concentrations in the supernatants (Figure 8.6).

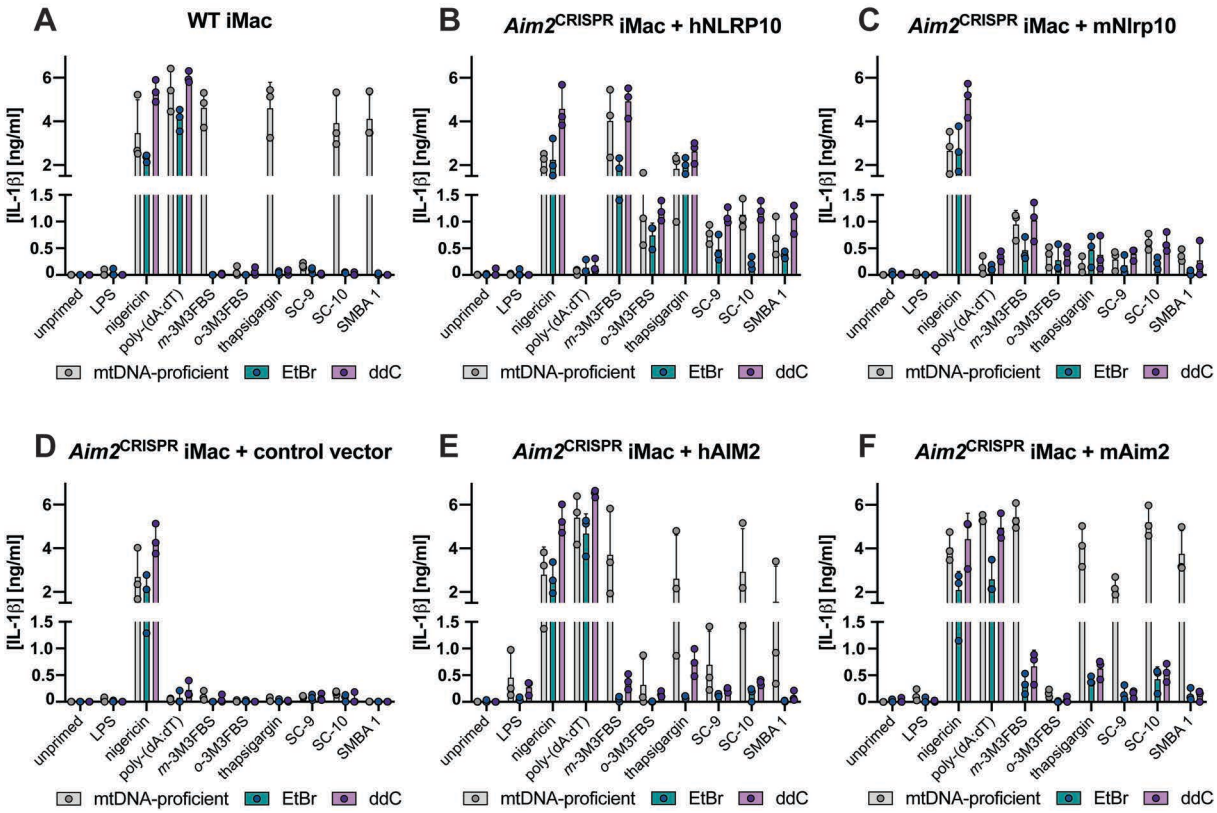

Figure 8.6. IL-1β responses in mtDNA-proficient or -depleted AIM2-deficient immortalized murine macrophages transduced with vectors encoding AIM2 or NLRP10
A-F: WT iMac cells (A) or *Aim2*^{CRISPR} iMac cells stably transduced with the control vector (D) or WT human (h) NLRP10 (B), WT murine (m) NLRP10 (C), WT hAIM2 (E), or WT mAim2 (F) were plated in 96-well plates at 2.5 × 10^3 cells per well, or ~7.8 × 10^3 cells/cm^2 and grown for 72-96 h in DMEM supplemented

with 10% FBS, penicillin, streptomycin, 1 mM sodium pyruvate and, where indicated, EtBr (75 ng/mL) or ddC (80 μg/mL). After reaching confluence, the cells were LPS-primed (200 ng/mL, 2 h) and stimulated with inflammasome activators in an extracellular medium consisting of (in mM) 123 NaCl, 5 KCl, 2 $MgCl_2$, 1 $CaCl_2$, 10 glucose, 10 HEPES, pH 7.4. The tested inflammasome activators were *m*-3M3FBS (85 μM), *o*-3M3FBS (85 μM), SC-9 (100 μM), SC-10 (100 μM), thapsigargin (20 μM), SMBA1 (50 μM), nigericin (10 μM), and poly-(dA:dT) (2 μg/mL complexed with 5 μL Lipofectamine 2000). The unprimed and LPS controls were subjected to medium alone. Immediately after addition of inflammasome activators, the plates were centrifuged at 340 × g for 5 min (RT). After 60 min, the supernatants were collected and IL-1β concentrations were measured by HTRF.
The results are plotted as means from 3 independent experiments performed in technical duplicate. Error bars represent SD. Individual data points represent means of the technical duplicate values from each of the independent experiments.

In all tested cell lines, the inflammasome responses to nigericin (NLRP3) and poly-(dA:dT) (AIM2) were partially sensitive to EtBr but fully insensitive to the mtDNA depletion with ddC[4]. In WT iMac cells, the responses to *m*-3M3FBS, thapsigargin, SC-10, and SMBA1 were fully abolished by mtDNA depletion. These cells did not secrete IL-1β after stimulations with *o*-3M3FBS and SC-9 (Figure 8.6 A). Consistent with previous observations (Sections 6.8, 6.9, and 6.16), the responses to *m*-3M3FBS, thapsigargin, SC-10, and SMBA1 were completely abolished in *Aim2*^{CRISPR} iMac cells overexpressing the empty vector, regardless of the mtDNA status (Figure 8.6 D). Human or murine NLRP10 overexpression in *Aim2*^{CRISPR} iMac cells enabled the responses to *m*-3M3FBS, thapsigargin, SC-10, and SMBA1 that were either unaffected (ddC) or only partially affected (EtBr) by mtDNA depletion. The inflammasome response to poly-(dA:dT) was not rescued by NLRP10 overexpression in *Aim2*^{CRISPR} iMac cells, but instead these macrophages secreted low levels of IL-1β upon stimulation with the NLRP10 activators *o*-3M3FBS and SC-9 (Figure 8.6 B, C). When *Aim2*^{CRISPR} iMac cells were reconstituted with human or murine AIM2, the responses to *m*-3M3FBS, thapsigargin, SC-10, and SMBA1 remained sensitive to mtDNA depletion. These cells were unresponsive to *o*-3M3FBS but, somewhat surprisingly, they exhibited a weak mtDNA-dependent response to SC-9 (Figure 8.6 E, F). This suggests that SC-9 might lead to minimal levels of mitochondrial damage that could be sensed by AIM2 overexpressed under the control of a strong constitutive promoter, but not by AIM2 at the endogenous expression levels (Figure 8.6 A). Collectively, the results presented in this Section indicate that the NLRP10 overexpression enables the inflammasome responses to *m*-3M3FBS, *o*-3M3FBS, SC-9, SC-10, thapsigargin, and SMBA1 in a manner independent of mtDNA and of AIM2.

[4] Of note, AIM2-deficient cells overexpressing NLRP10 did not secrete IL-1β upon stimulation with poly-(dA:dT), consistent with the results presented in Figures 7.7-7.9.

8.5. EtBr and ddC are not direct inhibitors of inflammasome activation

To exclude the possibility that the accumulation of EtBr or ddC in cells inhibits the *m*-3M3FBS- and thapsigargin-triggered AIM2 responses through a mechanism unrelated to mtDNA depletion, I performed a series of experiments to test whether short-time (5 min-2 h) incubations with the mtDNA replication inhibitors could affect inflammasome activation. Increasing doses of EtBr or ddC were administered to NLRP3/ASC^{mCerulean} reporter iMac cells, LPS-primed WT iMac cells, and NLRP10^{mCitrine}/ASC^{TagBFP} HEK cells either 2 h before (for WT iMac: at the onset of the LPS priming step), or 5 min before the challenge with the inflammasome activators. The inflammasome responses were assessed by measurement of the secreted IL-1β concentrations in WT iMac cells (Figure 8.7), and by imaging of ASC specks in NLRP3/ASC^{mCerulean} reporter iMac cells (Figure 8.8) and in NLRP10^{mCitrine}/ASC^{TagBFP} HEK cells (Figure 8.9).

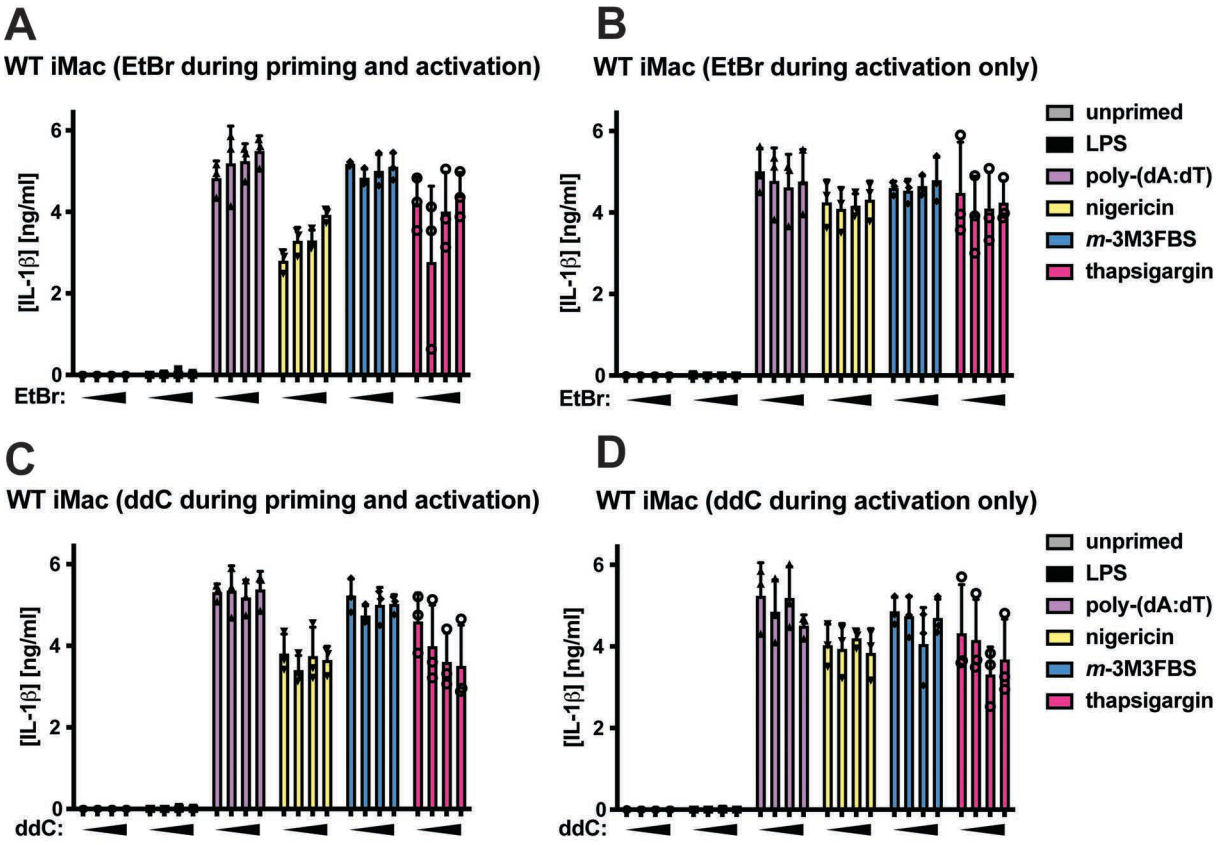

Figure 8.7. Short-term incubations with EtBr and ddC do not have an impact on IL-1β secretion by WT iMac cells treated with inflammasome activators
A-D: mtDNA-proficient WT iMac cells were primed with LPS (200 ng/mL, 2 h) in the presence of EtBr (0, 50, 75, or 100 ng/mL; A) or ddC (0, 40, 80, or 160 μg/mL; C) or pre-treated with EtBr (0, 50, 75, or 100 ng/mL; B) or ddC (0, 40, 80, or 160 μg/mL; D) for 5 min after the LPS priming was completed. Then, the cells were stimulated with *m*-3M3FBS (85 μM, blue bars), thapsigargin (20 μM, magenta bars), nigericin (10 μM, yellow bars), or poly-(dA:dT) (2 μg/mL complexed with 5 μL Lipofectamine 2000, purple bars) in

an extracellular medium consisting of (in mM) 123 NaCl, 5 KCl, 2 $MgCl_2$, 1 $CaCl_2$, 10 glucose, 10 HEPES, pH 7.4. The unprimed (grey bars) and LPS (black bars) controls were subjected to medium alone. Immediately after addition of inflammasome activators, the plates were centrifuged at 340 × g for 5 min (RT). After 60 min, the supernatants were collected and IL-1β concentrations were measured by HTRF.
The results are plotted as means from 3 independent experiments performed in technical duplicate. Error bars represent SD. Individual data points represent means of the technical duplicate values from each of the independent experiments.

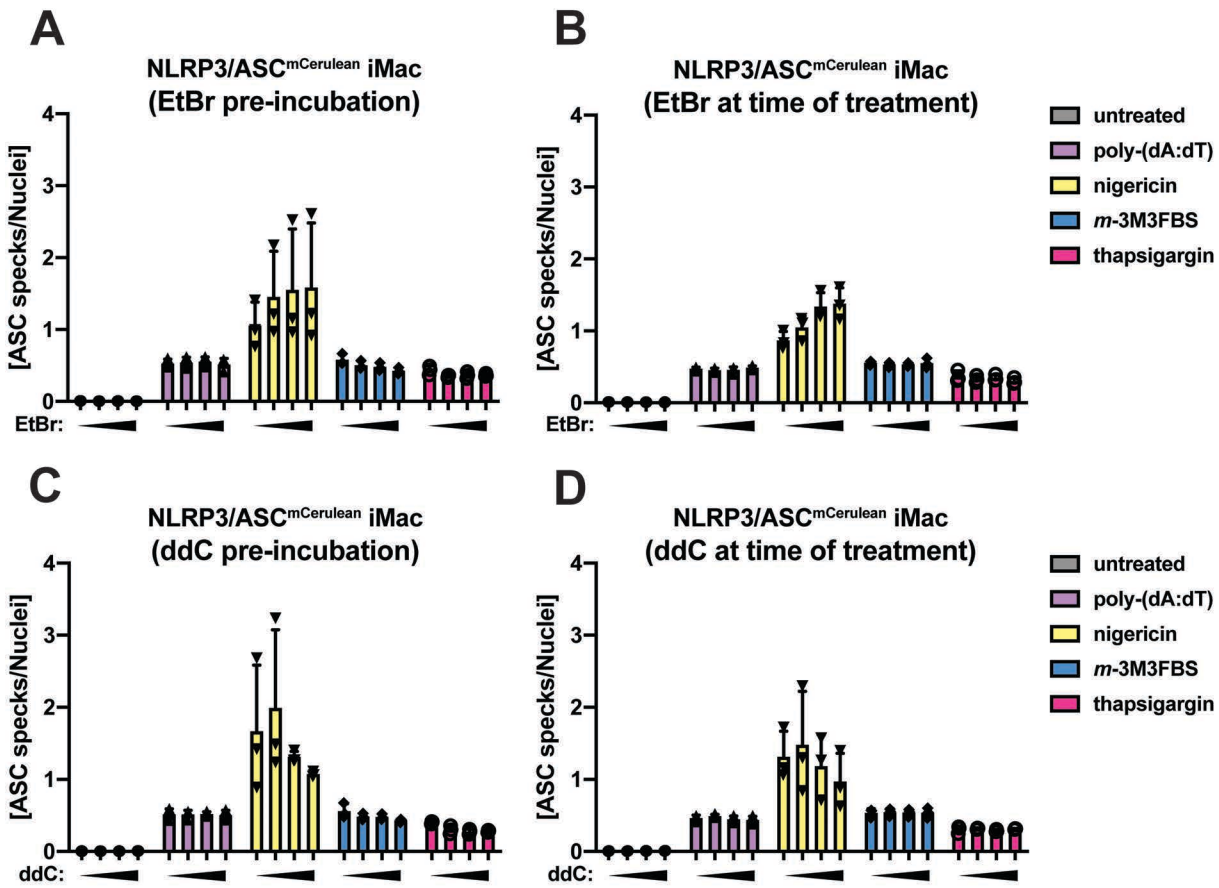

Figure 8.8. Short-term incubations with EtBr and ddC do not have an impact on ASC speck formation in NLRP3/ASC^{mCerulean} reporter iMac cells treated with inflammasome activators
A-D: mtDNA-proficient NLRP3/ASC^{mCerulean} reporter iMac cells were incubated for 2 h with EtBr (0, 50, 75, or 100 ng/mL; A) or ddC (0, 40, 80, or 160 μg/mL; C) or pre-treated with EtBr (0, 50, 75, or 100 ng/mL; B) or ddC (0, 40, 80, or 160 μg/mL; D) for 5 min directly before addition of inflammasome activators. Then, the cells were stimulated with *m*-3M3FBS (85 μM, blue bars), thapsigargin (20 μM, magenta bars), nigericin (10 μM, yellow bars), or poly-(dA:dT) (2 μg/mL complexed with 5 μL Lipofectamine 2000, purple bars) in an extracellular medium consisting of (in mM) 123 NaCl, 5 KCl, 2 $MgCl_2$, 1 $CaCl_2$, 10 glucose, 10 HEPES, pH 7.4. The untreated controls (grey bars) were subjected to medium alone. Immediately after addition of inflammasome activators, the plates were centrifuged at 340 × g for 5 min (RT). After 60 min, the cells were fixed with 4% formaldehyde, counterstained with the nuclear dye DRAQ5 (5 μM) and imaged using a widefield fluorescence microscope.
The results are plotted as means from 3 independent experiments performed in technical duplicate. Error bars represent SD. Individual data points represent means of the technical duplicate values from each of the independent experiments.

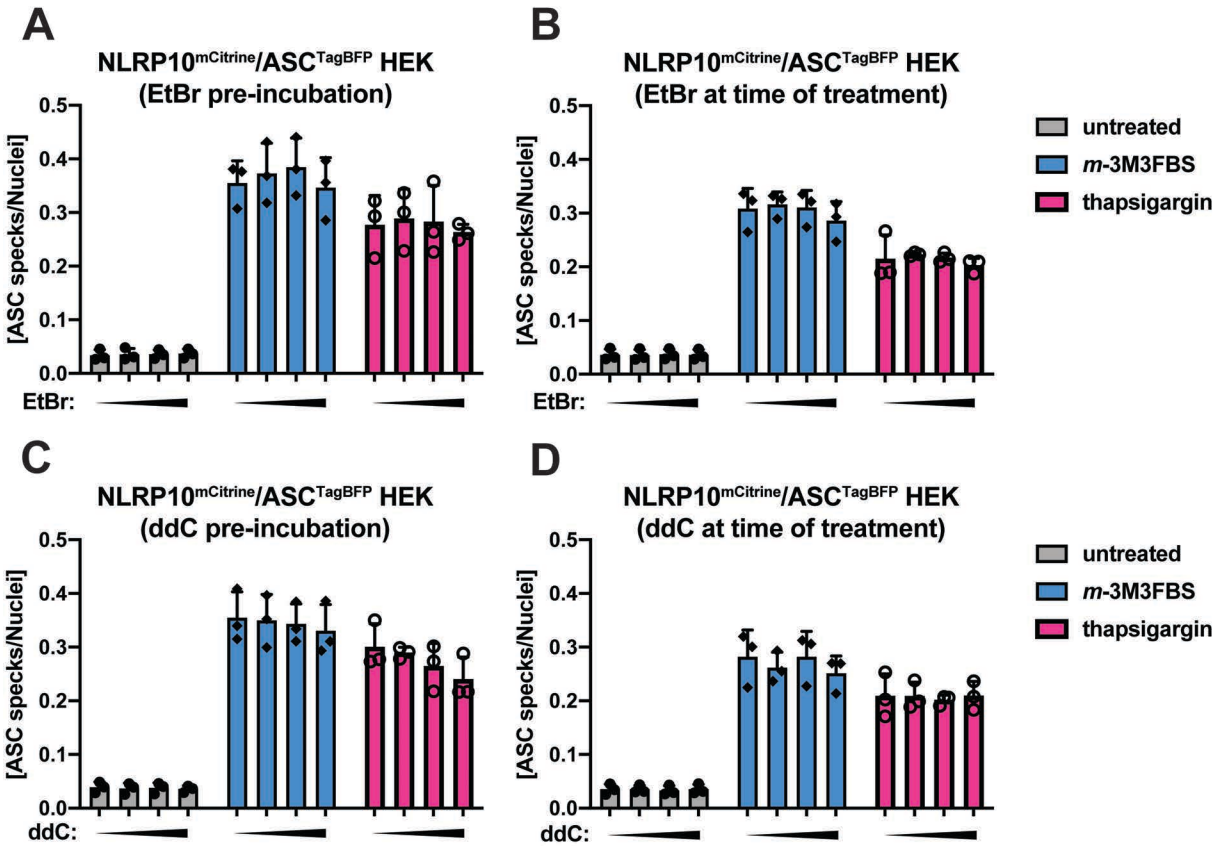

Figure 8.9. Short-term incubations with EtBr and ddC do not have an impact on ASC speck formation in NLRP10^{mCitrine}/ASC^{TagBFP} reporter HEK cells treated with inflammasome activators
A-D: mtDNA-proficient NLRP10^{mCitrine}/ASC^{TagBFP} HEK cells were incubated for 2 h with EtBr (0, 50, 75, or 100 ng/mL; A) or ddC (0, 40, 80, or 160 μg/mL; C) or pre-treated with EtBr (0, 50, 75, or 100 ng/mL; B) or ddC (0, 40, 80, or 160 μg/mL; D) for 5 min directly before addition of inflammasome activators. Then, the cells were stimulated with *m*-3M3FBS (85 μM, blue bars) or thapsigargin (20 μM, magenta bars) in an extracellular medium consisting of (in mM) 123 NaCl, 5 KCl, 2 $MgCl_2$, 1 $CaCl_2$, 10 glucose, 10 HEPES, pH 7.4. The untreated controls (grey bars) were subjected to medium alone. Immediately after addition of inflammasome activators, the plates were centrifuged at 340 × g for 5 min (RT). After 30 min, the cells were fixed with 4% formaldehyde, counterstained with the nuclear dye DRAQ5 (5 μM) and imaged using a widefield fluorescence microscope.
The results are plotted as means from 3 independent experiments performed in technical duplicate. Error bars represent SD. Individual data points represent means of the technical duplicate values from each of the independent experiments.

None of the tested inflammasome stimulations were affected by the 2-h or 5-min treatments with EtBr/ddC (Figures 8.7-8.9), indicating that these compounds are not direct AIM2/NLRP3/NLRP10 inhibitors. Instead, these results support the model where EtBr and ddC inhibit the *m*-3M3FBS- and thapsigargin-driven AIM2 activation by depleting mtDNA over the period of several days.

8.6. mtDNA is not required for the NLRP3 activation with the mitochondria-targeting compound R837 (imiquimod)

The observation that mtDNA depletion with EtBr/ddC had essentially no inhibitory effect on the NLRP3 activation with nigericin was surprising because multiple earlier studies argued that mtDNA is indispensable for the K^+ efflux-driven NLRP3 responses. Still, several other reports proposed models of NLRP3 activation that do not involve mitochondrial damage, even if they do not directly contradict the mitochondrial scenario (Chen and Chen, 2018; He et al., 2016; Samir et al., 2019). With that in mind, I went on to examine how mtDNA depletion would affect the NLRP3 activation with R837, an NLRP3 activator with a proven mitochondrial mechanism of action (Groß et al., 2016) (Figure 8.10).

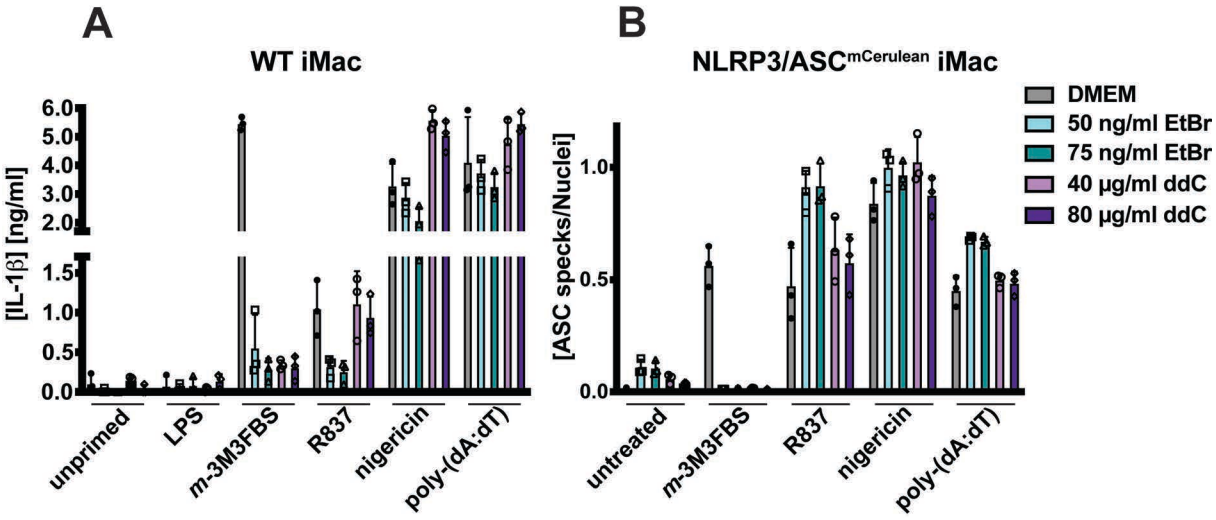

Figure 8.10. The NLRP3 responses to R837 (imiquimod) in mtDNA-depleted WT iMac and NLRP3/ASC^{mCerulean} reporter iMac cells

A-B: WT iMac cells (A) or NLRP3/ASC^{mCerulean} reporter iMac cells (B) were plated in 96-well plates at 2.5 × 10^3 cells per well, or ~7.8 × 10^3 cells/cm^2 and grown for 72-96 h in DMEM supplemented with 10% FBS, penicillin, streptomycin, 1 mM sodium pyruvate and, where indicated, EtBr (50 or 75 ng/mL; A, B, left panels) or ddC (40 or 80 µg/mL; A, B, right panels). After reaching confluence, the cells were LPS-primed (200 ng/mL, 2 h) and stimulated with inflammasome activators (A), or directly stimulated with inflammasome activators (B) in an extracellular medium consisting of (in mM) 123 NaCl, 5 KCl, 2 $MgCl_2$, 1 $CaCl_2$, 10 glucose, 10 HEPES, pH 7.4. The tested inflammasome activators were *m*-3M3FBS (85 µM), R837 (20 µg/mL), nigericin (10 µM), and poly-(dA:dT) (2 µg/mL complexed with 5 µL Lipofectamine 2000). The LPS (A) and unprimed (A, B) controls were subjected to medium alone. Immediately after addition of inflammasome activators, the plates were centrifuged at 340 × g for 5 min (RT). After 60 min, the supernatants were collected and IL-1β concentrations were measured by HTRF (A) or the cells were fixed with 4% formaldehyde, counterstained with the nuclear dye DRAQ5 (5 µM) and imaged using a widefield fluorescence microscope (B).

The results are plotted as means from 3 independent experiments performed in technical duplicate. Error bars represent SD. Individual data points represent means of the technical duplicate values from each of the independent experiments.

mtDNA depletion did not consistently inhibit the NLRP3 activation with R837. EtBr treatment resulted in inhibition of IL-1β secretion from R837-treated WT iMac cells, but this decrease was not observed in cells treated with ddC (Figure 8.10 A). Furthermore, ASC speck formation in NLRP3/ASC^{mCerulean} reporter iMac cells stimulated with R837 was not inhibited by either of the mtDNA depleting agents (Figure 8.10 B). Importantly, the *m*-3M3FBS-driven activation of the AIM2 inflammasome was completely abolished in both the EtBr- and the ddC-treated cells, confirming that the mtDNA depletion was efficient. Neither EtBr nor ddC affected the NLRP3 activation with nigericin or the AIM2 activation with poly-(dA:dT), which was consistent with my previous observations (Section 8.2). Based on these results, it appears that mtDNA is not required for the NLRP3 activation with R837.

The evidence presented so far implies that mtDNA may not be directly involved in the NLRP3 inflammasome activation but does not disprove the possibility that mitochondria as organelles play a role in this process. mtDNA depletion does not result in complete loss of the organelles, as mtDNA is not directly involved in mitochondrial biogenesis (Luo et al., 2013; Nacarelli et al., 2014). Taking this into account, a sensible interpretation of my data allows for the following conclusions:

1. mtDNA can act as an AIM2 inflammasome agonist when exposed to the cytosol.
2. Depletion of mtDNA to an extent that completely abolishes mtDNA sensing by AIM2 is not sufficient to inhibit the activation of the NLRP3 inflammasome.

In this light, it is unlikely that mtDNA serves as a ligand of NLRP3.

In the remaining part of this Chapter I will elaborate on two topics. First, I will attempt to reconcile the observation that *m*-3M3FBS and thapsigargin are both mitochondria-damaging agents but not NLRP3 activators with the notion that mitochondrial disruption could be involved in the NLRP3 activation. Then, I will present the evidence suggesting that in murine macrophages, the only inflammasome directly responding to cytosolic DNA is AIM2.

8.7. Interference between the signaling cascades elicited by the inflammasome activators *m*-3M3FBS, thapsigargin, and nigericin

My previous data demonstrated that the AIM2 activators poly-(dA:dT), *m*-3M3FBS, and thapsigargin lead to ASC speck formation at an earlier time point than the NLRP3 activator nigericin does (Section 6.13). In contrast to *m*-3M3FBS and thapsigargin, nigericin did not cause a leakage of fluorescent proteins from the mitochondrial matrix to the cytosol, indicating that the events in cells treated with nigericin are distinct from those observed upon treatment with thapsigargin/*m*-3M3FBS. This opens up the possibility that the damage inflicted by *m*-3M3FBS or thapsigargin could inhibit NLRP3 activation. To test this hypothesis, I pre-treated LPS-primed *Aim2*^{CRISPR} iMac cells stably transduced with the control vector with *m*-3M3FBS or thapsigargin and then stimulated them with nigericin (Figure 8.11 A). I assessed the degree of inflammasome activation by measuring the concentrations of secreted IL-1β (Figure 8.11 B).

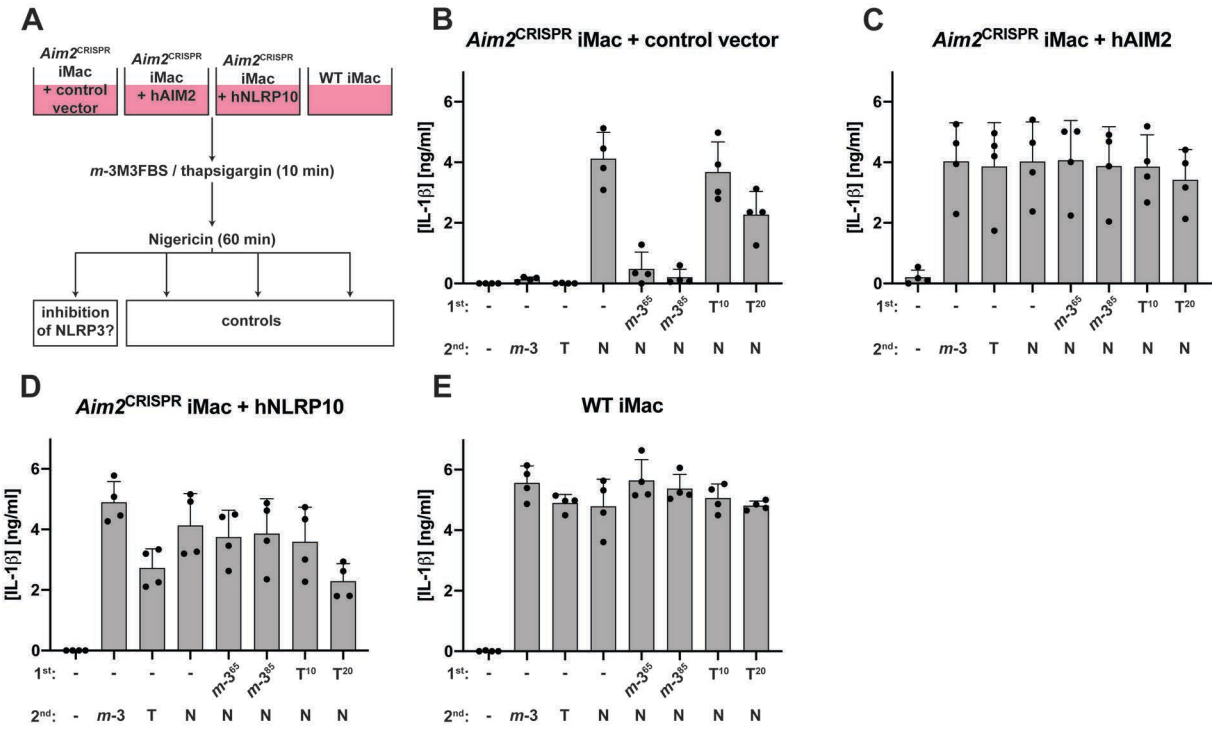

Figure 8.11. Influence of the AIM2/NLRP10 activators *m*-3M3FBS and thapsigargin on the NLRP3 inflammasome response to nigericin
A: Schematic overview of the experimental protocol.
B-E: LPS-primed (200 ng/mL, 2 h) *Aim2*^{CRISPR} iMac cells stably transduced with the empty vector (B), WT human (h) AIM2 (C), or WT hNLRP10 (D), or LPS-primed (200 ng/mL, 2 h) WT iMac cells (E) were shifted to an extracellular medium consisting of (in mM) 123 NaCl, 5 KCl, 2 $MgCl_2$, 1 $CaCl_2$, 10 glucose, 10 HEPES, pH 7.4 and treated for 10 min with *m*-3M3FBS (*m*-3; 65 or 85 μM), thapsigargin (T; 10 or 20 μM), or they were left untreated (the first treatment, indicated as *1st* in the figure panels). Immediately after administration of *m*-3M3FBS and thapsigargin, the cells were centrifuged at 340 × g for 5 min (RT). Then

the cells were stimulated with nigericin (N; 10 μM), or with *m*-3M3FBS (85 μM) or thapsigargin (20 μM; control treatments). Unstimulated controls were subjected to medium alone (the second treatment, indicated as *2nd* in the figure panels). Immediately after administration of the second set of stimuli, the cells were centrifuged at 340 × g for 2 min (RT). After 60 min, the supernatants were collected and IL-1β concentrations were measured by HTRF.
The results are plotted as means from 4 independent experiments performed in technical triplicate. Error bars represent SD. Individual data points represent means of the technical triplicate values from each of the independent experiments.

AIM2-deficient macrophages cannot activate the inflammasome in response to *m*-3M3FBS or thapsigargin, but all events upstream of AIM2 activation are expected to be uninterrupted. Consequently, the impact of *m*-3M3FBS and thapsigargin on the NLRP3 activation by nigericin can be examined in the absence of parallel AIM2 activation. WT iMac and *Aim2*^{CRISPR} iMac cells overexpressing human AIM2 or human NLRP10 served as control conditions in this experiment (Figure 8.11 C-E).

In *Aim2*^{CRISPR} iMac cells transduced with the control vector, the pre-treatment with *m*-3M3FBS almost completely abolished the NLRP3 activation by nigericin. In contrast, 20 μM thapsigargin (the concentration used for AIM2 activation) was only a partial NLRP3 inhibitor (Figure 8.11 B). In WT iMac and in *Aim2*^{CRISPR} iMac cells overexpressing human AIM2 or human NLRP10, the *m*-3M3FBS-mediated inhibition of NLRP3 could not be detected, presumably because the effect was concealed by the concurrent AIM2/NLRP10 activation (Figure 8.11 C-E). Partial inhibition of inflammasome activation was observed upon thapsigargin pre-treatment of *Aim2*^{CRISPR} cells overexpressing human NLRP10 and stimulated with nigericin (Figure 8.11 D), suggesting that there may be negative interference between these two triggers.

The results presented in Figure 8.11 indicate that some of the cellular events elicited by *m*-3M3FBS and thapsigargin negatively affect the NLRP3 activation by nigericin. Could a reverse scenario also be true? To determine whether nigericin could inhibit the AIM2/NLRP10 responses to *m*-3M3FBS and thapsigargin, I pre-treated LPS-primed WT iMac, NLRP3/ASC^{mCerulean} reporter iMac, and LPS-primed *Aim2*^{CRISPR} iMac cells transduced with the control vector or human AIM2 or NLRP10 with nigericin in the presence of the NLRP3 inhibitor CRID3 (to prevent the NLRP3-downstream effects), and then stimulated them with the AIM2/NLRP10 activators (Figure 8.12 A). I assessed the level of inflammasome activation by measuring the concentrations of secreted IL-1β and by imaging of ASC specks (Figure 8.12 B-F).

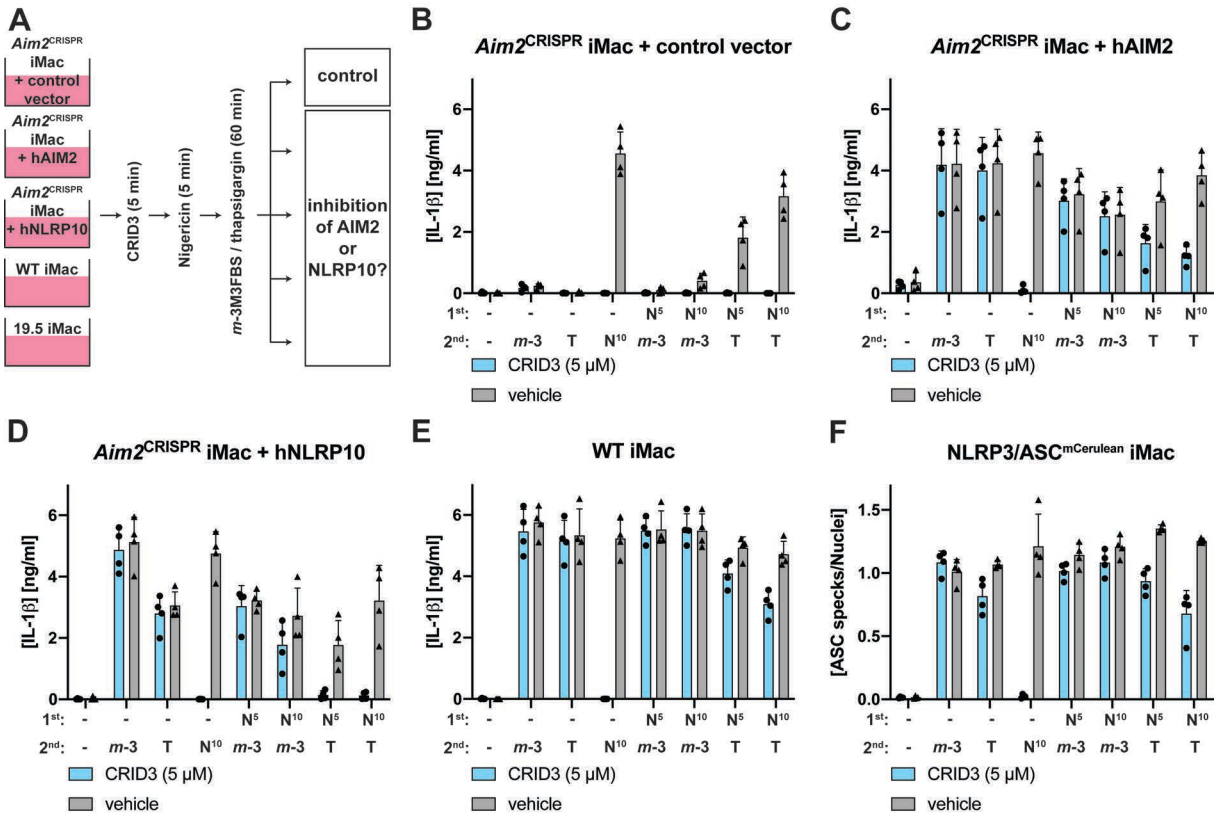

Figure 8.12. Impact of nigericin on the AIM2 and NLRP10 inflammasome responses to *m*-3M3FBS and thapsigargin

A: Schematic overview of the experimental protocol.

B-F: LPS-primed (200 ng/mL, 2 h) *Aim2*^{CRISPR} iMac cells stably transduced with the empty vector (B), WT human (h) AIM2 (C), or WT hNLRP10 (D), LPS-primed (200 ng/mL, 2 h) WT iMac cells (E), or NLRP3/ASC^{mCerulean} reporter iMac cells (F) were shifted to an extracellular medium consisting of (in mM) 123 NaCl, 5 KCl, 2 $MgCl_2$, 1 $CaCl_2$, 10 glucose, 10 HEPES, pH 7.4 containing the NLRP3 inhibitor CRID3 (5 μM; blue bars) or vehicle (ethanol; grey bars) and treated for 10 min with nigericin (N; 5 or 10 μM) or they were left untreated (the first treatment, indicated as *1st* in the figure panels). Immediately after administration of nigericin, the cells were centrifuged at 340 × g for 5 min (RT). Then the cells were stimulated with *m*-3M3FBS (*m*-3; 85 μM) or thapsigargin (T; 20 μM), or with nigericin (10 μM; control treatment). Unstimulated controls were subjected to medium alone (the second treatment, indicated as *2nd* in the figure panels). Immediately after administration of the second set of stimuli, the cells were centrifuged at 340 × g for 2 min (RT). After 60 min, the supernatants were collected and IL-1β concentrations were measured by HTRF (B-E) or the cells were fixed with 4% formaldehyde, counterstained with the nuclear dye DRAQ5 (5 μM) and imaged using a widefield fluorescence microscope (F).

The results are plotted as means from 4 independent experiments performed in technical triplicate. Error bars represent SD. Individual data points represent means of the technical triplicate values from each of the independent experiments.

The nigericin pre-treatment (in the presence of CRID3) fully inhibited the NLRP10 response to thapsigargin and partially – to *m*-3M3FBS (Figure 8.12 D). The AIM2 response to *m*-3M3FBS was not inhibited by nigericin, whereas the thapsigargin-driven AIM2 activation was inhibited only partially (Figure 8.12 C, E, F). These results indicate that the thapsigargin-triggered pathway of AIM2/NLRP10 activation may be sensitive to the loss of intracellular K^+ ions.

An unexpected observation in *Aim2*^{CRISPR} iMac cells transduced with the control vector was that *m*-3M3FBS was able to fully inhibit the NLRP3 response to nigericin even when it was administered *after* nigericin (Figure 8.12 B). Partial interference between nigericin and thapsigargin was also observed when thapsigargin was administered after nigericin (Figure 8.12 B).

To explore in more detail how various NLRP3 agonists could impact on the AIM2/NLRP10 responses to *m*-3M3FBS/thapsigargin, I pre-treated NLRP3/ASC^{mCerulean} reporter iMac cells, LPS-primed WT iMac cells, or NLRP10^{mCitrine}/ASC^{TagBFP} HEK cells with nigericin in the presence of CRID3 (Figure 8.13), valinomycin (Figure 8.14), R837 (Figure 8.15), or Leu-Leu-O-Me in the presence or absence of CRID3 (Figure 8.16), and then stimulated them with the AIM2/NLRP10 activators. The stimuli used here as pre-treatments cover a broad range of NLRP3 activation mechanisms. Nigericin and valinomycin are both K^+ ionophores (Prochnicki et al., 2016). Nigericin mediates fast electroneutral K^+ efflux and is a strong NLRP3 agonist, whereas valinomycin-driven K^+ efflux is electrogenic, leading to only negligible levels of NLRP3 activation (Perregaux and Gabel, 1994) (Figure 8.14). R837 is an inhibitor of the mitochondrial electron transport chain complex I and is reported to trigger NLRP3 activation independently of K^+ efflux (Groß et al., 2016). Finally, Leu-Leu-O-Me is a dipeptide that gets processed by lysosomal cathepsins yielding toxic intermediates that cause a leakage of the lysosomal contents (Hornung et al., 2008; Thiele and Lipsky, 1985; 1990). Of note, this process has been shown to activate the NLRP3 inflammasome through K^+ efflux (Muñoz-Planillo et al., 2013).

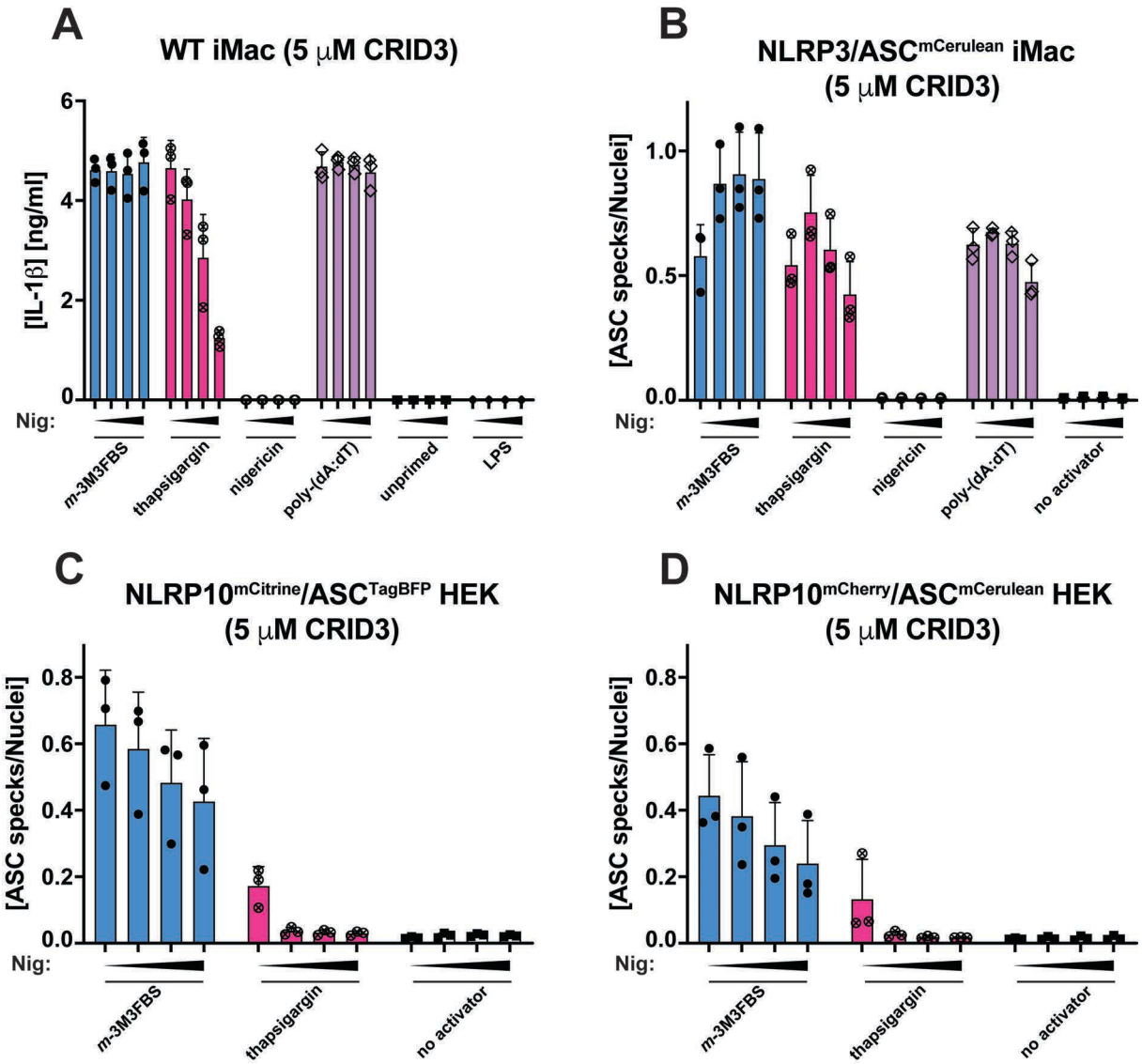

Figure 8.13. Impact of nigericin in the presence of CRID3 on the AIM2 and NLRP10 inflammasome responses to *m*-3M3FBS and thapsigargin

A-D: LPS-primed (200 ng/mL, 2 h) WT iMac cells (A), NLRP3/ASC^{mCerulean} reporter iMac cells (B), NLRP10^{mCitrine}/ASC^{TagBFP} HEK cells (C), and NLRP10^{mCherry}/ASC^{mCerulean} HEK cells (D) were shifted to an extracellular medium consisting of (in mM) 123 NaCl, 5 KCl, 2 $MgCl_2$, 1 $CaCl_2$, 10 glucose, 10 HEPES, pH 7.4 and supplemented with 5 μM CRID3 and then treated for 10 min with nigericin (Nig; 0, 5, 10, or 20 μM). Then the cells were subjected to the inflammasome activators *m*-3M3FBS (85 μM), thapsigargin (20 μM), nigericin (10 μM) or poly-(dA:dT) (2 μg/mL complexed with 5 μL Lipofectamine 2000). The LPS (A) and unprimed (A-D) controls were subjected to medium alone. Immediately after addition of inflammasome activators, the plates were centrifuged at 340 × g for 5 min (RT). After 30 min (C, D) or 60 min (A, B), the supernatants were collected and IL-1β concentrations were measured by HTRF (A) or the cells were fixed with 4% formaldehyde, counterstained with the nuclear dye DRAQ5 (5 μM) and imaged using a widefield fluorescence microscope (B-D).

The results are plotted as means from 3 independent experiments performed in technical duplicate. Error bars represent SD. Individual data points represent means of the technical duplicate values from each of the independent experiments.

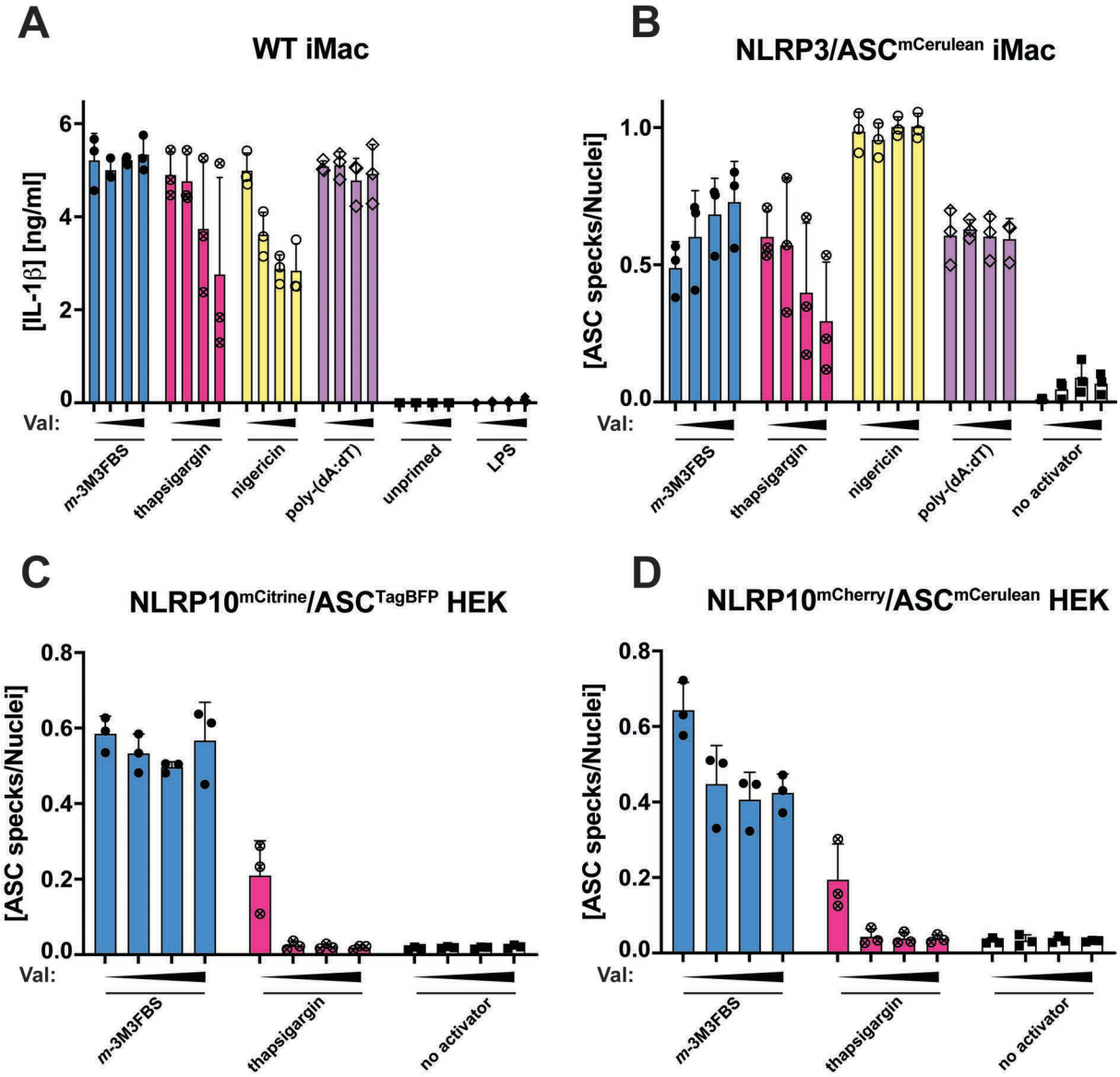

Figure 8.14. Impact of valinomycin on the AIM2 and NLRP10 inflammasome responses to *m*-3M3FBS and thapsigargin

A-D: LPS-primed (200 ng/mL, 2 h) WT iMac cells (A), NLRP3/ASC^{mCerulean} reporter iMac cells (B), NLRP10^{mCitrine}/ASC^{TagBFP} HEK cells (C), and NLRP10^{mCherry}/ASC^{mCerulean} HEK cells (D) were shifted to an extracellular medium consisting of (in mM) 123 NaCl, 5 KCl, 2 $MgCl_2$, 1 $CaCl_2$, 10 glucose, 10 HEPES, pH 7.4 and then treated for 10 min with valinomycin (Val; 0, 5, 10, or 15 μM). Then the cells were subjected to the inflammasome activators *m*-3M3FBS (85 μM), thapsigargin (20 μM), nigericin (10 μM) or poly-(dA:dT) (2 μg/mL complexed with 5 μL Lipofectamine 2000). The LPS (A) and unprimed (A-D) controls were subjected to medium alone. Immediately after addition of inflammasome activators, the plates were centrifuged at 340 × g for 5 min (RT). After 30 min (C, D) or 60 min (A, B), the supernatants were collected and IL-1β concentrations were measured by HTRF (A) or the cells were fixed with 4% formaldehyde, counterstained with the nuclear dye DRAQ5 (5 μM) and imaged using a widefield fluorescence microscope (B-D).

The results are plotted as means from 3 independent experiments performed in technical duplicate. Error bars represent SD. Individual data points represent means of the technical duplicate values from each of the independent experiments.

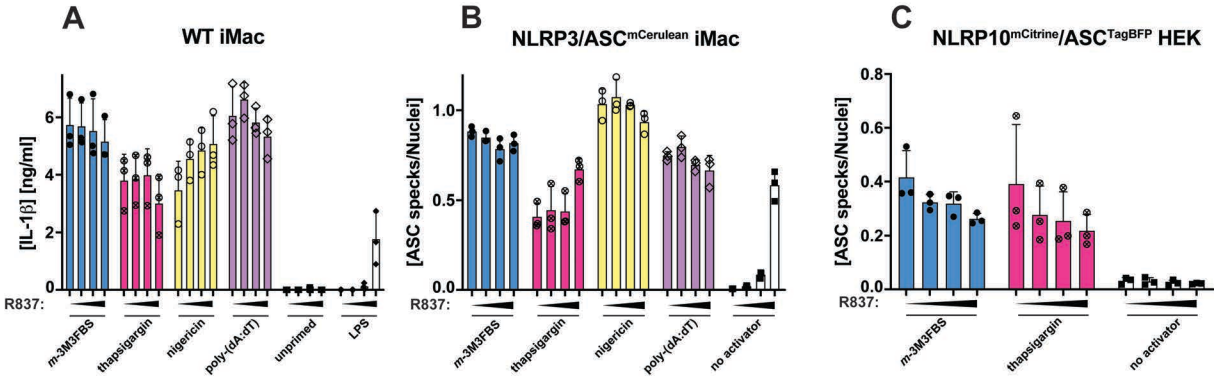

Figure 8.15. Impact of R837 (imiquimod) on the AIM2 and NLRP10 inflammasome responses to *m*-3M3FBS and thapsigargin

A-D: LPS-primed (200 ng/mL, 2 h) WT iMac cells (A), NLRP3/ASC^{mCerulean} reporter iMac cells (B), and NLRP10^{mCitrine}/ASC^{TagBFP} HEK cells (C) were shifted to an extracellular medium consisting of (in mM) 123 NaCl, 5 KCl, 2 $MgCl_2$, 1 $CaCl_2$, 10 glucose, 10 HEPES, pH 7.4 and then treated for 10 min with R837 (imiquimod; 0, 5, 10, or 25 μg/mL). Then the cells were subjected to the inflammasome activators *m*-3M3FBS (85 μM), thapsigargin (20 μM), nigericin (10 μM) or poly-(dA:dT) (2 μg/mL complexed with 5 μL Lipofectamine 2000). The LPS (A) and unprimed (A-C) controls were subjected to medium alone. Immediately after addition of inflammasome activators, the plates were centrifuged at 340 × g for 5 min (RT). After 30 min (C) or 60 min (A, B), the supernatants were collected and IL-1β concentrations were measured by HTRF (A) or the cells were fixed with 4% formaldehyde, counterstained with the nuclear dye DRAQ5 (5 μM) and imaged using a widefield fluorescence microscope (B, C).

The results are plotted as means from 3 independent experiments performed in technical duplicate. Error bars represent SD. Individual data points represent means of the technical duplicate values from each of the independent experiments.

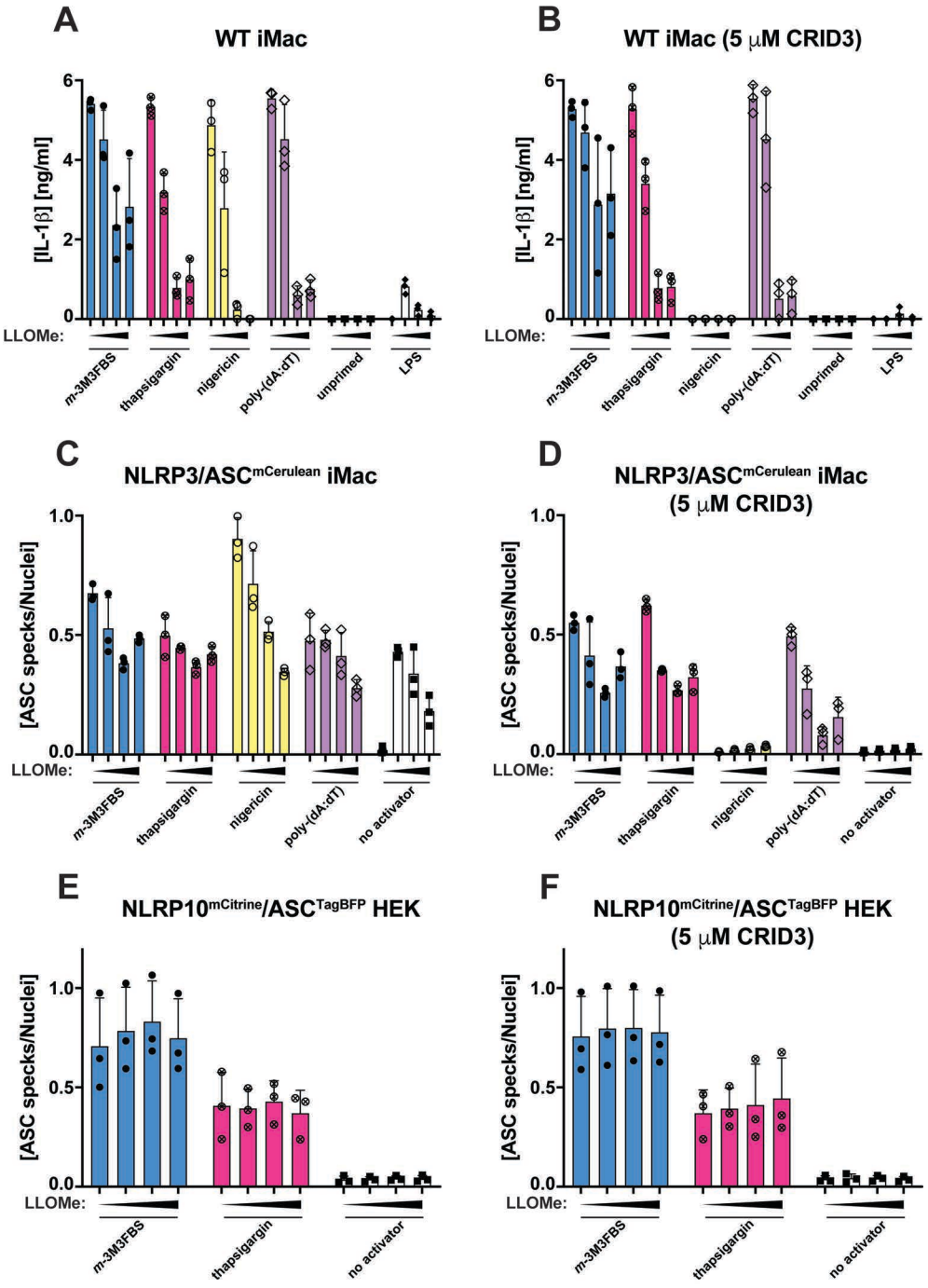

Figure 8.16. Impact of the Leu-Leu-O-Me in the presence or absence of CRID3 on the AIM2 and NLRP10 inflammasome responses to *m*-3M3FBS and thapsigargin

A-D: LPS-primed (200 ng/mL, 2 h) WT iMac cells (A, B), NLRP3/ASC^{mCerulean} reporter iMac cells (C, D), and NLRP10^{mCitrine}/ASC^{TagBFP} HEK cells (E, F) were shifted to an extracellular medium consisting of (in mM) 123 NaCl, 5 KCl, 2 $MgCl_2$, 1 $CaCl_2$, 10 glucose, 10 HEPES, pH 7.4 and supplemented with 5 μM CRID3 (B, D, F) or vehicle (ethanol; A, C, E) and then treated for 10 min with Leu-Leu-O-Me (LLOMe; 0, 0.5, 1, or 2.5 mM). Then the cells were subjected to the inflammasome activators *m*-3M3FBS (85 μM), thapsigargin (20 μM), nigericin (10 μM) or poly-(dA:dT) (2 μg/mL complexed with 5 μL Lipofectamine 2000). The LPS (A, B) and unprimed (A-F) controls were subjected to medium alone. Immediately after addition of inflammasome activators, the plates were centrifuged at 340 × g for 5 min (RT). After 30 min (E, F) or 60 min (A-D), the supernatants were collected and IL-1β concentrations were measured by HTRF (A, B) or the cells were fixed with 4% formaldehyde, counterstained with the nuclear dye DRAQ5 (5 μM) and imaged using a widefield fluorescence microscope (C-F).

The results are plotted as means from 3 independent experiments performed in technical duplicate. Error bars represent SD. Individual data points represent means of the technical duplicate values from each of the independent experiments.

Among the tested NLRP3 agonists, R837 did not inhibit the AIM2 and NLRP10 responses (Figure 8.15). High concentrations (1 mM and 2.5 mM) of Leu-Leu-O-Me caused non-specific inhibition of all tested inflammasome responses on the level of IL-1β release, including the NLRP3 activation by nigericin. This inhibitory effect was observed regardless of the presence of CRID3 in the stimulation medium (Figure 8.16 A, B) and was consistent with the report that high doses of Leu-Leu-O-Me are toxic and block NLRP3 activation (Katsnelson et al., 2016). The pan-inflammasome-blocking activity of Leu-Leu-O-Me was less pronounced in macrophages on the level of ASC speck formation (Figure 8.16 C, D) and completely absent in NLRP10^{mCitrine}/ASC^{TagBFP} HEK cells (Figure 8.16 E, F), despite the fact that Leu-Leu-O-Me elicited robust lysosomal damage in this cell type (Supplementary Figure S30). Importantly, Leu-Leu-O-Me alone did not activate the NLRP10 inflammasome (Figure 8.16 E, F), and neither did other treatments that disrupt the ER/endolysosomal compartment (Supplementary Figure S31). An interpretation of these observations could be that NLRP10 activation can proceed undisturbed in cells undergoing lysosomal damage. Another possible explanation is that in my experimental setup the *m*-3M3FBS- and thapsigargin-induced events were simply faster than the damage triggered by Leu-Leu-O-Me.

In agreement with my earlier observations (Figure 8.12 D), both nigericin and valinomycin were strong inhibitors of the NLRP10 response to thapsigargin in NLRP10^{mCitrine}/ASC^{TagBFP} HEK cells (Figures 8.13 C, D and 8.14 C, D), whereas the response to *m*-3M3FBS was only minorly affected. In macrophages, a slight K^+ efflux-mediated inhibition of the AIM2 response to thapsigargin was also observed, whereas the AIM2 activation by *m*-3M3FBS was not sensitive to nigericin and valinomycin (Figures 8.13 A, B and 8.14 A, B). Notably, none of the NLRP3 agonists tested here were able to activate NLRP10 in NLRP10^{mCitrine}/ASC^{TagBFP} HEK cells. This observation further confirms that the NLRP3 and NLRP10 activation pathways are distinct sequences of events.

How do the results above fit into the models proposing that NLRP3 is activated by mitochondrial damage? First, *m*-3M3FBS and, to a lesser extent, thapsigargin appear to mediate fast inhibition of NLRP3 activation. It is difficult to propose what the

mechanism behind it could be[5], but the possible consequence is that any NLRP3-activating events occurring in *m*-3M3FBS-/thapsigargin-treated cells may be counteracted by the overall inhibitory effect. As the signaling events triggered by NLRP3 agonists do not activate AIM2 and NLRP10, it remains possible that the NLRP3 activators affect a different mitochondrial subcompartment than do *m*-3M3FBS and thapsigargin do, or that they target the same subcompartment in a different way.

8.8. Oxidized dsDNA activates the inflammasome in an AIM2-dependent but NLRP3-independent manner

I have demonstrated that the cytosolic exposure of the macrophage mitochondrial matrix contents leads to mtDNA-dependent AIM2 inflammasome activation, that depletion of mtDNA does not inhibit activation of the NLRP3 and NLRP10 inflammasomes, and that *m*-3M3FBS and thapsigargin negatively interfere with NLRP3 activation[6]. Where do these observations leave the model of direct NLRP3 activation with oxidized mtDNA (Nakahira et al., 2010; Shimada et al., 2012; Zhong et al., 2018)?

To address this question, I generated (ox-)dsDNA fragments in a series of PCR reactions in the presence of increasing concentrations of 8-oxo-dGTP. (8-oxo-guanine is the most common oxidative modification of DNA (Kanvah et al., 2010).) I confirmed the incorporation of oxidized nucleotide residues into the PCR products by fluorescence microscopy, using an anti-8-oxo-dG antibody (Figure 8.17). The images in Figure 8.17 show NLRP3/ASC^{mCerulean} reporter iMac cells transfected with complexes of PCR-generated (ox-)dsDNA with Lipofectamine 2000. Unexpectedly, the 8-oxo-dG staining had a very high intracellular background signal. Nevertheless, examination of the extracellular DNA-Lipofectamine 2000 complexes allows for the conclusion that 8-oxo-dG is incorporated into the PCR products when 8-oxo-dGTP is present in the PCR mixes. By far the highest level of 8-oxo-dG was detected in the PCR products generated in the presence of 0.5 mM 8-oxo-dGTP (Figure 8.17).

[5] One culprit would be an increase in the cytosolic Ca^{2+} concentration. Even though I did not directly address this issue in my thesis, both thapsigargin and *m*-3M3FBS are expected to produce Ca^{2+} fluxes, respectively through the inhibition of the SERCA Ca^{2+} pump or the activation of IP_3Rs in the ER membrane. Katsnelson et al. (2016) demonstrated that elevated cytosolic Ca^{2+} concentrations may interfere with the NLRP3 inflammasome activation, which I also observed here (Figure 6.18).

[6] Of note, the observation that *m*-3M3FBS and thapsigargin impede NLRP3 activation does not necessarily mean that this effect relies on the IMM disruption.

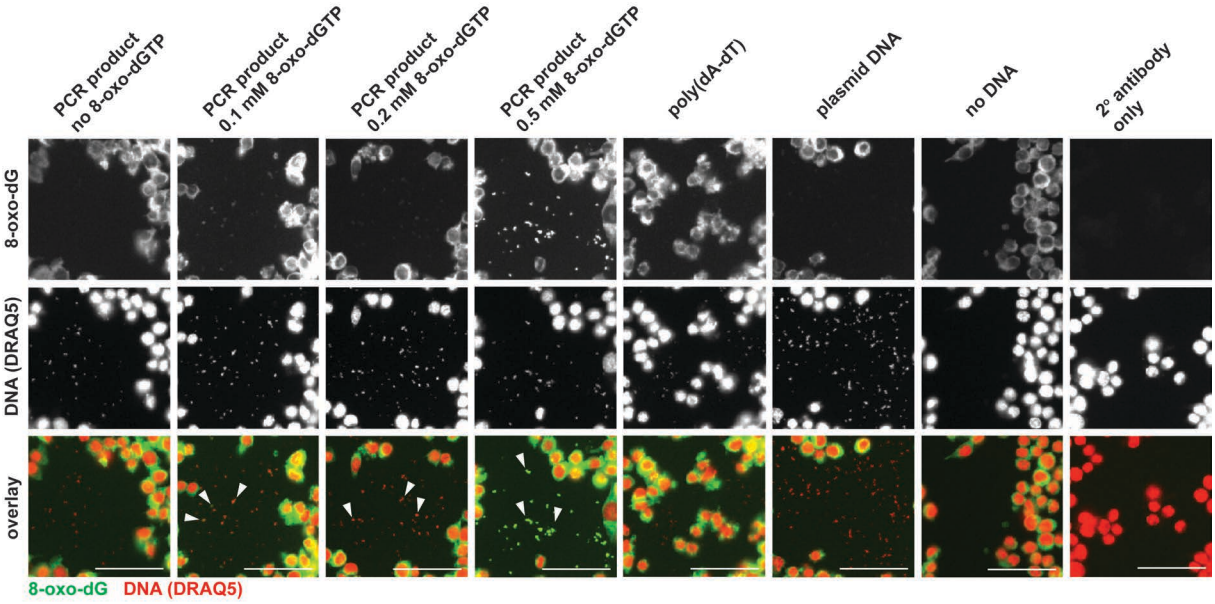

Figure 8.17. Confirmation of the incorporation of 8-oxo-dG into the PCR reaction products generated in the presence of 8-oxo-dGTP
NLRP3/ASC^{mCerulean} reporter iMac cells plated in a 96-well plate were shifted to an extracellular medium consisting of (in mM) 123 NaCl, 5 KCl, 2 $MgCl_2$, 1 $CaCl_2$, 10 glucose, 10 HEPES, pH 7.4 supplemented with VX-765 (caspase-1 inhibitor; 40 μM) and transfected with the following DNA species: dsDNA products of PCR performed in the presence of 0, 0.1, 0.2, or 0.5 mM 8-oxo-dGTP, poly-(dA:dT), or plasmid DNA. All tested DNA species were administered at 100 ng/well, complexed with 0.25 μL Lipofectamine 2000 transfection reagent (corresponding to 1 μg/mL DNA complexed with 2.5 μL Lipofectamine 2000). DNA-free and secondary (2°) antibody controls were subjected to medium alone. Immediately after addition of DNA transfection complexes, the plates were centrifuged at 340 × g for 5 min (RT). After 60 min, the cells were fixed with 4% formaldehyde, stained for oxidized DNA with an anti-8-oxo-dG antibody, counterstained with the nuclear dye DRAQ5 (5 μM; DRAQ5 also stains DNA within transfection complexes) and imaged using a widefield fluorescence microscope.
The images are representative of 3 independent experiments. Scale bars correspond to 50 μm.

I transfected the unoxidized and oxidized PCR products, in the presence or absence of the NLRP3 inhibitor CRID3, into LPS-primed NLRP3/ASC^{mCerulean} reporter iMac cells, NLRP3-deficient (*Nlrp3*$^{-/-}$) iMac cells, and *Aim2*^{CRISPR} iMac cells transduced with the control vector or human or murine AIM2. Lipofectamine 2000 was the transfection reagent. I evaluated the degree of inflammasome activation by measuring the concentrations of secreted IL-1β (Figure 8.18 A, C-F) and by imaging of ASC specks (Figure 8.18 B).

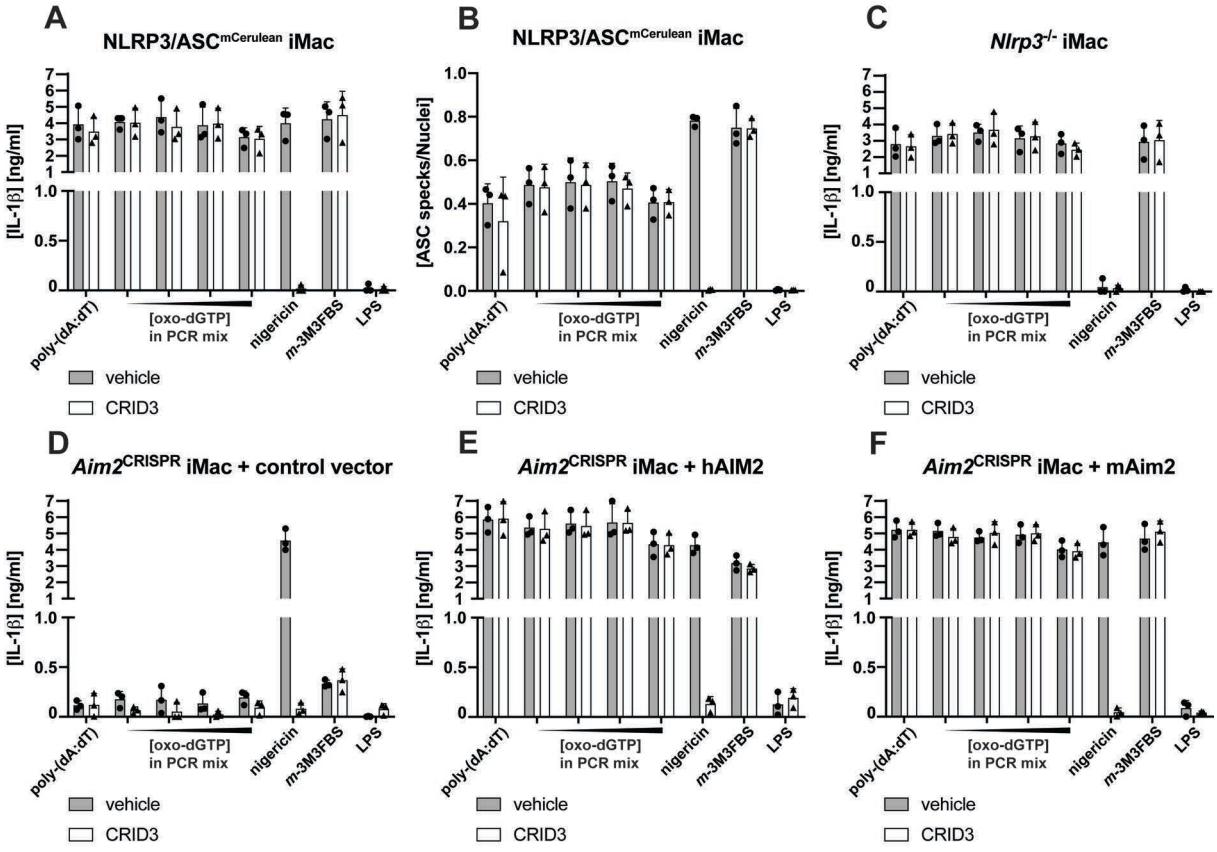

Figure 8.18. Immortalized murine macrophage inflammasome responses to dsDNA PCR products containing oxidative modifications

A-F: LPS-primed (200 ng/mL, 2 h) NLRP3/ASC^{mCerulean} reporter iMac cells (A, B), NLRP3-deficient (*Nlrp3*$^{-/-}$) iMac cells (C), or *Aim2*^{CRISPR} iMac cells stably transduced with the empty vector (D) or WT human (h) AIM2 (E) or WT murine (m) Aim2 (F) were shifted to an extracellular medium consisting of (in mM) 123 NaCl, 5 KCl, 2 $MgCl_2$, 1 $CaCl_2$, 10 glucose, 10 HEPES pH 7.4, supplemented with the NLRP3 inhibitor CRID3 (5 μM; white bars) or vehicle (ethanol; grey bars). Next, the cells were stimulated with the following agents: poly-(dA:dT) (2 μg/mL complexed with 5 μL Lipofectamine 2000), dsDNA PCR products generated in the presence of 0, 0.1, 0.2, or 0.5 mM 8-oxo-dGTP (model oxidized dsDNA molecules; 1.5 μg/mL complexed with 3.8 μL Lipofectamine 2000), nigericin (10 μM), or *m*-3M3FBS (85 μM). The LPS controls were subjected to medium alone. Immediately after addition of inflammasome activators, the plates were centrifuged at 340 × g for 5 min (RT). After 60 min, the supernatants were collected and IL-1β concentrations were measured by HTRF (A, C-F) or the cells were fixed with 4% formaldehyde, counterstained with the nuclear dye DRAQ5 (5 μM) and imaged using a widefield fluorescence microscope (B).

The results are plotted as means from 3 independent experiments performed in technical duplicate. Error bars represent SD. Individual data points represent means of the technical duplicate values from each of the independent experiments.

For an (ox-)dsDNA molecule to be designated as an NLRP3 activator, it would have to fulfill two criteria. First, it would have to cause an inflammasome response of a substantial level in AIM2-deficient macrophages. Secondly, this response should be sensitive to CRID3. As demonstrated in Figure 8.18, the PCR products triggered robust, CRID3-insensitive inflammasome responses in all tested cell lines (Figure 8.18 A-C, E, F) except for the *Aim2*^{CRISPR} iMac cells transduced with the control vector (Figure 8.18 D). Neither the strength nor the CRID3 sensitivity of these responses were dependent on

the concentration of 8-oxo-dGTP used for dsDNA generation. This observation indicates that dsDNA molecules selectively activate the AIM2 inflammasome regardless of whether or not they contain oxidative modifications[7].

Of note, very low levels of IL-1β were observed in the supernatants of *Aim2*^{CRISPR} iMac cells transduced with the control vector and transfected with the PCR products (250 pg/mL, more than a 90% decrease compared to *Aim2*^{CRISPR} iMac cells reconstituted with human or murine AIM2; Figure 8.18 D-F). Both the unoxidized and the oxidized PCR products led to the secretion of similar amounts of IL-1β. This IL-1β release was inhibited by CRID3, but the sensitivity to CRID3 was not dependent on the 8-oxo-dG incorporation (Figure 8.18 D). Collectively, these results do not provide evidence that the NLRP3 inflammasome could sense ox-dsDNA. Conversely, they support the notion that, in murine macrophages, the inflammasome responses to unoxidized and oxidized dsDNA are non-redundantly dependent on AIM2.

8.9. Oxidized ssDNA is not an activator of NLRP3

In ox-dsDNA, the oxidative modifications of guanylate residues are largely hidden inside of the double helix. To determine whether 8-oxo-dG residues exposed in a single-stranded (ss) DNA molecule could activate NLRP3, I generated unmodified and oxidized ssDNA fragments[8] by asymmetric PCR. In this reaction, one of the primers was 5'-phosphorylated. The products were subjected to digest with lambda exonuclease. This enzyme hydrolyzes 5'-phosphorylated, but not 5'-unphosphorylated DNA strands in dsDNA molecules. The resulting ssDNA reaction products were electrophoretically separated from the residual dsDNA substrate and isolated from the agarose gel. I transfected oxidized and unoxidized dsDNA and ssDNA PCR products, in the presence or absence of CRID3, into LPS-primed NLRP3/ASC^{mCerulean} reporter iMac cells, NLRP3-deficient (*Nlrp3*$^{-/-}$) iMac cells, and *Aim2*^{CRISPR} iMac cells transduced with the control vector or human or murine AIM2. I assessed the level of inflammasome activation by measuring the concentrations of secreted IL-1β (Figure 8.19 A, C-F) and by imaging of ASC specks (Figure 8.19 B). To ensure efficient delivery of the ssDNA fragments into the

[7] This is consistent with the report by Shimada et al. (2012), but not with the study by Zhong et al. (2018), who recorded a more pronounced shift from the AIM2-mediated to the NLRP3-mediated sensing of oxDNA.

[8] Here, I only tested the PCR products generated in the absence of 8-oxo-dGTP or in the presence of 0.5 mM 8-oxo-dGTP, without including the intermediate concentrations of the modified nucleotide.

cells, I used Lipofectamine 3000 with the P3000 reagent as a transfection agent for the PCR products. Poly-(dA:dT), the AIM2-specific control, was transfected using Lipofectamine 2000, as in all other experiments discussed in my thesis. As before, the criterium for designating a DNA molecule as an NLRP3 activator was the ability to trigger CRID3-sensitive IL-1β secretion from AIM2-deficient cells.

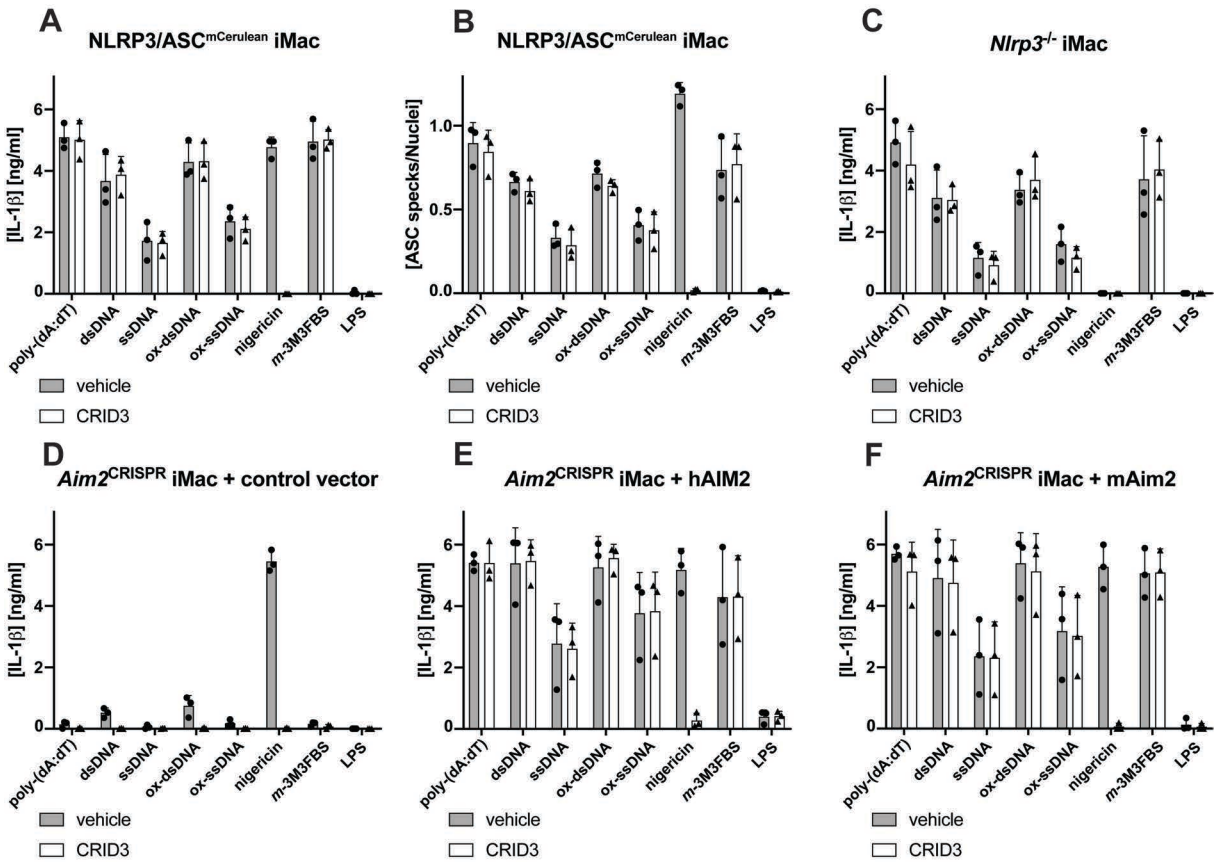

Figure 8.19. Immortalized murine macrophage inflammasome responses to ssDNA PCR products containing oxidative modifications

A-F: LPS-primed (200 ng/mL, 2 h) NLRP3/ASC^{mCerulean} reporter iMac cells (A, B), NLRP3-deficient (*Nlrp3*$^{-/-}$) iMac cells (C), or *Aim2*^{CRISPR} iMac cells stably transduced with the empty vector (D) or WT human (h) AIM2 (E) or WT murine (m) Aim2 (F) were shifted to an extracellular medium consisting of (in mM) 123 NaCl, 5 KCl, 2 $MgCl_2$, 1 $CaCl_2$, 10 glucose, 10 HEPES pH 7.4, supplemented with the NLRP3 inhibitor CRID3 (5 μM; white bars) or vehicle (ethanol; grey bars). Next, the cells were stimulated with the following agents: poly-(dA:dT) (2 μg/mL complexed with 5 μL Lipofectamine 2000), dsDNA PCR products generated in the presence of 0 or 0.5 mM 8-oxo-dGTP (model oxidized [ox-] dsDNA molecules; 1 μg/mL complexed with 2.5 μL Lipofectamine 3000 and 2 μL of the P3000 reagent), ssDNA PCR products generated in the presence of 0 or 0.5 mM 8-oxo-dGTP and subjected to lambda exonuclease (model ox-ssDNA molecules; 1 μg/mL complexed with 2.5 μL Lipofectamine 3000 and 2 μL of the P3000 reagent), nigericin (10 μM), or *m*-3M3FBS (85 μM). The LPS controls were subjected to medium alone. Immediately after addition of inflammasome activators, the plates were centrifuged at 340 × g for 5 min (RT). After 60 min, the supernatants were collected and IL-1β concentrations were measured by HTRF (A, C-F) or the cells were fixed with 4% formaldehyde, counterstained with the nuclear dye DRAQ5 (5 μM) and imaged using a widefield fluorescence microscope (B).

The results are plotted as means from 3 independent experiments performed in technical duplicate. Error bars represent SD. Individual data points represent means of the technical duplicate values from each of the independent experiments.

This experiment yielded two striking observations. First, ssDNA fragments elicited an AIM2-dependent inflammasome response regardless of the presence of oxidative modifications (Figure 8.19). The strength of the response to ssDNA was about 50% of the response to dsDNA (Figure 8.19 A-C, E, F). A possible explanation of this phenomenon is the formation of secondary structures in the transfected ssDNA molecules, as the ssDNA PCR products were relatively large (approximately 1000 nucleotide residues). Secondly, while the inflammasome response to poly-(dA:dT) was completely abolished in AIM2-deficient iMac cells, transfection with dsDNA PCR products led to a weak CRID3-sensitive inflammasome response in *Aim2*$^{\text{CRISPR}}$ cells transduced with the control vector. This response was observed both for the unoxidized and the oxidized dsDNA molecules (Figure 8.19 D). This observation was not consistent with the result presented in Figure 8.18, and it is difficult to explain in the context of the current knowledge. The only difference between the experimental setups in Figures 8.18 and 8.19 was the transfection reagent used for DNA delivery. Lipofectamine 2000 was used for the dsDNA PCR product delivery in Figure 8.18, whereas Lipofectamine 3000 with the P3000 reagent served as a transfection agent for the dsDNA and ssDNA PCR products in Figure 8.19. To test whether the use of transfection reagent could be the source of discrepancy between my results, I compared the relative levels of the NLRP3 and AIM2 inflammasome responses to dsDNA delivered with Lipofectamine 2000 or with Lipofectamine 3000 combined with the P3000 reagent.

8.10. DNA complexed with Lipofectamine 3000 and the P3000 reagent is a weak NLRP3 activator

Could the transfection reagent be the determining factor deciding whether only AIM2 or both AIM2 and NLRP3 get activated upon the delivery of dsDNA into murine macrophages? To answer this question, I prepared transfection complexes of unmodified dsDNA, ox-dsDNA (PCR reaction products), and plasmid DNA with either Lipofectamine 2000 or Lipofectamine 3000 and the P3000 reagent. These complexes were then administered to *Aim2*$^{\text{CRISPR}}$ iMac cells transduced with the control vector or human AIM2, or to NLRP3/ASC$^{\text{mCerulean}}$ reporter iMac cells. The NLRP3 inhibitor CRID3 was used to establish whether the inflammasome activation with a given stimulus is NLRP3-dependent. I assessed the degree of inflammasome activation by measuring the concentrations of secreted IL-1β (Figure 8.20 A-C) and by imaging of ASC specks (Figure 8.20 D).

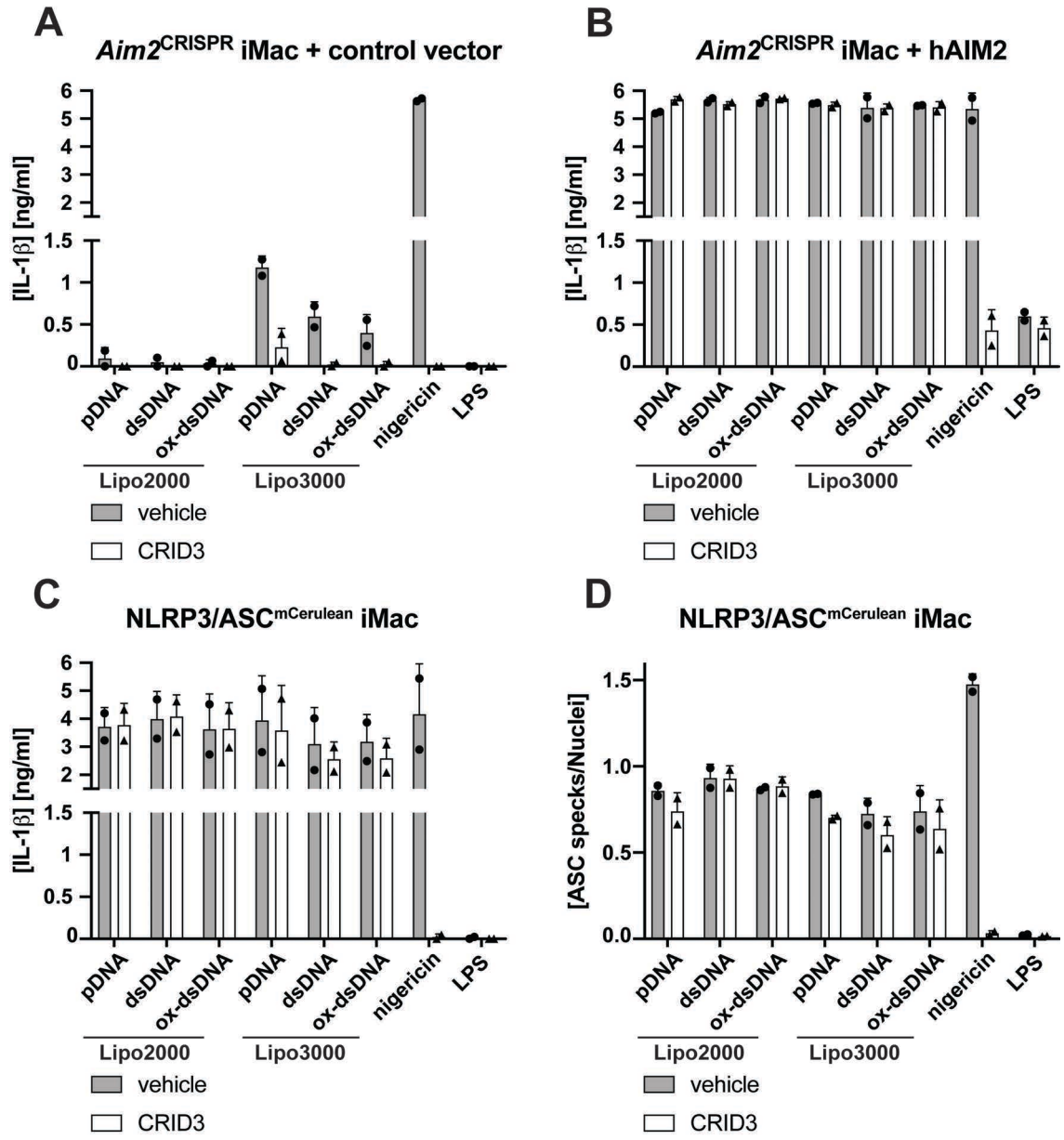

Figure 8.20. Comparison of the inflammasome responses to unoxidized and oxidized dsDNA molecules delivered into immortalized murine macrophages using Lipofectamine 2000 or Lipofectamine 3000 with the P3000 reagent

A-D: LPS-primed (200 ng/mL, 2 h) *Aim2*^{CRISPR} iMac cells stably transduced with the empty vector (A) or WT human (h) AIM2 (B), or LPS-primed (200 ng/mL, 2 h) NLRP3/ASC^{mCerulean} reporter iMac cells (C, D) were shifted to an extracellular medium consisting of (in mM) 123 NaCl, 5 KCl, 2 $MgCl_2$, 1 $CaCl_2$, 10 glucose, 10 HEPES pH 7.4, supplemented with the NLRP3 inhibitor CRID3 (5 μM; white bars) or vehicle (ethanol; grey bars). Next, the cells were stimulated with the following agents: plasmid (p) DNA (2 μg/mL complexed either with 5 μL Lipofectamine 2000 or 5 μL Lipofectamine 3000 and 4 μL of the P3000 reagent), dsDNA PCR products generated in the presence of 0 or 0.5 mM 8-oxo-dGTP (1 μg/mL complexed either with 2.5 μL Lipofectamine 2000 or 2.5 μL Lipofectamine 3000 and 2 μL of the P3000 reagent), or nigericin (10 μM). The LPS controls were subjected to medium alone. Immediately after addition of inflammasome activators, the plates were centrifuged at 340 × g for 5 min (RT). After 60 min, the supernatants were collected and IL-1β concentrations were measured by HTRF (A-C) or the cells were fixed with 4% formaldehyde, counterstained with the nuclear dye DRAQ5 (5 μM) and imaged using a widefield fluorescence microscope (D).

The results are plotted as means from 2 independent experiments performed in technical duplicate. Error bars represent SD. Individual data points represent means of the technical duplicate values from each of the independent experiments.

Strikingly, but in agreement with the results presented in Figures 8.18 and 8.19, dsDNA complexes with Lipofectamine 3000 and the P3000 reagent were capable of eliciting a weak NLRP3 inflammasome response in AIM2-deficient macrophages (Figure 8.20 A). This response was not dependent on the oxidative modifications as both the unoxidized and the oxidized PCR products triggered the release of similar amounts of IL-1β. Accordingly, plasmid DNA, which does not appear to be oxidized (Figure 8.17), also elicited this NLRP3 inflammasome response when delivered using Lipofectamine 3000 and the P3000 reagent. In contrast, complexes of dsDNA (PCR products and plasmid DNA) with Lipofectamine 2000 could not activate the NLRP3 inflammasome (Figure 8.20 A). All of the tested DNA transfection complexes activated the inflammasome in AIM2-proficient cells (Figure 8.20 B-D) in a manner not sensitive to CRID3, confirming efficient DNA delivery under the conditions of the experiment. Based on these results, a cautious conclusion could be drawn that DNA complexes with Lipofectamine 2000 are exclusively activating the AIM2 inflammasome, whereas DNA complexes with Lipofectamine 3000 and the P3000 reagent have a strong AIM2-triggering activity *and* a low NLRP3-triggering activity. Importantly, the oxidative modifications in the tested DNA molecules had no impact on which inflammasome was activated.

None of my observations support the notion that the introduction of oxidative modifications into DNA molecules could transform them from AIM2 ligands into NLRP3 agonists. Combined with the remaining evidence presented in this Chapter, these results indicate that DNA is not an NLRP3 activator in murine macrophages.

8.11. 8-OH-dG is not an NLRP3 inhibitor and mitochondria-targeting antibiotics are not inflammasome activators

Before I close this chapter, I would like to address two more pieces of evidence suggesting that NLRP3 activation *in vitro* could occur downstream of mitochondrial damage. First, Shimada et al. (2012) reported that monomeric 8-hydroxy-2'-deoxyguanosine (8-OH-dG) nucleosides added to cell culture medium inhibit the NLRP3 inflammasome responses to ATP and nigericin. The interpretation of this observation was that oxidative guanine modifications in a long DNA molecule can trigger NLRP3 clustering and inflammasome nucleation. Monomeric nucleosides were suggested to block this process by 'plugging' the NLRP3 ox-DNA binding site. I attempted to

reproduce this experiment in WT iMac cells and NLRP3/ASC^{mCerulean} reporter iMac cells. I tested impact of 8-OH-dG on inflammasome activation when added at the onset of LPS priming[9] or directly before the administration of inflammasome activators (Figure 8.21).

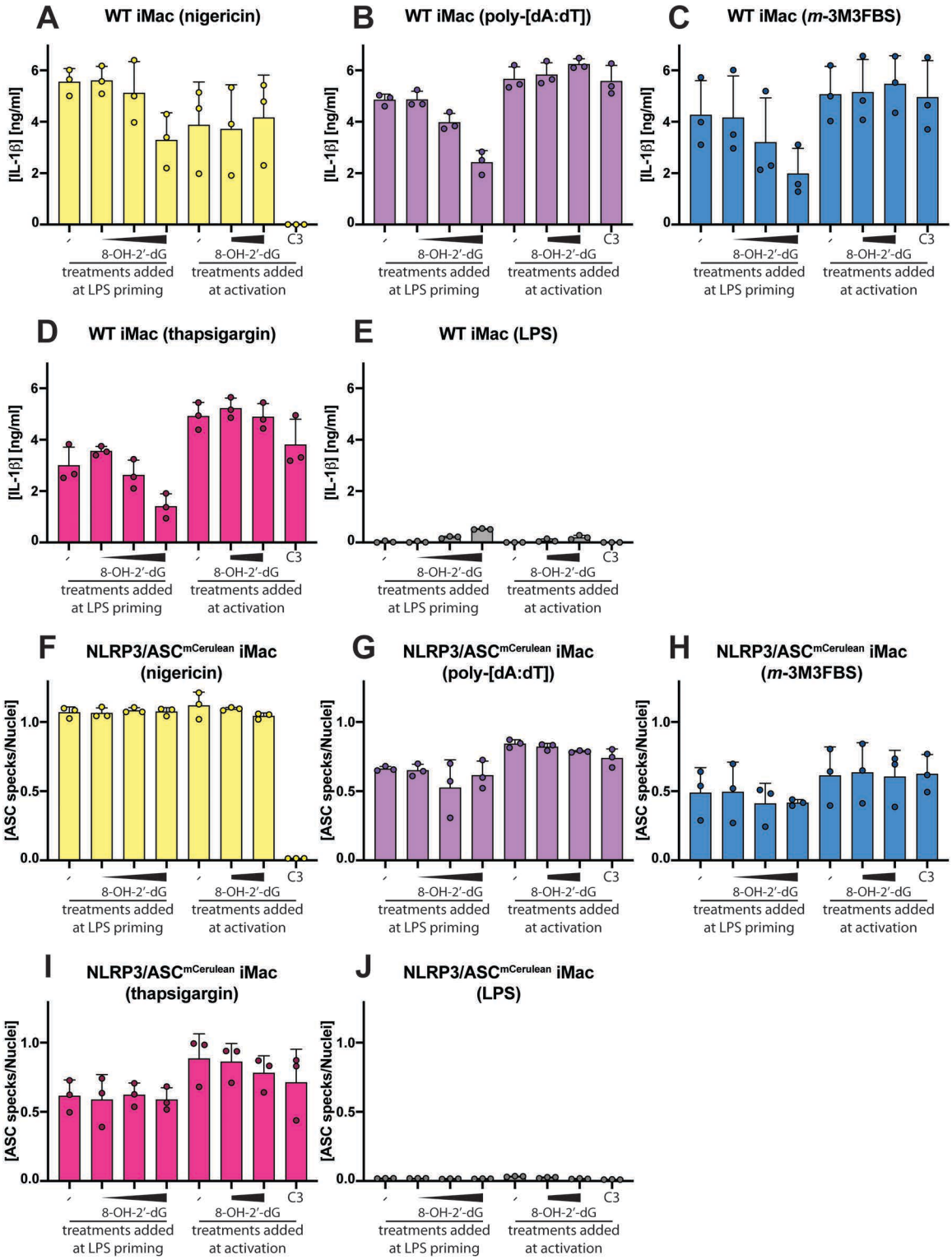

Figure 8.21. Impact of 8-hydroxy-2'-deoxyguanosine (8-OH-2'-dG) on the inflammasome responses to nigericin, poly-(dA:dT), *m*-3M3FBS, and thapsigargin

[9] This was the original experimental setup reported by Shimada et al. (2012).

◂ **A-J:** WT iMac cells (A-E) and NLRP3/ASC^{mCerulean} reporter iMac cells (F-J) were subjected to 8-OH-2'-dG (0, 50, 200, or 500 μM) during LPS priming (200 ng/mL for 2 h; 'treatments added at LPS priming') or were treated with 8-OH-2'-dG (0, 200, or 500 μM) or the NLRP3 inhibitor CRID 3 (C3; 5 μM) after the LPS priming step (200 ng/mL for 2 h), 5 min before administration of inflammasome activators ('treatments added at activation'). Then, the cells were stimulated with nigericin (10 μM; A, F), poly-(dA:dT) (2 μg/mL complexed with 5 μL Lipofectamine 2000; B, G), *m*-3M3FBS (85 μM; C, H), or thapsigargin (20 μM; D, I). The LPS controls (E, J) were subjected to medium alone. The stimulations designated as 'treatments added at LPS priming' were performed in OptiMEM supplemented with 1% FBS, whereas the stimulations designated as 'treatments added at activation' were performed in an extracellular medium consisting of (in mM) 123 NaCl, 5 KCl, 2 $MgCl_2$, 1 $CaCl_2$, 10 glucose, 10 HEPES pH 7.4. Immediately after addition of inflammasome activators, the plates were centrifuged at 340 × g for 5 min (RT). After 60 min, the supernatants were collected and IL-1β concentrations were measured by HTRF (A-E) or the cells were fixed with 4% formaldehyde, counterstained with the nuclear dye DRAQ5 (5 μM) and imaged using a widefield fluorescence microscope (F-J).
The results are plotted as means from 3 independent experiments performed in technical duplicate. Error bars represent SD. Individual data points represent means of the technical duplicate values from each of the independent experiments.

In the original report (Shimada et al., 2012), 200 μM 8-OH-dG was shown to inhibit the NLRP3 response to nigericin by about 50%. In my experiment, I also observed partial inhibition of the nigericin-induced NLRP3 activation, but only at 500 μM 8-OH-dG and only when the oxidized nucleoside was added together with LPS (that is, 2 h before administration of inflammasome activators; Figure 8.21 A). When 8-OH-dG was added directly before the administration of nigericin, the inhibitory effect was not detected. Importantly, the inflammasome responses to the AIM2 activators poly-(dA:dT), *m*-3M3FBS, and thapsigargin were also partially inhibited by 500 μM 8-OH-dG (Figure 8.21 B-D). This suggests that 8-OH-dG may interfere with the LPS-mediated pro-IL-1β synthesis rather than with inflammasome activation. On the ASC specking level (Figure 8-21 F-I), I did not observe any inhibitory activity of 8-OH-dG. Of note, 8-OH-dG alone did not act as an inflammasome agonist (Figure 8.21 E, J).

Importantly, the experiment discussed here (Figure 8.21) is not the only instance where the effects of 8-OH-dG are put into question. In a recent study on the influenza virus-mediated NLRP3 activation (Moriyama et al., 2020), 8-OH-dG co-administration actually *enhanced* NLRP3 activation[10]. Even though Moriyama et al. (2020) cited the early study by Shimada et al. (2012), they did not comment on this discrepancy.

The final experiment that I would like to discuss in this chapter concerns the mitochondrial damage caused by mitochondria-targeting antibiotics. Iyer et al. (2013) reported that linezolid, an antibiotic that also targets mitochondrial ribosomes, activates

[10] The relevant data can be inspected in Figure 4 C, D in the cited paper.

the NLRP3 inflammasome. To test whether I could reproduce this result, and whether other antibiotics with mitochondrial off-target effects could activate the inflammasome, I stimulated LPS-primed WT iMac cells, NLRP3/ASC^{mCerulean} reporter iMac cells, NLRP10^{mCitrine}/ASC^{TagBFP} HEK cells, and NLRP10^{mCherry}/ASC^{mCerulean} HEK cells with linezolid, eperezolid (McKee et al., 2006), chloramphenicol (Li et al., 2010), tetracycline (Moullan et al., 2015), and minocycline (Kupsch et al., 2009) for 24 h. I used IL-1β concentration measurements and ASC speck imaging as readouts of inflammasome activation (Figure 8.22).

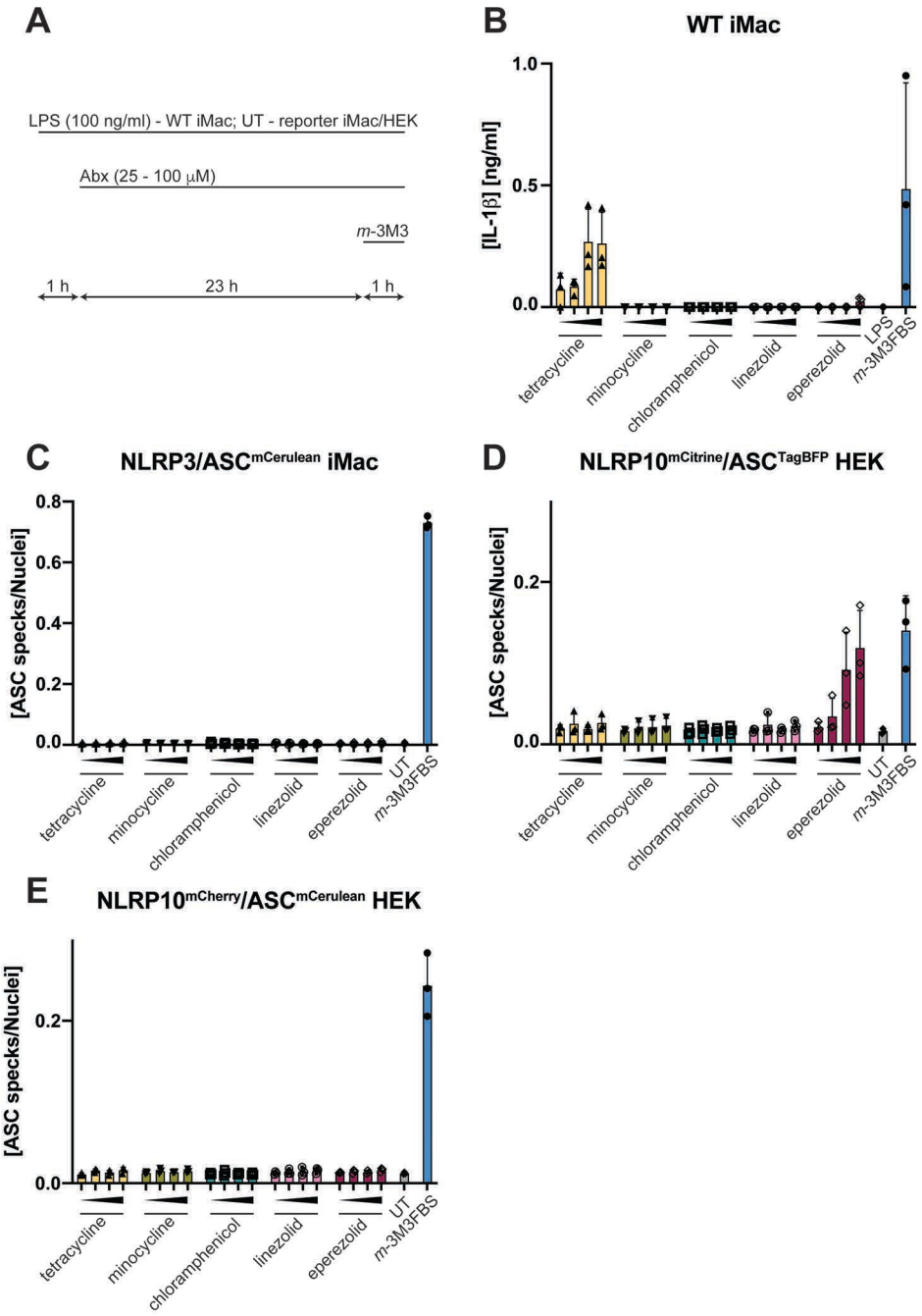

Figure 8.22. Mitochondria-targeting antibiotics do not activate the inflammasome

◂ **A:** Schematic overview of the experimental procedure.
B-E: LPS-primed (100 ng/mL, 1 h; LPS was left in the medium for entire duration of the experiment) WT iMac cells (B), NLRP3/ASC^{mCerulean} reporter iMac cells (C), NLRP10^{mCitrine}/ASC^{TagBFP} HEK cells (D), and NLRP10^{mCherry}/ASC^{mCerulean} HEK cells (E) were stimulated for 24 h with the following antibiotics: tetracycline (25, 50, 75, or 100 μM), minocycline (25, 50, 75, or 100 μM), chloramphenicol (25, 50, 75, or 100 μM), linezolid (25, 50, 75, or 100 μM), or eperezolid (25, 50, 75, or 100 μM) in DMEM supplemented with 10% FBS. During the final 60 min of the experiment, positive control (*m*-3M3FBS) cells were shifted to an extracellular medium consisting of (in mM) 123 NaCl, 5 KCl, 2 $MgCl_2$, 1 $CaCl_2$, 10 glucose, 10 HEPES pH 7.4 and stimulated with 85 μM *m*-3M3FBS. The LPS (B) or untreated (C-E) controls were subjected to medium alone. Immediately after addition of the tested stimuli, the plates were centrifuged at 340 × g for 5 min (RT). After 24 h (mitochondria-targeting antibiotics) or 60 min (*m*-3M3FBS), the supernatants were collected and IL-1β concentrations were measured by HTRF (B) or the cells were fixed with 4% formaldehyde, counterstained with the nuclear dye DRAQ5 (5 μM) and imaged using a widefield fluorescence microscope (C-E).
The results are plotted as means from 3 independent experiments performed in technical duplicate. Error bars represent SD. Individual data points represent means of the technical duplicate values from each of the independent experiments.

The results of this experiment indicated that the tested antibiotics are not inflammasome activators. Of note, high doses (75 μM and 100 μM) of tetracycline led to the secretion of low amounts of IL-1β into the tissue culture supernatant (Figure 8.22 B), but no ASC speck formation was observed (Figure 8.22 C). Furthermore, minocycline, another tetracycline antibiotic, caused neither IL-1β secretion nor ASC speck formation (Figure 8.22 B,C).

In NLRP10^{mCitrine}/ASC^{TagBFP} HEK cells, high doses (75 μM and 100 μM) of eperezolid seemingly produced an ASC specking signal (Figure 8.22 D) but upon closer visual inspection it came to light that eperezolid is autofluorescent in the BFP channel, leading to a false-positive result. When I repeated this experiment in NLRP10^{mCherry}/ASC^{mCerulean} HEK cells, I did not detect ASC speck formation in eperezolid-stimulated cells (Figure 8.22 E). In conclusion, in the experimental models used in my Thesis, the tested mitochondria-targeting antibiotics are not inflammasome agonists.

Collectively, the data presented in this Chapter indicate that *m*-3M3FBS, SC-10, thapsigargin, and SMBA1 activate the AIM2 inflammasome through exposure of mtDNA. mtDNA is not required and not involved in the activation of the NLRP3 inflammasome by K^+ efflux agonists such as nigericin as well as by R837 (imiquimod). These observations are in conflict with the studies supporting the role of mtDNA as the endogenous NLRP3 agonist (Nakahira et al., 2010; Shimada et al., 2012; Zhong et al., 2018), but partially in agreement with the reports indicating that AIM2 may be activated by mtDNA (Dang et al., 2017; Li et al., 2019).

Of note, I tested whether I could also observe AIM2 inflammasome activation in cholesterol-overloaded macrophages (Dang et al., 2017), but I did not detect an inflammasome response under these experimental conditions (Supplementary Figure S11). Correspondingly, cholesterol delivery to NLRP10^{mCitrine}/ASC^{TagBFP} HEK cells did not result in NLRP10 activation either (Supplementary Figure S12). The MRE11A inhibitor mirin, which was suggested to activate the AIM2 and/or NLRP3 inflammasomes through mitochondrial destabilization in CD4^{+} T cells (Li et al., 2019), was not an inflammasome activator in murine macrophages (Supplementary Figures S32 C, S33 C, S35, S36 A) and in NLRP10^{mCitrine}/ASC^{TagBFP} HEK cells (Supplementary Figure S34 C, S36 B-D). Similarly, other treatments expected to trigger or negatively interfere with mitochondrial permeabilization were neither AIM2/NLRP10 activators (Figure 6.43 E-G, Supplementary Figures S32 A, D, S33 A, D, S34 A, D, S35, S36) nor inhibitors (Supplementary Figures S32 B, S33 B, S34 B). This suggests that *m*-3M3FBS and thapsigargin might not engage the well-known mitochondrial permeabilization mechanisms, such as those involved in the induction of the intrinsic apoptosis pathway (Bock and Tait, 2019). In Chapter 9, I will compare the *m*-3M3FBS-/thapsigargin-induced mitochondrial rupture with other models of mitochondrial damage that had been characterized in more detail.

9. The *m*-3M3FBS- and thapsigargin-induced cellular events do not follow the known pathways of mitochondrial damage

Mitochondria are constantly exchanging information with their external environment, chiefly the cytosol and the nucleus but also other organelles such as the ER (Diogo et al., 2018; Mottis et al., 2019; Raimundo and Krisko, 2019; Xia et al., 2019). In molecular terms, this translates into an exchange of molecules and ions across the mitochondrial membranes through import and export pathways. Of particular interest to my research are processes that enable transport of large biomolecules: peptides, proteins, and nucleic acids. Several mechanisms involving such translocations have been described, including the normal physiological mitochondrial protein import (Wiedemann and Pfanner, 2017), the initiation of intrinsic apoptosis by Bak/Bax pores in the outer mitochondrial membrane (Bock and Tait, 2019), the GsdmD-/E-mediated permeabilization of the outer mitochondrial membrane during pyroptosis and/or apoptosis (Rogers et al., 2019), the mitochondrial unfolded protein response (Fessler et al., 2020; Guo et al., 2020), and the mitochondrial permeability transition, a poorly defined process during which the inner mitochondrial membrane becomes permeable to solutes below 1.5 kDa, resulting in mitochondrial matrix swelling and the outer mitochondrial membrane rupture (Halestrap, 2004; Izzo et al., 2016). The cytosolic leakage of the IMS contents during these processes is well documented but it has only recently been convincingly demonstrated that the contents of the mitochondrial matrix may also become exposed (McArthur et al., 2018; Riley et al., 2018).

In the final set of experiments discussed in my thesis, I will explore whether there are any points of convergence between the *m*-3M3FBS-/thapsigargin-induced mitochondrial damage, the known processes involving the mitochondrial membrane permeabilization, and the AIM2 and NLRP10 activations. Two questions are central here: (1) how *m*-3M3FBS and thapsigargin permeabilize the mitochondrial membranes; and (2) whether previously described processes involving mitochondrial disruption could also trigger the AIM2 and NLRP10 inflammasomes.

I have already touched on these topics in Section 6.9, in which I have demonstrated that the mPT agonist thapsigargin triggers the AIM2/NLRP10 activation, and in Section 6.16, where I showed that targeting Bax with SMBA1, but not with BAM7, leads to the

AIM2/NLRP10 activation. However, there is no consensus about the mechanistic target of thapsigargin responsible for the mitochondrial disruption, and the observation that one Bax agonist activated AIM2/NLRP10, but another one did not was puzzling rather than explanatory. Here, I will address the issue of how the AIM2 and NLRP10 activations with *m*-3M3FBS/thapsigargin fit into the previously described mechanisms of mitochondrial damage.

9.1. No evidence of AIM2/NLRP10 activation by stimuli triggering the intrinsic apoptosis pathway

Intrinsic apoptosis involves MOMP, the release of cytochrome c from the IMS, and the APAF1-mediated activation of the apoptotic caspases. Recently, independent reports demonstrated that (1) stimuli triggering MOMP also enable release of mtDNA to the cytosol (McArthur et al., 2018; Riley et al., 2018), and (2) intrinsic apoptosis can lead to IL-1β maturation and secretion in a manner partially dependent on NLRP3 (Chauhan et al., 2018; Chen et al., 2020; 2019; Vince et al., 2018). Specifically, the combined treatment with the MCL-1 inhibitor S63845 (Kotschy et al., 2016) and the BCL-2/BCL-XL/BCL-W inhibitor ABT737 (Oltersdorf et al., 2005) elicits secretion of cleaved IL-1β from macrophages (Chen et al., 2019; 2020; Vince et al., 2018). In a different model, the combination of S63845 and ABT737, in addition to MOMP, resulted in the IMM permeabilization and mtDNA-mediated activation of the cytosolic DNA sensor cGAS (Riley et al., 2018).

In cells stimulated with S63845 and ABT737, MOMP is mediated by the formation of Bak/Bax pores in the OMM, but the mechanistic details of the IMM damage are not well understood. Given the similarity between the observations reported by McArthur et al. (2018) and Riley et al. (2018) and my observations of mitochondrial matrix contents leakage upon stimulation with *m*-3M3FBS/thapsigargin, I examined whether the combined inhibition of BCL-2, BCL-XL, BCL-W, and MCL-1 could activate the AIM2 and/or NLRP10 inflammasomes.

To probe a maximally broad range of pro-apoptotic treatments, I tested the inflammasome responses to 24-h stimulations with two BCL-2/BCL-XL/BCL-W inhibitors, ABT263 (Navitoclax; Figure 9.1 A-C) and ABT737 (Figure 9.1 D-F) in

combination with S63845 or actinomycin D (a transcription inhibitor, which facilitates depletion of the rapidly degraded MCL-1), and in the presence or absence of the pan-caspase inhibitor Q-Vd-OPh. Q-Vd-OPh was added to prevent rapid cell death (Riley et al., 2018); the caspase-1-mediated IL-1β secretion is not significantly inhibited by Q-Vd-OPh (Supplementary Figure S42 A-C). The experiment was performed in LPS-primed WT iMac cells to assess the capacity for IL-1β secretion (Figure 9.1 A, D), and in NLRP3/ASC^{mCerulean} reporter iMac cells (Figure 9.1 B, E) and NLRP10^{mCitrine}/ASC^{TagBFP} HEK cells (Figure 9.1 C, F) to determine the levels of ASC speck formation.

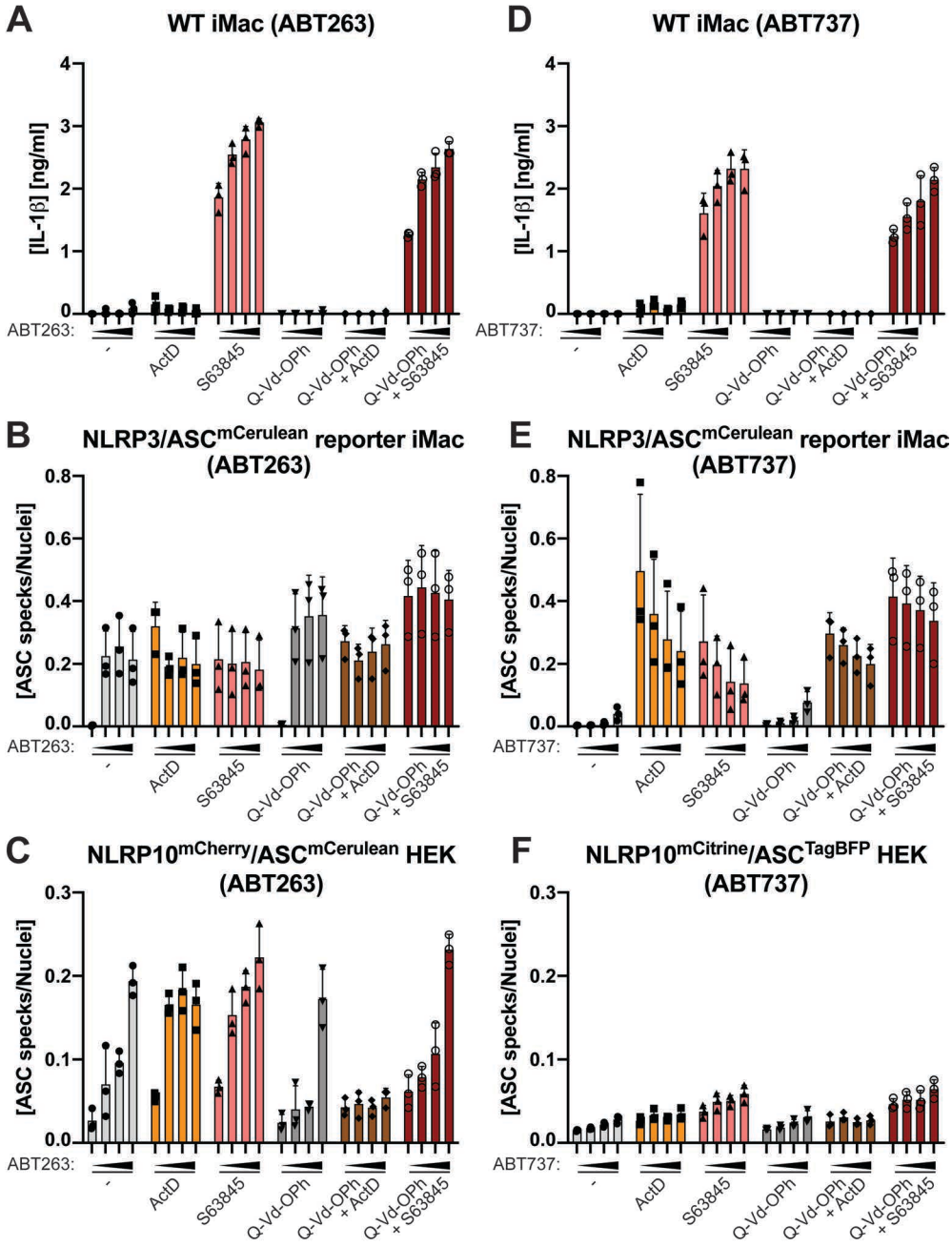

Figure 9.1. IL-1β and ASC specking responses to the mitochondrial outer membrane permeabilization triggered by inhibition of BCL-2 family proteins

◂ **A-F:** LPS-primed (100 ng/mL, 1 h; LPS was present in the stimulation medium for the duration of the entire experiment) WT iMac cells (A, D), unprimed NLRP3/ASC^{mCerulean} reporter iMac cells (B, E), unprimed NLRP10^{mCherry}/ASC^{mCerulean} HEK cells (C), and unprimed NLRP10^{mCitrine}/ASC^{TagBFP} HEK cells (F) were subjected to the transcription inhibitor actinomycin D (ActD; 2 μM) or the MCL-1 inhibitor S63845 (5 μM), or left untreated (-) in the presence or absence of the pan-caspase inhibitor Q-Vd-OPh (20 μM). Immediately after administration of these treatments, the cells were stimulated with the BCL-2 family inhibitors ABT263 (0, 10, 25, or 50 μM; A-C) or ABT737 (0, 10, 25, or 50 μM; D-F). All stimulations were performed in DMEM supplemented with 5% FBS. Immediately after addition of inflammasome activators, the plates were centrifuged at 340 × g for 5 min (RT). After 24 h, the supernatants were collected and IL-1β concentrations were measured by HTRF (A, D) or the cells were fixed with 4% formaldehyde, counterstained with the nuclear dye DRAQ5 (5 μM) and imaged using a widefield fluorescence microscope (B, C, E, F).
The results are plotted as means from 3 independent experiments performed in technical duplicate. Error bars represent SD. Individual data points represent means of the technical duplicate values from each of the independent experiments.

Alone, neither ABT263 nor ABT737 were capable of eliciting IL-1β release from LPS-primed WT iMac cells (Figure 9.1 A, D). IL-1β secretion was also not observed when the BCL-2/BCL-XL/BCL-W inhibitors were co-administered with actinomycin D. In contrast, the MCL-1 inhibitor S63845 alone elicited robust IL-1β secretion, which was synergistically and dose-dependently enhanced by ABT263 and ABT737. Addition of Q-Vd-OPh did not have an impact on the IL-1β responses under the tested conditions (Figure 9.1 A, B).

In NLRP3/ASC^{mCerulean} reporter iMac cells, ABT263 alone induced ASC speck formation at all tested concentrations (10-50 μM), whereas the ASC specking response to ABT737 was negligible (Figure 9.1 B, E). S63845 alone was capable of eliciting an ASC specking response as well, but in contrast to the trend observed in IL-1β secretion, this was not enhanced by co-treatment with ABT263/ABT737. In further opposition to the IL-1β results (Figure 9.1 A, B), actinomycin D alone elicited an ASC specking response (Figure 9.1 B, E).

In NLRP10^{mCitrine}/ASC^{TagBFP} HEK cells, ABT263 alone (but not ABT737) triggered ASC speck formation, which was potentiated by co-treatment with actinomycin D and S63845 in a caspase-dependent manner (Figure 9.1 C, F). Actinomycin D and S63845 administered alone led to slightly elevated ASC specking levels.

These results confirm that the inhibition of BCL-2 family members may activate an inflammasome response and IL-1β maturation and secretion (Chen et al., 2019; 2020; Vince et al., 2018). One important difference with the previously published observations

was that I recorded remarkably high ASC specking and IL-1β responses to S63845 alone (Figure 9.1 A, B, D, E), whereas Vince et al. (2018) reported that the IL-1β response to S63845 requires concomitant inactivation of other BCL-2 family members (inhibition of BCL-2/BCL-XL/BCL-W with ABT737 or genetic deficiency of BCL-XL). This discrepancy is difficult to interpret. One possibility is the difference in the employed cellular models (immortalized macrophages in my Thesis *versus* primary BMDMs in the study by Vince et al. (2018)).

The observation that the treatment with ABT263 led to ASC speck formation in NLRP10^{mCitrine}/ASC^{TagBFP} HEK cells suggested that intrinsic apoptosis might promote the NLRP10 activation. To test whether the detected ASC specking response could be attributed to the NLRP10 overexpression, and in an attempt to identify a non-redundant inflammasome-forming sensor activated by S63845 in macrophages, I stimulated LPS primed WT iMac cells (in the presence or absence of CRID3), NLRP3-deficient (*Nlrp3*$^{-/-}$) iMac cells, and AIM2-deficient (*Aim2*^{CRISPR}) iMac cells transduced with the empty vector, human AIM2, or human NLRP10 with S63845 in combination with ABT263/ABT737 (Figure 9.2). To further establish whether the observed responses are caspase-dependent, additional stimulations were performed in the presence of the pan-caspase inhibitor emricasan or the caspase-1 inhibitor VX-765.

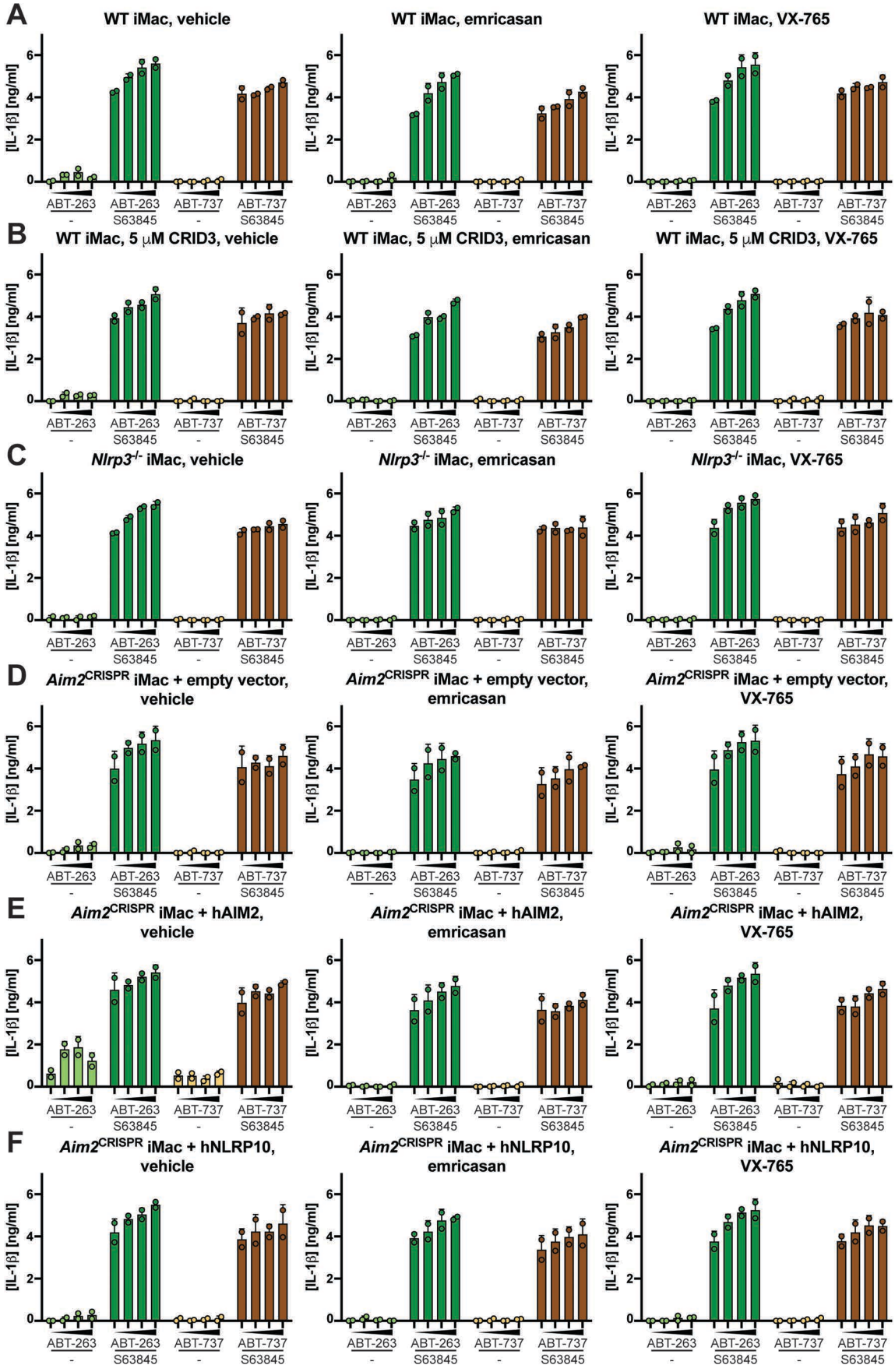

Figure 9.2. IL-1β secretion from NLRP3-/AIM2-proficient, NLRP3-deficient, and AIM2-deficient immortalized murine macrophages transduced with the empty vector, human AIM2, or human NLRP10, and stimulated with BCL-2 family inhibitors in the presence or absence of the pan-caspase inhibitor emricasan or the caspase-1 inhibitor VX-765

◂ **A-F:** LPS-primed (100 ng/mL, 1 h; LPS was present in the stimulation medium for the duration of the entire experiment) WT iMac cells in the absence (A) or presence (B) of the NLRP3 inhibitor CRID3 (5 μM), NLRP3-deficient (*Nlrp3*$^{-/-}$) iMac cells (C), and *Aim2*^{CRISPR} iMac cells stably transduced with the empty vector (D), WT human (h) AIM2 (E), or WT hNLRP10 (F) were subjected to the MCL-1 inhibitor S63845 (5 μM) or left untreated (-) in the presence of the pan-caspase inhibitor emricasan (20 μM), the caspase-1 inhibitor VX-765 (20 μM), or vehicle (DMSO). Immediately after administration of these treatments, the cells were stimulated with the BCL-2 family inhibitors ABT263 (0, 10, 25, or 50 μM) or ABT737 (0, 10, 25, or 50 μM). All stimulations were performed in DMEM supplemented with 5% FBS. Immediately after addition of inflammasome activators, the plates were centrifuged at 340 × g for 5 min (RT). After 24 h, the supernatants were collected and IL-1β concentrations were measured by HTRF.
The results are plotted as means from 2 independent experiments performed in technical duplicate. Error bars represent SD. Individual data points represent means of the technical duplicate values from each of the independent experiments.

In parallel, I examined the S63845-/ABT263-/ABT737-stimulated ASC speck formation in NLRP3/ASC^{mCerulean} reporter iMac cells (Figure 9.3 A), NLRP10^{mCherry}/ASC^{mCerulean} HEK cells (Figure 9.3 B), NLRP10^{mCitrine}/ASC^{TagBFP} HEK cells (Figure 9.3 C), and ASC^{mCerulean} HEK cells (Figure 9.3 D). These assays were also performed under caspase-proficient conditions (vehicle), or in the presence of the pan-caspase inhibitor emricasan or the caspase-1 inhibitor VX-765.

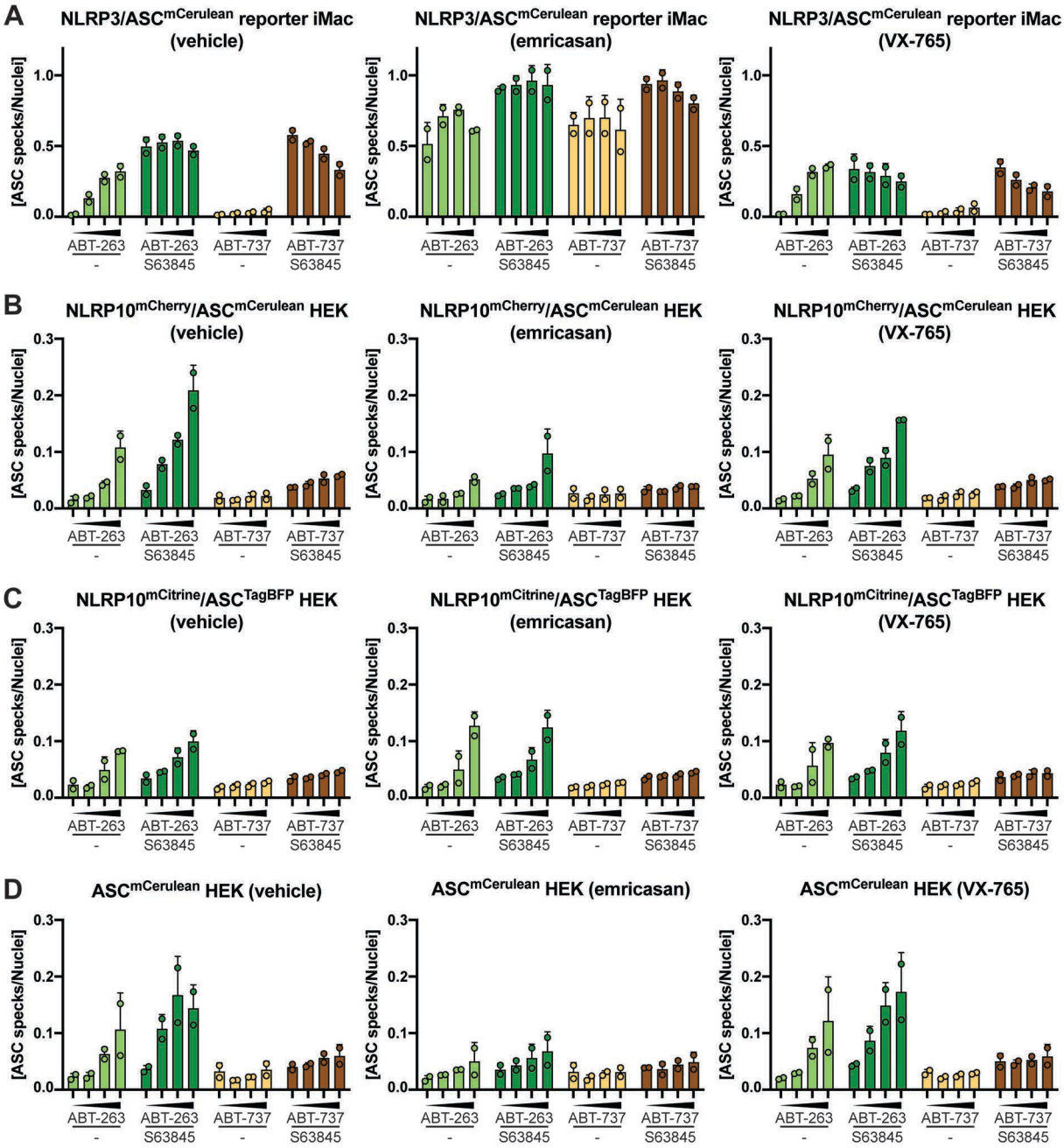

Figure 9.3. ASC speck formation in NLRP3/ASC^{mCerulean} reporter iMac cells, and HEK cells overexpressing fluorescently labelled ASC with or without NLRP10, stimulated with BCL-2 family inhibitors under caspase-proficient or caspase-inhibited conditions

A-D: LPS-primed (100 ng/mL, 1 h; LPS was present in the stimulation medium for the duration of the entire experiment) NLRP3/ASC^{mCerulean} reporter iMac cells (A), NLRP10^{mCherry}/ASC^{mCerulean} HEK cells (B), NLRP10^{mCitrine}/ASC^{TagBFP} HEK cells (C), and ASC^{mCerulean} HEK cells (D) were subjected to the MCL-1 inhibitor S63845 (5 μM) or left untreated (-) in the presence of the pan-caspase inhibitor emricasan (20 μM), the caspase-1 inhibitor VX-765 (20 μM), or vehicle (DMSO). Immediately after administration of these treatments, the cells were stimulated with the BCL-2 family inhibitors ABT263 (0, 10, 25, or 50 μM) or ABT737 (0, 10, 25, or 50 μM). All stimulations were performed in DMEM supplemented with 5% FBS. Immediately after addition of inflammasome activators, the plates were centrifuged at 340 × g for 5 min (RT). After 24 h, the cells were fixed with 4% formaldehyde, counterstained with the nuclear dye DRAQ5 (5 μM) and imaged using a widefield fluorescence microscope.

The results are plotted as means from 2 independent experiments performed in technical duplicate. Error bars represent SD. Individual data points represent means of the technical duplicate values from each of the independent experiments.

Strikingly, I detected similar activation patterns under all tested conditions, regardless of the genotype of the tested cells and of the presence of caspase inhibitors: S63845 alone was a potent inducer of IL-1β release, and the co-administration of ABT263/ABT737 enhanced this effect (Figure 9.2). With the exception of *Aim2*^{CRISPR} iMac cells reconstituted with human AIM2 (Figure 9.2 E), ABT263 and ABT737 alone were not able to trigger IL-1β release. Overall, the IL-1β secretion data do not provide any evidence that AIM2, NLRP3, or NLRP10 could be non-redundantly involved in the S63845-/ABT263-/ABT737-induced IL-1β response. This proves also appeared to occur in a caspase-independent manner.

On the level of ASC speck formation, the behavior of NLRP3/ASC^{mCerulean} reporter iMac cells (Figure 9.3 A) differed from that of HEK cells (Figure 9.3 B-D), consistent with the observations summarized in Figure 9.1. In macrophages, both ABT263 and S63845 administered alone produced ASC specking responses (Figure 9.3 A). Co-treatment with these agents did not lead to a synergistic effect. Unexpectedly, the background ASC specking levels of NLRP3/ASC^{mCerulean} reporter iMac cells cultured in the presence of emricasan were much higher than in the presence of VX-765 or DMSO (vehicle).

In HEK cells overexpressing fluorescently labeled ASC, ABT263 treatment resulted in ASC speck formation regardless of the NLRP10 overexpression status and of the addition of caspase inhibitors (Figure 9.3 B-D). This observation indicates that the ASC speck formation observed in HEK cells stimulated with ABT263 cannot be attributed to NLRP10. Future research could determine whether the ABT263-induced ASC specking response in HEK cells is an *in vitro* artifact linked to the prolonged stimulation time, an intrinsic property of ASC, or a result of ASC speck nucleation by a sensor expressed in HEK cells either constitutively or in a manner induced by ABT263.

Collectively, my results are only in partial agreement with the observations published by Vince et al. (2018). Vince et al. (2018) reported that the IL-1β response to S63845/ABT737 is independent of AIM2 and partially dependent on NLRP3 and on caspase-1. My results indicated that this response is independent of all three of these factors. Furthermore, Vince et al. (2018) observed that the S63845/ABT737-elicited IL-1β secretion is abolished in caspase-3/-7 double-deficient cells in the presence of the

NLRP3 inhibitor CRID3. In my experimental model, treatment with the pan-caspase inhibitor emricasan combined with the genetic or pharmacological NLRP3 inactivation still allowed for substantial IL-1β secretion when the cells were stimulated with S63845.

To exclude the possibility that S63845 led to IL-1β detection as an artifact resulting from the compound interference with the fluorescence-based IL-1β HTRF assay, I tested whether the addition of S63845 to DPBS could produce artifactual cytokine detection signal in the absence of cells (Supplementary Figure S37). Indeed, addition of S63845 to DPBS was associated with a weak HTRF signal compared to buffer control (Supplementary Figure S37 A) but the strength of this signal for 5 μM S63845 corresponded with the IL-1β concentration of 300 pg/mL (Supplementary Figure S37 B). The levels of the cytokine detected in the supernatants of cells treated with 5 μM S63845 were typically 4000-6000 pg/mL, so the S63845-induced IL-1β secretion cannot be explained by an autofluorescence artifact.

The possible sources of discrepancies between my results and the observations reported by Vince et al. (2018) are the cellular models employed in the studies, the time courses of the experiments, and the different approaches to caspase inactivation (pan-caspase inhibition with emricasan in my thesis *versus* caspase-3/-7 genetic deficiency in the article by Vince et al. (2018)). As there was no indication that S63845, ABT263, or ABT737 could activate AIM2 or NLRP10, alone or in combination, I did not proceed to investigate this matter in more depth. However, to gain more insight into the mechanism of the inflammasome responses to S63845/ABT263/ABT737, I went on to establish whether these processes could be inhibited by a range of cell death and mitochondrial damage blockers. The molecules tested in this context included the NLRP3 inhibitor CRID3, the tBid inhibitor BI-6C9 (Becattini et al., 2006), the caspase-1 inhibitor VX-765, the cell lysis inhibitor glycine (Brennan and Cookson, 2000; DiPeso et al., 2017; Heilig et al., 2018; Rashidi et al., 2019), and the mitoprotective agent CsA. Briefly, I pre-treated LPS-primed WT iMac cells (Figure 9.4) and NLRP3/ASC^{mCerulean} reporter iMac cells (Figure 9.5) with these compounds for 10 min, in the presence or absence of the pan-caspase inhibitor Q-Vd-OPh, and then administered S63845 and/or ABT263/ABT737. The IL-1β concentrations and ASC specking levels were measured after 24 h of stimulation.

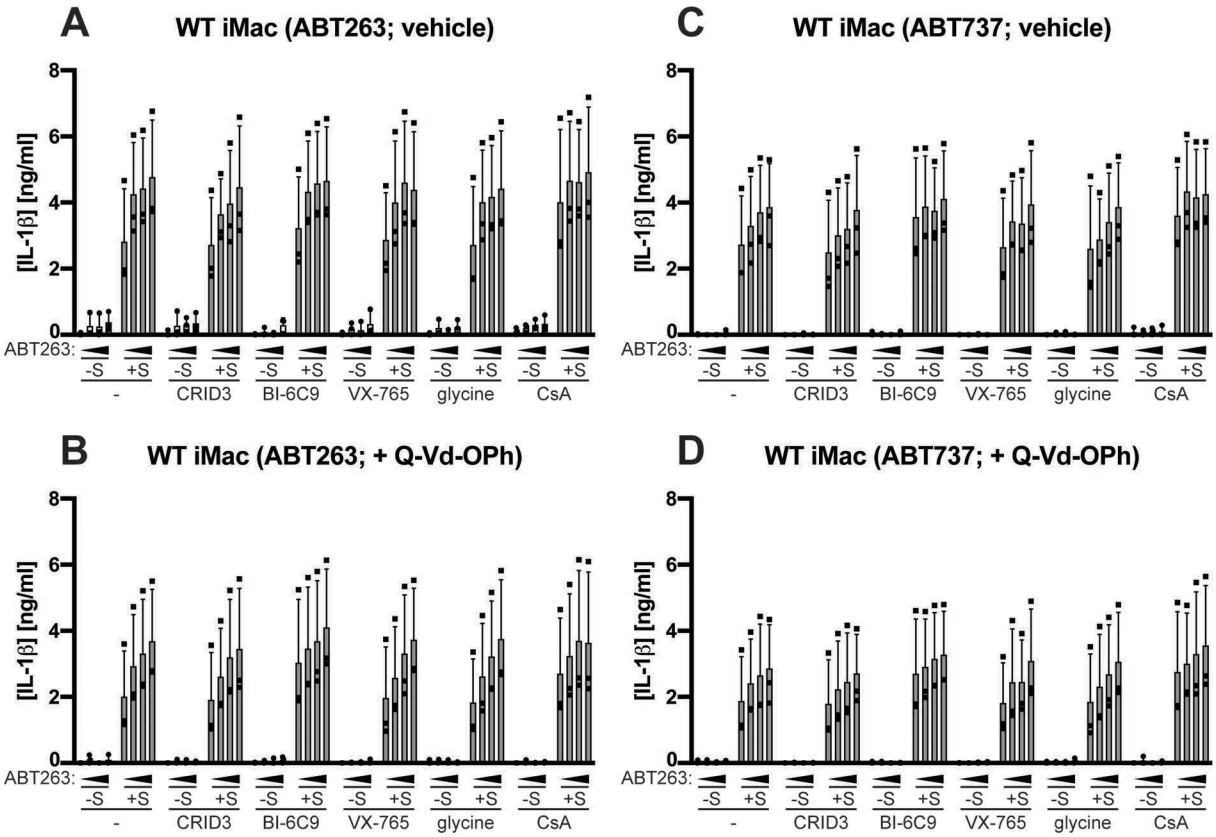

Figure 9.4. Sensitivity of the S63845- and ABT263-/ABT737-induced IL-1β release to CRID3, BI-6C9, VX-765, glycine, and cyclosporin A

A-D: LPS-primed (100 ng/mL, 2 h; LPS was present in the stimulation medium for the duration of the entire experiment) WT iMac cells were subjected to the MCL-1 inhibitor S63845 (+S; 5 μM), or left untreated (-S) in the presence or absence of the NLRP3 inhibitor CRID3 (5 μM), the tBid inhibitor BI-6C9 (25 μM), the caspase-1 inhibitor VX-765 (20 μM), the lytic cell death inhibitor glycine (5 mM), or the mitoprotective agent cyclosporin A (CsA; 10 μM). The stimulation media contained the pan-caspase inhibitor Q-Vd-OPh (20 μM; B, D) or vehicle (DMSO; A, C). Directly after administration of these treatments, the cells were stimulated with the BCL-2 family inhibitors ABT263 (0, 10, 25, or 50 μM; A, B) or ABT737 (0, 10, 25, or 50 μM; C, D). All stimulations were performed in DMEM supplemented with 5% FBS. Immediately after addition of inflammasome activators, the plates were centrifuged at 340 × g for 5 min (RT). After 24 h, the supernatants were collected and IL-1β concentrations were measured by HTRF. The results are plotted as means from 3 independent experiments performed in technical duplicate. Error bars represent SD. Individual data points represent means of the technical duplicate values from each of the independent experiments.

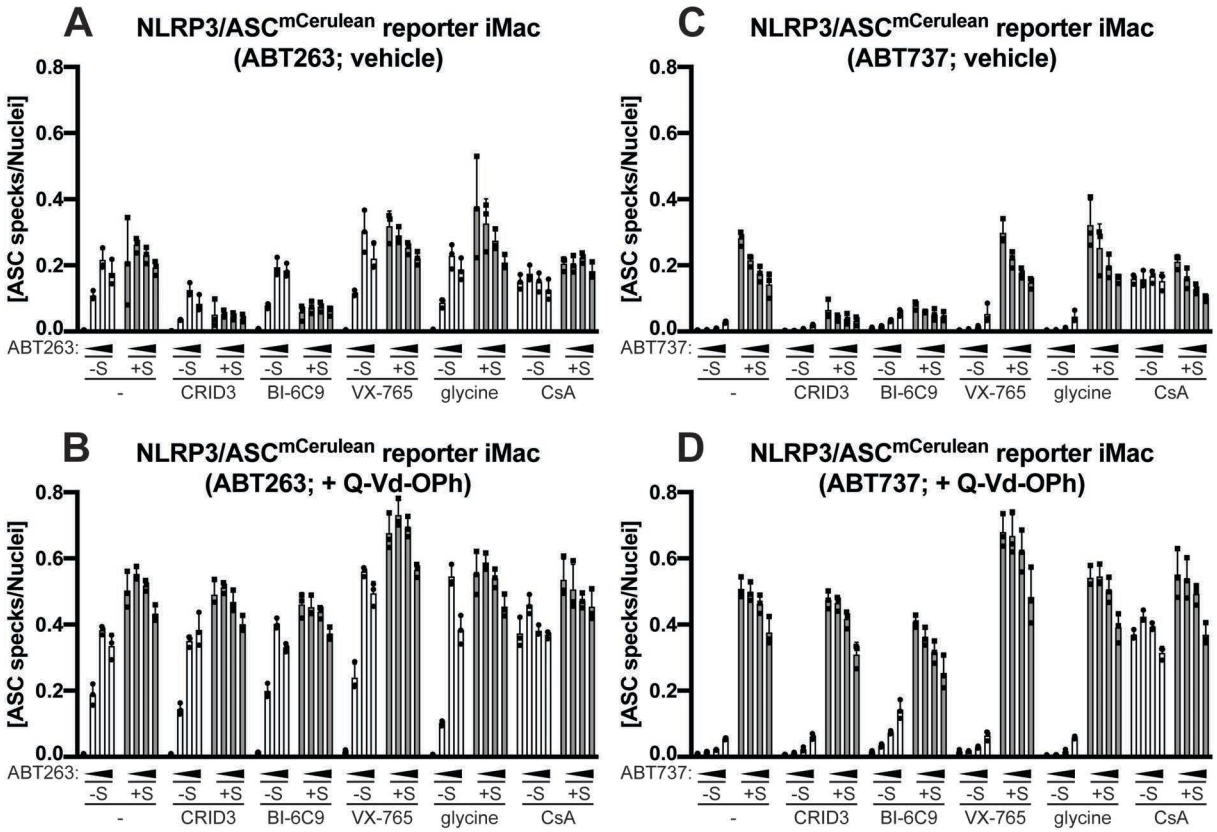

Figure 9.5 Sensitivity of the S63845- and ABT263-/ABT737-induced ASC speck formation to CRID3, BI-6C9, VX-765, glycine, and cyclosporin A

A-D: LPS-primed (100 ng/mL, 2 h; LPS was present in the stimulation medium for the duration of the entire experiment) NLRP3/ASC^{mCerulean} reporter iMac cells were subjected to the MCL-1 inhibitor S63845 (+S; 5 μM), or left untreated (-S) in the presence or absence of the NLRP3 inhibitor CRID3 (5 μM), the tBid inhibitor BI-6C9 (25 μM), the caspase-1 inhibitor VX-765 (20 μM), the lytic cell death inhibitor glycine (5 mM), or the mitoprotective agent cyclosporin A (CsA; 10 μM). The stimulation media contained the pan-caspase inhibitor Q-Vd-OPh (20 μM; B, D) or vehicle (DMSO; A, C). Directly after administration of these treatments, the cells were stimulated with the BCL-2 family inhibitors ABT263 (0, 10, 25, or 50 μM; A, B) or ABT737 (0, 10, 25, or 50 μM; C, D). All stimulations were performed in DMEM supplemented with 5% FBS. Immediately after addition of inflammasome activators, the plates were centrifuged at 340 × g for 5 min (RT). After 24 h, the cells were fixed with 4% formaldehyde, counterstained with the nuclear dye DRAQ5 (5 μM) and imaged using a widefield fluorescence microscope.
The results are plotted as means from 3 independent experiments performed in technical duplicate. Error bars represent SD. Individual data points represent means of the technical duplicate values from each of the independent experiments.

On the level of IL-1β secretion, none of the tested cytoprotective treatments could inhibit the S63845-induced cytokine release or the ABT263-/ABT737-mediated enhancement (Figure 9.4). This observation, combined with the results presented in Figure 9.2, suggests that multiple highly redundant pathways might be involved in the MOMP-elicited IL-1β response.

On the level of ASC speck formation, CRID3 and BI-6C9 were moderately potent inhibitors of the S63845- and ABT263-induced responses under caspase-proficient

conditions (Figure 9.5 A, C). The CRID3-mediated inhibition is in agreement with the report by Vince et al. (2018). None of the other tested treatments had an impact on the S63845-/ABT263-elicited ASC speck formation. Of note, the prolonged (24 h) treatment with CsA led to a high background ASC specking signal (Figure 9.5), which was not reflected by IL-1β secretion (Figure 9.4).

According to the model of inflammasome activation with S63845/ABT737 proposed by Vince et al. (2018), K^+ efflux is involved in the MOMP-induced NLRP3 response. To test whether I could reproduce this observation in my experimental system, I stimulated LPS-primed WT iMac cells and NLRP3/ASC^{mCerulean} reporter iMac cells with S63845, with or without ABT263/ABT737, in the presence of increased (60-100 mM) KCl concentrations (Figure 9.6 A, B). Media with increased NaCl concentrations served as an osmolarity control (Figure 9.6 C, D). The level of inflammasome activation was assessed by measurement of secreted IL-1β concentrations and imaging of ASC specks.

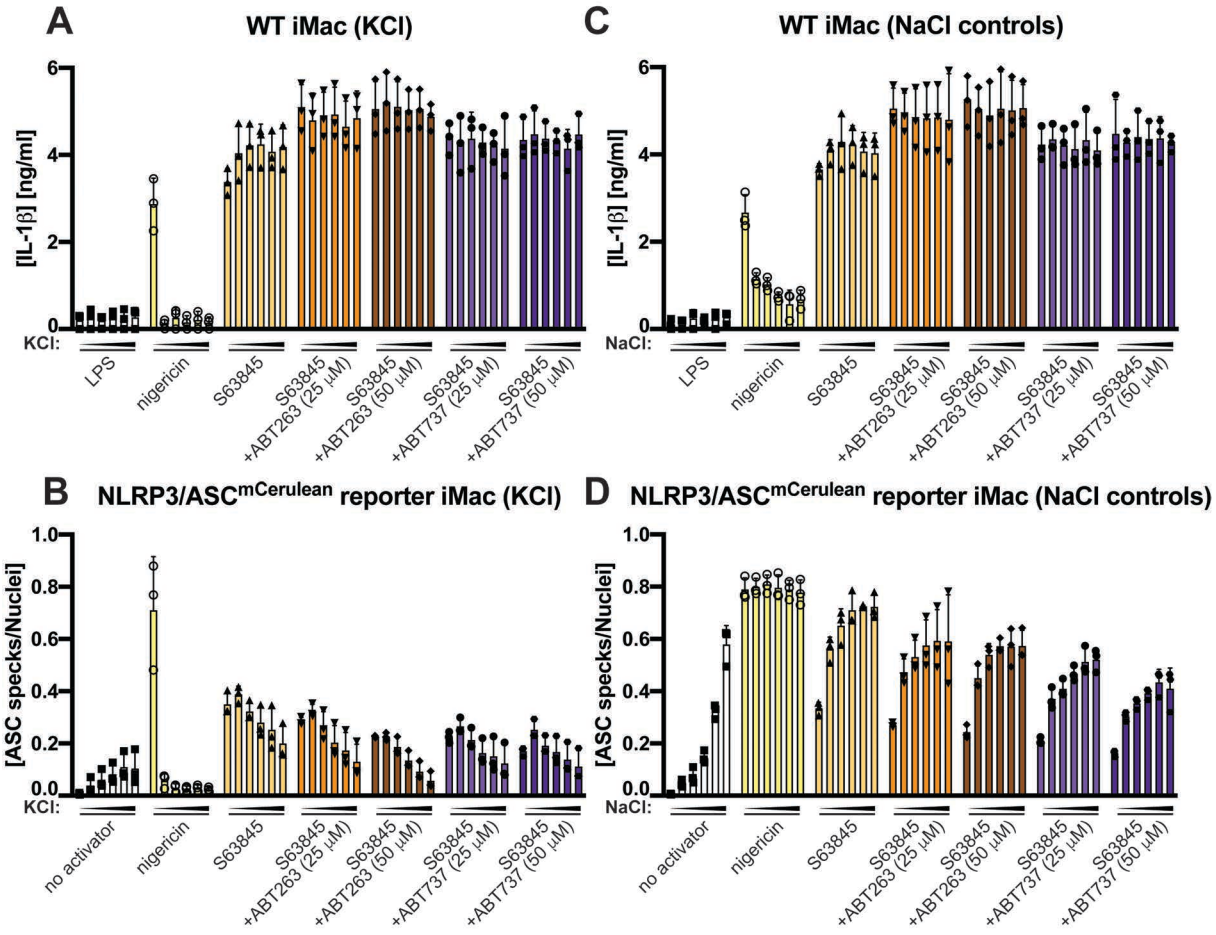

Figure 9.6 Sensitivity of the S63845- and ABT263-/ABT737-induced IL-1β release and ASC speck formation to high extracellular KCl concentrations

◂ **A-D:** LPS-primed (100 ng/mL, 1 h; LPS was present in the stimulation medium for the duration of the entire experiment) WT iMac cells (A, C) and unprimed NLRP3/ASC^{mCerulean} reporter iMac cells (B, D) were shifted to DMEM supplemented with 10% FBS and containing increased concentrations of KCl (5, 65, 75, 85, 95, or 105 mM; A, B) or NaCl (5, 65, 75, 85, 95, or 105 mM; C, D). Next, the cells were subjected to the MCL-1 inhibitor S63845 (5 μM) with or without the BCL-2 family inhibitors ABT263 (25 or 50 μM; A, B) or ABT737 (25 or 50 μM; C, D). The untreated control was subjected to medium alone, and the nigericin (10 μM) control was performed in the absence of MCL-1 and BCL-2 inhibitors. Immediately after addition of inflammasome activators, the plates were centrifuged at 340 × g for 5 min (RT). After 24 h, the supernatants were collected and IL-1β concentrations were measured by HTRF (A, C), or the cells were fixed with 4% formaldehyde, counterstained with the nuclear dye DRAQ5 (5 μM) and imaged using a widefield fluorescence microscope (B, D).
The results are plotted as means from 3 independent experiments performed in technical duplicate. Error bars represent SD. Individual data points represent means of the technical duplicate values from each of the independent experiments.

Whereas the nigericin-induced NLRP3 activation was completely abolished by increased KCl concentrations (Figure 9.6 A, B), the IL-1β secretion induced by S63845 (alone or in combination with ABT263/ABT737) was not sensitive to the increased KCl levels (Figure 9.6 A). In contrast, the MOMP-elicited ASC speck formation was partially sensitive to high KCl concentrations (Figure 9.6 B), suggesting that K^+ efflux may be required for ASC speck formation as increased NaCl concentrations did not have the inhibitory effect.

In conclusion, the partial sensitivity of the MOMP-driven ASC speck formation to CRID3 (Figure 9.5 A, C) and high KCl concentrations (Figure 9.6 B) are consistent with the previously reported results (Vince et al., 2018), but my observations regarding the IL-1β release from cells undergoing MOMP are not in agreement with the proposed model of the inflammasome activation by intrinsic apoptosis agonists. My results provide no evidence that MOMP could activate the AIM2 and NLRP10 inflammasomes.

The interpretation of my observations is difficult. Earlier in my thesis I have shown that the Bax agonist SMBA1 rapidly activates AIM2 and NLRP10, whereas BAM7, a different Bax activator, does not cause inflammasome formation (Section 6.16). Presently, I observed no signs of AIM2/NLRP10 activation in cells undergoing Bak-/Bax-mediated MOMP (Figures 9.2, 9.3). The easiest explanation of the observed discrepancy would be that SMBA1 induces mitochondrial damage through a Bak-/Bax-independent off-target effect. However, this scenario may be too simplistic in the light of the recent reports on the MOMP-induced leakage of mtDNA to the cytosol (McArthur et al., 2018; Riley et al., 2018). One possibility is that the biophysical and cellular characteristics of Bak/Bax pores may differ depending on the type of MOMP agonist. In principle this is possible, as

the sizes of Bak/Bax pores are variable and may be regulated (Bleicken et al., 2013). Another plausible scenario is that relatively slow processes, such as MOMP induced by S63845/ABT263/ABT737, could engage repair or clearance mechanisms that mask or degrade the AIM2/NLRP10 ligands, whereas the speed with which *m*-3M3FBS and thapsigargin permeabilize the IMM could prevent activation of such mechanisms. Finally, if the ligands of AIM2 and NLRP10 are released at a slower rate than cytochrome c (the APAF1 ligand) during the apoptotic MOMP, it is possible that the apoptotic cell death prevents AIM2/NLRP10 activation. The proposed scenarios are not mutually exclusive and given the current state of knowledge, it would be difficult to experimentally distinguish between them.

Because of the difficulties in interpreting the results obtained with BCL-2 family inhibitors, I went on to test a more direct way of triggering MOMP as a prospective NLRP10 activator. A recent report demonstrated that overexpression of the N-terminal domains of GsdmD and GsdmE may lead to the cytosolic leakage of the IMS contents and to pyroptotic cell death (Rogers et al., 2019). To examine whether overexpression of the GsdmD/E N-terminal domains could trigger NLRP10 activation, I transfected NLRP10$^{\text{mCitrine}}$/ASC$^{\text{TagBFP}}$ HEK cells and ASC$^{\text{TagBFP}}$ HEK cells (background control), with constructs encoding GsdmD/E (full-length or the N-terminal domains) as fusion proteins with mCherry or with mCherry co-expression driven by an IRES sequence. After 48 h of transfection, I inspected the ASC specking levels by fluorescence microscopy. The positive control samples were treated with *m*-3M3FBS during the final 30 min of the experiment (Figure 9.7).

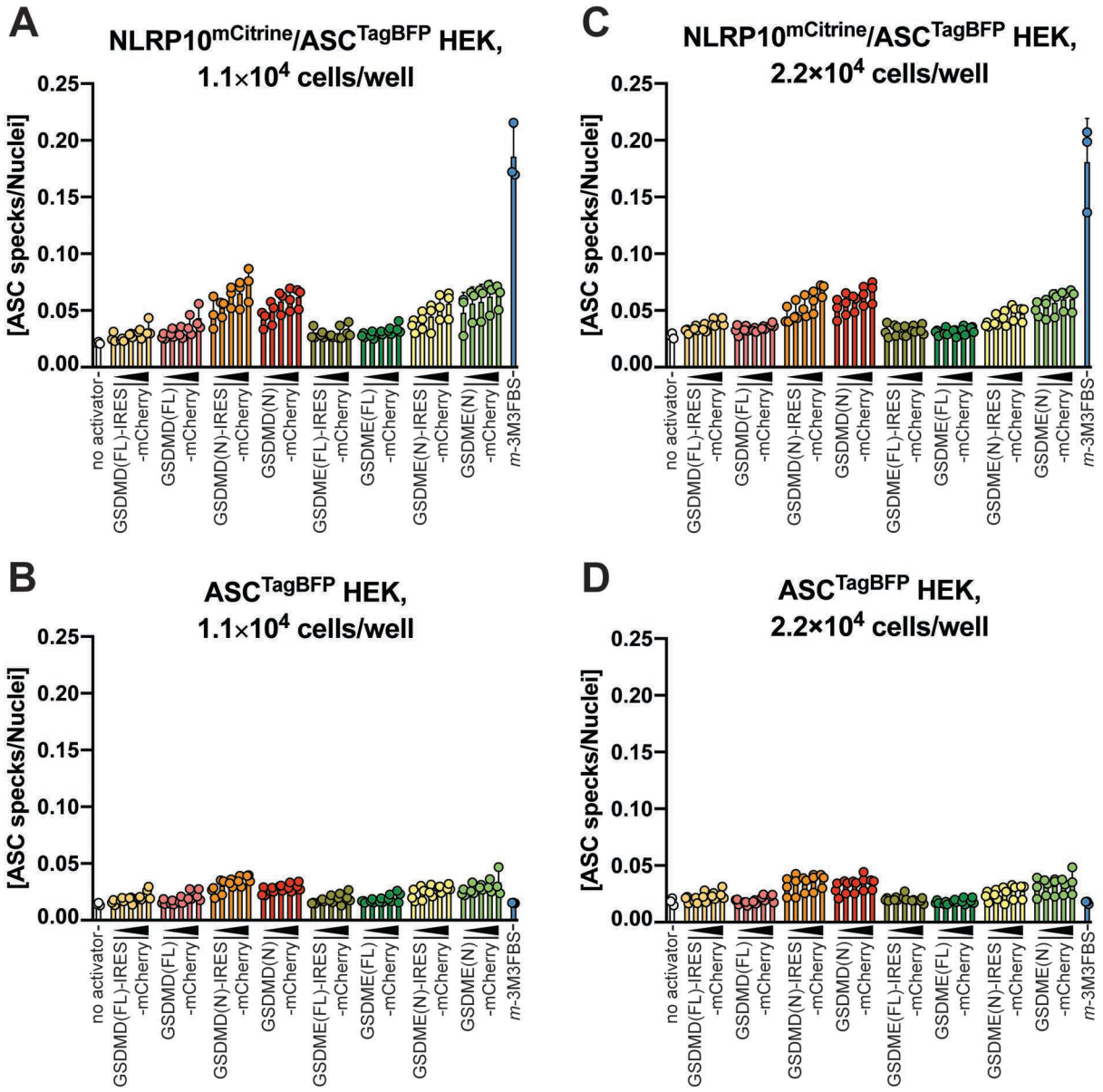

Figure 9.7. ASC specking levels in NLRP10^{mCitrine}/ASC^{TagBFP} HEK cells and ASC^{TagBFP} HEK cells transiently transfected with vectors encoding full-length gasdermin D/E or the gasdermin D/E N-terminal domains

A-D: NLRP10^{mCitrine}/ASC^{TagBFP} HEK cells (A, C) and ASC^{TagBFP} HEK cells (B, D) were plated in 96-well plates at 1.1 × 10^4 cells/well, or ~3.4 × 10^4 cells/cm^2 (A, B) or at 2.2 × 10^4 cells/well, or ~6.8 × 10^4 cells/cm^2 (C, D) and, after an overnight incubation, transfected with the following constructs (50, 75, 100, 150, or 200 ng of DNA per well) encoding human gasdermin (GSDM) D and E proteins or their N-terminal domains: full-length (FL) GSDMD-IRES-mCherry, GSDMD(FL)-linker-mCherry, N-terminal domain (N) of GSDMD-IRES-mCherry, GSDMD(N)-linker-mCherry, GSDME(FL)-IRES-mCherry, GSDME(FL)-linker-mCherry, GSDME(N)-IRES-mCherry, and GSDME(N)-linker-mCherry. The transfection reagent was Gene Juice and it was used at 2.7 μL of transfection reagent per 1 μg of DNA. After 24 h of stimulation, the cells were fixed with 4% formaldehyde, counterstained with the nuclear dye DRAQ5 (5 μM) and imaged using a widefield fluorescence microscope. The untreated (no activator) control was not transfected with DNA. The positive (*m*-3M3FBS) control cells were shifted to an extracellular medium consisting of (in mM) 123 NaCl, 5 KCl, 2 $MgCl_2$, 1 $CaCl_2$, 10 glucose, 10 HEPES pH 7.4 during the final 30 min of the experiment and stimulated with 85 μM *m*-3M3FBS.

The results are plotted as means from 3 independent experiments performed in technical duplicate. Error bars represent SD. Individual data points represent means of the technical duplicate values from each of the independent experiments.

In ASC^{TagBFP} HEK cells (without the NLRP10 overexpression), neither *m*-3M3FBS nor the overexpression of the GsdmD/E N-terminal domains caused ASC speck formation (Figure 9.7 B, D). In $NLRP10^{mCitrine}/ASC^{TagBFP}$ HEK cells, transfection with GsdmD/E N-terminal domains, but not the full-length variants, led a slight increase in ASC specking compared to the background signal (Figure 9.7 A, C). This ASC specking response was much lower than the response to *m*-3M3FBS, suggesting that the mitochondrial damage inflicted by the GsdmD/E N-terminal domains is not sufficient to activate NLRP10.

To ensure that cell death associated with the GsdmD/E N-terminal domain overexpression did not interfere with NLRP10 activation, I examined whether these proteins fragments could activate NLRP10 when the lytic cell death is blocked by the pan-caspase inhibitor Q-Vd-OPh, the osmoprotectant glycine, or the combination of these two agents (Figures 9.8.1 and 9.8.2).

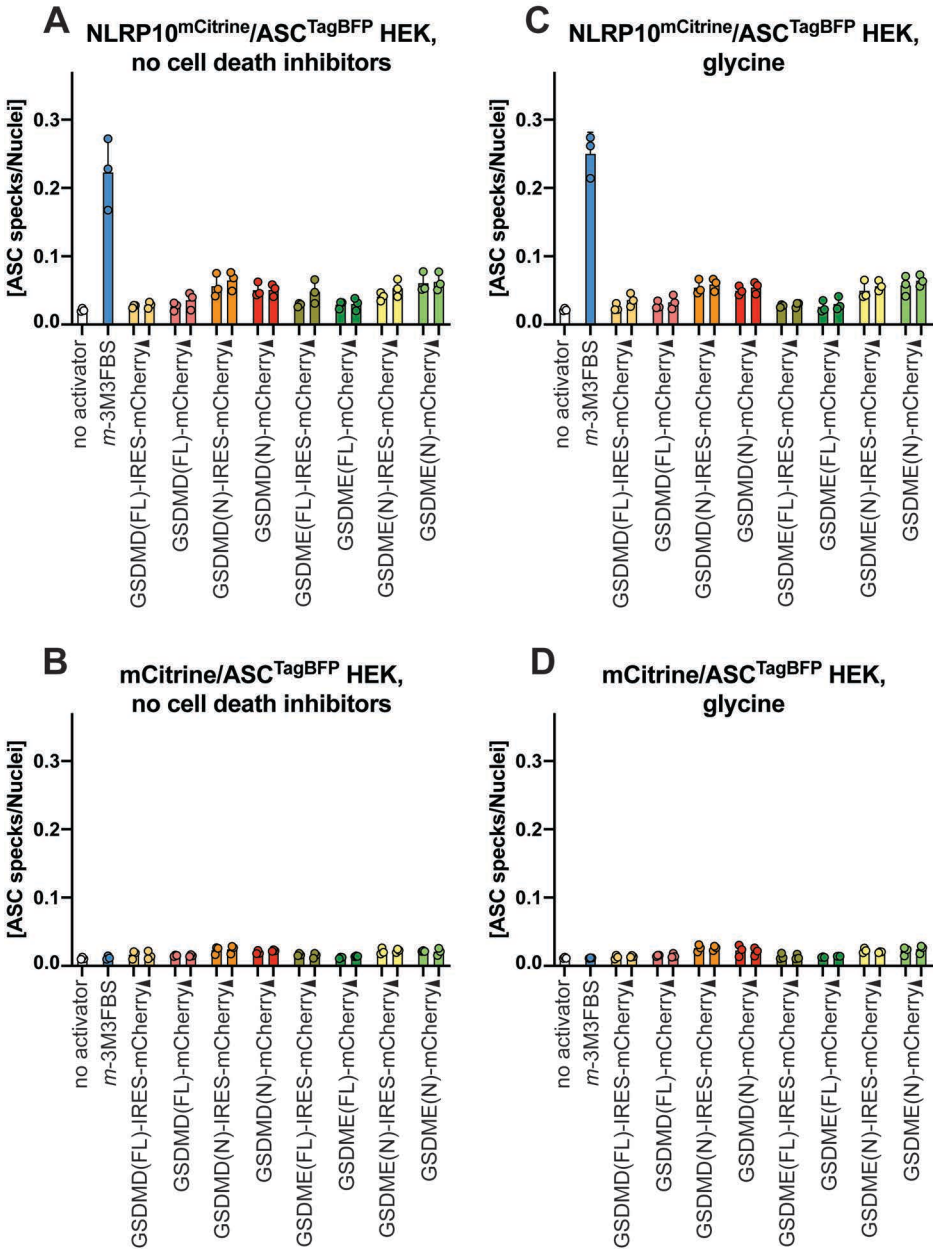

Figure 9.8.1 ASC specking levels in NLRP10^{mCitrine}/ASC^{TagBFP} HEK cells and ASC^{TagBFP} HEK cells transiently transfected with vectors encoding full-length gasdermin D/E or the gasdermin D/E N-terminal domains in the absence of cell death inhibitors or in the presence of glycine

A-D: NLRP10^{mCitrine}/ASC^{TagBFP} HEK cells (A, C) and ASC^{TagBFP} HEK cells (B, D) were plated in 96-well plates at 1.5 × 10^4 cells/well, or ~4.7 × 10^4 cells/cm^2 and, after an overnight incubation, transfected with the following constructs (150 or 200 ng of DNA per well) encoding human gasdermin (GSDM) D and E proteins or their N-terminal domains: full-length (FL) GSDMD-IRES-mCherry, GSDMD(FL)-linker-mCherry, N-terminal domain (N) of GSDMD-IRES-mCherry, GSDMD(N)-linker-mCherry, GSDME(FL)-IRES-mCherry, GSDME(FL)-linker-mCherry, GSDME(N)-IRES-mCherry, and GSDME(N)-linker-mCherry in the absence of cytoprotective agents ('no cell death inhibitors'; A, B) or in the presence of the lytic cell death inhibitor glycine (5 mM; C, D). The transfection reagent was Gene Juice and it was used at 2.7 µL of transfection reagent per 1 µg of DNA. After 24 h of stimulation, the cells were fixed with 4% formaldehyde, counterstained with the nuclear dye DRAQ5 (5 µM) and imaged using a widefield fluorescence microscope. The untreated (no activator) control was not transfected with DNA. The positive (*m*-3M3FBS) control cells were shifted to an extracellular medium consisting of (in mM) 123 NaCl, 5 KCl, 2 $MgCl_2$, 1 $CaCl_2$, 10 glucose, 10 HEPES pH 7.4 during the final 30 min of the experiment and stimulated with 85 µM *m*-3M3FBS.

The results are plotted as means from 3 independent experiments performed in technical duplicate. Error bars represent SD. Individual data points represent means of the technical duplicate values from each of the independent experiments.

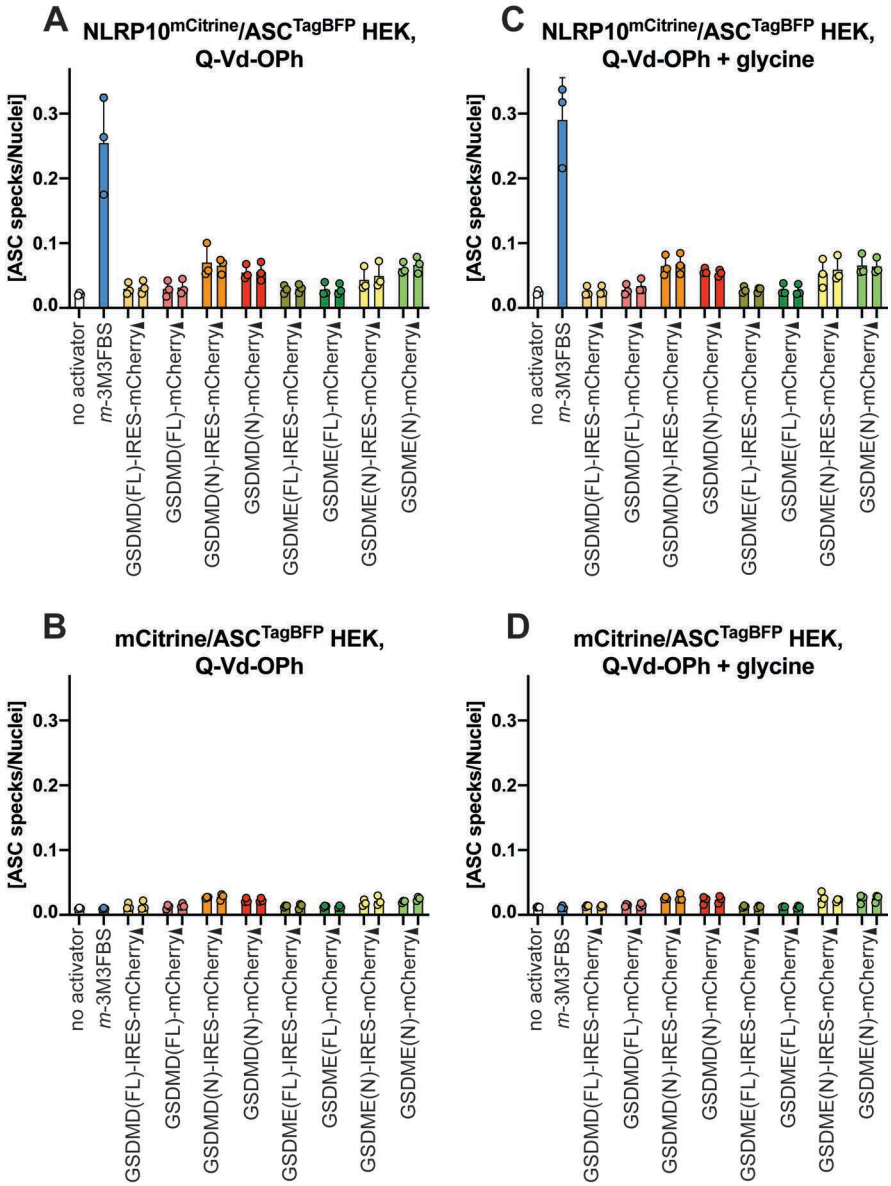

Figure 9.8.2 ASC specking levels in NLRP10^{mCitrine}/ASC^{TagBFP} HEK cells and ASC^{TagBFP} HEK cells transiently transfected with vectors encoding full-length gasdermin D/E or the gasdermin D/E N-terminal domains in the presence of Q-Vd-OPh or of the combination of glycine and Q-Vd-OPh

A-D: NLRP10^{mCitrine}/ASC^{TagBFP} HEK cells (A, C) and ASC^{TagBFP} HEK cells (B, D) were plated in 96-well plates at 1.5 × 10^4 cells/well, or ~4.7 × 10^4 cells/cm^2 and, after an overnight incubation, transfected with the following constructs (150 or 200 ng of DNA per well) encoding human gasdermin (GSDM) D and E proteins or their N-terminal domains: full-length (FL) GSDMD-IRES-mCherry, GSDMD(FL)-linker-mCherry, N-terminal domain (N) of GSDMD-IRES-mCherry, GSDMD(N)-linker-mCherry, GSDME(FL)-IRES-mCherry, GSDME(FL)-linker-mCherry, GSDME(N)-IRES-mCherry, and GSDME(N)-linker-mCherry in the presence of the pan-caspase inhibitor Q-Vd-OPh (20 μM; A, B) or of the combination of Q-Vd-OPh (20 μM) and the lytic cell death inhibitor glycine (5 mM; C, D). The transfection reagent was Gene Juice and it was used at 2.7 μL of transfection reagent per 1 μg of DNA. After 24 h of stimulation, the cells were fixed with 4% formaldehyde, counterstained with the nuclear dye DRAQ5 (5 μM) and imaged using a widefield fluorescence microscope. The untreated (no activator) control was not transfected with DNA. The positive (*m*-3M3FBS) control cells were shifted to an extracellular medium consisting of (in mM) 123 NaCl, 5 KCl, 2 $MgCl_2$, 1 $CaCl_2$, 10 glucose, 10 HEPES pH 7.4 during the final 30 min of the experiment and stimulated with 85 μM *m*-3M3FBS.

The results are plotted as means from 3 independent experiments performed in technical duplicate. Error bars represent SD. Individual data points represent means of the technical duplicate values from each of the independent experiments.

Under all tested conditions, the overexpression of the GsdmD/E N-terminal domains, but not the full-length proteins, led to a slight increase in ASC speck formation in NLRP10^{mCitrine}/ASC^{TagBFP} HEK cells (Figures 9.8.1 A, C and 9.8.2 A, C). This was not observed in ASC^{TagBFP} HEK cells without the NLRP10 overexpression. None of the tested cytoprotective treatments enhanced the ASC specking signal, consistent with the notion that permeabilization of the outer mitochondrial membrane by the GsdmD/E N-terminal domains is likely not sufficient to activate NLRP10. Collectively, my observations indicate that the apoptotic MOMP is not sufficient for the AIM2/NLRP10 activation.

9.2. Pharmacological targeting of BCL-2 family members provides no evidence of their involvement in AIM2/NLRP10 activation

The results presented in Section 9.1 suggest that induction of MOMP and/or intrinsic apoptosis does not act as a trigger for AIM2/NLRP10 activation, despite the reports suggesting that Bak/Bax pores could expose the mitochondrial matrix contents to the cytosol (McArthur et al., 2018; Riley et al., 2018).

Earlier in my thesis, I showed that the BCL-2 inhibitor HA14-1 and the BCL-2/BCL-XL/MCL-1 inhibitor TW37 were not capable of eliciting an inflammasome response during a short stimulation (Supplementary Figures S32 A, D, S33 A, D, and S34 A,D); in fact HA14-1 acted as a potent, non-selective inhibitor of multiple inflammasome responses. During an overnight incubation, HA14-1 and TW37 also did not consistently elicit the inflammasome activation (Supplementary Figures S35 and S36). Correspondingly, the Bax inhibitor iMAC2 did not inhibit the inflammasome responses to any of the tested stimuli (Supplementary Figures S32 B, S33 B, and S34 B).

To complete this picture, I tested whether the Bax agonist BTSA1 (Reyna et al., 2017) could activate the inflammasome in LPS-primed WT iMac cells, NLRP3/ASC^{mCerulean} reporter iMac cells, NLRP10^{mCitrine}/ASC^{TagBFP} HEK cells, or NLRP10^{mCherry}/ASC^{mCerulean} HEK cells (Figure 9.9). No inflammasome activation was detected when cells were treated with BTSA1 alone, whereas combined with the known inflammasome activators this compound behaved as a weak, non-selective inhibitor of multiple inflammasome responses (Figure 9.9). Interestingly, BTSA1 binds to the N-terminal portion of Bax (Reyna et al., 2017), similar to BAM7 (Gavathiotis et al., 2012). Neither of these two Bax

agonists activates the inflammasome. In contrast, SMBA1, the Bax activator that also activates AIM2 and NLRP10, binds to the C-terminal part of Bax (Xin et al., 2014).

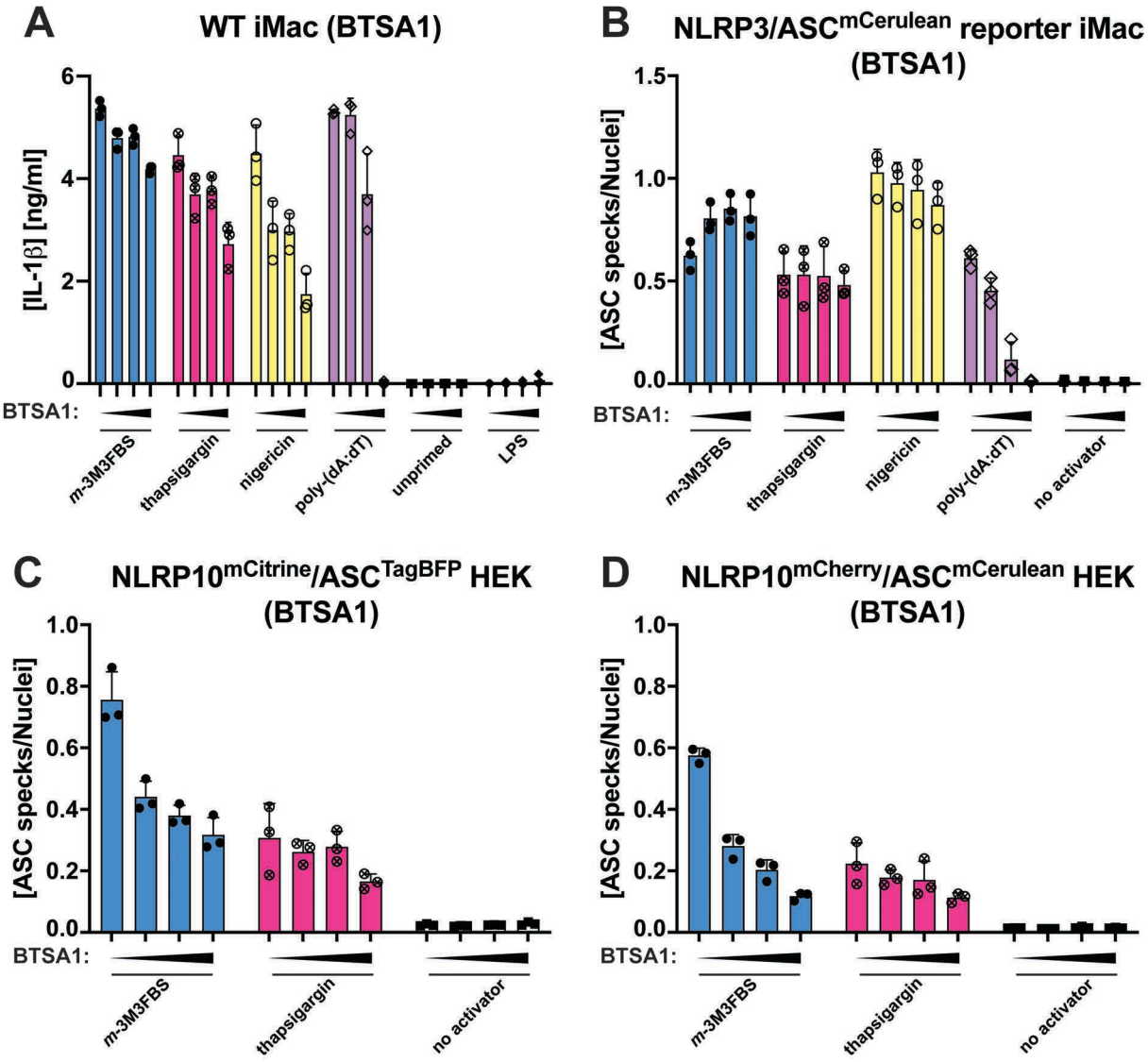

Figure 9.9. Influence of the Bax agonist BTSA1 on the inflammasome responses to *m*-3M3FBS, thapsigargin, nigericin, and poly-(dA:dT)

A-D: LPS-primed (200 ng/mL, 2 h) WT iMac cells (A), NLRP3/ASC^{mCerulean} reporter iMac cells (B), NLRP10^{mCitrine}/ASC^{TagBFP} HEK cells (C), and NLRP10^{mCherry}/ASC^{mCerulean} HEK cells (D) were shifted to an extracellular medium consisting of (in mM) 123 NaCl, 5 KCl, 2 $MgCl_2$, 1 $CaCl_2$, 10 glucose, 10 HEPES pH 7.4 and pre-treated for 10 min with BTSA1 (0, 5, 10, or 50 μM). Then, the cells were stimulated with the following inflammasome activators: *m*-3M3FBS (85 μM), thapsigargin (20 μM), nigericin (10 μM) or poly-(dA:dT) (2 μg/mL complexed with 5 μL Lipofectamine 2000). The LPS (A) and unprimed (A-D) controls were subjected to medium alone. Immediately after addition of inflammasome activators, the plates were centrifuged at 340 × g for 5 min (RT). After 30 min (C, D) or 60 min (A, B), the supernatants were collected and IL-1β concentrations were measured by HTRF (A) or the cells were fixed with 4% formaldehyde, counterstained with the nuclear dye DRAQ5 (5 μM) and imaged using a widefield fluorescence microscope (B-D).

The results are plotted as means from 3 independent experiments performed in technical duplicate. Error bars represent SD. Individual data points represent means of the technical duplicate values from each of the independent experiments.

I further tested the influence of AT406, LCL161, and birinapant on the inflammasome responses to multiple stimuli. These molecules, known as SMAC mimetics, promote apoptotic caspase activity by antagonizing proteins called inhibitors of apoptosis (cIAP and XIAP) (Fulda, 2015). I examined whether SMAC mimetics could trigger or inhibit inflammasome activation in LPS-primed WT iMac cells, NLRP3/ASC^{mCerulean} reporter iMac cells, and NLRP10^{mCitrine}/ASC^{TagBFP} HEK cells (Figures 9.10 and 9.11 A-C). In the same setup, I also examined whether the pan-BCL-2 family inhibitor gambogic acid has an influence on the inflammasome activation (Figure 9.11 D-F). Of note birinapant was strongly autofluorescent in the BFP channel so the results on the impact of this molecule on NLRP10 activation in NLRP10^{mCitrine}/ASC^{TagBFP} HEK cells are uninterpretable (Figure 9.11 C).

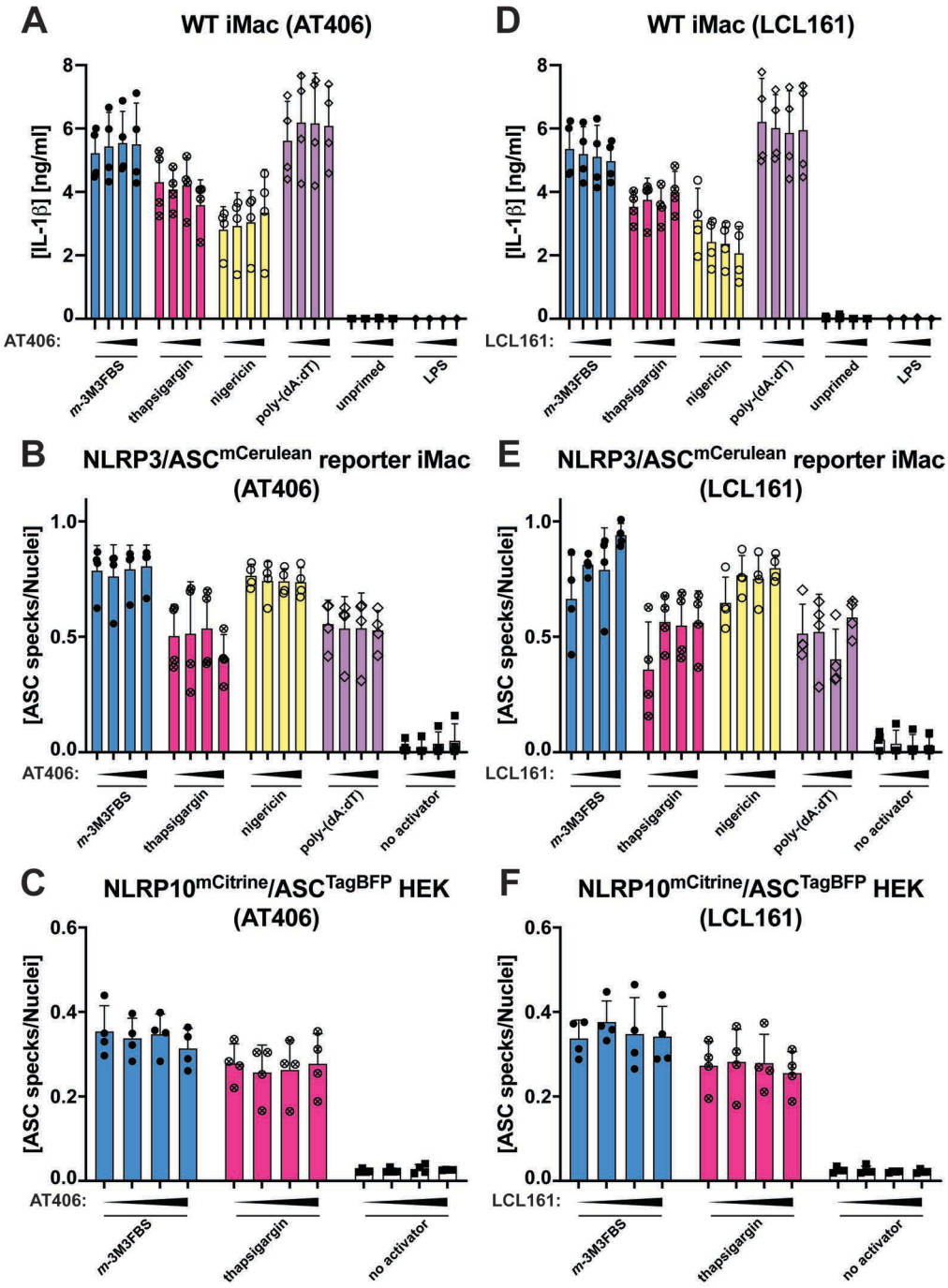

Figure 9.10. Influence of the SMAC mimetics AT406 and LCL161 on the inflammasome responses to *m*-3M3FBS, thapsigargin, nigericin, and poly-(dA:dT)

A-F: LPS-primed (200 ng/mL, 2 h) WT iMac cells (A, D), NLRP3/ASC^{mCerulean} reporter iMac cells (B, E), and NLRP10^{mCitrine}/ASC^{TagBFP} HEK cells (C, F) were shifted to an extracellular medium consisting of (in mM) 123 NaCl, 5 KCl, 2 $MgCl_2$, 1 $CaCl_2$, 10 glucose, 10 HEPES pH 7.4 and pre-treated for 10 min with AT406 (0, 5, 10, or 50 μM; A-C) or LCL161 (0, 5, 10, or 50 μM; D-F). Then, the cells were stimulated with the following inflammasome activators: *m*-3M3FBS (85 μM), thapsigargin (20 μM), nigericin (10 μM) or poly-(dA:dT) (2 μg/mL complexed with 5 μL Lipofectamine 2000). The LPS (A, D) and unprimed (A-F) controls were subjected to medium alone. Immediately after addition of inflammasome activators, the plates were centrifuged at 340 × g for 5 min (RT). After 30 min (C, F) or 60 min (A, B, D, E), the supernatants were collected and IL-1β concentrations were measured by HTRF (A, D) or the cells were fixed with 4% formaldehyde, counterstained with the nuclear dye DRAQ5 (5 μM) and imaged using a widefield fluorescence microscope (B, C, E, F).

The results are plotted as means from 4 independent experiments performed in technical duplicate. Error bars represent SD. Individual data points represent means of the technical duplicate values from each of the independent experiments.

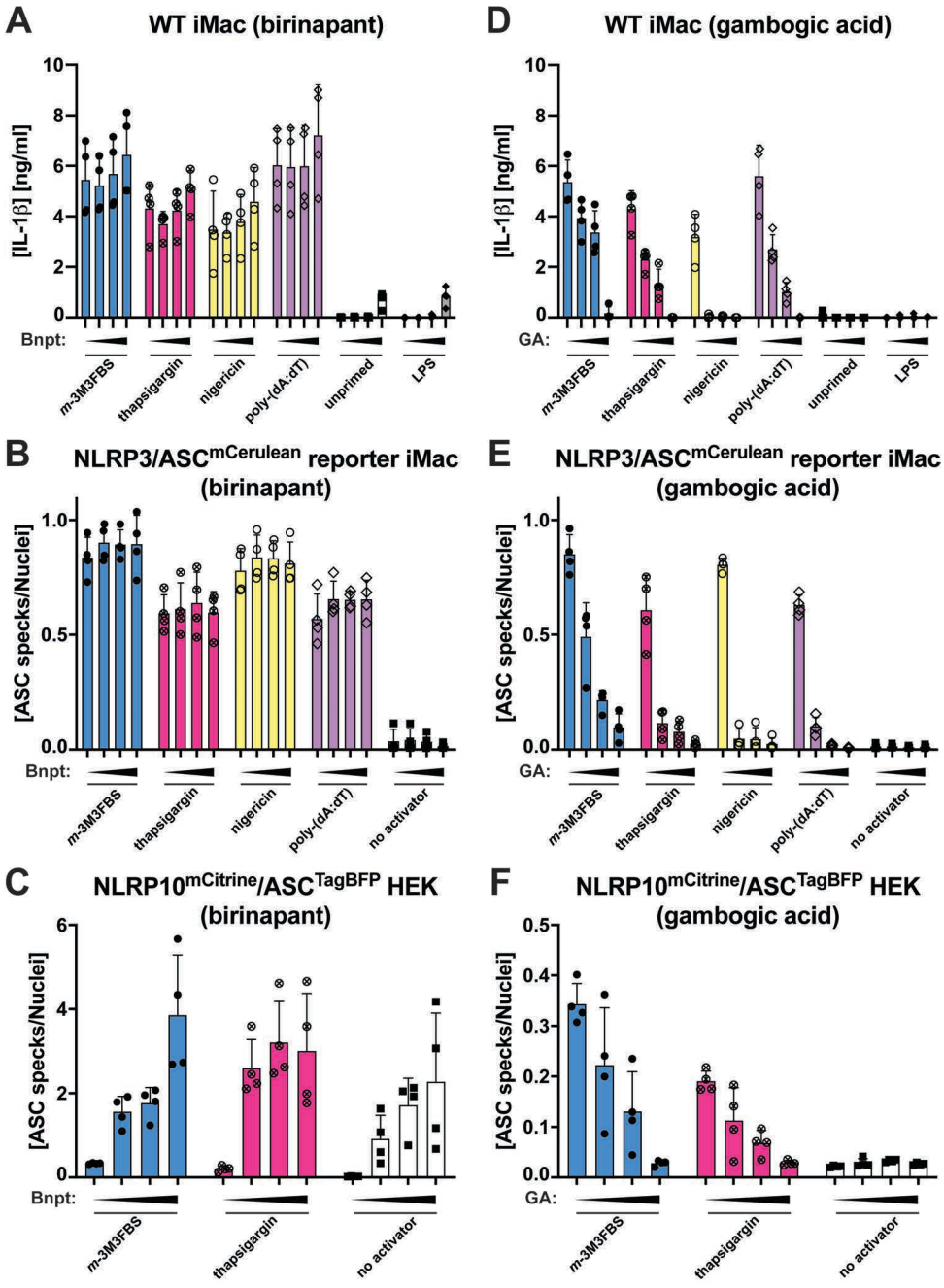

Figure 9.11. Impact of the SMAC mimetic birinapant and the BCL-2 family inhibitor gambogic acid on the inflammasome responses to *m*-3M3FBS, thapsigargin, nigericin, and poly-(dA:dT)

A-F: LPS-primed (200 ng/mL, 2 h) WT iMac cells (A, D), NLRP3/ASC^{mCerulean} reporter iMac cells (B, E), and NLRP10^{mCitrine}/ASC^{TagBFP} HEK cells (C, F) were shifted to an extracellular medium consisting of (in mM) 123 NaCl, 5 KCl, 2 $MgCl_2$, 1 $CaCl_2$, 10 glucose, 10 HEPES pH 7.4 and pre-treated for 10 min with birinapant (Bnpt; 0, 1, 5, or 50 μM; A-C) or gambogic acid (GA; 0, 5, 10, or 50 μM; D-F). Then, the cells were stimulated with the following inflammasome activators: *m*-3M3FBS (85 μM), thapsigargin (20 μM), nigericin (10 μM) or poly-(dA:dT) (2 μg/mL complexed with 5 μL Lipofectamine 2000). The LPS (A, D) and unprimed (A-F) controls were subjected to medium alone. Immediately after addition of inflammasome activators, the plates were centrifuged at 340 × g for 5 min (RT). After 30 min (C, F) or 60 min (A, B, D, E), the supernatants were collected and IL-1β concentrations were measured by HTRF (A, D) or the cells were fixed with 4% formaldehyde, counterstained with the nuclear dye DRAQ5 (5 μM) and imaged using a widefield fluorescence microscope (B, C, E, F).

The results are plotted as means from 4 independent experiments performed in technical duplicate. Error bars represent SD. Individual data points represent means of the technical duplicate values from each of the independent experiments.

None of the tested SMAC mimetics had the ability to activate the inflammasome (Figures 9.10 and 9.11 A, B). Short treatments with these agents also did not act as blockers of inflammasome activation. In contrast, the pan-BCL-2 family inhibitor gambogic acid strongly inhibited all tested inflammasome responses (Figure 9.11 D-F), in particular the NLRP3 response to nigericin (Figure 9.11 D, E). This is likely linked to the chemical reactivity of gambogic acid, which contains the Michael acceptor moiety (Sections 5.1-5.3).

Collectively, my results indicate that the induction of MOMP by BCL-2 family inhibition or by GsdmD/E N-terminal domains does not activate the AIM2/NLRP10 inflammasomes. Correspondingly, MOMP inhibitors do not inhibit the inflammasome activation by *m*-3M3FBS/thapsigargin. Among the three direct agonists of Bax tested in my thesis, one was a potent AIM2/NLRP10 activator (SMBA1), but two did not trigger inflammasome responses (BAM7 and BTSA1). The results presented in Sections 6.16, 9.1, and 9.2 do not exclude the possibility that the AIM2/NLRP10 activators and pro-apoptotic stimuli could share their targets. However, they clearly do not share the mechanisms of action.

The observed discrepancies suggest that many questions remain to be answered about the interactions between mitochondrial damage, cell death, and inflammasome activation. Some of the immediate topics for future research are: (1) how certain pro-apoptotic stimuli trigger IL-1β release, (2) how the IL-1β-inducing pro-apoptotic stimuli differ from those that do not induce IL-1β secretion, and (3) how the *m*-3M3FBS-/thapsigargin-induced mitochondrial disruption differs from the damage caused by S63845 and ABT263/ABT737.

9.3 Triggering the mitochondrial unfolded protein response does not activate the AIM2/NLRP10 inflammasomes

I found no evidence to link the intrinsic apoptosis pathway to AIM2/NLRP10 activation. Another axis of mitochondria-cytosol-nucleus communication, gaining more attention in the past ten years, is the mitochondrial unfolded protein response (UPR^{mt}) (Fessler et al., 2020; Guo et al., 2020; Melber and Haynes, 2018; Münch and Harper, 2016). The UPR^{mt} relays the information about the accumulation of unfolded proteins in the

mitochondrial matrix and along the mitochondrial protein import routes in a mechanism involving regulated proteolysis and translocation of signaling proteins from the IMS to the cytosol (Fessler et al., 2020; Guo et al., 2020). Pharmacologically, UPR^{mt} can be triggered by the inhibition of the mitochondrial protease Lon (using its LMW inhibitors CDDO or CDDO-Me; Bernstein et al., 2012), or by mitochondrially-targeted heat shock protein 90 (HSP90) inhibitors (such as GTPP; Kang et al., 2010; 2011; 2009; Karpel-Massler et al., 2017; Siegelin et al., 2011). I set out to examine whether cells undergoing UPR^{mt} could activate the AIM2 and NLRP10 inflammasomes.

First, I tested whether the UPR^{mt}-triggering stimuli could activate inflammasome responses in a 24-h setup, in the presence or absence of the NLRP3 inhibitor CRID3. I evaluated the ASC specking responses to CDDO, CDDO-Me, and GTPP in HEK cells overexpressing $NLRP10^{mCitrine}/ASC^{TagBFP}$, $NLRP10^{mCherry}/ASC^{mCerulean}$, or $mCitrine/ASC^{TagBFP}$ (Figure 9.12), and in $NLRP3/ASC^{mCerulean}$ reporter iMac cells overexpressing human/murine NLRP10 or transduced with the empty vector (Figure 9.13).

In HEK cells, regardless of the NLRP10 overexpression status, CDDO did not elicit ASC speck formation, whereas CDDO-Me and GTPP produced non-monotonic dose-response ASC specking curves. The maximal ASC specking levels were detected at intermediate concentrations of the UPR^{mt} agonists (Figure 9.12). Importantly, the observed ASC speck formation could not be attributed to the NLRP10 overexpression because $NLRP10^{mCitrine}/ASC^{TagBFP}$ HEK cells (Figure 9.12 A), $NLRP10^{mCherry}/ASC^{mCerulean}$ HEK cells (Figure 9.12 B), and $mCitrine/ASC^{TagBFP}$ HEK cells (Figure 9.12 C) all responded to CDDO-Me and GTPP with similar strength.

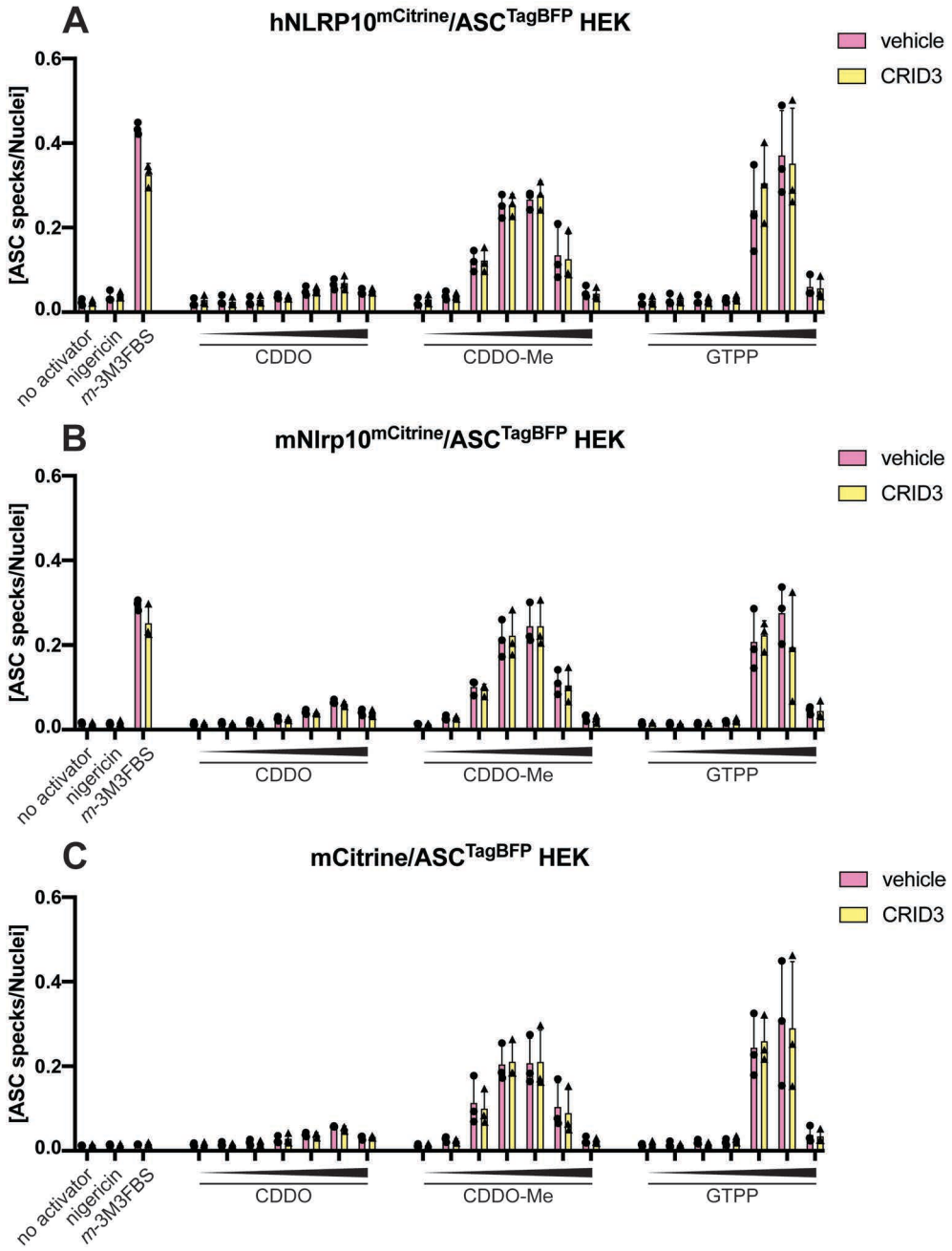

Figure 9.12. ASC specking levels in NLRP10^{mCitrine}/ASC^{TagBFP} HEK cells, NLRP10^{mCherry}/ASC^{mCerulean} HEK cells, and mCitrine/ASC^{TagBFP} HEK cells treated with the mitochondrial unfolded protein response agonists CDDO, CDDO-Me, and GTPP for 24 h

A-C: Human (h) NLRP10^{mCitrine}/ASC^{TagBFP} HEK cells (A), murine (m) Nlrp10^{mCitrine}/ASC^{TagBFP} HEK cells (B), and mCitrine/ASC^{TagBFP} HEK cells (C) were stimulated with CDDO (0.1, 0.5, 1, 2.5, 5, 10, or 20 μM), CDDO-Me (0.1, 0.5, 1, 2.5, 5, 10, or 20 μM), or GTPP (0.1, 0.5, 1, 2.5, 5, 10, or 20 μM) for 24 h in the presence (yellow bars) or absence (vehicle – ethanol; pink bars) of the NLRP3 inhibitor CRID3 (5 μM). During the last 60 min of experiment, the control cells were stimulated with nigericin (10 μM) or *m*-3M3FBS (85 μM). The untreated (no activator) controls were subjected to medium alone. Immediately after administration of the stimuli, the plates were centrifuged at 340 × g for 5 min (RT). With the exception of the nigericin and *m*-3M3FBS controls (which were performed in an extracellular medium consisting of [in mM] 123 NaCl, 5 KCl, 2 $MgCl_2$, 1 $CaCl_2$, 10 glucose, 10 HEPES pH 7.4), all stimulations were performed in DMEM supplemented with 10% FBS. After completion of the experiment, the cells were fixed with 4% formaldehyde, counterstained with the nuclear dye DRAQ5 (5 μM) and imaged using a widefield fluorescence microscope.

The results are plotted as means from 3 independent experiments performed in technical duplicate. Error bars represent SD. Individual data points represent means of the technical duplicate values from each of the independent experiments.

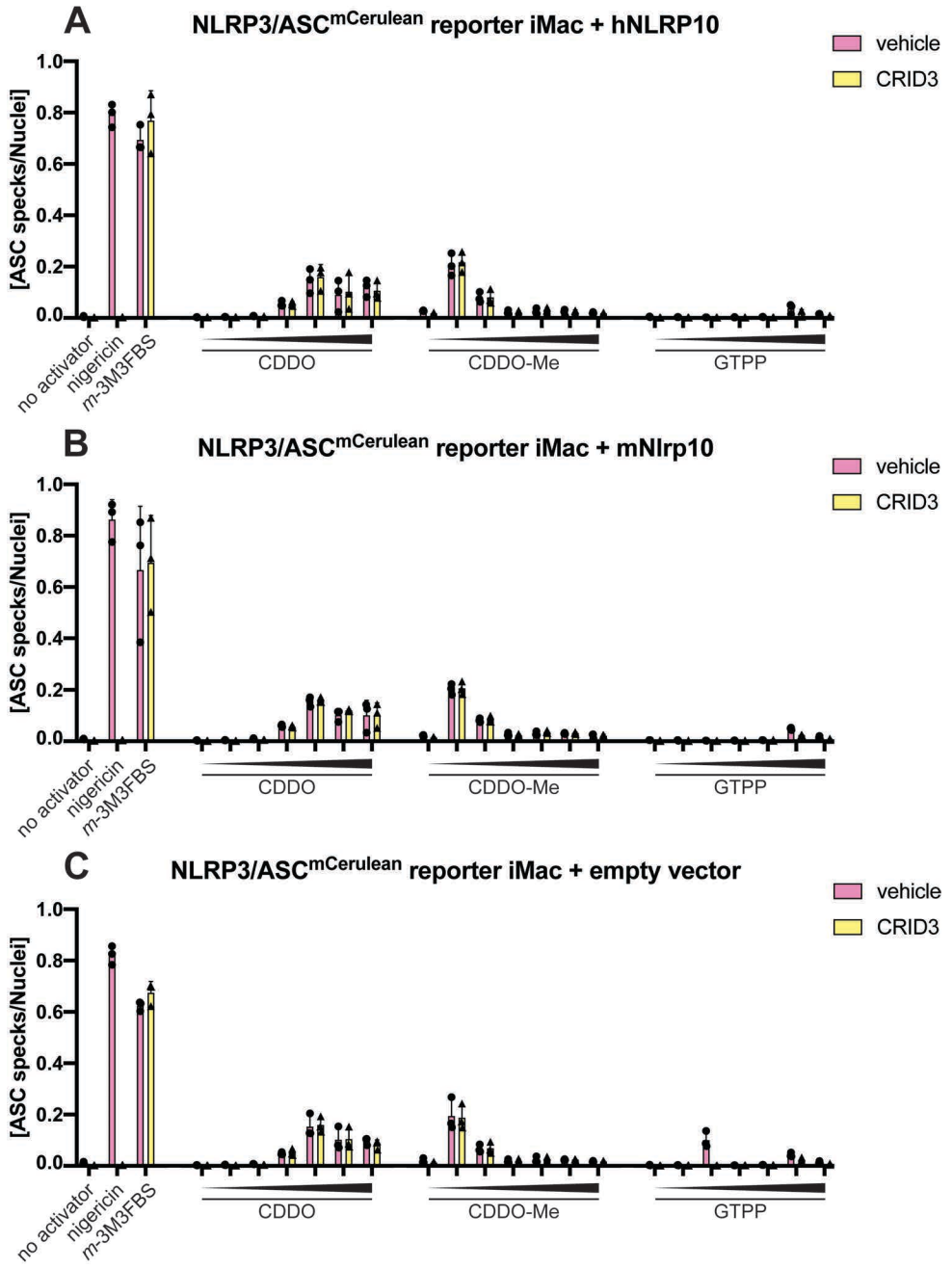

Figure 9.13 ASC specking levels in NLRP3/ASC^{mCerulean} reporter iMac cells overexpressing human/murine NLRP10 or transduced with the empty vector, and treated with the mitochondrial unfolded protein response agonists CDDO, CDDO-Me, and GTPP for 24 h

A-C: NLRP3/ASC^{mCerulean} reporter iMac cells overexpressing WT human (h) NLRP10 (A), WT murine (m) NLRP10 (B), or the empty vector (C) were stimulated with CDDO (0.1, 0.5, 1, 2.5, 5, 10, or 20 μM), CDDO-Me (0.1, 0.5, 1, 2.5, 5, 10, or 20 μM), or GTPP (0.1, 0.5, 1, 2.5, 5, 10, or 20 μM) for 24 h in the presence (yellow bars) or absence (vehicle – ethanol; pink bars) of the NLRP3 inhibitor CRID3 (5 μM). During the last 60 min of experiment, the control cells were stimulated with nigericin (10 μM) or *m*-3M3FBS (85 μM). The untreated (no activator) controls were subjected to medium alone. Immediately after administration of the stimuli, the plates were centrifuged at 340 × g for 5 min (RT). With the exception of the nigericin and *m*-3M3FBS controls (which were performed in an extracellular medium consisting of [in mM] 123 NaCl, 5 KCl, 2 $MgCl_2$, 1 $CaCl_2$, 10 glucose, 10 HEPES pH 7.4), all stimulations were performed in DMEM supplemented with 10% FBS. After completion of the experiment, the cells were fixed with 4% formaldehyde, counterstained with the nuclear dye DRAQ5 (5 μM) and imaged using a widefield fluorescence microscope.

The results are plotted as means from 3 independent experiments performed in technical duplicate. Error bars represent SD. Individual data points represent means of the technical duplicate values from each of the independent experiments.

In NLRP3/ASC^{mCerulean} reporter iMac cells, intermediate concentrations of CDDO and low concentrations of CDDO-Me produced weak ASC specking responses that were not inhibited by CRID3 and not linked to the NLRP10 overexpression status. Stimulations with GTPP only led to negligible levels of ASC specking (Figure 9.13).

I went on to determine whether the ASC speck formation observed in the UPR^{mt} agonist-stimulated cells (Figure 9.14 B-D) would be reflected by IL-1β secretion from LPS-primed WT iMac cells treated with CDDO, CDDO-Me, or GTPP (Figure 9.14 A). However, while NLRP3/ASC^{mCerulean} reporter iMac cells (Figure 9.14 B), NLRP10^{mCitrine}/ASC^{TagBFP} HEK cells (Figure 9.14 C), and NLRP10^{mCherry}/ASC^{mCerulean} HEK cells (Figure 9.14 D) all exhibited substantial levels of ASC specking after UPR^{mt} induction, the IL-1β concentrations detected in the supernatants of CDDO-, CDDO-Me-, and GTPP-stimulated LPS-primed WT iMac cells were only slightly higher than the background IL-1β levels secreted by cells treated with LPS alone (Figure 9.14 A). This observation suggests that the ASC specks detected in cells undergoing UPR^{mt} might not represent active inflammasomes. (Another example of ASC speck formation without inflammasome activation was reported by Green et al. (2018).) Collectively, there was no indication that CDDO, CDDO-Me, or GTPP could activate AIM2/NLRP10, and overall these treatments did not exhibit typical characteristics of inflammasome agonists.

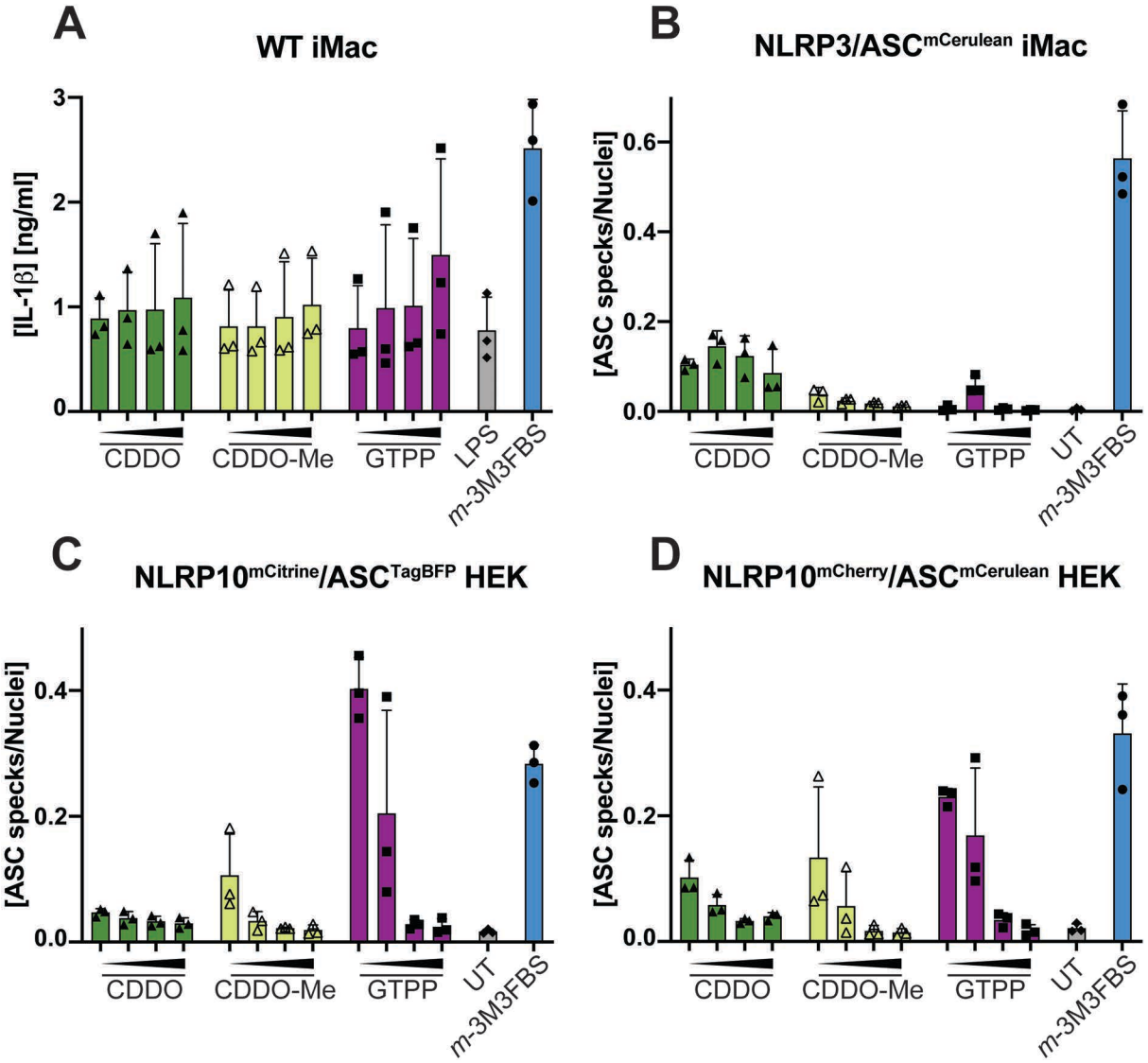

Figure 9.14. IL-1β and ASC specking responses to the UPR^{mt} agonists CDDO, CDDO-Me, and GTPP in LPS-primed WT iMac cells, NLRP3/ASC^{mCerulean} iMac cells, NLRP10^{mCitrine}/ASC^{TagBFP} HEK cells, and NLRP10^{mCherry}/ASC^{mCerulean} HEK cells

A-D: LPS-primed (100 ng/mL, 1 h; LPS was kept in the medium for the duration of the entire experiment) WT iMac cells (A), NLRP3/ASC^{mCerulean} reporter iMac cells (B), NLRP10^{mCitrine}/ASC^{TagBFP} HEK cells (C), and NLRP10^{mCherry}/ASC^{mCerulean} HEK cells (D) were stimulated with CDDO (5, 10, 25, or 50 μM), CDDO-Me (5, 10, 25, or 50 μM), or GTPP (5, 10, 25, or 50 μM) for 24 h in DMEM supplemented with 10% FBS. During the final 60 min of the experiment, the *m*-3M3FBS control cells were shifted to an extracellular medium consisting of (in mM) 123 NaCl, 5 KCl, 2 $MgCl_2$, 1 $CaCl_2$, 10 glucose, 10 HEPES pH 7.4 and stimulated with m-3M3FBS (85 μM). The LPS (A) and untreated (UT; B-D) controls were subjected to medium alone. Immediately after administration of the stimuli, the plates were centrifuged at 340 × g for 5 min (RT). After completion of the experiment, the supernatants were collected and IL-1β concentrations were measured by HTRF (A), or the cells were fixed with 4% formaldehyde, counterstained with the nuclear dye DRAQ5 (5 μM) and imaged using a widefield fluorescence microscope (B-D).
The results are plotted as means from 3 independent experiments performed in technical triplicate. Error bars represent SD. Individual data points represent means of the technical triplicate values from each of the independent experiments.

As the induction of UPR^{mt} did not lead to AIM2/NLRP10 activation, I proceeded to test whether the UPR^{mt} agonists could instead negatively interfere with inflammasome formation. To address this question, I pre-treated LPS-primed WT iMac cells,

NLRP3/ASC^{mCerulean} reporter iMac cells, NLRP10^{mCitrine}/ASC^{TagBFP} HEK cells (Figure 9.15), and NLRP10^{mCherry}/ASC^{mCerulean} HEK cells (Supplementary Figure S38) with CDDO, CDDO-Me, or GTPP, and then challenged them with the inflammasome agonists *m*-3M3FBS, thapsigargin, nigericin, and poly-(dA:dT). To assess the level of inflammasome activation, I measured the IL-1β concentrations in cell culture supernatants and imaged ASC specks by fluorescence microscopy.

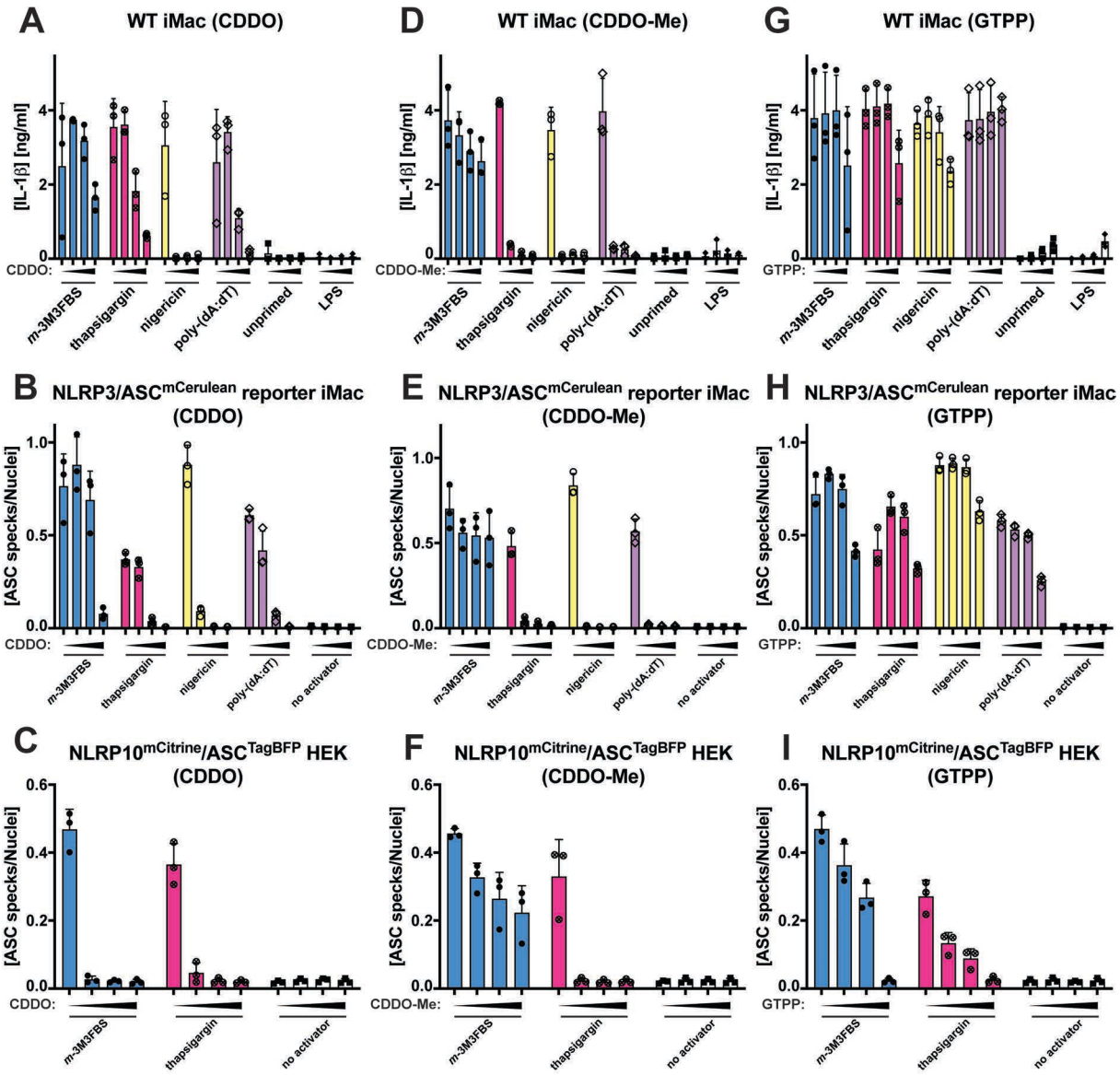

Figure 9.15. Influence of the UPR^{mt} agonists CDDO, CDDO-Me, and GTPP on the inflammasome responses to *m*-3M3FBS, thapsigargin, nigericin, and poly-(dA:dT)

A-I: LPS-primed (200 ng/mL, 2 h) WT iMac cells (A, D, G), NLRP3/ASC^{mCerulean} reporter iMac cells (B, E, H), and NLRP10^{mCitrine}/ASC^{TagBFP} HEK cells (C, F, I) were treated for 10 min with CDDO (0, 10, 25, or 50 μM; A-C), CDDO-Me (0, 10, 25, or 50 μM; D-F), or GTPP (0, 5, 10, or 50 μM; G-I) and then subjected to the inflammasome activators *m*-3M3FBS (85 μM), thapsigargin (20 μM), nigericin (10 μM) or poly-(dA:dT) (2 μg/mL complexed with 5 μL Lipofectamine 2000) in an extracellular medium consisting of (in mM) 123 NaCl, 5 KCl, 2 $MgCl_2$, 1 $CaCl_2$, 10 glucose, 10 HEPES, pH 7.4. The LPS (A, D, G) and unprimed (A-I) controls were subjected to medium alone. Immediately after addition of inflammasome activators, the plates were centrifuged at 340 × g for 5 min (RT). After 30 min (C, F, I) or 60 min (A, B, D, E, G, H), the supernatants

were collected and IL-1β concentrations were measured by HTRF (A, D, G) or the cells were fixed with 4% formaldehyde, counterstained with the nuclear dye DRAQ5 (5 μM) and imaged using a widefield fluorescence microscope (B, C, E, F, H, I).
The results are plotted as means from 3 independent experiments performed in technical duplicate. Error bars represent SD. Individual data points represent means of the technical duplicate values from each of the independent experiments.

None of the tested UPR^{mt} agonists elicited substantial levels of ASC speck formation or IL-1β release in the short incubation setup. In contrast, CDDO was a strong inhibitor of the NLRP3 response to nigericin, and an intermediately potent blocker of the AIM2 responses to thapsigargin and poly-(dA:dT) in macrophages (Figure 9.15 A, B). In this cell type, CDDO inhibited the AIM2 response to *m*-3M3FBS very weakly. Interestingly, in NLRP10-overexpressing HEK cells, CDDO potently inhibited the NLRP10 responses to both *m*-3M3FBS and thapsigargin (Figure 9.15 C).

CDDO-Me strongly inhibited the inflammasome responses to thapsigargin, nigericin, and poly-(dA:dT), but had no influence on the inflammasome activation with *m*-3M3FBS (Figure 9.15 D-F). Finally, GTPP was not a potent inflammasome inhibitor in macrophages (the highest tested GTPP concentrations only led to partial reduction in the inflammasome responses; Figure 9.15 G, H). Conversely, GTPP was a moderately potent inhibitor of the NLRP10 response to thapsigargin and weak inhibitor of the response to *m*-3M3FBS in NLRP10^{mCitrine}/ASC^{TagBFP} HEK cells (Figure 9.15 I). All the observations made in NLRP10^{mCitrine}/ASC^{TagBFP} HEK cells (Figure 9.15 C, F, I) were fully reproducible in NLRP10^{mCherry}/ASC^{mCerulean} HEK cells (Supplementary Figure S38).

The UPR^{mt} agonists in the short-term experimental setup had the ability to inhibit inflammasome activation. This effect was not selectively targeted at a specific inflammasome sensor molecule and not universally inflicted by all tested UPR^{mt} triggers: CDDO and CDDO-Me were more potent at inhibiting the inflammasome responses than GTPP, and NLRP3 activation was affected stronger than AIM2 and NLRP10 activations. It is likely that the CDDO-/CDDO-Me-mediated NLRP3 inhibition was linked to the Michael acceptor moieties in the CDDO and CDDO-Me molecules (Maucher et al., 2017; Sections 5.1-5.3). While the interplay between the UPR^{mt} and innate immune sensing may be an important topic for future research, I found no evidence that the UPR^{mt} activation could selectively activate or inhibit the AIM2/NLRP10 inflammasome responses.

9.4. Inorganic ion fluxes across the mitochondrial membranes are likely not involved in the inflammasome responses to *m*-3M3FBS and thapsigargin

So far, my results suggested that the well-known mitochondrial protein egress routes are not mediators of the AIM2/NLRP10 activation. What other mechanisms could explain the rapid cytosolic leakage of the mitochondrial matrix contents? One possible scenario is the rupture of the IMM due to osmotic stress. Such mechanism would explain the fast rate and the apparent lack of specificity of the *m*-3M3FBS-/thapsigargin-induced mitochondrial permeabilization, but it is questionable whether any cellular solute could contribute to an osmotic damage of this caliber.

In theory, the solutes that could be transported into the mitochondria during *m*-3M3FBS/thapsigargin stimulation are small inorganic ions. Consequently, it could be expected that the removal of an ionic species important for the AIM2/NLRP10 activation from the extracellular medium would partially or fully inhibit the inflammasome assembly. I already determined that the AIM2/NLRP10 responses proceed uninterrupted in the absence of K^+, Na^+, and Ca^{2+} ions (Sections 4.4, 6.3, and 6.11). Two relatively easily manipulatable species that remained to be tested were Mg^{2+} and Cl^- ions.

To examine whether the inflammasome activation with *m*-3M3FBS/thapsigargin could occur in Mg^{2+}- and Cl^--free media, I shifted LPS-primed WT iMac cells, NLRP3/ASC^{mCerulean} reporter iMac cells, and NLRP^{10mCitrine}/ASC^{TagBFP} HEK cells to a Ca^{2+}-/Mg^{2+}-free buffer (131 mM NaCl, 5 mM KCl, 10 mM glucose, 10 mM HEPES, pH 7.4) or to Ca^{2+}-/Mg^{2+}-/Cl^--free buffers (gluconate-based: 131 mM sodium gluconate, 5 mM potassium gluconate, 10 mM glucose, 10 mM HEPES, pH 7.4, or acetate-based: 131 mM sodium acetate, 5 mM potassium acetate, 10 mM glucose, 10 mM HEPES, pH 7.4). Next, I stimulated the cells with *m*-3M3FBS, thapsigargin, nigericin, and poly-(dA:dT), and measured the concentrations of secreted IL-1β (Figure 9.16 A) or performed imaging of ASC specks to determine the degree of inflammasome activation (Figure 9.16 B, C).

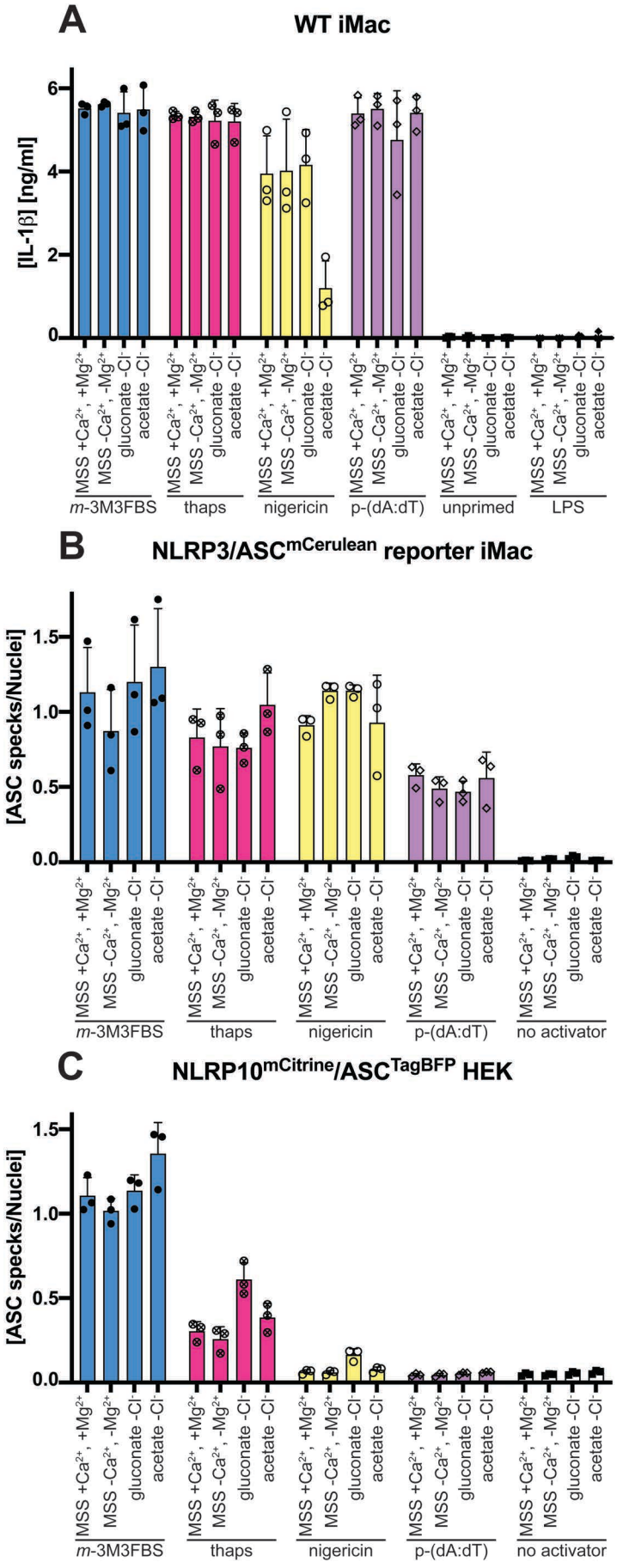

Figure 9.16. Inflammasome responses to *m*-3M3FBS, thapsigargin, nigericin, and poly-(dA:dT) in extracellular media depleted of Ca^{2+}, Mg^{2+}, and/or Cl^- ions

◂ **A-C:** LPS-primed (200 ng/mL, 2 h) WT iMac cells (A), NLRP3/ASC^{mCerulean} reporter iMac cells (B), and NLRP10^{mCitrine}/ASC^{TagBFP} HEK cells (C) were shifted to extracellular media containing (in mM; corresponding to the identifiers in the figure panels):

- MSS +Ca^{2+}, +Mg^{2+}: 123 NaCl, 5 KCl, 2 $MgCl_2$, 1 $CaCl_2$, 10 glucose, 10 HEPES, pH 7.4,
- MSS -Ca^{2+}, -Mg^{2+}: 131 NaCl, 5 KCl, 10 glucose, 10 HEPES, pH 7.4,
- gluconate -Cl^-: 131 sodium gluconate, 5 potassium gluconate, 10 glucose, 10 HEPES pH 7.4,
- acetate -Cl^-: 131 sodium acetate, 5 potassium acetate, 10 glucose, 10 HEPES, pH 7.4.

Then, the cells were subjected to the inflammasome activators *m*-3M3FBS (85 μM), thapsigargin (thaps; 20 μM), nigericin (10 μM) or poly-(dA:dT) (p-(dA:dT); 2 μg/mL complexed with 5 μL Lipofectamine 2000) in an extracellular medium consisting of (in mM) 123 NaCl, 5 KCl, 2 $MgCl_2$, 1 $CaCl_2$, 10 glucose, 10 HEPES, pH 7.4. The LPS (A) and unprimed (A-C) controls were subjected to medium alone. Immediately after addition of inflammasome activators, the plates were centrifuged at 340 × g for 5 min (RT). After 30 min (C) or 60 min (A, B), the supernatants were collected and IL-1β concentrations were measured by HTRF (A) or the cells were fixed with 4% formaldehyde, counterstained with the nuclear dye DRAQ5 (5 μM) and imaged using a widefield fluorescence microscope (B, C).
The results are plotted as means from 3 independent experiments performed in technical duplicate. Error bars represent SD. Individual data points represent means of the technical duplicate values from each of the independent experiments.

I observed no impact of the extracellular Mg^{2+} and Cl^- depletion on the inflammasome activations with the tested stimuli. On the level of IL-1β secretion, the acetate-based medium reduced the response to nigericin (Figure 9.16 A), but this reduction was not observed on the level of ASC speck formation (Figure 9.16 B) and in the gluconate-based medium (Figure 9.16 A, B). This suggests that the high acetate concentration, rather than the Cl^- deficiency, was responsible the inhibitory effect. In NLRP10^{mCitrine}/ASC^{TagBFP} HEK cells, the acetate-based medium led to a slightly increased ASC specking response to *m*-3M3FBS, whereas the gluconate-based buffer enhanced the response to thapsigargin (Figure 9.16 C). These effects therefore appeared to be linked to the Cl^--exchanging anion (acetate/gluconate), and not directly to Cl^- depletion. While these observations do not completely exclude the possibility that inorganic ion fluxes could be involved in the *m*-3M3FBS-/thapsigargin-induced mitochondrial damage, the fact that acute removal of Ca^{2+} and Mg^{2+} and replacement of Cl^- with acetate/gluconate still allow for robust inflammasome responses suggests that these ions are not important in this process.

Notably, Cl^- transport across the inner mitochondrial membrane has been implicated in the mPT in the past (De Marchi et al., 2008; Ponnalagu et al., 2019). Specifically, a Cl^- channel sensitive to DIDS but not to IAA-94 was linked to mPTP opening by (De Marchi et al., 2008), while (Ponnalagu et al., 2019) reported that the mPTP-dependent mitochondrial Ca^{2+} retention capacity could be reduced by IAA-94. Taking these observations into consideration, I tested whether the *m*-3M3FBS- or thapsigargin-

elicited inflammasome activations in LPS-primed WT iMac cells, NLRP3/ASC^{mCerulean} reporter iMac cells, and NLRP10^{mCherry}/ASC^{mCerulean} HEK cells are sensitive to DIDS (Figure 9.17 A-C) or IAA-94 (Figure 9.17 D-F).

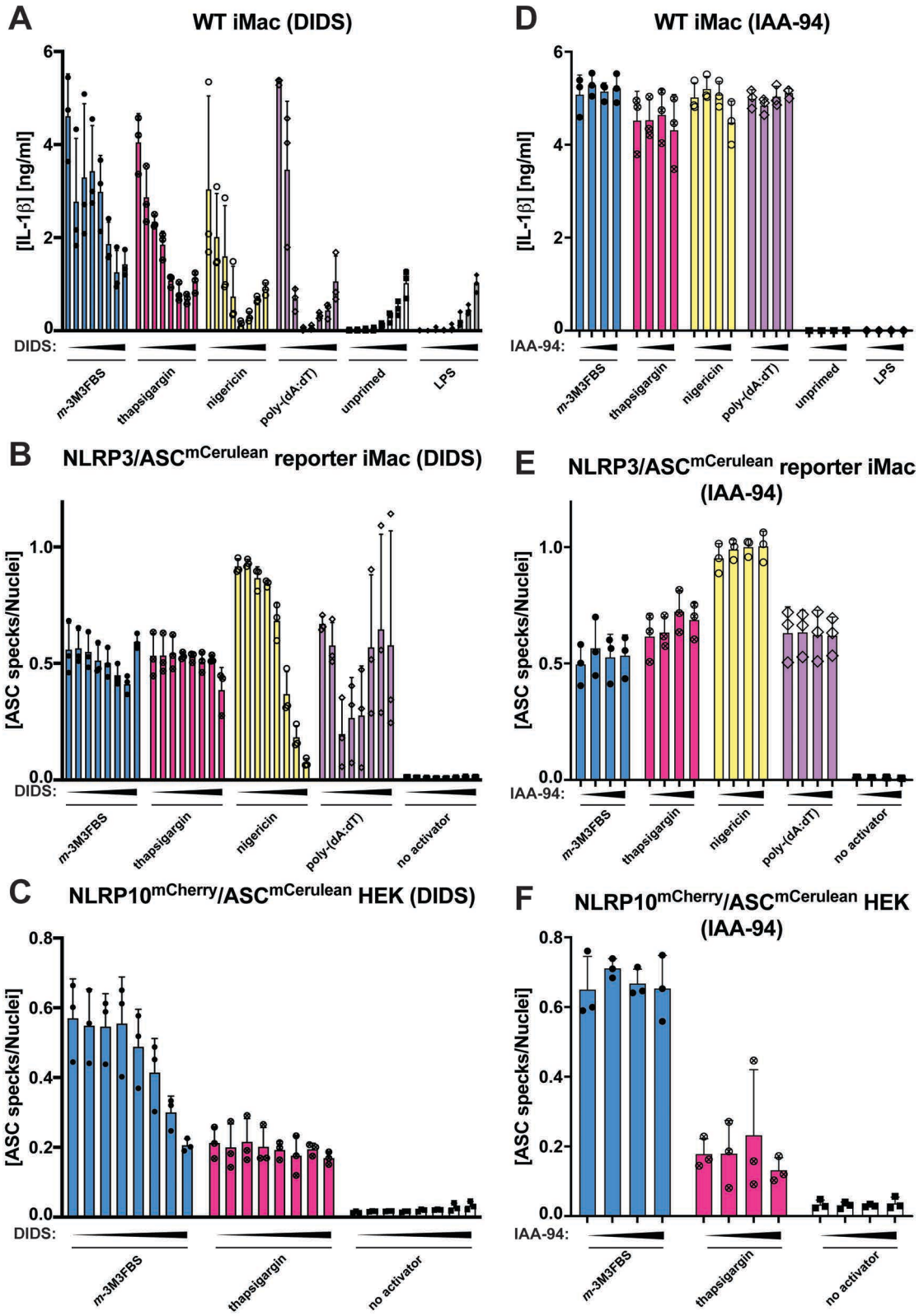

Figure 9.17. Influence of the Cl$^-$ channel blockers DIDS and IAA-94 on the inflammasome responses to *m*-3M3FBS, thapsigargin, nigericin, and poly-(dA:dT)

◂ **A-F:** LPS-primed (200 ng/mL, 2 h) WT iMac cells (A, D), NLRP3/ASC^{mCerulean} reporter iMac cells (B, E), and NLRP10^{mCherry}/ASC^{mCerulean} HEK cells (C, F) were treated for 10 min with DIDS (0, 10, 25, 50, 100, 250, 500, or 1000 μM; A-C) or IAA-94 (0, 25, 50, or 100 μM; D-F) and then subjected to the inflammasome activators *m*-3M3FBS (85 μM), thapsigargin (20 μM), nigericin (10 μM) or poly-(dA:dT) (2 μg/mL complexed with 5 μL Lipofectamine 2000) in an extracellular medium consisting of (in mM) 123 NaCl, 5 KCl, 2 $MgCl_2$, 1 $CaCl_2$, 10 glucose, 10 HEPES, pH 7.4. The LPS (A, D) and unprimed (A-F) controls were subjected to medium alone. Immediately after addition of inflammasome activators, the plates were centrifuged at 340 × g for 5 min (RT). After 30 min (C, F) or 60 min (A, B, D, E), the supernatants were collected and IL-1β concentrations were measured by HTRF (A, D) or the cells were fixed with 4% formaldehyde, counterstained with the nuclear dye DRAQ5 (5 μM) and imaged using a widefield fluorescence microscope (B, C, E, F).
The results are plotted as means from 3 independent experiments performed in technical duplicate. Error bars represent SD. Individual data points represent means of the technical duplicate values from each of the independent experiments.

IAA-94 had no impact on the inflammasome responses to the tested stimuli (Figure 9.17 D-F), whereas DIDS non-selectively inhibited all tested inflammasome responses on the level of IL-1β secretion (Figure 9.17 A). Unexpectedly, very high concentrations of DIDS (250-1000 μM) appeared to *elicit* an IL-1β response; however, it is possible that this signal was a result of a positive interference of the compound with the HTRF readout, as equal levels of IL-1β were detected in the supernatants from unprimed and LPS-primed cells. In macrophages, on the level of ASC speck formation, DIDS was a weak inhibitor of the nigericin-induced NLRP3 activation (Figure 9.17 B) but had no influence on the ASC specking responses to *m*-3M3FBS and thapsigargin, whereas the impact on the response to poly-(dA:dT) was biphasic. In NLRP10^{mCherry}/ASC^{mCerulean} HEK cells, DIDS was a weak, partial inhibitor of the NLRP10 response to *m*-3M3FBS, but not to thapsigargin (Figure 9.17 C). The IAA-94 results were fully reproducible in NLRP10^{mCitrine}/ASC^{TagBFP} HEK cells (Supplementary Figure S39 B), whereas the observations on the impact of DIDS on the inflammasome formation in these cells were uninterpretable because of the inhibitor's autofluorescence (Supplementary Figure S39 A). Collectively, my results provide no evidence that transmembrane fluxes of the most physiologically abundant inorganic ions could be involved in the activation of the AIM2/NLRP10 inflammasomes.

Another anion channel proposed to be involved in the mitochondrial membrane permeabilization is VDAC (Madesh and Hajnóczky, 2001; Tomasello et al., 2009). Importantly, this channel has already been implicated in one of the K^+ efflux-independent NLRP3 activation mechanisms (Wolf et al., 2016). Recently, VBIT-4, a specific inhibitor of VDAC, has been demonstrated to inhibit a pathological process whereby mtDNA fragment are released into the cytosol to induce interferon signaling (Kim et al., 2019). I proceeded to test whether VBIT-4 could prevent the inflammasome

responses to *m*-3M3FBS and thapsigargin in LPS-primed WT iMac cells, NLRP3/ASC^{mCerulean} reporter iMac cells, and NLRP10^{mCitrine}/ASC^{TagBFP} HEK cells (Figure 9.18).

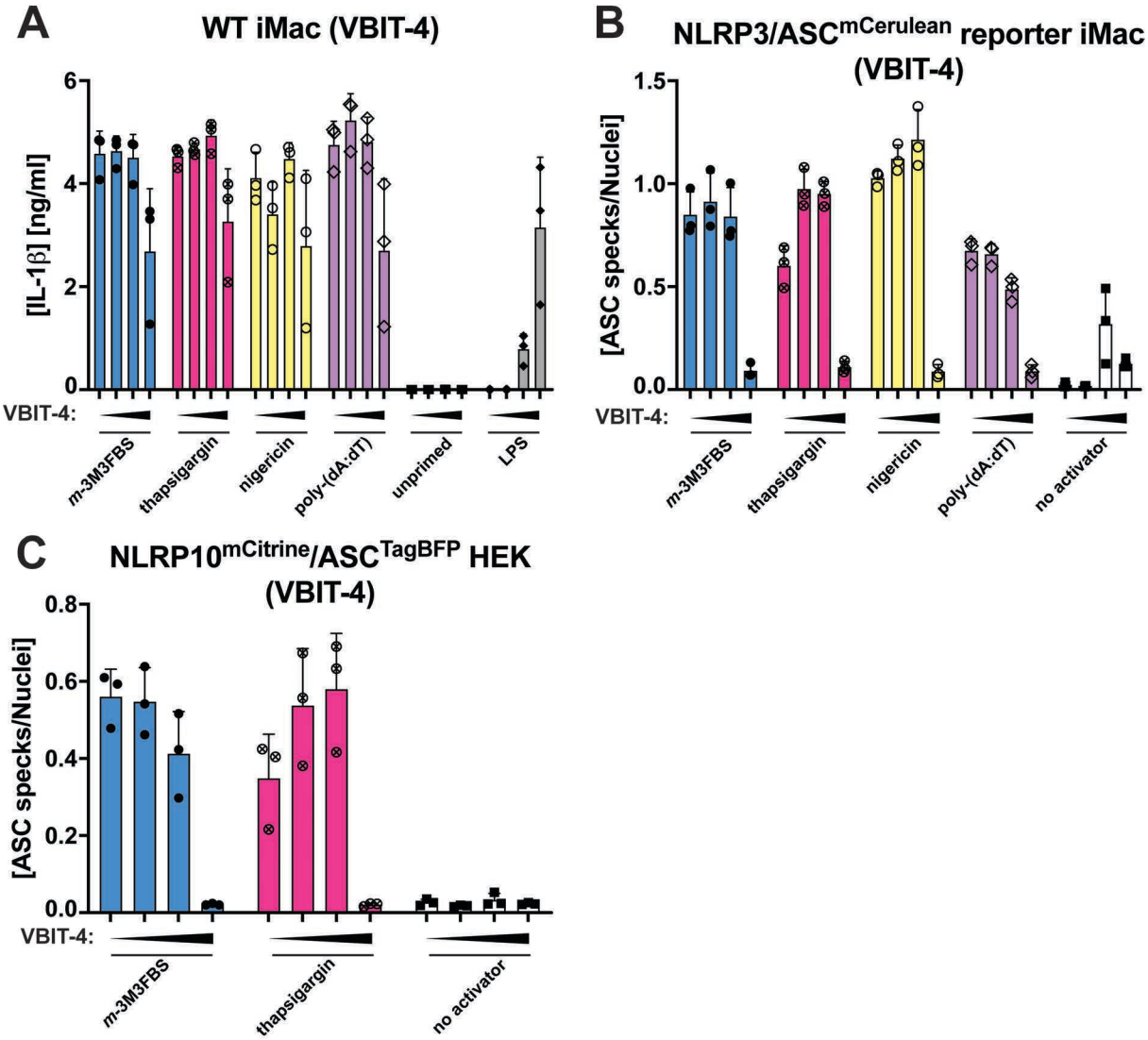

Figure 9.18. Influence of the VDAC blocker VBIT-4 on the inflammasome responses to *m*-3M3FBS, thapsigargin, nigericin, and poly-(dA:dT)

A-C: LPS-primed (200 ng/mL, 2 h) WT iMac cells (A), NLRP3/ASC^{mCerulean} reporter iMac cells (B), and NLRP10^{mCitrine}/ASC^{TagBFP} HEK cells (C) were treated for 10 min with VBIT-4 (0, 10, 25, or 50 μM) and then subjected to the inflammasome activators *m*-3M3FBS (85 μM), thapsigargin (20 μM), nigericin (10 μM) or poly-(dA:dT) (2 μg/mL complexed with 5 μL Lipofectamine 2000) in an extracellular medium consisting of (in mM) 123 NaCl, 5 KCl, 2 $MgCl_2$, 1 $CaCl_2$, 10 glucose, 10 HEPES, pH 7.4. The LPS (A) and unprimed (A-C) controls were subjected to medium alone. Immediately after addition of inflammasome activators, the plates were centrifuged at 340 × g for 5 min (RT). After 30 min (C) or 60 min (A, B), the supernatants were collected and IL-1β concentrations were measured by HTRF (A), or the cells were fixed with 4% formaldehyde, counterstained with the nuclear dye DRAQ5 (5 μM) and imaged using a widefield fluorescence microscope (B, C).

The results are plotted as means from 3 independent experiments performed in technical duplicate. Error bars represent SD. Individual data points represent means of the technical duplicate values from each of the independent experiments.

On the level of ASC speck formation, only the highest concentration (50 μM) of VBIT-4 appeared to inhibit the inflammasome responses, and it appeared to non-selectively target all tested inflammasome activations (Figure 9.18 B, C). This inhibitory effect was not observed on the level of IL-1β secretion (Figure 9.18 A). Instead, surprisingly, the intermediate and high concentrations (25-50 μM) of VBIT-4 alone were able to elicit IL-1β release from LPS-primed WT iMac cells (Figure 9.18 A). The observed IL-1β secretion was reflected by ASC speck formation in NLRP3/ASC^{mCerulean} reporter iMac cells (Figure 9.18 B), but not in NLRP10^{mCitrine}/ASC^{TagBFP} HEK cells (Figure 9.18 C). These observations indicate that VDAC is likely not involved in the NLRP10/AIM2 activations, but the VDAC inhibitor VBIT-4 may itself be an inflammasome trigger.

Finally, I examined whether the VBIT-4-induced inflammasome activation in macrophages was dependent on NLRP3 and on caspase-1 (Figure 9.19). In LPS-primed WT iMac cells, VBIT-4 induced IL-1β secretion in a manner inhibitable by the caspase-1 inhibitor VX-765, but not by the NLRP3 inhibitor CRID3 (Figure 9.19 A), indicating that the VDAC blocker triggers an NLRP3-independent inflammasome response. Consistent with the results presented in Figure 9.18 B, VBIT-4 elicited ASC speck formation in NLRP3/ASCmCerulean reporter iMac cells, but this response was markedly lower than the response to nigericin (Figure 9.19 B). The VBIT-4-induced ASC speck formation was not inhibited by CRID3, consistent with the IL-1β result (Figure 9.19 A). As expected, VX-765 did not inhibit the ASC specking responses to either of the tested stimuli. Collectively, these observations suggest that VBIT-4 may be a novel inflammasome activator. However, I did not pursue this topic, as there were no indications that VBIT-4 could activate NLRP10 (Figure 9.18 C) or that the VDAC opening could link the *m*-3M3FBS/thapsigargin stimulations to mitochondrial damage.

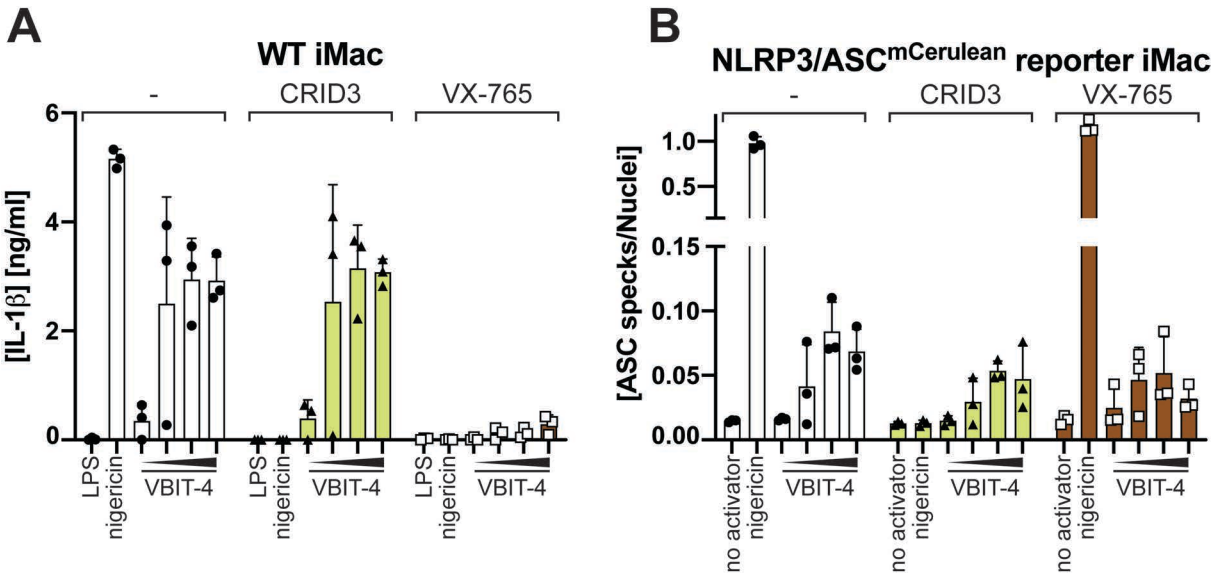

Figure 9.19. Sensitivity of the VBIT-4-induced IL-1β secretion and ASC speck formation to the NLRP3 inhibitor CRID3 and the caspase-1 inhibitor VX-765
A-B: LPS-primed (200 ng/mL, 2 h) WT iMac cells (A) and NLRP3/ASC^{mCerulean} reporter iMac cells (B) were shifted to an extracellular medium consisting of (in mM) 123 NaCl, 5 KCl, 2 $MgCl_2$, 1 $CaCl_2$, 10 glucose, 10 HEPES pH 7.4 and, where indicated, pre-treated (10 min) with the NLRP3 inhibitor CRID3 (5 μM) or the caspase-1 inhibitor VX-765 (40 μM). Then, the cells were stimulated with the inflammasome activators VBIT-4 (20, 30, 40, or 50 μM) or nigericin (10 μM). The LPS (A) and untreated (no activator; B) controls were subjected to medium alone. Immediately after addition of inflammasome activators, the plates were centrifuged at 340 × g for 5 min (RT). After 60 min, the supernatants were collected and IL-1β concentrations were measured by HTRF (A), or the cells were fixed with 4% formaldehyde, counterstained with the nuclear dye DRAQ5 (5 μM) and imaged using a widefield fluorescence microscope (B).
The results are plotted as means from 3 independent experiments performed in technical duplicate. Error bars represent SD. Individual data points represent means of the technical duplicate values from each of the independent experiments.

9.5. No evidence that the inhibition of the mitochondrial protein import could selectively activate the AIM2/NLRP10 inflammasomes

The mitochondrial protein import pathways can be seen as a way of communication between the cell and the mitochondria. The protein import route consists of translocases resident in the OMM and the IMM, and a number of accessory proteins. The polypeptide chains cross the mitochondrial membranes in an unfolded state, assisted by chaperones. Though relatively well described, this system is not easily targetable.

Here, I hypothesized that blocking the mitochondrial protein import might lead to accumulation of mitochondrial proteins in the cytosol and possibly result in NLRP10 activation. (The AIM2 inflammasome assembly in this scenario is less likely because the mitochondrial nucleoids undergo replication inside of the organelles and do not have to be imported.) To test this hypothesis, I used two of the few commercially available

inhibitors of the mitochondrial protein import: MitoBloCK-6 (Dabir et al., 2013) and MitoBloCK-12 (Miyata et al., 2014).

First, I tested whether MitoBloCK-6 or MitoBloCK-12 could activate the inflammasome in LPS-primed WT iMac cells (Figure 9.20), NLRP3/ASC^{mCerulean} reporter iMac cells (Figure 9.21), and NLRP10^{mCitrine}/ASC^{TagBFP} HEK cells (Figure 9.22) over the course of 1-h and 6-h stimulations. As it is conceivable that the mitochondrial proteins accumulating in the cytosol could be targeted for proteasomal degradation (Taylor and Rutter, 2011), I performed the MitoBloCK-6/12 challenges in the presence or absence of the proteasome inhibitor bortezomib. The treatment with *m*-3M3FBS served as a positive control (Figures 9.20-9.22).

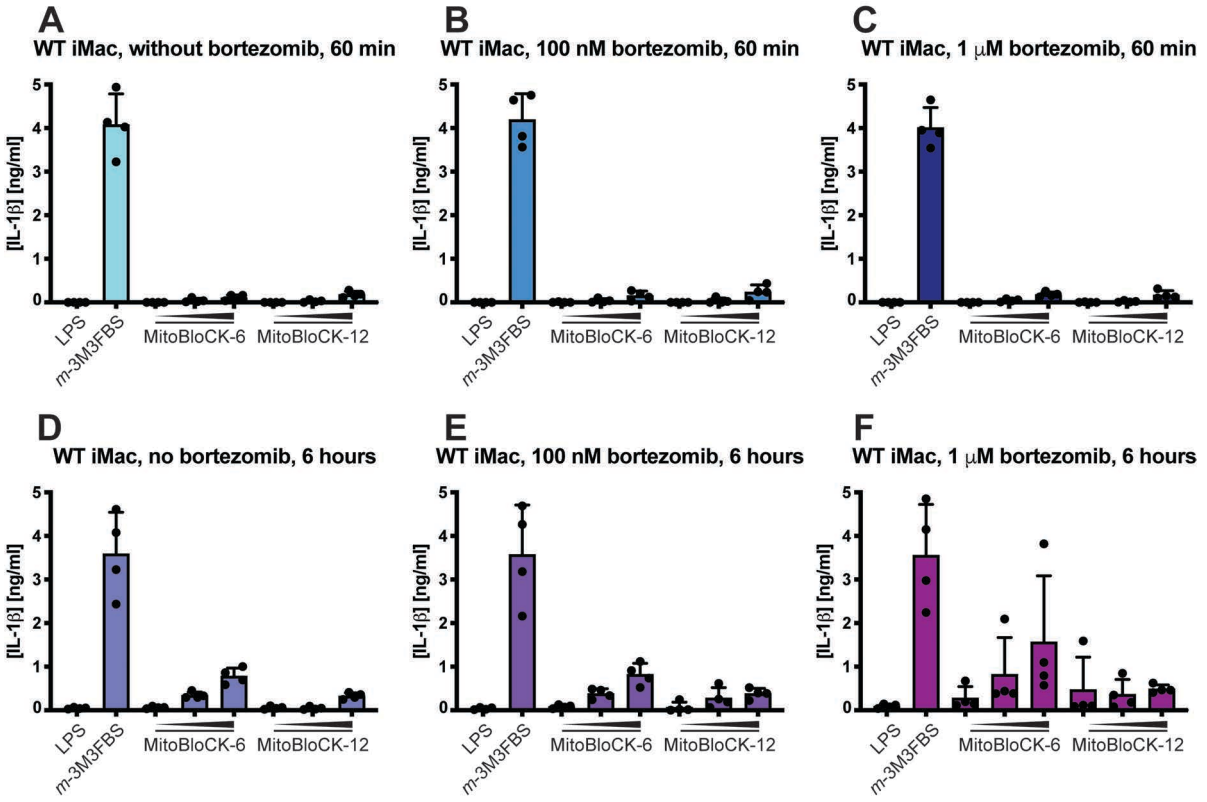

Figure 9.20. IL-1β secretion from LPS-primed WT iMac cells stimulated with the mitochondrial protein import inhibitors MitoBloCK-6 and MitoBloCK-12 in the presence or absence of the proteasome inhibitor bortezomib

A-F: LPS-primed (200 ng/mL, 2 h) WT iMac cells were stimulated with MitoBloCK-6 (10, 50, or 100 μM), MitoBloCK-12 (10, 50, or 100 μM), or *m*-3M3FBS (85 μM) for 60 min (A-C) or 6 h (D-F) in the absence (A, D) or presence of 100 nM (B, E) or 1 μM (C, F) bortezomib. The 60-min stimulations were performed in an extracellular medium consisting of (in mM) 123 NaCl, 5 KCl, 2 $MgCl_2$, 1 $CaCl_2$, 10 glucose, 10 HEPES pH 7.4 (A-C). The 6-h stimulations were performed in DMEM supplemented with 2.5% FBS (D-F; under these conditions LPS was kept in the medium for the duration of the entire experiment). The LPS controls were subjected to media alone. Immediately after administration of the stimuli, the plates were centrifuged at 340 × g for 5 min (RT). After 60 min (A-C) or 6 h (D-F), the supernatants were collected and IL-1β concentrations were measured by HTRF.

The results are plotted as means from 4 independent experiments performed in technical quadruplicate. Error bars represent SD. Individual data points represent means of the technical quadruplicate values from each of the independent experiments.

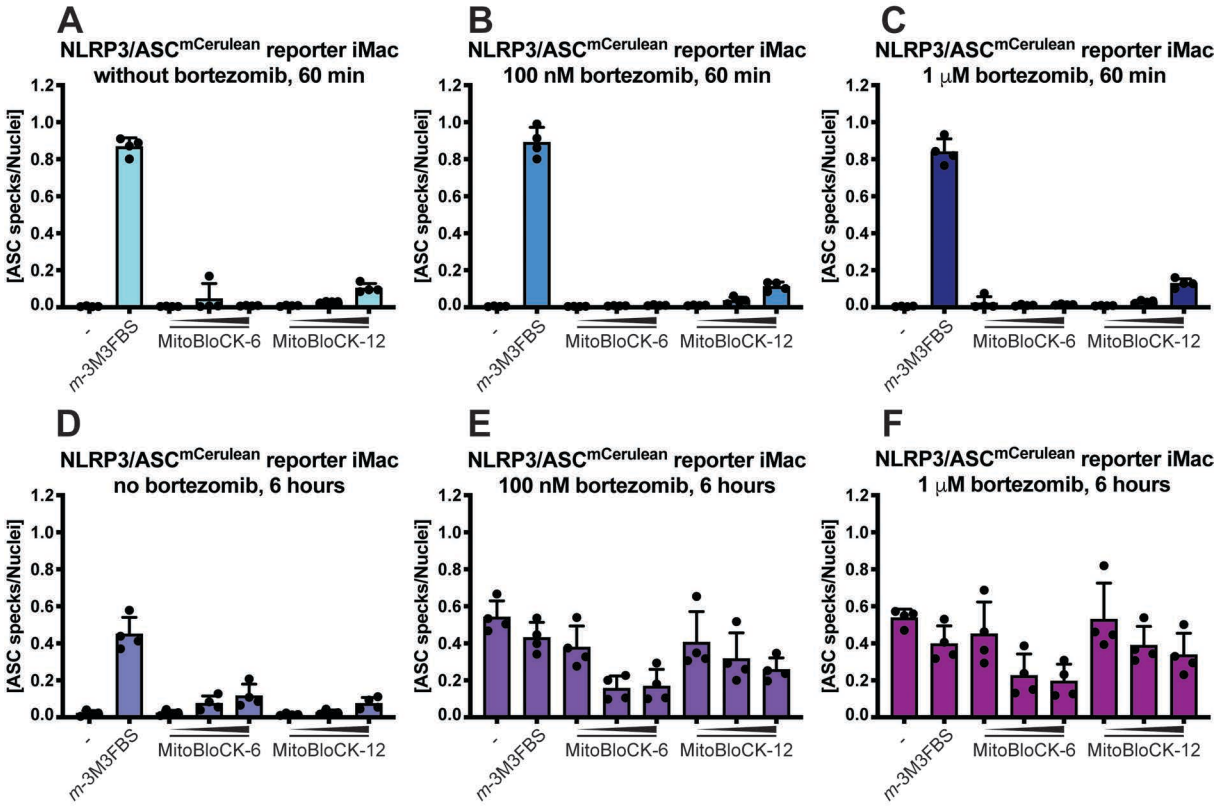

Figure 9.21. ASC specking levels in NLRP3/ASC^{mCerulean} reporter iMac cells stimulated with the mitochondrial protein import inhibitors MitoBloCK-6 and MitoBloCK-12 in the presence or absence of the proteasome inhibitor bortezomib

A-F: NLRP3/ASC^{mCerulean} reporter iMac cells were stimulated with MitoBloCK-6 (10, 50, or 100 μM), MitoBloCK-12 (10, 50, or 100 μM), or *m*-3M3FBS (85 μM) for 60 min (A-C) or 6 h (D-F) in the absence (A, D) or presence of 100 nM (B, E) or 1 μM (C, F) bortezomib. The 60-min stimulations were performed in an extracellular medium consisting of (in mM) 123 NaCl, 5 KCl, 2 $MgCl_2$, 1 $CaCl_2$, 10 glucose, 10 HEPES pH 7.4 (A-C). The 6-h stimulations were performed in DMEM supplemented with 2.5% FBS (D-F). The untreated (-) controls were subjected to media alone. Immediately after administration of the stimuli, the plates were centrifuged at 340 × g for 5 min (RT). After 60 min (A-C) or 6 h (D-F), the cells were fixed with 4% formaldehyde, counterstained with the nuclear dye DRAQ5 (5 μM) and imaged using a widefield fluorescence microscope.

The results are plotted as means from 4 independent experiments performed in technical quadruplicate. Error bars represent SD. Individual data points represent means of the technical quadruplicate values from each of the independent experiments.

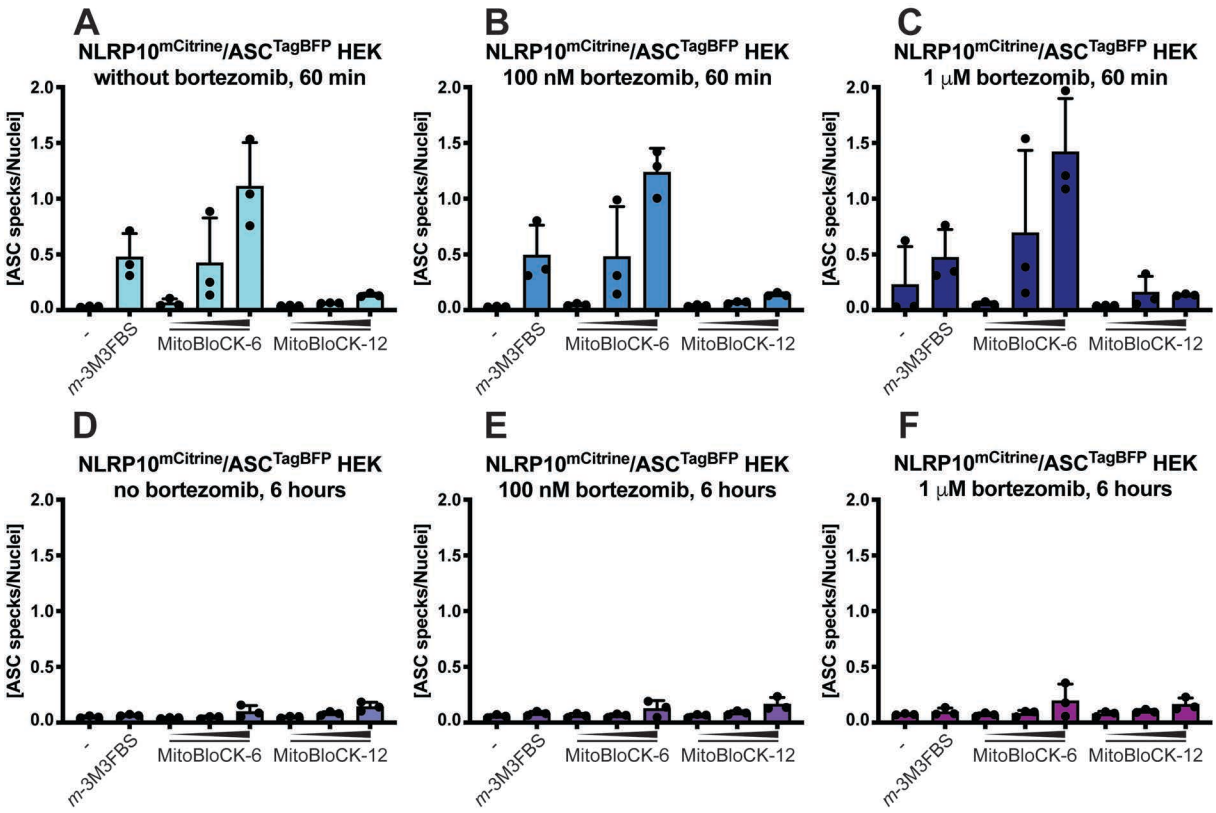

Figure 9.22. ASC specking levels in NLRP10^{mCitrine}/ASC^{TagBFP} HEK cells stimulated with the mitochondrial protein import inhibitors MitoBloCK-6 and MitoBloCK-12 in the presence or absence of the proteasome inhibitor bortezomib

A-F: NLRP10^{mCitrine}/ASC^{TagBFP} HEK cells were stimulated with MitoBloCK-6 (10, 50, or 100 μM), MitoBloCK-12 (10, 50, or 100 μM), or *m*-3M3FBS (85 μM) for 60 min (A-C) or 6 h (D-F) in the absence (A, D) or presence of 100 nM (B, E) or 1 μM (C, F) bortezomib. The 60-min stimulations were performed in an extracellular medium consisting of (in mM) 123 NaCl, 5 KCl, 2 $MgCl_2$, 1 $CaCl_2$, 10 glucose, 10 HEPES pH 7.4 (A-C). The 6-h stimulations were performed in DMEM supplemented with 2.5% FBS (D-F). The untreated (-) controls were subjected to media alone. Immediately after administration of the stimuli, the plates were centrifuged at 340 × g for 5 min (RT). After 60 min (A-C) or 6 h (D-F), the cells were fixed with 4% formaldehyde, counterstained with the nuclear dye DRAQ5 (5 μM) and imaged using a widefield fluorescence microscope.

The results are plotted as means from 3 independent experiments performed in technical quadruplicate. Error bars represent SD. Individual data points represent means of the technical quadruplicate values from each of the independent experiments.

In LPS-primed WT iMac cells, high concentrations (50-100 μM) of MitoBloCK-6/12 produced a substantial release of IL-1β after 6 h (Figure 9.20 D-F), but not at the 1-h time point (Figure 9.20 A-C), regardless of the presence of bortezomib. Treatments with both MitoBloCK-6 and -12 resulted in modest but detectable ASC specking responses in NLRP3/ASC^{mCerulean} reporter iMac cells at the 6-h time point (Figure 9.21 D), but not at the 1-h time point (Figure 9.21 A-C). Unexpectedly, the 6-h treatment with bortezomib resulted in a very high background ASC specking level in NLPR3/ASC^{mCerulean} reporter iMac cells (Figure 9.21 E, F). Consequently, the interpretation of the ASC specking assay results obtained at this time point in the presence of bortezomib is impossible. Of note,

the bortezomib-elicited ASC speck formation (Figure 9.21 E, F) was not reflected by IL-1β secretion (Figure 9.20 E, F), suggesting that the observed ASC specks may not represent active inflammasomes.

In NLRP10^{mCitrine}/ASC^{TagBFP} HEK cells the effects of MitoBloCK-6/-12 were less clear. At the 1-h time point, MitoBloCK-6, but not -12, produced a strong ASC specking response that was independent of the bortezomib co-administration (Figure 9.22 A-C). However, at the 6-h time point, this ASC specking response was no longer observed (Figure 9.22 D-F)[1].

I proceeded to determine whether the ASC speck formation observed in MitoBloCK-6-stimulated NLRP10^{mCitrine}/ASC^{TagBFP} HEK cells could be attributed to the NLRP10 overexpression, and whether a non-redundant sensor activated by MitoBloCK-6/12 in macrophages could be identified. To this end, I performed 24-h stimulations with MitoBloCK-6/-12 in the presence or absence of bortezomib in LPS-primed WT iMac cells (with or without the NLRP3 inhibitor CRID3), NLRP3-deficient (*Nlrp3*$^{-/-}$) iMac cells, and AIM2-deficient (*Aim2*^{CRISPR}) iMac cells transduced with the empty vector, human AIM2, or human NLRP10. I evaluated the levels of inflammasome responses by measuring the concentrations of secreted IL-1β (Figure 9.23).

[1] Importantly, at the 6-h time point, the *m*-3M3FBS-induced ASC speck formation was also not observed. This can be explained by the use of DMEM supplemented with 10% FBS for the 6-h stimulation. The *m*-3M3FBS-driven NLRP10 activation is suppressed under these conditions (Supplementary Methods Figure SM1 A, B).

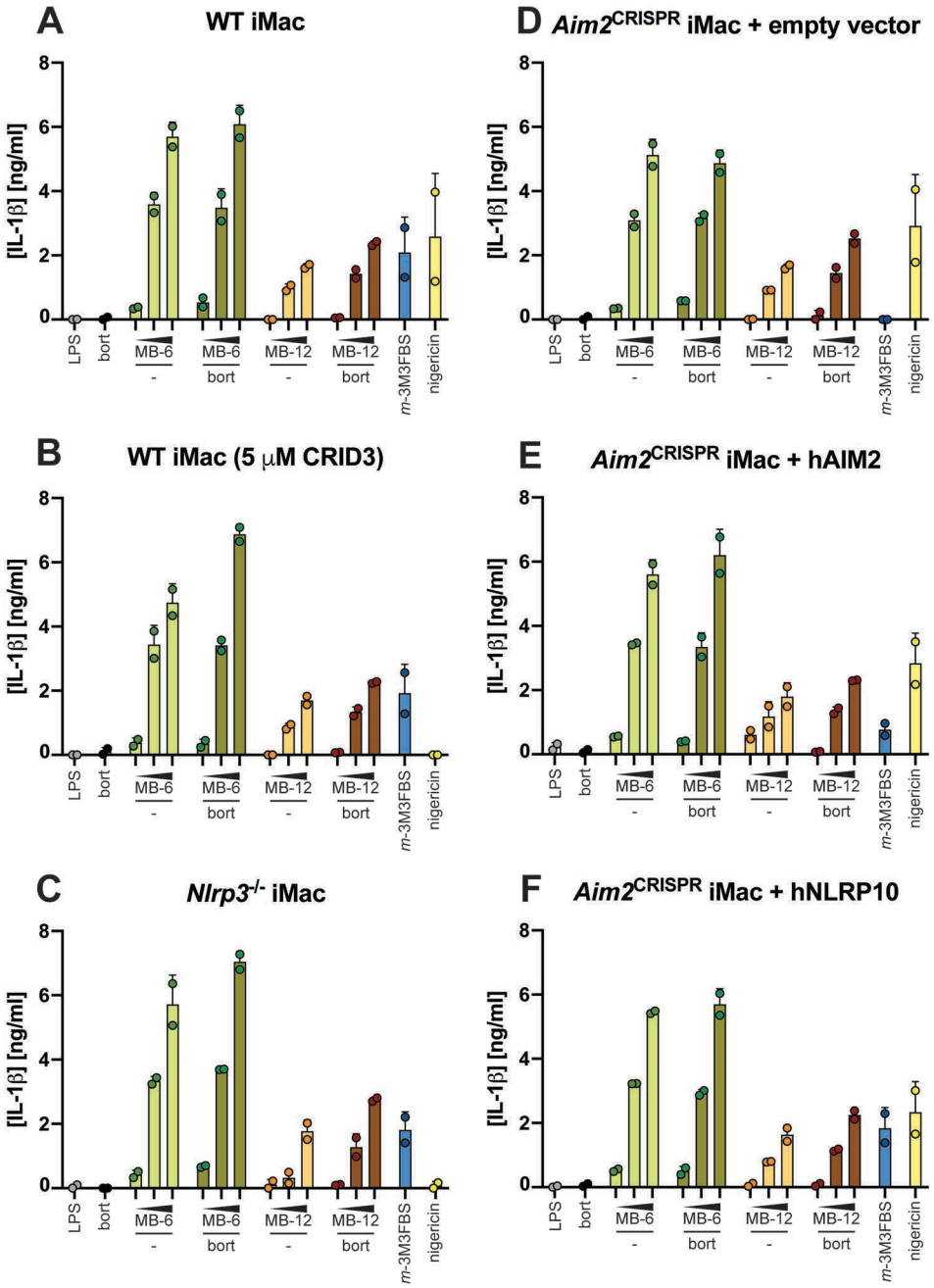

Figure 9.23. IL-1β secretion from NLRP3-/AIM2-proficient, NLRP3-deficient, and AIM2-deficient macrophages transduced with human AIM2, human NLRP10, or the empty vector, and stimulated with the mitochondrial protein import inhibitors MitoBloCK-6 and -12 in the presence or absence of the proteasome inhibitor bortezomib

A-F: LPS-primed (100 ng/mL, 1 h; LPS was kept in the media for the duration of the entire experiment) WT iMac cells in the absence (A) or presence of the NLRP3 inhibitor CRID3 (5 μM; B), NLRP3-deficient (*Nlrp3*$^{-/-}$) iMac cells (C), and *Aim2*^{CRISPR} iMac cells stably transduced with the empty vector (D), WT human (h) AIM2 (E), or WT hNLRP10 (F) were stimulated with MitoBloCK-6 (MB-6; 10, 50, or 100 μM) or MitoBloCK-12 (MB-12; 10, 50, or 100 μM) in presence or absence (-) of 500 nM bortezomib (bort). The following control treatments were included: LPS alone, bortezomib (500 nM) alone, *m*-3M3FBS (85 μM), and nigericin (10 μM). With the exception of the *m*-3M3FBS control (which was performed after shifting the cells to an extracellular medium consisting of [in mM] 123 NaCl, 5 KCl, 2 $MgCl_2$, 1 $CaCl_2$, 10 glucose, 10 HEPES pH 7.4), all stimulations were performed in DMEM supplemented with 5% FBS. Immediately after administration of the stimuli, the plates were centrifuged at 340 × g for 5 min (RT). After 24 h, the supernatants were collected and IL-1β concentrations were measured by HTRF.

The results are plotted as means from 2 independent experiments performed in technical triplicate. Error bars represent SD. Individual data points represent means of the technical triplicate values from each of the independent experiments.

I observed high levels of IL-1β secretion after MitoBloCK-6 treatment and intermediate IL-1β levels after MitoBloCK-12 treatment regardless of the cells' genotype, the presence or absence of bortezomib, and the presence or absence of CRID3. Therefore, the IL-1β secretion from MitoBloCK-6-/12-stimulated cells could not be attributed to any of the inflammasome sensor proteins investigated in this thesis (AIM2, NLRP3, and NLRP10). Instead, there might exist redundant mechanisms for sensing of the changes inflicted by MitoBloCK-6 and MitoBloCK-12.

Finally, to establish whether the MitoBloCK-6-/-12-induced ASC speck formation could be attributed to NLRP10, I performed 24-h stimulations with MitoBloCK-6/12, in the presence or absence of bortezomib, in NLRP10^{mCherry}/ASC^{mCerulean} HEK cells, NLRP10^{mCitrine}/ASC^{TagBFP} HEK cells, ASC^{mCerulean} HEK cells, and NLRP3/ASC^{mCerulean} reporter iMac cells (Figure 9.24).

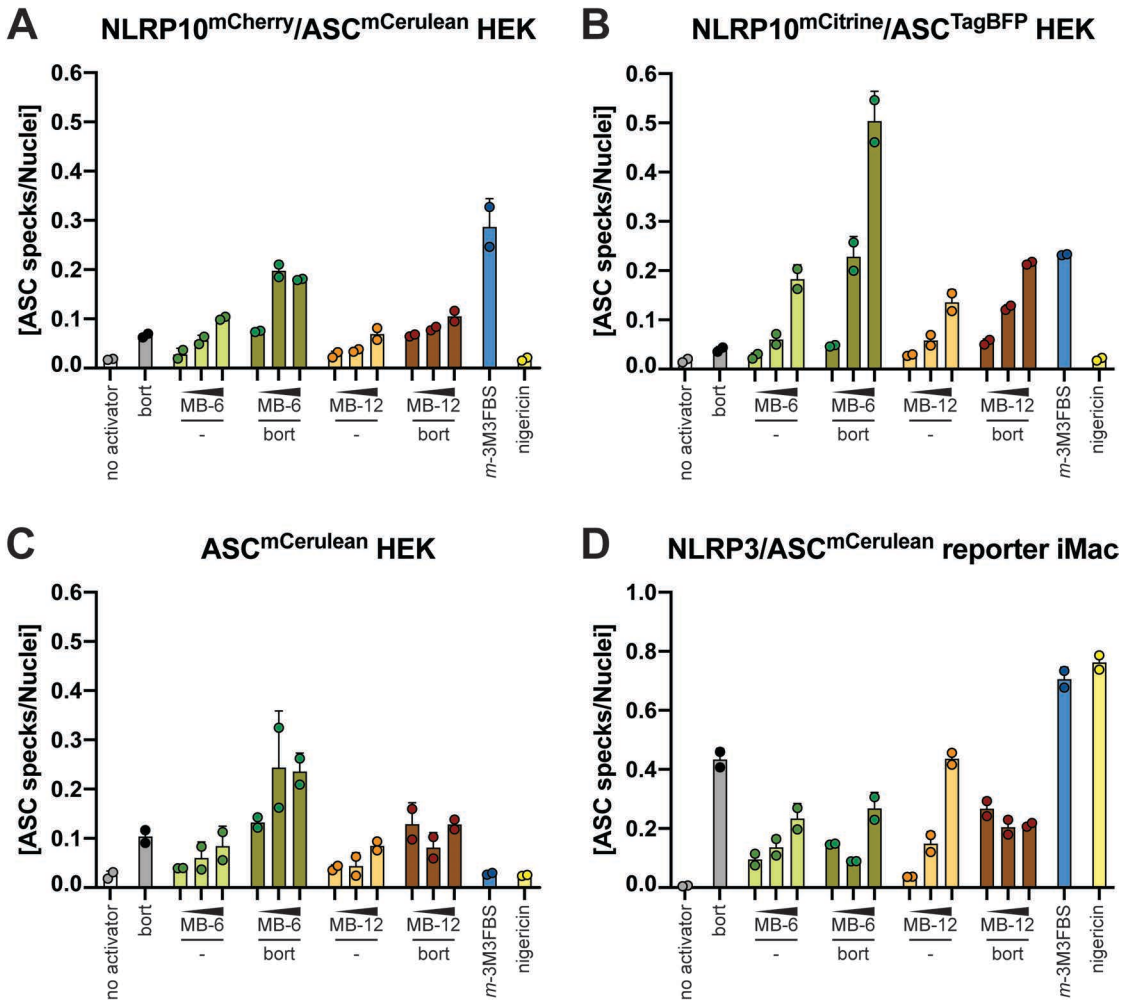

Figure 9.24. ASC specking levels in NLRP10^{mCherry}/ASC^{mCerulean} HEK cells, NLRP10^{mCitrine}/ASC^{TagBFP} HEK cells, ASC^{mCerulean} HEK cells, and NLRP3/ASC^{mCerulean} reporter iMac cells treated with the mitochondrial protein import inhibitors MitoBloCK-6 and MitoBloCK-12 in the presence or absence of the proteasome inhibitor bortezomib

◂ **A-D:** NLRP10^{mCherry}/ASC^{mCerulean} HEK cells (A), NLRP10^{mCitrine}/ASC^{TagBFP} HEK cells (B), ASC^{mCerulean} HEK cells (C), and NLRP3/ASC^{mCerulean} reporter iMac cells (D) were stimulated with MitoBloCK-6 (MB-6; 10, 50, or 100 μM) or MitoBloCK-12 (MB-12; 10, 50, or 100 μM) in presence or absence (-) of 500 nM bortezomib (bort). The following control treatments were included: LPS alone, bortezomib (500 nM) alone, *m*-3M3FBS (85 μM), and nigericin (10 μM). With the exception of the *m*-3M3FBS control (which was performed after shifting the cells to an extracellular medium consisting of [in mM] 123 NaCl, 5 KCl, 2 $MgCl_2$, 1 $CaCl_2$, 10 glucose, 10 HEPES pH 7.4), all stimulations were performed in DMEM supplemented with 5% FBS. Immediately after administration of the stimuli, the plates were centrifuged at 340 × g for 5 min (RT). After 24 h, the cells were fixed with 4% formaldehyde, counterstained with the nuclear dye DRAQ5 (5 μM) and imaged using a widefield fluorescence microscope.
The results are plotted as means from 2 independent experiments performed in technical triplicate. Error bars represent SD. Individual data points represent means of the technical triplicate values from each of the independent experiments.

In ASC^{mCerulean} HEK cells (Figure 9.24 C), treatments with MitoBloCK-6/-12 with or without bortezomib led to ASC specking responses similarly strong to those observed in NLRP10^{mCherry}/ASC^{mCerulean} HEK cells (Figure 9.24 A), indicating that the MitoBloCK-6-/-12-induced ASC speck formation cannot be attributed to the NLRP10 overexpression. The results obtained at the 24-h time point in NLRP10^{mCitrine}/ASC^{TagBFP} HEK cells (Figure 9.24 B) were consistent with the observations from NLRP10^{mCherry}/ASC^{mCerulean} HEK cells (Figure 9.24 A) and in ASC^{mCerulean} HEK cells (Figure 9.24 C). In NLRP3/ASC^{mCerulean} reporter iMac cells, bortezomib alone as well as the highest (100 μM) concentrations of the MitoBloCK inhibitors produced high levels of ASC speck formation (Figure 9.24 D).

Collectively, the mitochondrial protein import inhibitors appear to have the ability to trigger ASC speck formation and IL-1β secretion, but I found no evidence to link these responses to activation of the AIM2, NLRP3, or NLRP10 inflammasomes.

9.6. No evidence of the involvement of the mitochondrial permeability transition pore in the AIM2 and NLRP10 responses to *m*-3M3FBS and thapsigargin

The final process whose potential involvement in the *m*-3M3FBS-/thapsigargin-induced inflammasome activation I will address in my thesis is the opening of mPTP. The mPTP opening, or the mPT, is an incompletely defined pathway that begins with the inner mitochondrial membrane permeabilization to molecules and ions smaller than 1.5 kDa and may result in mitochondrial swelling and rupture (Kwong and Molkentin, 2015). In inflammasome studies, the mPT has been proposed to be involved in NLRP3 activation (Iyer et al., 2013; Nakahira et al., 2010), but this attribution has been questioned (Allam et al., 2014).

Investigating mPT is not easy. mPTP is likely a protein-lined channel in the IMM, possibly also bridging to the OMM, but there is no consensus as to which genes encode mPTP components. Several proteins have been proposed to 'moonlight' as mPTP; most prominently VDAC (Crompton et al., 1998; Szabo and Zoratti, 1993; Szabo et al., 1993; Zheng et al., 2003), the mitochondrial phosphate carrier (Kwong et al., 2014; Leung et al., 2008), ATP synthase (Alavian et al., 2014a; Bonora et al., 2014; Carraro et al., 2014; Giorgio et al., 2013; Mnatsakanyan et al., 2019), Slc25a4 (adenine nucleotide translocase) (Bauer et al., 1999; Beutner et al., 1999; Halestrap and Brenner, 2003a; Karch et al., 2019; Marzo et al., 1998), and TSPO (peripheral benzodiazepine receptor) (Azarashvili et al., 2007; Berson et al., 2001; Li et al., 2007; Pastorino et al., 1994). In addition, mitochondrial cyclophilin (cyclophilin F encoded by the gene named *PPIF*)[2] is proposed to act as an essential soluble proteinaceous component of mPTP (Azzolin et al., 2010; Baines et al., 2005; Basso et al., 2005; Matas et al., 2009; Nakagawa et al., 2005; Schinzel et al., 2005). Multiple stimuli for the mPTP opening are proposed, including Ca^{2+} fluxes, mtROS, and inorganic phosphate ions (Kwong and Molkentin, 2015).

My results provide arguments both for and against the involvement of mPTP in the AIM2/NLRP10 activation. The observation that the *m*-3M3FBS-/thapsigargin-induced inflammasome responses are not sensitive to perturbations of Ca^{2+} signaling (Section 6.11) hints at the lack of mPTP involvement. However, the fact that the thapsigargin-induced AIM2/NLRP10 activation is completely abolished by CsA (Section 6.15), an mPTP inhibitor (Baines et al., 2005; Basso et al., 2005; Nakagawa et al., 2005; Schinzel et al., 2005), suggests that the possible role of mPTP should not be excluded. To probe this issue in greater detail, I examined to which extent the AIM2/NLRP10 responses to *m*-3M3FBS and thapsigargin conform to the pharmacological characteristics of mPTP reported in the literature. To this end, I tested whether the AIM2/NLRP10 activations could be affected by $BaCl_2$ (Figure 9.25 A-C), $GdCl_3$ (Figure 9.25 D-F), oligomycin A (Figure 9.26 A-C ; all three treatments proposed to inhibit mPTP by Mnatsakanyan et al. (2019)), rotenone (Figure 9.26 D-G; proposed to inhibit mPTP by Chauvin et al. (2001) and Rekuviene et al. (2017)), two mitochondrial uncouplers (Figure 9.27; CCCP was

[2] To add to the confusion, mitochondrial cyclophilin, correctly termed cyclophilin F and encoded by the gene named *PPIF* (for peptidyl-prolyl isomerase F), was initially named cyclophilin D. However, the *real* cyclophilin D (encoded by the gene named *PPID*, for peptidyl-prolyl isomerase D) is a cytosolic protein and it is not involved in mPT (Gutiérrez-Aguilar and Baines, 2015). Studies on the role of cyclophilin D in mitochondrial damage frequently do not specify whether PPIF or PPID was experimentally targeted.

proposed to activate mPTP by Lim et al. (2001), Yang et al. (2001), and Minamikawa et al. (1999), while FCCP was implicated in the same process in the studies by Kowaltowski et al. (1996) and Gordan et al. (2016), although dissenting opinions were also published, for example by Petronilli et al. (2001)), the adenine nucleotide translocator 1 (ANT, or Slc25a4) inhibitors bongkrekic acid (Figure 9.28 A-C; reported to inhibit the mPTP opening) and carboxyatractyloside (Figure 9.28 D-F; reported to trigger the mPT, both reviewed in Halestrap and Brenner (2003b)), and the mitoprotective compounds dexpramipexole dihydrochloride (Figure 9.29 A-D; suggested to inhibit mPTP by Alavian et al. (2012; 2014b)), ER000444793 (Figure 9.29 E-H; reported to inhibit mPTP by Briston et al. (2016)), and TRO 19622 (Figure 9.30; reported to inhibit mPTP by Bordet et al. (2010)). For all experiments, LPS-primed WT iMac cells, NLRP3/ASC^{mCerulean} reporter iMac cells, and NLRP10/ASC fluorescent reporter HEK cells were pre-treated (10 min) with the mPT-active agents, followed by stimulation with the inflammasome activators *m*-3M3FBS, thapsigargin, nigericin, and poly-(dA:dT). The degree of the inflammasome responses was assessed by measurement of secreted IL-1β concentrations or by imaging of ASC specks.

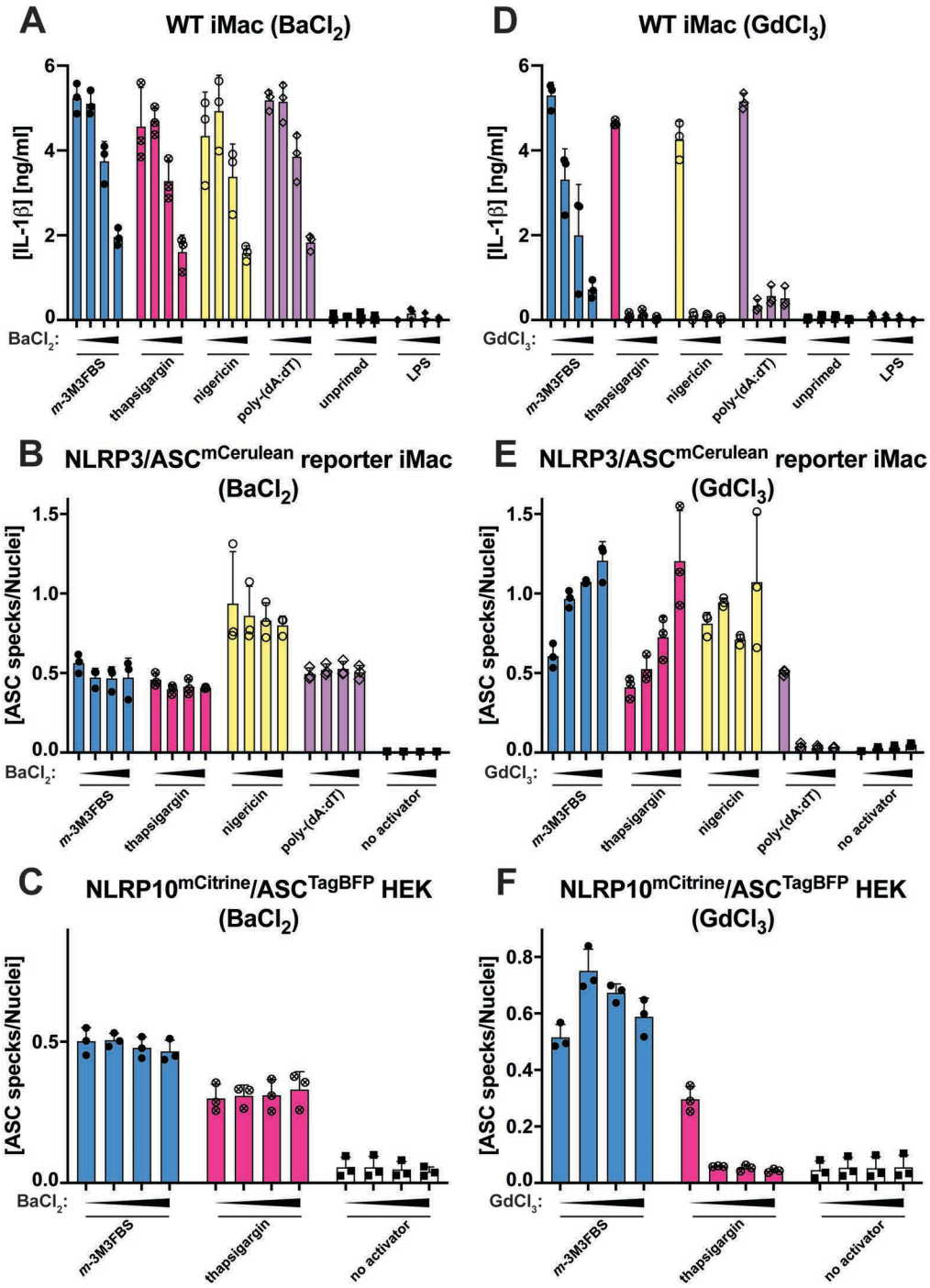

Figure 9.25. Influence of the reported mPTP blockers $BaCl_2$ and $GdCl_3$ on the inflammasome responses to *m*-3M3FBS, thapsigargin, nigericin, and poly-(dA:dT)

A-F: LPS-primed (200 ng/mL, 2 h) WT iMac cells (A, D), NLRP3/ASC^{mCerulean} reporter iMac cells (B, E), and NLRP10^{mCitrine}/ASC^{TagBFP} HEK cells (C, F) were treated for 10 min with $BaCl_2$ (0, 1, 2.5, or 5 mM; A-C) or $GdCl_3$ (0, 1, 2.5, or 5 mM; D-F) and then subjected to the inflammasome activators *m*-3M3FBS (85 μM), thapsigargin (20 μM), nigericin (10 μM) or poly-(dA:dT) (2 μg/mL complexed with 5 μL Lipofectamine 2000) in an extracellular medium consisting of (in mM) 123 NaCl, 5 KCl, 2 $MgCl_2$, 1 $CaCl_2$, 10 glucose, 10 HEPES, pH 7.4. The LPS (A, D) and unprimed (A-F) controls were subjected to medium alone. Immediately after addition of inflammasome activators, the plates were centrifuged at 340 × g for 5 min (RT). After 30 min (C, F) or 60 min (A, B, D, E), the supernatants were collected and IL-1β concentrations were measured by HTRF (A, D) or the cells were fixed with 4% formaldehyde, counterstained with the nuclear dye DRAQ5 (5 μM) and imaged using a widefield fluorescence microscope (B, C, E, F).

The results are plotted as means from 3 independent experiments performed in technical duplicate. Error bars represent SD. Individual data points represent means of the technical duplicate values from each of the independent experiments.

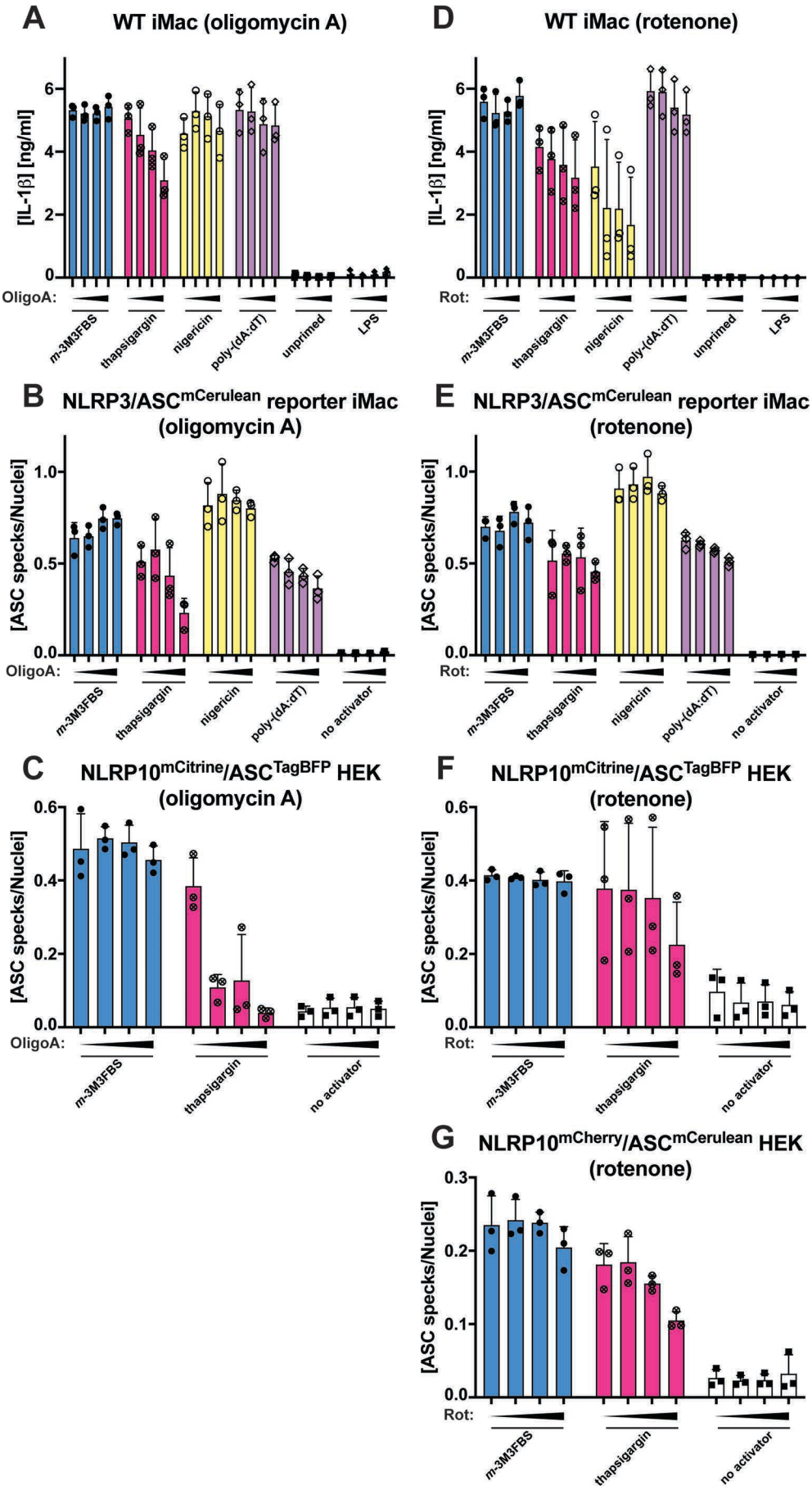

Figure 9.26. Influence of the reported mPTP inhibitors oligomycin A and rotenone on the inflammasome responses to *m*-3M3FBS, thapsigargin, nigericin, and poly-(dA:dT)

◂ **A-G:** LPS-primed (200 ng/mL, 2 h) WT iMac cells (A, D), NLRP3/ASC^{mCerulean} reporter iMac cells (B, E), NLRP10^{mCitrine}/ASC^{TagBFP} HEK cells (C, F), and NLRP10^{mCherry}/ASC^{mCerulean} HEK cells (G) were treated for 10 min with oligomycin A (OligoA; 0, 5, 10, or 20 μM; A-C) or rotenone (Rot; 0, 1, 5, or 10 μM; D-G) and then subjected to the inflammasome activators *m*-3M3FBS (85 μM), thapsigargin (20 μM), nigericin (10 μM) or poly-(dA:dT) (2 μg/mL complexed with 5 μL Lipofectamine 2000) in an extracellular medium consisting of (in mM) 123 NaCl, 5 KCl, 2 $MgCl_2$, 1 $CaCl_2$, 10 glucose, 10 HEPES, pH 7.4. The LPS (A, D) and unprimed (A-G) controls were subjected to medium alone. Immediately after addition of inflammasome activators, the plates were centrifuged at 340 × g for 5 min (RT). After 30 min (C, F, G) or 60 min (A, B, D, E), the supernatants were collected and IL-1β concentrations were measured by HTRF (A, D) or the cells were fixed with 4% formaldehyde, counterstained with the nuclear dye DRAQ5 (5 μM) and imaged using a widefield fluorescence microscope (B, C, E, F, G).
The results are plotted as means from 3 independent experiments performed in technical duplicate. Error bars represent SD. Individual data points represent means of the technical duplicate values from each of the independent experiments.

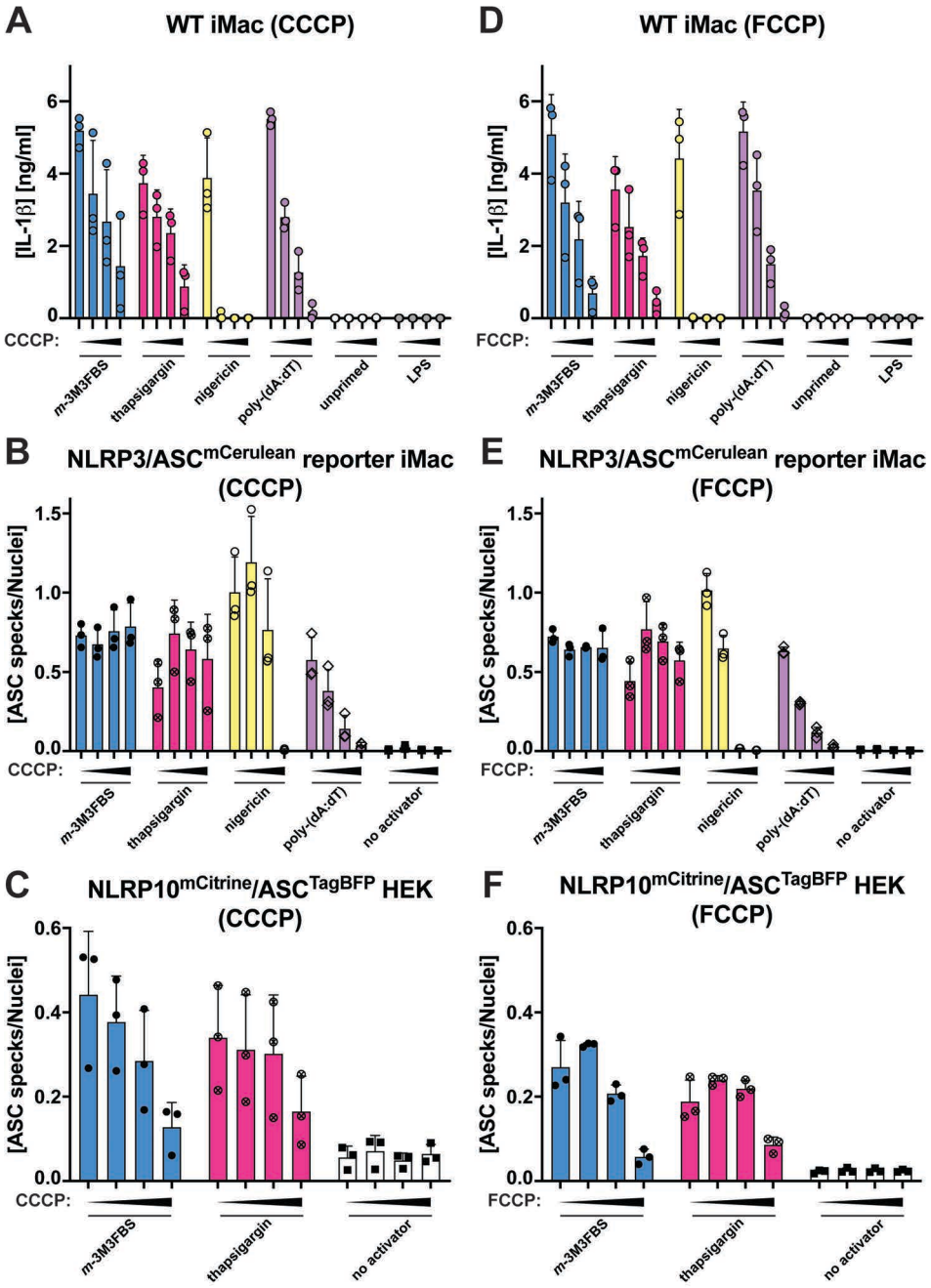

Figure 9.27. Influence of the mitochondrial uncouplers and reported mPTP agonists CCCP and FCCP on the inflammasome responses to *m*-3M3FBS, thapsigargin, nigericin, and poly-(dA:dT)

◂ **A-F:** LPS-primed (200 ng/mL, 2 h) WT iMac cells (A, D), NLRP3/ASC^{mCerulean} reporter iMac cells (B, E), and NLRP10^{mCitrine}/ASC^{TagBFP} HEK cells (C, F) were treated for 10 min with CCCP (0, 10, 25, or 50 μM; A-C) or FCCP (0, 10, 25, or 50 μM; D-F) and then subjected to the inflammasome activators *m*-3M3FBS (85 μM), thapsigargin (20 μM), nigericin (10 μM) or poly-(dA:dT) (2 μg/mL complexed with 5 μL Lipofectamine 2000) in an extracellular medium consisting of (in mM) 123 NaCl, 5 KCl, 2 $MgCl_2$, 1 $CaCl_2$, 10 glucose, 10 HEPES, pH 7.4. The LPS (A, D) and unprimed (A-F) controls were subjected to medium alone. Immediately after addition of inflammasome activators, the plates were centrifuged at 340 × g for 5 min (RT). After 30 min (C, F) or 60 min (A, B, D, E), the supernatants were collected and IL-1β concentrations were measured by HTRF (A, D) or the cells were fixed with 4% formaldehyde, counterstained with the nuclear dye DRAQ5 (5 μM) and imaged using a widefield fluorescence microscope (B, C, E, F).
The results are plotted as means from 3 independent experiments performed in technical duplicate. Error bars represent SD. Individual data points represent means of the technical duplicate values from each of the independent experiments.

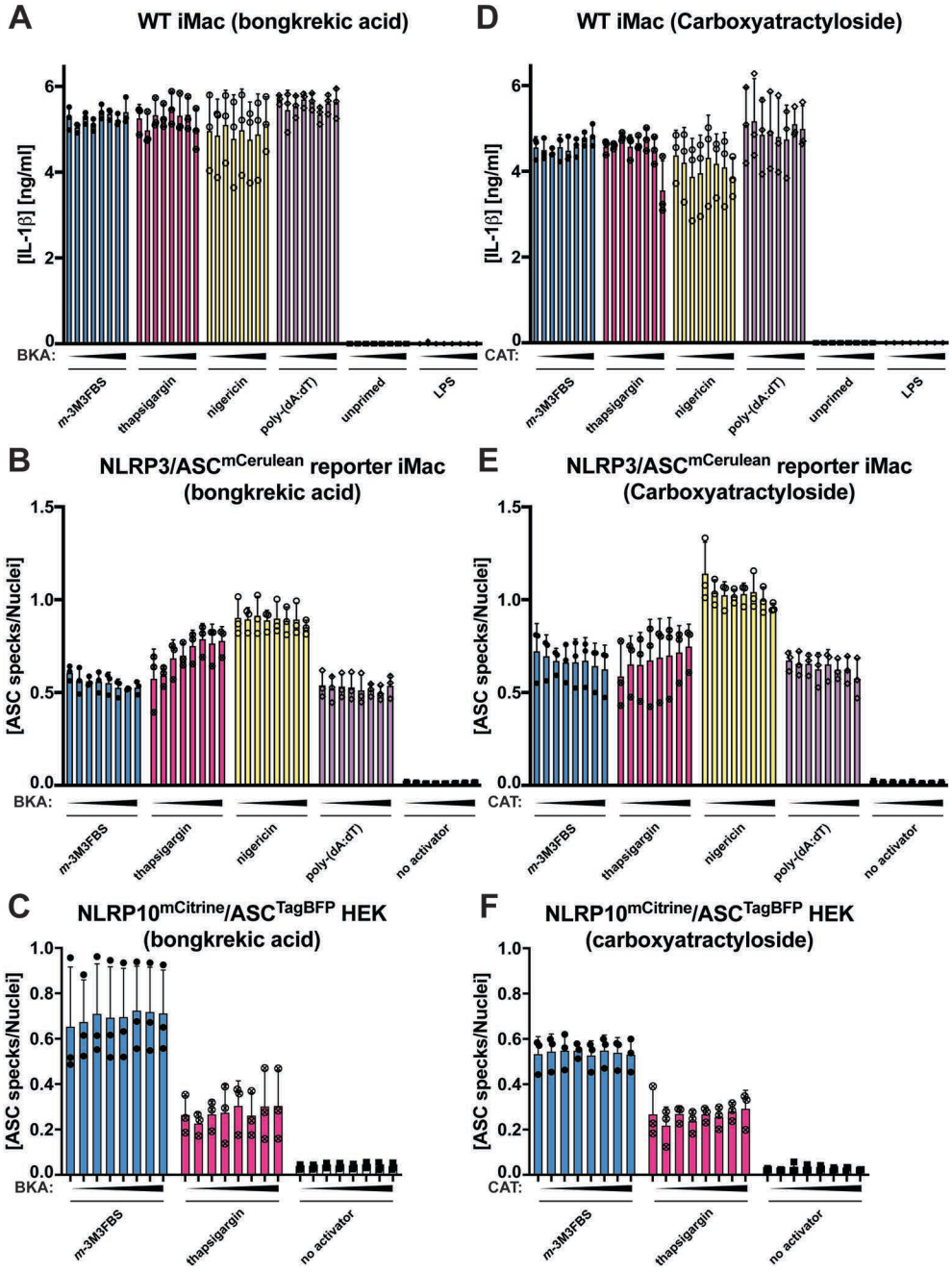

Figure 9.28. Influence of the adenine nucleotide translocase (Slc25a4) inhibitors bongkrekic acid and carboxyatractyloside on the inflammasome responses to *m*-3M3FBS, thapsigargin, nigericin, and poly-(dA:dT)

◂ **A-F:** LPS-primed (200 ng/mL, 2 h) WT iMac cells (A, D), NLRP3/ASC^{mCerulean} reporter iMac cells (B, E), and NLRP10^{mCitrine}/ASC^{TagBFP} HEK cells (C, F) were treated for 10 min with bongkrekic acid (BKA; 0, 1, 2.5, 5, 10, 15, 20, or 25 μM; A-C) or carboxyatractyloside (CAT; 0, 0.1, 0.5, 1, 2.5, 10, 25, or 50 μM; D-F) and then subjected to the inflammasome activators *m*-3M3FBS (85 μM), thapsigargin (20 μM), nigericin (10 μM) or poly-(dA:dT) (2 μg/mL complexed with 5 μL Lipofectamine 2000) in an extracellular medium consisting of (in mM) 123 NaCl, 5 KCl, 2 $MgCl_2$, 1 $CaCl_2$, 10 glucose, 10 HEPES, pH 7.4. The LPS (A, D) and unprimed (A-F) controls were subjected to medium alone. Immediately after addition of inflammasome activators, the plates were centrifuged at 340 × g for 5 min (RT). After 30 min (C, F) or 60 min (A, B, D, E), the supernatants were collected and IL-1β concentrations were measured by HTRF (A, D) or the cells were fixed with 4% formaldehyde, counterstained with the nuclear dye DRAQ5 (5 μM) and imaged using a widefield fluorescence microscope (B, C, E, F).
The results are plotted as means from 3 independent experiments performed in technical duplicate. Error bars represent SD. Individual data points represent means of the technical duplicate values from each of the independent experiments.

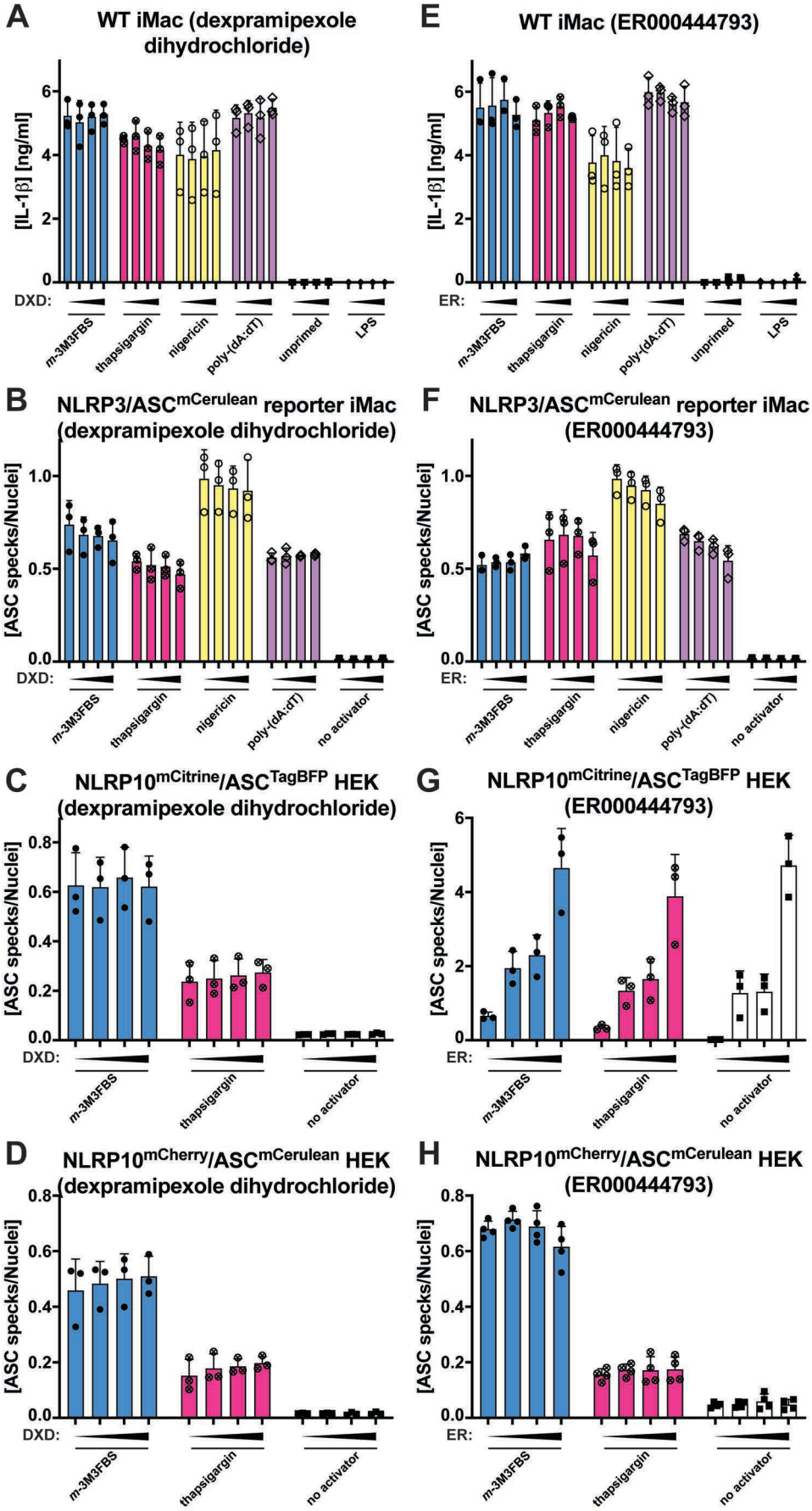

Figure 9.29. Influence of the mitoprotective agents dexpramipexole dihydrochloride and ER000444793 on the inflammasome responses to *m*-3M3FBS, thapsigargin, nigericin, and poly-(dA:dT)

◂ **A-H:** LPS-primed (200 ng/mL, 2 h) WT iMac cells (A, E), NLRP3/ASC^{mCerulean} reporter iMac cells (B, F), NLRP10^{mCitrine}/ASC^{TagBFP} HEK cells (C, G), and NLRP10^{mCherry}/ASC^{mCerulean} HEK cells (D, H) were treated for 10 min with dexpramipexole dihydrochloride (DXD; 0, 5, 10, or 50 μM; A-D) or ER000444793 (ER; 0, 5, 10, or 50 μM; E-H) and then subjected to the inflammasome activators *m*-3M3FBS (85 μM), thapsigargin (20 μM), nigericin (10 μM) or poly-(dA:dT) (2 μg/mL complexed with 5 μL Lipofectamine 2000) in an extracellular medium consisting of (in mM) 123 NaCl, 5 KCl, 2 $MgCl_2$, 1 $CaCl_2$, 10 glucose, 10 HEPES, pH 7.4. The LPS (A, E) and unprimed (A-H) controls were subjected to medium alone. Immediately after addition of inflammasome activators, the plates were centrifuged at 340 × g for 5 min (RT). After 30 min (C, D, G, H) or 60 min (A, B, E, F), the supernatants were collected and IL-1β concentrations were measured by HTRF (A, E) or the cells were fixed with 4% formaldehyde, counterstained with the nuclear dye DRAQ5 (5 μM) and imaged using a widefield fluorescence microscope (B-D, F-H).
The results are plotted as means from 3 (A-G) or 4 (H) independent experiments performed in technical duplicate. Error bars represent SD. Individual data points represent means of the technical duplicate values from each of the independent experiments.

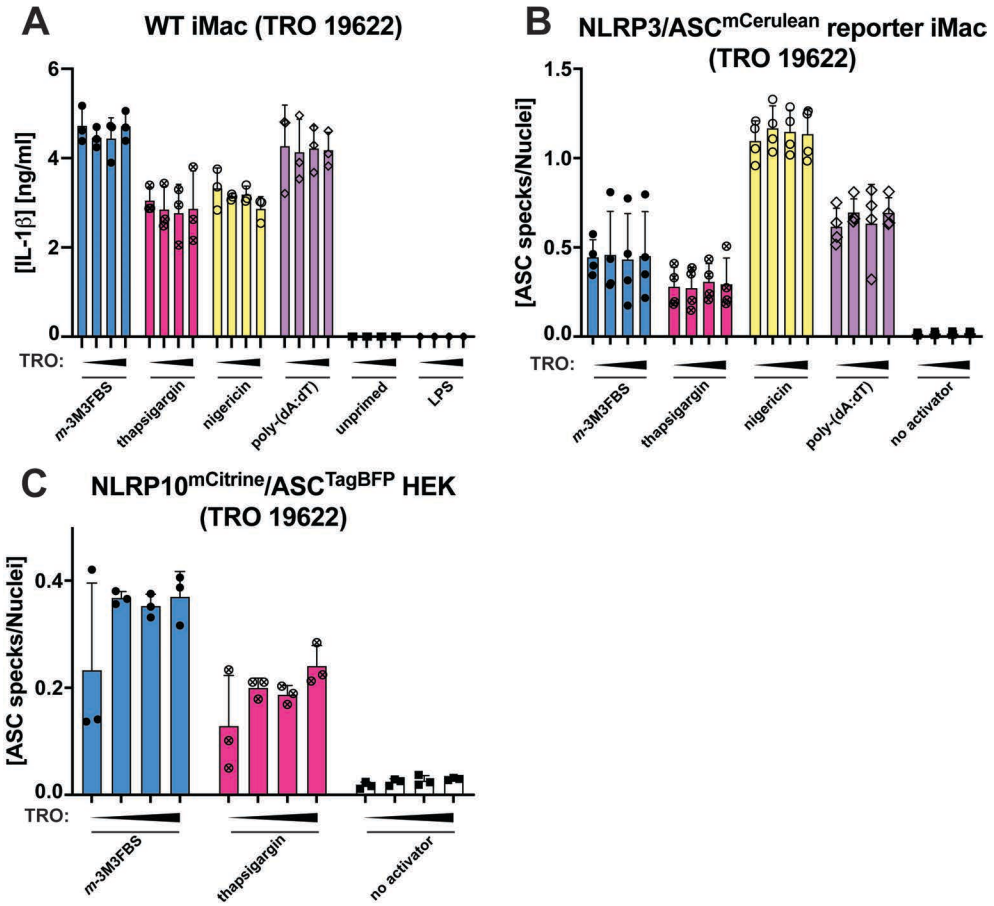

Figure 9.30. Influence of the mitoprotective agent TRO 19622 on the inflammasome responses to *m*-3M3FBS, thapsigargin, nigericin, and poly-(dA:dT)
A-C: LPS-primed (200 ng/mL, 2 h) WT iMac cells (A), NLRP3/ASC^{mCerulean} reporter iMac cells (B), and NLRP10^{mCitrine}/ASC^{TagBFP} HEK cells (C) were treated for 10 min with TRO 19622 (TRO; 0, 10, 25, or 50 μM) and then subjected to the inflammasome activators *m*-3M3FBS (85 μM), thapsigargin (20 μM), nigericin (10 μM) or poly-(dA:dT) (2 μg/mL complexed with 5 μL Lipofectamine 2000) in an extracellular medium consisting of (in mM) 123 NaCl, 5 KCl, 2 $MgCl_2$, 1 $CaCl_2$, 10 glucose, 10 HEPES, pH 7.4. The LPS (A) and unprimed (A-C) controls were subjected to medium alone. Immediately after addition of inflammasome activators, the plates were centrifuged at 340 × g for 5 min (RT). After 30 min (C) or 60 min (A, B), the supernatants were collected and IL-1β concentrations were measured by HTRF (A) or the cells were fixed with 4% formaldehyde, counterstained with the nuclear dye DRAQ5 (5 μM) and imaged using a widefield fluorescence microscope (B, C).
The results are plotted as means from 3 (A, C) or 4 (B) independent experiments performed in technical duplicate. Error bars represent SD. Individual data points represent means of the technical duplicate values from each of the independent experiments.

Testing of the influence of mPTP-targeting agents on the AIM2/NLRP10 activation did not provide a definitive answer about the involvement of mPT in these inflammasome responses. $BaCl_2$ did not inhibit the inflammasome activation with any of the tested stimuli (Figure 9.25 A-C). In contrast, $GdCl_3$ was a potent inhibitor of IL-1β secretion from LPS-primed WT iMac cells (Figure 9.25 D) but did not inhibit ASC speck formation with any of the tested stimuli in NLRP3/$ASC^{mCerulean}$ reporter iMac cells (Figure 9.25 E) and was a selective inhibitor of the thapsigargin-induced ASC speck formation in $NLRP10^{mCitrine}$/ASC^{TagBFP} HEK cells (Figure 9.25 F). Neither $BaCl_2$ nor $GdCl_3$ exhibited inflammasome-activating properties.

Rotenone neither activated the inflammasome nor inhibited the inflammasome responses to any of the tested stimuli (Figure 9.26 D-G), whereas oligomycin A somewhat selectively inhibited the thapsigargin-induced NLRP10 activation in $NLRP10^{mCitrine}$/ASC^{TagBFP} HEK cells (Figure 9.26 C) but had no influence on the thapsigargin-mediated AIM2 activation in macrophages (Figure 9.26 A, B). The mitochondrial uncouplers CCCP (Figure 9.27 A-C) and FCCP (Figure 9.27 D-F) did not cause inflammasome activation in any of the tested models but were instead potent inhibitors of the nigericin-induced NLRP3-mediated IL-1β secretion (Figure 9.27 A, D) and moderately strong inhibitors of the nigericin-elicited ASC speck formation (Figure 9.27 B, E). The highest concentrations (50 μM) of CCCP and FCCP acted as non-selective inhibitors of multiple inflammasome responses (Figure 9.27).

The reported mPTP inhibitor bongkrekic acid (Figure 9.28 A-C) and the mPTP agonist carboxyatractyloside (Figure 9.28 D-F) neither activated the inflammasome nor inhibited the inflammasome responses to any of the tested stimuli. Finally, the mitoprotective agents dexpramipexole dihydrochloride (Figure 9.29 A-D), ER000444793 (Figure 9.29 E, F, H), and TRO 19622 (Figure 9.30) were also neither inflammasome activators nor inhibitors. Of note, ER000444793 exhibited strong autofluorescence in the BFP channel (Figure 9.29 G), so the results obtained with this compound in $NLRP10^{mCitrine}$/ASC^{TagBFP} HEK cells are uninterpretable.

Collectively, my results suggest that the *m*-3M3FBS-driven AIM2/NLRP10 activation is not mediated by mPTP opening. The thapsigargin-induced AIM2/NLRP10 activation is sensitive to CsA, indicating that mPT might be involved in this process (Halestrap et al.,

1997). Furthermore, the thapsigargin-driven NLRP10 activation is sensitive to $GdCl_3$ and oligomycin A, which were both proposed to act as mPTP inhibitors (Mnatsakanyan et al., 2019). Conversely, multiple other mPTP inhibitors did not have an impact on the thapsigargin-induced inflammasome responses, providing an argument against the involvement of mPTP. Importantly, the permeability cutoff of the canonical mPTP is 1.5 kDa, which cannot explain the thapsigargin-induced cytosolic leakage of the mitochondrial matrix proteins and the cytosolic exposure of mtDNA.

Based on the comparisons with previously described mitochondrial stress mechanisms, I was unable to determine how *m*-3M3FBS and thapsigargin induce mitochondrial membrane permeabilization and AIM2/NLRP10 activation. Interference with intrinsic apoptosis, mPTP opening, or inorganic ion fluxes across the mitochondrial membranes did not selectively block the AIM2/NLRP10 inflammasome responses. None of the attempts to trigger mitochondrial membrane permeabilization led to inflammasome activation that could be unequivocally attributed to AIM2 or NLRP10. The induction of UPR^{mt} did not elicit AIM2/NLRP10 activation, and neither did blocking of the mitochondrial protein import. Of note, different ways of targeting the same pathway of mitochondrial damage frequently led to different conclusions. Together, these observations suggest the AIM2 and NLRP10 inflammasome responses may only be triggered by specific mitochondria-linked events, and not by any type of mitochondrial perturbation.

The results presented in this Chapter suggest that the mitochondria still hold many secrets. In the context of the current knowledge, it is impossible to make reliable predictions about the role of mitochondrial membrane permeabilization in the inflammasome activation, or to explain the phenotypes observed in cells treated with *m*-3M3FBS, thapsigargin, SC-10, and SMBA1. A detailed investigation of the mechanisms through which *m*-3M3FBS and thapsigargin permeabilize the mitochondria may lead to the discovery of new mitochondrial damage pathways and help improve the understanding of those that are already known. I will discuss how these topics could be followed up in Section 10.6.

10. Discussion

10.1. Assumptions underlying data interpretation

The results presented in my thesis have broad implications for the understanding of the activation mechanisms of three inflammasomes: AIM2, NLRP3, and NLRP10. Before I discuss how these data fit into, amend, or challenge the existing models, and how they could be followed up, I would like to briefly list the assumptions behind the interpretation of my observations.

First, I consider the signaling pathways leading to the activation of the AIM2 and NLRP3 inflammasomes as unconnected sequences of events that do not share common nodes upstream of ASC speck formation. I also assume that within the typical time frame of my experiments (up to 60 min of stimulation with inflammasome activators), the NLRP3 activation does not lead to 'secondary' AIM2 activation, and, correspondingly, the AIM2 activation does not promote the NLRP3 activation. Based on the literature (Fernandes-Alnemri et al., 2009; Hornung et al., 2009; Jin et al., 2012), such model is generally accepted for murine macrophages. It is also consistent with my data. Given the recent report that in human myeloid cells, dsDNA sensing may be dependent on NLRP3 and independent of AIM2 (Gaidt et al., 2017; discussed in Section 10.3), caution should be taken in extrapolating some of my results to the human system.

Secondly, I assume that the AIM2 activation is a simple process initiated by oligomerization of the receptor on dsDNA molecules in the cytosol and followed by the recruitment of ASC and caspase-1. According to such model, as soon as dsDNA is delivered to the cytosol, no additional 'licensing' steps are required for the AIM2 inflammasome assembly.

Finally, I assume that both the IL-1β concentration in the supernatant and the number of ASC specks in a population of cells monotonically increase with time after the administration of an inflammasome activator. Because of the generally short stimulation times employed in my thesis, this assumption does not have consequences for the majority of the results presented here. However, it remains important for the interpretation of the data obtained after longer stimulation times (Sections 9.1, 9.3, and

9.5) as well as for comparisons with previous studies in which longer stimulation times had been applied.

10.2. Involvement of PLC and Ca^{2+} signaling in the inflammasome activation

Multiple molecular events have been proposed to trigger the NLRP3 inflammasome activation but there is no universally accepted model linking all of them. It is widely accepted that the canonical NLRP3 activation is regulated by fluxes of inorganic ions across the plasma membrane. The central ionic species involved in the NLRP3 activation with nigericin, ATP, and lysosome-damaging agents is K^+. The intracellular K^+ concentration decreases during the NLRP3 activation (Mariathasan et al., 2006; Muñoz-Planillo et al., 2013; Perregaux and Gabel, 1994; Perregaux et al., 1992; Walev et al., 1995). Next to K^+, other inorganic ions have also been implicated in the NLRP3 responses, most importantly Cl^- (Domingo-Fernández et al., 2017; Green et al., 2018; Tang et al., 2017), and Ca^{2+} (Lee et al., 2012; Murakami et al., 2012; Rossol et al., 2012). The reports on the impact of Cl^- ions on the NLRP3 activation are mostly consistent with the K^+ efflux model and they have not been challenged by the literature. In contrast, the studies suggesting the involvement of Ca^{2+} ions have been in significant part based on false premises (Baldwin et al., 2017; Katsnelson et al., 2016; 2015; Muñoz-Planillo et al., 2013).

I commented on the conflict around the role of Ca^{2+} in the NLRP3 inflammasome activation in Chapter 5 to explain the rationale behind my experimental design. Briefly, in a set of independent articles (Lee et al., 2012; Murakami et al., 2012; Rossol et al., 2012), it was proposed that PLC activation and Ca^{2+} fluxes could be the proximal mediators of the NLRP3 activation. These conclusions were based on the observations that the NLRP3 responses were blocked by the PLC inhibitor U 73122, the intracellular Ca^{2+} chelator BAPTA-AM, and the IP_3R antagonist 2-APB. Additionally, Lee et al. (2012) and Rossol et al. (2012) suggested that an increase in the extracellular Ca^{2+} concentration could drive the NLRP3 activation, whereas Murakami et al. (2012) posited that the NLRP3 activation is impeded by depletion of extracellular Ca^{2+}.

Alternative explanations for many of these observations have been provided in subsequent studies. Muñoz-Planillo et al. (2013) demonstrated that solvated

extracellular Ca^{2+} ions do not serve as an NLRP3 activator. Instead, the authors linked the reported extracellular Ca^{2+}-induced NLRP3 activation (Lee et al., 2012; Rossol et al., 2012) to the precipitation of calcium phosphate crystals, followed by their phagocytosis and lysosomal damage-induced NLRP3 activation. Katsnelson et al. (2015) demonstrated that the NLRP3 activation is not affected by the extracellular Ca^{2+} depletion and that the Ca^{2+} chelator BAPTA-AM as well as the IP_3R antagonist 2-APB inhibit the NLRP3 responses through off-target effects. Baldwin et al. (2017) described a series of 2-APB-related NLRP3 inhibitors that did not interfere with Ca^{2+} signaling. Finally, Katsnelson et al. (2016) hinted at the possibility that overloading the cells with Ca^{2+} ions may inhibit the NLRP3 activation.

Despite these revisions, a number of studies employed BAPTA-AM and/or 2-APB to suggest that stimulation with an agent of interest activates the NLRP3 inflammasome by engaging PLC and Ca^{2+} signaling. Non-comprehensive lists of such studies include for BAPTA-AM: Chae et al., 2015; Chen et al., 2017; Deng et al., 2019; Elliott et al., 2018; Freeman et al., 2017; Hao et al., 2017; Martín-Nalda et al., 2020; Mishra et al., 2019; Yao et al., 2017; Zewinger et al., 2019; Zhang et al., 2017; and for 2-APB: Baron et al., 2015; Chae et al., 2015; Deng et al., 2019; Freeman et al., 2017; Swanson et al., 2017; Yao et al., 2017; Yeon et al., 2016; Zhang et al., 2018; 2017. It is likely that some of the NLRP3 activation mechanisms proposed in these studies are not valid.

The data presented in Chapters 4 and 5 of my Thesis as well as in Sections 6.1, 6.2, 6.8, 6.9, 6.11, and 6.13 can be regarded as a continuation of the four studies amending the Ca^{2+}-based model of the NLRP3 activation (Baldwin et al., 2017; Katsnelson et al., 2015; 2016; Muñoz-Planillo et al., 2013). In this respect, I have demonstrated that the canonical NLRP3 activator nigericin does not trigger PLC activation (Figures 5.5-5.7). I also provided an explanation for how the PLC inhibitor U 73122 blocks the NLRP3 inflammasome. This occurs through an off-target alkylation of one or more protein cysteinyl residues (Figures 5.1 and 5.2). Edelfosine, another commercially available PLC inhibitor, non-selectively blocks both the NLRP3 and the AIM2 inflammasome responses with similar potencies (Figure 4.3). Finally, the phosphatidylcholine (PC)-PLC inhibitor D609 does not inhibit the inflammasome activation (Supplementary Figure S40). This observation is consistent with the fact that the mammalian genomes do not have genes encoding PC-PLC enzymes (Kadamur and Ross, 2013; Nakamura and Fukami, 2017).

Some of my data provided validation for previously reported results. For instance, I detected no extracellular Ca^{2+}-induced inflammasome activation (Figure 4.4 D, E; Muñoz-Planillo et al., 2013), and I found no evidence that the depletion of extracellular Ca^{2+} could interfere with the NLRP3 responses (Figure 4.4 D, E; Katsnelson et al., 2015). I also confirmed that overloading the cells with Ca^{2+} ions could block the NLRP3 activation (Figures 6.18 A, C and 8.16 A, C; Katsnelson et al., 2016).

In a further attempt to systematize the knowledge on the PLC involvement in the inflammasome activation, I discovered that the reported PLC agonist *m*-3M3FBS triggers the inflammasome in an NLRP3-independent manner (Figure 4.5). Instead, in murine macrophages, *m*-3M3FBS activates AIM2 (Figure 6.11). Importantly, this observation was not in agreement with the report by Muñoz-Planillo et al. (2013), who suggested that *m*-3M3FBS could activate the inflammasome in an NLRP3-dependent manner[1]. It is difficult to comment on this discrepancy. In my opinion, the most likely explanation is the fact that *m*-3M3FBS does not have the ability to activate the inflammasome in media containing high concentrations of FBS (Supplementary Methods Figures SM1 and SM2). If Muñoz-Planillo et al. (2013) performed the experiments under suboptimal conditions[2], it is possible that the variation in the range of the observed responses was interpreted as dependence on NLRP3.

The *m*-3M3FBS-driven AIM2 activation does not rely on PLC. Instead, it involves mitochondrial damage, which is an off-target effect of *m*-3M3FBS (Figures 6.27 and 6.28). The endogenous AIM2 ligand exposed by *m*-3M3FBS is mtDNA (Figure 8.2; discussed in detail in Section 10.3). Collectively, my results highlight the need for a significant revision of the existing inflammasome literature. Numerous studies employed U 73122 to suggest a mechanistic link between a stimulus of interest and the inflammasome activation. A non-comprehensive list of such papers includes Baron et al., 2015; Chae et al., 2015; Deng et al., 2019; Freeman et al., 2017; Gutiérrez-López et al., 2018; Irmscher et al., 2019; Lee et al., 2012; Martín-Nalda et al., 2020; Murakami et al., 2012; Negash et al., 2019; Rossol et al., 2012; Yeon et al., 2016; Zhou et al., 2015. Furthermore, studies in which *m*-3M3FBS was used to demonstrate the link between

[1] The study by Muñoz-Planillo et al. (2013) is the only published article in which the inflammasome activation by *m*-3M3FBS has been assessed in an NLRP3-deficient model.
[2] The Methods section and the Figure Legend do not include information on the type of medium and the concentration of FBS in the experiment under consideration.

PLC activation and the NLRP3 inflammasome (Chae et al., 2015; Deng et al., 2019; Lee et al., 2012; Muñoz-Planillo et al., 2013) may also need to be re-evaluated.

An important conclusion from my work was that PLC was not the mediator through which *m*-3M3FBS induced the AIM2 activation. This statement is backed by three lines of argumentation. First, my results indicated that the *m*-3M3FBS-induced AIM2 activation is not very sensitive to PLC inhibitors (Figure 4.3) and to interference with Ca^{2+} signaling (Figures 6.16 A-D and 6.17 A-D). Secondly, I detected strong induction of PLC activity in murine macrophages transfected with poly-(dA:dT) (Figures 5.5-5.7). In this cell type, it is well-established that poly-(dA:dT) activates the AIM2 inflammasome through direct binding. Because of that, it is likely that the IP_1 surge observed in poly-(dA:dT)-transfected cells is a byproduct of DNA delivery and that it does not represent a step in the AIM2 inflammasome activation[3]. Thirdly, transfection with poly-(dA:dT) did not lead to mitochondrial damage (Figures 6.27 and 6.28), indicating that at least the global PLC activation induced with poly-(dA:dT) is not sufficient disrupt the mitochondria. Correspondingly, the other AIM2 activators identified in my study (thapsigargin, SC-10, and SMBA1) trigger the mitochondrial contents leakage but have not been reported to activate PLC. Finally, I would like to comment on the scenario that PLC could 'digest its way' through the mitochondrial membranes after activation with *m*-3M3FBS. This is highly unlikely for the following reason: the mitochondrial membranes are not enriched in inositol lipids (van Meer and de Kroon, 2010; van Meer et al., 2008); the estimated content of all such lipids in the mitochondria is 6% (Casares et al., 2019). Lipid membranes have self-sealing properties, and PIP_2 hydrolysis by PLC is, in fact, not expected to physically damage the membrane, as DAG, one of the PLC reaction products, remains in the lipid layer. Notably, the possibility of PLC-unrelated effects of *m*-3M3FBS administration has been suggested in previous studies performed by Krjukova et al. (2004) and Dwyer et al. (2010).

A piece of evidence on the PLC involvement in the inflammasome activation that I did not address experimentally in my Thesis is the observation that APLAID patients harboring hypermorphic mutations in the gene encoding PLCγ2 suffer from symptoms

[3] Such interpretation is supported by the low sensitivity of the AIM2 inflammasome activation to the PLC inhibitors U 73122 and edelfosine (Figure 4.3). In contrast, U 73122 and edelfosine strongly inhibit PLC activation caused by poly-(dA:dT) transfection (Figure 5.5).

of autoinflammation. Monocytes isolated from these patients spontaneously release IL-1β in response to LPS. This phenotype has been linked to aberrant activation of the NLRP3 inflammasome (Chae et al., 2015; Martín-Nalda et al., 2020). Importantly, neither of the cited studies proved the NLRP3 involvement in the observed IL-1β secretion[4], and the supporting mechanistic data were all obtained with the use of BAPTA-AM, 2-APB, U 73122, and *m*-3M3FBS. All of these molecules have been demonstrated to act through off-target effects in previous studies or in my Thesis. In the future, it would be interesting to establish whether the inflammatory response in APLAID is NLRP3-dependent, and to mechanistically explore the link between the PLCγ2 mutations and the onset of inflammation. Genetic systems could be employed to investigate this, such as inducible overexpression of the hypermorphic PLCγ2 variants in immortalized murine macrophages or in THP-1 cells. Interestingly, one of the models of the NLRP3 activation proposes that NLRP3 interacts with the Golgi inositol lipid PI4P (Bittner et al., 2020; Chen and Chen, 2018). Could hypermorphic PLC mutants upregulate the levels of PI4P? A direct effect is unlikely because PI4P is neither a substrate, nor a product of the PLC-catalyzed reaction. Even so, the amounts of inositol phospholipids could theoretically be linked to PLC activity through feedback mechanisms not directly related to the PLC-catalyzed reaction.

Martín-Nalda et al. (2020) further proposed that the inflammasome responses in APLAID patients might be mediated by the alternative pathway of the NLRP3 activation, which was initially described by Gaidt et al. (2016). This attribution may be incorrect for several reasons. The alternative NLRP3 activation is an LPS-induced response observed in human monocytes and dependent on TLR4, NLRP3, ASC, and caspase-1. In contrast to the canonical pathway, the alternative NLRP3 activation does not involve K^+ efflux and is not associated with ASC speck formation. The rate of this process is slow, for example Gaidt et al. (2016) report a 14-h stimulation. Mechanistically, the alternative NLRP3 activation requires TRIF, RIPK1, FADD, and caspase-8 (Gaidt et al., 2016). In contrast to this original report, the response observed by Martín-Nalda et al. (2020) in monocytes from APLAID patients is fast (2-h stimulations) and is associated with ASC speck formation. The involvement of factors such as NLRP3, K^+ efflux, TRIF, RIPK1, FADD, and

[4] For example by employing the NLRP3 inhibitor CRID3 (Coll et al., 2019; 2015; Tapia-Abellán et al., 2019; Vande Walle et al., 2019). Notably, the K^+ efflux involvement in the inflammasome activation in monocytes from APLAID patients has also not been experimentally addressed.

caspase-8 has not been tested. More data is required to support the notion that enhanced alternative NLRP3 activation is a feature of monocytes isolated from APLAID patients.

***

A separate topic related to Ca^{2+} signaling and inflammasome responses is the influence of thapsigargin on the NLRP3 activation. My experiments, which were all performed using high thapsigargin concentrations (~20 μM) and short stimulation times, indicated that in murine macrophages thapsigargin selectively activates the AIM2 inflammasome (Figure 6.13)[5]. I found no evidence that NLRP3 could be involved in this response. Instead, in AIM2-deficient cells, thapsigargin acted as a weak, partial inhibitor of the NLRP3 activation with nigericin (Figure 8.11). These results are not fully consistent with what has previously been reported on the impact of thapsigargin on the inflammasome activation. However, the published reports on this topic also reach divergent conclusions. One explanation for these discrepancies could be the variation in thapsigargin concentrations and stimulation times between studies. Below, I provide an outline of the literature addressing the impact of thapsigargin on the NLRP3 inflammasome activation.

The first report suggesting that thapsigargin activates the NLRP3 inflammasome was a paper by Menu et al. (2012), which proposed that the NLRP3 inflammasome can be activated by the thapsigargin-induced ER stress through mechanisms independent of the UPR. The authors demonstrated that in BMDMs, but not in THP-1 cells, 6-h stimulations with 5-10 μM thapsigargin lead to the inflammasome activation. This process was considered to be NLRP3-dependent, but the evidence supporting this statement is limited[6]. Lee et al. (2012) then showed that 50 nM thapsigargin could

[5] This process was dependent on the recognition of the exposed mtDNA (Figure 8.2) and could be fully inhibited with CsA (Figure 6.37), which correlated with protection from the thapsigargin-induced mitochondrial damage (Figure 6.40). I discuss these topics in detail in Sections 10.3 and 10.4.

[6] It can be inspected in Figure 2 A in the cited article. In this figure, the release of cleaved caspase-1 into the supernatant is assessed by western blotting. The amounts of caspase-1 secreted by thapsigargin-treated NLRP3-proficient and -deficient BMDMs are compared, and the caspase-1 release from NLRP3-deficient cells is reduced but not completely absent. With no additional evidence, a cautious interpretation of this result would be that the inflammasome activation with thapsigargin is less potent in NLRP3-deficient cells. In my opinion, these data are insufficient as a proof that the thapsigargin-induced inflammasome activation is non-redundantly NLRP3-dependent.

trigger IL-1β secretion from and ASC oligomerization in LPS-primed BMDMS within 30 min. This result was used as evidence that an increase in the cytosolic Ca^{2+} concentration can trigger the NLRP3 inflammasome, even though an NLRP3-deficient control was not tested. To prove the same point, Rossol et al. (2012) demonstrated that thapsigargin (50 nM - 2 μM) triggers a robust IL-1β response, also without employing an NLRP3-deficient control[7]. Lerner et al. (2012) reported that thapsigargin (1 μM at the 4-h time point, but not after only 2 h) could trigger the inflammasome activation in THP-1 cells, which is not consistent with the study by Menu et al. (2012), who did not detect inflammasome activation with thapsigargin in THP-1 cells. The thapsigargin-induced inflammasome activation in THP-1 cells was abolished by NLRP3 deficiency and by an inhibitor of inositol-requiring enzyme 1 α (IRE1α), a downstream effector of ER stress-sensing mechanisms (Lerner et al., 2012). In a similar set of experiments, Oslowski et al. (2012) demonstrated that a 6-h treatment of THP-1 cells with 1 μM thapsigargin leads to IL-1β secretion and caspase-1 cleavage, although here the data from an NLRP3-deficient model were not provided. The model proposed by Lerner et al. (2012) and Oslowski et al. (2012), which suggests the involvement of PERK/IRE1α as mediators of the NLRP3 inflammasome response to ER stress, is not in agreement with the model proposed by Menu et al. (2012), where PERK and IRE1α were shown not be required for the NLRP3 activation by ER stress inducers.

In subsequent years, Shin et al. (2013) proposed that thapsigargin (5 μM for 4 h) activates the NLRP3 inflammasome through ROS formation and lysosomal damage. This observation was presented in support of the model according to which the proteotoxic stress activates NLRP3, even though the NLRP3 dependence of the thapsigargin-induced inflammasome activation was not confirmed. Rada et al. (2014) observed that thapsigargin (100 nM - 1 μM for 24-48 h) elicits a weak IL-1β response and interpreted this result as indicative of the involvement of Ca^{2+} ions in the NLRP3 inflammasome activation, despite the lack of an NLRP3-deficient control. Bronner et al. (2015) reported that 10 μM thapsigargin triggers the NLRP3 activation in BMDMs over the course of a 4-h stimulation (the NLRP3-deficient control was employed). Finally, Robblee et al. (2016) used thapsigargin as a control ER stress inducer in a study on the inflammasome activation by saturated fatty acids. This was proposed to be mediated by the ER stress,

[7] The stimulation time is not reported in the cited article.

IRE1α engagement, and NLRP3 activation[8]. In this report, 200 nM thapsigargin triggered the inflammasome activation over the course of 20-24 h, which could be blocked by IRE1α inhibition, consistent with the observations reported by Lerner et al. (2012) and Oslowski et al. (2012), but not by Menu et al. (2012).

To add to the confusion, one study suggested that thapsigargin may inhibit the NLRP3 activation. Murakami et al. (2012) reported that a 30-min pre-treatment with thapsigargin (to deplete the ER Ca^{2+} stores; the thapsigargin concentration was not disclosed) inhibited the NLRP3 activation with ATP in LPS-primed BMDMs. Upon closer inspection of the data[9], the response to LPS and ATP in thapsigargin-treated cells is reduced compared to the untreated control, but still robust. It is difficult to interpret these data without knowledge of the detailed experimental protocol (thapsigargin concentration, incorporation of washing steps between the thapsigargin pre-treatment and the ATP stimulation). In opposition to Murakami et al. (2012), Katsnelson et al. (2015) reported that, in Ca^{2+}-free media, thapsigargin (300 nM) did not inhibit the NLRP3 inflammasome activation, or only acted as a weak inhibitor. Under these conditions, Katsnelson et al. (2015) did not observe the inflammasome activation with thapsigargin, which was not fully consistent with the results reported by Lee et al. (2012) and Rossol et al. (2012)[10].

My observation that thapsigargin is an inflammasome activator (Figure 6.12) is in agreement with most of the discussed studies. However, three of these studies (Bronner et al., 2015; Lerner et al., 2012; Menu et al., 2012) linked the thapsigargin stimulation to the NLRP3 inflammasome activation using NLRP3-deficient models, whereas my results suggest complete dependence on AIM2 (Figure 6.13). I have not determined whether longer treatments with thapsigargin could trigger the NLRP3 inflammasome in an AIM2-deficient model. Regardless of the result, such experiment would not explain why some authors reported a *complete* dependence of the thapsigargin-induced inflammasome

[8] This was a bold statement on the part of the authors, given that none of the experiments in the cited article feature an NLRP3-deficient control.
[9] Figure 1 B in the cited article.
[10] Importantly, Katsnelson et al. (2015) performed the stimulations with thapsigargin under Ca^{2+}-free conditions, whereas Lee et al. (2012) and Rossol et al. (2012) used Ca^{2+}-containing media. In my experiments (Figures 6.16-6.18), removal of the extracellular Ca^{2+} did not have an impact on the AIM2 response to thapsigargin but the concentration of thapsigargin used throughout my Thesis was much higher than it was in the cited studies.

activation on NLRP3, whereas I observed a *complete* dependence on AIM2. Overall, attempting to reconcile all published observations on the impact of thapsigargin on the inflammasome activation is probably a futile task. Experimentally, the discrepancies I pointed out could be addressed by a time- and concentration-resolved thapsigargin stimulation of murine and human macrophages, ideally employing AIM2-deficient, NLRP3-deficient, and AIM2/NLRP3 double-deficient models. I did not perform such an experiment because I used thapsigargin to trigger mitochondrial damage, and not to target the ER Ca^{2+} stores or to induce ER stress.

In summary, my research on the involvement of PLC in the NLRP3 inflammasome activation provided the final arguments that the previously proposed PLC-Ca^{2+}-NLRP3 signaling axis is thoroughly a product of experimental artifacts. I could reproduce the observations that *m*-3M3FBS and thapsigargin activate the inflammasome but in my experimental models, these responses were completely dependent on AIM2 and independent of NLRP3. The mechanism through which *m*-3M3FBS and thapsigargin activate the AIM2 inflammasome is mitochondrial damage, which I discuss in Sections 10.3 and 10.4.

10.3. Sensing of mtDNA by the inflammasome

An unresolved question on the mechanism of the canonical NLRP3 activation is how the information about K^+ efflux is transmitted to NLRP3. A number of downstream mediators have been proposed to be engaged by K^+ efflux agonists: (ox-)mtDNA (Nakahira et al., 2010; Shimada et al., 2012; Zhong et al., 2018), cardiolipin (Iyer et al., 2013), the Golgi phospholipid PI4P (Bittner et al., 2020; Chen and Chen, 2018), TXNIP (Lerner et al., 2012; Zhou et al., 2009; 2010), MAVS (Subramanian et al., 2013), NEK7 (He et al., 2016; Schmid-Burgk et al., 2016; Shi et al., 2015), DDX3X (Samir et al., 2019), and SCAP (Guo et al., 2018). An integrative interpretation of these studies is difficult for several reasons. First, validation studies are scarce, so it is often not clear whether the identified NLRP3 interaction partners are required for the inflammasome activation universally or only in specific model systems (that is, they are context-dependent). For example, MAVS had been initially proposed to be 'required for optimal NLRP3 inflammasome activity' (Subramanian et al., 2013; I allowed myself to directly quote from the cited article) but was later demonstrated to be in fact dispensable in this

process (Allam et al., 2014; Park et al., 2013). NEK7 may also not be universally involved in the NLRP3 activation, as Schmacke et al. (2019) proposed an inflammasome priming mechanism that circumvents the requirement for NEK7. Another example of such discrepancy is the model proposed by Zhong et al. (2018), whereby the priming signal induces mtDNA synthesis in an IRF1-dependent manner, with NLRP3 responses significantly diminished in IRF1-deficient cells. Yet two other studies reported unaltered levels of NLRP3 activation in an IRF1-deficient model (Kuriakose et al., 2018; Man et al., 2015). Secondly, the reports claiming to have discovered a 'new' NLRP3 interaction partner rarely include data on how this newly described interaction fits into the existing models of the NLRP3 activation. Consequently, it is currently unclear whether mtDNA, cardiolipin, PI4P, NEK7, MAVS, TXNIP, DDX3X, and SCAP all form one large signaling complex with NLRP3, whether NLRP3 sequentially interacts with all these molecules collecting 'posttranslational marks' licensing the inflammasome activation, or whether the NLRP3 inflammasome formation represents a combination of both scenarios.

In my Thesis research, somewhat inadvertently, I had to confront the notion that NLRP3 is activated by mtDNA. Notably, mtDNA has been implicated in the activation of multiple inflammasomes: NLRP3 (Li et al., 2019; Nakahira et al., 2010; Shimada et al., 2012; Zhong et al., 2018), AIM2 (Dang et al., 2017; Li et al., 2019), and NLRC4 (Jabir et al., 2014). It is not likely that mtDNA is actually involved in all these inflammasome responses; if it was, much more redundancy would be observed in this signaling system. I provided an example in the introduction to Chapter 8: if the canonical NLRP3 activators cause a cytosolic leakage of mtDNA (Nakahira et al., 2010; Shimada et al., 2012), why do they not activate the AIM2 inflammasome, especially in the light of the observation that cytosolic mtDNA in cholesterol-overloaded macrophages acts as an AIM2 ligand (Dang et al., 2017)?

Another concern about the early studies suggesting that mtDNA translocates to the cytosol in cells treated with the canonical NLRP3 stimuli is that this conclusion relies on qPCR quantifications of cytosolic mtDNA. These measurements were always presented as a value relative to the resting conditions. The cytosolic mtDNA level was reported to increase up to fivefold after LPS and ATP treatment, compared to LPS alone (Nakahira et al., 2010). How biologically meaningful is such a value? Under resting conditions, when mtDNA is shielded by two mitochondrial membranes, the cytosolic mtDNA content can

be expected to be close to zero. For the sake of the calculation, it could be assumed that one in every ten cells would have one copy of cytosolically translocated mtDNA (or, on the average, 0.1 copies of mtDNA per cell), accounting for spontaneous mitochondrial damage and systematic errors related to sample contamination. If a treatment with an NLRP3 activator leads to one in every two cells having one copy of mtDNA translocated to the cytosol (or 0.5 copies of mtDNA per cell), this already results in a fivefold increase when normalized to the resting state. None of the studies on the mtDNA involvement in the NLRP3 activation proposed a threshold cytosolic mtDNA concentration enabling NLRP3 activation; providing such estimate would probably be challenging[11]. The calculation above puts into perspective the magnitude of the initially reported mtDNA leakage: fivefold increase over a very low initial value may not indicate translocation of large quantities of mtDNA during NLRP3 activation. Notably, whereas I detected *m*-3M3FBS-, SC-10-, thapsigargin-, and SMBA1-induced leakage of the mitochondrial contents in cells overexpressing a fluorescent protein targeted to the mitochondrial matrix (Figures 6.27 and 6.28), I did not observe a similar event in cells stimulated with nigericin. This suggests that the treatment with nigericin does not lead to an exposure of the mitochondrial contents to the cytosol.

The data presented in my Thesis contradict the model proposed by Nakahira et al. (2010), Shimada et al. (2012), and Zhong et al. (2018). First, my results indicate that the NLRP3 activation is not affected by mtDNA depletion. Secondly, they suggest that in the event of mtDNA exposure to the cytosol, the inflammasome response is mediated by AIM2 and independent of NLRP3 (Sections 8.2, 8.5, and 8.6). Depletion of mtDNA with ddC or EtBr completely abolished the AIM2-driven (Figures 6.11, 6.13, and 6.44) IL-1β and ASC specking responses to *m*-3M3FBS, thapsigargin, SC-10, and SMBA1 (Figures 8.2 and 8.6). In contrast, ddC had no impact on the IL-1β and ASC specking responses to poly-(dA:dT) (AIM2) and nigericin (NLRP3), whereas EtBr partially inhibited the IL-1β responses to both poly-(dA:dT) and nigericin, but was not an inhibitor of the ASC speck formation triggered by these stimuli (Figure 8.2). The observation that the AIM2 activation induced by poly-(dA:dT) is not blocked by mtDNA depletion indicated that the loss of mtDNA does not lead to a global inhibition of the AIM2 inflammasome responses.

[11] At present, super-resolution microscopy could potentially be employed to resolve such issues. McArthur et al. (2018) and Riley et al. (2018) succeeded in imaging the cytosolic translocation of mitochondrial nucleoids in cells treated with pro-apoptotic stimuli so similar visualization techniques could be applied to cells stimulated with NLRP3 agonists.

Interestingly, the K^+ efflux-independent mitochondria-targeting NLRP3 agonist R837 also triggered the NLRP3 activation in a manner independent of mtDNA (Figure 8.10). Overall, my observations are in agreement with the study by Dang et al. (2017), who reported that the cytosolic translocation of mtDNA in macrophages overloaded with cholesterol causes activation of the AIM2 inflammasome. Consistent with my conclusions on the canonical NLRP3 activation, Dang et al. (2017) did not observe a defect in the IL-1β response to LPS and ATP upon mtDNA depletion.

The inflammasome responses to synthetically generated oxDNA fragments were previously used as a proof that NLRP3 is activated by ox-mtDNA. I tested whether I could reproduce these observations. I generated dsDNA (~1000 bp) and ssDNA (~1000 nt) PCR products with or without the oxidized variant of guanylate residues (8-OH-dG) and examined whether they could activate the NLRP3 inflammasome in AIM2-deficient cells (Sections 8.8 and 8.9). I found no evidence that ss- or dsDNA fragments could activate NLRP3, regardless of the presence of the oxidative modification. Furthermore, I discovered that in my experimental model, any residual NLRP3 activation in AIM2-deficient cells transfected with DNA could be explained by the transfection reagent used for DNA delivery (Section 8.10). Finally, I was unable to reproduce the earlier observation (Shimada et al., 2012) that monomeric 8-OH-dG could selectively inhibit NLRP3 (Figure 8.21). These results indicated that (ox-)ds-/ssDNA molecules are not NLRP3 ligands in murine macrophages.

Collectively, my data provide strong arguments against the involvement of mtDNA in the NLRP3 activation. They also demonstrate that AIM2 can be directly activated by mtDNA in murine macrophages. Given the chemical and biochemical properties of mtDNA, which, unlike nuclear DNA, is not bound to histones, this is not surprising, but so far has been directly proposed in the literature only once (Dang et al., 2017)[12].

Of note, this picture may be more complicated in the human system. In human monocytes, the inflammasome response to cytosolic DNA is dependent on NLRP3 (Gaidt et al., 2017). This has been demonstrated in a model of transfection-mediated DNA

[12] The report by Dang et al. (2017) is the only publication known to me demonstrating that endogenously released mtDNA non-redundantly activates AIM2. Earlier studies did demonstrate that transfected dsDNA molecules, with or without oxidative modifications, may activate the AIM2 inflammasome (Shimada et al., 2012), whereas Li et al. (2019) hinted at the possibility of the AIM2 activation by mtDNA in $CD4^+$ T cells.

delivery but presumably is also valid for endogenous DNA from ruptured mitochondria. The mechanism proposed by Gaidt et al. (2017) relies on cytosolic DNA recognition by cGAS, generation of cGAMP, cGAMP-induced translocation of STING to the lysosomal membrane, lysosomal damage, and K^+ efflux. This last event enables the NLRP3 activation. Importantly, the authors do not propose an explanation for why AIM2 is 'silent' in this scenario, even though it is present in the cells. Based on my results, such lack of sensitivity to transfected DNA is not an intrinsic property of human AIM2, as AIM2-deficient murine macrophages reconstituted with human AIM2 were as efficient in responding to cytosolic DNA as were cells reconstituted with murine AIM2 (Figures 7.7, 7.8, 7.9, and 8.6)[13]. This suggests that AIM2 might be actively shut down in the human system. Whether this is the case, and what the mechanism could be, will have to be determined by future research. If a mechanism for the AIM2 inactivation in human monocytes exists, it would be interesting to determine whether it could be defect in any autoinflammatory or autoimmune disorders, possibly contributing to the pathology. Finally, it is important to point out a major caveat in the study by Gaidt et al. (2017): all the experiments in this article were performed in TLR ligand-primed cells, even though the AIM2 activation, at least in the murine system, does not require the priming step (Figure 4.4 A and Supplementary Figure S6 C). Consequently, it is conceivable that the priming stimulus could re-route the DNA sensing mechanism from AIM2 to NLRP3.

Unfortunately, the main genetically manipulatable cellular model employed in the study by Gaidt et al. (2017) (BlaER1 cells; Gaidt et al., 2018; Rapino et al., 2013) is not available anymore due to a retroviral contamination. In the remaining model system for human monocytes and macrophages, THP-1 cells, the response to cytosolic DNA is AIM2-dependent (Fernandes-Alnemri et al., 2009; Gaidt et al., 2017), narrowing the scope of possible experiments. Besides the two cited studies, surprisingly little research has been done on the inflammasome-mediated cytosolic DNA sensing in human myeloid cells. In the absence of an explanation for why AIM2 is not responsive to DNA in human monocytes even though it is expressed, it may be prudent not to completely dismiss the possibility that AIM2 remains a functional DNA sensor in some human cell types.

[13] The AIM2 activation, even by transfected DNA, was also very fast in my experimental model (Figure 6.28), with ASC specks appearing within 10 min of DNA administration.

It is impossible to present so many results contradicting the conclusions from previous studies without a commentary. First, I would like to emphasize that revisions in the inflammasome signaling field occur frequently and the part of my Thesis concerning the impact of PLC on the inflammasome activation can be seen as a continuation of earlier validation studies (Baldwin et al., 2017; Katsnelson et al., 2015; 2016; Muñoz-Planillo et al., 2013). My conclusions on the mtDNA involvement in the AIM2 and NLRP3 activations are essentially unprecedented but the inconsistencies between the studies on the role of mitochondria in the inflammasome activation have already been pointed out in several reviews and opinion articles (Holley and Schroder, 2020; Lawlor and Vince, 2014; Yabal et al., 2018). Of note, a major revision has also recently been published regarding the regulation of the NLRC4 inflammasome (Tenthorey et al., 2020), providing a simplified model of NLRC4 activation. In my opinion, it is important to highlight the explanatory, rather than the disruptive, power of such findings.

Even adopting such a cautious approach, it cannot be denied that inconsistencies are abundant in the inflammasome literature. This has led to a view expressed by many that the NLRP3 inflammasome is activated under any conditions triggering 'cell stress'. I believe this is an oversimplification, not least because 'cell stress' is an umbrella term encompassing multiple responses (the list includes heat shock response, mechanical and osmotic stress, the UPR and the ISR, infection, permeabilization of the plasma membrane or organelle membranes, response to DNA damage, and response to oxidative agents). That all of these conditions produce signals converging on NLRP3 is unlikely. Instead, the NLRP3 activation appears to be a well-regulated process, triggered by several sets of stimuli: K^+ efflux (the so-called canonical NLRP3 activation as well as the non-canonical NLRP3 pathway), certain disruptors of glycolysis or mitochondrial respiration (the thoroughly characterized agonists of this pathway are R837, ENOblock, koningic acid, and N-acetylglucosamine), and signaling complexes linked to TLR activation and cell death (examples include the alternative NLRP3 activation and the ZBP1-mediated NLRP3 activation).

NLRP3 is a protein, not a sentient being, and as such it does not 'monitor' the cellular environment, but instead engages in physical and chemical interactions with the components of the cell. These interactions may promote or suppress the inflammasome activation, they may be stable or transient, they may involve large biomolecules or LMW

metabolites, they may be non-covalent or covalent, and if they are covalent, they may result from nonenzymatic chemical reactions or they may be enzymatically catalyzed. In this light, NLRP3 cannot be activated as a consequence of a loosely specified 'stress state' unless there exists a sequence/set of molecular events that can transmit the information about the stressor to NLRP3, resulting in a state permissive for the inflammasome nucleation. Such state is likely a product of a specific NLRP3 conformation[14], posttranslational modifications, or a combination of these two factors.

The data presented in my Thesis allow to simplify the existing model of the canonical NLRP3 activation by providing evidence that PLC and mtDNA are not involved in this response. In the future, this model will likely undergo further rounds of expansion, validation, and refinement, hopefully producing a version that explains how all of the identified NLRP3-activating and -inhibitory inputs regulate the inflammasome formation.

10.4. Sensing of mitochondrial damage by the AIM2 and NLRP10 inflammasomes

In Sections 10.2 and 10.3 I commented on how my Thesis research fits into and modifies the existing models of the NLRP3 inflammasome activation. I also discussed how AIM2 can be activated by endogenous mtDNA in the murine system. Another important discovery presented in my thesis is the identification and characterization of four LMW compounds that trigger leakage of the mitochondrial matrix contents into the cytosol (Figures 6.27 and 6.28). In murine macrophages, these compounds (*m*-3M3FBS, SC-10, thapsigargin, and SMBA1) elicit inflammasome activation in an AIM2-dependent manner (Figures 6.11, 6.13, and 6.44). This process relies on sensing of the exposed mtDNA (Figures 8.2 and 8.6). Collectively, my results indicate that mitochondrial damage resulting in mtDNA exposure is necessary and sufficient for the AIM2 activation with *m*-3M3FBS, SC-10, thapsigargin, and SMBA1.

Unexpectedly, during the initial screening to identify the prospective inflammasome-forming proteins activated by *m*-3M3FBS, I observed that the transfection with NLRP10 renders ASC^{TagBFP} HEK cells responsive to this molecule (Figure 6.2). Using two

[14] This includes the possibility that new binding interfaces may be exposed as a result of NLRP3 association with a binding partner, or NLRP3 dissociation from a binding partner.

overexpression systems, AIM2-deficient murine macrophages transduced with NLRP10 and HEK cells transduced with fluorescently labeled ASC and NLRP10, I further determined that NLRP10 enables inflammasome responses to *o*-3M3FBS, SC-9, SC-10, thapsigargin, and SMBA1 (Figures 6.4, 6.14, 6.24, 6.43, 7.7, 7.8, and 7.9).

In contrast to the AIM2 activation, the NLRP10 responses were independent of mtDNA (Figures 8.3 and 8.6). The implication of this observation is that the 'products' of mtDNA – the mitochondrial rRNA/tRNA molecules and the mitochondrially encoded proteins containing N-formylmethionyl residues – are also not required for the NLRP10 activation.

Under resting conditions, NLRP10 is a soluble cytosolic protein. In HEK cells treated with *m*-3M3FBS, thapsigargin, or SMBA1 (the NLRP10 agonists that are mitochondrially active in HEK cells), NLRP10 translocates to the mitochondria (Figures 6.10, 6.15, and 6.55), suggesting that a ligand for NLRP10 could be exposed following mitochondrial disruption, leading to the NLRP10 recruitment. The part of NLRP10 involved in the mitochondrial translocation likely resides in the NACHT domain or in the linker between the PYD and the NACHT domains, as NLRP10 without the PYD domain can still translocate to the mitochondria, whereas the PYD domain alone does not change its localization upon *m*-3M3FBS stimulation (Figures 7.5 and 7.6).

I did not identify the mechanism governing the NLRP10 aggregation at the mitochondria. My imaging data suggest that, when a mitochondria-disrupting activator such as *m*-3M3FBS is employed, NLRP10 rapidly translocates to the mitochondria and remains stably associated with these organelles (Figure 6.51). This could represent an interaction with a ligand that is either a resident component of the IMM[15], or is recruited to a molecular pattern exposed by the damaged organelles. When NLRP10 is activated with mitochondrially-inactive molecules such as *o*-3M3FBS, SC-9, and (in HEK cells) SC-10, the NLRP10 puncta formation is still observed (Figures 6.51 and 6.54), but these aggregates do not colocalize with the mitochondria (Figures 6.52 and 6.55). Under such conditions, it is not conceivable that NLRP10 could be recruited to an IMM component,

[15] I also base this conclusion on the observation that treatments that exclusively permeabilize the OMM do not activate NLRP10, suggesting that the exposure of the IMS contents and of the outer leaflet of the IMM is not sufficient for the NLRP10 inflammasome activation (Figures 9.1-9.3, 9.7-9.10).

indicating that NLRP10 may also get activated in the absence of mitochondrial membranes permeabilization. Could *o*-3M3FBS, SC-9, and (in HEK cells) SC-10 somehow mimic the downstream events triggered by the mitochondrial rupture without the need for the damage to occur? Theoretically yes, but it is impossible to answer this question without a detailed understanding of the molecular targets of *m*-3M3FBS, *o*-3M3FBS, SC-9, SC-10, thapsigargin, and SMBA1.

At present, none of these NLRP10 activators have well-defined targets. *m*-3M3FBS is marketed as an activator of PLC (Bae et al., 2003), but I have provided substantial evidence that it activates the NLRP10 inflammasome through mitochondrial damage in a PLC-independent manner. Multiple arguments speak against the involvement of PLC in the NLRP10 inflammasome activation and most of them are related to the arguments for why PLC activation does not trigger the AIM2 inflammasome assembly. The PLC inhibitors U 73122 and edelfosine are only weak inhibitors of the *m*-3M3FBS-mediated NLRP10 inflammasome activation (Figure 6.5), overexpression of a hyperactive PLCγ2 variant or of a constitutively active G_q protein does not lead to the NLRP10 inflammasome activation (Supplementary Figure S5), interfering with Ca^{2+} signaling does not inhibit the NLRP10 inflammasome (Figures 6.16 and 6.17), Ca^{2+} fluxes do not activate NLRP10 (Figures 6.18 and 6.35), multiple activators without reported PLC-inducing activity are able to activate NLRP10 (Figures 6.4, 6.14, 6.24, and 6.43), and poly-(dA:dT) transfection, which, in macrophages, is capable of eliciting PLC activation (Figure 5.5 and Supplementary Figure S1) does not activate the NLRP10 inflammasome in this cellular model (Figures 7.7-7.9). *o*-3M3FBS is even more mysterious than *m*-3M3FBS because till now it has solely been used as a PLC-inactive isomer of *m*-3M3FBS (Bae et al., 2003). SC-9 and SC-10 are suggested to act as PKC agonists (Ito et al., 1986) but they activate the NLRP10 inflammasome in a manner not inhibitable by the pan-kinase inhibitor staurosporine (Figure 6.46)[16]. Instead, they likely act through mechanisms similar to *m*-3M3FBS and *o*-3M3FBS, as all four compounds are structurally related (Supplementary Figure S15). Thapsigargin, best known as a SERCA inhibitor, activates the NLRP10 inflammasome through a mechanism independent of SERCA blockade (Supplementary Figure S12) but instead linked to an unidentified mitochondrial target. Finally, SMBA1 is a reported Bax activator binding to the C-

[16] Additionally, two better characterized PKC agonists, PMA and bryostatin 1, are not NLRP10 activators (Figure 6.23).

terminal part of the protein (Xin et al., 2014). Whether Bax is the SMBA1 target engaged in the NLRP10 inflammasome activation is unclear. Two other direct Bax agonists tested, BAM7 (Figure 6.43; Gavathiotis et al., 2012) and BTSA1 (Figure 9.9; Reyna et al., 2017), bind to the N-terminal part of the protein and are incapable of eliciting the NLRP10 inflammasome activation. Induction of MOMP and intrinsic apoptosis with S63845 and ABT263/ABT737 (Vince et al., 2018) is also not a trigger for the NLRP10 inflammasome activation (Figures 9.1-9.3).

Importantly, CsA blocked the thapsigargin- and SMBA1-induced mitochondrial damage in both macrophages (Figures 6.50) and HEK cells (Figure 6.49). This mitoprotective effect correlated with complete inhibition of the AIM2 and NLRP10 inflammasome responses (Figures 6.37 and 6.46). Of note, the thapsigargin-induced AIM2 and NLRP10 activations were also blocked by non-immunosuppressive analogs of CsA: NIM811 and Debio025/alisporivir (Figure 6.38). In contrast, the *m*-3M3FBS- and (in macrophages) SC-10-induced mitochondrial damage could not be prevented by CsA (Figures 6.49 and 6.50), and the AIM2/NLRP10 responses to these stimuli were not inhibited by CsA (Figures 6.37 and 6.46). These observations provide an argument for the involvement of mitochondria during the NLRP10 activation by *m*-3M3FBS, thapsigargin, and SMBA1. However, they do not suggest an explanation for why NLRP10 can also be activated by a set of stimuli that do not inflict mitochondrial damage – *o*-3M3FBS, SC-9, and (in HEK cells) SC-10.

The observation that the SMBA1-induced NLRP10 activation was inhibited by CsA suggests that SMBA1 and thapsigargin could share a common target. There is only one report that thapsigargin could trigger Bax activation (Yamaguchi et al., 2003) and there are no mechanistic reports on the sensitivity of Bax pores to CsA. Therefore, it is very difficult to conclude what this common target could be based on the literature. The potential involvement of Bax could be addressed by inspecting whether thapsigargin/SMBA1 treatments lead to Bax translocation to the mitochondria. Bax-deficient and Bak/Bax double-deficient models could also be employed. In Section 10.6, I will speculate on the possible pathways that might be induced by *m*-3M3FBS, SC-10 (in macrophages), thapsigargin, and SMBA1 to permeabilize the mitochondria. There, I will also outline the possible strategies for target identification of the mitochondria-damaging molecules.

My results provide both arguments for and against the mitochondrial rupture involvement in the NLRP10 activation. The notion that the NLRP10 activation is triggered by mitochondrial damage is supported by the observations that (1) *m*-3M3FBS, SC-10 (in macrophages), thapsigargin, and SMBA1 disrupt the mitochondria, (2) NLRP10 translocates to the mitochondria in HEK cells treated with *m*-3M3FBS, thapsigargin, or SMBA1, (3) CsA blocks both the thapsigargin-/SMBA1-incuced mitochondrial damage and NLRP10 activation but not the *m*-3M3FBS-induced mitochondrial damage and NLRP10 activation, and (4) the non-immunosuppressive CsA analogs NIM811 and Debio025/alisporivir block the inflammasome activation with thapsigargin. The following observations speak against the mitochondrial involvement in the NLRP10 activation: (1) *o*-3M3FBS, SC-9, and (in HEK cells) SC-10 trigger the NLRP10 inflammasome without inflicting mitochondrial damage, and (2) in HEK cells treated with *o*-3M3FBS, SC-9, or SC-10, NLRP10 forms puncta that do not colocalize with the mitochondria.

So far, I have not addressed the possibility that *m*-3M3FBS, *o*-3M3FBS, SC-9, SC-10, thapsigargin, and SMBA1 could all directly bind to NLRP10. This could be tested using biophysical techniques such as isothermal titration calorimetry or surface plasmon resonance; but there are several arguments suggesting that direct binding is not the mechanism by which the NLRP10 activators identified in my Thesis trigger the inflammasome. First, although *m*-3M3FBS, *o*-3M3FBS, SC-9, and SC-10 are all structurally related, thapsigargin and SMBA1 are not similar to them or to each other. Therefore, to enable direct activation, NLRP10 would have to have at least three agonist-binding pockets to accommodate three classes of molecules. Furthermore, agonist binding at each of these sites would have to result in the same conformational change, leading to ASC recruitment and the inflammasome formation. Secondly, the thapsigargin- and SMBA1-induced NLRP10 activation can be inhibited by CsA, but CsA does not inhibit the NLRP10 activation with *m*-3M3FBS, SC-9, and SC-10[17]. If the NLRP10 activation was mediated by direct agonist binding, CsA would have to mask the thapsigargin- and SMBA1-binding pockets, but not the *m*-3M3FBS-binding pocket (in a competitive inhibition scenario), or it would have to engage a fourth binding site, whose occupancy impairs the NLRP10 activation with thapsigargin and SMBA1, but not with *m*-

[17] I did not test whether the *o*-3M3FBS-induced NLRP10 activation could be blocked by CsA.

3M3FBS (in an allosteric inhibition scenario). Thirdly, thapsigargin, *m*-3M3FBS, and SMBA1 all trigger not only mitochondrial rupture and the NLRP10 activation, but also NLRP10 translocation to the mitochondria. Direct binding of the activators to NLRP10 does not explain how this translocation could occur. Finally, the fact that CsA inhibits both the thapsigargin-/SMBA1-elicited mitochondrial damage and the NLRP10 activation by these compounds suggests that these events may be linked.

In conclusion, a definitive answer as to the role of mitochondrial damage in the NLRP10 activation will only become available when the targets of *m*-3M3FBS, *o*-3M3FBS, SC-9, SC-10, thapsigargin, and SMBA1 as well as the cellular ligands of NLRP10 are identified. Based on my observations, the NLRP10 inflammasome can get activated when the mitochondrial matrix contents are exposed to the cytosol, but this requirement for mitochondrial rupture may be circumvented through a mechanism that I did not succeed at identifying.

10.5. NLRP10 as an inflammasome-forming NLRP subfamily member

My thesis provides the first, to my knowledge, description of NLRP10 as an inflammasome-forming member of the NLRP subfamily. I initially identified NLRP10 as a prospective PYD-containing protein mediating ASC speck formation in cells stimulated with *m*-3M3FBS (Figure 6.2). I validated this finding (Figure 6.4), and subsequently identified five more NLRP10 activators: *o*-3M3FBS (Figure 6.4), thapsigargin (Figure 6.14), SC-9, SC-10 (Figure 6.24), and SMBA1 (Figure 6.43). All of these stimuli were capable of inducing NLRP10 colocalization with the inflammasome adaptor ASC (Figure 7.1 and Supplementary Figures S27 and S28). I employed AIM2-deficient macrophages stably transduced with NLRP10 to determine whether the ASC specks assembled by NLRP10 represented functional inflammasomes. In this model, all NLRP10 activators identified in ASC speck formation assays were also capable of eliciting IL-1β release in a manner attributable to NLRP10 (Figures 7.7-7.9). Importantly, this IL-1β response could be blocked by the caspase-1 inhibitor VX-765, providing evidence of caspase-1 involvement (Figure 7.8).

Consistent with the knowledge on the NLRP3-driven inflammasome responses (Duncan et al., 2007), the ability of NLRP10 to trigger inflammasome formation is completely

dependent on the ATPase activity of the NACHT domain, as it was disrupted by mutations in the Walker A and B motifs (Figures 7.3 and 7.7). Of note, Lautz et al. (2012) previously demonstrated that the NLRP10-mediated chemokine (C-X-C motif) ligand 8 (CXCL8) production in a *Shigella* infection model also depends on the intact sequences of the Walker A and B motifs. Importantly, these sequences are completely conserved among the inspected sequences of mammalian NLRP10 orthologs (Figure 7.3). I provide a more detailed commentary on the evolutionary history of NLRP10 in Section 10.7, so here I would like to only highlight that in mammals, NLRP10 is well conserved from platypus[18] to human, although some of the mammalian lineages lost the NLRP10-encoding gene.

Of note, the other cellular factors involved in the NLRP10 activation also appear to be conserved, at least between mouse and human, given that in (human) HEK cells, human NLRP10 responded to all identified NLRP10 activators, and murine NLRP10 responded to *m*-3M3FBS, *o*-3M3FBS, and thapsigargin (Figures 6.4 and 6.14; I did not test the murine NLRP10 responses to SC-9, SC-10, and SMBA1 in this model). Correspondingly, in AIM2-deficient murine macrophages overexpressing NLRP10, both the human and the murine orthologs enabled the responses to all the identified NLRP10 activators (Figures 7.7-7.9).

Full-length NLRP10 protein is required for the inflammasome assembly (Figures 7.2 and 7.7). The NLRP10 NACHT domain (including a short N-terminal linker between the PYD and NACHT domains) is sufficient for the translocation of NLRP10 to the mitochondria upon stimulation with the mitochondria-targeting activator *m*-3M3FBS (Figures 7.5 and 7.6). The NLRP10 PYD domain alone does not translocate to the mitochondria and in contrast to what is reported on the NLRP3 PYD domain (Stutz et al., 2017), it does not spontaneously engage in homotypic interactions (Figures 7.5 and 7.6).

My data indicate that NLRP10, the NLRP subfamily member without the LRR domain, is capable of assembling an ASC speck possessing the typical inflammasome characteristics (caspase-1 recruitment, IL-1β release). The NLRP10 NACHT domain and/or the linker

[18] The nucleotide sequences for platypus NLRP10, which is predicted to be expressed as two isoforms, can be retrieved from the Nucleotide database using the accession numbers XM_029058185.1 and XM_029058186.1 (NCBI Resource Coordinators et al., 2017).

located between the PYD and the NACHT domains is sufficient for the NLRP10 translocation to the mitochondria and aggregation, so it is likely that both the oligomerization and the ligand-binding sites are located in this portion of the protein. Of note, this is not the first report of an NLRP protein without the LRR domain assembling an inflammasome. It has been demonstrated that engineered NLRP3 without the LRR domain can mediate the inflammasome formation in response to the canonical NLRP3 activator nigericin (Hafner-Bratkovič et al., 2018). In contrast to the cited study, my description of NLRP10 is the first instance where an NLRP protein endogenously lacking the LRR domain is shown to assemble an inflammasome.

Finally, my results dispel with the notion that NLRP10 could act as a direct inhibitor of inflammasome formation (Imamura et al., 2010; Murphy et al., 2013; Wang et al., 2004). This idea was likely initially developed because it was 'intuitively plausible' that an NLRP protein without the LRR domain could act in a manner similar to decoy receptors. A crucial structural difference between NLRP10 and typical decoy receptors is that the latter usually lack the signaling domains, not the putative ligand recognition domains, whereas the NLRP10 signaling domains are essentially intact. The experimental evidence behind the hypothesis that NLRP10 is an inflammasome inhibitor is questionable. The first report of the inflammasome-inhibiting properties of NLRP10 proposed that NLRP10 overexpression 'inhibits ASC-mediated NF-κB activation'[19] and demonstrated that IL-1β release resulting from combined overexpression of ASC, pro-caspase-1, and pro-IL-1β in HEK cells (in the absence of an inflammasome sensor molecule and an inflammasome activator) is reduced when NLRP10 is additionally overexpressed (Wang et al., 2004). The problem with the first observation is that 'ASC-mediated NF-κB activation' does not represent a biological phenomenon (ASC is an adaptor protein for inflammasome signaling but does not play a role in the NF-κB activation). The second observation is also difficult to fit into the current model of inflammasome activation because co-expression of ASC, pro-caspase-1, and pro-IL-1β without a sensor protein and in the absence of an inflammasome-activating stimulus is generally not considered to be sufficient to trigger the inflammasome response.

[19] I quote from Wang et al. (2004).

Imamura et al. (2010) reproduced the results reported by Wang et al. (2004) and proceeded to generate NLRP10-transgenic mice with constitutive NLRP10 overexpression. Peritoneal macrophages from these animals exhibited reduced inflammasome responses to *Salmonella* infection and to R837. The NLRP10-transgenic mice were also protected from endotoxic shock after LPS injection. However, ASC speck formation and caspase-1 activation were not directly inhibited, putting into question whether the overexpressed NLRP10 physically interferes with the inflammasome activation. The final paper proposing that NLRP10 is an inflammasome inhibitor does so based on the observation that a pre-treatment of microglia with recombinant NLRP10 protein added to the culture medium (*sic*) abolishes the inflammasome activation in response to LPS and Aβ aggregates[20] (Murphy et al., 2013). Given that NLRP10 is a cytosolic protein, it is not clear why the authors decided to determine its impact on the inflammasome activation by adding NLRP10 to the extracellular medium. The conclusions based on such experimental design are debatable.

In my experimental models, overexpression of NLRP10 in macrophages did not interfere with the NLRP3 responses to nigericin (Figures 7.7-7.9 and 8.4-8.6) and AIM2 responses to poly-(dA:dT) (Figures 8.4 and 8.5). These observations indicate that NLRP10 does not act as an inhibitor of the NLRP3 and AIM2 activations. In contrast, NLRP10 overexpression in macrophages enables robust mtDNA-independent ASC specking and IL-1β responses to *m*-3M3FBS, *o*-3M3FBS, thapsigargin, SC-9, SC-10, and SMBA1 (Figures 6.4, 6.14, 6.24, 6.43, 7.7-7.9, and 8.3-8.6). These results are sufficient to challenge the previous model that NLRP10 is an inhibitory member of the NLRP subfamily. Nevertheless, it would still be interesting to determine why the NLRP10-overexpressing transgenic mice were protected from death induced by LPS injection and why peritoneal macrophages isolated from these animals had decreased inflammasome responses to *Salmonella* and R837 (Imamura et al., 2010). Importantly, NLRP10-deficient animals are not reported to manifest with spontaneous autoimmune or autoinflammatory phenotypes (Nakajima et al., 2018), suggesting that, at least under specific pathogen-free conditions of animal facilities, NLRP10 is not involved in the homeostatic regulation of inflammation.

[20] Aβ aggregates activate the NLRP3 inflammasome in microglia through the lysosomal damage pathway (Halle et al., 2008)

10.6. Mechanisms of mitochondrial damage triggered by the AIM2/NLRP10 activators

A puzzling observation I made in my Thesis research was the rapid leakage of the mitochondrial matrix contents in cells treated with *m*-3M3FBS, SC-10 (in macrophages), thapsigargin, and SMBA1. The leakage of the IMS contents, including cytochrome c (Goldstein et al., 2000; Kluck, 1997; Liu et al., 1996) and the protease HtrA2/OMI (Rogers et al., 2019), is a well-defined feature of intrinsic apoptosis and a secondary event during extrinsic apoptosis. In contrast, there are only two detailed accounts of the exposure of the mitochondrial matrix contents during programmed cell death (McArthur et al., 2018; Riley et al., 2018). McArthur et al. (2018) and Riley et al. (2018) demonstrated that over the course of the intrinsic apoptosis cascade, Bax/Bak pores formed in the OMM allow for the extrusion and – presumably – mechanical rupture of the IMM, leading to the cytosolic release of mitochondrial nucleoids and cGAS/STING activation. The processes and molecular events described by McArthur et al. (2018) and Riley et al. (2018) occur over the course of hours, consistent with the general descriptions of intrinsic apoptosis (Gelles and Chipuk, 2016).

There are two major differences between the observations reported by McArthur et al. (2018) and Riley et al. (2018) and the results presented in my Thesis. First, I observed a very fast onset of mitochondrial damage (within 5 min of the administration of the stimuli; Figures 6.27 and 6.28). The leakage of the mitochondrial matrix contents was essentially complete within 10 min of the stimulus administration. Similarly, the AIM2-mediated macrophage ASC speck formation elicited by *m*-3M3FBS and thapsigargin occurred within the first 10 min of the stimulus administration (Figure 6.28), indicating that this period was sufficient for mtDNA exposure. Secondly, the types of stimuli applied by McArthur et al. (2018) and Riley et al. (2018) to permeabilize the mitochondria (combination of a genetic or pharmacological inactivation of MCL-1 with ABT-737, a pan-BCL-2 family inhibitor) did not appear to selectively activate the AIM2 and NLRP10 inflammasomes in my experimental models (Section 9.1). These discrepancies suggest that intrinsic apoptotic stimuli and *m*-3M3FBS/thapsigargin elicit the mitochondrial disruption through distinct mechanisms.

Importantly, McArthur et al. (2018) and Riley et al. (2018) used mtDNA staining to visualize permeabilization of the mitochondrial membranes, whereas I employed tracking of fluorescent proteins targeted to the mitochondrial matrix. Future experiments could establish how the outcomes of these two readouts compare between cells treated with intrinsic apoptotic stimuli and those treated with AIM2/NLRP10 activators. If an additional marker of the IMS is used (cytochrome c or HtrA2/OMI), more insight could be gained into which submitochondrial compartments are affected by these treatments. The possible outcomes of the OMM and IMM permeabilization are outlined in Scheme 10.1. Determining which areas within the mitochondria are targeted by AIM2/NLRP10 activators could provide hints as to how exactly they damage these organelles.

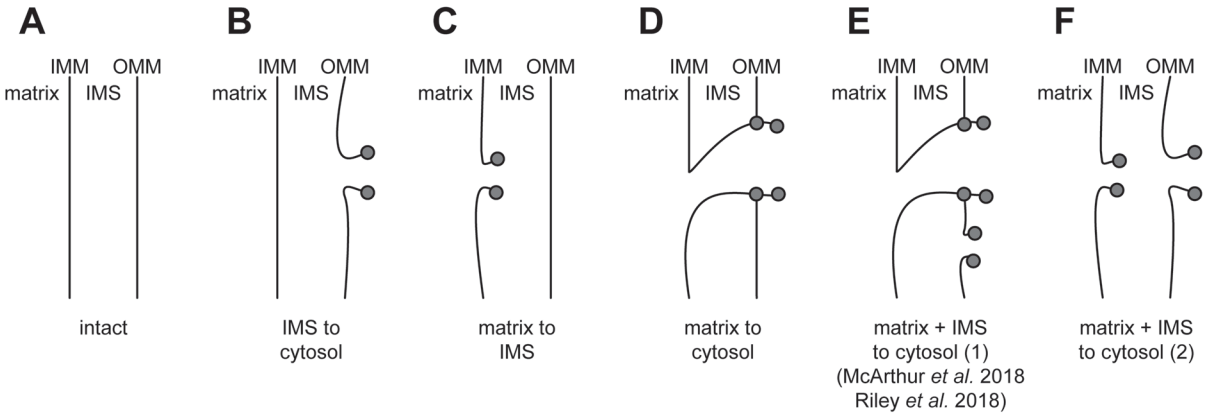

Scheme 10.1. The possible topologies of mitochondrial membranes permeabilization
The scheme presents the possible ways in which the mitochondrial membranes could be permeabilized.
A: Both the inner mitochondrial membrane (IMM) and the outer mitochondrial membrane (OMM) are intact. The contents of the intermembrane space (IMS) are separated from the cytosol and from the mitochondrial matrix.
B: Permeabilization of the OMM: the contents of the IMS and the cytosol may mix.
C: Permeabilization of the IMM: the contents of the IMS and the mitochondrial matrix may mix.
D: Hypothetical permeabilization of the IMM through extrusion of the IMM folds through pores in the OMM. In this scenario, the contents of the mitochondrial matrix and the cytosol may mix, but the contents of the IMS remain sealed between the IMM and the OMM.
E: Permeabilization of the OMM coincidental with permeabilization of the IMM through extrusion of the IMM folds through pores in the OMM. The mitochondrial matrix and IMS context may mix with the cytosol and with each other. This mitochondrial membranes permeabilization scenario was described by McArthur et al. (2018) and Riley et al. (2018).
F: Pore-mediated permeabilizations of both the IMM and the OMM. The mitochondrial matrix and IMS context may mix with the cytosol and with each other.

Collectively, my observations suggested that *m*-3M3FBS, SC-10 (in macrophages), thapsigargin, and SMBA1 might engage previously unidentified factors to cause mitochondrial damage. Furthermore, given the pharmacological differences between the AIM2/NLRP10 activators (Figures 6.37, 6.38, 6.49, and 6.50), *m*-3M3FBS and SC-10 (in

macrophages) might act through a different mechanism than do thapsigargin and SMBA1.

I considered two non-mutually exclusive scenarios of how the observed mitochondrial damage could occur. First, high-diameter protein-lined pores could open in the inner and/or outer mitochondrial membranes, allowing for the exposure of the mitochondrial contents to the cytosol. Secondly, osmotic pressure could build up in the mitochondrial matrix, leading to organelle rupture and free diffusion of the soluble mitochondrial contents into the cytosol. The second scenario is particularly attractive because it provides explanations for both the fast rate and the apparent lack of selectivity of the mitochondrial permeabilization by AIM2/NLRP10 activators. The arguments against it are (1) that it is not likely that any cellular solute has a concentration gradient across the IMM steep enough to account for the observed mitochondrial rupture, and (2) that my attempts to modify the ionic compositions of the extracellular milieu had absolutely no influence on the inflammasome activations with *m*-3M3FBS and thapsigargin (Figures 4.4 and 6.6, and Section 9.4).

Could the AIM2/NLRP10 activators engage previously described mechanisms of mitochondrial damage, but with a more dramatic outcome? I attempted to answer this question in Chapter 9 and found no evidence that the 'mitochondrial cell death' and mitochondrial stress pathways could share common steps with the damage inflicted by *m*-3M3FBS and thapsigargin. Importantly, this lack of evidence does not mean that common steps cannot be shared. To test whether any intracellular pore-forming proteins mediate the effects of the *m*-3M3FBS/thapsigargin administration, the following targets could be genetically inactivated: Bak, Bax[21], Bok, Gsdm family members (in spite of the fact that overexpression of the GsdmD/E N-terminal domains was not sufficient to elicit the NLRP10 inflammasome activation; Figures 9.7-9.8.2), VDAC isoforms (despite the fact that high concentrations of the VDAC blocker VBIT-4 appeared to cause inflammasome activation; Figures 9.18 and 9.19), MLKL, subunits of the TOM and TIM complexes, or even subunits of ATP synthase. Alternatively, broader and more unbiased chemical biology techniques could be applied to identify the *m*-3M3FBS and thapsigargin targets. For example, a library of mutant cells could be

[21] Bak/Bax double-deficient model could also be tested, as it is believed that these two proteins have at least partially redundant functions (Bock and Tait, 2019).

generated and challenged with *m*-3M3FBS/thapsigargin to select resistant mutants based on differential survival (Brammeld et al., 2017; Lin and Sheltzer, 2020; Lin et al., 2019). Considering that most of the identified AIM2/NLRP10 activators have multiple off-target effects and are toxic to the cells, such screen would likely be difficult to set up. The need to develop a cell-based assay could be circumvented by proteomic methods for identification of binding partners of LMW compounds in cell lysates (Franken et al., 2015).

Of note, I selected a number of cell death and cellular damage response pathways and tested whether there are any indications of their involvement in the AIM2/NLRP10 activations. Activation of caspases does not seem to be the mediator of the *m*-3M3FBS and thapsigargin effects as the pan-caspase inhibitors emricasan (Supplementary Figure S41) and Q-Vd-OPh (Supplementary Figure S42 A-C), the caspase-2[22] inhibitor ICH-1 (Supplementary Figure S42 G-I), and the caspase-8 inhibitor Z-IETD-FMK (Supplementary Figure S42 D-F) did not block the inflammasome responses to the AIM2/NLRP10 activators. Furthermore, the necroptosis inhibitors necrostatin-1 (Supplementary Figure S43 A-C) and necrosulfonamide (Supplementary Figure S43 D-F) as well as the lytic cell death inhibitor glycine (Supplementary Figures S43 G-I and S44) also did not inhibit the AIM2/NLRP10 activations, suggesting that programmed cell death pathways are not engaged in this process. One study proposed that Bid cleavage resulting from accumulation of unfolded proteins could serve as a trigger for activation of the AIM2 and NLRP3 inflammasomes (Liao et al., 2019) but the chemical chaperone 4-phenylbutyrate (Supplementary Figure S45 A-C) and the tBid inhibitor BI-6C9 (Supplementary Figure S45 D-F) did not block the inflammasome responses to *m*-3M3FBS and thapsigargin in the experimental models employed in my Thesis.

The ISR has been implicated in the inflammasome activation through mechanisms linked to the PKR kinase (Lu et al., 2012) and the kinase HRI (Abdel-Nour et al., 2019). However, in my experimental models, LMW inhibitors of the ISR kinases did not have a consistent impact on the AIM2 and NLRP10 activations. The GCN2 inhibitor A-92 (Supplementary Figure S46 A-D) and the PKR inhibitor C16 (Supplementary Figure S46 E-H) did not inhibit the inflammasome responses to *m*-3M3FBS and thapsigargin. The

[22] Caspase-2 was previously implicated in mitochondrial damage, including the cytosolic leakage of mtDNA, in a model of NLRP3 activation during *Brucella abortus* infection (Bronner et al., 2015).

PERK inhibitor AMG PERK 44 led to an uninterpretable phenotype in cells treated with the AIM2/NLRP10 activators (Supplementary Figure S47 A-D), whereas another PERK inhibitor, GSK2606414, selectively blocked the NLRP10 activation with thapsigargin, but not the AIM2 response to the same treatment (Supplementary Figure S47 E-H).

Serum and glucocorticoid-regulated kinases (SGKs) have also been suggested to be involved in multiple stress responses (Lang et al., 2018) but the SGK inhibitors CkI 7 (Supplementary Figure S48 A-C) and GSK650394 (Supplementary Figure S48 D-F) did not have an impact on the AIM2/NLRP10 inflammasome responses. Combined with the observation that the pan-kinase inhibitor staurosporine was generally incapable of blocking the AIM2 and NLRP10 activations (Figures 6.19, 6.45, and 6.46), it is unlikely that the ISR kinases and SGKs could be engaged by *m*-3M3FBS and thapsigargin.

I invested a significant effort into determining whether the mPTP opening could contribute to the AIM2/NLRP10 activations. This investigation did not yield a definitive answer, partially because of the poorly defined molecular composition and pharmacological characteristics of mPTP. The overall evidence suggested that the mPTP opening is not involved in the inflammasome responses to *m*-3M3FBS and thapsigargin (Section 9.6). I attempted to gain further insight into the influence of mitoprotective as well as mitochondria-disrupting treatments on the AIM2 and NLRP10 inflammasome responses, hoping that such results could suggest the potential mechanisms of action of *m*-3M3FBS and thapsigargin. The mitochondrial fragmentation inhibitor Mdivi-1 (Supplementary Figure S49 A-C), the mitoprotective agent PF543 (Supplementary Figure S49 D-F), idebenone, a coenzyme Q mimic that inhibits the NLRP3 activation with R837 (Groß et al., 2016; Supplementary Figure S50), and two compounds suggested to possess a mitoprotective activity, diazoxide (Supplementary Figure S51 A-D), and metformin (Supplementary Figure S51 E-G) were all neither consistent nor selective inhibitors of the *m*-3M3FBS-/thapsigargin- induced inflammasome activations. Mitochondria-disrupting agents such as the mtROS inducers Bz-423 (Supplementary Figures S52 A-C and S53) and auranofin (Supplementary Figures S52 D-F and S53) did not have a selective impact on the inflammasome responses to the tested activators; auranofin appeared to act as a pan-inflammasome inhibitor. Lonidamine, a cytostatic compound that likely acts through limiting the metabolite flux to the mitochondria, also did not inhibit the AIM2/NLRP10 activations with *m*-3M3FBS/thapsigargin

(Supplementary Figure S54). Collectively, neither my main line of research nor the follow-up experiments provided reliable evidence for the involvement of previously described mitochondrial damage pathways in the AIM2 and NLRP10 inflammasome responses.

As *m*-3M3FBS was proposed to induce localization changes of the ezrin/radixin/moesin family proteins (Hao et al., 2009), I tested whether the ezrin inhibitor NSC668394 would have an impact on the AIM2/NLRP10 responses (Supplementary Figure S55). NSC668394 did not affect the inflammasome activations by *m*-3M3FBS and thapsigargin, whereas it inhibited the NLRP3 response to nigericin (Supplementary Figure S55 A, B). Finally, I examined whether pathways broadly implicated in the regulation of other inflammasomes could explain the activity of *m*-3M3FBS and thapsigargin. The autophagy inhibitor 3-methyladenine (Supplementary Figure S56), the microtubule polymerization inhibitor colchicine (Supplementary Figure S57), and hyperosmotic shock caused by high NaCl concentrations (Supplementary Figure S58) did not selectively or consistently inhibit the AIM2/NLRP10 inflammasome responses. Lower concentrations of the PKD inhibitor CRT0066101 selectively blocked the NLRP3 inflammasome activation, consistent with a previous report (Zhang et al., 2017), and at higher concentrations, CRT0066101 had a pan-inflammasome inhibitory effect[23] (Supplementary Figure S59 A-C). The Akt activator SC79 was a pan-inflammasome inhibitor (Supplementary Figure S59 D-G).

My extensive comparison of the AIM2/NLRP10 activation-triggering mitochondrial damage to previously described pathways did not allow for the identification of the mechanisms of action of *m*-3M3FBS, SC-10, thapsigargin, and SMBA1. I have proposed that *m*-3M3FBS and SC-10 could act through the same target based on their structural similarity. It is also likely that thapsigargin and SMBA1 share a common target, as the mitochondrial damage and inflammasome activation triggered by these molecules can be inhibited with CsA. In the future, genetic inactivation of prospective targets as well as more unbiased chemical biology approaches could help establish how the AIM2/NLRP10 activators disrupt the mitochondria.

[23] High concentrations of CRT0066101 also appeared to be autofluorescent in the ASC speck detection channel.

10.7. Hypotheses on the physiological and pathological processes involving NLRP10

Are there any physiological processes in which NLRP10 is involved? This is a big question and it may be worth to break it down into smaller steps that can be experimentally addressed:

1. In which organs and cell types is NLRP10 constitutively expressed? Based on the literature, NLRP10 is mainly expressed in the skin (Damm et al., 2016; Lachner et al., 2017; Lautz et al., 2012; Nakajima et al., 2018) and in the heart (Joly et al., 2012; Vacca et al., 2017; Wang et al., 2004), whereas the myeloid cell expression levels are low.

2. Are there any examples of inducible expression of NLRP10? To my knowledge, the only such instance reported in the literature is the increase in the NLRP10 level in bone marrow-derived dendritic cells stimulated with the TLR9 ligand CpG (Vacca et al., 2017).

3. Are there any patients with mutations in the NLRP10-encoding gene? Observation of such patients could help link their phenotype to the processes in which NLRP10 plays a role. Till now, mutations in the NLRP10 locus have only been associated with an increased risk of developing atopic dermatitis in a Japanese cohort (Hirota et al., 2012) but no mechanistic links have been proposed.

4. What are the phenotypes of NLRP10-deficient mice? This question has already been addressed in the context of sterile damage (Damm et al., 2016), infection (Clay et al., 2017), and the general characteristics of the immune responses (Nakajima et al., 2018; Vacca et al., 2017) but areas such as aging or cardiovascular health have not been investigated.

5. Can any insights about NLRP10 be gained by tracking its evolutionary history? I have already brought up the high conservation of the NLRP10 Walker A and B

motifs while Lachner et al. (2017) identified several mammalian lineages that lost the NLRP10-encoding gene over the course of evolution.

Answering the questions above in more detail may help selecting cellular and animal models in which to test the potential function of NLRP10 in the future. The results presented in my Thesis may provide further inspiration as to the possible processes in which NLRP10 plays a role. Cardiac homeostasis and disorders are a particularly attractive point of focus in this respect, as NLRP10 is expressed in the heart and the high energy demand of cardiomyocytes is supplied by a system of mitochondria that takes up 25-30% of their total cell volume (Brown et al., 2016). There are reports of mitochondrial disruption and cardiac inflammation during coxsackievirus B3 infection (Lin et al., 2017; Wei et al., 2014). mPTP opening and mitochondrial damage have also been implicated in the myocardial ischemia/reperfusion injury. Based on this hypothesis, CsA, which inhibits the thapsigargin-induced NLRP10 activation in my models (Figure 6.37), has been tested in clinical trials to target myocardial infarction (Chiari et al., 2014; Cung et al., 2015; Ghaffari et al., 2013; Hausenloy et al., 2014; Mewton et al., 2010; Piot et al., 2008). The results of these studies were not encouraging but it is important to point out that – considering my observation that most of the reported mPTP blockers did not prevent the NLRP10 activation by thapsigargin and essentially none could inhibit the NLRP10 activation with *m*-3M3FBS (Section 9.6) – the properties of mPTP are still not very well understood. My data provide two insights into the process of mitochondrial rupture that could be relevant here. First, I observed two pharmacologically distinguishable modes of mitochondrial disruption in cells treated with the mitochondria-targeting NLRP10 agonists: the damage induced by thapsigargin and SMBA1 could be inhibited by CsA, whereas the damage inflicted by *m*-3M3FBS and (in macrophages) SC-10 was not sensitive to CsA (Figures 6.49 and 6.50). If the *m*-3M3FBS-elicited mitochondrial rupture represents a mechanism that could also be triggered *in vivo*, possibly both the CsA-sensitive and the CsA-unresponsive arms of mitochondrial damage would have to be targeted to achieve reliable mitoprotection. Secondly, if NLRP10 were to be activated during myocardial infarction, it would suggest that this condition could potentially be targeted with NLRP10[24] and caspase-1 inhibitors, or even with the IL-1 family scavengers/antagonists.

[24] Direct NLRP10 inhibitors are not yet available but the fact that NLRP3 can be efficiently targeted by LMW compounds that bind to the NACHT domain (Coll et al., 2015; 2019; Tapia-Abellán et al., 2019;

Speculating on the potential involvement of NLRP10 in cardiac ischemia/reperfusion damage may be futile but it would be interesting to examine the outcomes of a myocardial infarction model in NLRP10-deficient mice compared to WT animals. Of note, I performed a series of preliminary experiments to determine whether chemically-induced hypoxia (triggered by $CoCl_2$; Supplementary Figures S60-S62; Muñoz Sánchez and Chánez Cárdenas, 2018) or ischemia-reperfusion (triggered by incubation with NaN_3 followed by a series of washes; Supplementary Figure S63) could elicit the AIM2/NLRP10 activation. My observations did not provide any indication that this could be the case.

NLRP10 is also proposed to be involved in skin diseases. In this respect, it has been identified as a susceptibility locus for atopic dermatitis in a Japanese cohort (Hirota et al., 2012). Two *in vivo* mouse models demonstrated a role for NLRP10 in cutaneous immunological events. NLRP10 deficiency was protective in a chemical-induced model of contact hypersensitivity, which was likely linked to a cell-autonomous NLRP10 function in keratinocytes (Damm et al., 2016). In a cutaneous leishmaniasis model, NLRP10 expression was protective, as NLRP10-deficient mice were unable to contain the infection (Clay et al., 2017).

***

Can any insights into the role of NLRP10 be gained from an analysis of the NLRP10 evolutionary history? I will focus here on mammalian NLRP10. In mammals, the gene encoding this protein can be considered fairly ancient, as NLRP10 orthologs have been identified in the platypus[25] (Duéñez-Guzmán and Haig, 2014). According to the Nucleotide database (accession numbers XM_029058185.1 and XM_029058186.1; NCBI Resource Coordinators et al., 2017), there are two isoforms of platypus NLRP10, the longer of which is 698-amino-acid-long (as a comparison, murine NLRP10 is 673-amino-acid-long, and human NLRP10 is 655-amino-acid-long), indicating that the loss of the

Vande Walle et al., 2019) indicates that development of direct inhibitors of the NLRP subfamily proteins is possible.

[25] Of note, according to Duéñez-Guzmán and Haig (2014), there are five genes encoding NLRP subfamily members in the platypus genome, which are orthologs of human NLRP3, NLRP6, NLRP10 (two copies), and NLRP12. This may represent the prototypic set of mammalian NLRP proteins but it is also possible that platypuses lost other NLRP-encoding genes over the course of evolution. To complete the picture, there is no AIM2 ortholog in the platypus genome according to the Ensembl database (Yates et al., 2019).

NLRP10 LRR domain occurred very early in mammalian evolution. Importantly, both the Walker A motif lysine residue and the Walker B motif aspartic acid residue are conserved between the platypus, mouse, and human proteins. Other regions of the NLRP10 protein sequence are not equally strongly conserved. For example, exon 2 of the human NLRP10-encoding gene is ~2.7 kb shorter than the corresponding region in the chimpanzee gene (Ha et al., 2009). As can be seen throughout my thesis, this deletion does not affect the NLRP10 capacity for inflammasome formation, whereas experimentally introduced mutations in the conserved Walker A and B motifs completely abolish the NLRP10 inflammasome responses (Figures 7.3 and 7.7).

The genes encoding the NLRP subfamily proteins are products of several rounds of duplications, starting with the ancestral NLRP gene, after which the NLRP paralogs were passed down to later generations (a simplified scenario for one such duplication round is presented in Scheme 10.2 A). As speciation progressed, it can be assumed that the NLRP orthologs were evolving independently between species (that is, the mutations accumulating in an ortholog from species 1 were not passed to species 2). Based on the comparison of mammalian NLRP10 protein sequences (Figure 7.3 A), it appears that there was a pressure against mutations in the Walker A and B motifs that would interfere with the NLRP10 inflammasome-forming properties. I made this conclusion based on the following reasoning. Genetic mutations are random, so they occur at equal rates along the NLRP10-encoding gene. However, in part due to phenotypic differences between mutation-bearing individuals, the random mutations are not passed down to the progeny with equal success: many mutations are neutral, some are deleterious, and few – beneficial. When comparing the protein sequences of an ortholog between several species (Scheme 10.2 B), the frequency of mutations at a given amino acid position can be assessed; the lower this frequency, the more conserved a given residue. If the frequency of mutations does not change with the position of the amino acid residue in the polypeptide chain, it either suggests that there was no pressure to conserve this sequence (uniformly high mutation frequency), or that the pressure was extremely high (uniformly low mutation frequency). If a particular residue at a particular position is essential for the protein function, the mutation frequency at this position will likely be lower than in the neighboring regions, manifesting as dips in the plot of mutation frequency *versus* amino acid position. Finally, there is the hypothetical option where the

selection pressure favors variation at a given position, which would manifest as peaks in the plot[26].

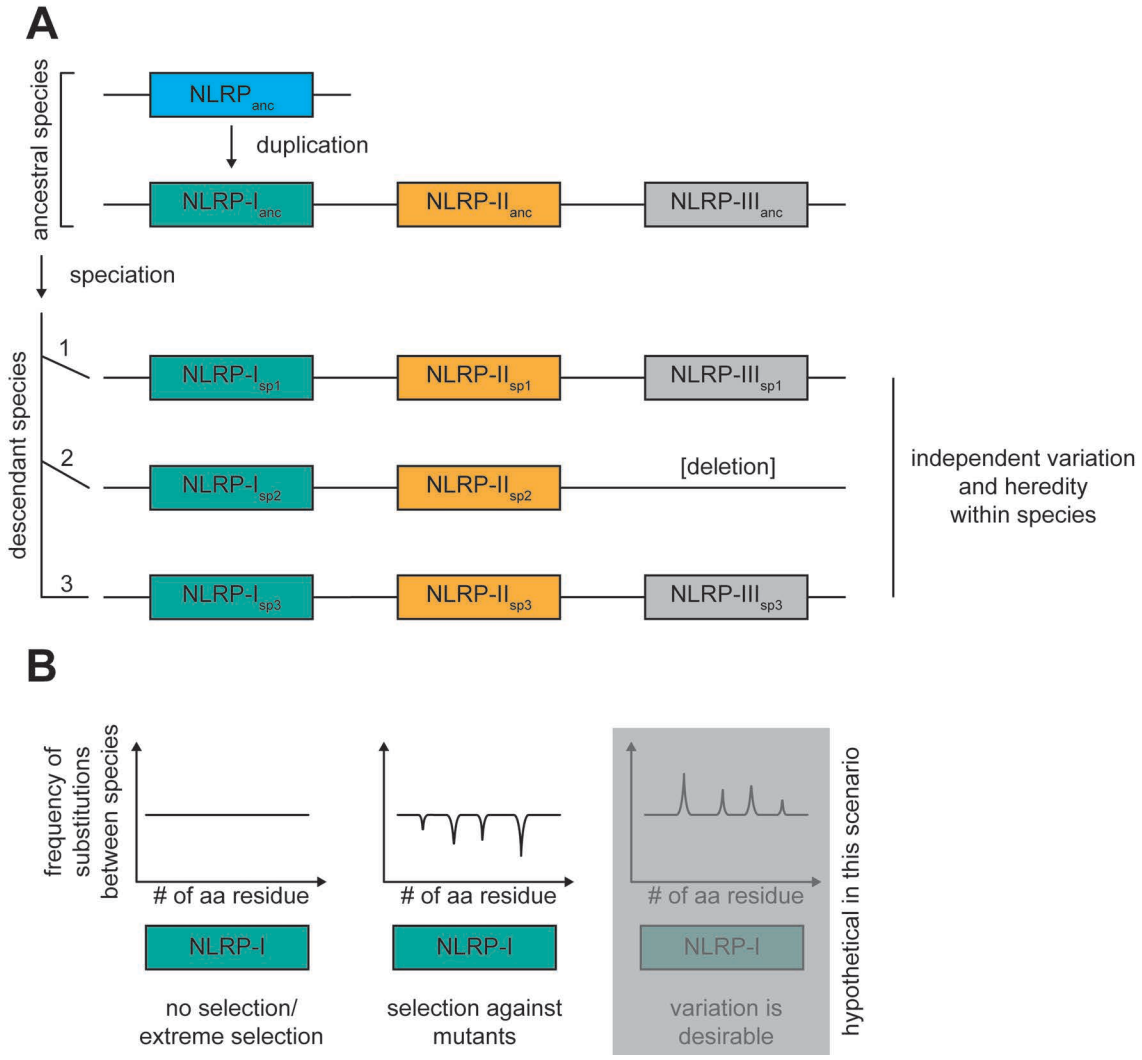

Scheme 10.2. The evolutionary history of a hypothetical member of the NLRP subfamily
A: Duplications of a founding member of the NLRP subfamily ($NLRP_{anc}$) in an ancestral species, leading to three NLRP paralogs ($NLRP\text{-}I_{anc}$, $NLRP\text{-}II_{anc}$, and $NLRP\text{-}III_{anc}$), followed by independent evolution of the NLRP subfamily in descendant species (sp1, sp2, sp3). Point mutations, deletions (middle line), or further duplications (not shown) may occur.
B: Comparison of the amino acid sequences of NLRP-I orthologs between descendant species. The plots indicate the frequency of substitutions as a function of the amino acid position in the polypeptide chain. No pressure to conserve amino acid residues would result in a stochastic accumulation of mutations and an approximately uniform, relatively high rate of substitutions along the polypeptide sequence. Similarly, extremely high pressure for amino acid residues conservation would result in an approximately uniform, very low rate of substitutions along the polypeptide sequence (**left**). When certain regions of the polypeptide sequence are functionally important and their activity is dependent on the chemical and/or physical properties of the amino acid residues at the given positions (for example, coordination of metal ions, involvement in a post-translational modification, participation in the catalytic center of an enzyme), there may be a selection pressure to conserve such sequences (**center**). In cases where variation in the amino acid sequence is desirable (for example for greater diversity in antigen binding), sites with elevated substitution rates compared to the neighboring regions may be observed (**right**).

[26] Such variation-enriched sequences *within* an *individual* are the complementarity-determining regions of T-cell receptors and B cell-receptors/antibodies, and *within* a *species* this type of variability can also be observed in the amino acid sequences of MHC class I and II molecules.

Of note, I do not wish to claim that NLRP10 is essential for survival of mammals. In fact, there are several mammalian lineages that have lost the NLRP10-encoding gene. Such deletions occurred in the ancestor of armadillos[27] as well as during speciation of ungulates (Lachner et al., 2017). According to the Ensembl database (Yates et al., 2019), the species closest to human that have lost NLRP10 are orangutan and vervet monkey. The existence of these deletions indicates that there are mechanisms robustly compensating for NLRP10 deficiency. At the same time, it would be wrong to assume that the NLRP10 losses had had an adaptive value. At least some of them were probably a result of genetic drift and not natural selection.

Combining the evolutionary history of mammalian NLRP10 and the data presented in my thesis, it appears that the regions of NLRP10 required for inflammasome activation are conserved between species that did not lose the NLRP10-encoding gene. While this observation is suggestive that the capacity to assemble the NLRP10 inflammasome, possibly in response to mitochondrial damage, is more beneficial than lack thereof, it is not a proof that NLRP10 forms inflammasomes *in vivo* and it cannot replace further experimentation.

10.8. Conclusions and implications

The findings reported in my Thesis contribute to three fields of research. With respect to signaling biochemistry, I described an off-target effect of the reported PLC agonist *m*-3M3FBS, which may have significant consequences for the interpretation of earlier studies as well as for planning future research. *m*-3M3FBS, in a manner independent of its activity on PLC, disrupts the integrity of the mitochondria, leading to the cytosolic leakage of the soluble components of the mitochondrial matrix and to the exposure of the mitochondrial contents. I identified three more molecules triggering a similar type of damage: SC-10 (originally described as a PKC agonist; the mitochondrial activity has, to

[27] The loss of NLRP10 in armadillos may be interesting from the perspective of infection biology. These animals are vectors for *Mycobacterium* (*M.*) *leprae*, the causative agent of leprosy (Balamayooran et al., 2015; Oliveira et al., 2019; Sharma et al., 2012). The reason why armadillos develop a systemic infection with *M. leprae* is probably their low body temperature (~34°C), which is optimal for *M. leprae* growth, and not the NLRP10 deletion. Nevertheless, it might be worth testing whether *M. leprae*, an intracellular pathogen, could activate the NLRP10 inflammasome. In a zebrafish infection model, *M. leprae* has been shown to cause swelling and/or loss of mitochondria (Madigan et al., 2017). Furthermore, single nucleotide polymorphisms in genes encoding PINK1 and PARL, two proteins involved in mitochondrial homeostasis, were reported to be associated with leprosy risk in a Han Chinese cohort (Wang et al., 2016).

my knowledge, never been reported), thapsigargin (previously implicated in mitochondrial damage), and SMBA1 (a Bax agonist, which is expected to permeabilize the OMM but has not yet been shown to cause a leakage of the mitochondrial matrix contents).

Regarding the research on the mitochondrial stress responses, I provided a description and partial characterization of an acute damage pathway that leads to the cytosolic exposure of the mitochondrial matrix contents within minutes of the initiation of the process. I did not find other reports of a similar type of damage in the literature and I was unable to determine whether the process I observed is a variant of an already known mechanism of mitochondrial disruption or a novel type of mitochondrial stress response.

Finally, I contributed to the inflammasome research by simplifying the current model of the NLRP3 activation, by providing the evidence of a direct activation of AIM2 by mtDNA, and by characterizing NLRP10 as a novel inflammasome-forming NLRP subfamily member. I demonstrated that PLC activation is neither necessary nor sufficient for the NLRP3 inflammasome assembly in murine macrophages. I also provided the evidence that in this cell type, the cytosolic exposure of mtDNA leads to the AIM2, not NLRP3, inflammasome activation. Conversely, the NLRP3 inflammasome responses were not dependent on mtDNA. My work provides the second, after the study by Dang et al. (2017), dataset demonstrating cell-autonomous activation of AIM2 by endogenous mtDNA exposed to the cytosol. It is also the first report to identify *m*-3M3FBS, as well as SC-10, thapsigargin, and SMBA1 to be AIM2 activators. The revised molecular model of the AIM2 and NLRP3 activations in murine macrophages is proposed in Scheme 10.3.

In parallel to my work on the mechanisms of the AIM2 and NLRP3 activations, I described a new inflammasome-forming sensor – NLRP10. Collectively, I identified six NLRP10-triggering stimuli: *m*-3M3FBS, *o*-3M3FBS, SC-9, SC-10, thapsigargin, and SMBA1. My observations challenge the view that this protein is an inhibitor of inflammasome activation. Instead, NLRP10 can assemble a functional inflammasome, both in response to mitochondrial damage and the cytosolic exposure of the

mitochondrial matrix contents and in cells stimulated with the mitochondrially inactive NLRP10 activators.

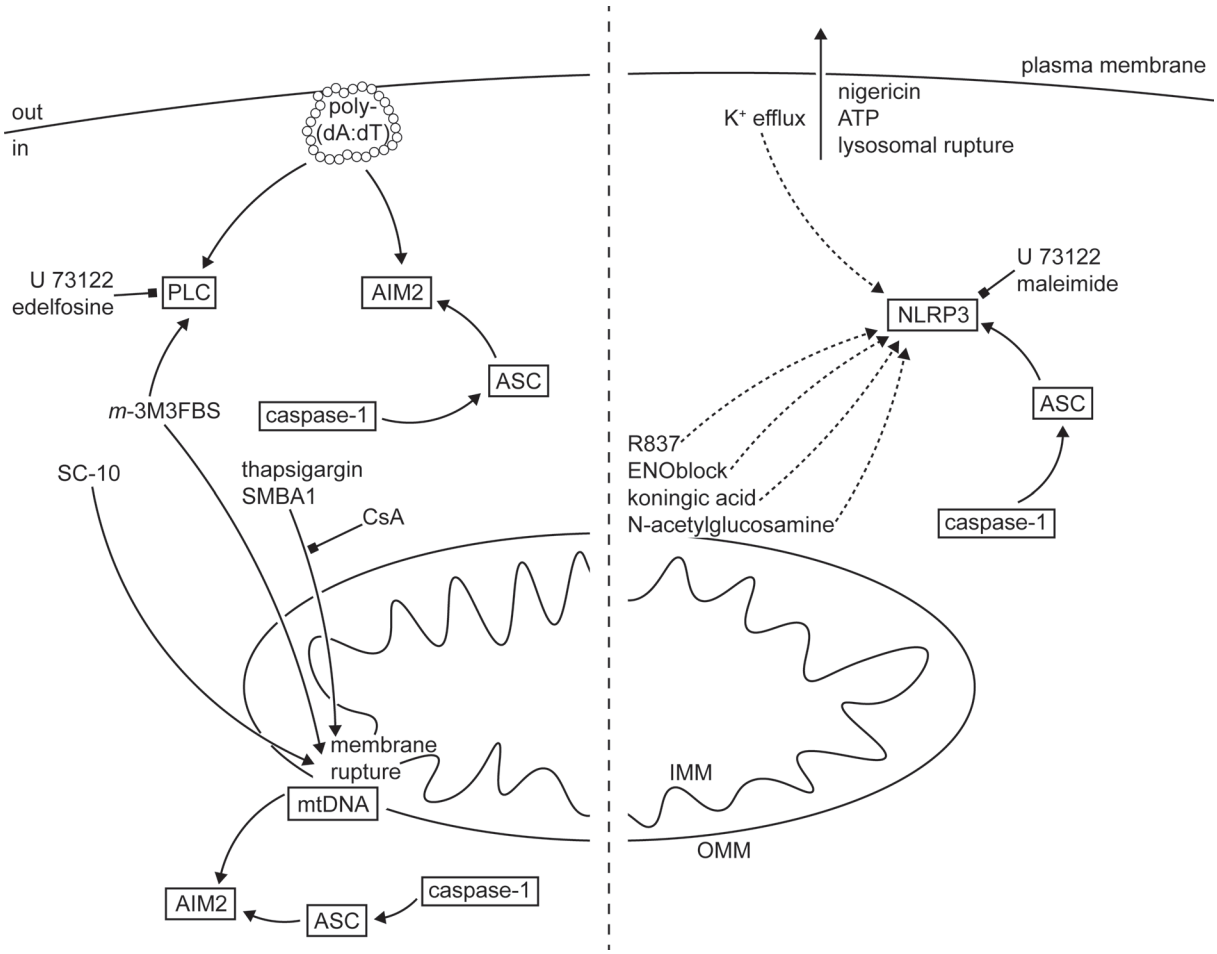

Scheme 10.3. A revised molecular model of the activation mechanisms of the AIM2 and NLRP3 inflammasomes
Based on my Thesis research, the models for both the AIM2 and the NLRP3 activation can be updated.
Left: Transfection-mediated delivery of the AIM2 ligand poly-(dA:dT) leads to AIM2 activation through direct binding, but also elicits phospholipase C (PLC) activation through an unrelated mechanism. Administration of *m*-3M3FBS, SC-10, thapsigargin, or SMBA1 triggers mitochondrial rupture and exposure of mtDNA to the cytosol, enabling AIM2 activation by this endogenous ligand. The *m*-3M3FBS-induced mitochondrial membrane permeabilization and AIM2 activation do not rely on PLC activation.
Right: K^+ efflux-inducing stimuli such as nigericin, ATP, and lysosomal damage trigger NLRP3 activation in a manner independent of mtDNA and of PLC. NLRP3 activation is inhibited by the PLC inhibitor U 73122 through an off-target effect that can be mimicked by the administration of maleimide, the active moiety of U 73122 that does not target PLC. Several NLRP3 activators (R837, ENOblock, koningic acid, and N-acetylglucosamine) directly target the mitochondria. R837 activates NLRP3 in a manner independent of mtDNA, whereas the mtDNA-dependence of ENOblock, koningic acid, and N-acetylglucosamine has not been experimentally addressed.

I believe that my data are relevant for all three fields outlined above. In the area of cell signaling, my work highlights the necessity to develop better tools to target PLC to study physiological processes. Importantly, concerns have already been raised about the

quality of U 73122 (Horowitz et al., 2005; Maucher et al., 2017) and *m*-3M3FBS (Dwyer et al., 2010; Horowitz et al., 2005; Krjukova et al., 2004) as pharmacological tools for PLC targeting. In certain cases, this issue can be solved by selectively activating signaling pathways upstream of PLC such as G_q-coupled GPCRs or receptor tyrosine kinases. Correspondingly, selective genetic targeting of individual PLC isoforms is also possible. For broader questions – such as the inflammasome activation – the availability of low-toxicity PLC inhibitors without promiscuous off-target effects could help address the existing discrepancies.

My observations on the characteristics of the mitochondrial damage triggered by *m*-3M3FBS, SC-10, thapsigargin, and SMBA1 serve as an example that 'mitochondrial stress' may encompass multiple types of organelle disruption and consequently trigger different types of responses in the cell. Which pathway is engaged likely depends on the specific characteristics of the stressor, for example the ability to cause OMM/IMM permeabilization, the type of molecules to which a membrane becomes permeable, the maintenance or loss of the mitochondrial $\Delta\Psi$, and the generation or absence of mtROS.

I discovered that, at least *in vitro*, there exists a mechanism allowing for rapid permeabilization of the IMM and resulting in the cytosolic exposure of the mitochondrial matrix contents. How this process is mediated and whether it has further significance *in vitro* (beyond serving as a tool for dissecting the inflammasome activation pathways) or *in vivo* (as a physiological/pathophysiological mechanism or as a potential trojan horse to destroy the mitochondria in tumor cells or in autoreactive lymphocytes) may be questions for future research.

In the area of inflammasome studies, my results provide explanations for several previous discrepant observations and re-route the currently proposed map of inflammasome activation. My findings on the NLRP3 activation mechanism allow for the removal of two factors (PLC and mtDNA) from the current model of the NLRP3 inflammasome assembly. As NLRP3 is emerging as a therapeutic target (Mangan et al., 2018; Swanson et al., 2019), these results may have far-reaching implications. This is true both for the presumably monogenic disease APLAID, in which patients with the hyperactive PLCγ2 variant suffer from symptoms of autoinflammation, and for other, complex diseases involving the activation of PLC-linked pathways and/or sensing of

mtDNA. Aberrant PLC activation may not be an indication of NLRP3 involvement and when mitochondrial damage is observed, the potential involvement of AIM2 ought to be considered. Possibly, adjustments need to be made when comparing the results from the murine and human systems, as there is evidence that in certain human cell types the DNA-induced inflammasome response is NLRP3-dependent and does not involve AIM2 (Gaidt et al., 2017).

Finally, it is possible that the discovery of the NLRP10 inflammasome-forming capacity will help explain certain phenotypes, both in laboratory animals and in humans, where severe mitochondrial damage is linked to inflammation and/or cell death. I did not address the question of whether NLRP10 assembles the inflammasome *in vivo* but such response would theoretically be possible both during pathological mitochondrial disruption events and during physiological processes that eliminate cells with damaged or otherwise compromised mitochondria.

10.9. Outstanding questions and future directions

The work presented in my Thesis opens the way for several future studies. In my opinion, the following are the most interesting questions that could be addressed:

1. What are the molecular targets of *m*-3M3FBS, *o*-3M3FBS, SC-9, SC-10, thapsigargin, and SMBA1?

2. How do *m*-3M3FBS, SC-10 (in macrophages), thapsigargin, and SMBA1 permeabilize the mitochondria? How is it possible that SC-10 permeabilizes the mitochondria in macrophages, but not in HEK cells? Answering these questions is linked to point (1.), because the molecular targets of the mitochondria-disrupting compounds will likely suggest their mechanisms of action. Of note, this could lead to the discovery of a novel pathway of mitochondrial damage.

3. What is the ligand of NLRP10? This question will probably have to be addressed by proteomics combined with loss-of-function (reverse-genetics) follow-up experiments. A different option is a CRISPR or chemical mutagenesis forward screen using ASC specking as a readout in NLRP10/ASC fluorescent reporter HEK

cells, or IL-1β secretion as a readout in AIM2-deficient macrophages overexpressing NLRP10.

4. Which innate immune pathways are engaged by *m*-3M3FBS, *o*-3M3FBS, SC-9, SC-10, thapsigargin, and SMBA1 in human myeloid cells, in which cytosolic DNA is sensed by the NLRP3 inflammasome (Gaidt et al., 2017)? Could the identified mitochondria-damaging molecules trigger the cGAS-STING-NLRP3 or cGAS-STING-IFN responses?

5. Are there any physiological (development, repair, regeneration) or pathological processes in which NLRP10 is involved? What could have been the nature of the evolutionary pressures that promoted the conservation of the NLRP10 amino acid sequence in mammals?

11. Supplementary Data Figures S1-S63

Supplementary Figure S1:

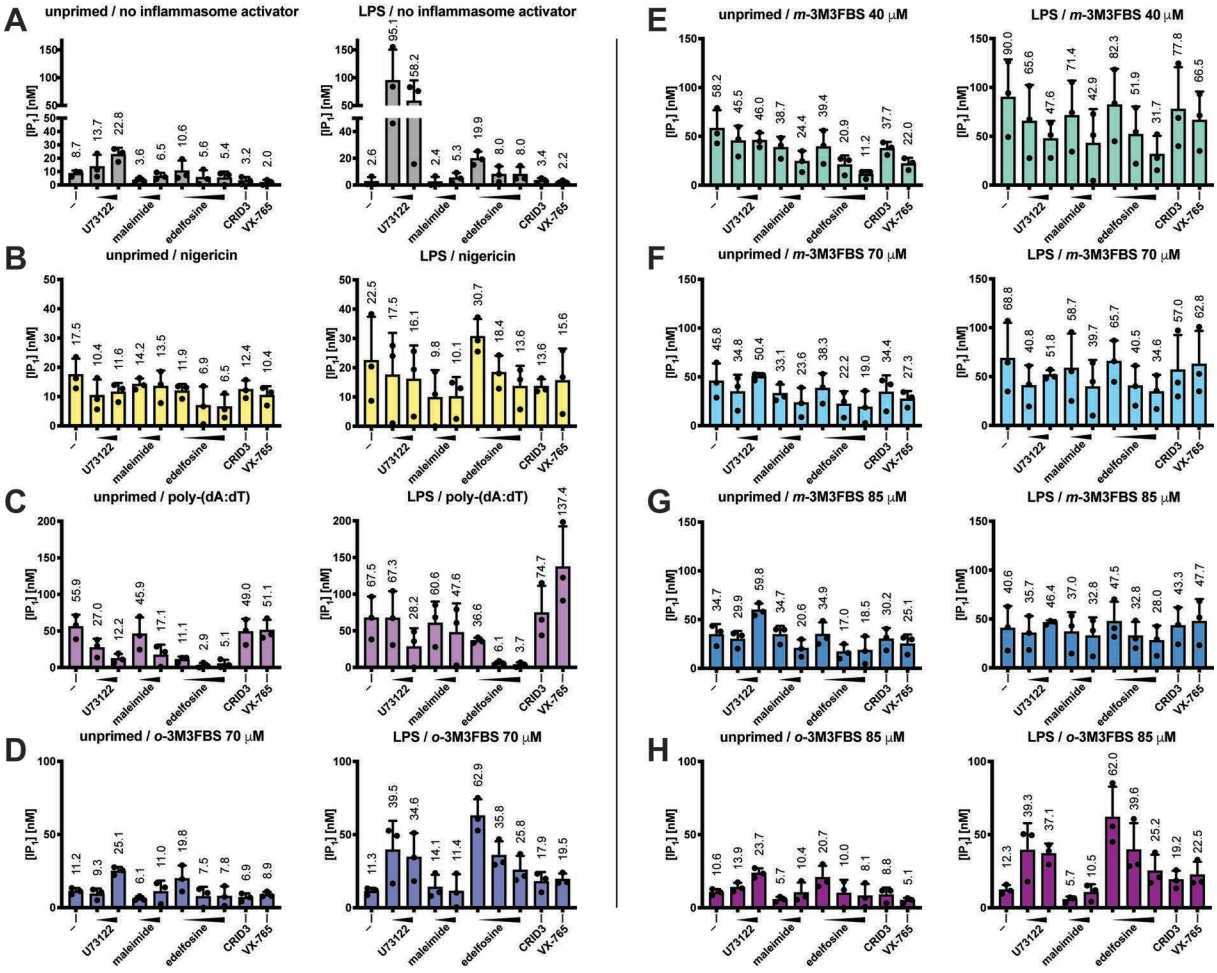

Supplementary Figure S1: IP_1 levels in unprimed or LPS-primed WT iMac cells treated with inflammasome activators in a minimal salt solution containing 50 mM LiCl and 125 mM NaCl

A-H: To determine whether the inflammasome activators nigericin, poly-(dA:dT), and *m*-3M3FBS are capable of eliciting PLC activation, unprimed or LPS-primed (200 ng/mL, 2 h) WT iMac cells were shifted to an extracellular medium consisting of (in mM): 50 LiCl, 125 NaCl, 5 KCl, 2 $MgCl_2$, 1 $CaCl_2$, 10 glucose, 10 HEPES, pH 7.4. Then the cells were left untreated or pre-treated for 10 min with U 73122 (5 or 25 μM), maleimide (5 or 25 μM), edelfosine (10, 25, or 50 μM), CRID3 (5 μM), or VX-765 (40 μM). This pre-incubation was followed by administration of the inflammasome activators: 10 μM nigericin (B), 2 μg/mL poly-(dA:dT) complexed with 5 μL lipofectamine (C), 40-85 μM *m*-3M3FBS (E-G), or 70-85 μM *o*-3M3FBS (D, H; PLC-inactive isomer of *m*-3M3FBS). The negative controls (A) were subjected to the medium alone. Immediately after addition of inflammasome activators, the plates were centrifuged at 340 × g for 5 min (RT). After 45 min of stimulation, the cells were lysed by addition of Triton X-100 (final concentration 0.5%) and the concentrations of IP_1 in the supernatants were assessed by HTRF.

Because the tested treatments led to a relatively wide range of detected IP_1 concentrations, the scales on the y-axes differ between panels A-H. To enable easier comparisons, absolute mean values are specified above each bar or within the bars.

The results are plotted as means from 3 independent experiments performed in technical duplicate. Error bars represent SD. Individual data points represent means of the technical duplicate values from each of the independent experiments.

Supplementary Figure S2:

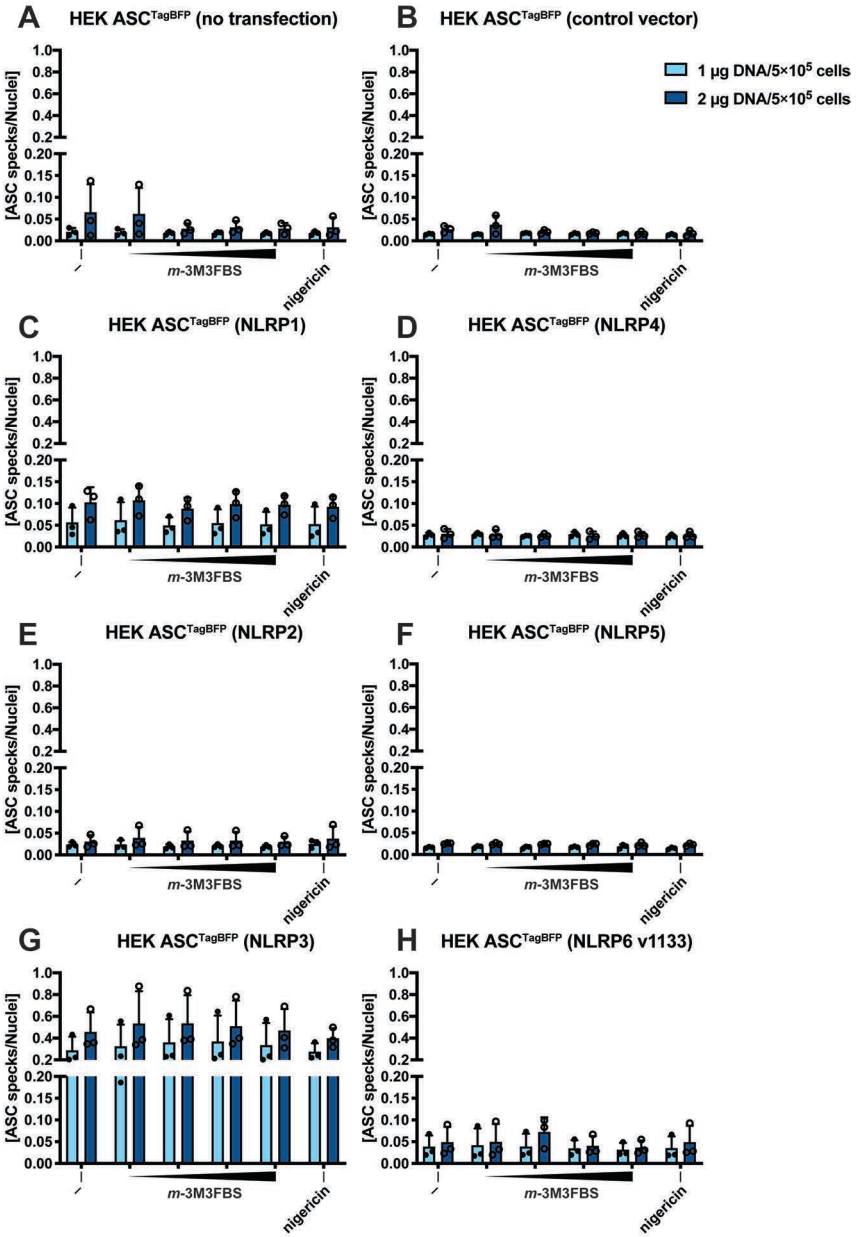

Supplementary Figure S2: Non-normalized values of the ASC specks/Nuclei ratio in response to *m*-3M3FBS in ASC^{TagBFP} reporter HEK cells overexpressing human NLRP1, human NLRP2, human NLRP3, human NLRP4, human NLRP5, or human NLRP6

A-H: ASC^{TagBFP} HEK cells were left untransfected (A) or were transiently transfected in wells of a 6-well plate with the empty vector (B) or with vectors encoding human (h) NLRP1 (C), hNLRP2 (E), hNLRP3 (G), hNLRP4 (D), hNLRP5 (F), or hNLRP6 (H; plasmid ID in the Institute of Innate Immunity database was 1133). The transfected DNA amount was 1 µg per 5×10^5 cells (light blue bars; the number of cells refers to the initial cell population) or 2 µg per 5×10^5 cells (dark blue bars; the number of cells refers to the initial cell population). The transfection reagent was Gene Juice and it was combined with DNA at the ratio of 2.3 µL of Gene Juice per 1 µg of DNA. After 24 h of transfection, the cells were replated into 96-well plates, and after additional 24 h they were shifted to an extracellular medium consisting of (in mM) 123 NaCl, 5 KCl, 2 $MgCl_2$, 1 $CaCl_2$, 10 glucose, 10 HEPES pH 7.4. Then, the cells were left untreated (-), or they were stimulated with *m*-3M3FBS (40, 55, 70, or 85 µM) or with nigericin (10 µM). Immediately after addition of inflammasome activators, the plates were centrifuged at 340 × g for 5 min (RT). After 30 min, the cells were fixed with 4% formaldehyde, counterstained with the nuclear dye DRAQ5 (5 µM) and imaged using a widefield fluorescence microscope.

The results are plotted as means from 3 independent experiments performed in technical duplicate. Error bars represent SD. Individual data points represent means of the technical duplicate values from each of the independent experiments.

Supplementary Figure S3:

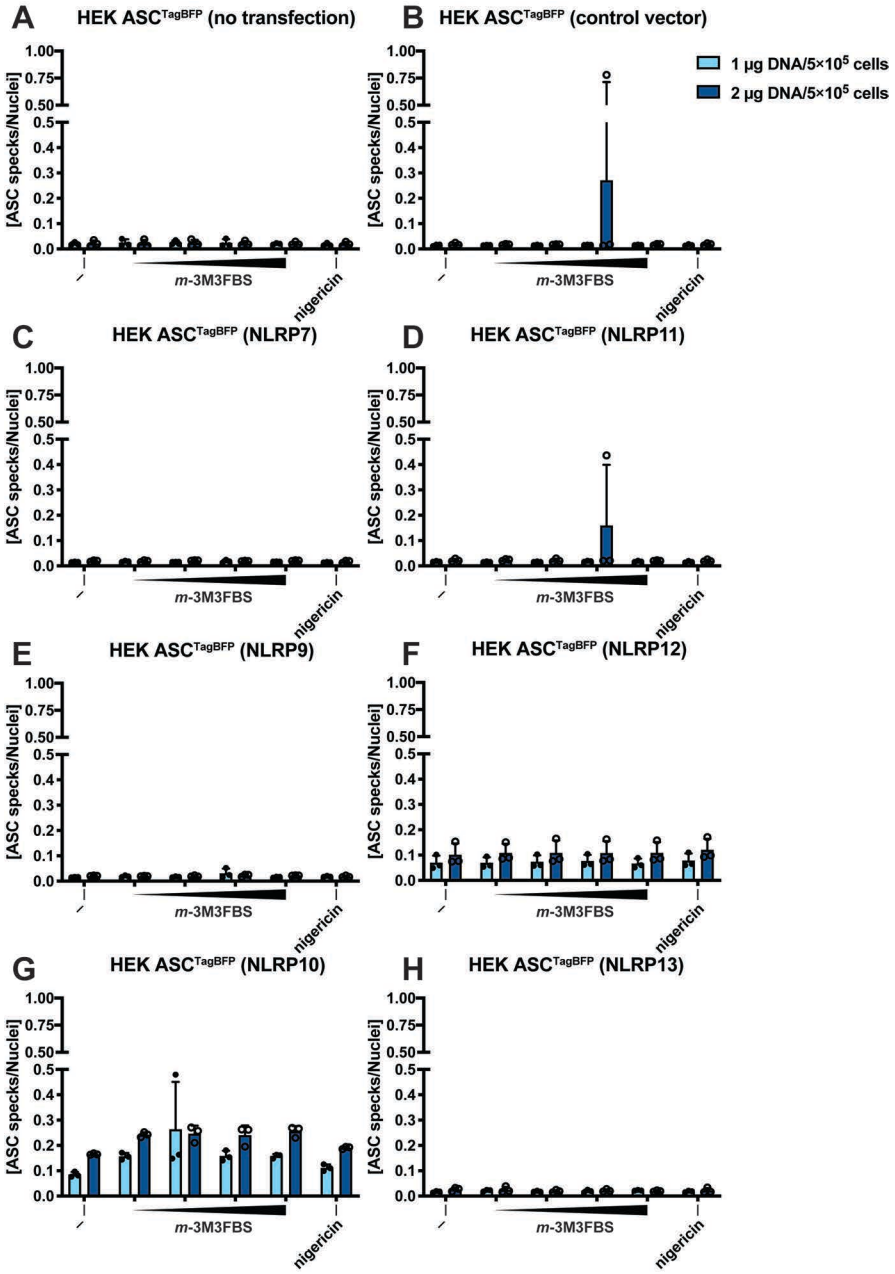

Supplementary Figure S3: Non-normalized values of the ASC specks/Nuclei ratio in response to *m*-3M3FBS in ASC^{TagBFP} reporter HEK cells overexpressing human NLRP7, human NLRP9, human NLRP10, human NLRP11, human NLRP12, or human NLRP13

A-H: ASC^{TagBFP} HEK cells were left untransfected (A) or were transiently transfected in wells of a 6-well plate with the empty vector (B) or with vectors encoding human (h) NLRP7 (C), hNLRP9 (E), hNLRP10 (G), hNLRP11 (D), hNLRP12 (F), or hNLRP13 (H). The transfected DNA amount was 1 µg per 5×10^5 cells (light blue bars; the number of cells refers to the initial cell population) or 2 µg per 5×10^5 cells (dark blue bars; the number of cells refers to the initial cell population). The transfection reagent was Gene Juice and it was combined with DNA at the ratio of 2.3 µL of Gene Juice per 1 µg of DNA. After 24 h of transfection, the cells were replated into 96-well plates, and after additional 24 h they were shifted to an extracellular medium consisting of (in mM) 123 NaCl, 5 KCl, 2 $MgCl_2$, 1 $CaCl_2$, 10 glucose, 10 HEPES pH 7.4. Then, the cells were left untreated (-), or they were stimulated with *m*-3M3FBS (40, 55, 70, or 85 µM) or with nigericin (10 µM). Immediately after addition of inflammasome activators, the plates were centrifuged at $340 \times g$ for 5 min (RT). After 30 min, the cells were fixed with 4% formaldehyde, counterstained with the nuclear dye DRAQ5 (5 µM) and imaged using a widefield fluorescence microscope.

The results are plotted as means from 3 independent experiments performed in technical duplicate. Error bars represent SD. Individual data points represent means of the technical duplicate values from each of the independent experiments.

Supplementary Figure S4:

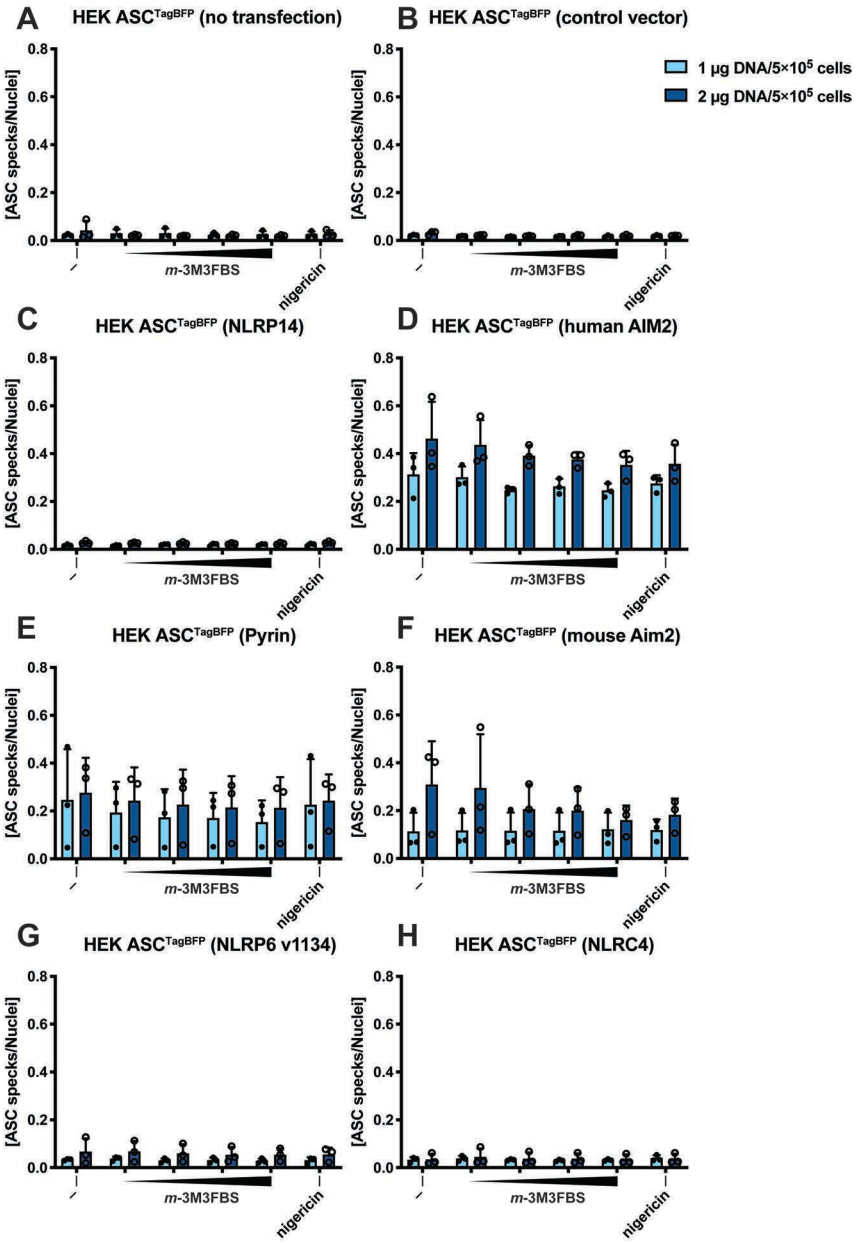

Supplementary Figure S4: Non-normalized values of the ASC specks/Nuclei ratio in response to *m*-3M3FBS in ASC^{TagBFP} reporter HEK cells overexpressing human NLRP14, human pyrin, human AIM2, murine AIM2, human NLRP6, or human NLRC4

A-H: ASC^{TagBFP} HEK cells were left untransfected (A) or were transiently transfected in wells of a 6-well plate with the empty vector (B) or with vectors encoding human (h) NLRP14 (C), hPyrin (E), hNLRP6 (G; the vector ID in the Institute of Innate Immunity database was 1134), hAIM2 (D), murine Aim2 (F), or hNLRC4 (H). The transfected DNA amount was 1 µg per 5 × 10^5 cells (light blue bars; the number of cells refers to the initial cell population) or 2 µg per 5 × 10^5 cells (dark blue bars; the number of cells refers to the initial cell population). The transfection reagent was Gene Juice and it was combined with DNA at the ratio of 2.3 µL of Gene Juice per 1 µg of DNA. After 24 h of transfection, the cells were replated into 96-well plates, and after additional 24 h they were shifted to an extracellular medium consisting of (in mM) 123 NaCl, 5 KCl, 2 $MgCl_2$, 1 $CaCl_2$, 10 glucose, 10 HEPES pH 7.4. Then, the cells were left untreated (-), or they were stimulated with *m*-3M3FBS (40, 55, 70, or 85 µM) or with nigericin (10 µM). Immediately after addition of inflammasome activators, the plates were centrifuged at 340 × g for 5 min (RT). After 30 min, the cells were fixed with 4% formaldehyde, counterstained with the nuclear dye DRAQ5 (5 µM) and imaged using a widefield fluorescence microscope.

The results are plotted as means from 3 independent experiments performed in technical duplicate. Error bars represent SD. Individual data points represent means of the technical duplicate values from each of the independent experiments.

Supplementary Figure S5:

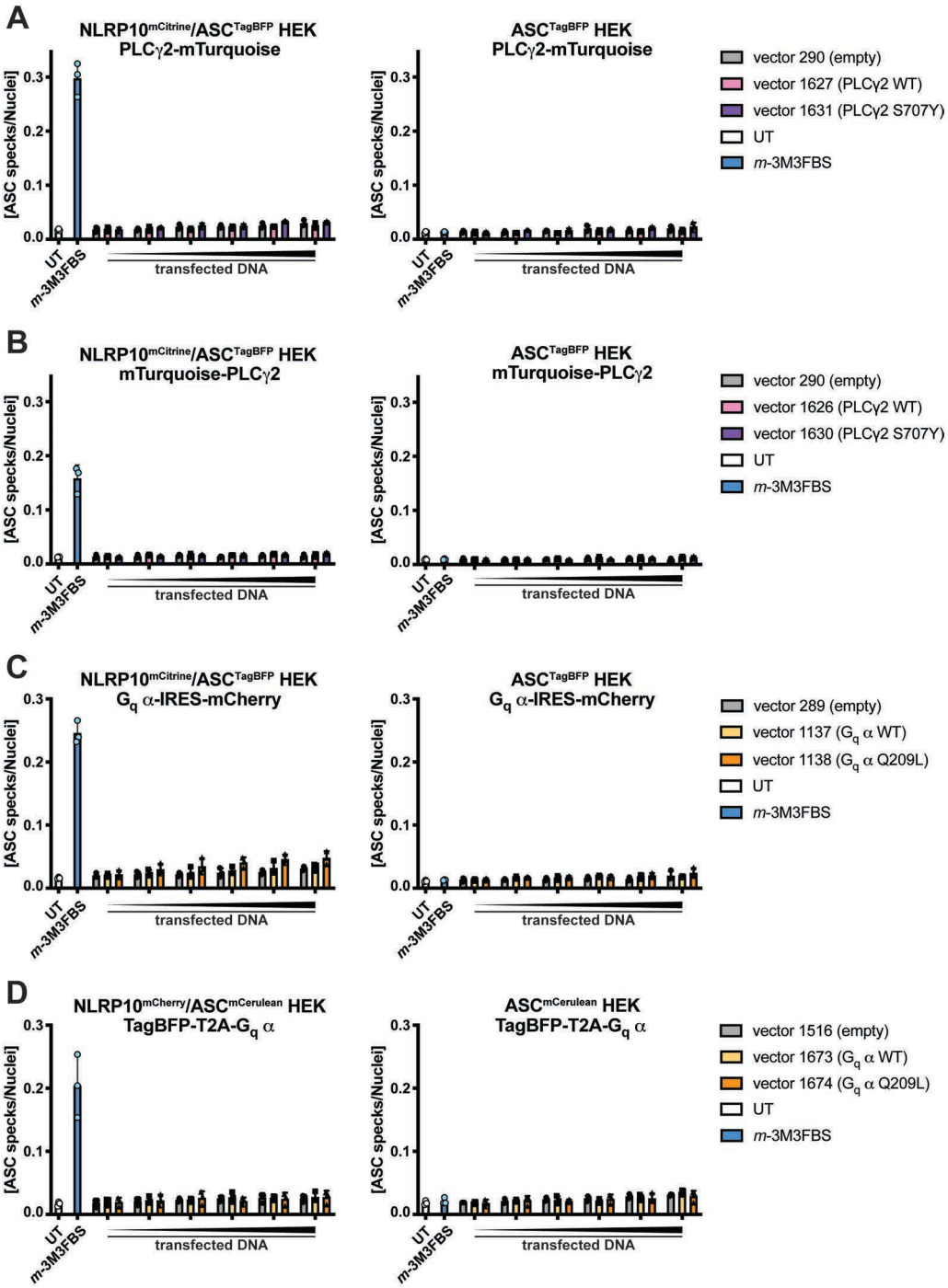

Supplementary Figure S5: NLRP10 is not activated by the hyperactive human PLCγ2 variant (p.S707Y) or by the constitutively active G_q protein mutant (Q209L)

A, B: NLRP10^{mCitrine}/ASC^{TagBFP} HEK cells (A, B, left panels) and ASC^{TagBFP} HEK cells (A, B, right panels; NLRP10-negative control) were transfected with the empty vector (#290 in the Institute of Innate Immunity database) or with vectors encoding C-terminal (A) or N-terminal (B) mTurquoise fusion proteins with WT or hypermorphic human PLCγ2 (WT PLCγ2: #1626 for N-terminal fusion and #1627 for C-terminal fusion in the Institute of Innate Immunity database; hypermorphic PLCγ2-S707Y: #1630 for N-terminal fusion and #1631 for C-terminal fusion in the Institute of Innate Immunity database). The transfected DNA amounts were 10, 50, 75, 100, 150, or 200 ng/well, combined with Gene Juice [transfection reagent] at the ratio of 2.5 µL of Gene Juice per 1 µg of DNA. After 24 h of transfection, the cells were fixed, counterstained for the nuclei (5 µM DRAQ5) and imaged using a widefield fluorescence microscope. During the final 30 min of the experiment, the positive control (*m*-3M3FBS) cells were shifted to an extracellular medium consisting of (in mM) 123 NaCl, 5 KCl, 2 $MgCl_2$, 1 $CaCl_2$, 10 glucose, 10 HEPES pH 7.4 and stimulated with 85 µM *m*-3M3FBS.

C, D: NLRP10^{mCitrine}/ASC^{TagBFP} HEK cells (C, right panel), ASC^{TagBFP} HEK cells (C, right panel; NLRP10-negative control), NLRP10^{mCherry}/ASC^{mCerulean} HEK cells (D, left panel) and ASC^{mCerulean} HEK cells (D, right panel; NLRP10-negative control) were transfected with the empty vector (#289 [C] and #1516 [D] in the Institute of Innate Immunity database) or with vectors encoding the normal (WT) or the constitutively active (Q209L) variant of the G_q α protein in an IRES-mCherry expression cassette (C) or a TagBFP-T2A expression cassette (D; WT G_q α: #1137 for the IRES-mCherry expression cassette and #1673 for the TagBFP-T2A expression cassette in the Institute of Innate Immunity database; constitutively active [Q209L] G_q α: #1138 for the IRES-mCherry expression cassette and #1674 for the TagBFP-T2A expression cassette in the Institute of Innate Immunity database). The transfected DNA amounts were 10, 50, 75, 100, 150, or 200 ng/well, combined with Gene Juice [transfection reagent] at the ratio of 2.5 µL of Gene Juice per 1 µg of DNA. After 24 h of transfection, the cells were fixed, counterstained for the nuclei (5 µM DRAQ5) and imaged using a widefield fluorescence microscope. During the final 30 min of the experiment, the positive control (*m*-3M3FBS) cells were shifted to an extracellular medium consisting of (in mM) 123 NaCl, 5 KCl, 2 $MgCl_2$, 1 $CaCl_2$, 10 glucose, 10 HEPES pH 7.4 and stimulated with 85 µM *m*-3M3FBS.

Supplementary Figure S6:

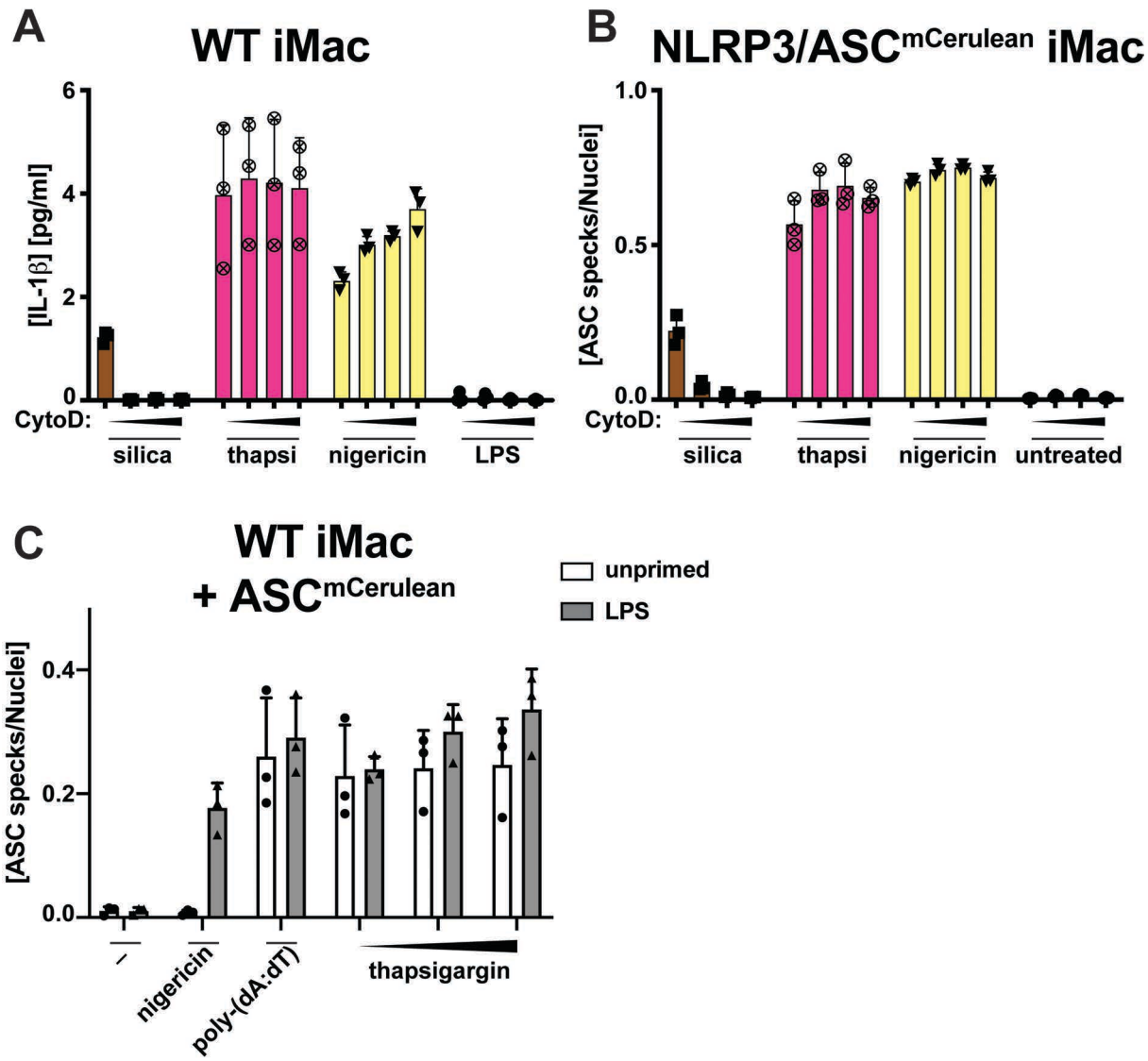

Supplementary Figure S6: The AIM2 inflammasome activation with thapsigargin is independent of phagocytosis and does not rely on LPS priming

A, B: For the assessment of the sensitivity of the inflammasome activation to cytochalasin D (CytoD; phagocytosis inhibitor), LPS-primed (200 ng/mL, 2 h) WT iMac cells (A) or unprimed NLRP3/ASC^{mCerulean} reporter iMac cells (B) were pre-treated with CytoD (0 [DMSO control], 10, 25, or 50 µM) for 10 min, and then stimulated with silica crystals (0.5 mg/mL, 6 h), thapsigargin (thapsi; 20 µM, 60 min), or nigericin (10 µM, 60 min). The silica stimulations as well as the unprimed and LPS control stimulations (6 h) were

performed in DMEM supplemented with 10% FBS. The thapsigargin and nigericin stimulations were performed in an extracellular medium consisting of (in mM) 123 NaCl, 5 KCl, 2 $MgCl_2$, 1 $CaCl_2$, 10 glucose, 10 HEPES, pH 7.4. Immediately after addition of inflammasome activators, the plates were centrifuged at 340 × g for 5 min (RT). After the stimulations were completed, the supernatants were collected and IL-1β concentrations were measured by HTRF (A), or the cells were fixed, counterstained for the nuclei and imaged using a fluorescence microscope (B).

C: To determine whether the thapsigargin-induced inflammasome activation requires the priming step, $ASC^{mCerulean}$-overexpressing WT iMac cells were primed with LPS (200 ng/mL, 2 h) or left unprimed, and then stimulated with thapsigargin (15, 20, or 25 μM), nigericin (10 μM), or poly-(dA:dT) (2 μg/mL complexed with 5 μL Lipofectamine 2000) in an extracellular medium consisting of (in mM) 123 NaCl, 5 KCl, 2 $MgCl_2$, 1 $CaCl_2$, 10 glucose, 10 HEPES, pH 7.4. The negative controls were subjected to medium alone. Immediately after addition of inflammasome activators, the plates were centrifuged at 340 × g for 5 min (RT). After 60 min, the cells were fixed, counterstained for the nuclei and imaged using a fluorescence microscope.

Supplementary Figure S7:

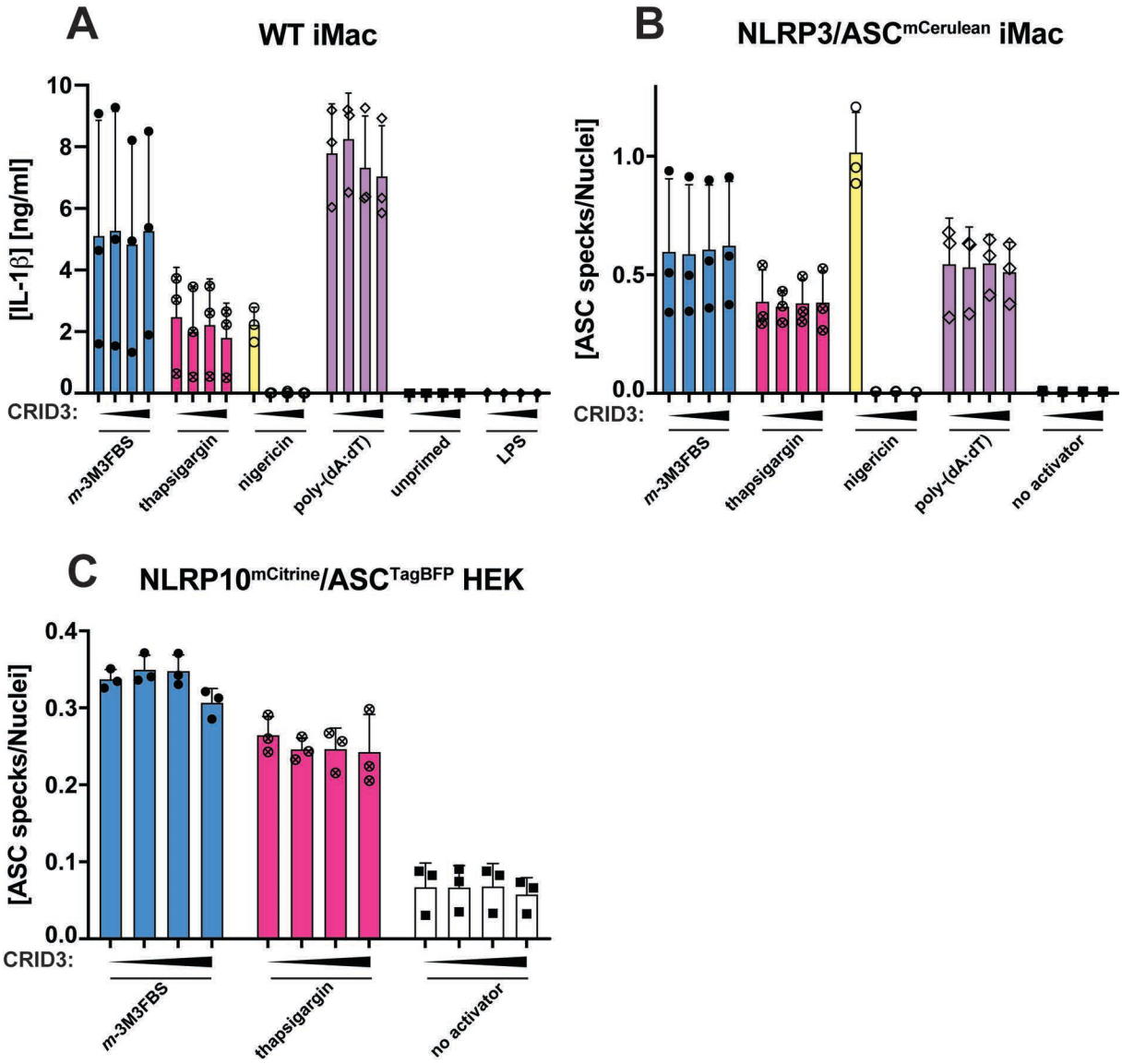

Supplementary Figure S7: The NLRP3 inhibitor CRID3 does not block the AIM2/NLRP10 inflammasome responses to *m*-3M3FBS and thapsigargin

A-C: LPS-primed (200 ng/mL, 2 h) WT iMac cells (A), $NLRP3/ASC^{mCerulean}$ reporter iMac cells (B), and $NLRP10^{mCitrine}/ASC^{TagBFP}$ HEK cells (C) were treated for 10 min with CRID3 (0, 1, 5, or 10 μM) and then subjected to the inflammasome activators *m*-3M3FBS (85 μM), thapsigargin (20 μM), nigericin (10 μM) or poly-(dA:dT) (2 μg/mL complexed with 5 μL Lipofectamine 2000) in an extracellular medium consisting

of (in mM) 123 NaCl, 5 KCl, 2 $MgCl_2$, 1 $CaCl_2$, 10 glucose, 10 HEPES, pH 7.4. The LPS (A) and unprimed (A-C) controls were subjected to medium alone. Immediately after addition of inflammasome activators, the plates were centrifuged at 340 × g for 5 min (RT). After 30 min (C) or 60 min (A, B), the supernatants were collected and IL-1β concentrations were measured by HTRF (A) or the cells were fixed with 4% formaldehyde, counterstained with the nuclear dye DRAQ5 (5 μM) and imaged using a widefield fluorescence microscope (B, C).
The results are plotted as means from 3 independent experiments performed in technical duplicate. Error bars represent SD. Individual data points represent means of the technical duplicate values from each of the independent experiments.

Supplementary Figure S8:

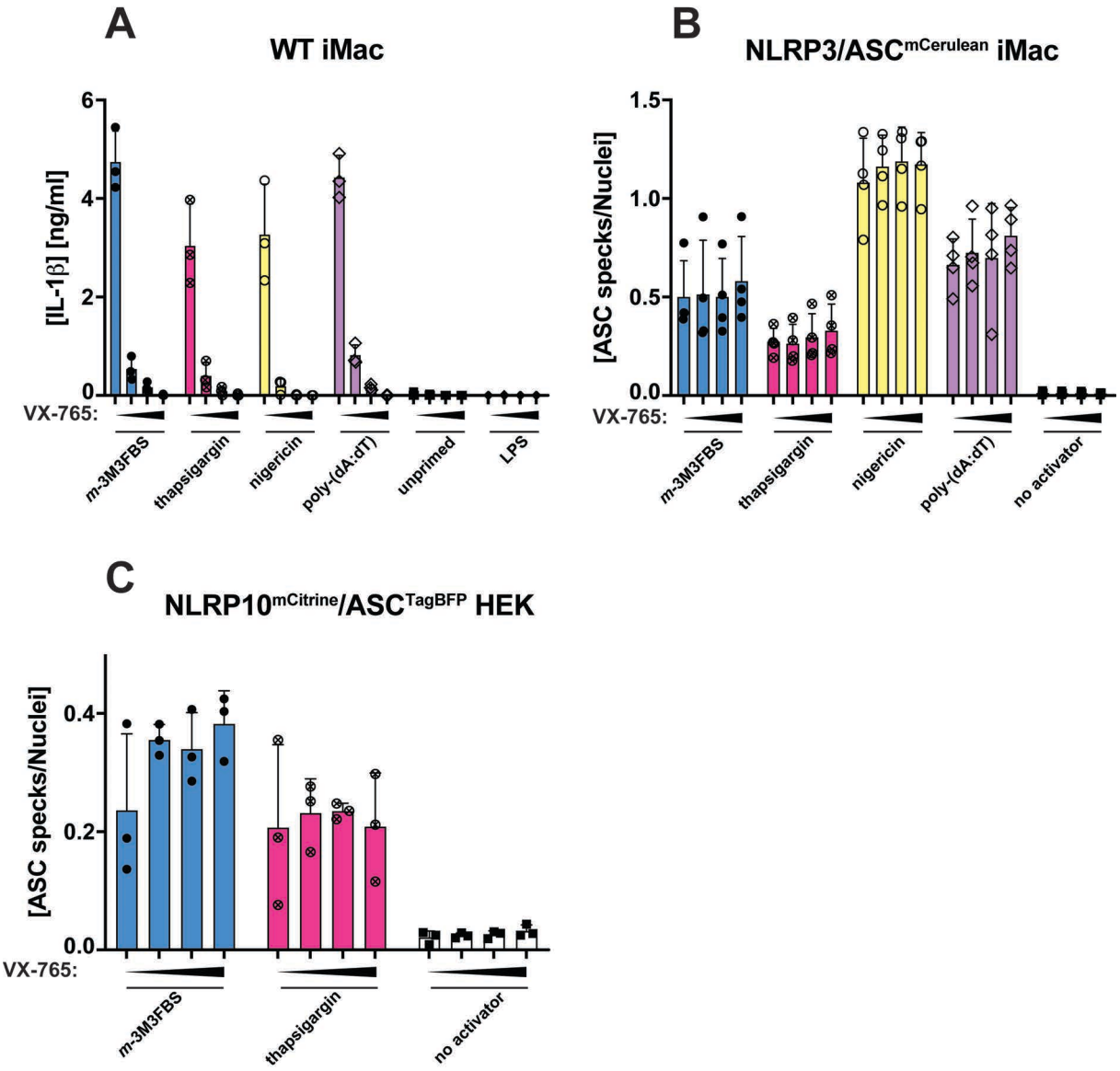

Supplementary Figure S8: The caspase-1 inhibitor VX-765 blocks thapsigargin-induced IL-1β secretion, but not ASC speck formation
A-C: LPS-primed (200 ng/mL, 2 h) WT iMac cells (A), NLRP3/$ASC^{mCerulean}$ reporter iMac cells (B), and $NLRP10^{mCitrine}$/ASC^{TagBFP} HEK cells (C) were treated for 10 min with VX-765 (0, 10, 25, or 50 μM) and then subjected to the inflammasome activators *m*-3M3FBS (85 μM), thapsigargin (20 μM), nigericin (10 μM) or poly-(dA:dT) (2 μg/mL complexed with 5 μL Lipofectamine 2000) in an extracellular medium consisting of (in mM) 123 NaCl, 5 KCl, 2 $MgCl_2$, 1 $CaCl_2$, 10 glucose, 10 HEPES, pH 7.4. The LPS (A) and unprimed (A-C) controls were subjected to medium alone. Immediately after addition of inflammasome activators, the plates were centrifuged at 340 × g for 5 min (RT). After 30 min (C) or 60 min (A, B), the supernatants were collected and IL-1β concentrations were measured by HTRF (A) or the cells were fixed with 4%

formaldehyde, counterstained with the nuclear dye DRAQ5 (5 µM) and imaged using a widefield fluorescence microscope (B, C).
The results are plotted as means from 3 independent experiments performed in technical duplicate. Error bars represent SD. Individual data points represent means of the technical duplicate values from each of the independent experiments.

Supplementary Figure S9:

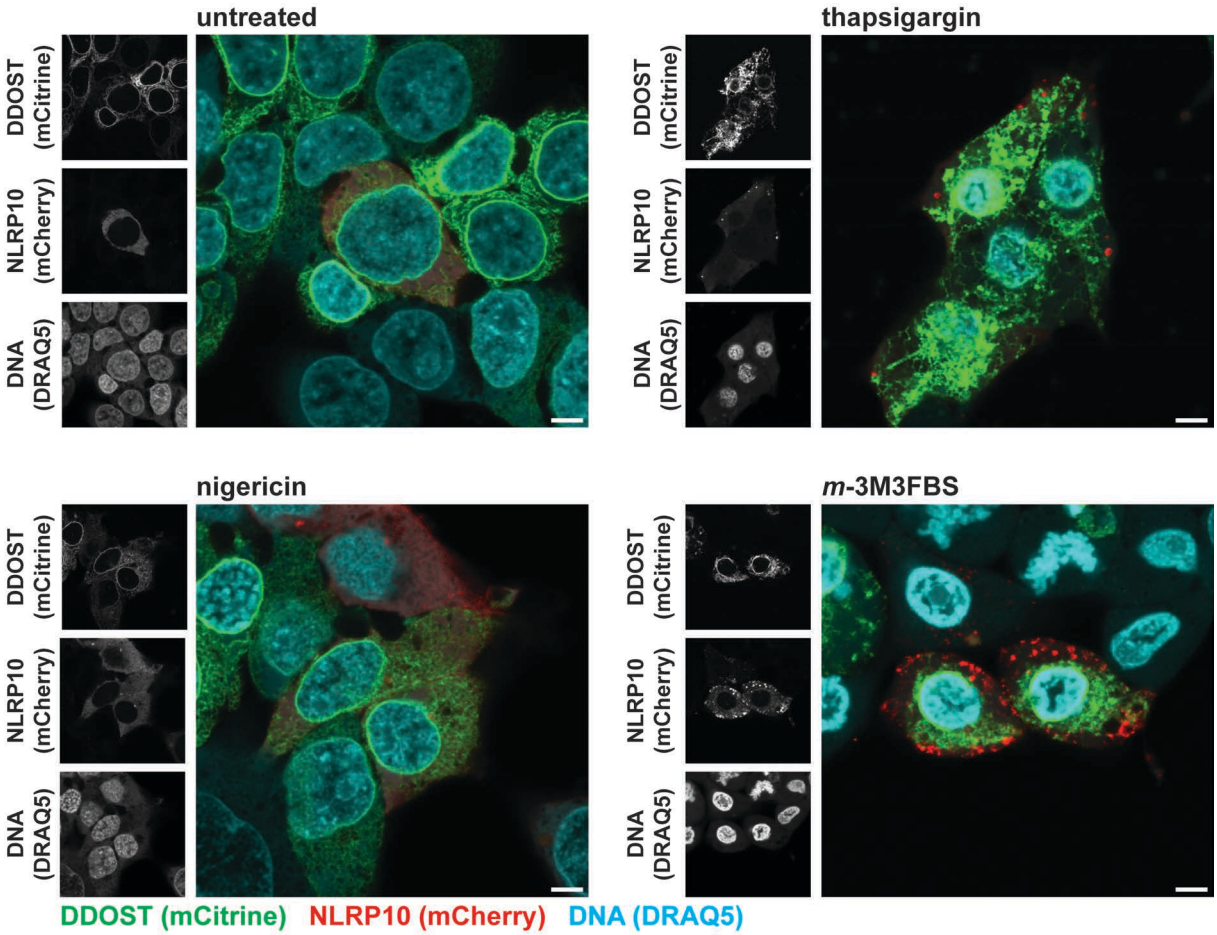

Supplementary Figure S9: Thapsigargin and *m*-3M3FBS do not trigger NLRP10 colocalization with the endoplasmic reticulum in NLRP10^{mCherry} reporter HEK cells overexpressing DDOST^{mCitrine}
Human NLRP10^{mCherry} HEK cells were transiently transfected (200 ng of DNA per well of a 96-well plate combined with 0.5 µL of Gene Juice [transfection reagent], or 2 µg/mL of DNA combined with 5 µL of Gene Juice) with a vector encoding the ER marker DDOST expressed as a fusion protein with mCitrine. After 24 h of transfection, the cells were shifted to an extracellular medium consisting of (in mM) 123 NaCl, 5 KCl, 2 $MgCl_2$, 1 $CaCl_2$, 10 glucose, 10 HEPES pH 7.4 and left untreated, or were stimulated with thapsigargin (20 µM), *m*-3M3FBS (85 µM) or nigericin (10 µM). After 30 min, the cells were fixed with 4% formaldehyde, counterstained with the nuclear dye DRAQ5 (5 µM) and imaged using a confocal microscope.
Images are representative of 3 independent experiments. Scale bars correspond to 5 µm.

Supplementary Figure S10:

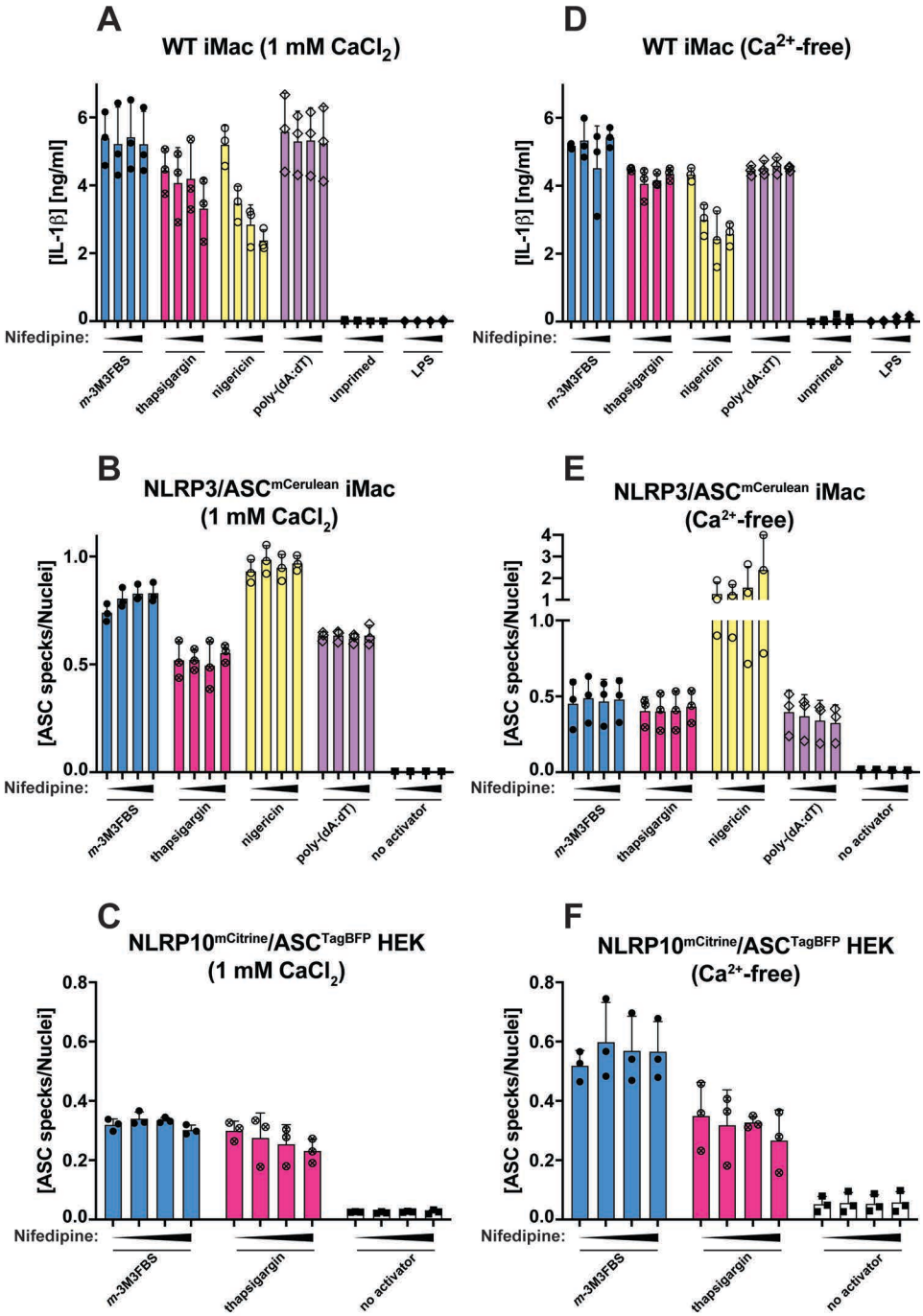

Supplementary Figure S10: Nifedipine does not inhibit inflammasome activation

A-F: LPS-primed (200 ng/mL, 2 h) WT iMac cells (A, D), NLRP3/ASC^{mCerulean} reporter iMac cells (B, E), and NLRP10^{mCitrine}/ASC^{TagBFP} HEK cells (C, F) were treated for 10 min with nifedipine (0, 10, 25, or 50 μM) in the presence (A-C) or absence (D-F) of extracellular Ca^{2+} and then subjected to the inflammasome activators *m*-3M3FBS (85 μM), thapsigargin (20 μM), nigericin (10 μM) or poly-(dA:dT) (2 μg/mL complexed with 5 μL Lipofectamine 2000) in an extracellular medium consisting of (in mM) 123 NaCl, 5 KCl, 2 $MgCl_2$, 0 or 1 $CaCl_2$, 10 glucose, 10 HEPES, pH 7.4. The LPS (A, D) and unprimed (A-F) controls were subjected to medium alone. Immediately after addition of inflammasome activators, the plates were centrifuged at 340 × g for 5 min (RT). After 30 min (C, F) or 60 min (A, B, D, E), the supernatants were collected and IL-1β concentrations were measured by HTRF (A, D) or the cells were fixed with 4% formaldehyde, counterstained with the nuclear dye DRAQ5 (5 μM) and imaged using a widefield fluorescence microscope (B, C, E, F).

The results are plotted as means from 3 independent experiments performed in technical duplicate. Error bars represent SD. Individual data points represent means of the technical duplicate values from each of the independent experiments.

Supplementary Figure S11:

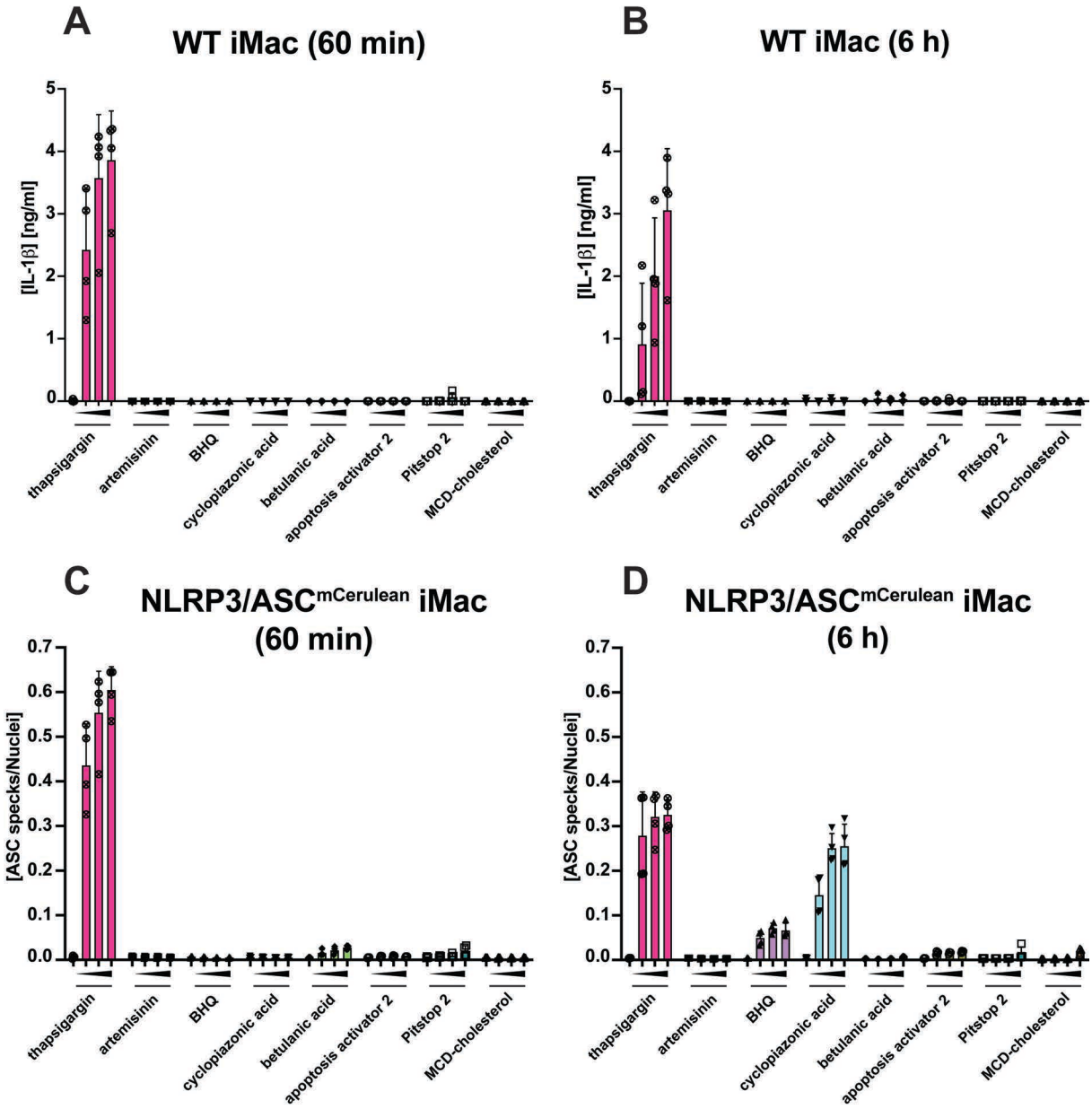

Supplementary Figure S11: The sarco/endoplasmic reticulum Ca^{2+} ATPase (SERCA) inhibitors artemisinin, BHQ, and cyclopiazonic acid, the pro-apoptotic agents betulinic acid and apoptosis activator 2, the nuclear permeability inducer Pitstop-2, and methylcyclodextrin (MCD)-cholesterol are not inflammasome activators in murine macrophages

A-D: LPS-primed (200 ng/mL, 2 h) WT iMac cells (A, B) and NLRP3/ASC^{mCerulean} reporter iMac cells (C, D) were stimulated with thapsigargin (0, 15, 20, or 25 μM), artemisinin (0, 10, 25, or 50 μM), BHQ (0, 10, 25, or 50 μM), cyclopiazonic acid (0, 10, 25, or 50 μM), betulinic acid (0, 25, 50, or 100 μM), apoptosis activator 2 (0, 10, 25, or 50 μM), Pitstop 2 (0, 25, 50, or 100 μM), or MCD-cholesterol complexes (0, 100, 250, or 500 μg/mL) for 60 min (A, C) or 6 h (B, D). The 6-h stimulations were performed in DMEM supplemented with 10% FBS (B, D; panel B – LPS was kept in the medium for the duration of the entire experiment), whereas the 60-min stimulations were performed in an extracellular medium consisting of (in mM) 123 NaCl, 5 KCl, 2 $MgCl_2$, 1 $CaCl_2$, 10 glucose, 10 HEPES pH 7.4 (A, C). Immediately after addition of the stimuli, the plates were centrifuged at 340 × g for 5 min (RT). After 60 min (A, C) or 6 h (B, D), the supernatants were collected and IL-1β concentrations were measured by HTRF (A, B) or the cells were fixed with 4% formaldehyde, counterstained with the nuclear dye DRAQ5 (5 μM) and imaged using a widefield fluorescence microscope (C, D).

The results are plotted as means from 4 independent experiments performed in technical triplicate. Error bars represent SD. Individual data points represent means of the technical triplicate values from each of the independent experiments.

Supplementary Figure S12:

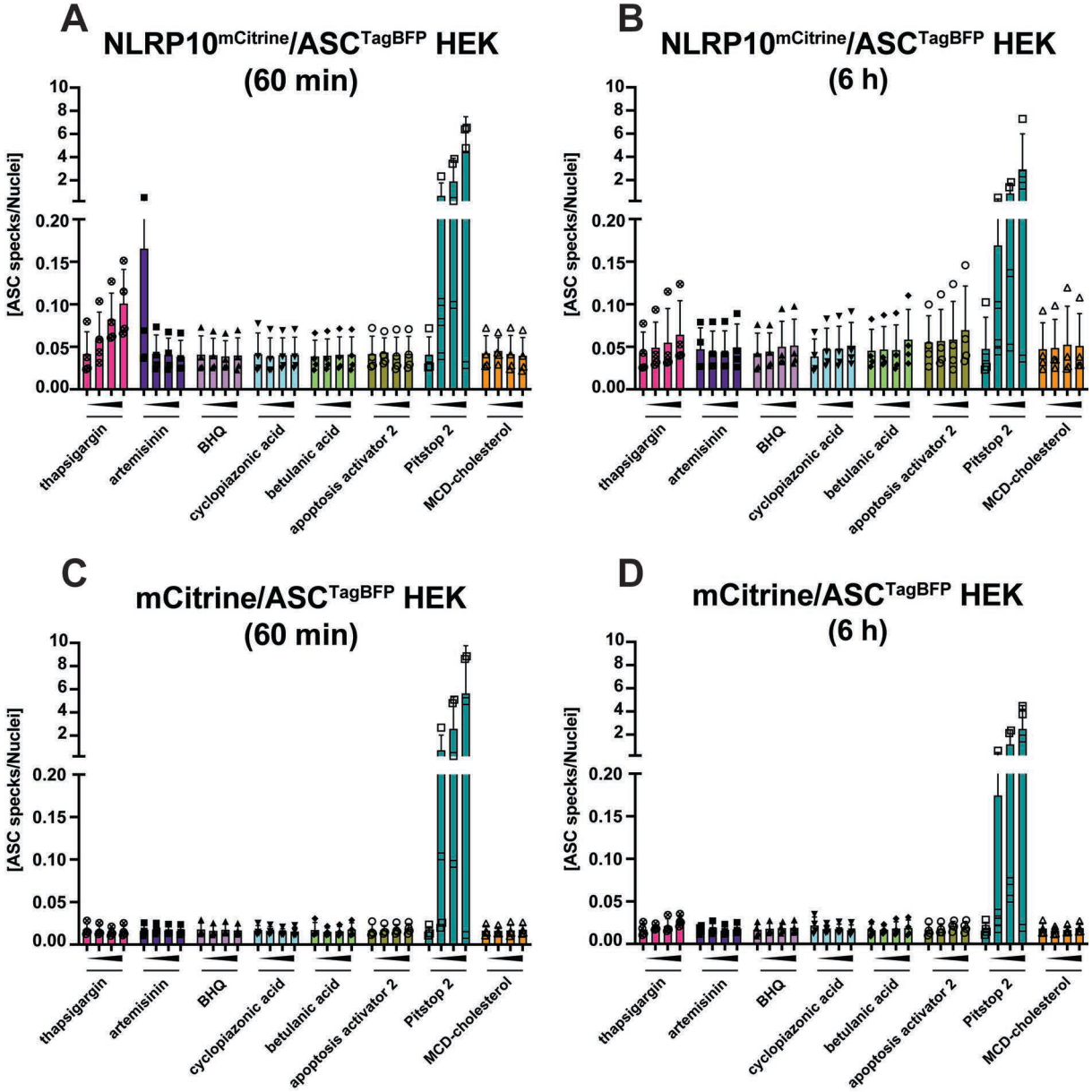

Supplementary Figure S12: The sarco/endoplasmic reticulum Ca^{2+} ATPase (SERCA) inhibitors artemisinin, BHQ, and cyclopiazonic acid, the pro-apoptotic agents betulinic acid and apoptosis activator 2, the nuclear permeability inducer Pitstop-2, and methylcyclodextrin (MCD)-cholesterol are not inflammasome activators in NLRP10^{mCitrine}/ASC^{TagBFP} reporter HEK cells

A-D: NLRP10^{mCitrine}/ASC^{TagBFP} HEK cells (A, B) and mCitrine/ASC^{TagBFP} HEK cells (C, D; NLRP10-negative control) were stimulated with thapsigargin (0, 15, 20, or 25 μM), artemisinin (0, 10, 25, or 50 μM), BHQ (0, 10, 25, or 50 μM), cyclopiazonic acid (0, 10, 25, or 50 μM), betulinic acid (0, 25, 50, or 100 μM), apoptosis activator 2 (0, 10, 25, or 50 μM), Pitstop 2 (0, 25, 50, or 100 μM), or MCD-cholesterol complexes (0, 100, 250, or 500 μg/mL) for 60 min (A, C) or 6 h (B, D). The 6-h stimulations were performed in DMEM supplemented with 10% FBS (B, D), whereas the 60-min stimulations were performed in an extracellular medium consisting of (in mM) 123 NaCl, 5 KCl, 2 $MgCl_2$, 1 $CaCl_2$, 10 glucose, 10 HEPES pH 7.4 (A, C). Immediately after addition of the stimuli, the plates were centrifuged at 340 × g for 5 min (RT). After 60 min (A, C) or 6 h (B, D), the cells were fixed with 4% formaldehyde, counterstained with the nuclear dye DRAQ5 (5 μM) and imaged using a widefield fluorescence microscope.

The results are plotted as means from 4 independent experiments performed in technical triplicate. Error bars represent SD. Individual data points represent means of the technical triplicate values from each of the independent experiments.

Supplementary Figure S13:

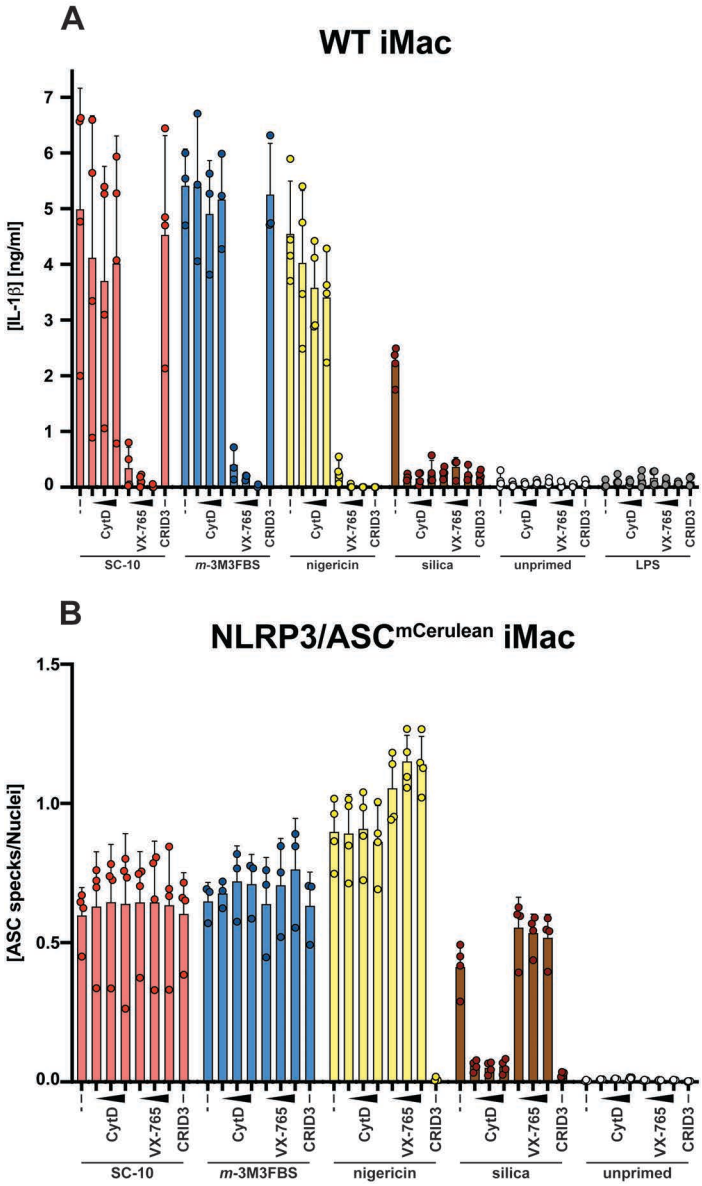

Supplementary Figure S13: Sensitivity of the SC-10-induced inflammasome activation to the phagocytosis inhibitor cytochalasin D, the caspase-1 inhibitor VX-765, and the NLRP3 inhibitor CRID3

A, B: LPS-primed WT iMac cells (A) and NLRP3/ASC^{mCerulean} reporter iMac cells (B) were shifted to an extracellular medium consisting of (in mM) 123 NaCl, 5 KCl, 2 $MgCl_2$, 1 $CaCl_2$, 10 glucose, 10 HEPES pH 7.4 and left untreated (-) or pre-treated for 10 min with cytochalasin D (CytD; 10, 25, or 50 μM), VX-765 (10, 25, or 50 μM) or CRID3 (5 μM). (Importantly, the cells under the silica-stimulated, unprimed, and LPS control conditions were kept in DMEM supplemented with 10% FBS; the shift to the minimal medium was not performed. Consequently, all pre-treatments and stimulations for these conditions were performed in DMEM supplemented with 10% FBS.) Next, the cells were left untreated or were stimulated with the following inflammasome activators: SC-10 (100 μM; red bars), *m*-3M3FBS (85 μM; blue bars), nigericin (10 μM; yellow bars), or silica crystals (500 μg/mL; brown bars). Immediately after addition of inflammasome activators, the plates were centrifuged at 340 × g for 5 min (RT). After 60 min (SC-10, *m*-3M3FBS, and nigericin stimulations) or 6 h (silica stimulation and the LPS and unprimed controls), the supernatants were collected and IL-1β concentrations were measured by HTRF (A) or the cells were fixed with 4% formaldehyde, counterstained with the nuclear dye DRAQ5 (5 μM) and imaged using a widefield fluorescence microscope (B).

The results are plotted as means from 4 independent experiments for all activators except *m*-3M3FBS, and 3 independent experiments for *m*-3M3FBS. The experiments were performed in technical duplicate. Error bars represent SD. Individual data points represent means of the technical duplicate values from each of the independent experiments.

Supplementary Figure S14:

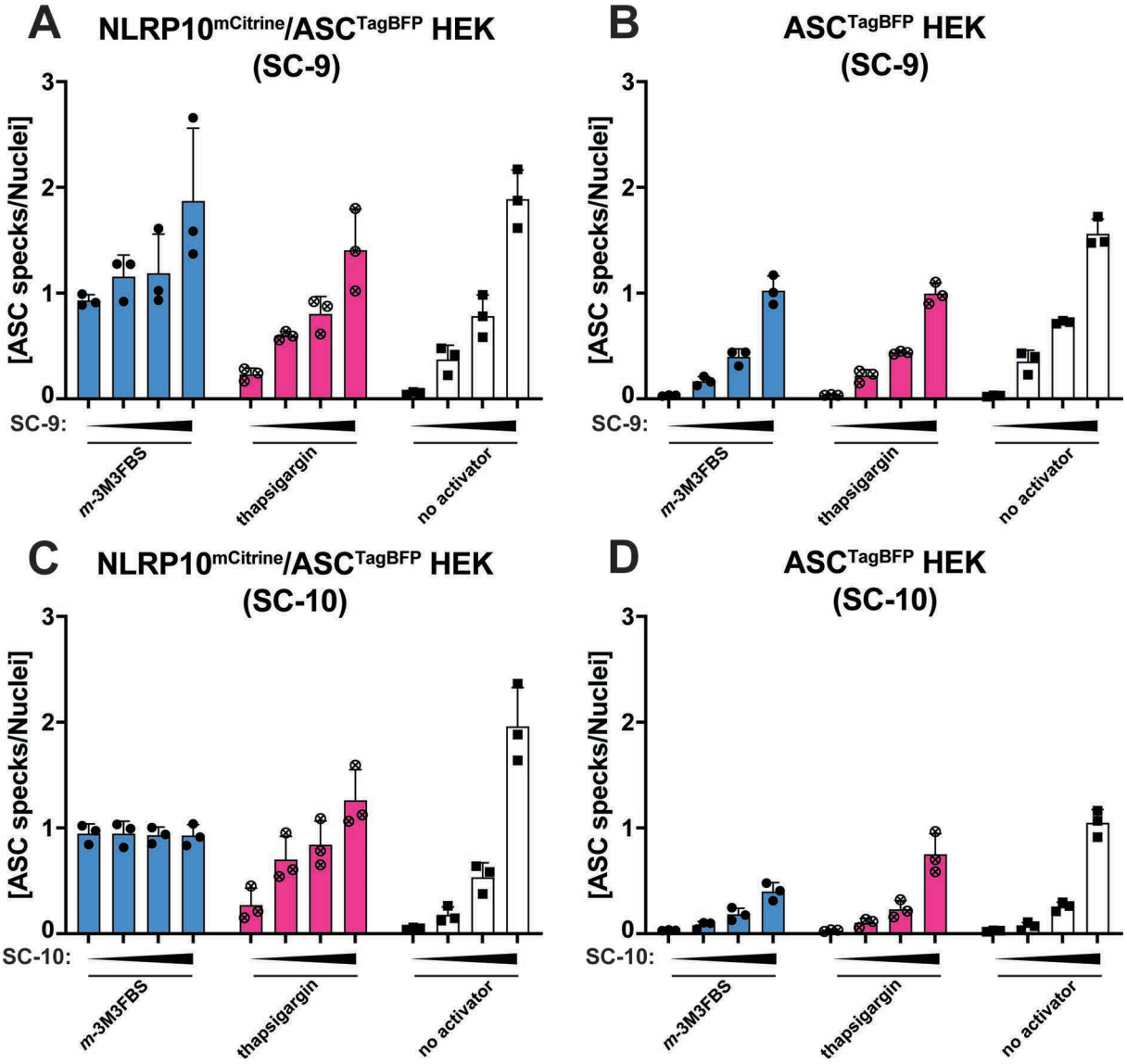

Supplementary Figure S14: SC-9 and SC-10 are autofluorescent in the BFP channel and interfere with ASC^{TagBFP} speck detection

A-D: NLRP10^{mCitrine}/ASC^{TagBFP} HEK cells (A, C) and ASC^{TagBFP} HEK cells (NLRP10-negative control; B, D) were treated for 10 min with SC-9 (0, 25, 50, or 100 μM; A, B) or SC-10 (0, 25, 50, or 100 μM; C, D) and then subjected to the inflammasome activators *m*-3M3FBS (85 μM) or thapsigargin (20 μM) in an extracellular medium consisting of (in mM) 123 NaCl, 5 KCl, 2 $MgCl_2$, 1 $CaCl_2$, 10 glucose, 10 HEPES, pH 7.4. The untreated controls were subjected to medium alone. Immediately after addition of inflammasome activators, the plates were centrifuged at 340 × g for 5 min (RT). After 30 min, the cells were fixed with 4% formaldehyde, counterstained with the nuclear dye DRAQ5 (5 μM) and imaged using a widefield fluorescence microscope.

The results are plotted as means from 3 independent experiments performed in technical duplicate. Error bars represent SD. Individual data points represent means of the technical duplicate values from each of the independent experiments.

Supplementary Figure S15:

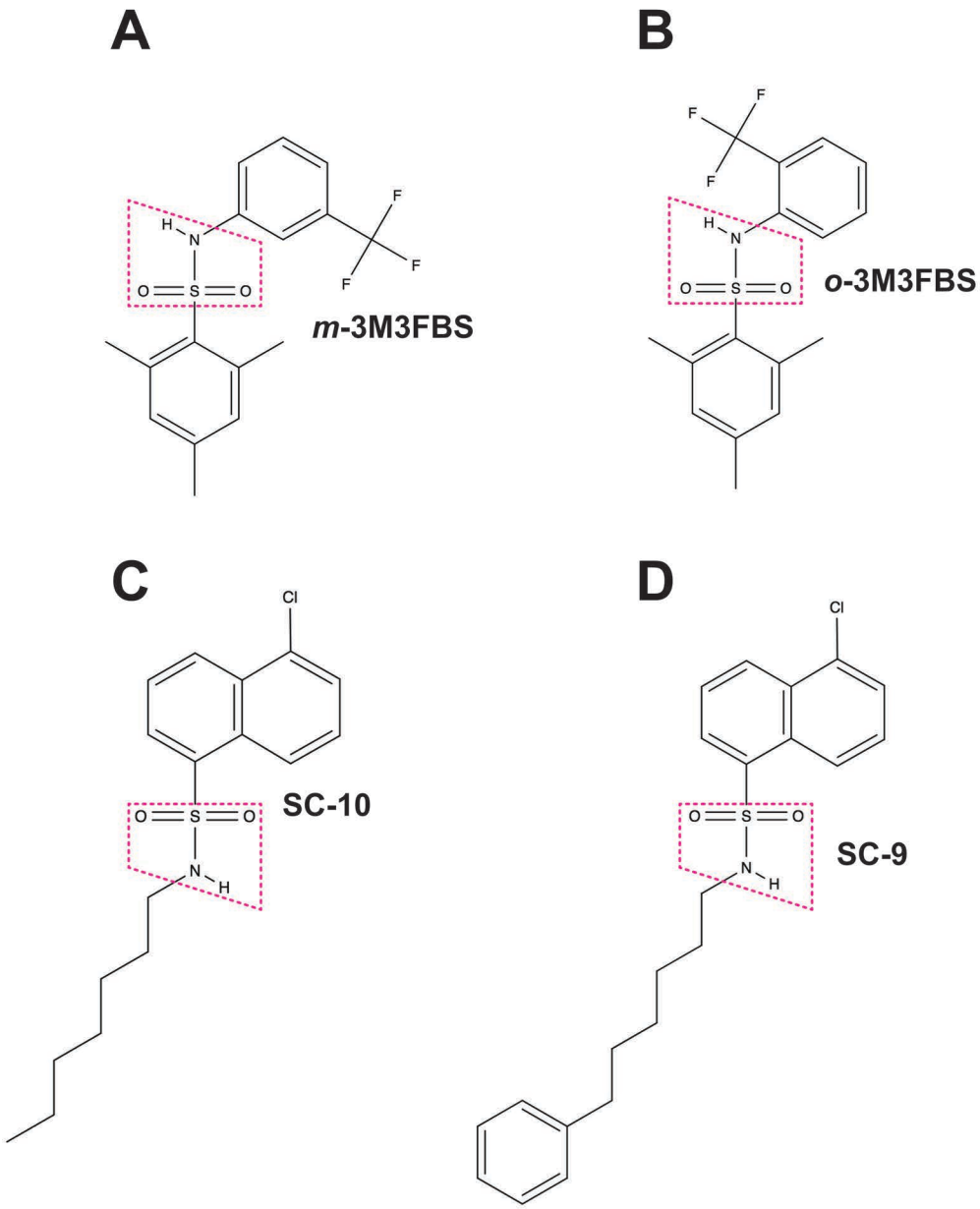

Supplementary Figure S15: Comparison of the chemical structures of the PLC activator *m*-3M3FBS, its 'inactive' isomer *o*-3M3FBS, and the PKC activators SC-9 and SC-10
A: structural formula of the reported PLC activator *m*-3M3FBS;
B: structural formula of *o*-3M3FBS, a reported inactive isomer of *m*-3M3FBS;
C: structural formula of the reported PKC activator SC-10;
D: structural formula of the reported PKC activator SC-9.

Supplementary Figure S16:

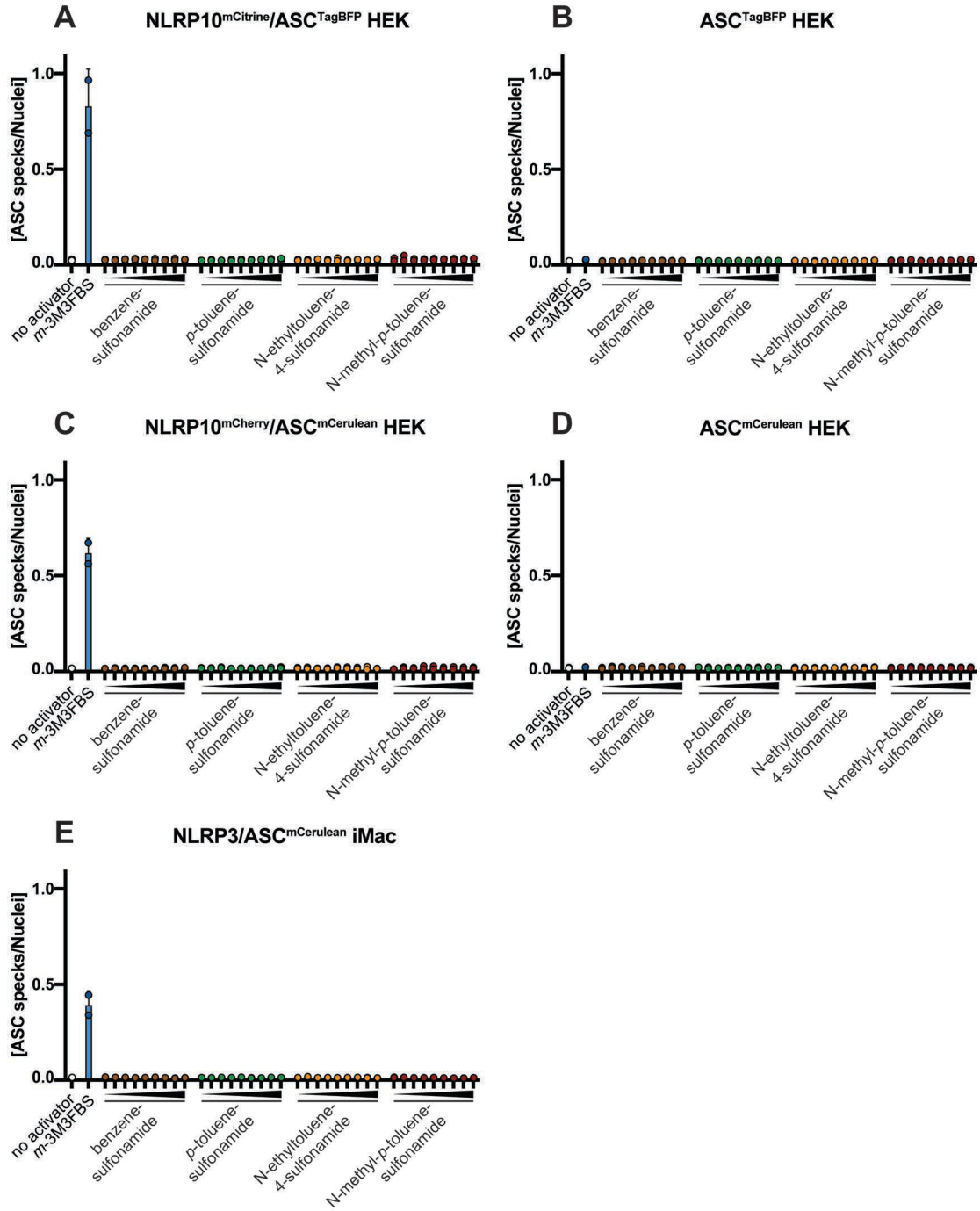

Supplementary figure S16: Simple benzenesulfonamide derivatives are not inflammasome activators

A-E: NLRP10^{mCitrine}/ASC^{TagBFP} HEK cells (A), ASC^{TagBFP} HEK cells (B), NLRP10^{mCherry}/ASC^{mCerulean} HEK cells (C), ASC^{mCerulean} HEK cells (D), and NLRP3/ASC^{mCerulean} reporter iMac cells (E) were shifted to an extracellular medium consisting of (in mM) 123 NaCl, 5 KCl, 2 $MgCl_2$, 1 $CaCl_2$, 10 glucose, 10 HEPES pH 7.4 and then stimulated with *m*-3M3FBS (85 μM; positive control) or with increasing doses (10, 25, 50, 75, 100, 200, 300, 400, or 500 μM) of benzenesulfonamide, *p*-toluenesulfonamide, N-ethyltoluene-4-sulfonamide, or N-methyl-*p*-toluenesulfonamide. The untreated ('no activator') controls were subjected to medium alone. Immediately after addition of the stimuli, the plates were centrifuged at 340 × g for 5 min (RT). After 60 min, the cells were fixed with 4% formaldehyde, counterstained with the nuclear dye DRAQ5 (5 μM) and imaged using a widefield fluorescence microscope.
The results are plotted as means from 2 independent experiments performed in technical duplicate. Error bars represent SD. Individual data points represent means of the technical duplicate values from each of the independent experiments.

Supplementary Figure S17:

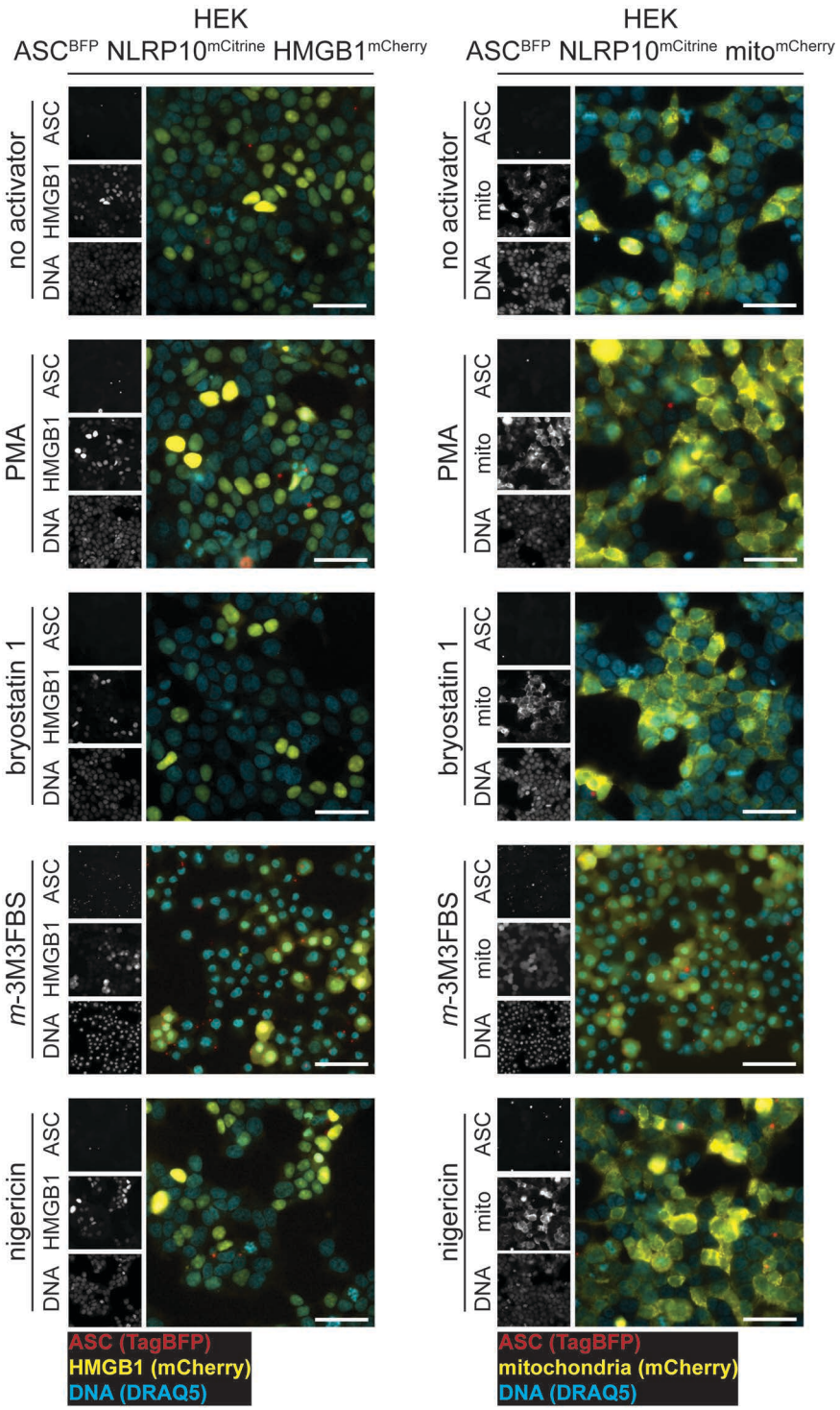

Supplementary figure S17: The PKC activators PMA and bryostatin 1 do not induce nuclear and mitochondrial contents leakage in NLRP10^{mCitrine}/ASC^{TagBFP}/HMGB1^{mCherry} reporter and NLRP10^{mCitrine}/ASC^{TagBFP}/mito^{mCherry} reporter HEK cells

HEK cells stably overexpressing NLRP10^{mCitrine}, ASC^{TagBFP}, and the nuclear marker HMGB1^{mCherry} (left column) or the mitochondrial marker mito^{mCherry} (right column) were shifted to an extracellular medium consisting of (in mM) 123 NaCl, 5 KCl, 2 $MgCl_2$, 1 $CaCl_2$, 10 glucose, 10 HEPES pH 7.4 supplemented with 40 μM VX-765 and stimulated with PMA (5 μM), bryostatin 1 (500 nM), *m*-3M3FBS (85 μM), or nigericin (10 μM). The untreated ('no activator') controls were subjected to medium alone. Immediately after addition of the stimuli, the plates were centrifuged at 340 × g for 5 min (RT). After 30 min, the cells were fixed with 4% formaldehyde, counterstained with the nuclear dye DRAQ5 (5 μM) and imaged using a widefield fluorescence microscope.

The images are representative of 3 independent experiments. Scale bars correspond to 50 μm.

Supplementary Figure S18:

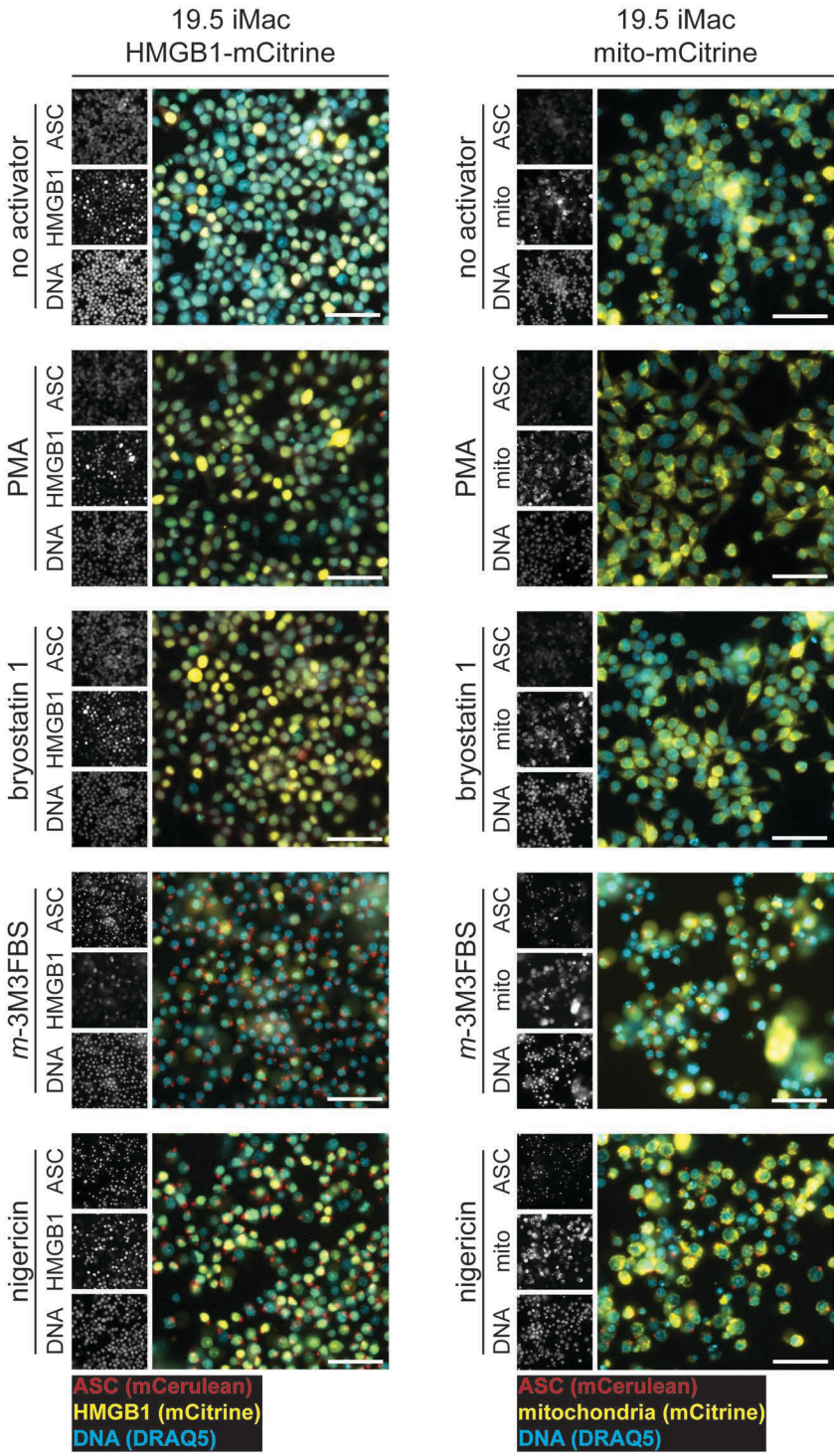

Supplementary figure S18: The PKC activators PMA and bryostatin 1 do not induce nuclear and mitochondrial contents leakage in NLRP3/ASC^{mCerulean}/HMGB1^{mCitrine} reporter and NLRP3/ASC^{mCerulean}/mito^{mCitrine} reporter iMac cells

NLRP3/ASC^{mCerulean} reporter iMac cells stably overexpressing the nuclear marker HMGB1^{mCitrine} (left column) or the mitochondrial marker mito^{mCitrine} (right column) were shifted to an extracellular medium consisting of (in mM) 123 NaCl, 5 KCl, 2 $MgCl_2$, 1 $CaCl_2$, 10 glucose, 10 HEPES pH 7.4 supplemented with 40 μM VX-765 and stimulated with PMA (5 μM), bryostatin 1 (500 nM), *m*-3M3FBS (85 μM), or nigericin (10 μM). The untreated ('no activator') controls were subjected to medium alone. Immediately after addition of the stimuli, the plates were centrifuged at 340 × g for 5 min (RT). After 30 min, the cells were fixed with 4% formaldehyde, counterstained with the nuclear dye DRAQ5 (5 μM) and imaged using a widefield fluorescence microscope.

The images are representative of 3 independent experiments. Scale bars correspond to 50 μm.

Supplementary Figure S19:

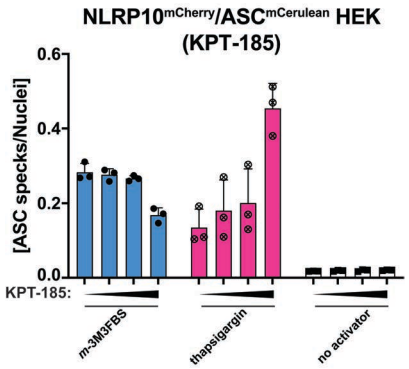

Supplementary figure S19: The nuclear export inhibitor KPT-185 does not inhibit the NLRP10 inflammasome activation

NLRP10^{mCherry}/ASC^{mCerulean} HEK cells were treated for 10 min with KPT-185 (0, 5, 10, or 50 μM; A-C) and then subjected to the inflammasome activators *m*-3M3FBS (85 μM) and thapsigargin (20 μM) in an extracellular medium consisting of (in mM) 123 NaCl, 5 KCl, 2 $MgCl_2$, 1 $CaCl_2$, 10 glucose, 10 HEPES, pH 7.4. The untreated ('no activator') controls were subjected to medium alone. Immediately after addition of inflammasome activators, the plates were centrifuged at 340 × g for 5 min (RT). After 30 min, the cells were fixed with 4% formaldehyde, counterstained with the nuclear dye DRAQ5 (5 μM) and imaged using a widefield fluorescence microscope.

The results are plotted as means from 3 independent experiments performed in technical duplicate. Error bars represent SD. Individual data points represent means of the technical duplicate values from each of the independent experiments.

Supplementary Figure S20:

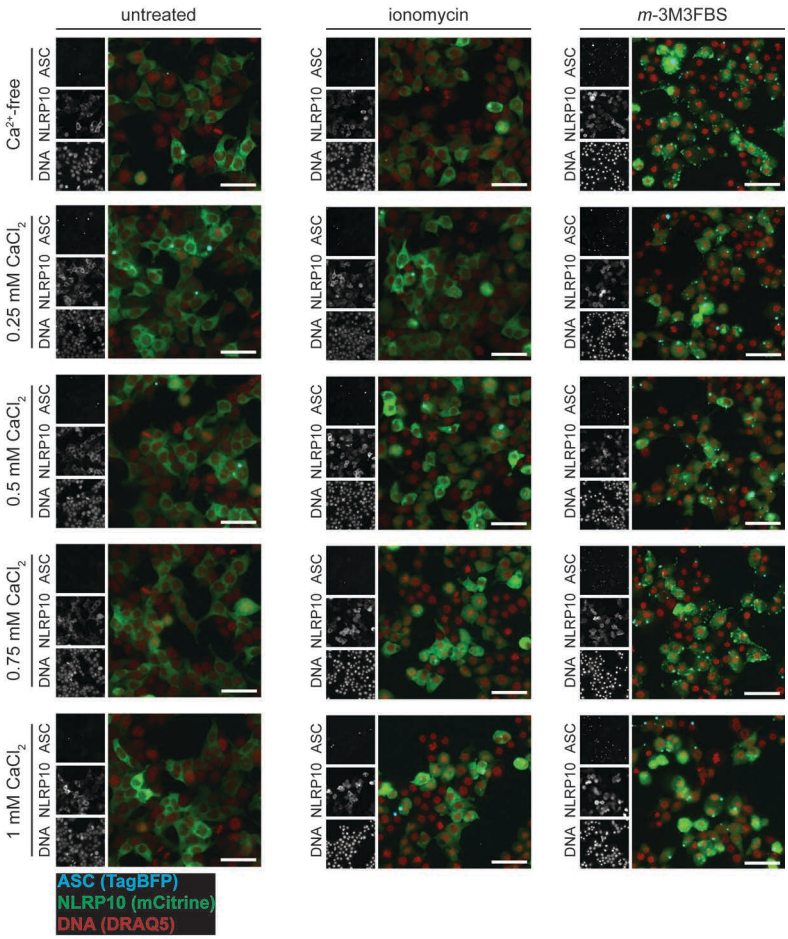

Supplementary figure S20: Treatments with ionomycin in the presence of $CaCl_2$ and with *m*-3M3FBS counteract the NLRP10 nuclear exclusion, indicating mixing of nuclear and cytosolic contents

◂ Representative images of the ASC^{TagBFP}, $NLRP10^{mCitrine}$, and DRAQ5 (DNA) channels recorded from $NLRP10^{mCitrine}/ASC^{TagBFP}$ HEK cells analyzed in Figure 6.35. Under all *m*-3M3FBS-treated conditions (right column) and 10 μM ionomycin-treated conditions at 750 μM and 1 mM $CaCl_2$ (central column, rows 4 and 5), the loss of nuclear exclusion of NLRP10 can be observed, compared to the untreated conditions (left column).
$NLRP10^{mCitrine}/ASC^{TagBFP}$ HEK cells were shifted to extracellular media consisting of (in mM) 123 NaCl, 5 KCl, 2 $MgCl_2$, 10 glucose, 10 HEPES pH 7.4 with the addition of 0, 62.5, 125, 250, 500, 600, 750, or 1000 μM $CaCl_2$. Then the cells were stimulated with ionomycin (10 μM) or m-3M3FBS (85 μM). The untreated controls were subjected to media alone. Immediately after addition of the stimuli, the plates were centrifuged at 340 × g for 5 min (RT). After 60 min, the cells were fixed with 4% formaldehyde, counterstained with the nuclear dye DRAQ5 (5 μM) and imaged using a widefield fluorescence microscope.
The images are representative of 3 independent experiments. Scale bars correspond to 50 μm.

Supplementary Figure S21:

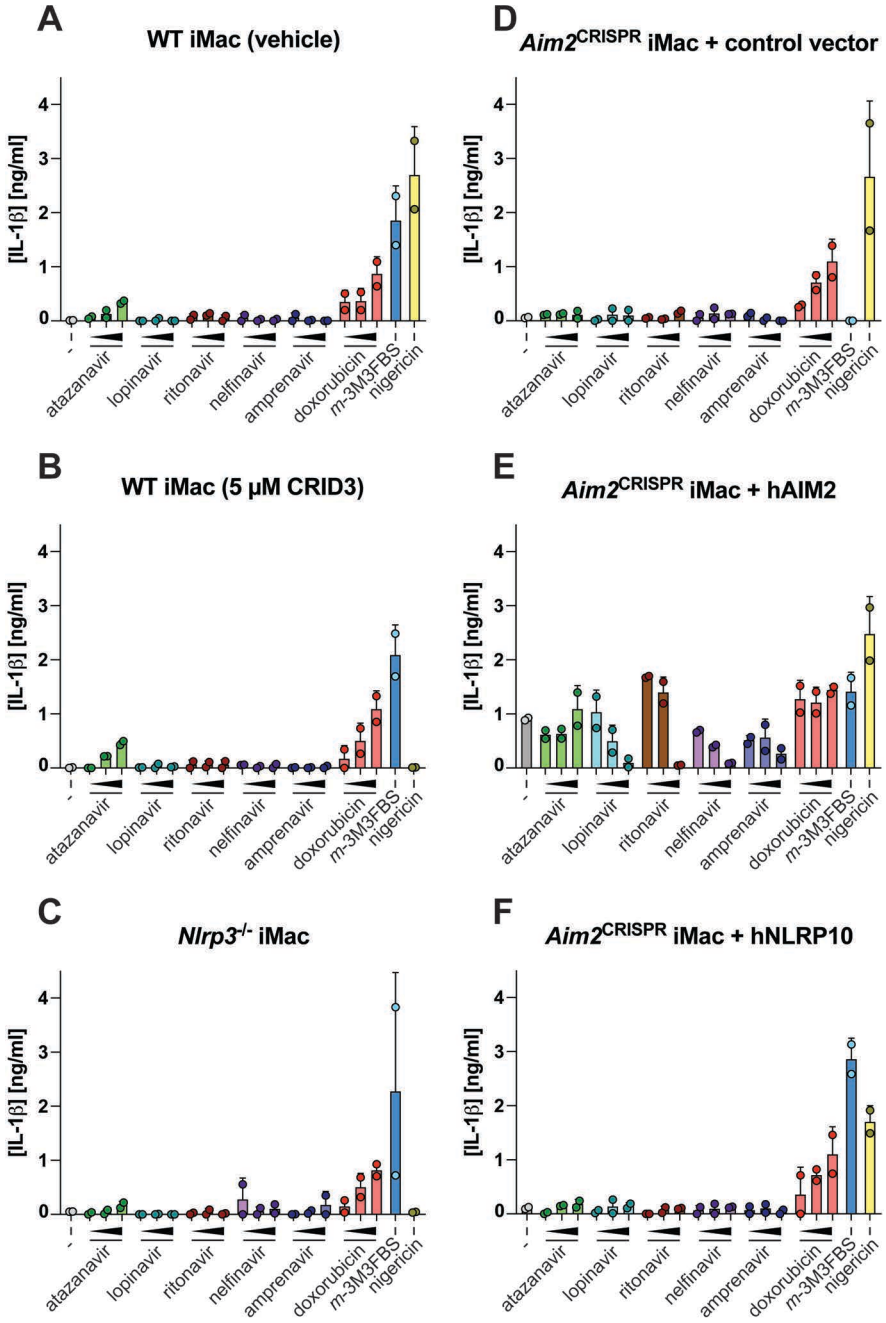

Supplementary figure S21: Concentrations of IL-1β secreted by macrophages stimulated with the HIV protease inhibitors atazanavir, lopinavir, ritonavir, nelfinavir, and amprenavir, and the antitumor drug doxorubicin

◂ **A-F:** LPS-primed (100 ng/mL, 1 h; LPS was present in the stimulation medium for the duration of the entire experiment) WT iMac cells in the absence (A) or presence (B) of the NLRP3 inhibitor CRID3 (5 μM), NLRP3-deficient (*Nlrp3*$^{-/-}$) iMac cells (C), and *Aim2*^{CRISPR} iMac cells stably transduced with the empty vector (D), WT human (h) AIM2 (E), or WT hNLRP10 (F) were subjected to the HIV protease inhibitors atazanavir (10, 25, or 50 μM), lopinavir (10, 25, or 50 μM), ritonavir (10, 25, or 50 μM), nelfinavir (10, 25, or 50 μM), or amprenavir (10, 25, or 50 μM), or to the antitumor drug doxorubicin (1, 5, or 10 μM). The LPS (-) controls were subjected to medium alone. All stimulations were performed in DMEM supplemented with 5% FBS. Immediately after addition of inflammasome activators, the plates were centrifuged at 340 × g for 5 min (RT). After 24 h, the supernatants were collected and IL-1β concentrations were measured by HTRF. 60 min before the completion of the experiment, the positive control (*m*-3M3FBS and nigericin) cells were shifted to an extracellular medium consisting of (in mM) 123 NaCl, 5 KCl, 2 $MgCl_2$, 1 $CaCl_2$, 10 glucose, 10 HEPES pH 7.4 and stimulated with *m*-3M3FBS (85 μM) or nigericin (10 μM).

The results are plotted as means from 2 independent experiments performed in technical duplicate. Error bars represent SD. Individual data points represent means of the technical duplicate values from each of the independent experiments.

Supplementary Figure S22:

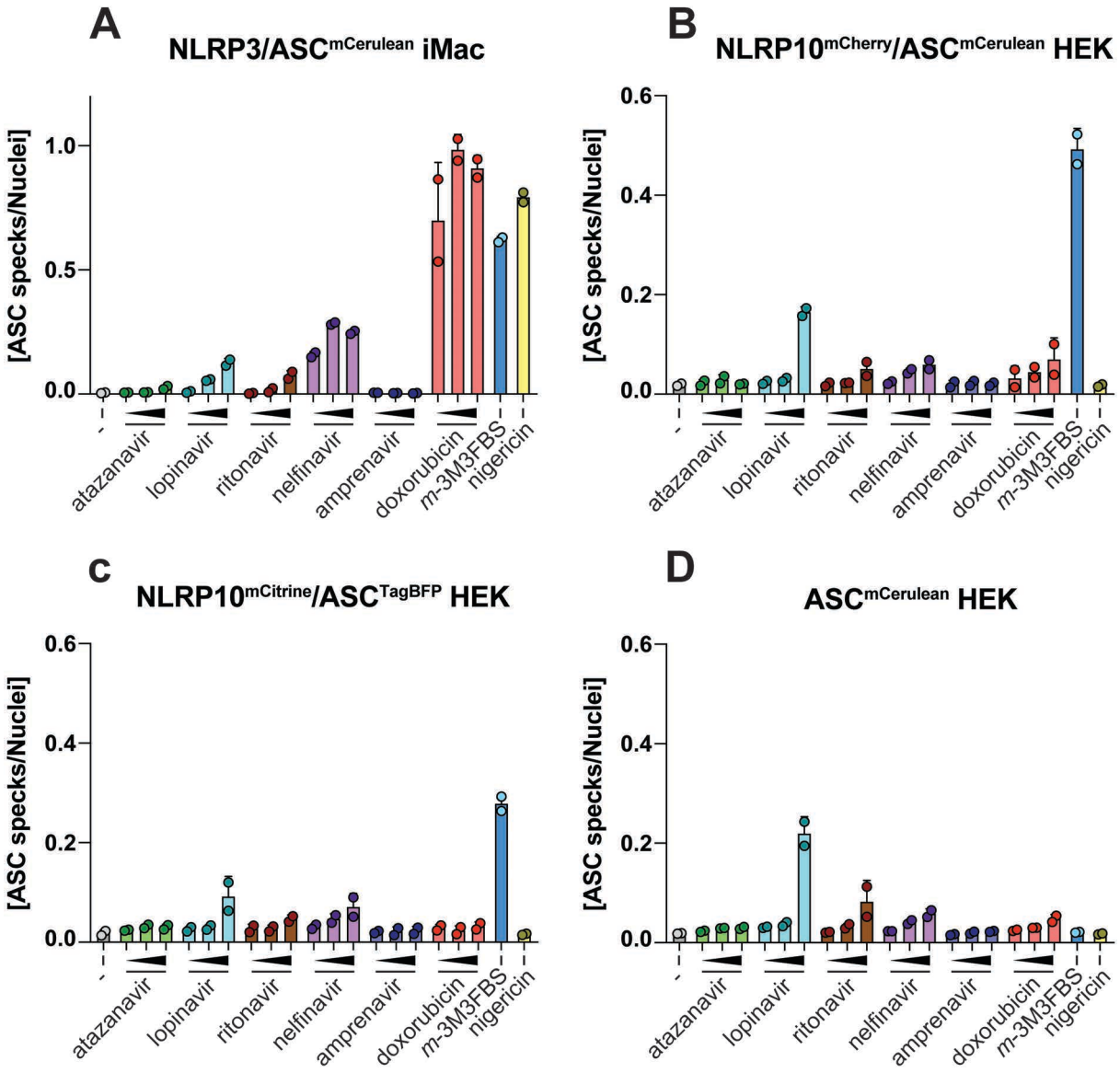

Supplementary figure S22: ASC specking in NLRP3/ASC^{mCerulean} reporter iMac cells and (NLRP10)/ASC fluorescent reporter HEK cells stimulated with the HIV protease inhibitors atazanavir, lopinavir, ritonavir, nelfinavir, and amprenavir, and the antitumor drug doxorubicin

◂ **A-D:** NLRP3/ASC^{mCerulean} reporter iMac cells (A), NLRP10^{mCherry}/ASC^{mCerulean} HEK cells (B), NLRP10^{mCitrine}/ASC^{TagBFP} HEK cells (C), and ASC^{mCerulean} HEK cells (D; NLRP10-negative control) were subjected to the HIV protease inhibitors atazanavir (10, 25, or 50 μM), lopinavir (10, 25, or 50 μM), ritonavir (10, 25, or 50 μM), nelfinavir (10, 25, or 50 μM), or amprenavir (10, 25, or 50 μM), or to the antitumor drug doxorubicin (1, 5, or 10 μM). The LPS (-) controls were subjected to medium alone. All stimulations were performed in DMEM supplemented with 5% FBS. Immediately after addition of inflammasome activators, the plates were centrifuged at 340 × g for 5 min (RT). After 24 h, the supernatants were collected and IL-1β concentrations were measured by HTRF. 60 min (A) or 30 min (B-D) before the completion of the experiment, the positive control (*m*-3M3FBS and nigericin) cells were shifted to an extracellular medium consisting of (in mM) 123 NaCl, 5 KCl, 2 $MgCl_2$, 1 $CaCl_2$, 10 glucose, 10 HEPES pH 7.4 and stimulated with *m*-3M3FBS (85 μM) or nigericin (10 μM).

The results are plotted as means from 2 independent experiments performed in technical duplicate. Error bars represent SD. Individual data points represent means of the technical duplicate values from each of the independent experiments.

Supplementary Figure S23:

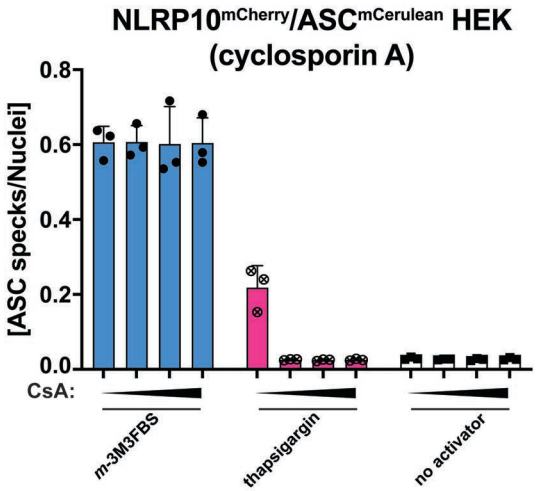

Supplementary figure S23: Cyclosporin A selectively inhibits the NLRP10-driven ASC specking response to thapsigargin

NLRP10^{mCherry}/ASC^{mCerulean} HEK cells were treated for 10 min with cyclosporin A (CsA; 0, 10, 15, or 20 μM; A-C) and then subjected to the inflammasome activators *m*-3M3FBS (85 μM) or thapsigargin (20 μM) in an extracellular medium consisting of (in mM) 123 NaCl, 5 KCl, 2 $MgCl_2$, 1 $CaCl_2$, 10 glucose, 10 HEPES, pH 7.4. The untreated ('no activator') controls were subjected to medium alone. Immediately after addition of inflammasome activators, the plates were centrifuged at 340 × g for 5 min (RT). After 30 min, the cells were fixed with 4% formaldehyde, counterstained with the nuclear dye DRAQ5 (5 μM) and imaged using a widefield fluorescence microscope.

The results are plotted as means from 3 independent experiments performed in technical duplicate. Error bars represent SD. Individual data points represent means of the technical duplicate values from each of the independent experiments.

Supplementary Figure S24:

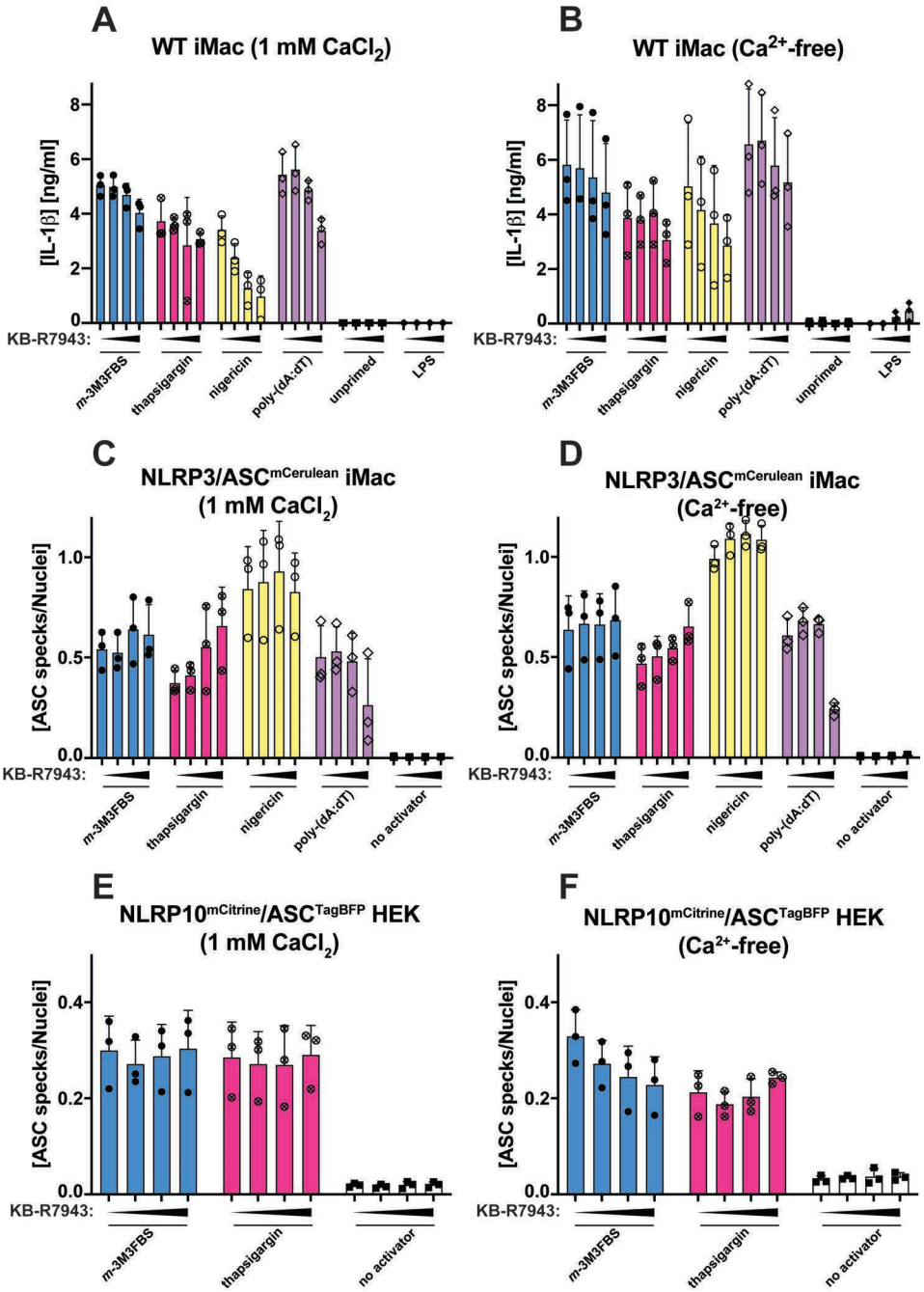

Supplementary figure S24: Influence of the mitochondrial calcium uniporter blocker KB-R7943 on the inflammasome activations with *m*-3M3FBS, thapsigargin, nigericin, and poly-(dA:dT)

A-F: LPS-primed (200 ng/mL, 2 h) WT iMac cells (A, B), NLRP3/ASC^{mCerulean} reporter iMac cells (C, D), and NLRP10^{mCitrine}/ASC^{TagBFP} HEK cells (E, F) were treated for 10 min with KB-R7943 (0, 10, 25, or 50 μM) in the presence (A, C, E) or absence (B, D, F) of extracellular Ca^{2+} and then subjected to the inflammasome activators *m*-3M3FBS (85 μM), thapsigargin (20 μM), nigericin (10 μM) or poly-(dA:dT) (2 μg/mL complexed with 5 μL Lipofectamine 2000) in an extracellular medium consisting of (in mM) 123 NaCl, 5 KCl, 2 $MgCl_2$, 0 or 1 $CaCl_2$, 10 glucose, 10 HEPES, pH 7.4. The LPS (A, B) and unprimed (A-F) controls were subjected to medium alone. Immediately after addition of inflammasome activators, the plates were centrifuged at 340 × g for 5 min (RT). After 30 min (E, F) or 60 min (A-D), the supernatants were collected and IL-1β concentrations were measured by HTRF (A, B) or the cells were fixed with 4% formaldehyde, counterstained with the nuclear dye DRAQ5 (5 μM) and imaged using a widefield fluorescence microscope (C-F).

The results are plotted as means from 3 independent experiments performed in technical duplicate. Error bars represent SD. Individual data points represent means of the technical duplicate values from each of the independent experiments.

Supplementary Figure S25:

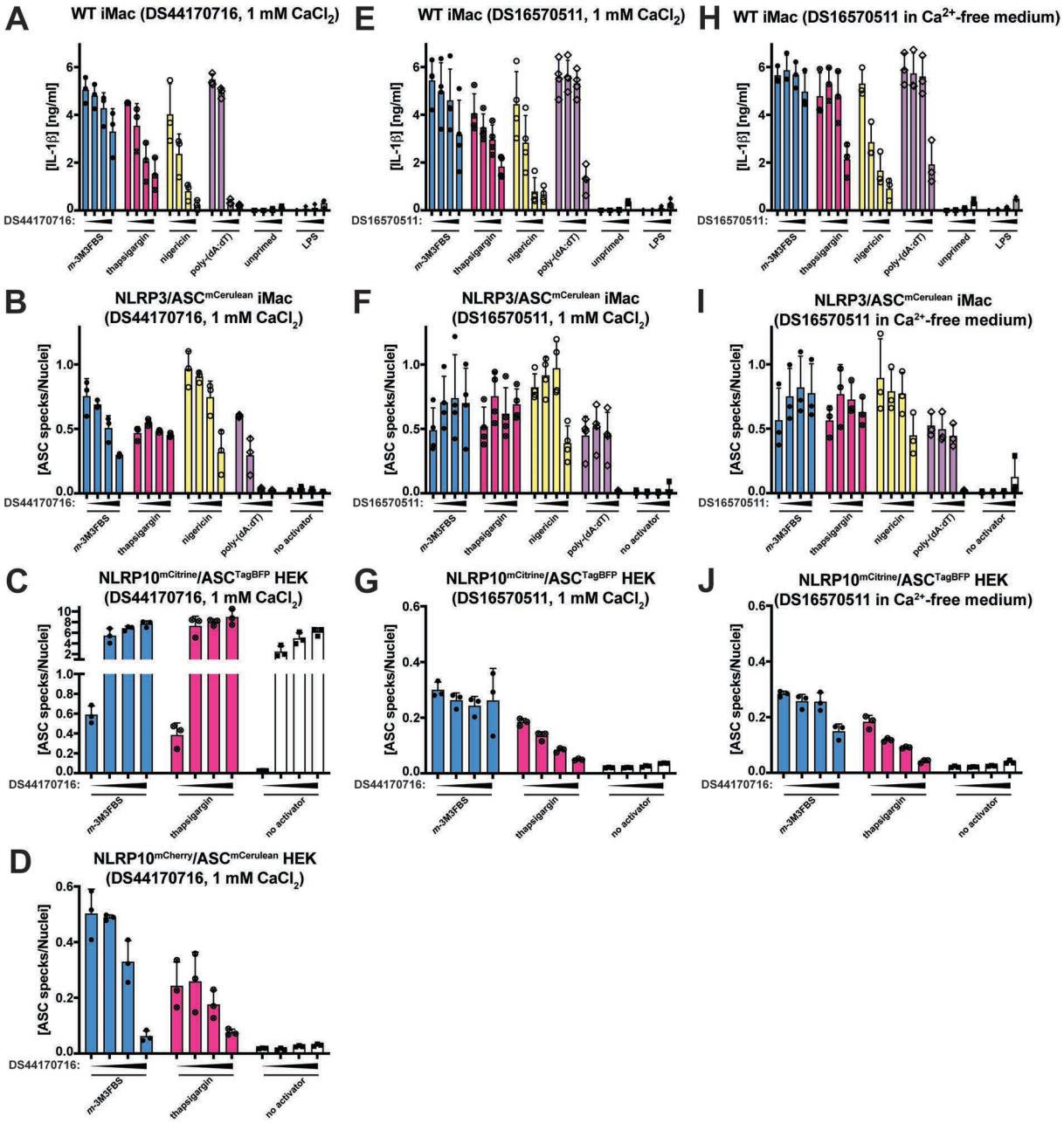

Supplementary figure S25: Influence of the mitoprotective agent DS44170716 and the mitochondrial calcium uniporter blocker DS16570511 on the inflammasome activations with *m*-3M3FBS, thapsigargin, nigericin, and poly-(dA:dT)

A-J: LPS-primed (200 ng/mL, 2 h) WT iMac cells (A, E, H), NLRP3/ASC^{mCerulean} reporter iMac cells (B, F, I), NLRP10^{mCitrine}/ASC^{TagBFP} HEK cells (C, G, I), and NLRP10^{mCherry}/ASC^{mCerulean} HEK cells (D) were treated for 10 min with DS44170716 (0, 10, 25, or 50 μM; A-D) in the presence of 1 mM extracellular Ca^{2+} or with DS16570511 (0, 25, 50, or 100 μM; E-J) in the presence (E-G) or absence (H-J) of extracellular Ca^{2+}. Then, the cells were subjected to the inflammasome activators *m*-3M3FBS (85 μM), thapsigargin (20 μM), nigericin (10 μM) or poly-(dA:dT) (2 μg/mL complexed with 5 μL Lipofectamine 2000) in an extracellular medium consisting of (in mM) 123 NaCl, 5 KCl, 2 $MgCl_2$, 0 or 1 $CaCl_2$, 10 glucose, 10 HEPES, pH 7.4. The LPS (A, E, H) and unprimed (A-J) controls were subjected to medium alone. Immediately after addition of inflammasome activators, the plates were centrifuged at 340 × g for 5 min (RT). After 30 min (C, D, G, J) or 60 min (A, B, E, F, H, I), the supernatants were collected and IL-1β concentrations were measured by HTRF (A, E, H) or the cells were fixed with 4% formaldehyde, counterstained with the nuclear dye DRAQ5 (5 μM) and imaged using a widefield fluorescence microscope (B-D, F, G, I, J).

The results are plotted as means from 3 (A-D, G-J) or 4 (E, F) independent experiments performed in technical duplicate. Error bars represent SD. Individual data points represent means of the technical duplicate values from each of the independent experiments.

Supplementary Figure S26:

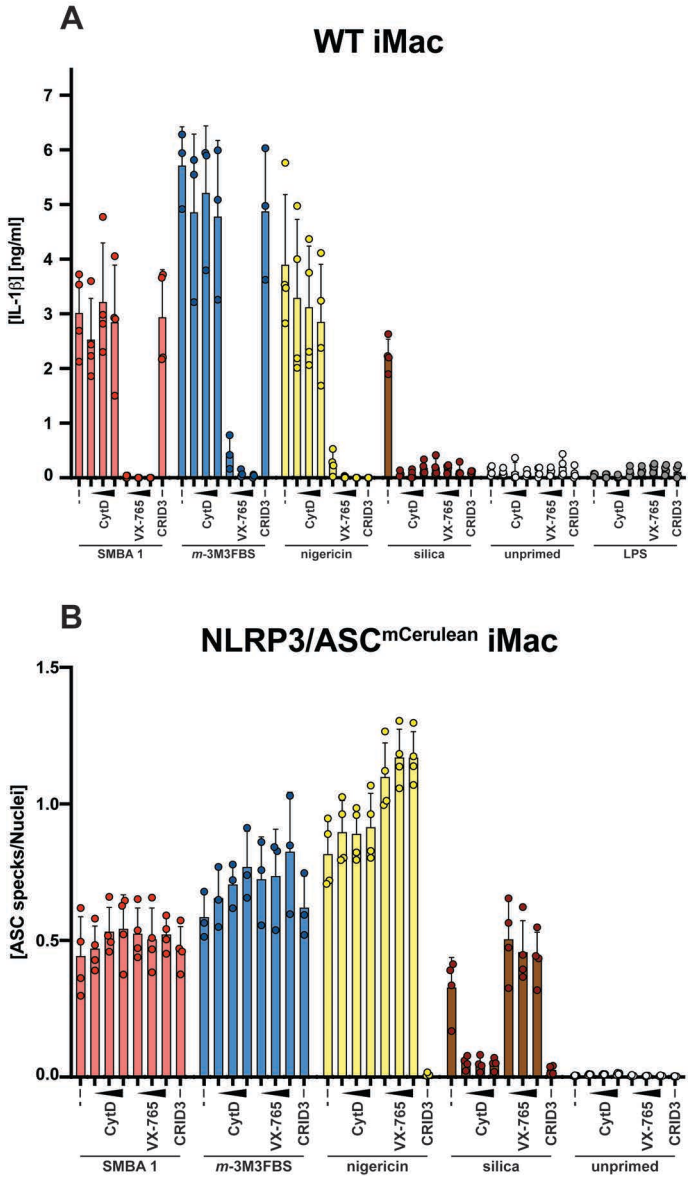

Supplementary figure S26: Sensitivity of the SMBA 1-induced inflammasome activation to the phagocytosis inhibitor cytochalasin D, the caspase-1 inhibitor VX-765, and the NLRP3 inhibitor CRID3

A, B: LPS-primed WT iMac cells (A) and NLRP3/ASC^{mCerulean} reporter iMac cells (B) were shifted to an extracellular medium consisting of (in mM) 123 NaCl, 5 KCl, 2 $MgCl_2$, 1 $CaCl_2$, 10 glucose, 10 HEPES pH 7.4 and left untreated (-) or pre-treated for 10 min with cytochalasin D (CytD; 10, 25, or 50 μM), VX-765 (10, 25, or 50 μM) or CRID3 (5 μM). (Importantly, the cells under the silica-stimulated, unprimed, and LPS control conditions were kept in DMEM supplemented with 10% FBS; the shift to the minimal medium was not performed. Consequently, all pre-treatments and stimulations for these conditions were performed in DMEM supplemented with 10% FBS.) Next, the cells were left untreated or were stimulated with the following inflammasome activators: SMBA1 (50 μM; red bars), *m*-3M3FBS (85 μM; blue bars), nigericin (10 μM; yellow bars), or silica crystals (500 μg/mL; brown bars). Immediately after addition of inflammasome activators, the plates were centrifuged at 340 × g for 5 min (RT). After 60 min (SMBA1, *m*-3M3FBS, and nigericin stimulations) or 6 h (silica stimulation and the LPS and unprimed controls), the supernatants were collected and IL-1β concentrations were measured by HTRF (A) or the cells were fixed with 4% formaldehyde, counterstained with the nuclear dye DRAQ5 (5 μM) and imaged using a widefield fluorescence microscope (B).

The results are plotted as means from 4 independent experiments for all activators except *m*-3M3FBS, and 3 independent experiments for *m*-3M3FBS. The experiments were performed in technical duplicate. Error bars represent SD. Individual data points represent means of the technical duplicate values from each of the independent experiments.

Supplementary Figure S27:

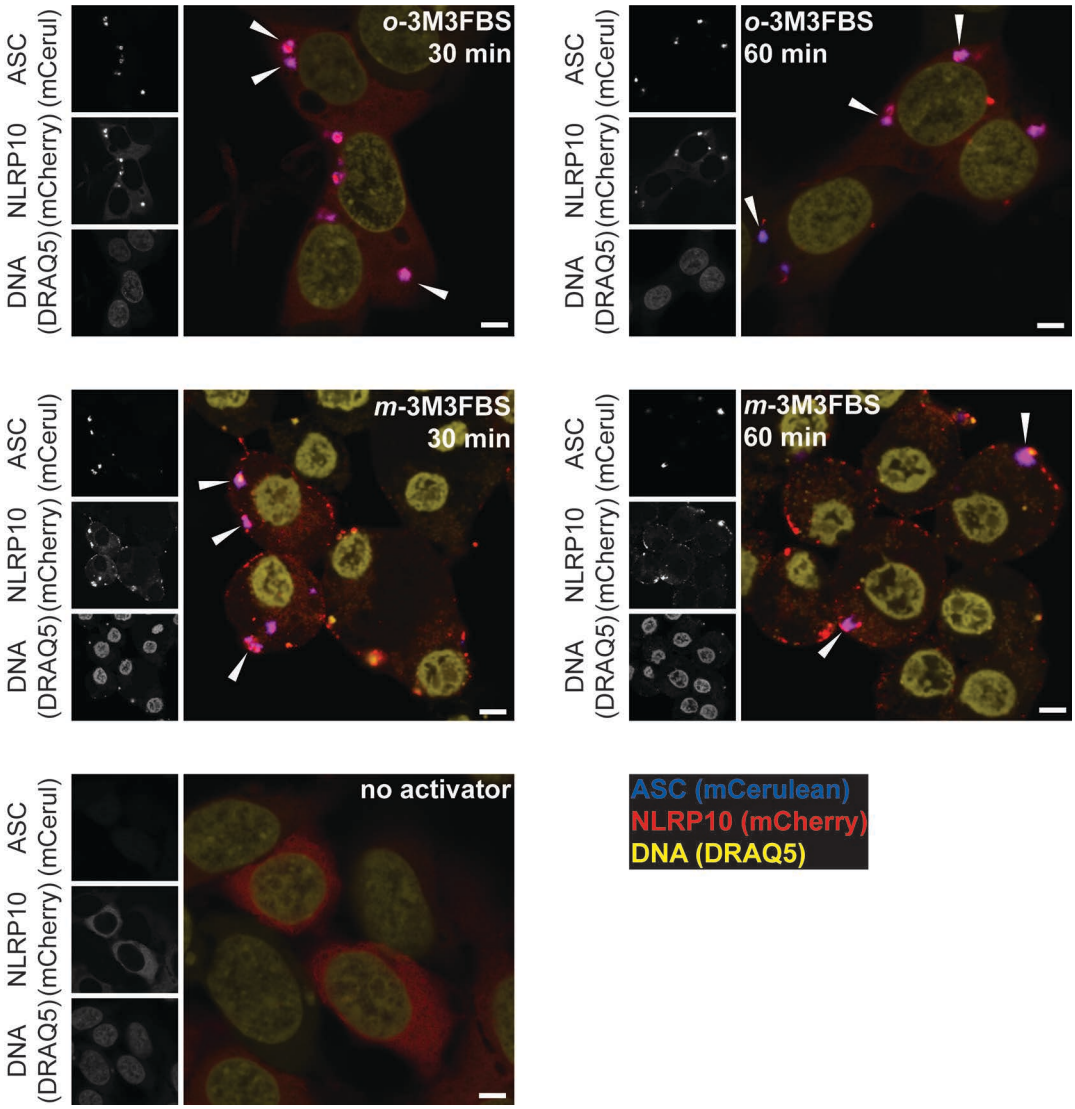

Supplementary Figure S27: NLRP10/ASC colocalization in NLRP10^{mCherry}/ASC^{mCerulean} reporter HEK cells stimulated with *m*-3M3FBS or *o*-3M3FBS

NLRP10^{mCherry}/ASC^{mCerulean} HEK cells were treated with *m*-3M3FBS (85 µM) or *o*-3M3FBS (85 µM) in an extracellular medium consisting of (in mM) 123 NaCl, 5 KCl, 2 $MgCl_2$, 1 $CaCl_2$, 10 glucose, 10 HEPES, pH 7.4. Directly after administration of inflammasome activators, the cells were centrifuged at RT, 340 × g for 5 min. The untreated controls were subjected to 60 min of medium alone. After 30 or 60 min of stimulation (as indicated in the panels), the cells were fixed with 4% formaldehyde, counterstained with the nuclear dye DRAQ5 (5 µM) and imaged using a confocal microscope.
Images are representative of 4 independent experiments. Scale bars correspond to 5 µm.

Supplementary Figure S28:

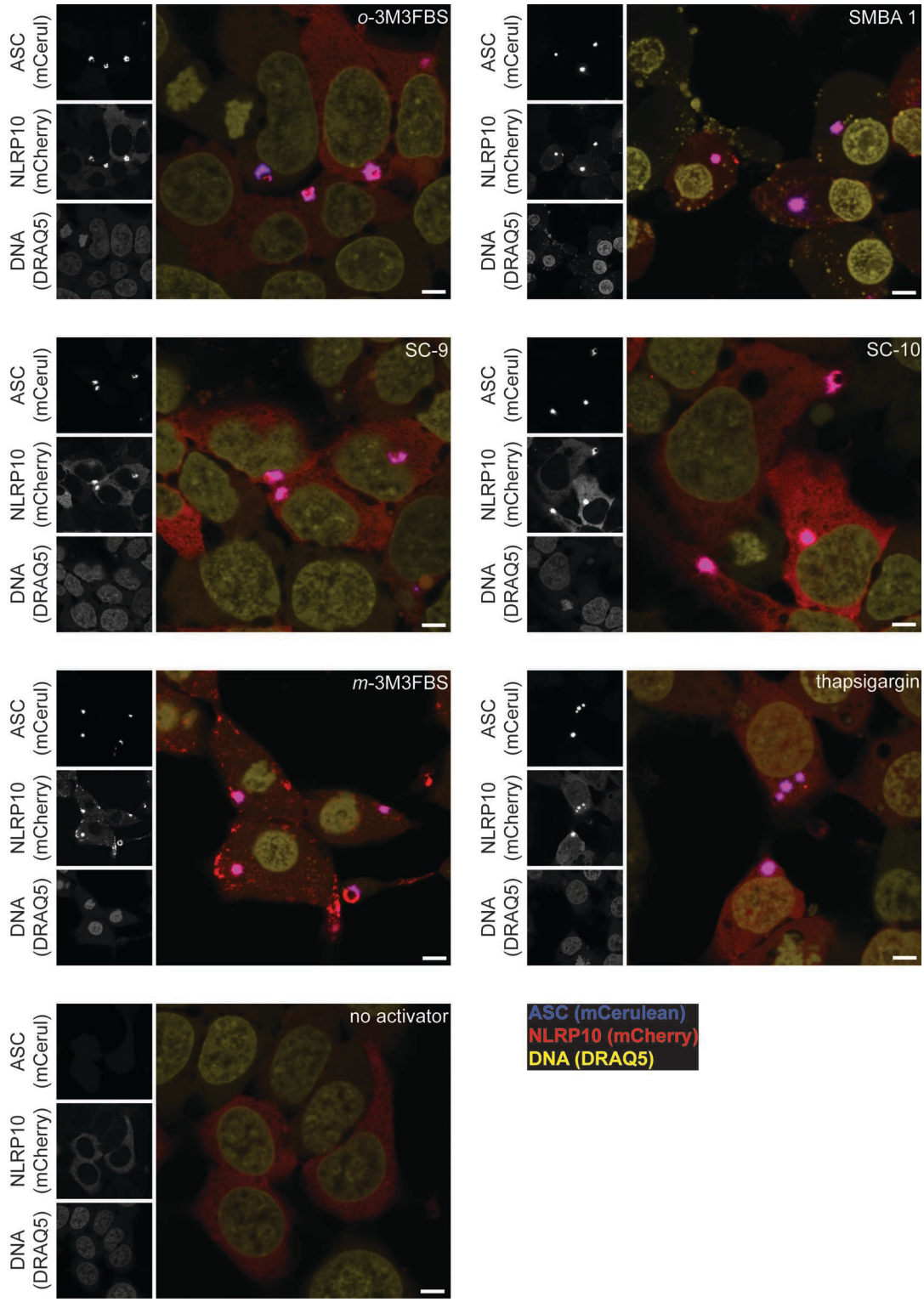

Supplementary Figure S28: NLRP10/ASC colocalization in NLRP10^{mCherry}/ASC^{mCerulean} reporter HEK cells stimulated with *m*-3M3FBS, *o*-3M3FBS, SC-9, SC-10, SMBA 1, or thapsigargin

NLRP10^{mCherry}/ASC^{mCerulean} HEK cells were treated with *m*-3M3FBS (85 µM), *o*-3M3FBS (85 µM), SC-9 (100 µM), SC-10 (100 µM), SMBA1 (50 µM), or thapsigargin (20 µM) in an extracellular medium consisting of (in mM) 123 NaCl, 5 KCl, 2 $MgCl_2$, 1 $CaCl_2$, 10 glucose, 10 HEPES, pH 7.4. The untreated controls were subjected to medium alone. Directly after administration of inflammasome activators, the cells were centrifuged at RT, 340 × g for 5 min. After 30 min of stimulation, the cells were fixed with 4% formaldehyde, counterstained with the nuclear dye DRAQ5 (5 µM) and imaged using a confocal microscope.

Images are representative of 3 independent experiments. Scale bars correspond to 5 µm.

Supplementary Figure S29:

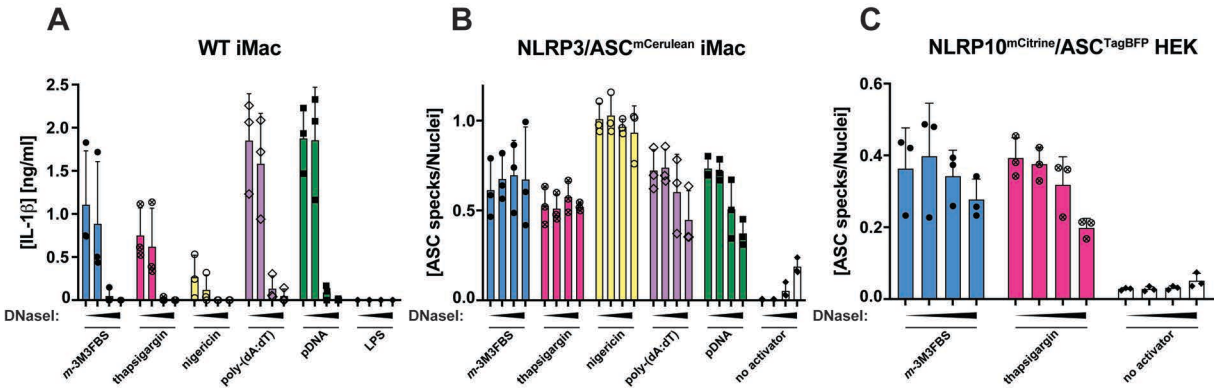

Supplementary Figure S29: Influence of DNase I protein transfection on the inflammasome responses to *m*-3M3FBS, thapsigargin, nigericin, and dsDNA in WT iMac cells, NLRP3/ASC^{mCerulean} reporter iMac cells, and NLRP10^{mCitrine}/ASC^{TagBFP} reporter HEK cells

Protein transfection with DNase I was performed as described by Jabir et al. (2014). WT iMac cells (A), NLR3/ASC^{mCerulean} reporter iMac cells (B), and NLRP10^{mCitrine}/ASC^{TagBFP} HEK cells (C) were loaded with DNase I (0, 60, 300, or 500 ng per well in a 96-well plate) using the PULSin protein transfection reagent (at the ratio of 4 μL of PULSin per 1 μg of protein). The loading step (5 h) was performed in OptiMEM **without** FBS supplementation. After the DNase I delivery, the cells were shifted to DMEM supplemented with 10% FBS and primed with LPS (200 ng/mL, 90 min; A) or left unprimed (90 min; B, C). Finally, the cells were shifted to an extracellular medium consisting of (in mM) 123 NaCl, 5 KCl, 2 $MgCl_2$, 1 $CaCl_2$, 10 glucose, 10 HEPES pH 7.4 and subjected to the following inflammasome activators: *m*-3M3FBS (85 μM), thapsigargin (20 μM), nigericin (10 μM), poly-(dA:dT) (2 μg/mL complexed with 5 μL Lipofectamine 2000) or plasmid (p) DNA (2 μg/mL complexed with 5 μL Lipofectamine 2000). The LPS (A) and unprimed (B, C) controls were subjected to medium alone. Immediately after addition of inflammasome activators, the plates were centrifuged at 340 × g for 5 min (RT). After 30 min (C) or 60 min (A, B), the supernatants were collected and IL-1β concentrations were measured by HTRF (A) or the cells were fixed with 4% formaldehyde, counterstained with the nuclear dye DRAQ5 (5 μM) and imaged using a widefield fluorescence microscope (B, C).

The results are plotted as means from 3 independent experiments performed in technical duplicate (A, B) or triplicate (C). Error bars represent SD. Individual data points represent means of the technical duplicate (A, B) or triplicate (C) values from each of the independent experiments. As evidenced in the figure, the data are not consistent between panels A and B (DNase I protein transfection appears to globally inhibit IL-1β secretion [A] but has no impact on ASC speck formation [B]). Importantly, the AIM2-driven ASC speck formation in response to transfected DNA (either poly-(dA:dT) or pDNA) was not inhibited (B), suggesting that DNase I delivered into the cells may not be active.

Supplementary Figure S30:

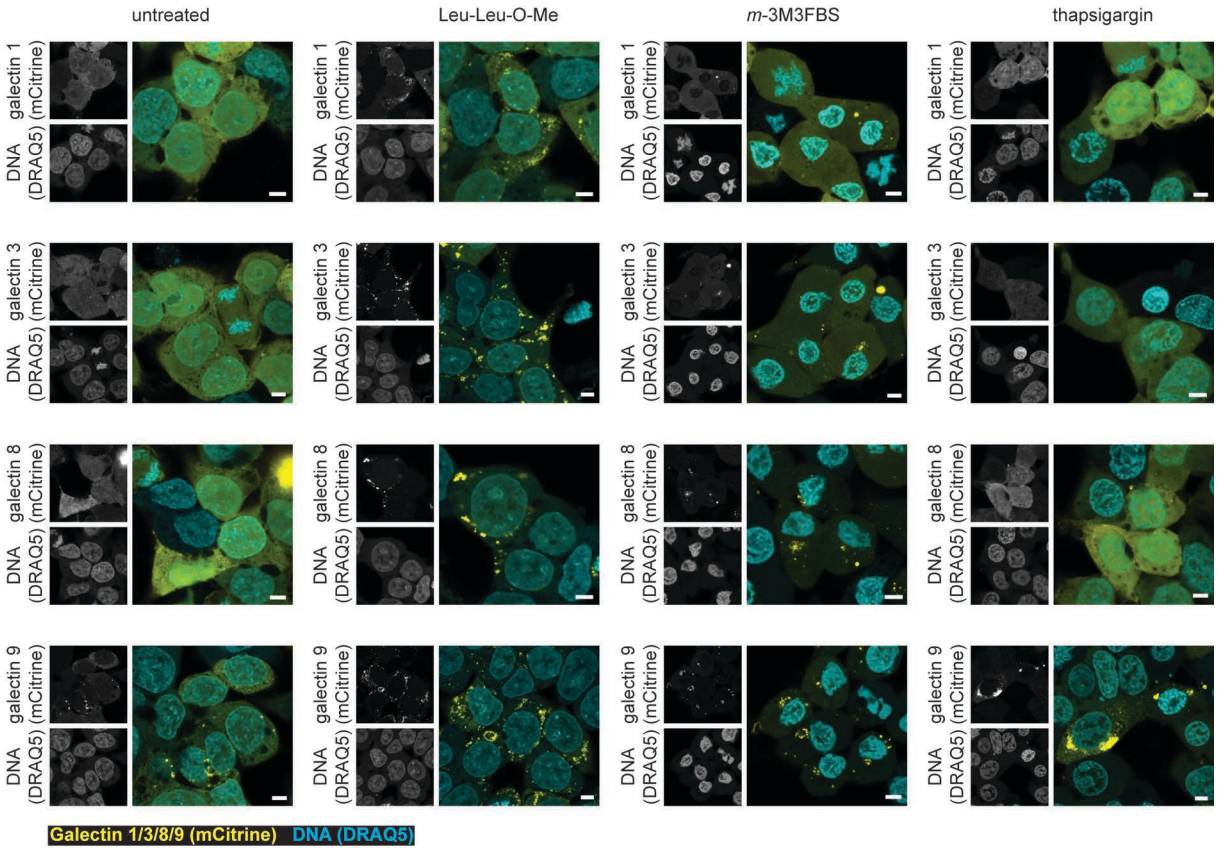

Supplementary figure S30: Influence of Leu-Leu-O-Me, *m*-3M3FBS, and thapsigargin on the distribution patterns of mCitrine-tagged galectin 1, 3, 8, and 9 in HEK cells

HEK cells were transiently transfected (100 ng of DNA per well in a 96-well plate; the transfection reagent was Gene Juice and it was used at the ratio of 2.7 µL of Gene Juice per 1 µg of DNA) with vectors encoding galectin 1 (row 1), galectin 3 (row 2), galectin 8 (row 3), or galectin 9 (row 4) expressed as fusion proteins with mCitrine. After 24 h of transfection, the cells were shifted to an extracellular medium consisting of (in mM) 123 NaCl, 5 KCl, 2 $MgCl_2$, 1 $CaCl_2$, 10 glucose, 10 HEPES pH 7.4 and subjected to the inflammasome activators *m*-3M3FBS (85 µM), thapsigargin (20 µM), or Leu-Leu-O-Me (1 mM). The untreated controls were subjected to medium alone. Immediately after addition of inflammasome activators, the plates were centrifuged at 340 × g for 5 min (RT). After 60 min, the cells were fixed with 4% formaldehyde, counterstained with the nuclear dye DRAQ5 (5 µM) and imaged using a confocal microscope.
Images are representative of 4 independent experiments. Scale bars correspond to 5 µm.

Supplementary Figure S31:

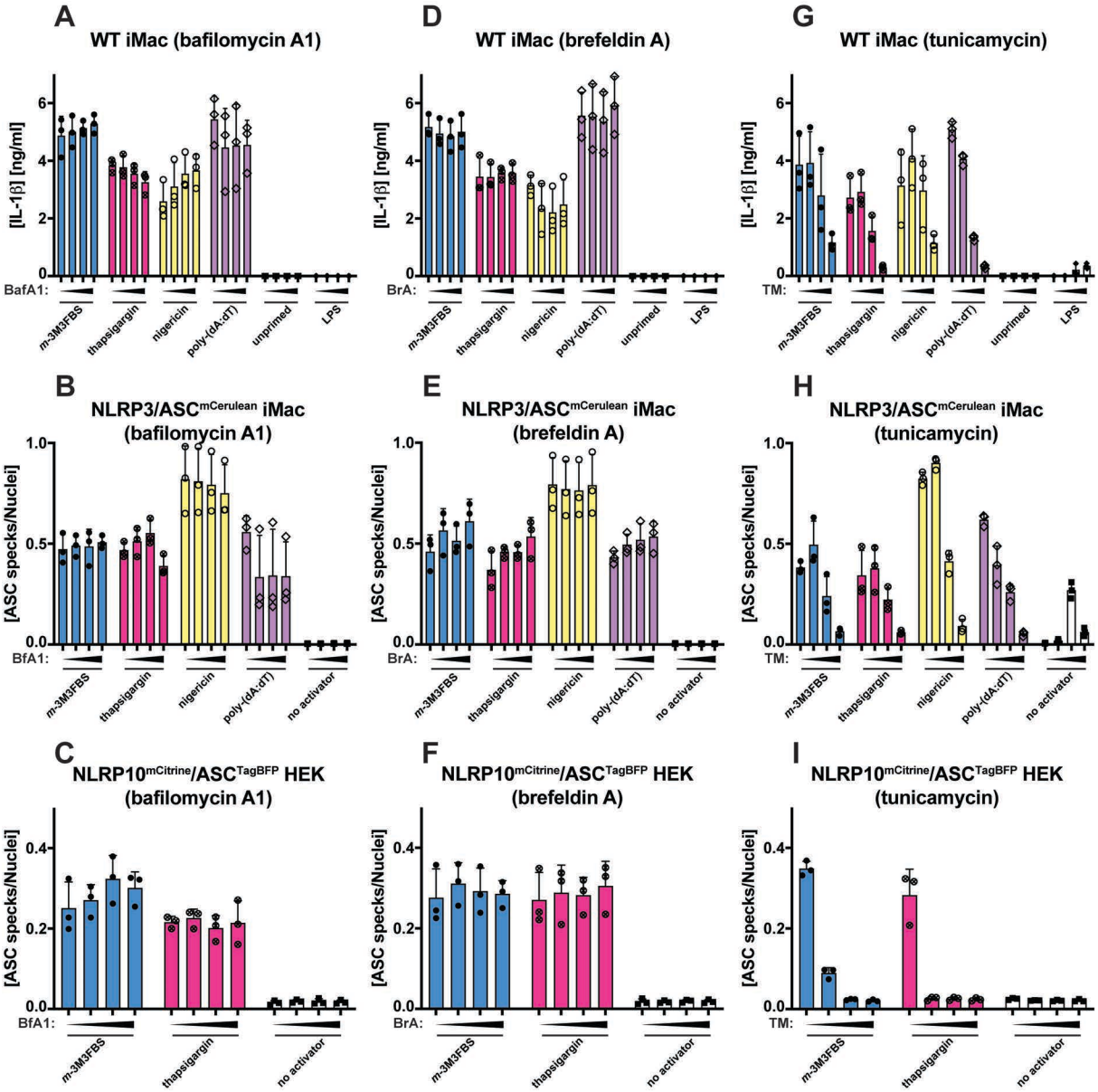

Supplementary figure S31: Influence of bafilomycin A1, brefeldin A and tunicamycin on the inflammasome responses to *m*-3M3FBS, thapsigargin, nigericin, and poly-(dA:dT)

A-I: LPS-primed (200 ng/mL, 2 h) WT iMac cells (A, D, G), NLRP3/ASC^{mCerulean} reporter iMac cells (B, E, H), and NLRP10^{mCitrine}/ASC^{TagBFP} HEK cells (C, F, I) were treated for 10 min with bafilomycin A1 (BfA1; 0, 50, 125, or 250 nM; A-C), brefeldin A (BrA; 0, 5, 10, or 25 μg/mL; D-F) or tunicamycin (TM; 0, 10, 25, or 50 μM; G-I). Then, the cells were subjected to the inflammasome activators *m*-3M3FBS (85 μM), thapsigargin (20 μM), nigericin (10 μM) or poly-(dA:dT) (2 μg/mL complexed with 5 μL Lipofectamine 2000) in an extracellular medium consisting of (in mM) 123 NaCl, 5 KCl, 2 $MgCl_2$, 1 $CaCl_2$, 10 glucose, 10 HEPES, pH 7.4. The LPS (A, D, G) and unprimed (A-I) controls were subjected to medium alone. Immediately after addition of inflammasome activators, the plates were centrifuged at 340 × g for 5 min (RT). After 30 min (C, F, I) or 60 min (A, B, D, E, G, H), the supernatants were collected and IL-1β concentrations were measured by HTRF (A, D, G) or the cells were fixed with 4% formaldehyde, counterstained with the nuclear dye DRAQ5 (5 μM) and imaged using a widefield fluorescence microscope (B, C, E, F, H, I).

The results are plotted as means from 3 independent experiments performed in technical duplicate. Error bars represent SD. Individual data points represent means of the technical duplicate values from each of the independent experiments.

Supplementary Figure S32:

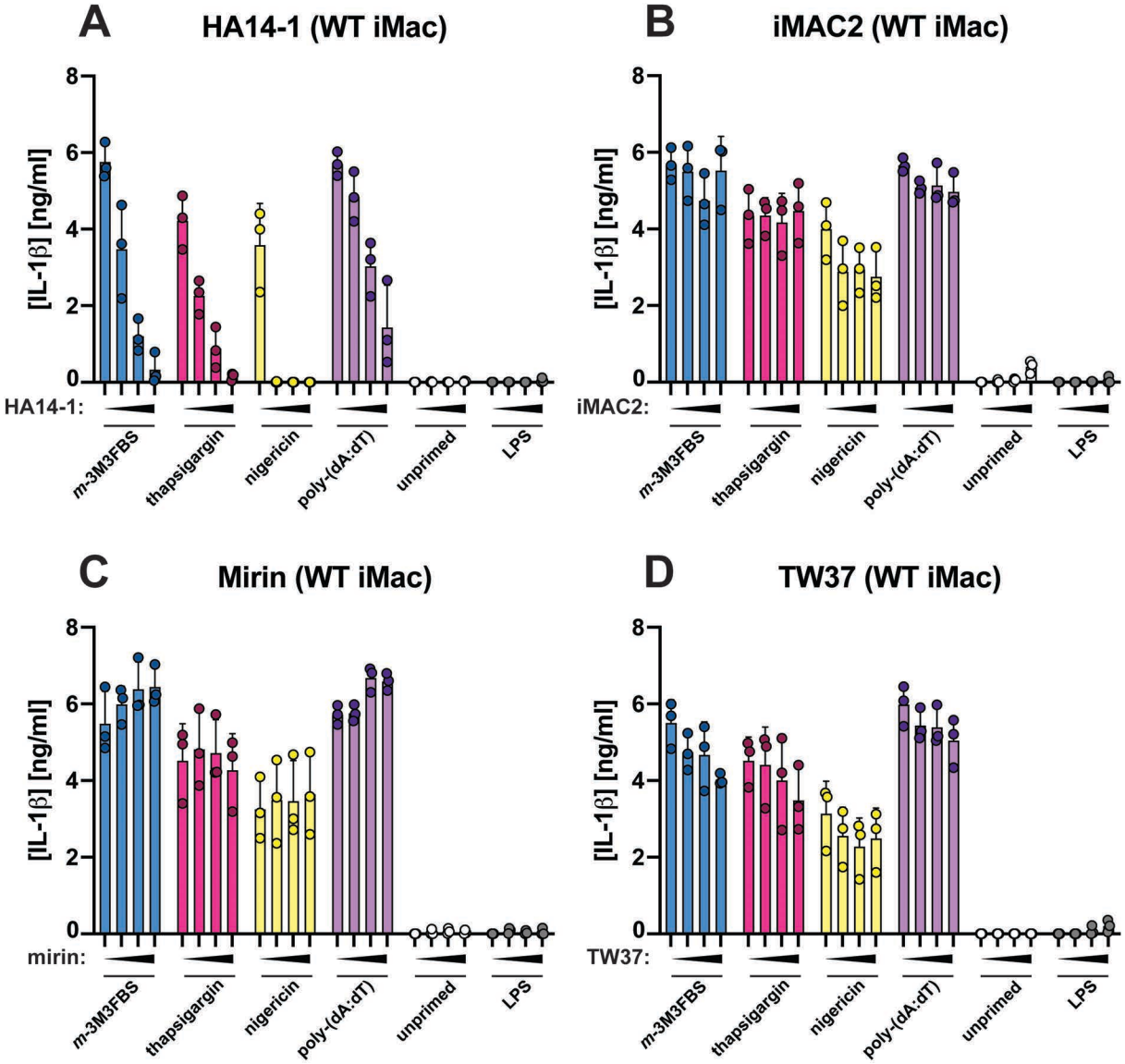

Supplementary figure S32: Influence of HA14-1, iMAC2, mirin, and TW37 on the inflammasome responses to *m*-3M3FBS, thapsigargin, nigericin, and poly-(dA:dT) in WT iMac cells

A-D: LPS-primed (200 ng/mL, 2 h) WT iMac cells were treated for 10 min with HA14-1 (0, 10, 25, or 50 μM; A), iMAC2 (0, 5, 10, or 50 μM; B), mirin (0, 20, 50, or 100 μM; C) or TW37 (0, 10, 25, or 50 μM; D). Then, the cells were subjected to the inflammasome activators *m*-3M3FBS (85 μM), thapsigargin (20 μM), nigericin (10 μM) or poly-(dA:dT) (2 μg/mL complexed with 5 μL Lipofectamine 2000) in an extracellular medium consisting of (in mM) 123 NaCl, 5 KCl, 2 $MgCl_2$, 1 $CaCl_2$, 10 glucose, 10 HEPES, pH 7.4. The LPS and unprimed controls were subjected to medium alone. Immediately after addition of inflammasome activators, the plates were centrifuged at 340 × g for 5 min (RT). After 60 min, the supernatants were collected and IL-1β concentrations were measured by HTRF.

The results are plotted as means from 3 independent experiments performed in technical duplicate. Error bars represent SD. Individual data points represent means of the technical duplicate values from each of the independent experiments.

Supplementary Figure S33:

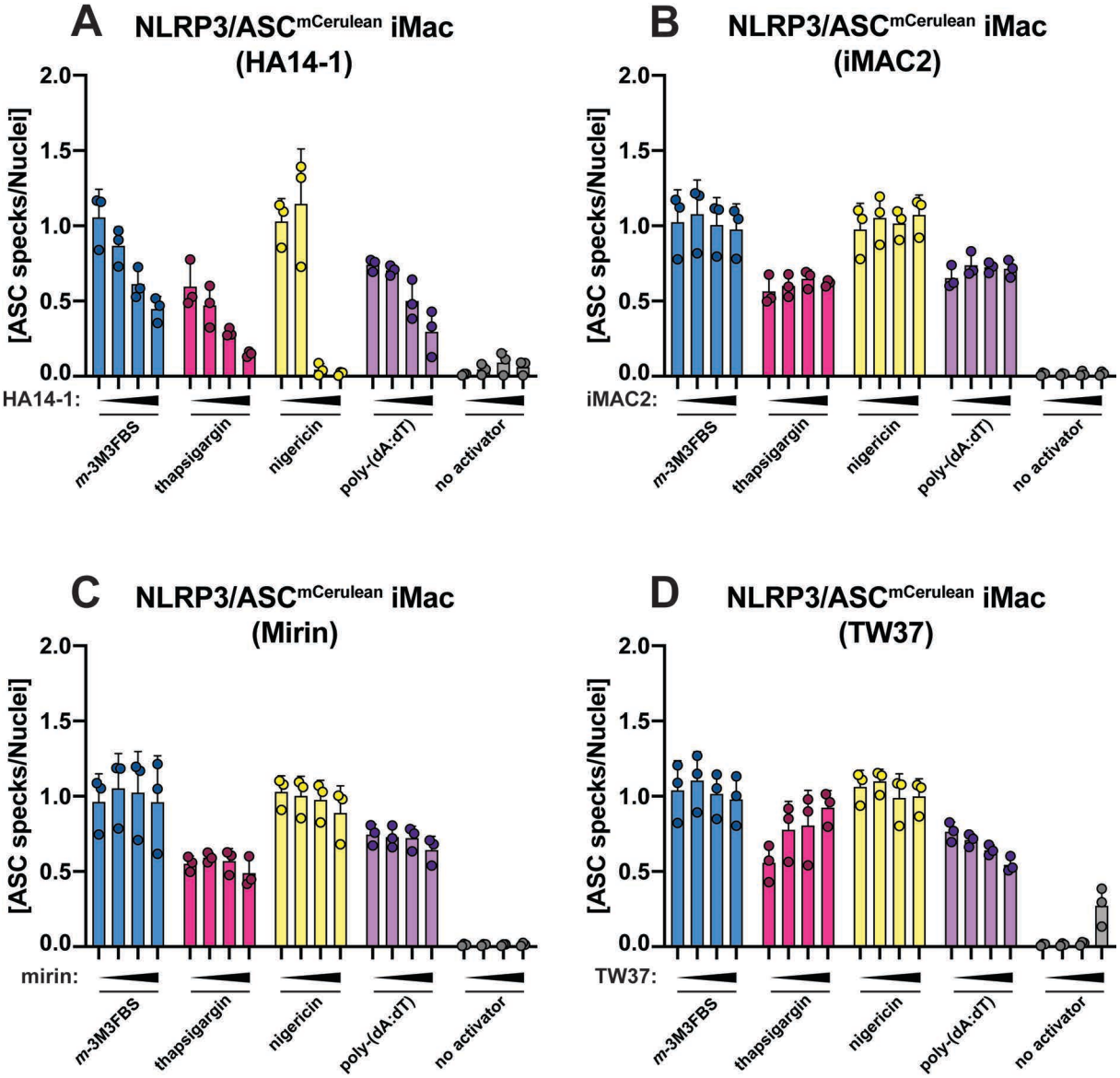

Supplementary figure S33: Influence of HA14-1, iMAC2, mirin, and TW37 on the inflammasome responses to *m*-3M3FBS, thapsigargin, nigericin, and poly-(dA:dT) in NLRP3/ASC^{mCerulean} reporter iMac cells

A-D: NLRP3/ASC^{mCerulean} reporter iMac cells were treated for 10 min with HA14-1 (0, 10, 25, or 50 μM; A), iMAC2 (0, 5, 10, or 50 μM; B), mirin (0, 20, 50, or 100 μM; C) or TW37 (0, 10, 25, or 50 μM; D). Then, the cells were subjected to the inflammasome activators *m*-3M3FBS (85 μM), thapsigargin (20 μM), nigericin (10 μM) or poly-(dA:dT) (2 μg/mL complexed with 5 μL Lipofectamine 2000) in an extracellular medium consisting of (in mM) 123 NaCl, 5 KCl, 2 $MgCl_2$, 1 $CaCl_2$, 10 glucose, 10 HEPES, pH 7.4. The untreated ('no activator') controls were subjected to medium alone. Immediately after addition of inflammasome activators, the plates were centrifuged at 340 × g for 5 min (RT). After 60 min, the cells were fixed with 4% formaldehyde, counterstained with the nuclear dye DRAQ5 (5 μM) and imaged using a widefield fluorescence microscope.

The results are plotted as means from 3 independent experiments performed in technical duplicate. Error bars represent SD. Individual data points represent means of the technical duplicate values from each of the independent experiments.

Supplementary Figure S34:

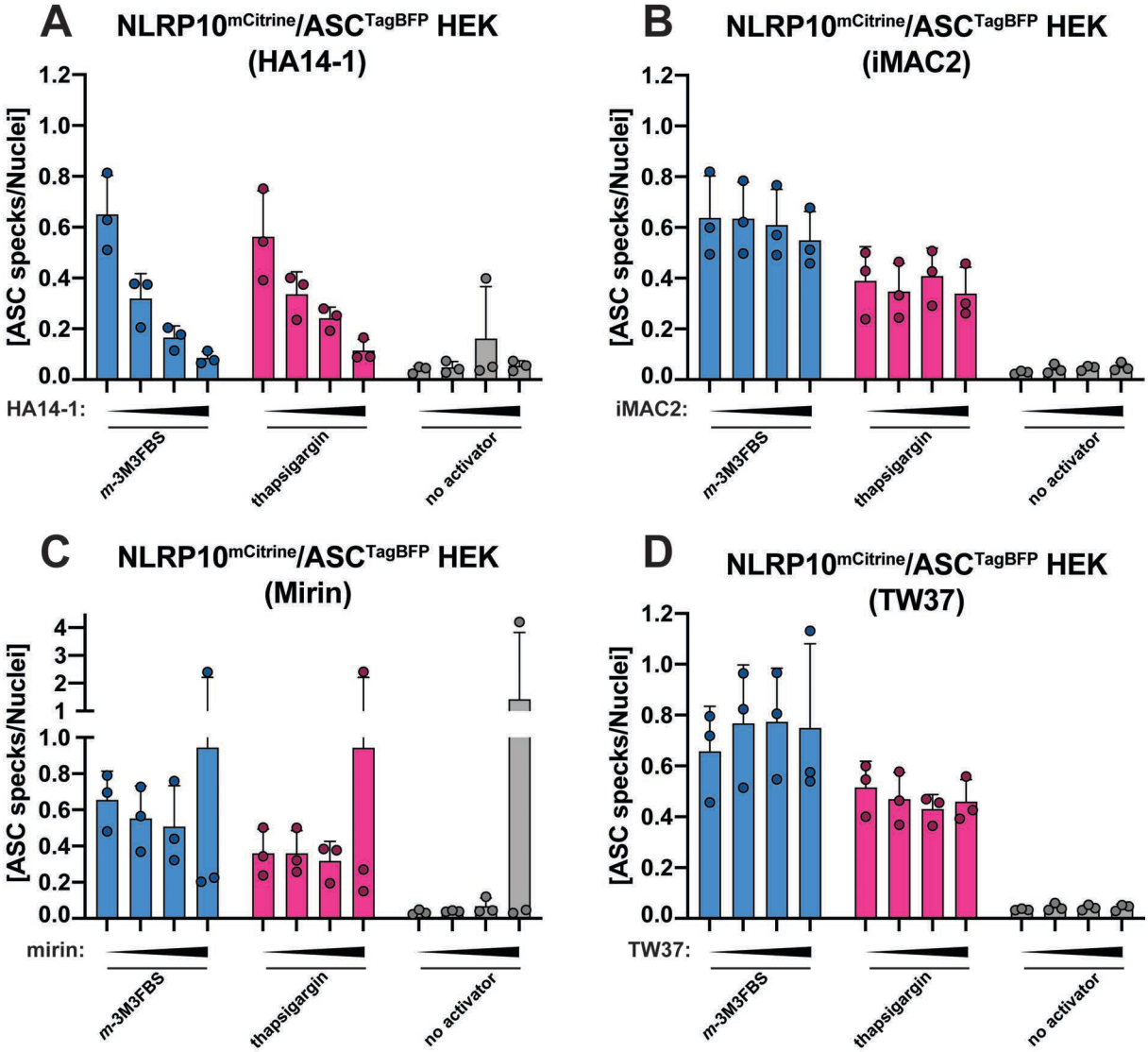

Supplementary figure S34: Influence of HA14-1, iMAC2, mirin, and TW37 on the inflammasome responses to *m*-3M3FBS and thapsigargin in NLRP10^{mCitrine}/ASC^{TagBFP} HEK cells

A-D: NLRP10^{mCitrine}/ASC^{TagBFP} HEK cells were treated for 10 min with HA14-1 (0, 10, 25, or 50 μM; A), iMAC2 (0, 5, 10, or 50 μM; B), mirin (0, 20, 50, or 100 μM; C) or TW37 (0, 10, 25, or 50 μM; D). Then, the cells were subjected to the inflammasome activators *m*-3M3FBS (85 μM) or thapsigargin (20 μM) in an extracellular medium consisting of (in mM) 123 NaCl, 5 KCl, 2 $MgCl_2$, 1 $CaCl_2$, 10 glucose, 10 HEPES, pH 7.4. The untreated ('no activator') controls were subjected to medium alone. Immediately after addition of inflammasome activators, the plates were centrifuged at 340 × g for 5 min (RT). After 30 min, the cells were fixed with 4% formaldehyde, counterstained with the nuclear dye DRAQ5 (5 μM) and imaged using a widefield fluorescence microscope.

The results are plotted as means from 3 independent experiments performed in technical duplicate. Error bars represent SD. Individual data points represent means of the technical duplicate values from each of the independent experiments.

Supplementary Figure S35:

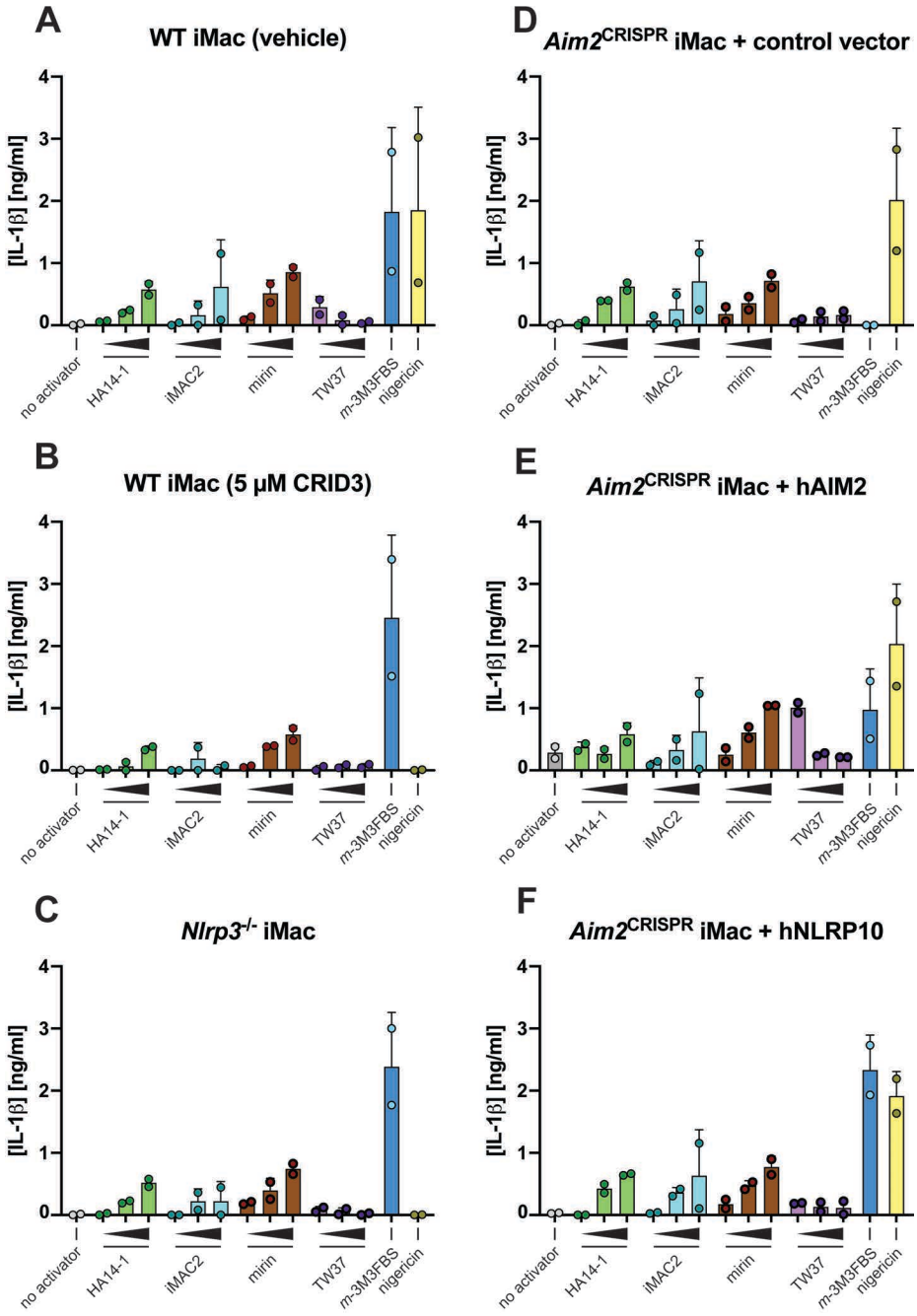

Supplementary figure S35: IL-1β secretion from immortalized murine macrophages stimulated for 24 h with HA14-1, iMAC2, mirin, or TW37

A-F: LPS-primed (100 ng/mL, 1 h; LPS was present in the stimulation medium for the duration of the entire experiment) WT iMac cells in the absence (A) or presence (B) of the NLRP3 inhibitor CRID3 (5 µM), NLRP3-deficient (*Nlrp3*$^{-/-}$) iMac cells (C), and *Aim2*^{CRISPR} iMac cells stably transduced with the empty vector (D), WT human (h) AIM2 (E), or WT hNLRP10 (F) were subjected to HA14-1 (0, 10, 25, or 50 µM), iMAC2 (0, 5, 10, or 50 µM), mirin (0, 20, 50, or 100 µM), or TW37 (0, 10, 25, or 50 µM). The LPS ('no activator') controls were subjected to medium alone. All stimulations were performed in DMEM supplemented with 5% FBS. Immediately after addition of the stimuli, the plates were centrifuged at 340 × g for 5 min (RT). After 24 h, the supernatants were collected and IL-1β concentrations were measured by HTRF. 60 min before the completion of the experiment, the positive control (*m*-3M3FBS and nigericin) cells were shifted to an extracellular medium consisting of (in mM) 123 NaCl, 5 KCl, 2 $MgCl_2$, 1 $CaCl_2$, 10 glucose, 10 HEPES pH 7.4 and stimulated with *m*-3M3FBS (85 µM) or nigericin (10 µM).
The results are plotted as means from 2 independent experiments performed in technical triplicate. Error bars represent SD. Individual data points represent means of the technical triplicate values from each of the independent experiments.

Supplementary Figure S36:

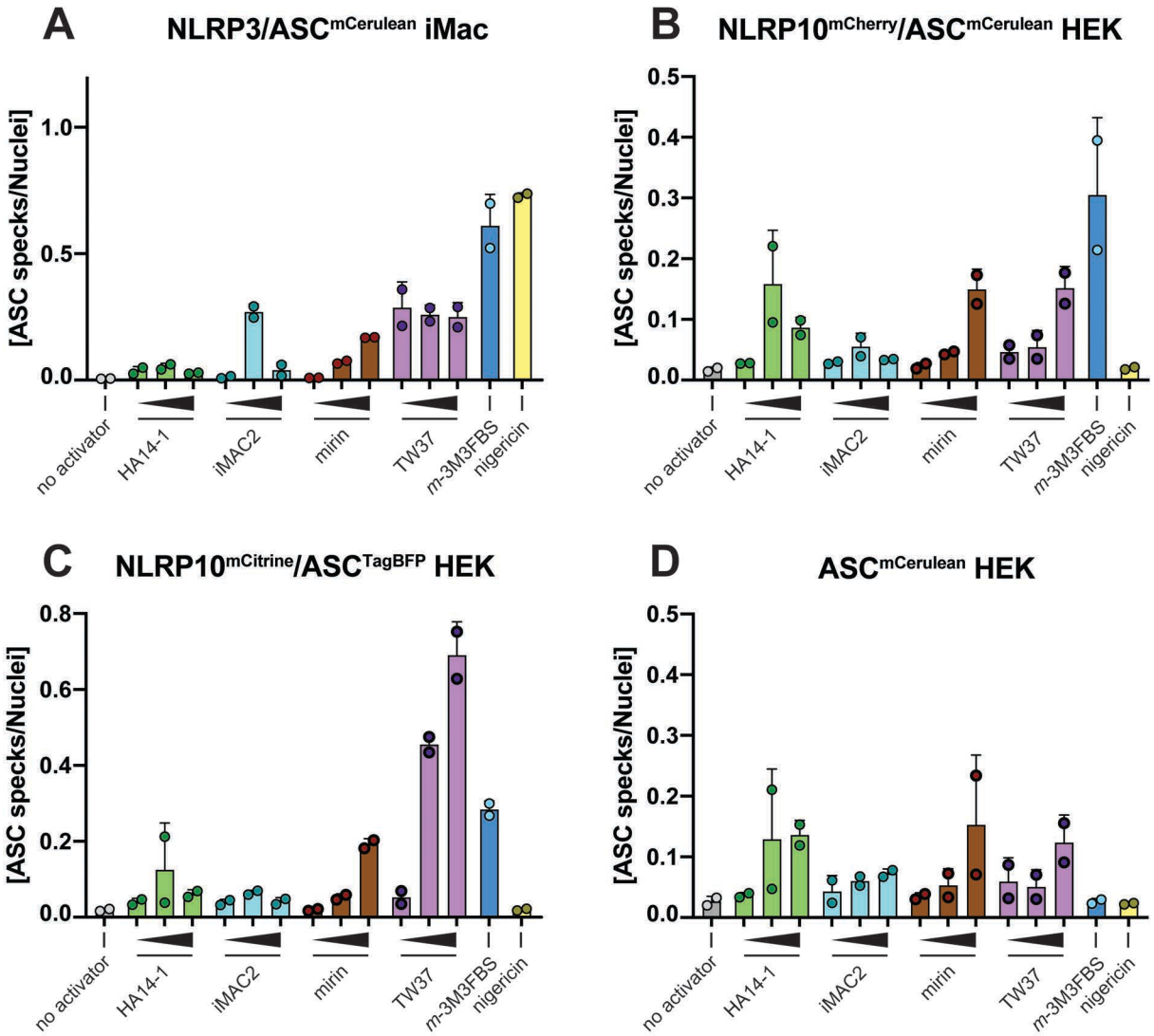

Supplementary Figure S36: ASC speck formation in NLRP3/ASC^{mCerulean} reporter iMac cells, NLRP10^{mCherry}/ASC^{mCerulean} HEK cells, NLRP10^{mCitrine}/ASC^{TagBFP} HEK cells, and ASC^{mCerulean} HEK cells stimulated for 24 h with HA14-1, iMAC2, mirin, or TW37

A-D: LPS-primed (100 ng/mL, 1 h; LPS was present in the stimulation medium for the duration of the entire experiment) NLRP3/ASC^{mCerulean} reporter iMac cells (A), NLRP10^{mCherry}/ASC^{mCerulean} HEK cells (B), NLRP10^{mCitrine}/ASC^{TagBFP} HEK cells (C), and ASC^{mCerulean} HEK cells (D; NLRP10-negative control) were subjected to HA14-1 (0, 10, 25, or 50 μM), iMAC2 (0, 5, 10, or 50 μM), mirin (0, 20, 50, or 100 μM), or TW37 (0, 10, 25, or 50 μM). The LPS ('no activator') controls were subjected to medium alone. All stimulations were performed in DMEM supplemented with 5% FBS. Immediately after addition of the stimuli, the plates were centrifuged at 340 × g for 5 min (RT). After 24 h, the cells were fixed with 4% formaldehyde, counterstained with the nuclear dye DRAQ5 (5 μM) and imaged using a widefield fluorescence microscope. 60 min before the completion of the experiment, the positive control (*m*-3M3FBS and nigericin) cells were shifted to an extracellular medium consisting of (in mM) 123 NaCl, 5 KCl, 2 $MgCl_2$, 1 $CaCl_2$, 10 glucose, 10 HEPES pH 7.4 and stimulated with *m*-3M3FBS (85 μM) or nigericin (10 μM).

The results are plotted as means from 2 independent experiments performed in technical triplicate. Error bars represent SD. Individual data points represent means of the technical triplicate values from each of the independent experiments.

Supplementary Figure S37:

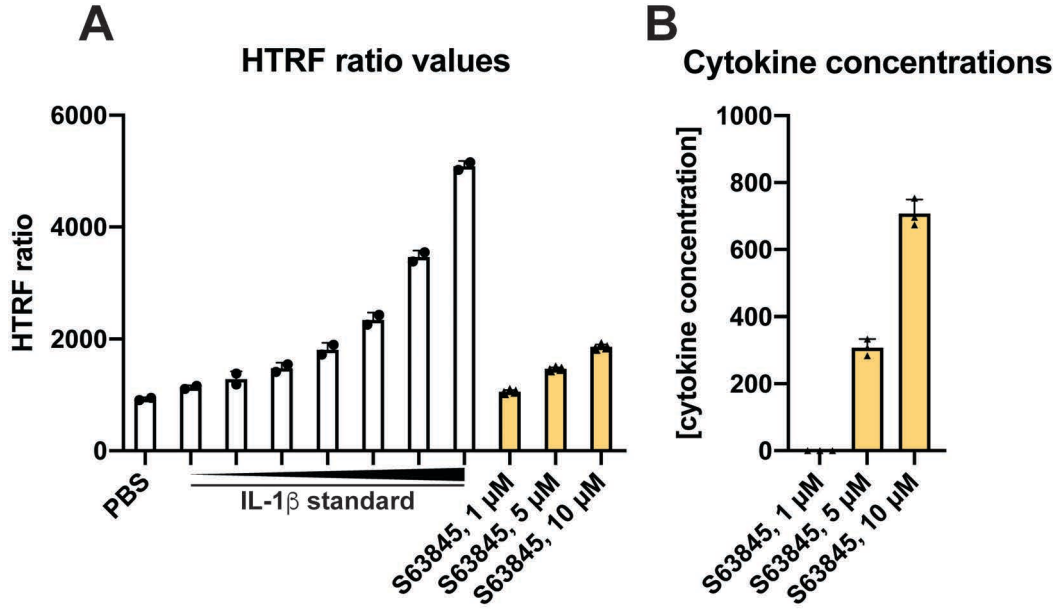

Supplementary Figure S37: S63845 positively interferes with the HTRF signal to a minimal extent
A: S63845 (1, 5, or 10 μM) was diluted in PBS (yellow bars) and the HTRF signal of these solutions was measured, compared to the IL-1β standard curve (white bars; 66-4200 pg/mL). Tissue culture supernatants were not added to the samples.
B: The productive levels of S63845 HTRF signal when diluted in PBS (as interpreted based on the IL-1β standard curve in [A]). 5 μM S63845 (the concentration used in the assays performed in this thesis) produces an HTRF signal that can be interpreted as ~300 pg/mL of IL-1β.
Results are presented as means of technical duplicates (IL-1β standard curve) or triplicates (S63845 samples) from 1 experiment. Error bars correspond with the SD values. Individual data points correspond to the individual values of the HTRF signal (A) or to the apparent cytokine concentrations calculated for each of the triplicate samples (B).

Supplementary Figure S38:

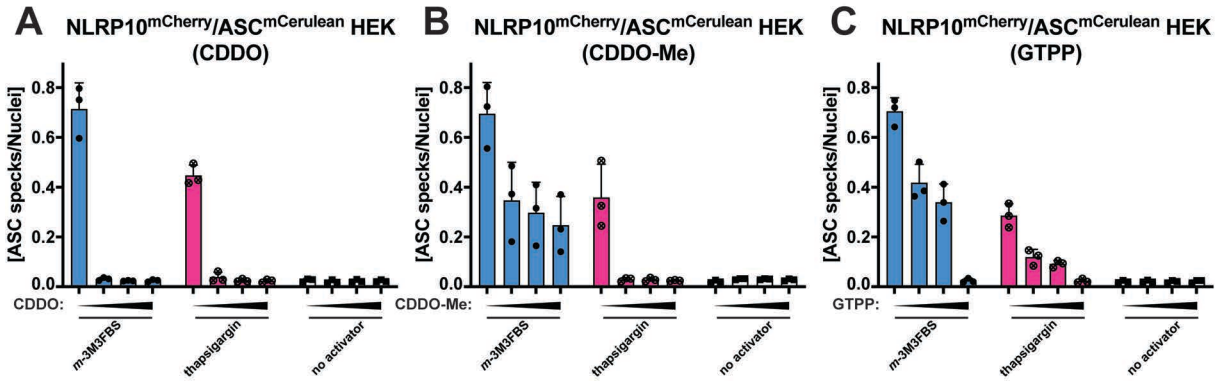

Supplementary Figure S38: Influence of the UPR^{mt} agonists CDDO, CDDO-Me, and GTPP on the inflammasome responses to *m*-3M3FBS and thapsigargin in NLRP10^{mCherry}/ASC^{mCerulean} HEK cells
A-C: NLRP10^{mCherry}/ASC^{mCerulean} HEK cells were treated for 10 min with CDDO (0, 10, 25, or 50 μM; A), CDDO-Me (0, 10, 25, or 50 μM; B), or GTPP (0, 5, 10, or 50 μM; C) and then subjected to the inflammasome activators *m*-3M3FBS (85 μM) or thapsigargin (20 μM) in an extracellular medium consisting of (in mM) 123 NaCl, 5 KCl, 2 $MgCl_2$, 1 $CaCl_2$, 10 glucose, 10 HEPES, pH 7.4. The untreated ('no activator') controls were subjected to medium alone. Immediately after addition of inflammasome activators, the plates were centrifuged at 340 × g for 5 min (RT). After 30 min, the cells were fixed with 4% formaldehyde, counterstained with the nuclear dye DRAQ5 (5 μM) and imaged using a widefield fluorescence microscope.
The results are plotted as means from 3 independent experiments performed in technical duplicate. Error bars represent SD. Individual data points represent means of the technical duplicate values from each of the independent experiments.

Supplementary Figure S39:

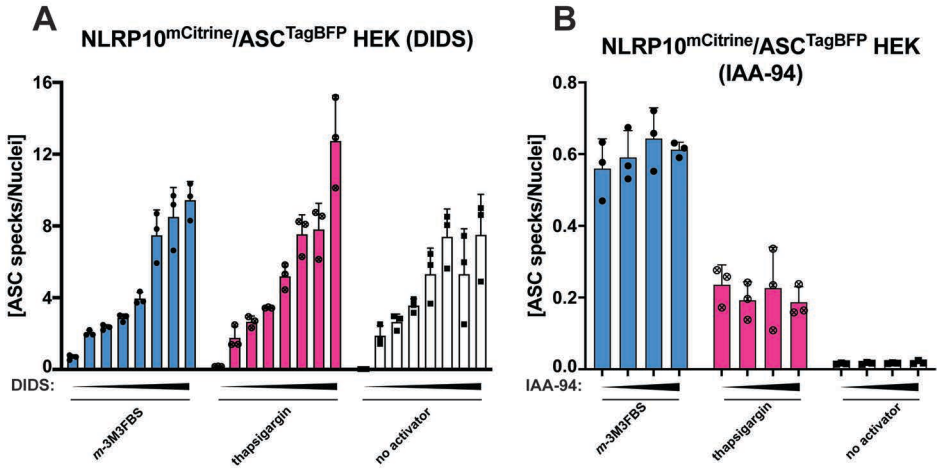

Supplementary Figure S39: Influence of the Cl^- channel blockers DIDS and IAA-94 on the inflammasome responses to *m*-3M3FBS and thapsigargin in NLRP10^{mCitrine}/ASC^{TagBFP} HEK cells

A, B: NLRP10^{mCitrine}/ASC^{TagBFP} HEK cells were treated for 10 min with DIDS (0, 10, 25, 50, 100, 250, 500, or 1000 μM; A) or IAA-94 (0, 25, 50, or 100 μM; B) and then subjected to the inflammasome activators *m*-3M3FBS (85 μM) or thapsigargin (20 μM), nigericin (10 μM) in an extracellular medium consisting of (in mM) 123 NaCl, 5 KCl, 2 $MgCl_2$, 1 $CaCl_2$, 10 glucose, 10 HEPES, pH 7.4. The untreated ('no activator') controls were subjected to medium alone. Immediately after addition of inflammasome activators, the plates were centrifuged at 340 × g for 5 min (RT). After 30 min, the cells were fixed with 4% formaldehyde, counterstained with the nuclear dye DRAQ5 (5 μM) and imaged using a widefield fluorescence microscope.

The results are plotted as means from 3 independent experiments performed in technical duplicate. Error bars represent SD. Individual data points represent means of the technical duplicate values from each of the independent experiments.

Supplementary Figure S40:

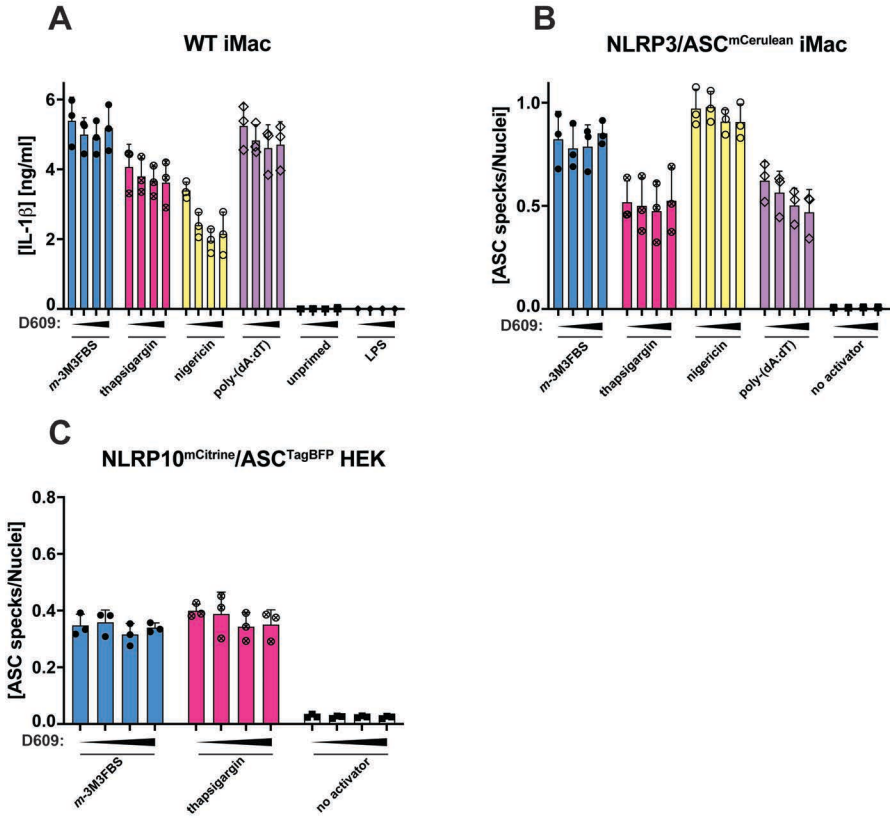

Supplementary figure S40: Influence of the phosphatidylcholine-PLC inhibitor D609 on the inflammasome responses to *m*-3M3FBS, thapsigargin, nigericin, and poly-(dA:dT)

◂ **A-C:** LPS-primed (200 ng/mL, 2 h) WT iMac cells (A), NLRP3/ASC^{mCerulean} reporter iMac cells (B), and NLRP10^{mCitrine}/ASC^{TagBFP} HEK cells (C) were treated for 10 min with D609 (0, 10, 25, or 50 μM). Then, the cells were subjected to the inflammasome activators *m*-3M3FBS (85 μM), thapsigargin (20 μM), nigericin (10 μM) or poly-(dA:dT) (2 μg/mL complexed with 5 μL Lipofectamine 2000) in an extracellular medium consisting of (in mM) 123 NaCl, 5 KCl, 2 $MgCl_2$, 1 $CaCl_2$, 10 glucose, 10 HEPES, pH 7.4. The LPS (A) and unprimed (A-C) controls were subjected to medium alone. Immediately after addition of inflammasome activators, the plates were centrifuged at 340 × g for 5 min (RT). After 30 min (C) or 60 min (A, B), the supernatants were collected and IL-1β concentrations were measured by HTRF (A) or the cells were fixed with 4% formaldehyde, counterstained with the nuclear dye DRAQ5 (5 μM) and imaged using a widefield fluorescence microscope (B, C).
The results are plotted as means from 3 independent experiments performed in technical duplicate. Error bars represent SD. Individual data points represent means of the technical duplicate values from each of the independent experiments.

Supplementary Figure S41:

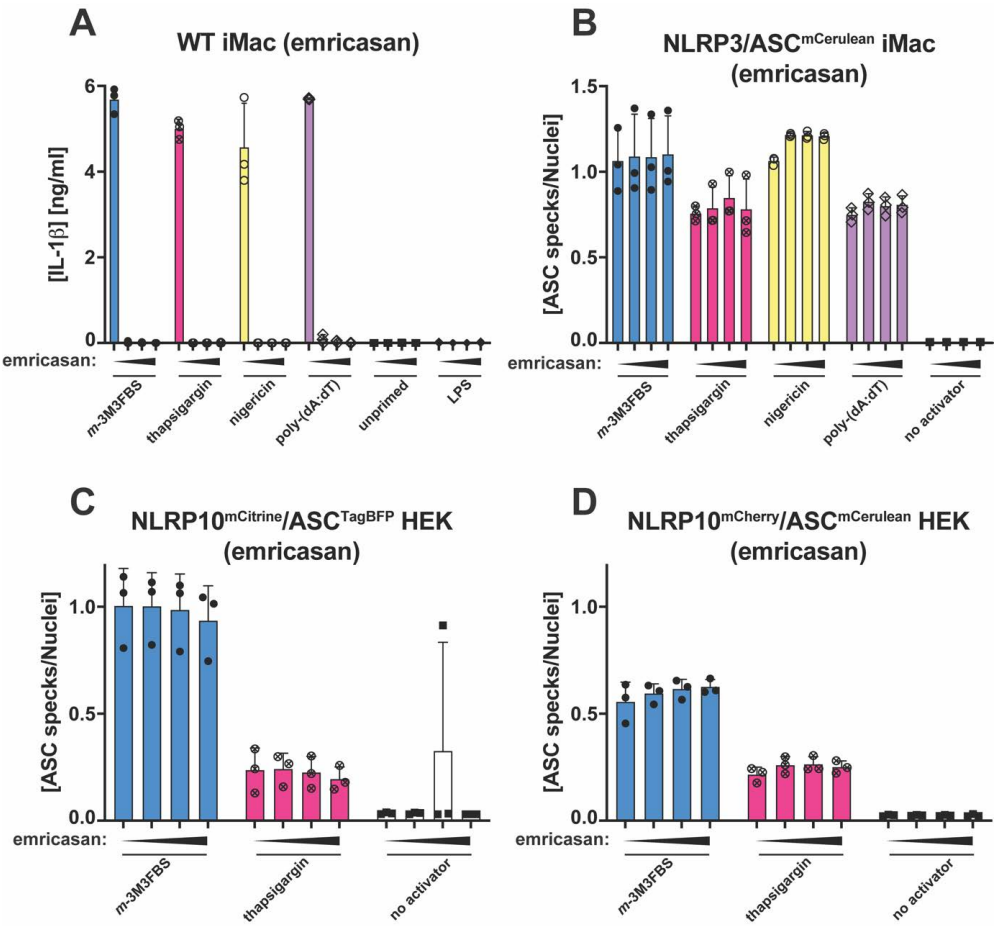

Supplementary Figure S41: Influence of the pan-caspase inhibitor emricasan on the inflammasome responses to *m*-3M3FBS, thapsigargin, nigericin, and poly-(dA:dT)
A-D: LPS-primed (200 ng/mL, 2 h) WT iMac cells (A), NLRP3/ASC^{mCerulean} reporter iMac cells (B), NLRP10^{mCitrine}/ASC^{TagBFP} HEK cells (C), and NLRP10^{mCherry}/ASC^{mCerulean} HEK cells (D) were treated for 10 min with emricasan (0, 5, 10, or 25 μM). Then, the cells were subjected to the inflammasome activators *m*-3M3FBS (85 μM), thapsigargin (20 μM), nigericin (10 μM) or poly-(dA:dT) (2 μg/mL complexed with 5 μL Lipofectamine 2000) in an extracellular medium consisting of (in mM) 123 NaCl, 5 KCl, 2 $MgCl_2$, 1 $CaCl_2$, 10 glucose, 10 HEPES, pH 7.4. The LPS (A) and unprimed (A-D) controls were subjected to medium alone. Immediately after addition of inflammasome activators, the plates were centrifuged at 340 × g for 5 min (RT). After 30 min (C, D) or 60 min (A, B), the supernatants were collected and IL-1β concentrations were measured by HTRF (A) or the cells were fixed with 4% formaldehyde, counterstained with the nuclear dye DRAQ5 (5 μM) and imaged using a widefield fluorescence microscope (B-D).
The results are plotted as means from 3 independent experiments performed in technical duplicate. Error bars represent SD. Individual data points represent means of the technical duplicate values from each of the independent experiments.

Supplementary Figure S42:

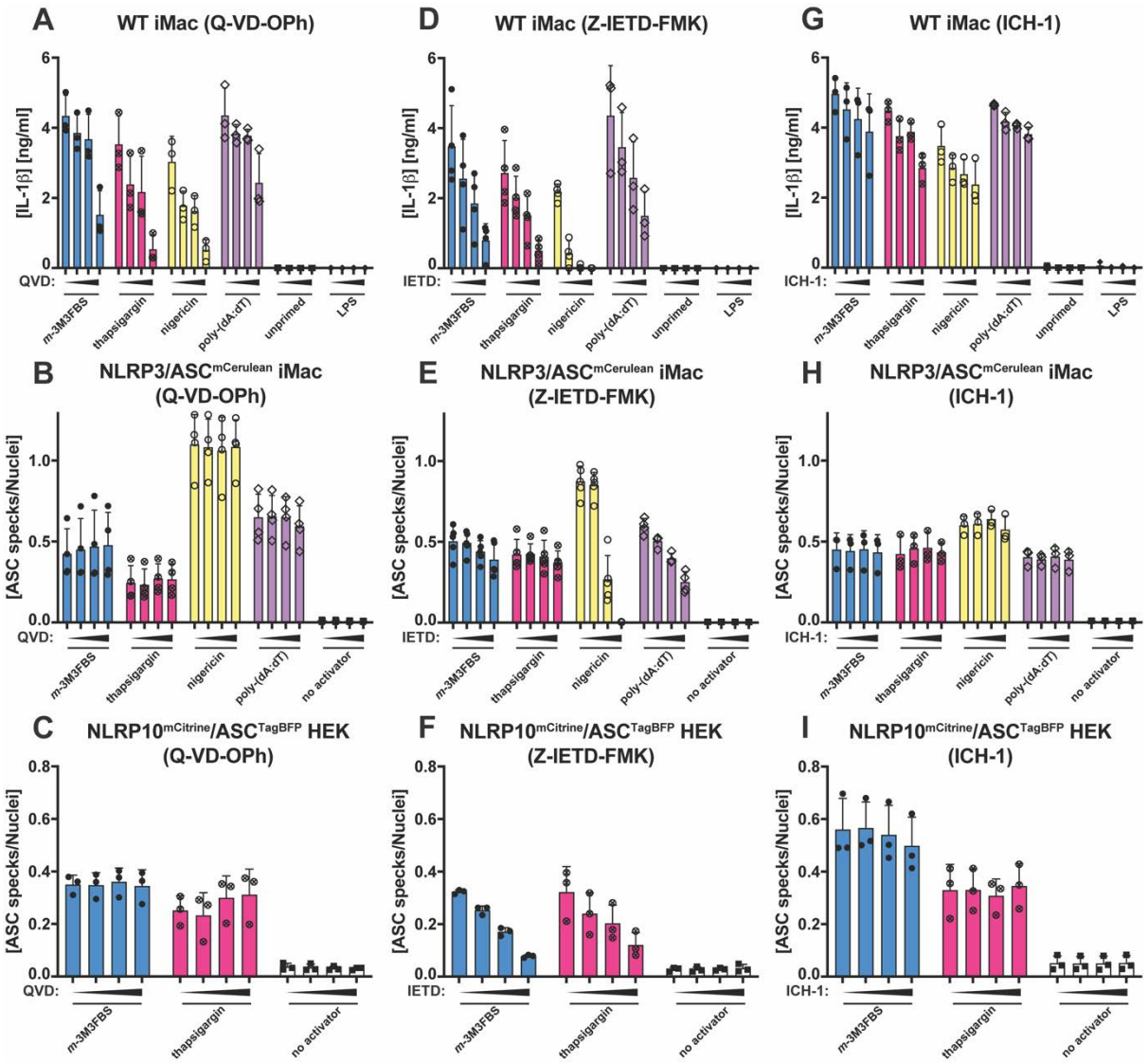

Supplementary Figure S42: Influence of the pan-caspase inhibitor Q-Vd-OPh, the caspase-8 inhibitor Z-IETD-FMK, and the caspase-2 inhibitor ICH-1 on the inflammasome responses to *m*-3M3FBS, thapsigargin, nigericin, and poly-(dA:dT)

A-I: LPS-primed (200 ng/mL, 2 h) WT iMac cells (A, D, G), NLRP3/ASC^{mCerulean} reporter iMac cells (B, E, H), and NLRP10^{mCitrine}/ASC^{TagBFP} HEK cells (C, F, I) were treated for 10 min with Q-Vd-OPh (QVD; 0, 5, 10, or 50 μM; A-C), Z-IETD-FMK (IETD; 0, 10, 25, or 50 μM; D-F), or ICH-1 (0, 5, 10, or 50 μM; G-I). Then, the cells were subjected to the inflammasome activators *m*-3M3FBS (85 μM), thapsigargin (20 μM), nigericin (10 μM) or poly-(dA:dT) (2 μg/mL complexed with 5 μL Lipofectamine 2000) in an extracellular medium consisting of (in mM) 123 NaCl, 5 KCl, 2 $MgCl_2$, 1 $CaCl_2$, 10 glucose, 10 HEPES, pH 7.4. The LPS (A, D, G) and unprimed (A-I) controls were subjected to medium alone. Immediately after addition of inflammasome activators, the plates were centrifuged at 340 × g for 5 min (RT). After 30 min (C, F, I) or 60 min (A, B, D, E, G, H), the supernatants were collected and IL-1β concentrations were measured by HTRF (A, D, G) or the cells were fixed with 4% formaldehyde, counterstained with the nuclear dye DRAQ5 (5 μM) and imaged using a widefield fluorescence microscope (B, C, E, F, H, I).

The results are plotted as means from 3 independent experiments performed in technical duplicate. Error bars represent SD. Individual data points represent means of the technical duplicate values from each of the independent experiments.

Supplementary Figure S43:

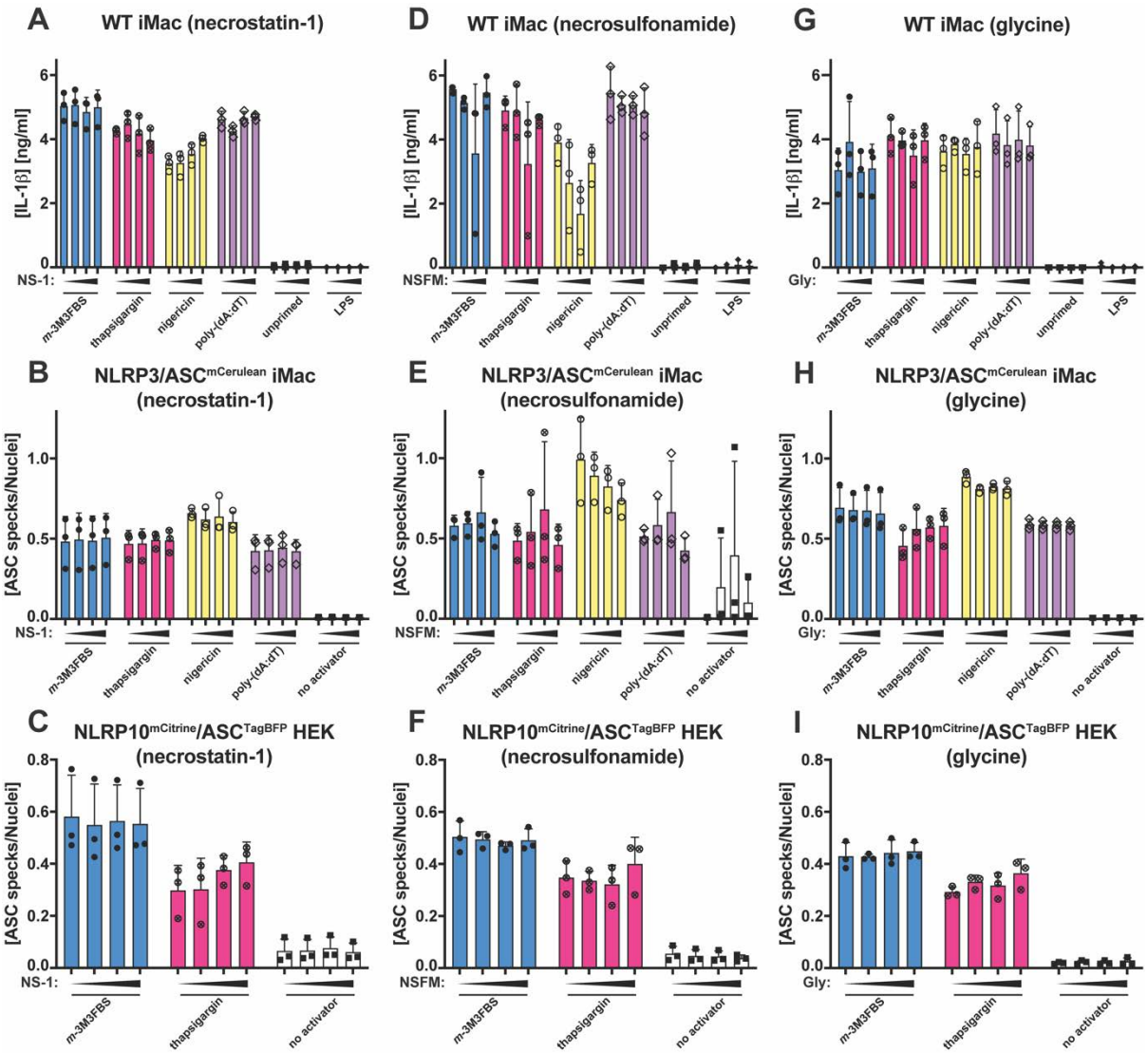

Supplementary Figure S43: Influence of the MLKL/necroptosis inhibitors necrostatin-1 and necrosulfonamide and the lytic cell death inhibitor glycine on the inflammasome responses to *m*-3M3FBS, thapsigargin, nigericin, and poly-(dA:dT)

A-I: LPS-primed (200 ng/mL, 2 h) WT iMac cells (A, D, G), NLRP3/ASC^{mCerulean} reporter iMac cells (B, E, H), and NLRP10^{mCitrine}/ASC^{TagBFP} HEK cells (C, F, I) were treated for 10 min with necrostatin-1 (NS-1; 0, 5, 10, or 50 μM; A-C), necrosulfonamide (NSFM; 0, 5, 10, or 50 μM; D-F), or glycine (Gly; 0, 2.5, 5, or 10 mM; G-I). Then, the cells were subjected to the inflammasome activators *m*-3M3FBS (85 μM), thapsigargin (20 μM), nigericin (10 μM) or poly-(dA:dT) (2 μg/mL complexed with 5 μL Lipofectamine 2000) in an extracellular medium consisting of (in mM) 123 NaCl, 5 KCl, 2 $MgCl_2$, 1 $CaCl_2$, 10 glucose, 10 HEPES, pH 7.4. The LPS (A, D, G) and unprimed (A-I) controls were subjected to medium alone. Immediately after addition of inflammasome activators, the plates were centrifuged at 340 × g for 5 min (RT). After 30 min (C, F, I) or 60 min (A, B, D, E, G, H), the supernatants were collected and IL-1β concentrations were measured by HTRF (A, D, G) or the cells were fixed with 4% formaldehyde, counterstained with the nuclear dye DRAQ5 (5 μM) and imaged using a widefield fluorescence microscope (B, C, E, F, H, I).

The results are plotted as means from 3 independent experiments performed in technical duplicate. Error bars represent SD. Individual data points represent means of the technical duplicate values from each of the independent experiments.

Supplementary Figure S44:

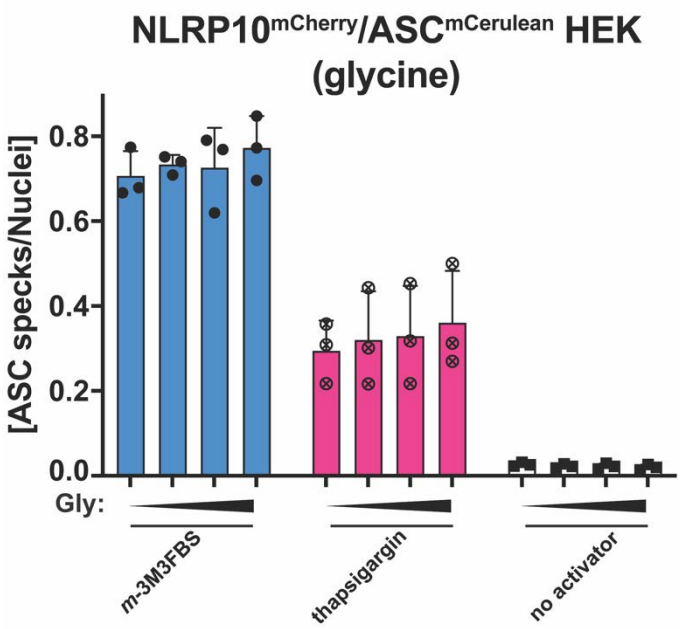

Supplementary Figure S44: Influence of the lytic cell death inhibitor glycine on the inflammasome responses to *m*-3M3FBS and thapsigargin in NLRP10^{mCherry}/ASC^{mCerulean} HEK cells

NLRP10^{mCherry}/ASC^{mCerulean} HEK cells were treated for 10 min with glycine (Gly; 0, 2.5, 5, or 10 mM). Then, the cells were subjected to the inflammasome activators *m*-3M3FBS (85 μM) or thapsigargin (20 μM) in an extracellular medium consisting of (in mM) 123 NaCl, 5 KCl, 2 $MgCl_2$, 1 $CaCl_2$, 10 glucose, 10 HEPES, pH 7.4. The untreated ('no activator') controls were subjected to medium alone. Immediately after addition of inflammasome activators, the plates were centrifuged at 340 × g for 5 min (RT). After 30 min, the cells were fixed with 4% formaldehyde, counterstained with the nuclear dye DRAQ5 (5 μM) and imaged using a widefield fluorescence microscope.

The results are plotted as means from 3 independent experiments performed in technical duplicate. Error bars represent SD. Individual data points represent means of the technical duplicate values from each of the independent experiments.

Supplementary Figure S45:

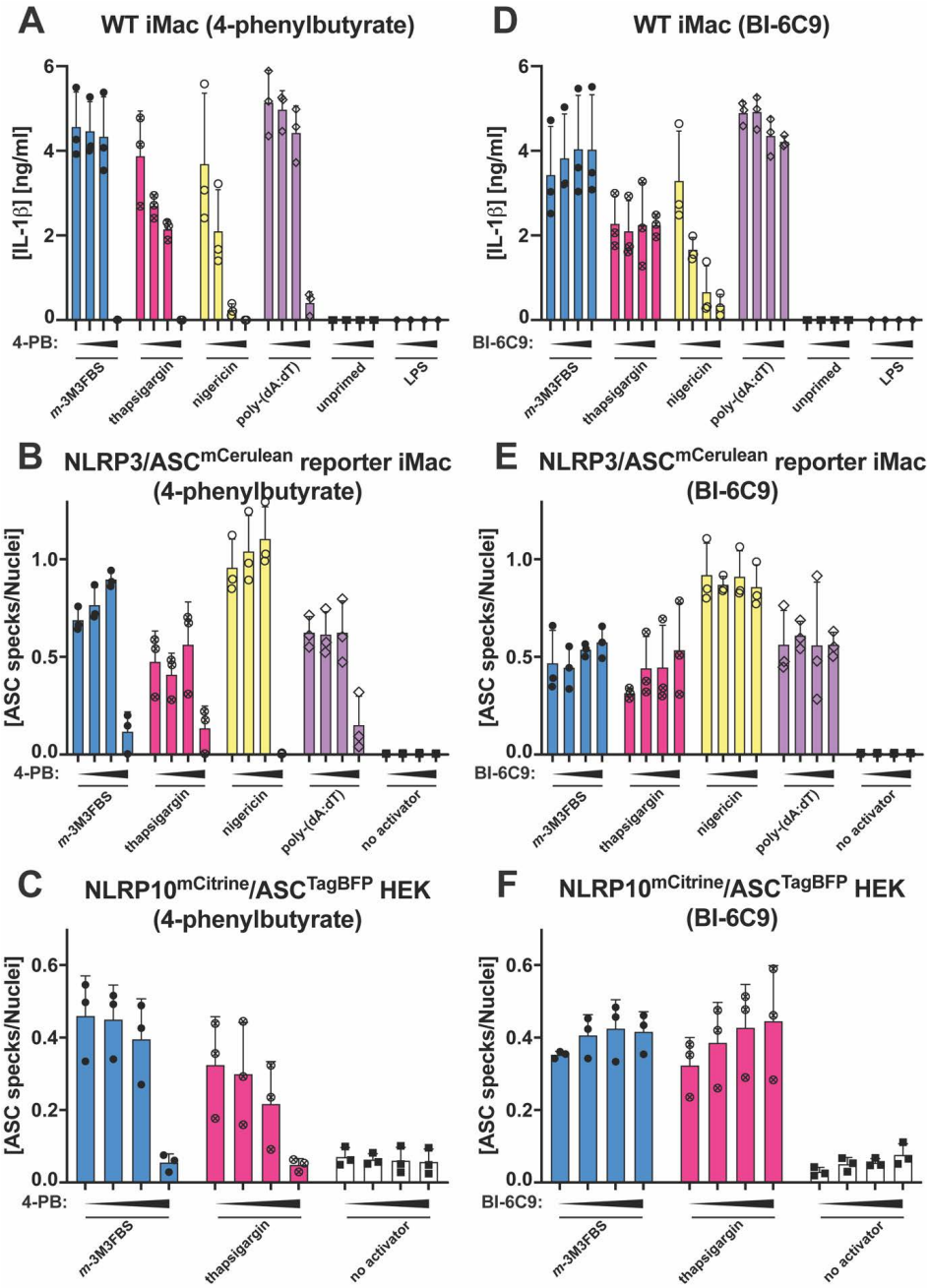

Supplementary Figure S45: Influence of the chemical chaperone 4-phenylbutyrate and the tBid inhibit BI-6C9 on the inflammasome responses to *m*-3M3FBS, thapsigargin, nigericin, and poly-(dA:dT)

A-F: LPS-primed (200 ng/mL, 2 h) WT iMac cells (A, D), NLRP3/ASC^{mCerulean} reporter iMac cells (B, E), and NLRP10^{mCitrine}/ASC^{TagBFP} HEK cells (C, F) were treated for 10 min with 4-phenylbutyrate (4-PB; 0, 5, 10, or 25 mM; A-C) or BI-6C9 (0, 10, 25, or 50 μM; D-F). Then, the cells were subjected to the inflammasome activators *m*-3M3FBS (85 μM), thapsigargin (20 μM), nigericin (10 μM) or poly-(dA:dT) (2 μg/mL complexed with 5 μL Lipofectamine 2000) in an extracellular medium consisting of (in mM) 123 NaCl, 5 KCl, 2 $MgCl_2$, 1 $CaCl_2$, 10 glucose, 10 HEPES, pH 7.4. The LPS (A, D) and unprimed (A-F) controls were subjected to medium alone. Immediately after addition of inflammasome activators, the plates were centrifuged at 340 × g for 5 min (RT). After 30 min (C, F) or 60 min (A, B, D, E), the supernatants were collected and IL-1β concentrations were measured by HTRF (A, D) or the cells were fixed with 4% formaldehyde, counterstained with the nuclear dye DRAQ5 (5 μM) and imaged using a widefield fluorescence microscope (B, C, E, F).

The results are plotted as means from 3 independent experiments performed in technical duplicate. Error bars represent SD. Individual data points represent means of the technical duplicate values from each of the independent experiments.

Supplementary Figure S46:

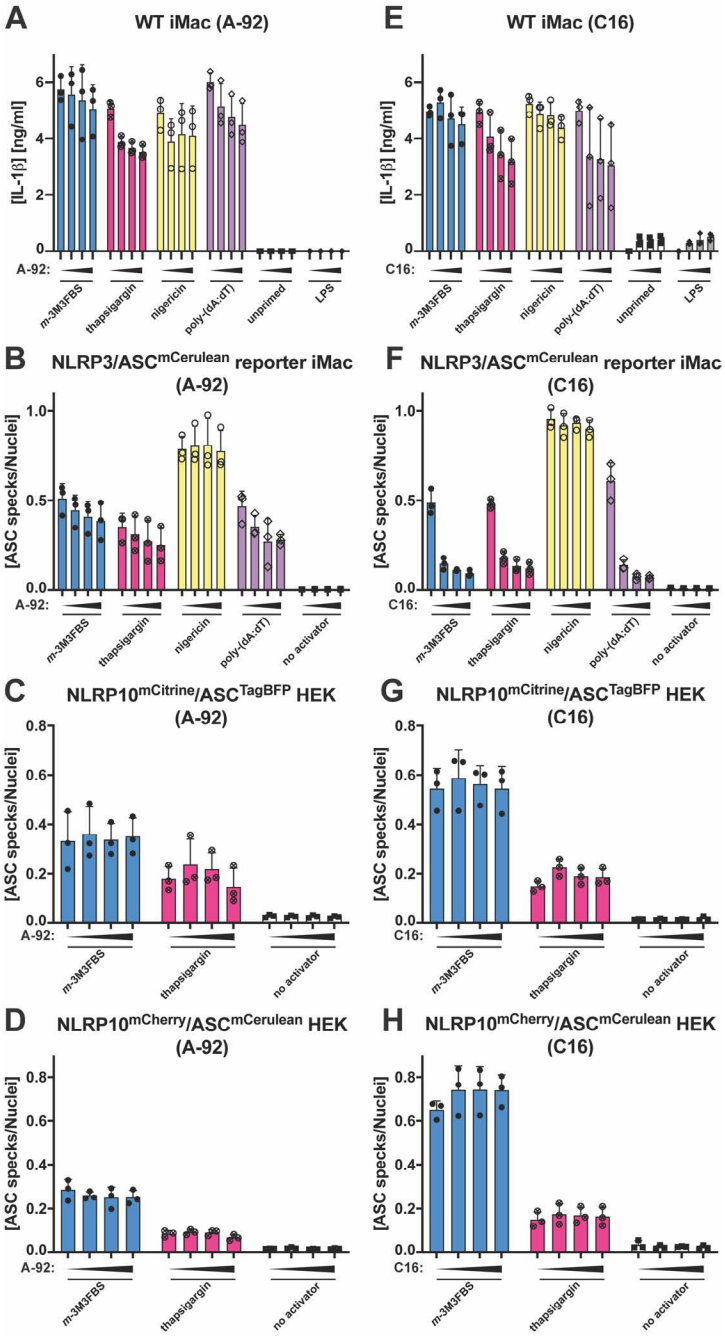

Supplementary Figure S46: Influence of the GCN2 kinase inhibitor A-92 and the PKR inhibitor C16 on the inflammasome responses to *m*-3M3FBS, thapsigargin, nigericin, and poly-(dA:dT)

A-H: LPS-primed (200 ng/mL, 2 h) WT iMac cells (A, E), NLRP3/ASC^{mCerulean} reporter iMac cells (B, F), NLRP10^{mCitrine}/ASC^{TagBFP} HEK cells (C, G), and NLRP10^{mCherry}/ASC^{mCerulean} HEK cells (D, H) were treated for 10 min with A-92 (0, 5, 10, or 50 μM; A-D) or C16 (0, 5, 10, or 25 μM; E-H). Then, the cells were subjected to the inflammasome activators *m*-3M3FBS (85 μM), thapsigargin (20 μM), nigericin (10 μM) or poly-(dA:dT) (2 μg/mL complexed with 5 μL Lipofectamine 2000) in an extracellular medium consisting of (in mM) 123 NaCl, 5 KCl, 2 $MgCl_2$, 1 $CaCl_2$, 10 glucose, 10 HEPES, pH 7.4. The LPS (A, E) and unprimed (A-H) controls were subjected to medium alone. Immediately after addition of inflammasome activators, the plates were centrifuged at 340 × g for 5 min (RT). After 30 min (C, D, G, H) or 60 min (A, B, E, F), the supernatants were collected and IL-1β concentrations were measured by HTRF (A, E) or the cells were fixed with 4% formaldehyde, counterstained with the nuclear dye DRAQ5 (5 μM) and imaged using a widefield fluorescence microscope (B-D, F-H).

The results are plotted as means from 3 independent experiments performed in technical duplicate. Error bars represent SD. Individual data points represent means of the technical duplicate values from each of the independent experiments.

Supplementary Figure S47:

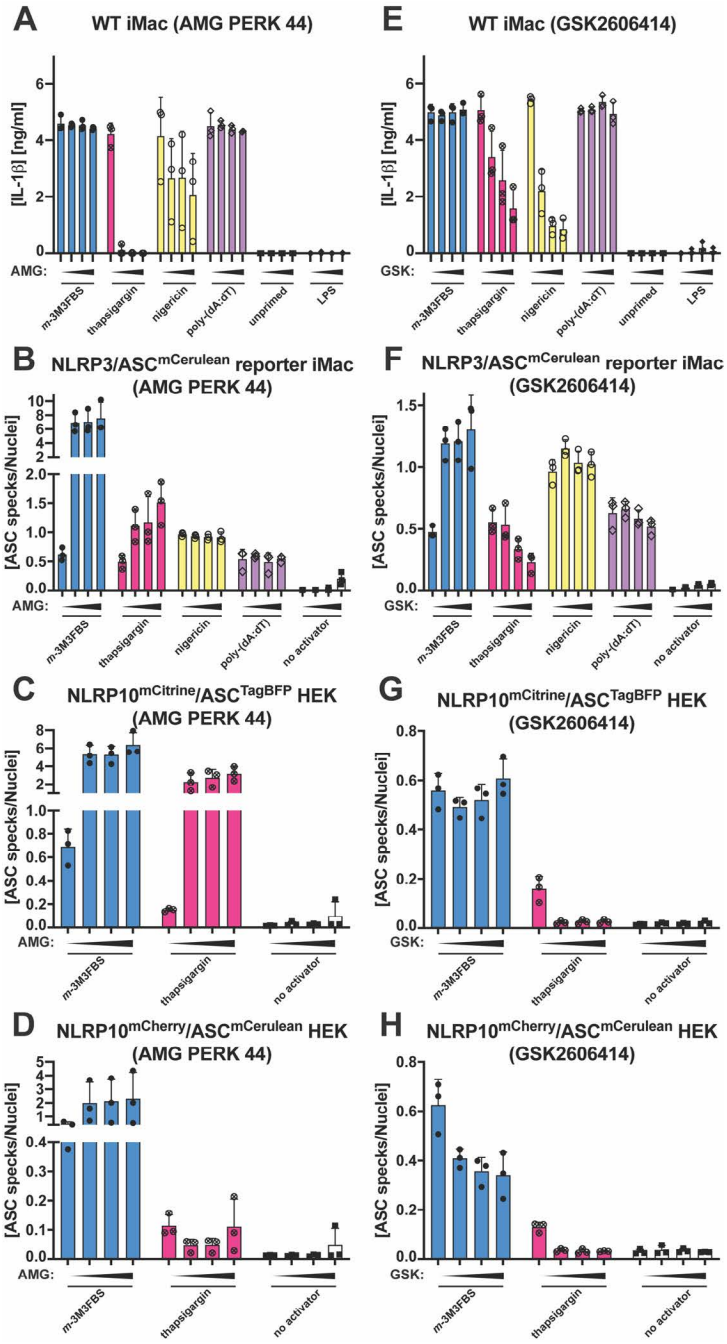

Supplementary Figure S47: Influence of the PERK inhibitors AMG PERK 44 and GSK2606414 on the inflammasome responses to *m*-3M3FBS, thapsigargin, nigericin, and poly-(dA:dT)

A-H: LPS-primed (200 ng/mL, 2 h) WT iMac cells (A, E), NLRP3/ASC^{mCerulean} reporter iMac cells (B, F), NLRP10^{mCitrine}/ASC^{TagBFP} HEK cells (C, G), and NLRP10^{mCherry}/ASC^{mCerulean} HEK cells (D, H) were treated for 10 min with AMG PERK 44 (AMG; 0, 5, 10, or 20 μM; A-D) or GSK2606414 (GSK; 0, 5, 10, or 25 μM; E-H). Then, the cells were subjected to the inflammasome activators *m*-3M3FBS (85 μM), thapsigargin (20 μM), nigericin (10 μM) or poly-(dA:dT) (2 μg/mL complexed with 5 μL Lipofectamine 2000) in an extracellular medium consisting of (in mM) 123 NaCl, 5 KCl, 2 $MgCl_2$, 1 $CaCl_2$, 10 glucose, 10 HEPES, pH 7.4. The LPS (A, E) and unprimed (A-H) controls were subjected to medium alone. Immediately after addition of inflammasome activators, the plates were centrifuged at 340 × g for 5 min (RT). After 30 min (C, D, G, H) or 60 min (A, B, E, F), the supernatants were collected and IL-1β concentrations were measured by HTRF (A, E) or the cells were fixed with 4% formaldehyde, counterstained with the nuclear dye DRAQ5 (5 μM) and imaged using a widefield fluorescence microscope (B-D, F-H).

The results are plotted as means from 3 independent experiments performed in technical duplicate. Error bars represent SD. Individual data points represent means of the technical duplicate values from each of the independent experiments.

Supplementary Figure S48:

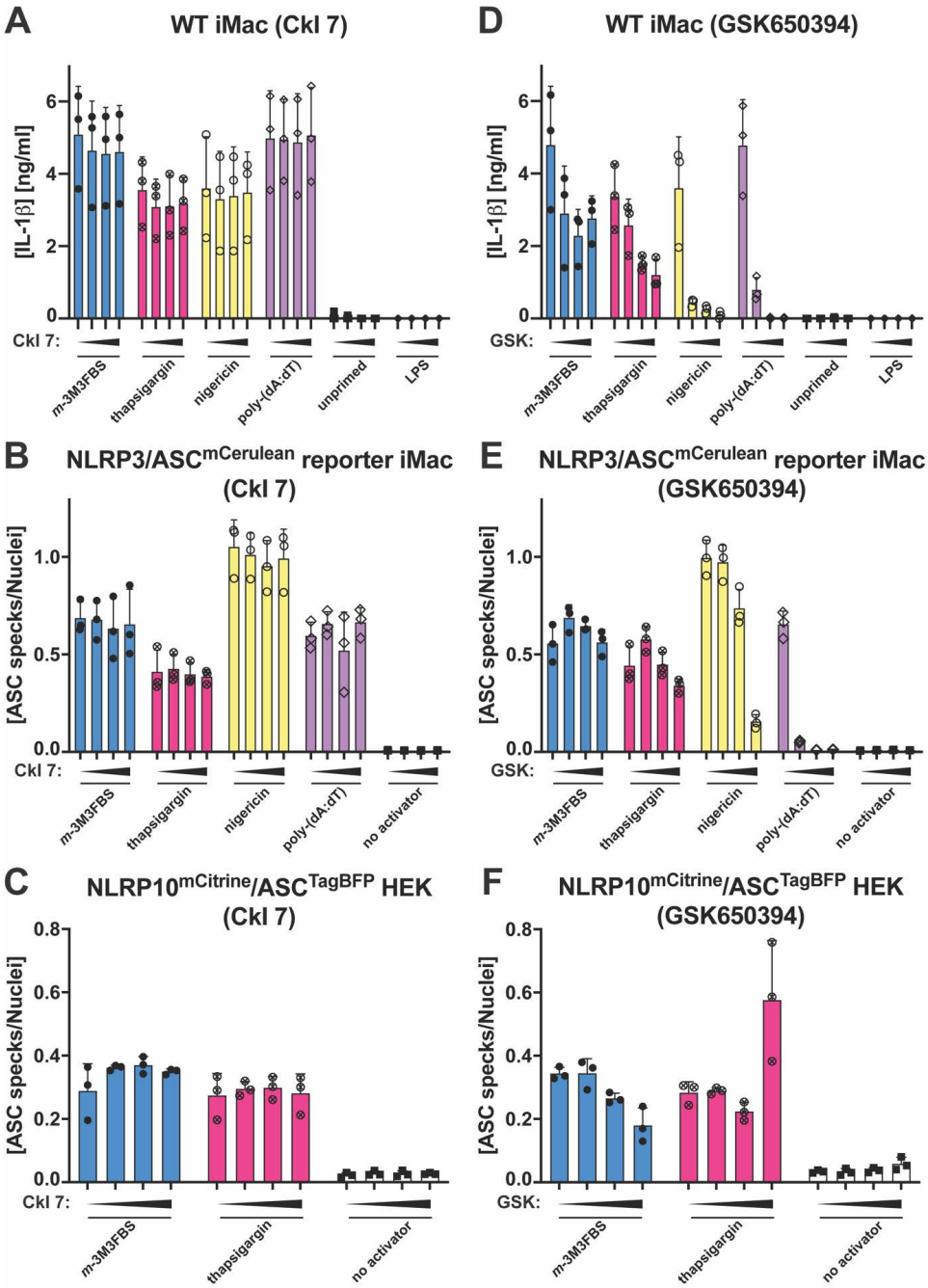

Supplementary Figure S48: Influence of the SGK inhibitors CkI 7 and GSK650394 on the inflammasome responses to *m*-3M3FBS, thapsigargin, nigericin, and poly-(dA:dT)

A-F: LPS-primed (200 ng/mL, 2 h) WT iMac cells (A, D), NLRP3/ASC^{mCerulean} reporter iMac cells (B, E), and NLRP10^{mCitrine}/ASC^{TagBFP} HEK cells (C, F) were treated for 10 min with CkI7 (0, 10, 25, or 50 μM; A-C) or GSK650394 (GSK; 0, 10, 25, or 50 μM; D-F). Then, the cells were subjected to the inflammasome activators *m*-3M3FBS (85 μM), thapsigargin (20 μM), nigericin (10 μM) or poly-(dA:dT) (2 μg/mL complexed with 5 μL Lipofectamine 2000) in an extracellular medium consisting of (in mM) 123 NaCl, 5 KCl, 2 $MgCl_2$, 1 $CaCl_2$, 10 glucose, 10 HEPES, pH 7.4. The LPS (A, D) and unprimed (A-F) controls were subjected to medium alone. Immediately after addition of inflammasome activators, the plates were centrifuged at 340 × g for 5 min (RT). After 30 min (C, F) or 60 min (A, B, D, E), the supernatants were collected and IL-1β concentrations were measured by HTRF (A, D) or the cells were fixed with 4% formaldehyde, counterstained with the nuclear dye DRAQ5 (5 μM) and imaged using a widefield fluorescence microscope (B, C, E, F).

The results are plotted as means from 3 independent experiments performed in technical duplicate. Error bars represent SD. Individual data points represent means of the technical duplicate values from each of the independent experiments.

Supplementary Figure S49:

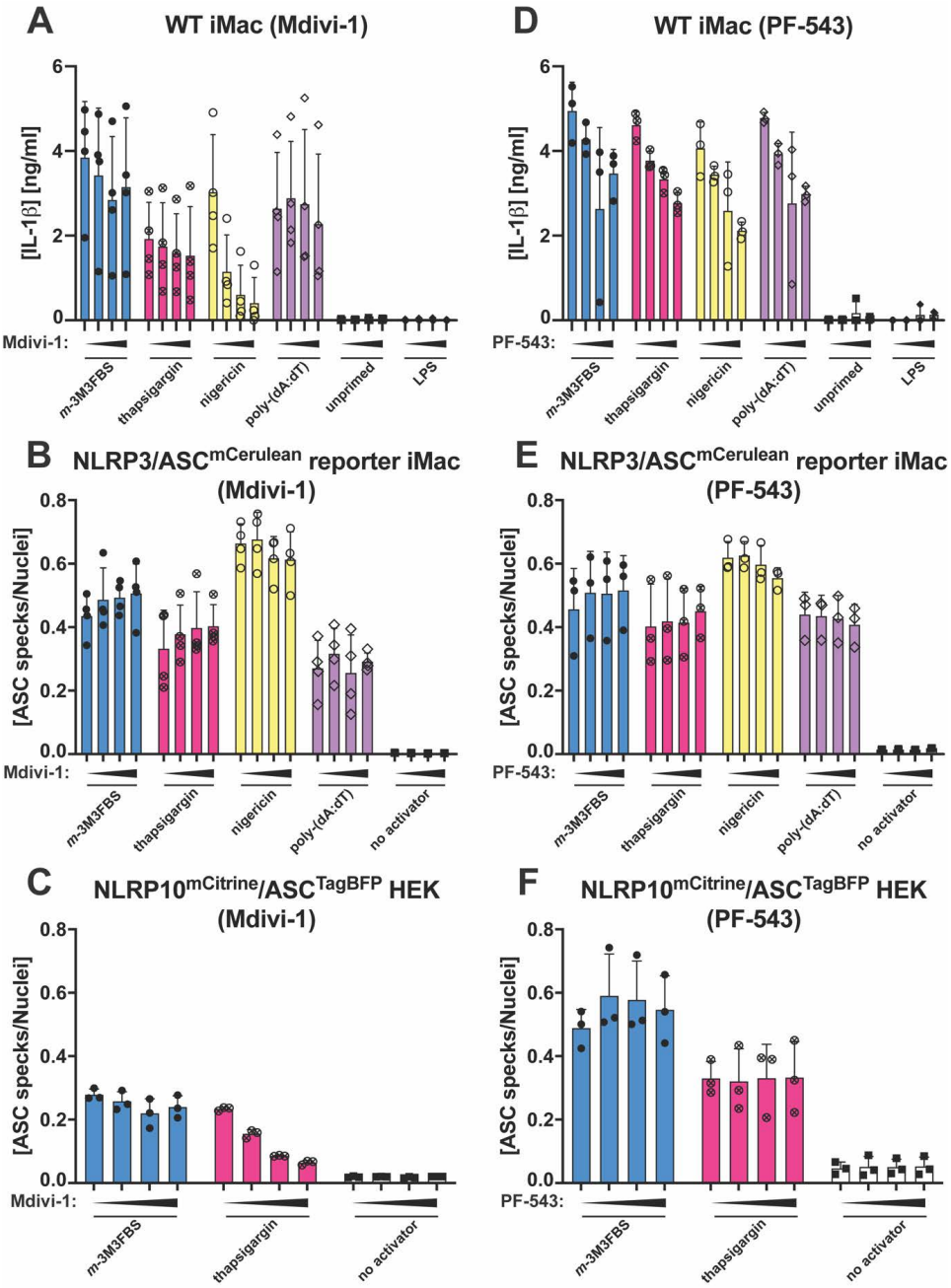

Supplementary Figure S49: Influence of the Drp1/mitochondrial fission inhibitor Mdivi-1 and the sphingosine kinase 1 inhibitor PF-543 on the inflammasome responses to *m*-3M3FBS, thapsigargin, nigericin, and poly-(dA:dT)

A-F: LPS-primed (200 ng/mL, 2 h) WT iMac cells (A, D), NLRP3/ASC^{mCerulean} reporter iMac cells (B, E), and NLRP10^{mCitrine}/ASC^{TagBFP} HEK cells (C, F) were treated for 10 min with Mdivi-1 (0, 25, 50, or 75 μM; A-C) or PF-543 (0, 10, 25, or 50 μM; D-F). Then, the cells were subjected to the inflammasome activators *m*-3M3FBS (85 μM), thapsigargin (20 μM), nigericin (10 μM) or poly-(dA:dT) (2 μg/mL complexed with 5 μL Lipofectamine 2000) in an extracellular medium consisting of (in mM) 123 NaCl, 5 KCl, 2 $MgCl_2$, 1 $CaCl_2$, 10 glucose, 10 HEPES, pH 7.4. The LPS (A, D) and unprimed (A-F) controls were subjected to medium alone. Immediately after addition of inflammasome activators, the plates were centrifuged at 340 × g for 5 min (RT). After 30 min (C, F) or 60 min (A, B, D, E), the supernatants were collected and IL-1β concentrations were measured by HTRF (A, D) or the cells were fixed with 4% formaldehyde, counterstained with the nuclear dye DRAQ5 (5 μM) and imaged using a widefield fluorescence microscope (B, C, E, F).

The results are plotted as means from 3 (C-F) or 4 (A, B) independent experiments performed in technical duplicate. Error bars represent SD. Individual data points represent means of the technical duplicate values from each of the independent experiments.

Supplementary Figure S50:

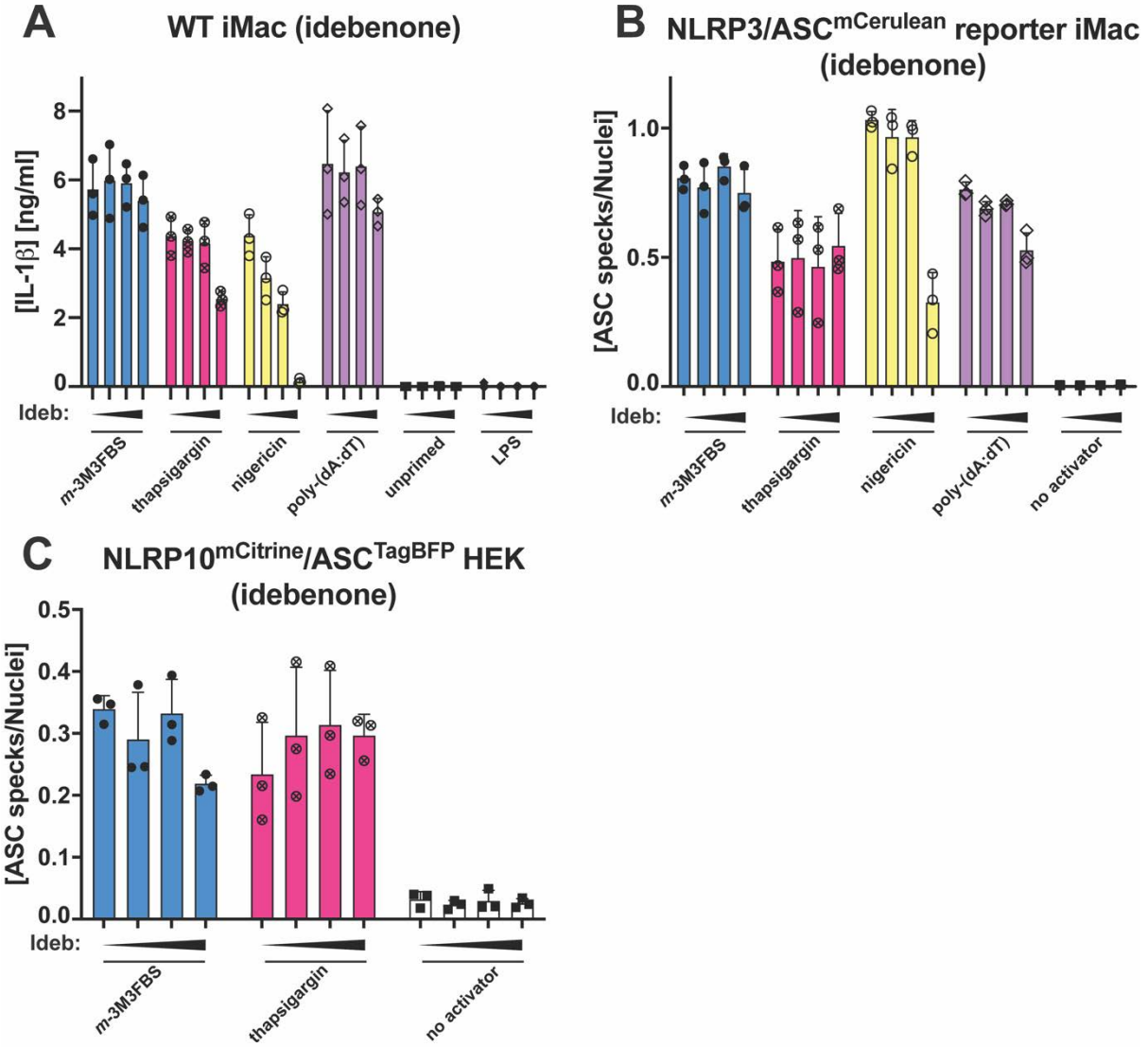

Supplementary Figure S50: Influence of the coenzyme Q synthetic analog idebenone on the inflammasome responses to *m*-3M3FBS, thapsigargin, nigericin, and poly-(dA:dT)

A-C: LPS-primed (200 ng/mL, 2 h) WT iMac cells (A), NLRP3/ASC^{mCerulean} reporter iMac cells (B), and NLRP10^{mCitrine}/ASC^{TagBFP} HEK cells (C) were treated for 10 min with idebenone (Ideb; 0, 5, 10, or 50 μM). Then, the cells were subjected to the inflammasome activators *m*-3M3FBS (85 μM), thapsigargin (20 μM), nigericin (10 μM) or poly-(dA:dT) (2 μg/mL complexed with 5 μL Lipofectamine 2000) in an extracellular medium consisting of (in mM) 123 NaCl, 5 KCl, 2 $MgCl_2$, 1 $CaCl_2$, 10 glucose, 10 HEPES, pH 7.4. The LPS (A) and unprimed (A-C) controls were subjected to medium alone. Immediately after addition of inflammasome activators, the plates were centrifuged at 340 × g for 5 min (RT). After 30 min (C) or 60 min (A, B), the supernatants were collected and IL-1β concentrations were measured by HTRF (A) or the cells were fixed with 4% formaldehyde, counterstained with the nuclear dye DRAQ5 (5 μM) and imaged using a widefield fluorescence microscope (B, C).

The results are plotted as means from 3 independent experiments performed in technical duplicate. Error bars represent SD. Individual data points represent means of the technical duplicate values from each of the independent experiments.

Supplementary Figure S51:

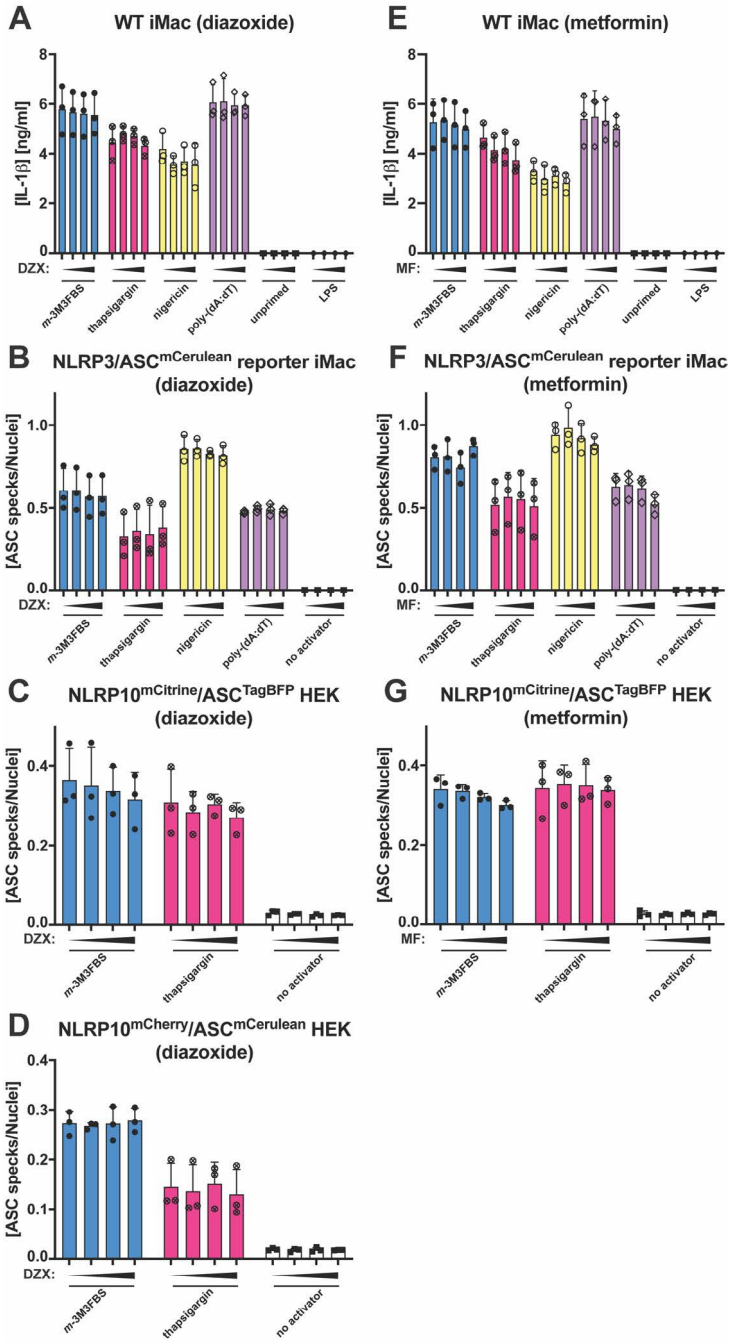

Supplementary Figure S51: Influence of diazoxide and metformin on the inflammasome responses to m-3M3FBS, thapsigargin, nigericin, and poly-(dA:dT)

A-G: LPS-primed (200 ng/mL, 2 h) WT iMac cells (A, E), NLRP3/ASC^{mCerulean} reporter iMac cells (B, F), NLRP10^{mCitrine}/ASC^{TagBFP} HEK cells (C, G), and NLRP10^{mCherry}/ASC^{mCerulean} HEK cells (D) were treated for 10 min with diazoxide (DZX; 0, 10, 50, or 100 μM; A-D) or metformin (MF; 0, 25, 50, or 100 μM; E-G). Then, the cells were subjected to the inflammasome activators *m*-3M3FBS (85 μM), thapsigargin (20 μM), nigericin (10 μM) or poly-(dA:dT) (2 μg/mL complexed with 5 μL Lipofectamine 2000) in an extracellular medium consisting of (in mM) 123 NaCl, 5 KCl, 2 $MgCl_2$, 1 $CaCl_2$, 10 glucose, 10 HEPES, pH 7.4. The LPS (A, E) and unprimed (A-G) controls were subjected to medium alone. Immediately after addition of inflammasome activators, the plates were centrifuged at 340 × g for 5 min (RT). After 30 min (C, D, G) or 60 min (A, B, E, F), the supernatants were collected and IL-1β concentrations were measured by HTRF (A, E) or the cells were fixed with 4% formaldehyde, counterstained with the nuclear dye DRAQ5 (5 μM) and imaged using a widefield fluorescence microscope (B-D, F, G).

The results are plotted as means from 3 independent experiments performed in technical duplicate. Error bars represent SD. Individual data points represent means of the technical duplicate values from each of the independent experiments.

Supplementary Figure S52:

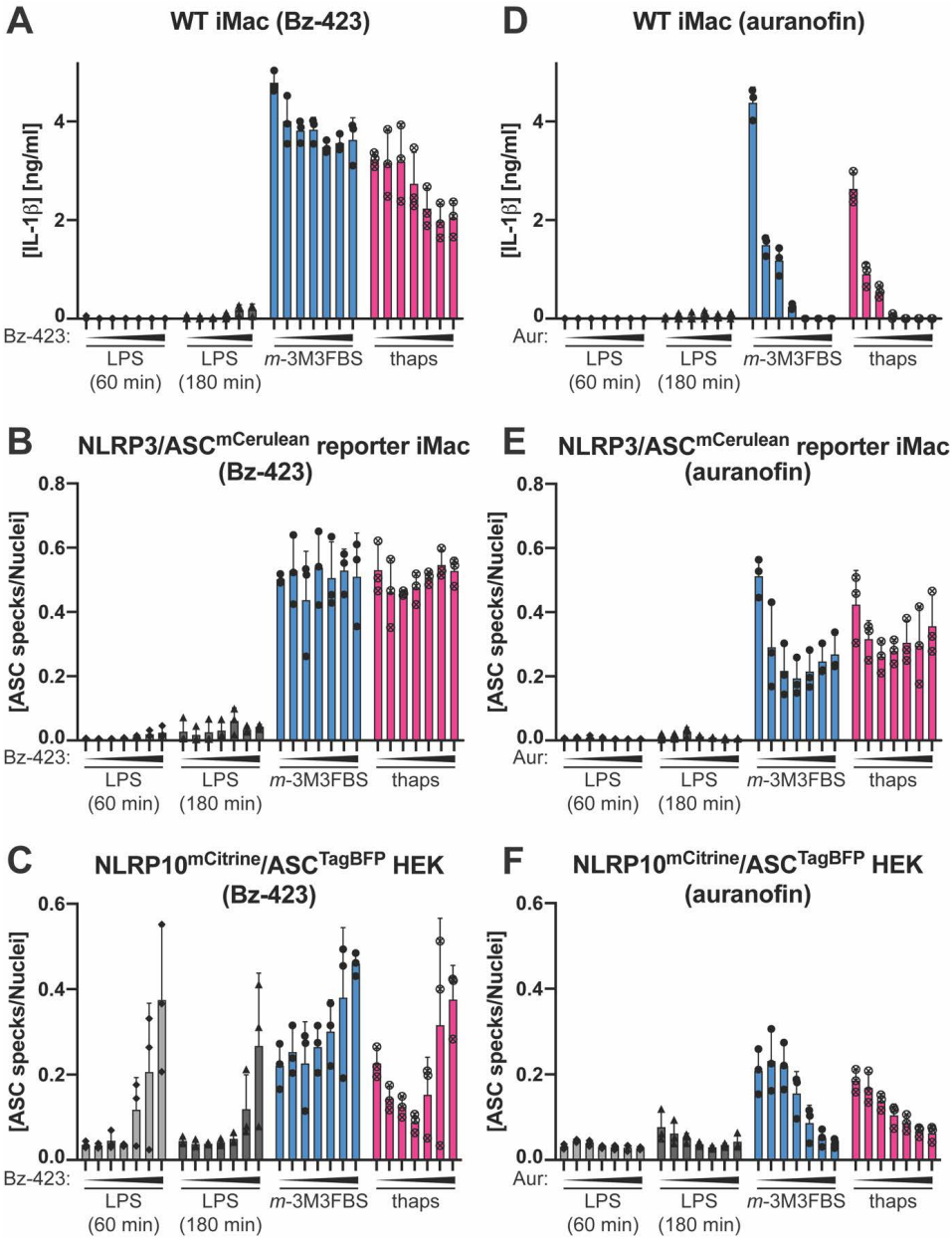

Supplementary Figure S52: Influence of Bz-423 and auranofin on the inflammasome responses to *m*-3M3FBS and thapsigargin in immortalized murine macrophages and in NLRP10^{mCitrine}/ASC^{TagBFP} HEK cells

A-F: WT iMac cells (A, D), NLRP3/ASC^{mCerulean} reporter iMac cells (B, E), and NLRP10^{mCitrine}/ASC^{TagBFP} HEK cells (C, F) were stimulated with LPS (200 ng/mL, 2 h) and then either kept in DMEM supplemented with 10% FBS and 200 ng/mL LPS (the 'LPS [180 min]' conditions) or shifted to an extracellular medium consisting of (in mM) 123 NaCl, 5 KCl, 2 $MgCl_2$, 1 $CaCl_2$, 10 glucose, 10 HEPES pH 7.4 (all the remaining conditions). Then, the cells were treated for 10 min with Bz-423 (0, 5, 10, 25, 50, 75, or 100 μM; A-C) or auranofin (Aur; 0, 5, 10, 25, 50, 75, or 100 μM; D-F) and either stimulated with these agents for a further 60 or 180 min (for the 180-min stimulations, the 100-μM concentrations of Bz-423 and auranofin were omitted), or subjected for 60 min to the inflammasome activators m-3M3FBS (85 μM) or thapsigargin (20 μM). Immediately after addition of inflammasome activators, the plates were centrifuged at 340 × g for 5 min (RT). After the completion of the experiment, the supernatants were collected and IL-1β concentrations were measured by HTRF (A, D) or the cells were fixed with 4% formaldehyde, counterstained with the nuclear dye DRAQ5 (5 μM) and imaged using a widefield fluorescence microscope (B, C, E, F).

The results are plotted as means from 3 independent experiments performed in technical duplicate. Error bars represent SD. Individual data points represent means of the technical duplicate values from each of the independent experiments.

Supplementary Figure S53:

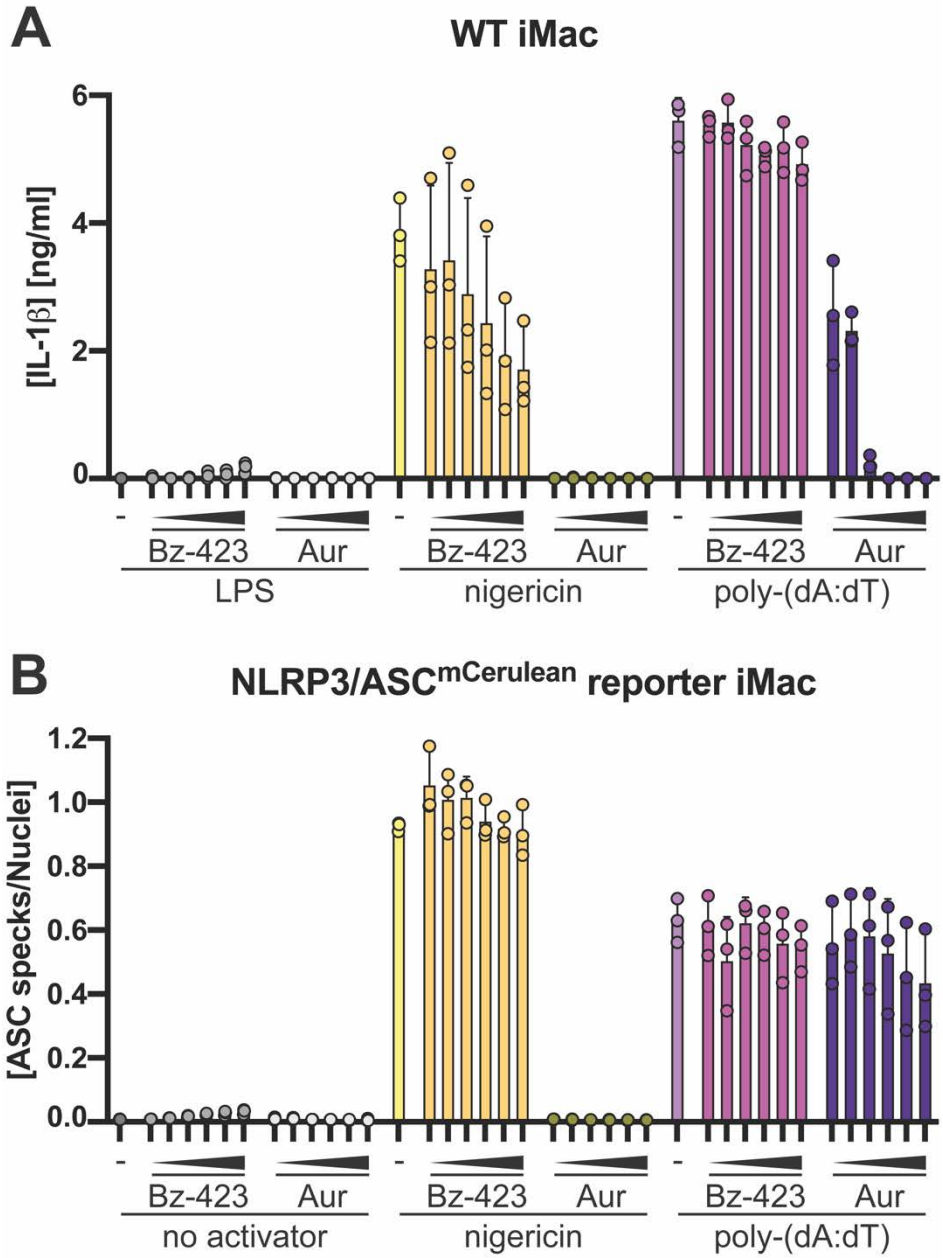

Supplementary Figure S53: Influence of Bz-423 and auranofin on the inflammasome responses to nigericin and poly-(dA:dT) in immortalized murine macrophages

A, B: LPS-primed (200 ng/mL, 2 h) WT iMac cells (A) and NLRP3/ASC^{mCerulean} reporter iMac cells (B) were shifted to an extracellular medium consisting of (in mM) 123 NaCl, 5 KCl, 2 $MgCl_2$, 1 $CaCl_2$, 10 glucose, 10 HEPES pH 7.4 and then left untreated (-) or treated for 10 min with Bz-423 (5, 10, 25, 50, 75, or 100 μM) or auranofin (Aur; 5, 10, 25, 50, 75, or 100 μM). Next, the cells were incubated with Bz-423 or auranofin for further 60 min ('no activator') or they were stimulated with nigericin (10 μM) or poly-(dA:dT) (2 μg/mL complexed with 5 μL Lipofectamine 2000). Immediately after addition of inflammasome activators, the plates were centrifuged at 340 × g for 5 min (RT). After 60 min, the supernatants were collected and IL-1β concentrations were measured by HTRF (A) or the cells were fixed with 4% formaldehyde, counterstained with the nuclear dye DRAQ5 (5 μM) and imaged using a widefield fluorescence microscope (B).

The results are plotted as means from 3 independent experiments performed in technical duplicate. Error bars represent SD. Individual data points represent means of the technical duplicate values from each of the independent experiments.

Supplementary Figure S54:

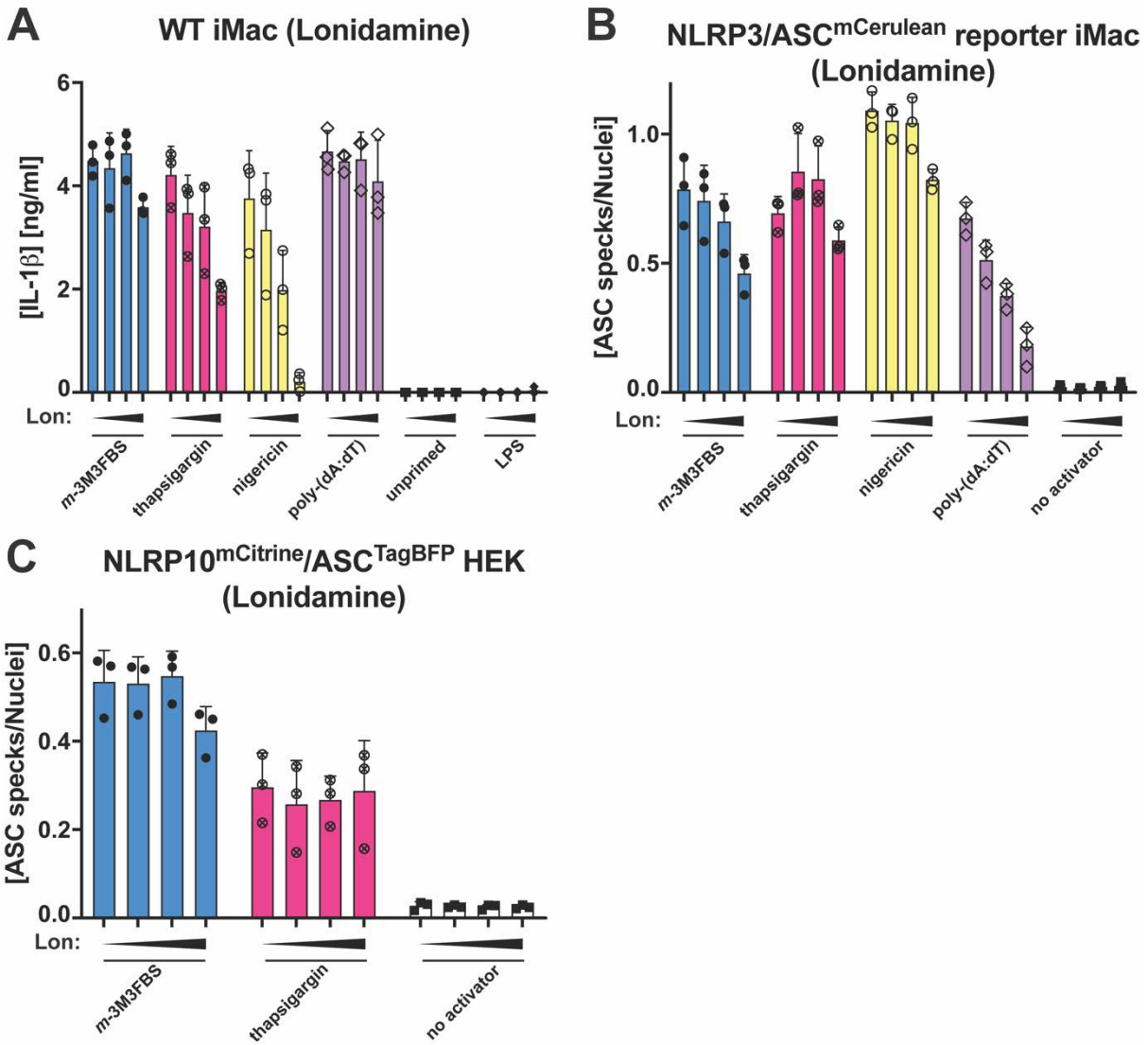

Supplementary Figure S54: Influence of lonidamine on the inflammasome responses to *m*-3M3FBS, thapsigargin, nigericin, and poly-(dA:dT)

A-C: LPS-primed (200 ng/mL, 2 h) WT iMac cells (A), NLRP3/ASC^{mCerulean} reporter iMac cells (B), and NLRP10^{mCitrine}/ASC^{TagBFP} HEK cells (C) were treated for 10 min with lonidamine (Lon; 0, 25, 50, or 100 μM). Then, the cells were subjected to the inflammasome activators *m*-3M3FBS (85 μM), thapsigargin (20 μM), nigericin (10 μM) or poly-(dA:dT) (2 μg/mL complexed with 5 μL Lipofectamine 2000) in an extracellular medium consisting of (in mM) 123 NaCl, 5 KCl, 2 $MgCl_2$, 1 $CaCl_2$, 10 glucose, 10 HEPES, pH 7.4. The LPS (A) and unprimed (A-C) controls were subjected to medium alone. Immediately after addition of inflammasome activators, the plates were centrifuged at 340 × g for 5 min (RT). After 30 min (C) or 60 min (A, B), the supernatants were collected and IL-1β concentrations were measured by HTRF (A) or the cells were fixed with 4% formaldehyde, counterstained with the nuclear dye DRAQ5 (5 μM) and imaged using a widefield fluorescence microscope (B, C).

The results are plotted as means from 3 independent experiments performed in technical duplicate. Error bars represent SD. Individual data points represent means of the technical duplicate values from each of the independent experiments.

Supplementary Figure S55:

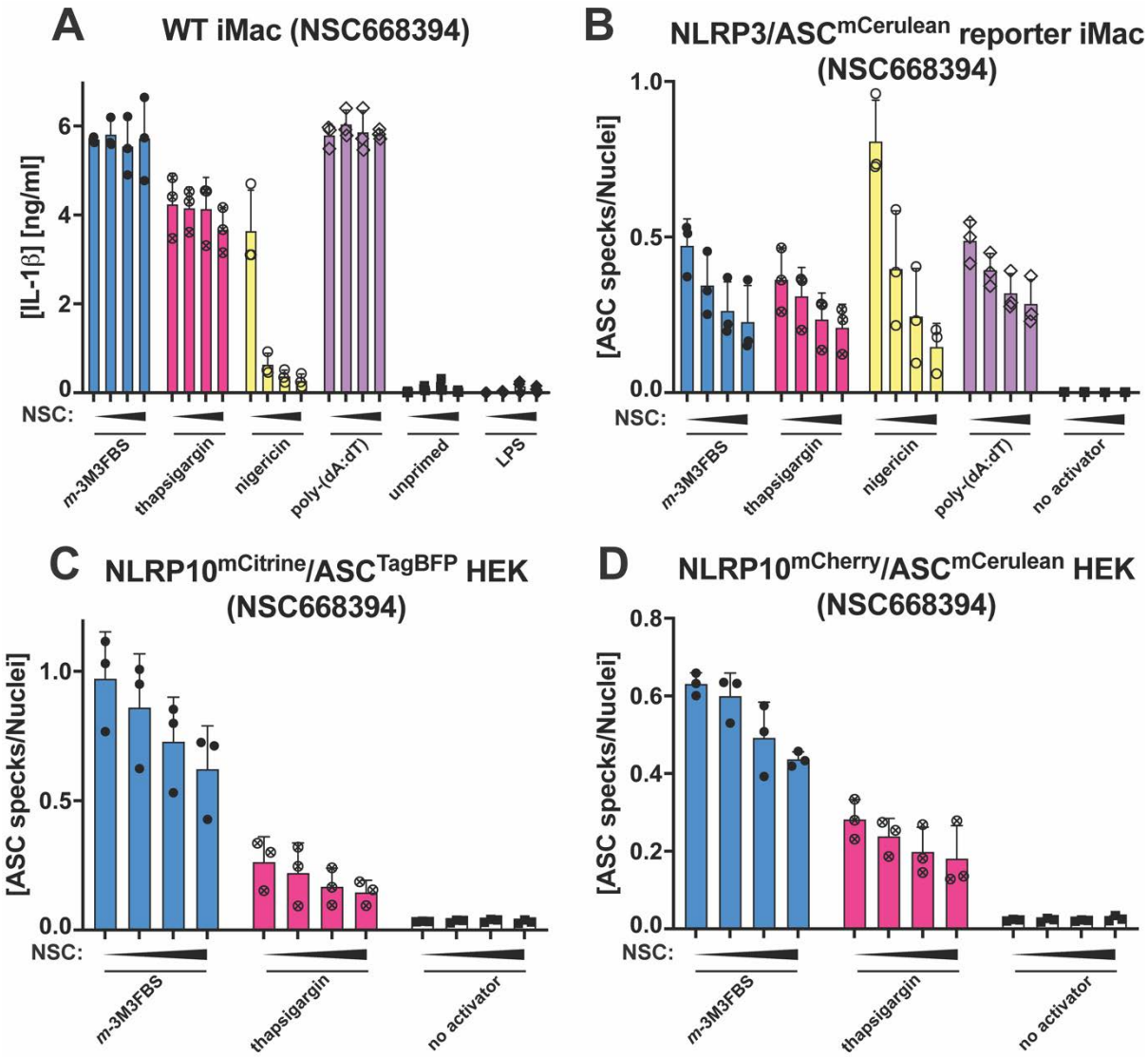

Supplementary Figure S55: Influence of the ezrin inhibitor NSC668394 on the inflammasome responses to *m*-3M3FBS, thapsigargin, nigericin, and poly-(dA:dT)

A-D: LPS-primed (200 ng/mL, 2 h) WT iMac cells (A), NLRP3/ASC^{mCerulean} reporter iMac cells (B), NLRP10^{mCitrine}/ASC^{TagBFP} HEK cells (C), and NLRP10^{mCherry}/ASC^{mCerulean} HEK cells (D) were treated for 10 min with NSC668394 (NSC; 0, 25, 50, or 100 μM). Then, the cells were subjected to the inflammasome activators *m*-3M3FBS (85 μM), thapsigargin (20 μM), nigericin (10 μM) or poly-(dA:dT) (2 μg/mL complexed with 5 μL Lipofectamine 2000) in an extracellular medium consisting of (in mM) 123 NaCl, 5 KCl, 2 $MgCl_2$, 1 $CaCl_2$, 10 glucose, 10 HEPES, pH 7.4. The LPS (A) and unprimed (A-D) controls were subjected to medium alone. Immediately after addition of inflammasome activators, the plates were centrifuged at 340 × g for 5 min (RT). After 30 min (C, D) or 60 min (A, B), the supernatants were collected and IL-1β concentrations were measured by HTRF (A) or the cells were fixed with 4% formaldehyde, counterstained with the nuclear dye DRAQ5 (5 μM) and imaged using a widefield fluorescence microscope (B-D).

The results are plotted as means from 3 independent experiments performed in technical duplicate. Error bars represent SD. Individual data points represent means of the technical duplicate values from each of the independent experiments.

Supplementary Figure S56:

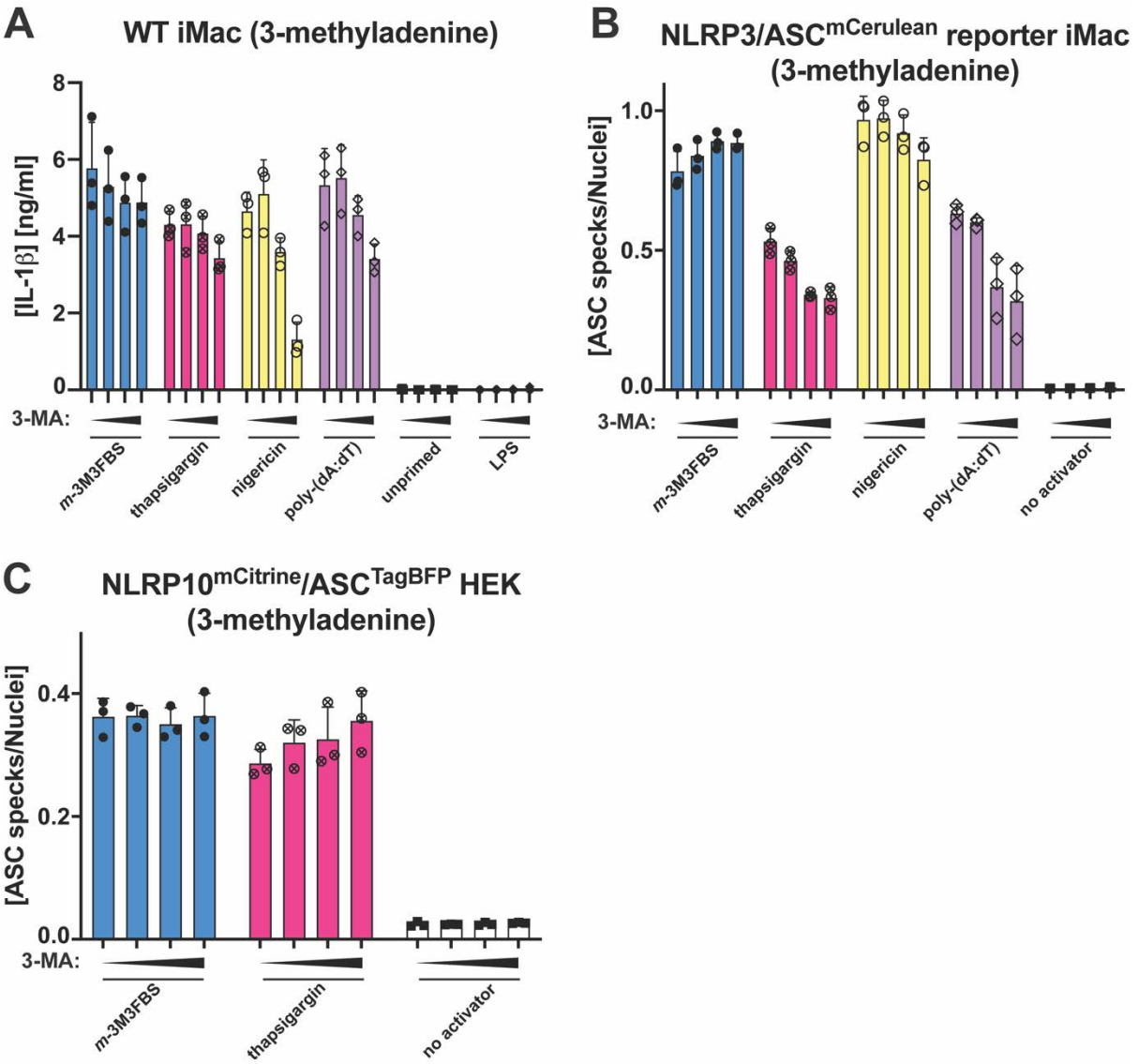

Supplementary Figure S56: Influence of 3-methyladenine on the inflammasome responses to *m*-3M3FBS, thapsigargin, nigericin, and poly-(dA:dT)

A-C: LPS-primed (200 ng/mL, 2 h) WT iMac cells (A), NLRP3/ASC^{mCerulean} reporter iMac cells (B), and NLRP10^{mCitrine}/ASC^{TagBFP} HEK cells (C) were treated for 10 min with 3-methyladenine (3-MA; 0, 1, 5, or 10 mM). Then, the cells were subjected to the inflammasome activators *m*-3M3FBS (85 μM), thapsigargin (20 μM), nigericin (10 μM) or poly-(dA:dT) (2 μg/mL complexed with 5 μL Lipofectamine 2000) in an extracellular medium consisting of (in mM) 123 NaCl, 5 KCl, 2 $MgCl_2$, 1 $CaCl_2$, 10 glucose, 10 HEPES, pH 7.4. The LPS (A) and unprimed (A-C) controls were subjected to medium alone. Immediately after addition of inflammasome activators, the plates were centrifuged at 340 × g for 5 min (RT). After 30 min (C) or 60 min (A, B), the supernatants were collected and IL-1β concentrations were measured by HTRF (A) or the cells were fixed with 4% formaldehyde, counterstained with the nuclear dye DRAQ5 (5 μM) and imaged using a widefield fluorescence microscope (B, C).

The results are plotted as means from 3 independent experiments performed in technical duplicate. Error bars represent SD. Individual data points represent means of the technical duplicate values from each of the independent experiments.

Supplementary Figure S57:

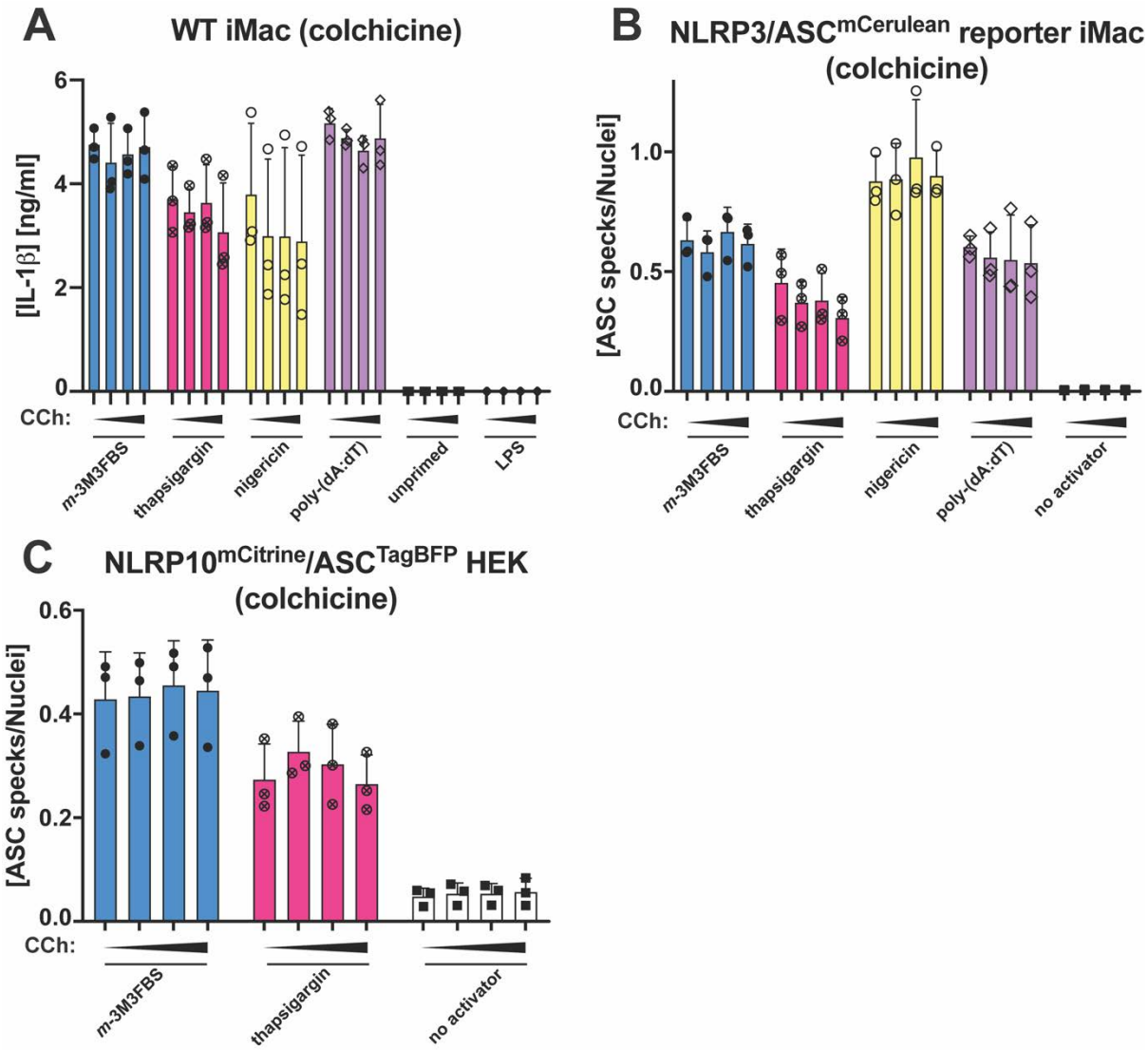

Supplementary Figure S57: Influence of colchicine on the inflammasome responses to *m*-3M3FBS, thapsigargin, nigericin, and poly-(dA:dT)

A-C: LPS-primed (200 ng/mL, 2 h) WT iMac cells (A), NLRP3/ASC^{mCerulean} reporter iMac cells (B), and NLRP10^{mCitrine}/ASC^{TagBFP} HEK cells (C) were treated for 10 min with colchicine (CCh; 0, 10, 25, or 50 μM). Then, the cells were subjected to the inflammasome activators *m*-3M3FBS (85 μM), thapsigargin (20 μM), nigericin (10 μM) or poly-(dA:dT) (2 μg/mL complexed with 5 μL Lipofectamine 2000) in an extracellular medium consisting of (in mM) 123 NaCl, 5 KCl, 2 $MgCl_2$, 1 $CaCl_2$, 10 glucose, 10 HEPES, pH 7.4. The LPS (A) and unprimed (A-C) controls were subjected to medium alone. Immediately after addition of inflammasome activators, the plates were centrifuged at 340 × g for 5 min (RT). After 30 min (C) or 60 min (A, B), the supernatants were collected and IL-1β concentrations were measured by HTRF (A) or the cells were fixed with 4% formaldehyde, counterstained with the nuclear dye DRAQ5 (5 μM) and imaged using a widefield fluorescence microscope (B, C).

The results are plotted as means from 3 independent experiments performed in technical duplicate. Error bars represent SD. Individual data points represent means of the technical duplicate values from each of the independent experiments.

Supplementary Figure S58:

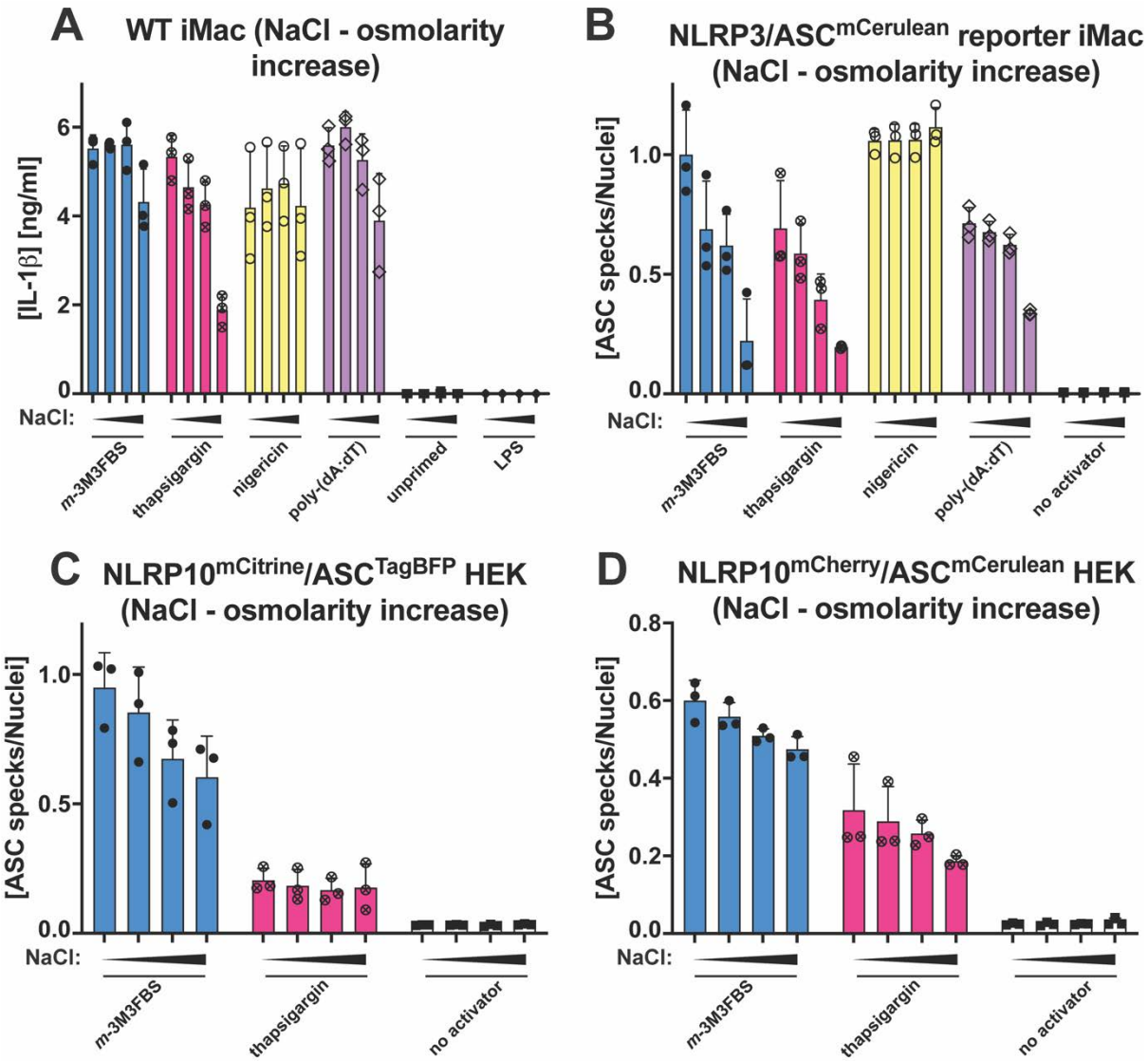

Supplementary Figure S58: Influence of increased osmolarity of the extracellular milieu on the inflammasome responses to *m*-3M3FBS, thapsigargin, nigericin, and poly-(dA:dT)

A-D: LPS-primed (200 ng/mL, 2 h) WT iMac cells (A), NLRP3/ASC^{mCerulean} reporter iMac cells (B), NLRP10^{mCitrine}/ASC^{TagBFP} HEK cells (C), and NLRP10^{mCherry}/ASC^{mCerulean} HEK cells (D) were treated for 10 min with media with supraphysiological concentrations of NaCl (0, 15, 30, or 60 mM) to increase the osmolarity of the extracellular fluid. Then, the cells were subjected to the inflammasome activators *m*-3M3FBS (85 μM), thapsigargin (20 μM), nigericin (10 μM) or poly-(dA:dT) (2 μg/mL complexed with 5 μL Lipofectamine 2000) in an extracellular medium consisting of (in mM) 123, 138, 153, or 183 NaCl, 5 KCl, 2 $MgCl_2$, 1 $CaCl_2$, 10 glucose, 10 HEPES, pH 7.4. The LPS (A) and unprimed (A-D) controls were subjected to medium alone. Immediately after addition of inflammasome activators, the plates were centrifuged at 340 × g for 5 min (RT). After 30 min (C, D) or 60 min (A, B), the supernatants were collected and IL-1β concentrations were measured by HTRF (A) or the cells were fixed with 4% formaldehyde, counterstained with the nuclear dye DRAQ5 (5 μM) and imaged using a widefield fluorescence microscope (B-D).

The results are plotted as means from 3 independent experiments performed in technical duplicate. Error bars represent SD. Individual data points represent means of the technical duplicate values from each of the independent experiments.

Supplementary Figure S59:

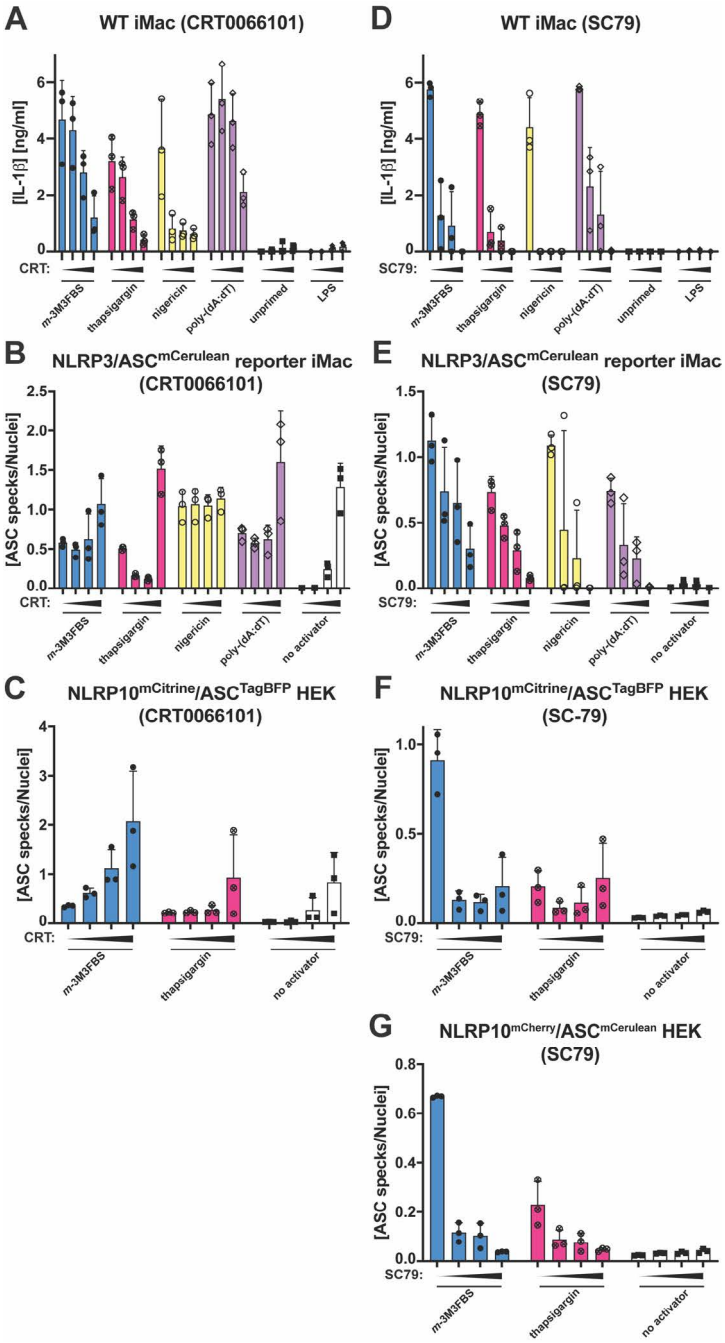

Supplementary Figure S59: Influence of CRT0066101 and SC79 on the inflammasome responses to *m*-3M3FBS, thapsigargin, nigericin, and poly-(dA:dT)

A-G: LPS-primed (200 ng/mL, 2 h) WT iMac cells (A, D), NLRP3/ASC^{mCerulean} reporter iMac cells (B, E), NLRP10^{mCitrine}/ASC^{TagBFP} HEK cells (C, F), and NLRP10^{mCherry}/ASC^{mCerulean} HEK cells (G) were treated for 10 min with CRT0066101 (CRT; 0, 10, 25, or 50 μM; A-C) or SC79 (0, 5, 10, or 50 μM; D-G). Then, the cells were subjected to the inflammasome activators *m*-3M3FBS (85 μM), thapsigargin (20 μM), nigericin (10 μM) or poly-(dA:dT) (2 μg/mL complexed with 5 μL Lipofectamine 2000) in an extracellular medium consisting of (in mM) 123 NaCl, 5 KCl, 2 $MgCl_2$, 1 $CaCl_2$, 10 glucose, 10 HEPES, pH 7.4. The LPS (A, D) and unprimed (A-G) controls were subjected to medium alone. Immediately after addition of inflammasome activators, the plates were centrifuged at 340 × g for 5 min (RT). After 30 min (C, F, G) or 60 min (A, B, D, E), the supernatants were collected and IL-1β concentrations were measured by HTRF (A, D) or the cells were fixed with 4% formaldehyde, counterstained with the nuclear dye DRAQ5 (5 μM) and imaged using a widefield fluorescence microscope (B, C, E-G).

The results are plotted as means from 3 independent experiments performed in technical duplicate. Error bars represent SD. Individual data points represent means of the technical duplicate values from each of the independent experiments.

Supplementary Figure S60:

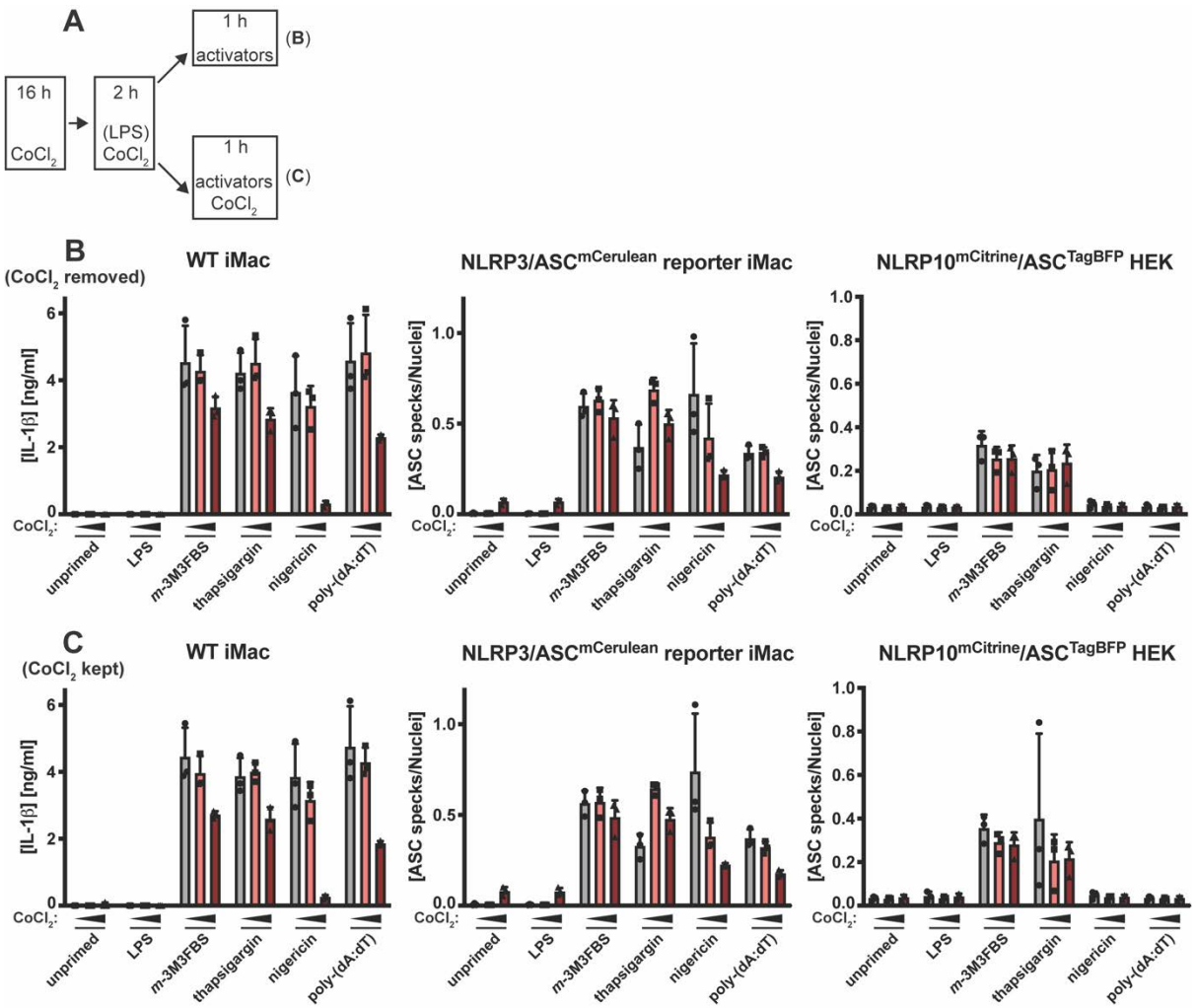

Supplementary Figure S60: The inflammasome responses to *m*-3M3FBS, thapsigargin, nigericin, and poly-(dA:dT) in immortalized murine macrophages and in NLRP10^{mCitrine}/ASC^{TagBFP} HEK cells after chemical induction of hypoxia using overnight incubations with $CoCl_2$

A: Schematic overview of the experimental protocol.

B, C: WT iMac cells (left column), NLRP3/ASC^{mCerulean} reporter iMac cells (central column), and NLRP10^{mCitrine}/ASC^{TagBFP} HEK cells (right column) were treated overnight (~16 h) with $CoCl_2$ (0, 100, or 250 μM) in DMEM supplemented with 10% FBS. On the next day, the cells were shifted to $CoCl_2$-free media and primed with LPS (200 ng/mL, 2 h; WT iMac cells) or left unprimed (NLRP3/ASC^{mCerulean} reporter iMac cells and NLRP10^{mCitrine}/ASC^{TagBFP} HEK cells) (B) or they were kept in $CoCl_2$ (0, 100, or 250 μM)-containing media and LPS-primed (200 ng/mL, 2 h; WT iMac cells) or left unprimed (NLRP3/ASC^{mCerulean} reporter iMac and NLRP10^{mCitrine}/ASC^{TagBFP} HEK cells) (C). Next, the cells were shifted to an extracellular medium consisting of (in mM) 123 NaCl, 5 KCl, 2 MgCl2, 1 CaCl2, 10 glucose, 10 HEPES pH 7.4 without (B) or with (C) $CoCl_2$ (0, 100, or 250 μM) and stimulated with the inflammasome activators *m*-3M3FBS (85 μM), thapsigargin (20 μM), nigericin (10 μM) or poly-(dA:dT) (2 μg/mL complexed with 5 μL Lipofectamine 2000). Immediately after addition of inflammasome activators, the plates were centrifuged at 340 × g for 5 min (RT). After 30 min (NLRP10^{mCitrine}/ASC^{TagBFP} HEK cells) or 60 min (WT iMac cells, NLRP3/ASC^{mCerulean} reporter iMac cells), the supernatants were collected and IL-1β concentrations were measured by HTRF (WT iMac cells) or the cells were fixed with 4% formaldehyde, counterstained with the nuclear dye DRAQ5 (5 μM) and imaged using a widefield fluorescence microscope (NLRP10^{mCitrine}/ASC^{TagBFP} HEK cells and NLRP3/ASC^{mCerulean} reporter iMac cells).

The results are plotted as means from 3 independent experiments performed in technical triplicate. Error bars represent SD. Individual data points represent means of the technical triplicate values from each of the independent experiments.

Supplementary Figure S61:

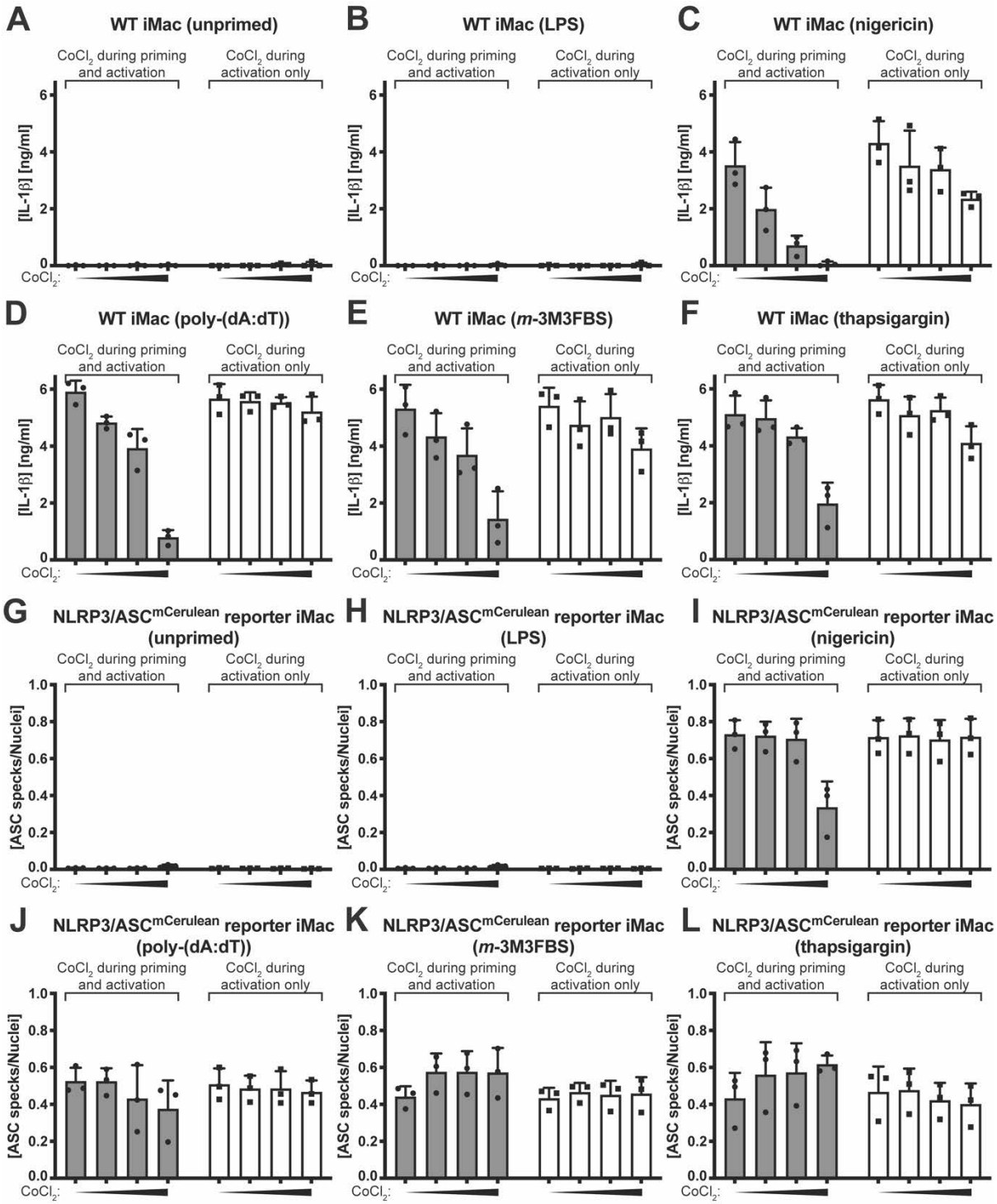

Supplementary Figure S61: Influence of short (5 min - 2h) incubations with $CoCl_2$ on the inflammasome responses to *m*-3M3FBS, thapsigargin, nigericin, and poly-(dA:dT) in immortalized murine macrophages

A-L: WT iMac cells (B-F) and NLRP3/ASC^{mCerulean} reporter iMac cells (H-L) were treated for 2 h with DMEM supplemented with 10% FBS, 200 ng/mL LPS and $CoCl_2$ (0, 100, 250, or 500 μM; '$CoCl_2$ during priming and activation'). The cells under conditions designated as '$CoCl_2$ during activation only' were subjected to DMEM with 10% FBS and 200 ng/mL LPS without addition of $CoCl_2$. The unprimed (A, G) controls were subjected to the same conditions but without addition of LPS. Next, the cells were shifted to an extracellular medium consisting of (in mM) 123 NaCl, 5 KCl, 2 $MgCl_2$, 1 $CaCl_2$, 10 glucose, 10 HEPES pH 7.4 supplemented with 0, 100, 250, or 500 μM $CoCl_2$, and stimulated with the following inflammasome activators: *m*-3M3FBS (85 μM; E, K), thapsigargin (20 μM; F, L), nigericin (10 μM; C, I) or poly-(dA:dT) (2 μg/mL complexed with 5 μL Lipofectamine 2000; D, J). The unprimed (A, G) and LPS controls (B, H) were

subjected to medium alone. Immediately after addition of inflammasome activators, the plates were centrifuged at 340 × g for 5 min (RT). After 60 min, the supernatants were collected and IL-1β concentrations were measured by HTRF (A-F) or the cells were fixed with 4% formaldehyde, counterstained with the nuclear dye DRAQ5 (5 μM) and imaged using a widefield fluorescence microscope (G-L).
The results are plotted as means from 3 independent experiments performed in technical duplicate. Error bars represent SD. Individual data points represent means of the technical duplicate values from each of the independent experiments.

Supplementary Figure S62:

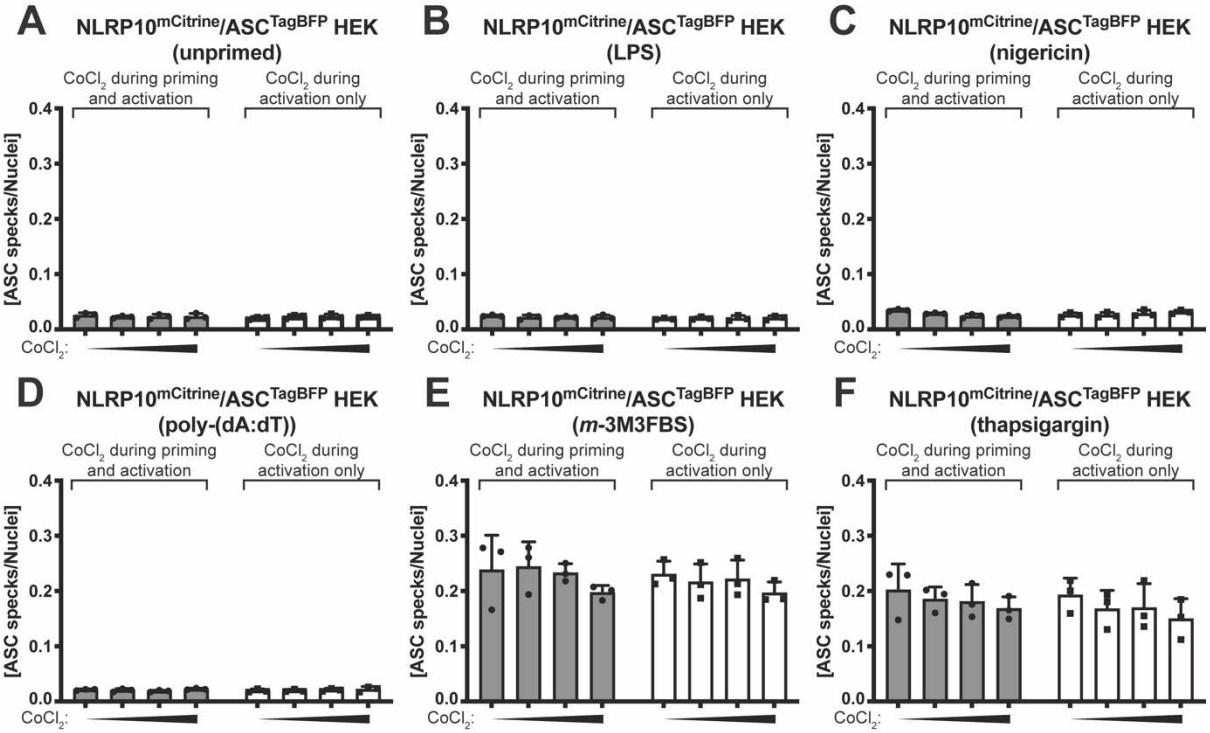

Supplementary Figure S62: Influence of short (5 min - 2h) incubations with $CoCl_2$ on the inflammasome responses to *m*-3M3FBS, thapsigargin, nigericin, and poly-(dA:dT) in NLRP10^{mCitrine}/ASC^{TagBFP} HEK cells

A-F: NLRP10^{mCitrine}/ASC^{TagBFP} HEK cells (B-F) were treated for 2 h with DMEM supplemented with 10% FBS, 200 ng/mL LPS and $CoCl_2$ (0, 100, 250, or 500 μM; '$CoCl_2$ during priming and activation'). The cells under conditions designated as '$CoCl_2$ during activation only' were subjected to DMEM with 10% FBS and 200 ng/mL LPS without addition of $CoCl_2$. The unprimed (A) controls were subjected to the same conditions but without addition of LPS. Next, the cells were shifted to an extracellular medium consisting of (in mM) 123 NaCl, 5 KCl, 2 $MgCl_2$, 1 $CaCl_2$, 10 glucose, 10 HEPES pH 7.4 supplemented with 0, 100, 250, or 500 μM $CoCl_2$, and stimulated with the following inflammasome activators: *m*-3M3FBS (85 μM; E), thapsigargin (20 μM; F), nigericin (10 μM; C) or poly-(dA:dT) (2 μg/mL complexed with 5 μL Lipofectamine 2000; D). The unprimed (A) and LPS controls (B) were subjected to medium alone. Immediately after addition of inflammasome activators, the plates were centrifuged at 340 × g for 5 min (RT). After 30 min, the cells were fixed with 4% formaldehyde, counterstained with the nuclear dye DRAQ5 (5 μM) and imaged using a widefield fluorescence microscope.
The results are plotted as means from 3 independent experiments performed in technical duplicate. Error bars represent SD. Individual data points represent means of the technical duplicate values from each of the independent experiments.

Supplementary Figure S63:

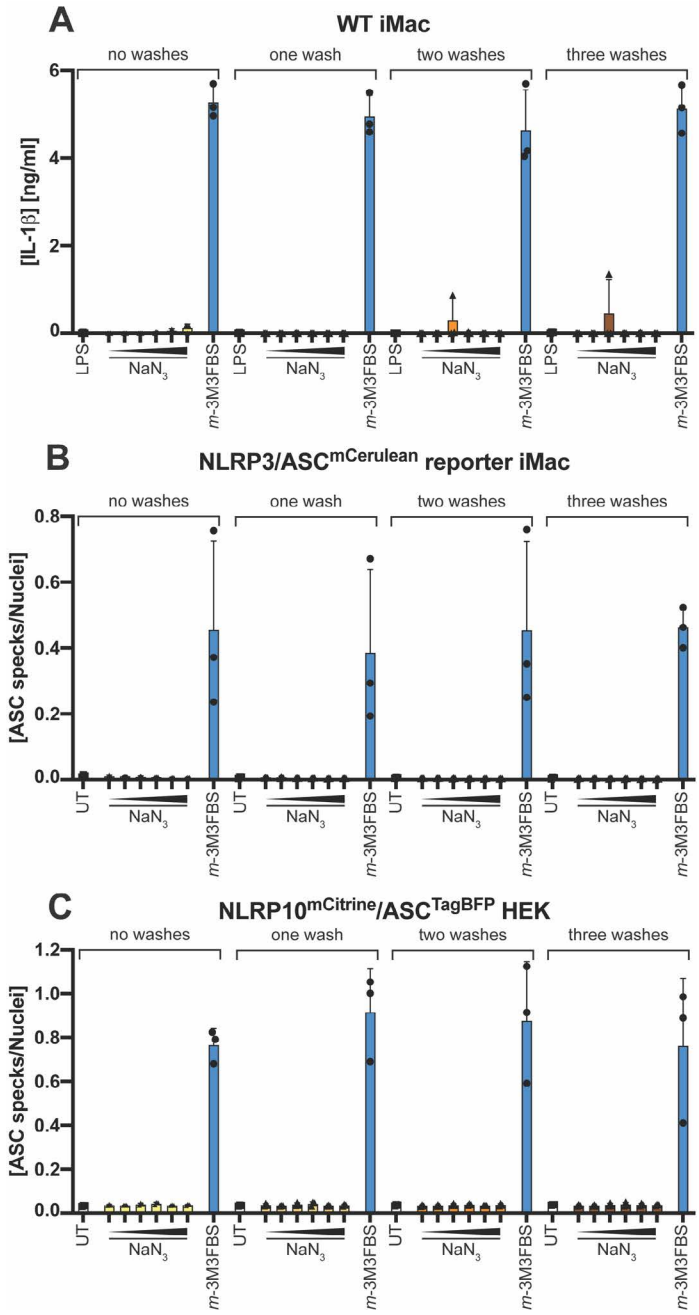

Supplementary Figure S63: IL-1β secretion from and ASC speck formation in immortalized murine macrophages and NLRP10^{mCitrine}/ASC^{TagBFP} HEK cells treated with NaN_3 to mimic an ischemia/reperfusion scenario

A-C: LPS-primed (200 ng/mL, 2 h) WT iMac cells (A), NLRP3/ASC^{mCerulean} reporter iMac cells (B), and NLRP10^{mCitrine}/ASC^{TagBFP} HEK cells (C) were shifted to an extracellular medium consisting of (in mM) 123 NaCl, 5 KCl, 2 $MgCl_2$, 1 $CaCl_2$, 10 glucose, 10 HEPES pH 7.4, without (LPS controls in panel A and untreated [UT] controls in panels B and C) or with NaN_3 (0.5, 1, 2.5, 5, 10, or 20 mM). The cells were incubated under these conditions for 30 min (the 'one wash', 'two washes', and 'three washes' conditions) or for 90 min (the 'no washes' conditions). After 30 min, NaN_3 was washed away (one, two, or three washes with the experimental medium, as indicated), and the cells were incubated for further 60 min in the experimental medium without NaN_3. At this point, the positive (*m*-3M3FBS) control cells were stimulated with 85 μM *m*-3M3FBS. At the completion of the experiment, the supernatants were collected and IL-1β concentrations were measured by HTRF (A) or the cells were fixed with 4% formaldehyde, counterstained with the nuclear dye DRAQ5 (5 μM) and imaged using a widefield fluorescence microscope (B, C).
The results are plotted as means from 3 independent experiments performed in technical triplicate. Error bars represent SD. Individual data points represent means of the technical triplicate values from each of the independent experiments.

12. Supplementary Methods Figures SM1-SM4

Supplementary Methods Figure SM1:

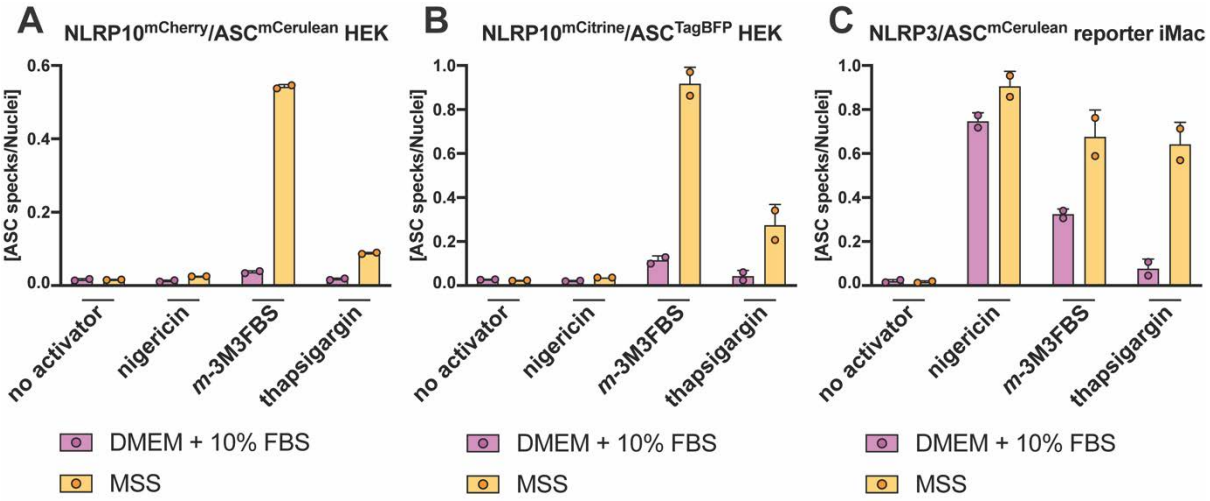

Supplementary Methods Figure SM1: Impact of the extracellular medium choice on the magnitude of the inflammasome responses to *m*-3M3FBS and thapsigargin

A-C: NLRP10^{mCherry}/ASC^{mCerulean} HEK cells (A), NLRP^{10mCitrine}/ASC^{TagBFP} HEK cells (B), and NLRP3/ASC^{mCerulean} reporter iMac cells (C) were stimulated with nigericin (10 μM), m-3M3FBS (85 μM), or thapsigargin (20 μM) in DMEM supplemented with 10% FBS (pink bars) or in minimal salt solution (MSS) consisting of (in mM) 123 NaCl, 5 KCl, 2 $MgCl_2$, 1 $CaCl_2$, 10 glucose, 10 HEPES pH 7.4. The untreated ('no activator') alone were subjected to media alone. After 30 min (A, B) or 60 min (C) of stimulation, the cells were fixed with 4% formaldehyde, counterstained with the nuclear dye DRAQ5 (5 μM) and imaged using a widefield fluorescence microscope.

The results are plotted as means from 2 independent experiments performed in technical quadruplicate. Error bars represent SD. Individual data points represent means of the technical quadruplicate values from each of the independent experiments.

Supplementary Methods Figure SM2:

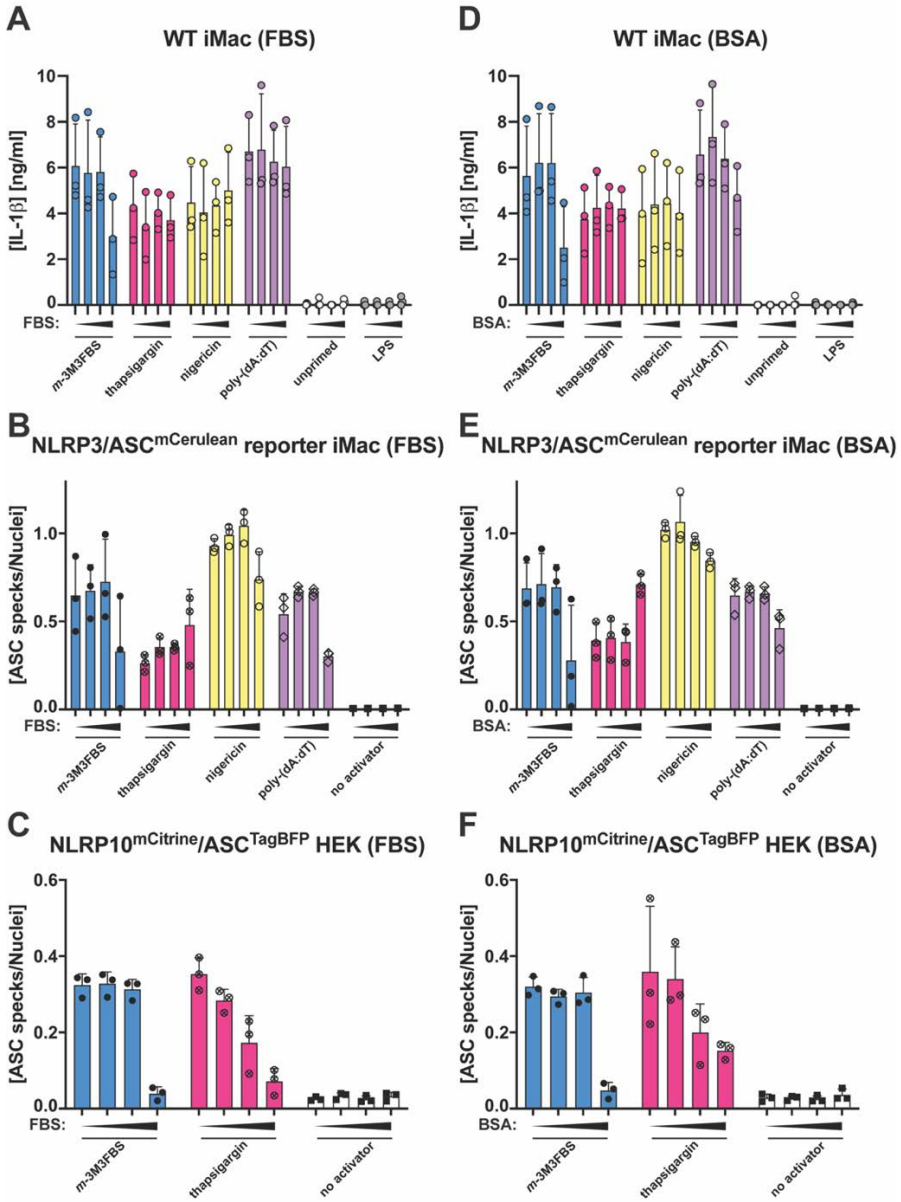

Supplementary Methods Figure SM2: Influence of fetal bovine serum and bovine serum albumin in the extracellular milieu on the inflammasome responses to *m*-3M3FBS, thapsigargin, nigericin, and poly-(dA:dT)

A-F: LPS-primed (200 ng/mL, 2 h) WT iMac cells (A, D), NLRP3/ASC^{mCerulean} reporter iMac cells (B, E), NLRP10^{mCitrine}/ASC^{TagBFP} HEK cells (C, F) were shifted to an extracellular medium consisting of (in mM) 123 NaCl, 5 KCl, 2 $MgCl_2$, 1 $CaCl_2$, 10 glucose, 10 HEPES pH 7.4 supplemented with increasing concentrations of fetal bovine serum (FBS; 0%, 0.1%, 1%, or 10%; A-C) or bovine serum albumin (BSA; 0, 0.05, 0.5, or 5 mg/mL; D-F). Of note, the tested BSA concentrations (D-F) correspond to the approximate **total protein** concentrations in the tested FBS dilutions (A-C). After a 10-min pre-incubation, the cells were challenged with the following inflammasome activators: *m*-3M3FBS (85 μM), thapsigargin (20 μM), nigericin (10 μM), and poly-(dA:dT) (2 μg/mL complexed with 5 μL Lipofectamine 2000). The LPS (A, D) and unprimed (A-F) controls were subjected to medium alone. Immediately after addition of inflammasome activators, the plates were centrifuged at 340 × g for 5 min (RT). After 30 min (C, F) or 60 min (A, B, D, E), the supernatants were collected and IL-1β concentrations were measured by HTRF (A, D) or the cells were fixed with 4% formaldehyde, counterstained with the nuclear dye DRAQ5 (5 μM) and imaged using a widefield fluorescence microscope (B, C, E, F).

The results are plotted as means from 3 independent experiments performed in technical duplicate. Error bars represent SD. Individual data points represent means of the technical duplicate values from each of the independent experiments.

Supplementary Methods Figure SM3:

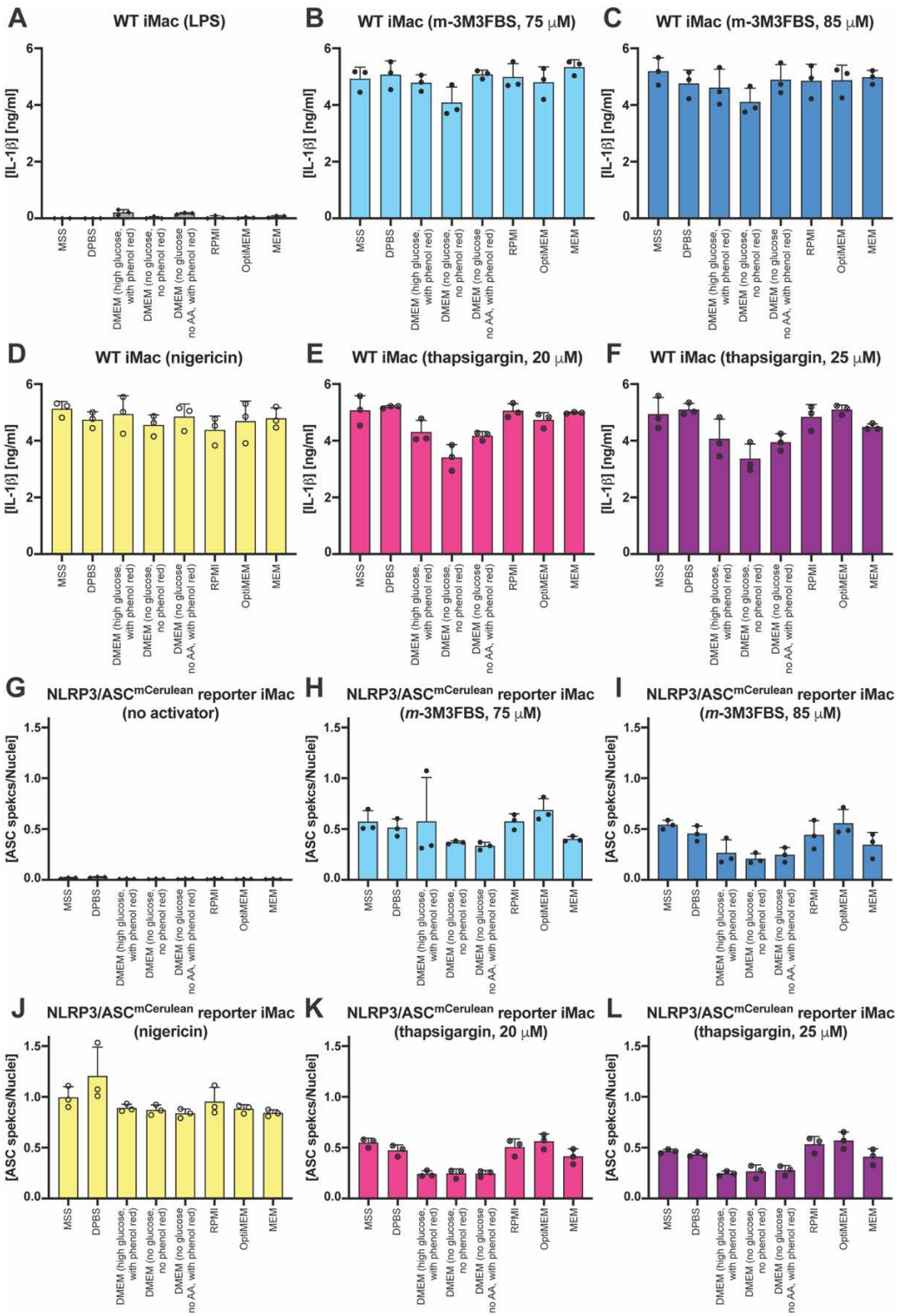

Supplementary Methods Figure SM3: Comparison of the magnitudes of the immortalized murine macrophage inflammasome responses to *m*-3M3FBS and thapsigargin in several commercially available cell culture media

A-L: LPS-primed (200 ng/mL, 2 h) WT iMac cells (A-F) and NLRP3/ASC^{mCerulean} reporter iMac cells (G-L) were shifted to the following extracellular media: Dulbecco's PBS (DPBS), DMEM (high glucose, that is 4.5 g/L, with phenol red), DMEM (without glucose, without phenol red), DMEM (without glucose, without amino acids, with phenol red), RPMI, OptiMEM, MEM, or to the extracellular medium consisting of (in mM)

123 NaCl, 5 KCl, 2 $MgCl_2$, 1 $CaCl_2$, 10 glucose, 10 HEPES pH 7.4 (minimal salt solution [MSS]). After a 10-min pre-incubation, the cells were challenged with the following inflammasome activators: *m*-3M3FBS (75 μM [B, H] or 85 μM [C, I]), thapsigargin (20 μM [E, K] or 25 μM [F, L]), or nigericin (10 μM [D, J]). The LPS (A) and untreated ('no activator'; G) controls were subjected to the tested media alone. Immediately after addition of inflammasome activators, the plates were centrifuged at 340 × g for 5 min (RT). After 60 min, the supernatants were collected and IL-1β concentrations were measured by HTRF (A-F) or the cells were fixed with 4% formaldehyde, counterstained with the nuclear dye DRAQ5 (5 μM) and imaged using a widefield fluorescence microscope (G-L).
The results are plotted as means from 3 independent experiments performed in technical duplicate. Error bars represent SD. Individual data points represent means of the technical duplicate values from each of the independent experiments.

Supplementary Methods Figure SM4:

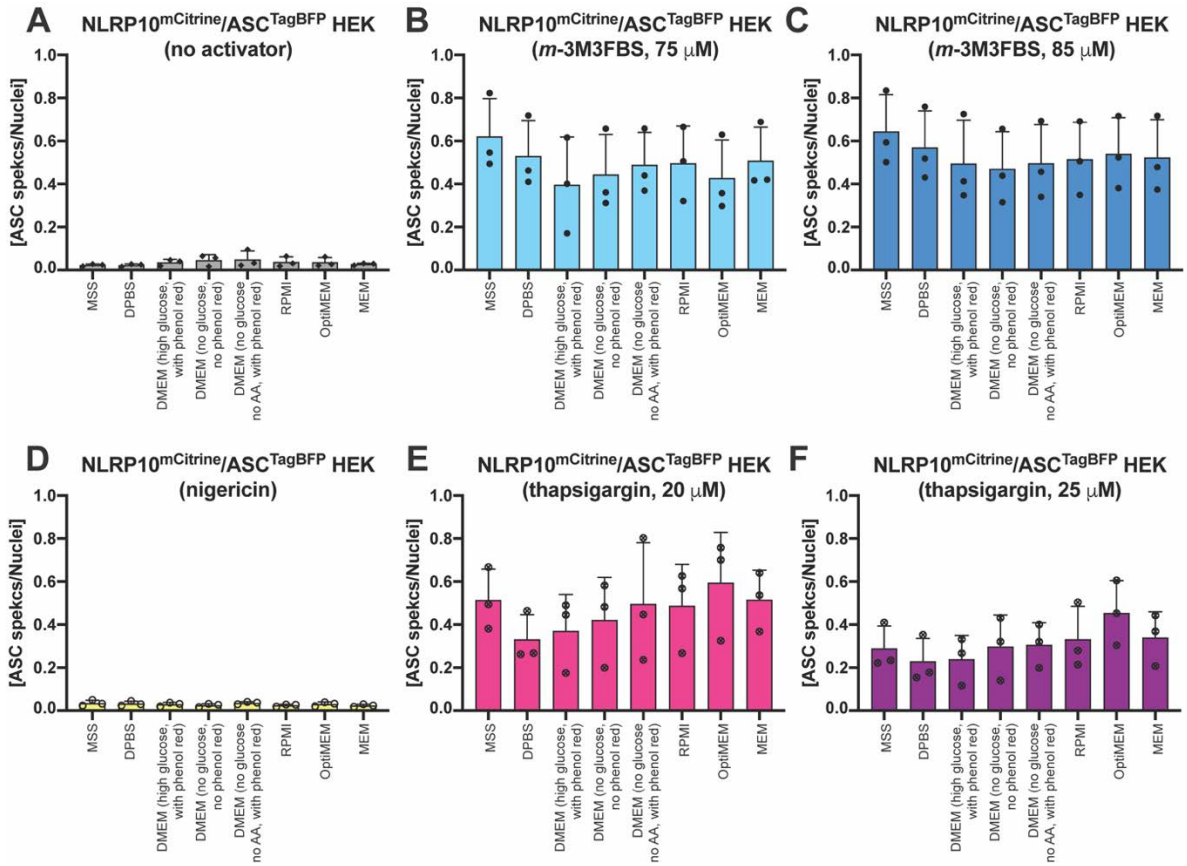

Supplementary Methods Figure SM4: Comparison of the magnitudes of the NLRP10^{mCitrine}/ASC^{TagBFP} HEK cell inflammasome responses to *m*-3M3FBS and thapsigargin in several commercially available cell culture media

A-F: NLRP10^{mCitrine}/ASC^{TagBFP} HEK cells were shifted to the following extracellular media: Dulbecco's PBS (DPBS), DMEM (high glucose, that is 4.5 g/L, with phenol red), DMEM (without glucose, without phenol red), DMEM (without glucose, without amino acids, with phenol red), RPMI, OptiMEM, MEM, or to the extracellular medium consisting of (in mM) 123 NaCl, 5 KCl, 2 $MgCl_2$, 1 $CaCl_2$, 10 glucose, 10 HEPES pH 7.4 (minimal salt solution [MSS]). After a 10-min pre-incubation, the cells were challenged with the following inflammasome activators: *m*-3M3FBS (75 μM [B] or 85 μM [C]), thapsigargin (20 μM [E] or 25 μM [F]), or nigericin (10 μM [D]). The untreated ('no activator'; A) controls were subjected to the tested media alone. Immediately after addition of inflammasome activators, the plates were centrifuged at 340 × g for 5 min (RT). After 30 min, the cells were fixed with 4% formaldehyde, counterstained with the nuclear dye DRAQ5 (5 μM) and imaged using a widefield fluorescence microscope.
The results are plotted as means from 3 independent experiments performed in technical duplicate. Error bars represent SD. Individual data points represent means of the technical duplicate values from each of the independent experiments.

13. Literature

Abdel-Nour, M., Carneiro, L.A.M., Downey, J., Tsalikis, J., Outlioua, A., Prescott, D., Da Costa, L.S., Hovingh, E.S., Farahvash, A., Gaudet, R.G., et al. (2019). The heme-regulated inhibitor is a cytosolic sensor of protein misfolding that controls innate immune signaling. Science *365*, eaaw4144.

Ablasser, A., Goldeck, M., Cavlar, T., Deimling, T., Witte, G., Röhl, I., Hopfner, K.-P., Ludwig, J., and Hornung, V. (2013). cGAS produces a 2′-5′-linked cyclic dinucleotide second messenger that activates STING. Nature *498*, 380–384.

Aiyar, A., Xiang, Y., and Leis, J. (1996). Site-Directed Mutagenesis Using Overlap Extension PCR. In In Vitro Mutagenesis Protocols, (New Jersey: Humana Press), pp. 177–192.

Alavian, K.N., Beutner, G., Lazrove, E., Sacchetti, S., Park, H.A., Licznerski, P., Li, H., Nabili, P., Hockensmith, K., Graham, M., et al. (2014a). An uncoupling channel within the c-subunit ring of the F1FO ATP synthase is the mitochondrial permeability transition pore. Proc Natl Acad Sci USA *111*, 10580–10585.

Alavian, K.N., Dworetzky, S.I., Bonanni, L., Zhang, P., Sacchetti, S., Li, H., Signore, A.P., Smith, P.J.S., Gribkoff, V.K., and Jonas, E.A. (2014b). The Mitochondrial Complex V–Associated Large-Conductance Inner Membrane Current Is Regulated by Cyclosporine and Dexpramipexole. Mol Pharmacol *87*, 1–8.

Alavian, K.N., Dworetzky, S.I., Bonanni, L., Zhang, P., Sacchetti, S., Mariggio, M.A., Onofrj, M., Thomas, A., Li, H., Mangold, J.E., et al. (2012). Effects of dexpramipexole on brain mitochondrial conductances and cellular bioenergetic efficiency. Brain Research *1446*, 1–11.

Alberts, B., Johnson, A., Lewis, J., Morgan, D., Raff, M., Roberts, K., and Walter, P. (2017). Molecular Biology of the Cell (Garland Science).

Alexopoulou, L., Holt, A.C., Medzhitov, R., and Flavell, R.A. (2001). Recognition of double-stranded RNA and activation of NF-κB by Toll-like receptor 3. Nature *413*, 732–738.

Allam, R., Darisipudi, M.N., Tschopp, J., and Anders, H.-J. (2013). Histones trigger sterile inflammation by activating the NLRP3 inflammasome. Eur. J. Immunol. *43*, 3336–3342.

Allam, R., Lawlor, K.E., Yu, E.C.W., Mildenhall, A.L., Moujalled, D.M., Lewis, R.S., Ke, F., Mason, K.D., White, M.J., Stacey, K.J., et al. (2014). Mitochondrial apoptosis is dispensable for NLRP3 inflammasome activation but non-apoptotic caspase-8 is required for inflammasome priming. EMBO Rep *15*, 982–990.

Allen, I.C., Scull, M.A., Moore, C.B., Holl, E.K., McElvania-TeKippe, E., Taxman, D.J., Guthrie, E.H., Pickles, R.J., and Ting, J.P.-Y. (2009). The NLRP3 Inflammasome Mediates In Vivo Innate Immunity to Influenza A Virus through Recognition of Viral RNA. Immunity *30*, 556–565.

Altan-Bonnet, G., and Mukherjee, R. (2019). Cytokine-mediated communication: a quantitative appraisal of immune complexity. Nat Rev Immunol *19*, 205–217.

Amulic, B., Knackstedt, S.L., Abu Abed, U., Deigendesch, N., Harbort, C.J., Caffrey, B.E., Brinkmann, V., Heppner, F.L., Hinds, P.W., and Zychlinsky, A. (2017). Cell-Cycle Proteins Control Production of Neutrophil Extracellular Traps. Developmental Cell *43*, 449–462.e5.

Antonsson, B. (1997). Inhibition of Bax Channel-Forming Activity by Bcl-2. Science *277*, 370–372.

Arbore, G., West, E.E., Spolski, R., Robertson, A.A.B., Klos, A., Rheinheimer, C., Dutow, P., Woodruff, T.M., Yu, Z.X., ONeill, L.A., et al. (2016). T helper 1 immunity requires complement-driven NLRP3 inflammasome activity in CD4+ T cells. Science *352*, aad1210–aad1210.

Azarashvili, T., Grachev, D., Krestinina, O., Evtodienko, Y., Yurkov, I., Papadopoulos, V., and Reiser, G. (2007). The peripheral-type benzodiazepine receptor is involved in control of Ca2+-induced permeability transition pore opening in rat brain mitochondria. Cell Calcium *42*, 27–39.

Azzolin, L., Stockum, von, S., Basso, E., Petronilli, V., Forte, M.A., and Bernardi, P. (2010). The mitochondrial permeability transition from yeast to mammals. FEBS Letters *584*, 2504–2509.

Bae, Y.-S., Lee, T.G., Park, J.C., Hur, J.H., Kim, Y., Heo, K., Kwak, J.-Y., Suh, P.-G., and Ryu, S.H. (2003). Identification of a Compound That Directly Stimulates Phospholipase C Activity. Mol Pharmacol *63*, 1043–1050.

Baines, C.P., Kaiser, R.A., Purcell, N.H., Blair, N.S., Osinska, H., Hambleton, M.A., Brunskill, E.W., Sayen, M.R., Gottlieb, R.A., Dorn, G.W., II, et al. (2005). Loss of cyclophilin D reveals a critical role for mitochondrial permeability transition in cell death. Nature *434*, 658–662.

Balamayooran, G., Pena, M., Sharma, R., and Truman, R.W. (2015). The armadillo as an animal model and reservoir host for Mycobacterium leprae. Clinics in Dermatology *33*, 108–115.

Baldwin, A.G., Rivers-Auty, J., Daniels, M.J.D., White, C.S., Schwalbe, C.H., Schilling, T., Hammadi, H., Jaiyong, P., Spencer, N.G., England, H., et al. (2017). Boron-Based Inhibitors of the NLRP3 Inflammasome. Cell Chemical Biology *24*, 1321–1335.e1325.

Baroja-Mazo, A., Martín-Sánchez, F., Gomez, A.I., Martínez, C.M., Amores-Iniesta, J., Compan, V., Barberà-Cremades, M., Yagüe, J., Ruiz-Ortiz, E., Antón, J., et al. (2014). The NLRP3 inflammasome is released as a particulate danger signal that amplifies the inflammatory response. Nat Immunol *15*, 738–748.

Baron, L., Gombault, A., Fanny, M., Villeret, B., Savigny, F., Guillou, N., Panek, C., Le Bert, M., Lagente, V., Rassendren, F., et al. (2015). The NLRP3 inflammasome is activated by nanoparticles through ATP, ADP and adenosine. Cell Death Dis *6*, e1629–e1629.

Bartok, E., and Hartmann, G. (2020). Immune Sensing Mechanisms that Discriminate Self from Altered Self and Foreign Nucleic Acids. Immunity *53*, 54–77.

Basso, E., Fante, L., Fowlkes, J., Petronilli, V., Forte, M.A., and Bernardi, P. (2005). Properties of the Permeability Transition Pore in Mitochondria Devoid of Cyclophilin D. Journal of Biological Chemistry *280*, 18558–18561.

Bauer, M.K.A., Schubert, A., Rocks, O., and Grimm, S. (1999). Adenine Nucleotide Translocase-1, a Component of the Permeability Transition Pore, Can Dominantly Induce Apoptosis. J Cell Biol *147*, 1493–1502.

Bauernfeind, F.G., Horvath, G., Stutz, A., Alnemri, E.S., MacDonald, K., Speert, D., Fernandes-Alnemri, T., Wu, J., Monks, B.G., Fitzgerald, K.A., et al. (2009). Cutting Edge: NF- B Activating Pattern Recognition and Cytokine Receptors License NLRP3 Inflammasome Activation by Regulating NLRP3 Expression. The Journal of Immunology *183*, 787–791.

Becattini, B., Culmsee, C., Leone, M., Zhai, D., Zhang, X., Crowell, K.J., Rega, M.F., Landshamer, S., Reed, J.C., Plesnila, N., et al. (2006). Structure-activity relationships by interligand NOE-based design and synthesis of antiapoptotic compounds targeting Bid. Proc Natl Acad Sci USA *103*, 12602–12606.

Bernstein, S.H., Venkatesh, S., Li, M., Lee, J., Lu, B., Hilchey, S.P., Morse, K.M., Metcalfe, H.M., Skalska, J., Andreeff, M., et al. (2012). The mitochondrial ATP-dependent Lon protease: a novel target in lymphoma death mediated by the synthetic triterpenoid CDDO and its derivatives. Blood *119*, 3321–3329.

Berson, A., Descatoire, V., Sutton, A., Fau, D., Maulny, B., Vadrot, N., Feldmann, G., Berthon, B., Tordjmann, T., and Pessayre, D. (2001). Toxicity of alpidem, a peripheral benzodiazepine receptor ligand, but not zolpidem, in rat hepatocytes: role of mitochondrial permeability transition and metabolic activation. J. Pharmacol. Exp. Ther. *299*, 793–800.

Bertheloot, D., Naumovski, A.L., Langhoff, P., Horvath, G.L., Jin, T., Xiao, T.S., Garbi, N., Agrawal, S., Kolbeck, R., and Latz, E. (2016). RAGE Enhances TLR Responses through Binding and Internalization of RNA. The Journal of Immunology *197*, 4118–4126.

Beutner, G., Rück, A., Riede, B., Welte, W., and Brdiczka, D. (1999). Complexes between kinases, mitochondrial porin and adenylate translocator in rat brain resemble the permeability transition pore. FEBS Letters *396*, 189–195.

Billich, A., Hammerschmid, F., Peichl, P., Wenger, R., Zenke, G., Quesniaux, V., and Rosenwirth, B. (1995). Mode of action of SDZ NIM 811, a nonimmunosuppressive cyclosporin A analog with activity against human immunodeficiency virus (HIV) type 1: interference with HIV protein-cyclophilin A interactions. J. Virol. *69*, 2451–2461.

Bittner, Z.A., Liu, X., Shankar, S., Tapia-Abellán, A., Kalbacher, H., Andreeva, L., Mangan, M., Düwell, P., Lovotti, M., Bosch, K., et al. (2020). BTK operates a phospho-tyrosine switch to regulate NLRP3 inflammasome activity. bioRxiv *9*, 864702.

Black, R.A., Kronheim, S.R., and Sleath, P.R. (1989). Activation of interleukin-1 beta by a co-induced protease. FEBS Letters *247*, 386–390.

Blander, J.M. (2008). Phagocytosis and antigen presentation: a partnership initiated by Toll-like receptors. Ann Rheum Dis *67*, iii44–iii49.

Bleicken, S., Landeta, O., Landajuela, A., Basañez, G., and García-Sáez, A.J. (2013). Proapoptotic Bax and Bak Proteins Form Stable Protein-permeable Pores of Tunable Size. Journal of Biological Chemistry *288*, 33241–33252.

Bock, F.J., and Tait, S.W.G. (2019). Mitochondria as multifaceted regulators of cell death. Nat Rev Mol Cell Biol *21*, 85–100.

Bonora, M., Bononi, A., De Marchi, E., Giorgi, C., Lebiedzinska, M., Marchi, S., Patergnani, S., Rimessi, A., Suski, J.M., Wojtala, A., et al. (2014). Role of the c subunit of the F OATP synthase in mitochondrial permeability transition. Cell Cycle *12*, 674–683.

Bordet, T., Berna, P., Abitbol, J.-L., and Pruss, R.M. (2010). Olesoxime (TRO19622): A Novel Mitochondrial-Targeted Neuroprotective Compound. Pharmaceuticals *3*, 345–368.

Boucher, D., Monteleone, M., Coll, R.C., Chen, K.W., Ross, C.M., Teo, J.L., Gomez, G.A., Holley, C.L., Bierschenk, D., Stacey, K.J., et al. (2018). Caspase-1 self-cleavage is an intrinsic mechanism to terminate inflammasome activity. J Exp Med *215*, 827–840.

Boyden, E.D., and Dietrich, W.F. (2006). Nalp1b controls mouse macrophage susceptibility to anthrax lethal toxin. Nat. Genet. *38*, 240–244.

Brammeld, J.S., Petljak, M., Martincorena, I., Williams, S.P., Alonso, L.G., Dalmases, A., Bellosillo, B., Robles-Espinoza, C.D., Price, S., Barthorpe, S., et al. (2017). Genome-wide chemical mutagenesis screens allow unbiased saturation of the cancer genome and identification of drug resistance mutations. Genome Res. *27*, 613–625.

Brennan, M.A., and Cookson, B.T. (2000). Salmonella induces macrophage death by caspase-1-dependent necrosis. Mol Microbiol *38*, 31–40.

Brinkmann, V. (2004). Neutrophil Extracellular Traps Kill Bacteria. Science *303*, 1532–1535.

Briston, T., Lewis, S., Koglin, M., Mistry, K., Shen, Y., Hartopp, N., Katsumata, R., Fukumoto, H., Duchen, M.R., Szabadkai, G., et al. (2016). Identification of ER-000444793, a Cyclophilin D-independent inhibitor of mitochondrial permeability transition, using a high-throughput screen in cryopreserved mitochondria. Sci. Rep. *6*, 1047.

Bronner, D.N., Abuaita, B.H., Chen, X., Fitzgerald, K.A., Núñez, G., He, Y., Yin, X.-M., and O'Riordan, M.X.D. (2015). Endoplasmic Reticulum Stress Activates the Inflammasome via NLRP3- and Caspase-2-Driven Mitochondrial Damage. Immunity *43*, 451–462.

Brown, D.A., Perry, J.B., Allen, M.E., Sabbah, H.N., Stauffer, B.L., Shaikh, S.R., Cleland, J.G.F., Colucci, W.S., Butler, J., Voors, A.A., et al. (2016). Mitochondrial function as a therapeutic target in heart failure. Nat Rev Cardiol *14*, 238–250.

Brown, G.D., and Gordon, S. (2001). A new receptor for β-glucans. Nature *413*, 36–37.

Broz, P., Moltke, von, J., Jones, J.W., Vance, R.E., and Monack, D.M. (2010). Differential Requirement for Caspase-1 Autoproteolysis in Pathogen-Induced Cell Death and Cytokine Processing. Cell Host & Microbe *8*, 471–483.

Cai, X., Chen, J., Xu, H., Liu, S., Jiang, Q.-X., Halfmann, R., and Chen, Z.J. (2014). Prion-like Polymerization Underlies Signal Transduction in Antiviral Immune Defense and Inflammasome Activation. Cell *156*, 1207–1222.

Carpenter, A.E., Jones, T.R., Lamprecht, M.R., Clarke, C., Kang, I.H., Friman, O., Guertin, D.A., Chang, J.H., Lindquist, R.A., Moffat, J., et al. (2006). CellProfiler: image analysis software for identifying and quantifying cell phenotypes. Genome Biol. *7*, R100–R111.

Carraro, M., Giorgio, V., Šileikytė, J., Sartori, G., Forte, M., Lippe, G., Zoratti, M., Szabò, I., and Bernardi, P. (2014). Channel Formation by Yeast F-ATP Synthase and the Role of Dimerization in the Mitochondrial Permeability Transition. Journal of Biological Chemistry *289*, 15980–15985.

Casares, D., Escribá, P.V., and Rosselló, C.A. (2019). Membrane Lipid Composition: Effect on Membrane and Organelle Structure, Function and Compartmentalization and Therapeutic Avenues. Ijms *20*, 2167.

Chae, J.J., Park, Y.H., Park, C., Hwang, I.-Y., Hoffmann, P., Kehrl, J.H., Aksentijevich, I., and Kastner, D.L. (2015). Brief Report: Connecting Two Pathways Through Ca 2+Signaling: NLRP3 Inflammasome Activation Induced by a Hypermorphic PLCG2Mutation. Arthritis & Rheumatology *67*, 563–567.

Chao, D.T., and Korsmeyer, S.J. (1998). BCL-2 FAMILY: Regulators of Cell Death. Annu. Rev. Immunol. *16*, 395–419.

Chauhan, D., Bartok, E., Gaidt, M.M., Bock, F.J., Herrmann, J., Seeger, J.M., Broz, P., Beckmann, R., Kashkar, H., Tait, S.W.G., et al. (2018). BAX/BAK-Induced Apoptosis Results in Caspase-8-Dependent IL-1β Maturation in Macrophages. Cell Reports *25*, 2354–2368.e2355.

Chauvin, C., De Oliveira, F., Ronot, X., Mousseau, M., Leverve, X., and Fontaine, E. (2001). Rotenone Inhibits the Mitochondrial Permeability Transition-induced Cell Death in U937 and KB Cells. Journal of Biological Chemistry *276*, 41394–41398.

Chen, H., Yang, D., Han, F., Tan, J., Zhang, L., Xiao, J., Zhang, Y., and Liu, Q. (2017a). The Bacterial T6SS Effector EvpP Prevents NLRP3 Inflammasome Activation by Inhibiting the Ca 2+ -Dependent MAPK-Jnk Pathway. Cell Host & Microbe *21*, 47–58.

Chen, J.-J., and London, I.M. (1995). Regulation of protein synthesis by heme-regulated eIF-2α kinase. Trends in Biochemical Sciences *20*, 105–108.

Chen, J., and Chen, Z.J. (2018). PtdIns4P on dispersed trans-Golgi network mediates NLRP3 inflammasome activation. Nature *564*, 71–76.

Chen, K.W., Demarco, B., and Broz, P. (2020). Pannexin-1 promotes NLRP3 activation during apoptosis but is dispensable for canonical or noncanonical inflammasome activation. Eur. J. Immunol. *50*, 170–177.

Chen, K.W., Demarco, B., Heilig, R., Shkarina, K., Boettcher, A., Farady, C.J., Pelczar, P., and Broz, P. (2019). Extrinsic and intrinsic apoptosis activate pannexin-1 to drive NLRP3 inflammasome assembly. The EMBO Journal *38*.

Chen, L., Wilson, J.E., Koenigsknecht, M.J., Chou, W.-C., Montgomery, S.A., Truax, A.D., Brickey, W.J., Packey, C.D., Maharshak, N., Matsushima, G.K., et al. (2017b). NLRP12 attenuates colon inflammation by

maintaining colonic microbial diversity and promoting protective commensal bacterial growth. Nat Immunol *123*, 700.

Chen, W.-C. (2014). Rise of [Ca^(2+)]i and Apoptosis Induced by M-3M3FBS in SCM1 Human Gastric Cancer Cells. Chin. J. Physiol. *57*, 31–40.

Cheng, Q.J., Ohta, S., Sheu, K.M., Spreafico, R., Adelaja, A., Taylor, B., and Hoffmann, A. (2020). NFκB dynamics determine the stimulus-specificity of epigenomic reprogramming in macrophages. *7*, 11772.

Chiari, P., Angoulvant, D., Mewton, N., Desebbe, O., Obadia, J.-F., Robin, J., Farhat, F., Jegaden, O., Bastien, O., Lehot, J.-J., et al. (2014). Cyclosporine Protects the Heart during Aortic Valve Surgery. Anesthesiology *121*, 232–238.

Chittenden, T., Flemington, C., Houghton, A.B., Ebb, R.G., Gallo, G.J., Elangovan, B., Chinnadurai, G., and Lutz, R.J. (1995). A conserved domain in Bak, distinct from BH1 and BH2, mediates cell death and protein binding functions. The EMBO Journal *14*, 5589–5596.

Chow, J.C., Young, D.W., Golenbock, D.T., Christ, W.J., and Gusovsky, F. (1999). Toll-like Receptor-4 Mediates Lipopolysaccharide-induced Signal Transduction. Journal of Biological Chemistry *274*, 10689–10692.

Chow, K.T., Gale, M., Jr, and Loo, Y.-M. (2018). RIG-I and Other RNA Sensors in Antiviral Immunity. Annu. Rev. Immunol. *36*, 667–694.

Chui, A.J., Okondo, M.C., Rao, S.D., Gai, K., Griswold, A.R., Johnson, D.C., Ball, D.P., Taabazuing, C.Y., Orth, E.L., Vittimberga, B.A., et al. (2019). N-terminal degradation activates the NLRP1B inflammasome. Science *364*, 82–85.

Civril, F., Deimling, T., de Oliveira Mann, C.C., Ablasser, A., Moldt, M., Witte, G., Hornung, V., and Hopfner, K.-P. (2013). Structural mechanism of cytosolic DNA sensing by cGAS. Nature *498*, 332–337.

Clay, G.M., Valadares, D.G., Graff, J.W., Ulland, T.K., Davis, R.E., Scorza, B.M., Zhanbolat, B.S., Chen, Y., Sutterwala, F.S., and Wilson, M.E. (2017). An Anti-Inflammatory Role for NLRP10 in Murine Cutaneous Leishmaniasis. The Journal of Immunology *199*, 2823–2833.

Cocco, M., Garella, D., Di Stilo, A., Borretto, E., Stevanato, L., Giorgis, M., Marini, E., Fantozzi, R., Miglio, G., and Bertinaria, M. (2014). Electrophilic Warhead-Based Design of Compounds Preventing NLRP3 Inflammasome-Dependent Pyroptosis. J. Med. Chem. *57*, 10366–10382.

Cocco, M., Miglio, G., Giorgis, M., Garella, D., Marini, E., Costale, A., Regazzoni, L., Vistoli, G., Orioli, M., Massulaha-Ahmed, R., et al. (2016). Design, Synthesis, and Evaluation of Acrylamide Derivatives as Direct NLRP3 Inflammasome Inhibitors. ChemMedChem n/a–n/a.

Cocco, M., Pellegrini, C., Martínez-Banaclocha, H., Giorgis, M., Marini, E., Costale, A., Miglio, G., Fornai, M., Antonioli, L., López-Castejón, G., et al. (2017). Development of an Acrylate Derivative Targeting the NLRP3 Inflammasome for the Treatment of Inflammatory Bowel Disease. J. Med. Chem. *60*, 3656–3671.

Coll, R.C., Hill, J.R., Day, C.J., Zamoshnikova, A., Boucher, D., Massey, N.L., Chitty, J.L., Fraser, J.A., Jennings, M.P., Robertson, A.A.B., et al. (2019). MCC950 directly targets the NLRP3 ATP-hydrolysis motif for inflammasome inhibition. Nat Chem Biol *15*, 556–559.

Coll, R.C., Robertson, A.A.B., Chae, J.J., Higgins, S.C., Muñoz-Planillo, R., Inserra, M.C., Vetter, I., Dungan, L.S., Monks, B.G., Stutz, A., et al. (2015). A small-molecule inhibitor of the NLRP3 inflammasome for the treatment of inflammatory diseases. Nat Med.

Compan, V., Baroja-Mazo, A., López-Castejón, G., Gomez, A.I., Martínez, C.M., Angosto, D., Montero, M.T., Herranz, A.S., Bazán, E., Reimers, D., et al. (2012). Cell Volume Regulation Modulates NLRP3 Inflammasome Activation. Immunity *37*, 487–500.

Crabtree, G.R., and Olson, E.N. (2002). NFAT Signaling. Cell *109*, S67–S79.

Crompton, M., Virji, S., and Ward, J.M. (1998). Cyclophilin-D binds strongly to complexes of the voltage-dependent anion channel and the adenine nucleotide translocase to form the permeability transition pore. European Journal of Biochemistry *258*, 729–735.

Cung, T.-T., Morel, O., Cayla, G., Rioufol, G., Garcia-Dorado, D., Angoulvant, D., Bonnefoy-Cudraz, E., Guérin, P., Elbaz, M., Delarche, N., et al. (2015). Cyclosporine before PCI in Patients with Acute Myocardial Infarction. N Engl J Med *373*, 1021–1031.

Dabir, D.V., Hasson, S.A., Setoguchi, K., Johnson, M.E., Wongkongkathep, P., Douglas, C.J., Zimmerman, J., Damoiseaux, R., Teitell, M.A., and Koehler, C.M. (2013). A Small Molecule Inhibitor of Redox-Regulated Protein Translocation into Mitochondria. Developmental Cell *25*, 81–92.

Damm, A., Giebeler, N., Zamek, J., Zigrino, P., and Kufer, T.A. (2016). Epidermal NLRP10 contributes to contact hypersensitivity responses in mice. Eur. J. Immunol.

Dang, E.V., McDonald, J.G., Russell, D.W., and Cyster, J.G. (2017). Oxysterol Restraint of Cholesterol Synthesis Prevents AIM2 Inflammasome Activation. Cell *171*, 1057–1071.e11.

De Marchi, U., Szabò, I., Cereghetti, G.M., Hoxha, P., Craigen, W.J., and Zoratti, M. (2008). A maxi-chloride channel in the inner membrane of mammalian mitochondria. Biochimica Et Biophysica Acta (BBA) - Bioenergetics *1777*, 1438–1448.

del Rey, A., Renigunta, V., Dalpke, A.H., Leipziger, J., Matos, J.E., Robaye, B., Zuzarte, M., Kavelaars, A., and Hanley, P.J. (2006). Knock-out Mice Reveal the Contributions of P2Y and P2X Receptors to Nucleotide-induced Ca 2+Signaling in Macrophages. Journal of Biological Chemistry *281*, 35147–35155.

Deng, M., Guo, H., Tam, J.W., Johnson, B.M., Brickey, W.J., New, J.S., Lenox, A., Shi, H., Golenbock, D.T., Koller, B.H., et al. (2019). Platelet-activating factor (PAF) mediates NLRP3-NEK7 inflammasome induction independently of PAFR. J Exp Med *216*, 2838–2853.

Deo, P., Chow, S.H., Han, M.-L., Speir, M., Huang, C., Schittenhelm, R.B., Dhital, S., Emery, J., Li, J., Kile, B.T., et al. (2020). Mitochondrial dysfunction caused by outer membrane vesicles from Gram-negative bacteria activates intrinsic apoptosis and inflammation. Nat Microbiol *15*, 375.

Deretic, V., Saitoh, T., and Akira, S. (2013). Autophagy in infection, inflammation and immunity. Nat Rev Immunol *13*, 722–737.

Dethlefsen, L., McFall-Ngai, M., and Relman, D.A. (2007). An ecological and evolutionary perspective on human–microbe mutualism and disease. Nature *449*, 811–818.

Dever, T.E., Chen, J.J., Barber, G.N., Cigan, A.M., Feng, L., Donahue, T.F., London, I.M., Katze, M.G., and Hinnebusch, A.G. (1993). Mammalian eukaryotic initiation factor 2 alpha kinases functionally substitute for GCN2 protein kinase in the GCN4 translational control mechanism of yeast. Proc Natl Acad Sci USA *90*, 4616–4620.

Dever, T.E., Feng, L., Wek, R.C., Cigan, A.M., Donahue, T.F., and Hinnebusch, A.G. (1992). Phosphorylation of initiation factor 2α by protein kinase GCN2 mediates gene-specific translational control of GCN4 in yeast. Cell *68*, 585–596.

Deveraux, Q.L. (1998). IAPs block apoptotic events induced by caspase-8 and cytochrome c by direct inhibition of distinct caspases. The EMBO Journal *17*, 2215–2223.

Di Micco, A., Frera, G., Lugrin, J., Jamilloux, Y., Hsu, E.-T., Tardivel, A., De Gassart, A., Zaffalon, L., Bujisic, B., Siegert, S., et al. (2016). AIM2 inflammasome is activated by pharmacological disruption of nuclear envelope integrity. Proc Natl Acad Sci USA *113*, E4671–E4680.

Dinarello, C.A. (2009). Interleukin-1β and the Autoinflammatory Diseases. N Engl J Med *360*, 2467–2470.

Dinarello, C.A. (2017). Overview of the IL-1 family in innate inflammation and acquired immunity. Immunol Rev *281*, 8–27.

Dinarello, C.A., Simon, A., and van der Meer, J.W.M. (2012). Treating inflammation by blocking interleukin-1 in a broad spectrum of diseases. Nat Rev Drug Discov *11*, 633–652.

Diogo, C.V., Yambire, K.F., Fernández Mosquera, L., Branco F, T., and Raimundo, N. (2018). Mitochondrial adventures at the organelle society. Biochemical and Biophysical Research Communications *500*, 87–93.

DiPeso, L., Ji, D.X., Vance, R.E., and Price, J.V. (2017). Cell death and cell lysis are separable events during pyroptosis. Cell Death Discovery *3*, 99.

Domingo-Fernández, R., Coll, R.C., Kearney, J., Breit, S., and O'Neill, L.A.J. (2017). The intracellular chloride channel proteins CLIC1 and CLIC4 induce IL-1β transcription and activate the NLRP3 inflammasome. Journal of Biological Chemistry *292*, 12077–12087.

Dorward, D.A., Lucas, C.D., Chapman, G.B., Haslett, C., Dhaliwal, K., and Rossi, A.G. (2015). The Role of Formylated Peptides and Formyl Peptide Receptor 1 in Governing Neutrophil Function during Acute Inflammation. The American Journal of Pathology *185*, 1172–1184.

Duewell, P., Kono, H., Rayner, K.J., Sirois, C.M., Vladimer, G., Bauernfeind, F.G., Abela, G.S., Franchi, L., Núñez, G., Schnurr, M., et al. (2010). NLRP3 inflammasomes are required for atherogenesis and activated by cholesterol crystals. Nature *464*, 1357–1361.

Duéñez-Guzmán, E.A., and Haig, D. (2014). The Evolution of Reproduction-Related NLRP Genes. J Mol Evol *78*, 194–201.

Duncan, J.A., Bergstralh, D.T., Wang, Y., Willingham, S.B., Ye, Z., Zimmermann, A.G., and Ting, J.P.Y. (2007). Cryopyrin/NALP3 binds ATP/dATP, is an ATPase, and requires ATP binding to mediate inflammatory signaling. Proc Natl Acad Sci USA *104*, 8041–8046.

Dupré-Crochet, S., Erard, M., and Nüβe, O. (2013). ROS production in phagocytes: why, when, and where? Journal of Leukocyte Biology *94*, 657–670.

Dwyer, L., Kim, H.J., Koh, B.H., and Koh, S.D. (2010). Phospholipase C-independent effects of 3M3FBS in murine colon. European Journal of Pharmacology *628*, 187–194.

Elinav, E., Strowig, T., Kau, A.L., Henao-Mejia, J., Thaiss, C.A., Booth, C.J., Peaper, D.R., Bertin, J., Eisenbarth, S.C., Gordon, J.I., et al. (2011). NLRP6 Inflammasome Regulates Colonic Microbial Ecology and Risk for Colitis. Cell *145*, 745–757.

Elliott, E.I., Miller, A.N., Banoth, B., Iyer, S.S., Stotland, A., Weiss, J.P., Gottlieb, R.A., Sutterwala, F.S., and Cassel, S.L. (2018). Cutting Edge: Mitochondrial Assembly of the NLRP3 Inflammasome Complex Is Initiated at Priming. The Journal of Immunology *200*, 3047–3052.

Elliott, J.M., Rouge, L., Wiesmann, C., and Scheer, J.M. (2009a). Crystal Structure of Procaspase-1 Zymogen Domain Reveals Insight into Inflammatory Caspase Autoactivation. Journal of Biological Chemistry *284*, 6546–6553.

Elliott, M.R., Chekeni, F.B., Trampont, P.C., Lazarowski, E.R., Kadl, A., Walk, S.F., Park, D., Woodson, R.I., Ostankovich, M., Sharma, P., et al. (2009b). Nucleotides released by apoptotic cells act as a find-me signal to promote phagocytic clearance. Nature *461*, 282–286.

Emmel, E., Verweij, C., Durand, D., Higgins, K., Lacy, E., and Crabtree, G. (1989). Cyclosporin A specifically inhibits function of nuclear proteins involved in T cell activation. Science *246*, 1617–1620.

Fang, Y.-C., Kuo, D.-H., Shieh, P., Chen, F.-A., Kuo, C.-C., and Jan, C.-R. (2009). Effect of m-3M3FBS on Ca2+ movement in Madin-Darby canine renal tubular cells. Hum Exp Toxicol *28*, 655–663.

Fernandes-Alnemri, T., Yu, J.-W., Datta, P., Wu, J., and Alnemri, E.S. (2009). AIM2 activates the inflammasome and cell death in response to cytoplasmic DNA. Nature *458*, 509–513.

Fessler, E., Eckl, E.-M., Schmitt, S., Mancilla, I.A., Meyer-Bender, M.F., Hanf, M., Philippou-Massier, J., Krebs, S., Zischka, H., and Jae, L.T. (2020). A pathway coordinated by DELE1 relays mitochondrial stress to the cytosol. Nature *579*, 433–437.

Flanagan, W.M., Corthésy, B., Bram, R.J., and Crabtree, G.R. (1991). Nuclear association of a T-cell transcription factor blocked by FK-506 and cyclosporin A. Nature *352*, 803–807.

Franchi, L., and Núñez, G. (2008). The Nlrp3 inflammasome is critical for aluminium hydroxide-mediated IL-1β secretion but dispensable for adjuvant activity. Eur. J. Immunol. *38*, 2085–2089.

Franken, H., Mathieson, T., Childs, D., Sweetman, G.M.A., Werner, T., Tögel, I., Doce, C., Gade, S., Bantscheff, M., Drewes, G., et al. (2015). Thermal proteome profiling for unbiased identification of direct and indirect drug targets using multiplexed quantitative mass spectrometry. Nat Protoc *10*, 1567–1593.

Franklin, B.S., Bossaller, L., De Nardo, D., Ratter, J.M., Stutz, A., Engels, G., Brenker, C., Nordhoff, M., Mirandola, S.R., Al-Amoudi, A., et al. (2014). The adaptor ASC has extracellular and "prionoid" activities that propagate inflammation. Nat Immunol *15*, 727–737.

Freeman, L., Guo, H., David, C.N., Brickey, W.J., Jha, S., and Ting, J.P.-Y. (2017). NLR members NLRC4 and NLRP3 mediate sterile inflammasome activation in microglia and astrocytes. J Exp Med *214*, 1351–1370.

Fulda, S. (2015). Promises and Challenges of Smac Mimetics as Cancer Therapeutics. Clinical Cancer Research *21*, 5030–5036.

Gaidt, M.M., Ebert, T.S., Chauhan, D., Ramshorn, K., Pinci, F., Zuber, S., O'Duill, F., Schmid-Burgk, J.L., Hoss, F., Buhmann, R., et al. (2017). The DNA Inflammasome in Human Myeloid Cells Is Initiated by a STING-Cell Death Program Upstream of NLRP3. Cell *171*, 1110–1124.e1118.

Gaidt, M.M., Ebert, T.S., Chauhan, D., Schmidt, T., Schmid-Burgk, J.L., Rapino, F., Robertson, A.A.B., Cooper, M.A., Graf, T., and Hornung, V. (2016). Human Monocytes Engage an Alternative Inflammasome Pathway. Immunity.

Gaidt, M.M., Rapino, F., Graf, T., and Hornung, V. (2018). Modeling Primary Human Monocytes with the Trans-Differentiation Cell Line BLaER1. Methods Mol. Biol. *1714*, 57–66.

Gao, W., Yang, J., Liu, W., Wang, Y., and Shao, F. (2016). Site-specific phosphorylation and microtubule dynamics control Pyrin inflammasome activation. Proc Natl Acad Sci USA *113*, E4857–E4866.

García, M.A., Meurs, E.F., and Esteban, M. (2007). The dsRNA protein kinase PKR: Virus and cell control. Biochimie *89*, 799–811.

Garlanda, C., Dinarello, C.A., and Mantovani, A. (2013). The Interleukin-1 Family: Back to the Future. Immunity *39*, 1003–1018.

Gavathiotis, E., Reyna, D.E., Bellairs, J.A., Leshchiner, E.S., and Walensky, L.D. (2012). Direct and selective small-molecule activation of proapoptotic BAX. Nat Chem Biol *8*, 639–645.

Gelles, J.D., and Chipuk, J.E. (2016). Robust high-throughput kinetic analysis of apoptosis with real-time high-content live-cell imaging. Cell Death Dis *7*, e2493–e2493.

Germic, N., Frangez, Z., Yousefi, S., and Simon, H.-U. (2019). Regulation of the innate immune system by autophagy: monocytes, macrophages, dendritic cells and antigen presentation. Cell Death Differ *26*, 715–727.

Gewirtz, A.T., Navas, T.A., Lyons, S., Godowski, P.J., and Madara, J.L. (2001). Cutting Edge: Bacterial Flagellin Activates Basolaterally Expressed TLR5 to Induce Epithelial Proinflammatory Gene Expression. The Journal of Immunology *167*, 1882–1885.

Ghaffari, S., Kazemi, B., Toluey, M., and Sepehrvand, N. (2013). The Effect of Prethrombolytic Cyclosporine-A Injection on Clinical Outcome of Acute Anterior ST-Elevation Myocardial Infarction. Cardiovasc Ther *31*, e34–e39.

Ghayur, T., Banerjee, S., Hugunin, M., Butler, D., Herzog, L., Carter, A., Quintal, L., Sekut, L., Talanian, R., Paskind, M., et al. (1997). Caspase-1 processes IFN-γ-inducing factor and regulates LPS-induced IFN- γ production. Nature *386*, 619–623.

Giorgio, V., Stockum, von, S., Antoniel, M., Fabbro, A., Fogolari, F., Forte, M., Glick, G.D., Petronilli, V., Zoratti, M., Szabo, I., et al. (2013). Dimers of mitochondrial ATP synthase form the permeability transition pore. Proc Natl Acad Sci USA *110*, 5887–5892.

Girardin, S.E., Boneca, I.G., Viala, J., Chamaillard, M., Labigne, A., Thomas, G., Philpott, D.J., and Sansonetti, P.J. (2003a). Nod2 Is a General Sensor of Peptidoglycan through Muramyl Dipeptide (MDP) Detection. Journal of Biological Chemistry *278*, 8869–8872.

Girardin, S.E., Travassos, L.H., Hervé, M., Blanot, D., Boneca, I.G., Philpott, D.J., Sansonetti, P.J., and Mengin-Lecreulx, D. (2003b). Peptidoglycan Molecular Requirements Allowing Detection by Nod1 and Nod2. Journal of Biological Chemistry *278*, 41702–41708.

Goldstein, J.C., Waterhouse, N.J., Juin, P., Evan, G.I., and Green, D.R. (2000). The coordinate release of cytochrome c during apoptosis is rapid, complete and kinetically invariant. Nat Cell Biol *2*, 156–162.

Gomes, L.C., and Dikic, I. (2014). Autophagy in Antimicrobial Immunity. Molecular Cell *54*, 224–233.

Gong, T., Liu, L., Jiang, W., and Zhou, R. (2019). DAMP-sensing receptors in sterile inflammation and inflammatory diseases. Nat Rev Immunol *20*, 95–112.

Gordan, R., Fefelova, N., Gwathmey, J.K., and Xie, L.-H. (2016). Involvement of mitochondrial permeability transition pore (mPTP) in cardiac arrhythmias: Evidence from cyclophilin D knockout mice. Cell Calcium *60*, 363–372.

Gordon, S. (2016). Phagocytosis: An Immunobiologic Process. Immunity *44*, 463–475.

Goujon, M., McWilliam, H., Li, W., Valentin, F., Squizzato, S., Paern, J., and Lopez, R. (2010). A new bioinformatics analysis tools framework at EMBL-EBI. Nucleic Acids Research *38*, W695–W699.

Green, J.P., Yu, S., Martín-Sánchez, F., Pelegrín, P., López-Castejón, G., Lawrence, C.B., and Brough, D. (2018). Chloride regulates dynamic NLRP3-dependent ASC oligomerization and inflammasome priming. Proc Natl Acad Sci USA *115*, E9371–E9380.

Griffith, J.W., Sokol, C.L., and Luster, A.D. (2014). Chemokines and Chemokine Receptors: Positioning Cells for Host Defense and Immunity. Annu. Rev. Immunol. *32*, 659–702.

Gritsenko, A., Yu, S., Martín-Sánchez, F., del Olmo, I.D., Nichols, E.-M., Davis, D.M., Brough, D., and López-Castejón, G. Priming is dispensable for NLRP3 inflammasome activation in human monocytes. *56*, 542.

Gross, A., Yin, X.-M., Wang, K., Wei, M.C., Jockel, J., Milliman, C., Erdjument-Bromage, H., Tempst, P., and Korsmeyer, S.J. (1999). Caspase Cleaved BID Targets Mitochondria and Is Required for Cytochrome cRelease, while BCL-X LPrevents This Release but Not Tumor Necrosis Factor-R1/Fas Death. Journal of Biological Chemistry *274*, 1156–1163.

Groß, C.J., Mishra, R., Schneider, K.S., Médard, G., Wettmarshausen, J., Dittlein, D.C., Shi, H., Gorka, O., Koenig, P.-A., Fromm, S., et al. (2016). K+ Efflux-Independent NLRP3 Inflammasome Activation by Small Molecules Targeting Mitochondria. Immunity *45*, 761–773.

Guo, C., Chi, Z., Jiang, D., Xu, T., Yu, W., Wang, Z., Chen, S., Zhang, L., Liu, Q., Guo, X., et al. (2018). Cholesterol Homeostatic Regulator SCAP-SREBP2 Integrates NLRP3 Inflammasome Activation and Cholesterol Biosynthetic Signaling in Macrophages. Immunity *49*, 842–856.e847.

Guo, C., Xie, S., Chi, Z., Zhang, J., Liu, Y., Zhang, L., Zheng, M., Zhang, X., Xia, D., Ke, Y., et al. (2016). Bile Acids Control Inflammation and Metabolic Disorder through Inhibition of NLRP3 Inflammasome. Immunity *45*, 944.

Guo, X., Aviles, G., Liu, Y., Tian, R., Unger, B.A., Lin, Y.-H.T., Wiita, A.P., Xu, K., Correia, M.A., and Kampmann, M. (2020). Mitochondrial stress is relayed to the cytosol by an OMA1–DELE1–HRI pathway. Nature *579*, 427–432.

Gutiérrez-Aguilar, M., and Baines, C.P. (2015). Structural mechanisms of cyclophilin D-dependent control of the mitochondrial permeability transition pore. Biochimica Et Biophysica Acta (BBA) - General Subjects *1850*, 2041–2047.

Gutiérrez-López, T.Y., Orduña-Castillo, L.B., Hernández-Vásquez, M.N., Vázquez-Prado, J., and Reyes-Cruz, G. (2018). Calcium sensing receptor activates the NLRP3 inflammasome via a chaperone-assisted degradative pathway involving Hsp70 and LC3-II. Biochemical and Biophysical Research Communications *505*, 1121–1127.

Ha, H.J., Kim, D.S., and Hahn, Y. (2009). A 2.7-kb Deletion in the Human NLRP10 Gene Exon 2 Occurred After the Human–Chimpanzee Divergence. Biochem Genet *47*, 665–670.

Hafner-Bratkovič, I., Sušjan, P., Lainšček, D., Tapia-Abellán, A., Cerović, K., Kadunc, L., Angosto-Bazarra, D., Pelegrín, P., and Jerala, R. (2018). NLRP3 lacking the leucine-rich repeat domain can be fully activated via the canonical inflammasome pathway. Nat Comms *9*, 666.

Halestrap, A. (2004). Mitochondrial permeability transition pore opening during myocardial reperfusion—a target for cardioprotection. Cardiovasc Res *61*, 372–385.

Halestrap, A.P., Connern, C.P., Griffiths, E.J., and Kerr, P.M. (1997). Cyclosporin A binding to mitochondrial cyclophilin inhibits the permeability transition pore and protects hearts from ischaemia/reperfusion injury. In Detection of Mitochondrial Diseases, (Boston, MA: Springer US), pp. 167–172.

Halestrap, A.P. (2009). What is the mitochondrial permeability transition pore? Journal of Molecular and Cellular Cardiology *46*, 821–831.

Halestrap, A.P., and Brenner, C. (2003a). The adenine nucleotide translocase: a central component of the mitochondrial permeability transition pore and key player in cell death. Curr. Med. Chem. *10*, 1507–1525.

Halestrap, A.P., and Brenner, C. (2003b). The adenine nucleotide translocase: a central component of the mitochondrial permeability transition pore and key player in cell death. Curr. Med. Chem. *10*, 1507–1525.

Halle, A., Hornung, V., Petzold, G.C., Stewart, C.R., Monks, B.G., Reinheckel, T., Fitzgerald, K.A., Latz, E., Moore, K.J., and Golenbock, D.T. (2008). The NALP3 inflammasome is involved in the innate immune response to amyloid-β. Nat Immunol *9*, 857–865.

Handschumacher, R., Harding, M., Rice, J., Drugge, R., and Speicher, D. (1984). Cyclophilin: a specific cytosolic binding protein for cyclosporin A. Science *226*, 544–547.

Hao, H., Cao, L., Jiang, C., Che, Y., Zhang, S., Takahashi, S., Wang, G., and Gonzalez, F.J. (2017). Farnesoid X Receptor Regulation of the NLRP3 Inflammasome Underlies Cholestasis-Associated Sepsis. Cell Metabolism *25*, 856–867.e5.

Hao, J.-J., Liu, Y., Kruhlak, M., Debell, K.E., Rellahan, B.L., and Shaw, S. (2009). Phospholipase C–mediated hydrolysis of PIP2 releases ERM proteins from lymphocyte membrane. J Cell Biol *184*, 451–462.

Hara, H., Seregin, S.S., Yang, D., Fukase, K., Chamaillard, M., Alnemri, E.S., Inohara, N., Chen, G.Y., and Núñez, G. (2018). The NLRP6 Inflammasome Recognizes Lipoteichoic Acid and Regulates Gram-Positive Pathogen Infection. Cell *175*, 1651–1664.e14.

Harding, H.P., Zhang, Y., and Ron, D. (1999). Protein translation and folding are coupled by an endoplasmic-reticulum-resident kinase. Nature *397*, 271–274.

Hashiguchi, K., and Zhang-Akiyama, Q.-M. (2009). Establishment of Human Cell Lines Lacking Mitochondrial DNA. In Mitochondrial DNA, (Totowa, NJ: Humana Press), pp. 383–391.

Hausenloy, D.J., Kunst, G., Boston-Griffiths, E., Kolvekar, S., Chaubey, S., John, L., Desai, J., and Yellon, D.M. (2014). The effect of cyclosporin-A on peri-operative myocardial injury in adult patients undergoing coronary artery bypass graft surgery: a randomised controlled clinical trial. Heart *100*, 544–549.

Hayashi, F., Smith, K.D., Ozinsky, A., Hawn, T.R., Yi, E.C., Goodlett, D.R., Eng, J.K., Akira, S., Underhill, D.M., and Aderem, A. (2001). The innate immune response to bacterial flagellin is mediated by Toll-like receptor 5. Nature *410*, 1099–1103.

He, W.-T., Wan, H., Hu, L., Chen, P., Wang, X., Huang, Z., Yang, Z.-H., Zhong, C.-Q., and Han, J. (2015). Gasdermin D is an executor of pyroptosis and required for interleukin-1β secretion. Cell Res *25*, 1285–1298.

He, Y., Varadarajan, S., Muñoz-Planillo, R., Burberry, A., Nakamura, Y., and Núñez, G. (2014). 3,4-Methylenedioxy-β-nitrostyrene Inhibits NLRP3 Inflammasome Activation by Blocking Assembly of the Inflammasome. Journal of Biological Chemistry *289*, 1142–1150.

He, Y., Zeng, M.Y., Yang, D., Motro, B., and Núñez, G. (2016). NEK7 is an essential mediator of NLRP3 activation downstream of potassium efflux. Nature *530*, 354–357.

Heilig, R., Dick, M.S., Sborgi, L., Meunier, E., Hiller, S., and Broz, P. (2018a). The Gasdermin-D pore acts as a conduit for IL-1β secretion in mice. Eur. J. Immunol. *48*, 584–592.

Heilig, R., Dick, M.S., Sborgi, L., Meunier, E., Hiller, S., and Broz, P. (2018b). The Gasdermin-D pore acts as a conduit for IL-1β secretion in mice. Eur. J. Immunol. *48*, 584–592.

Hellmich, K.A., Levinsohn, J.L., Fattah, R., Newman, Z.L., Maier, N., Sastalla, I., Liu, S., Leppla, S.H., and Moayeri, M. (2012). Anthrax Lethal Factor Cleaves Mouse Nlrp1b in Both Toxin-Sensitive and Toxin-Resistant Macrophages. PLoS ONE *7*, e49741.

Hemmi, H., Takeuchi, O., Kawai, T., Kaisho, T., Sato, S., Sanjo, H., Matsumoto, M., Hoshino, K., Wagner, H., Takeda, K., et al. (2000). A Toll-like receptor recognizes bacterial DNA. Nature *408*, 740–745.

Heneka, M.T., Kummer, M.P., Stutz, A., Delekate, A., Schwartz, S., Vieira-Saecker, A., Griep, A., Axt, D., Remus, A., Tzeng, T.-C., et al. (2012). NLRP3 is activated in Alzheimer's disease and contributes to pathology in APP/PS1 mice. Nature *493*, 674–678.

Hirota, T., Takahashi, A., Kubo, M., Tsunoda, T., Tomita, K., Sakashita, M., Yamada, T., Fujieda, S., Tanaka, S., Doi, S., et al. (2012). Genome-wide association study identifies eight new susceptibility loci for atopic dermatitis in the Japanese population. Nat. Genet. *44*, 1222–1226.

Hise, A.G., Tomalka, J., Ganesan, S., Patel, K., Hall, B.A., Brown, G.D., and Fitzgerald, K.A. (2009). An Essential Role for the NLRP3 Inflammasome in Host Defense against the Human Fungal Pathogen Candida albicans. Cell Host & Microbe *5*, 487–497.

Hoffman, H.M., Mueller, J.L., Broide, D.H., Wanderer, A.A., and Kolodner, R.D. (2001). Mutation of a new gene encoding a putative pyrin-like protein causes familial cold autoinflammatory syndrome and Muckle–Wells syndrome. Nat. Genet. *29*, 301–305.

Holley, C.L., and Schroder, K. (2020). The rOX-stars of inflammation: links between the inflammasome and mitochondrial meltdown. Clin Trans Immunol *9*, 133.

Holt, P.G., Strickland, D.H., Wikström, M.E., and Jahnsen, F.L. (2008). Regulation of immunological homeostasis in the respiratory tract. Nat Rev Immunol *8*, 142–152.

Hooftman, A., Angiari, S., Hester, S., Corcoran, S.E., Runtsch, M.C., Ling, C., Ruzek, M.C., Slivka, P.F., McGettrick, A.F., Banahan, K., et al. (2020). The Immunomodulatory Metabolite Itaconate Modifies NLRP3 and Inhibits Inflammasome Activation. Cell Metabolism *32*, 468–478.e7.

Horng, T. (2014). Calcium signaling and mitochondrial destabilization in the triggering of the NLRP3 inflammasome. Trends in Immunology *35*, 253–261.

Hornung, V., Ablasser, A., Charrel-Dennis, M., Bauernfeind, F., Horvath, G., Caffrey, D.R., Latz, E., and Fitzgerald, K.A. (2009). AIM2 recognizes cytosolic dsDNA and forms a caspase-1-activating inflammasome with ASC. Nature *458*, 514–518.

Hornung, V., Bauernfeind, F., Halle, A., Samstad, E.O., Kono, H., Rock, K.L., Fitzgerald, K.A., and Latz, E. (2008). Silica crystals and aluminum salts activate the NALP3 inflammasome through phagosomal destabilization. Nat Immunol *9*, 847–856.

Horowitz, L.F., Hirdes, W., Suh, B.-C., Hilgemann, D.W., Mackie, K., and Hille, B. (2005). Phospholipase C in Living Cells. The Journal of General Physiology *126*, 243–262.

Hsu, S.Y., Kaipia, A., McGee, E., Lomeli, M., and Hsueh, A.J.W. (1997). Bok is a pro-apoptotic Bcl-2 protein with restricted expression in reproductive tissues and heterodimerizes with selective anti-apoptotic Bcl-2 family members. Proc Natl Acad Sci USA *94*, 12401–12406.

Hu, J.J., Liu, X., Xia, S., Zhang, Z., Zhang, Y., Zhao, J., Ruan, J., Luo, X., Lou, X., Bai, Y., et al. (2020). FDA-approved disulfiram inhibits pyroptosis by blocking gasdermin D pore formation. Nat Immunol *21*, 736–745.

Huang, L.S., Hong, Z., Wu, W., Xiong, S., Zhong, M., Gao, X., Rehman, J., and Malik, A.B. (2020). mtDNA Activates cGAS Signaling and Suppresses the YAP-Mediated Endothelial Cell Proliferation Program to Promote Inflammatory Injury. Immunity *52*, 475–486.e475.

Humphries, F., Shmuel-Galia, L., Ketelut-Carneiro, N., Li, S., Wang, B., Nemmara, V.V., Wilson, R., Jiang, Z., Khalighinejad, F., Muneeruddin, K., et al. (2020). Succination inactivates gasdermin D and blocks pyroptosis. Science eabb9818.

Imamura, R., Wang, Y., Kinoshita, T., Suzuki, M., Noda, T., Sagara, J., Taniguchi, S., Okamoto, H., and Suda, T. (2010). Anti-Inflammatory Activity of PYNOD and Its Mechanism in Humans and Mice. The Journal of Immunology *184*, 5874–5884.

Inohara, N., Ogura, Y., Fontalba, A., Gutierrez, O., Pons, F., Crespo, J., Fukase, K., Inamura, S., Kusumoto, S., Hashimoto, M., et al. (2003). Host Recognition of Bacterial Muramyl Dipeptide Mediated through NOD2. Journal of Biological Chemistry *278*, 5509–5512.

Irmscher, S., Brix, S.R., Zipfel, S.L.H., Halder, L.D., Mutlutürk, S., Wulf, S., Girdauskas, E., Reichenspurner, H., Stahl, R.A.K., Jungnickel, B., et al. (2019). Serum FHR1 binding to necrotic-type cells activates monocytic inflammasome and marks necrotic sites in vasculopathies. Nat Comms *10*, 599.

Isaacs, A., and Lindenmann, J. (1957). Virus interference. I. The interferon. Proc. R. Soc. Lond., B, Biol. Sci. *147*, 258–267.

Isaacs, A., Lindenmann, J., and Valentine, R.C. (1957). Virus interference. II. Some properties of interferon. Proc. R. Soc. Lond., B, Biol. Sci. *147*, 268–273.

Ito, M., Tanaka, T., Inagaki, M., Nakanishi, K., and Hidaka, H. (1986). N-(6-phenylhexyl)-5-chloro-1-naphthalenesulfonamide, a novel activator of protein kinase C. Biochemistry *25*, 4179–4184.

Ivashkiv, L.B., and Donlin, L.T. (2013). Regulation of type I interferon responses. Nat Rev Immunol *14*, 36–49.

Iyer, S.S., He, Q., Janczy, J.R., Elliott, E.I., Zhong, Z., Olivier, A.K., Sadler, J.J., Knepper-Adrian, V., Han, R., Qiao, L., et al. (2013). Mitochondrial Cardiolipin Is Required for Nlrp3 Inflammasome Activation. Immunity *39*, 311–323.

Izzo, V., Bravo-San Pedro, J.M., Sica, V., Kroemer, G., and Galluzzi, L. (2016). Mitochondrial Permeability Transition: New Findings and Persisting Uncertainties. Trends in Cell Biology *26*, 655–667.

Jabir, M.S., Hopkins, L., Ritchie, N.D., Ullah, I., Bayes, H.K., Li, D., Tourlomousis, P., Lupton, A., Puleston, D., Simon, A.K., et al. (2014). Mitochondrial damage contributes to Pseudomonas aeruginosaactivation of the inflammasome and is downregulated by autophagy. Autophagy *11*, 166–182.

Jack, R., and Pasquier, Du, L. (2019). Evolutionary Concepts in Immunology (Cham: Springer International Publishing).

Jakubzick, C.V., Randolph, G.J., and Henson, P.M. (2017). Monocyte differentiation and antigen-presenting functions. Nat Rev Immunol *17*, 349–362.

Janeway, C.A. (1989). Approaching the Asymptote? Evolution and Revolution in Immunology. Cold Spring Harbor Symposia on Quantitative Biology *54*, 1–13.

Jayasinghe, M., Wang, Q., Schirmer, A., and Stan, G. (2016). Investigation of Inhibitory Potency of BHQ Derivatives as SERCA Inhibitors to use as Potential Drugs as well as Tools to Study the SERCA Function: Binding Free Energy Computation using FEP/MD Simulations. Biophysical Journal *110*, 540a–541a.

Jin, T., Curry, J., Smith, P., Jiang, J., and Xiao, T.S. (2013). Structure of the NLRP1 caspase recruitment domain suggests potential mechanisms for its association with procaspase-1. Proteins *81*, 1266–1270.

Jin, T., Perry, A., Jiang, J., Smith, P., Curry, J.A., Unterholzner, L., Jiang, Z., Horvath, G., Rathinam, V.A., Johnstone, R.W., et al. (2012). Structures of the HIN Domain:DNA Complexes Reveal Ligand Binding and Activation Mechanisms of the AIM2 Inflammasome and IFI16 Receptor. Immunity *36*, 561–571.

Joly, S., Eisenbarth, S.C., Olivier, A.K., Williams, A., Kaplan, D.H., Cassel, S.L., Flavell, R.A., and Sutterwala, F.S. (2012). Cutting Edge: Nlrp10 Is Essential for Protective Antifungal Adaptive Immunity against Candida albicans. The Journal of Immunology *189*, 4713–4717.

Jorgensen, I., Zhang, Y., Krantz, B.A., and Miao, E.A. (2016). Pyroptosis triggers pore-induced intracellular traps (PITs) that capture bacteria and lead to their clearance by efferocytosis. J Exp Med jem.20151613.

Juliana, C., Fernandes-Alnemri, T., Wu, J., Datta, P., Solorzano, L., Yu, J.W., Meng, R., Quong, A.A., Latz, E., Scott, C.P., et al. (2010). Anti-inflammatory Compounds Parthenolide and Bay 11-7082 Are Direct Inhibitors of the Inflammasome. Journal of Biological Chemistry *285*, 9792–9802.

Juliana, C., Fernandes-Alnemri, T., Kang, S., Farias, A., Qin, F., and Alnemri, E.S. (2012). Non-transcriptional Priming and Deubiquitination Regulate NLRP3 Inflammasome Activation. Journal of Biological Chemistry *287*, 36617–36622.

Kadamur, G., and Ross, E.M. (2013). Mammalian Phospholipase C. Annu. Rev. Physiol. *75*, 127–154.

Kale, J., Osterlund, E.J., and Andrews, D.W. (2017). BCL-2 family proteins: changing partners in the dance towards death. Cell Death Differ *25*, 65–80.

Kamentsky, L., Jones, T.R., Fraser, A., Bray, M.-A., Logan, D.J., Madden, K.L., Ljosa, V., Rueden, C., Eliceiri, K.W., and Carpenter, A.E. (2011). Improved structure, function and compatibility for CellProfiler: modular high-throughput image analysis software. Bioinformatics *27*, 1179–1180.

Kang, B.H., Siegelin, M.D., Plescia, J., Raskett, C.M., Garlick, D.S., Dohi, T., Lian, J.B., Stein, G.S., Languino, L.R., and Altieri, D.C. (2010). Preclinical Characterization of Mitochondria-Targeted Small Molecule Hsp90 Inhibitors, Gamitrinibs, in Advanced Prostate Cancer. Clinical Cancer Research *16*, 4779–4788.

Kang, B.H., Tavecchio, M., Goel, H.L., Hsieh, C.-C., Garlick, D.S., Raskett, C.M., Lian, J.B., Stein, G.S., Languino, L.R., and Altieri, D.C. (2011). Targeted inhibition of mitochondrial Hsp90 suppresses localised and metastatic prostate cancer growth in a genetic mouse model of disease. Br J Cancer *104*, 629–634.

Kang, B.H., Plescia, J., Song, H.Y., Meli, M., Colombo, G., Beebe, K., Scroggins, B., Neckers, L., and Altieri, D.C. (2009). Combinatorial drug design targeting multiple cancer signaling networks controlled by mitochondrial Hsp90. J. Clin. Invest. *119*, 454–464.

Kanvah, S., Joseph, J., Schuster, G.B., Barnett, R.N., Cleveland, C.L., and Landman, U. (2010). Oxidation of DNA: Damage to Nucleobases. Acc. Chem. Res. *43*, 280–287.

Karch, J., Bround, M.J., Khalil, H., Sargent, M.A., Latchman, N., Terada, N., Peixoto, P.M., and Molkentin, J.D. (2019). Inhibition of mitochondrial permeability transition by deletion of the ANT family and CypD. Sci. Adv. *5*, eaaw4597.

Karpel-Massler, G., Ishida, C.T., Bianchetti, E., Shu, C., Perez-Lorenzo, R., Horst, B., Banu, M., Roth, K.A., Bruce, J.N., Canoll, P., et al. (2017). Inhibition of Mitochondrial Matrix Chaperones and Antiapoptotic Bcl-2 Family Proteins Empower Antitumor Therapeutic Responses. Cancer Research *77*, 3513–3526.

Katsnelson, M.A., Lozada-Soto, K.M., Russo, H.M., Miller, B.A., and Dubyak, G.R. (2016). NLRP3 inflammasome signaling is activated by low-level lysosome disruption but inhibited by extensive lysosome disruption: roles for K +efflux and Ca 2+influx. AJP: Cell Physiology *311*, C83–C100.

Katsnelson, M.A., Rucker, L.G., Russo, H.M., and Dubyak, G.R. (2015). K+ Efflux Agonists Induce NLRP3 Inflammasome Activation Independently of Ca2+ Signaling. The Journal of Immunology *194*, 3937–3952.

Kayagaki, N., Stowe, I.B., Lee, B.L., O'Rourke, K., Anderson, K., Warming, S., Cuellar, T., Haley, B., Roose-Girma, M., Phung, Q.T., et al. (2015). Caspase-11 cleaves gasdermin D for non-canonical inflammasome signalling. Nature *526*, 666–671.

Kayagaki, N., Warming, S., Lamkanfi, M., Walle, L.V., Louie, S., Dong, J., Newton, K., Qu, Y., Liu, J., Heldens, S., et al. (2011). Non-canonical inflammasome activation targets caspase-11. Nature *479*, 117–121.

Kiefer, M.C., Brauer, M.J., Powers, V.C., Wu, J.J., Umansky, S.R., Tomei, L.D., and Barr, P.J. (1995). Modulation of apoptosis by the widely distributed Bcl-2 homologue Bak. Nature *374*, 736–739.

Kim, J., Gupta, R., Blanco, L.P., Yang, S., Shteinfer-Kuzmine, A., Wang, K., Zhu, J., Yoon, H.E., Wang, X., Kerkhofs, M., et al. (2019). VDAC oligomers form mitochondrial pores to release mtDNA fragments and promote lupus-like disease. Science *366*, 1531–1536.

Kirschning, C.J., and Schumann, R.R. (2002). TLR2: Cellular Sensor for Microbial and Endogenous Molecular Patterns. In Diverse Effects of Hypoxia on Tumor Progression, M.C. Simon, ed. (Berlin, Heidelberg: Springer Berlin Heidelberg), pp. 121–144.

Klein, R.R., Bourdon, D.M., Costales, C.L., Wagner, C.D., White, W.L., Williams, J.D., Hicks, S.N., Sondek, J., and Thakker, D.R. (2011). Direct Activation of Human Phospholipase C by Its Well Known Inhibitor U73122. Journal of Biological Chemistry *286*, 12407–12416.

Kluck, R.M. (1997). The Release of Cytochrome c from Mitochondria: A Primary Site for Bcl-2 Regulation of Apoptosis. Science *275*, 1132–1136.

Kofoed, E.M., and Vance, R.E. (2011). Innate immune recognition of bacterial ligands by NAIPs determines inflammasome specificity. Nature *477*, 592–595.

Korge, P., and Weiss, J.N. (1999). Thapsigargin directly induces the mitochondrial permeability transition. European Journal of Biochemistry *265*, 273–280.

Kostura, M.J., Tocci, M.J., Limjuco, G., Chin, J., Cameron, P., Hillman, A.G., Chartrain, N.A., and Schmidt, J.A. (1989). Identification of a monocyte specific pre-interleukin 1 beta convertase activity. Proc Natl Acad Sci USA *86*, 5227–5231.

Kotschy, A., Szlavik, Z., Murray, J., Davidson, J., Maragno, A.L., Le Toumelin-Braizat, G., Chanrion, M., Kelly, G.L., Gong, J.-N., Moujalled, D.M., et al. (2016). The MCL1 inhibitor S63845 is tolerable and effective in diverse cancer models. Nature *538*, 477–482.

Kowaltowski, A.J., Castilho, R.F., and Vercesi, A.E. (1996). Opening of the mitochondrial permeability transition pore by uncoupling or inorganic phosphate in the presence of Ca2+ is dependent on mitochondrial-generated reactive oxygen species. FEBS Letters *378*, 150–152.

Krishnaswamy, J.K., Singh, A., Gowthaman, U., Wu, R., Gorrepati, P., Sales Nascimento, M., Gallman, A., Liu, D., Rhebergen, A.M., Calabro, S., et al. (2015). Coincidental loss of DOCK8 function in NLRP10-deficient and C3H/HeJ mice results in defective dendritic cell migration. Proc Natl Acad Sci USA *112*, 3056–3061.

Krjukova, J., Holmqvist, T., Danis, A.S., Åkerman, K.E.O., and Kukkonen, J.P. (2004). Phospholipase C activator m-3M3FBS affects Ca 2+homeostasis independently of phospholipase C activation. British Journal of Pharmacology *143*, 3–7.

Kumar, H., Kawai, T., and Akira, S. (2011). Pathogen Recognition by the Innate Immune System. International Reviews of Immunology *30*, 16–34.

Kupsch, K., Hertel, S., Kreutzmann, P., Wolf, G., Wallesch, C.-W., Siemen, D., and Schönfeld, P. (2009). Impairment of mitochondrial function by minocycline. FEBS Journal *276*, 1729–1738.

Kuriakose, T., Man, S.M., Subbarao Malireddi, R.K., Karki, R., Kesavardhana, S., Place, D.E., Neale, G., Vogel, P., and Kanneganti, T.-D. (2016). ZBP1/DAI is an innate sensor of influenza virus triggering the NLRP3 inflammasome and programmed cell death pathways. Sci. Immunol. *1*, aag2045–aag2045.

Kuriakose, T., Zheng, M., Neale, G., and Kanneganti, T.-D. (2018). IRF1 Is a Transcriptional Regulator of ZBP1 Promoting NLRP3 Inflammasome Activation and Cell Death during Influenza Virus Infection. The Journal of Immunology *200*, 1489–1495.

Kwong, J.Q., Davis, J., Baines, C.P., Sargent, M.A., Karch, J., Wang, X., Huang, T., and Molkentin, J.D. (2014). Genetic deletion of the mitochondrial phosphate carrier desensitizes the mitochondrial permeability transition pore and causes cardiomyopathy. Cell Death Differ *21*, 1209–1217.

Kwong, J.Q., and Molkentin, J.D. (2015). Physiological and Pathological Roles of the Mitochondrial Permeability Transition Pore in the Heart. Cell Metabolism *21*, 206–214.

Lachner, J., Mlitz, V., Tschachler, E., and Eckhart, L. (2017). Epidermal cornification is preceded by the expression of a keratinocyte-specific set of pyroptosis-related genes. Sci. Rep. *7*, 107.

Land, W. (2003). Allograft injury mediated by reactive oxygen species: from conserved proteins of Drosophila to acute and chronic rejection of human transplants. Part III: interaction of (oxidative) stress-induced heat shock proteins with toll-like receptor-bearing cells of innate immunity and its consequences for the development of acute and chronic allograft rejection. Transplantation Reviews *17*, 67–86.

Lang, F., Stournaras, C., Zacharopoulou, N., Voelkl, J., and Alesutan, I. (2018). Serum- and glucocorticoid-inducible kinase 1 and the response to cell stress. Cell Stress *3*, 1–8.

Latz, E., Xiao, T.S., and Stutz, A. (2013). Activation and regulation of the inflammasomes. Nat Rev Immunol *13*, 397–411.

Lautz, K., Damm, A., Menning, M., Wenger, J., Adam, A.C., Zigrino, P., Kremmer, E., and Kufer, T.A. (2012). NLRP10 enhances Shigella-induced pro-inflammatory responses. Cell Microbiol *14*, 1568–1583.

Lawlor, K.E., and Vince, J.E. (2014). Ambiguities in NLRP3 inflammasome regulation: Is there a role for mitochondria? Biochimica Et Biophysica Acta (BBA) - General Subjects *1840*, 1433–1440.

Lawlor, K.E., Feltham, R., Yabal, M., Conos, S.A., Chen, K.W., Ziehe, S., Graß, C., Zhan, Y., Nguyen, T.A., Hall, C., et al. (2017). XIAP Loss Triggers RIPK3- and Caspase-8-Driven IL-1β Activation and Cell Death as a Consequence of TLR-MyD88-Induced cIAP1-TRAF2 Degradation. Cell Reports *20*, 668–682.

Lawlor, K.E., Khan, N., Mildenhall, A., Gerlic, M., Croker, B.A., D'Cruz, A.A., Hall, C., Kaur Spall, S., Anderton, H., Masters, S.L., et al. (2015). RIPK3 promotes cell death and NLRP3 inflammasome activation in the absence of MLKL. Nat Comms *6*, pii:a008730.

Lee, G.-S., Subramanian, N., Kim, A.I., Aksentijevich, I., Goldbach-Mansky, R., Sacks, D.B., Germain, R.N., Kastner, D.L., and Chae, J.J. (2012). The calcium-sensing receptor regulates the NLRP3 inflammasome through Ca2+ and cAMP. Nature *492*, 123–127.

Lee, M.S., and Kim, Y.-J. (2007). Signaling Pathways Downstream of Pattern-Recognition Receptors and Their Cross Talk. Annu. Rev. Biochem. *76*, 447–480.

Lerner, A.G., Upton, J.-P., Praveen, P.V.K., Ghosh, R., Nakagawa, Y., Igbaria, A., Shen, S., Nguyen, V., Backes, B.J., Heiman, M., et al. (2012). IRE1α Induces Thioredoxin-Interacting Protein to Activate the NLRP3 Inflammasome and Promote Programmed Cell Death under Irremediable ER Stress. Cell Metabolism *16*, 250–264.

Leung, A.W.C., Varanyuwatana, P., and Halestrap, A.P. (2008). The Mitochondrial Phosphate Carrier Interacts with Cyclophilin D and May Play a Key Role in the Permeability Transition. Journal of Biological Chemistry *283*, 26312–26323.

Levinsohn, J.L., Newman, Z.L., Hellmich, K.A., Fattah, R., Getz, M.A., Liu, S., Sastalla, I., Leppla, S.H., and Moayeri, M. (2012). Anthrax Lethal Factor Cleavage of Nlrp1 Is Required for Activation of the Inflammasome. PLoS Pathog *8*, e1002638.

Levy, M., Thaiss, C.A., Zeevi, D., Dohnalová, L., Zilberman-Schapira, G., Mahdi, J.A., David, E., Savidor, A., Korem, T., Herzig, Y., et al. (2015). Microbiota-Modulated Metabolites Shape the Intestinal Microenvironment by Regulating NLRP6 Inflammasome Signaling. Cell *163*, 1428–1443.

Li, C.-H., Cheng, Y.-W., Liao, P.-L., Yang, Y.-T., and Kang, J.-J. (2010). Chloramphenicol Causes Mitochondrial Stress, Decreases ATP Biosynthesis, Induces Matrix Metalloproteinase-13 Expression, and Solid-Tumor Cell Invasion. Toxicological Sciences *116*, 140–150.

Li, H., Zhu, H., Xu, C.-J., and Yuan, J. (1998). Cleavage of BID by Caspase 8 Mediates the Mitochondrial Damage in the Fas Pathway of Apoptosis. Cell *94*, 491–501.

Li, J., Wang, J., and Zeng, Y. (2007). Peripheral benzodiazepine receptor ligand, PK11195 induces mitochondria cytochrome c release and dissipation of mitochondria potential via induction of mitochondria permeability transition. European Journal of Pharmacology *560*, 117–122.

Li, P., Nijhawan, D., Budihardjo, I., Srinivasula, S.M., Ahmad, M., Alnemri, E.S., and Wang, X. (1997). Cytochrome c and dATP-Dependent Formation of Apaf-1/Caspase-9 Complex Initiates an Apoptotic Protease Cascade. Cell *91*, 479–489.

Li, Y., Shen, Y., Jin, K., Wen, Z., Cao, W., Wu, B., Wen, R., Tian, L., Berry, G.J., Goronzy, J.J., et al. (2019). The DNA Repair Nuclease MRE11A Functions as a Mitochondrial Protector and Prevents T Cell Pyroptosis and Tissue Inflammation. Cell Metabolism *30*, 477–492.e6.

Liao, Y., Hussain, T., Liu, C., Cui, Y., Wang, J., Yao, J., Chen, H., Song, Y., Sabir, N., Hussain, M., et al. (2019). Endoplasmic Reticulum Stress Induces Macrophages to Produce IL-1β During Mycobacterium bovis Infection via a Positive Feedback Loop Between Mitochondrial Damage and Inflammasome Activation. Front. Immunol. *10*, 768542.

Liashkovich, I., Pasrednik, D., Prystopiuk, V., Rosso, G., Oberleithner, H., and Shahin, V. (2015). Clathrin inhibitor Pitstop-2 disrupts the nuclear pore complex permeability barrier. Sci. Rep. *5*, 109.

Lightfield, K.L., Persson, J., Brubaker, S.W., Witte, C.E., Moltke, von, J., Dunipace, E.A., Henry, T., Sun, Y.-H., Cado, D., Dietrich, W.F., et al. (2008). Critical function for Naip5 in inflammasome activation by a conserved carboxy-terminal domain of flagellin. Nat Immunol *9*, 1171–1178.

Lim, M.L.R., Minamikawa, T., and Nagley, P. (2001). The protonophore CCCP induces mitochondrial permeability transition without cytochrome crelease in human osteosarcoma cells. FEBS Letters *503*, 69–74.

Lin, A., and Sheltzer, J.M. (2020). Discovering and validating cancer genetic dependencies: approaches and pitfalls. Nat Rev Genet *136*, 823.

Lin, A., Giuliano, C.J., Palladino, A., John, K.M., Abramowicz, C., Yuan, M.L., Sausville, E.L., Lukow, D.A., Liu, L., Chait, A.R., et al. (2019). Off-target toxicity is a common mechanism of action of cancer drugs undergoing clinical trials. Science Translational Medicine *11*, eaaw8412.

Lin, L., Zhang, M., Yan, R., Shan, H., Diao, J., and Wei, J. (2017). Inhibition of Drp1 attenuates mitochondrial damage and myocardial injury in Coxsackievirus B3 induced myocarditis. Biochemical and Biophysical Research Communications *484*, 550–556.

Liston, A., and Masters, S.L. (2017). Homeostasis-altering molecular processes as mechanisms of inflammasome activation. Nat Rev Immunol *17*, 208–214.

Liu, S.-I. (2013). M-3M3FBS-Induced Ca^(2+) Movement and Apoptosis in HA59T Human Hepatoma Cells. Chin. J. Physiol. *56*, 26–35.

Liu, X., Zhang, Z., Ruan, J., Pan, Y., Magupalli, V.G., Wu, H., and Lieberman, J. (2016). Inflammasome-activated gasdermin D causes pyroptosis by forming membrane pores. Nature *535*, 153–158.

Liu, X., Kim, C.N., Yang, J., Jemmerson, R., and Wang, X. (1996). Induction of Apoptotic Program in Cell-Free Extracts: Requirement for dATP and Cytochrome c. Cell *86*, 147–157.

Livak, K.J., and Schmittgen, T.D. (2001). Analysis of Relative Gene Expression Data Using Real-Time Quantitative PCR and the 2−ΔΔCT Method. Methods *25*, 402–408.

López-Castejón, G., Luheshi, N.M., Compan, V., High, S., Whitehead, R.C., Flitsch, S., Kirov, A., Prudovsky, I., Swanton, E., and Brough, D. (2013). Deubiquitinases Regulate the Activity of Caspase-1 and Interleukin-1β Secretion via Assembly of the Inflammasome. Journal of Biological Chemistry *288*, 2721–2733.

Lu, A., Magupalli, V.G., Ruan, J., Yin, Q., Atianand, M.K., Vos, M.R., Schröder, G.F., Fitzgerald, K.A., Wu, H., and Egelman, E.H. (2014). Unified Polymerization Mechanism for the Assembly of ASC-Dependent Inflammasomes. Cell *156*, 1193–1206.

Lu, B., Nakamura, T., Inouye, K., Li, J., Tang, Y., Lundbäck, P., Valdes-Ferrer, S.I., Olofsson, P.S., Kalb, T., Roth, J., et al. (2012). Novel role of PKR in inflammasome activation and HMGB1 release. Nature *488*, 670–674.

Lu, L.L., Suscovich, T.J., Fortune, S.M., and Alter, G. (2017). Beyond binding: antibody effector functions in infectious diseases. Nat Rev Immunol *18*, 46–61.

Luo, X., Budihardjo, I., Zou, H., Slaughter, C., and Wang, X. (1998). Bid, a Bcl2 Interacting Protein, Mediates Cytochrome c Release from Mitochondria in Response to Activation of Cell Surface Death Receptors. Cell *94*, 481–490.

Luo, Y., Hu, Y., Zhang, M., Xiao, Y., Song, Z., and Xu, Y. (2013). EtBr-induced selective degradation of mitochondria occurs via autophagy. Oncol. Rep. *30*, 1201–1208.

MacDonald, J.A., Wijekoon, C.P., Liao, K.-C., and Muruve, D.A. (2013). Biochemical and structural aspects of the ATP-binding domain in inflammasome-forming human NLRP proteins. IUBMB Life *65*, 851–862.

Madesh, M., and Hajnóczky, G. (2001). VDAC-dependent permeabilization of the outer mitochondrial membrane by superoxide induces rapid and massive cytochrome c release. J Cell Biol *155*, 1003–1016.

Madigan, C.A., Cambier, C.J., Kelly-Scumpia, K.M., Scumpia, P.O., Cheng, T.-Y., Zailaa, J., Bloom, B.R., Moody, D.B., Smale, S.T., Sagasti, A., et al. (2017). A Macrophage Response to Mycobacterium leprae Phenolic Glycolipid Initiates Nerve Damage in Leprosy. Cell *170*, 973–985.e10.

Maekawa, H., Inoue, T., Ouchi, H., Jao, T.-M., Inoue, R., Nishi, H., Fujii, R., Ishidate, F., Tanaka, T., Tanaka, Y., et al. (2019). Mitochondrial Damage Causes Inflammation via cGAS-STING Signaling in Acute Kidney Injury. Cell Reports *29*, 1261–1273.e1266.

Malik, A., and Kanneganti, T.-D. (2017). Inflammasome activation and assembly at a glance. Journal of Cell Science *130*, 3955–3963.

Man, S.M., Karki, R., and Kanneganti, T.-D. (2017). Molecular mechanisms and functions of pyroptosis, inflammatory caspases and inflammasomes in infectious diseases. Immunol Rev *277*, 61–75.

Man, S.M., Karki, R., Malireddi, R.K.S., Neale, G., Vogel, P., Yamamoto, M., Lamkanfi, M., and Kanneganti, T.-D. (2015). The transcription factor IRF1 and guanylate-binding proteins target activation of the AIM2 inflammasome by Francisella infection. Nat Immunol *16*, 467–475.

Mangan, M.S.J., Olhava, E.J., Roush, W.R., Seidel, H.M., Glick, G.D., and Latz, E. (2018). Targeting the NLRP3 inflammasome in inflammatory diseases. Nat Rev Drug Discov *17*, 588–606.

Manon, S., Chaudhuri, B., and Guérin, M. (1997). Release of cytochrome c and decrease of cytochrome c oxidase in Bax-expressing yeast cells, and prevention of these effects by coexpression of Bcl-x L. FEBS Letters *415*, 29–32.

Mariathasan, S., Weiss, D.S., Newton, K., McBride, J., O'Rourke, K., Roose-Girma, M., Lee, W.P., Weinrauch, Y., Monack, D.M., and Dixit, V.M. (2006). Cryopyrin activates the inflammasome in response to toxins and ATP. Nature *440*, 228–232.

Martinon, F., Burns, K., and Tschopp, J. (2002). The inflammasome: a molecular platform triggering activation of inflammatory caspases and processing of proIL-beta. Molecular Cell *10*, 417–426.

Martinon, F., Petrilli, V., Mayor, A., Tardivel, A., and Tschopp, J. (2006). Gout-associated uric acid crystals activate the NALP3 inflammasome. Nature *440*, 237–241.

Martín-Nalda, A., Fortuny, C., Rey, L., Bunney, T.D., Alsina, L., Esteve-Solé, A., Bull, D., Anton, M.C., Basagaña, M., Casals, F., et al. (2020). Severe Autoinflammatory Manifestations and Antibody Deficiency Due to Novel Hypermorphic PLCG2 Mutations. J Clin Immunol *18*, 832.

Marton, J., Albert, D., Wiltshire, S.A., Park, R., Bergen, A., Qureshi, S., Malo, D., Burelle, Y., and Vidal, S.M. (2015). Cyclosporine A Treatment Inhibits Abcc6-Dependent Cardiac Necrosis and Calcification following Coxsackievirus B3 Infection in Mice. PLoS ONE *10*, e0138222.

Marzo, I., Brenner, C., Zamzami, N., Jürgensmeier, J.M., Susin, S.A., Vieira, H.L., Prévost, M.C., Xie, Z., Matsuyama, S., Reed, J.C., et al. (1998). Bax and adenine nucleotide translocator cooperate in the mitochondrial control of apoptosis. Science *281*, 2027–2031.

Matas, J., Tien Sing Young, N., Bourcier-Lucas, C., Ascah, A., Marcil, M., Deschepper, C.F., and Burelle, Y. (2009). Increased expression and intramitochondrial translocation of cyclophilin-D associates with

increased vulnerability of the permeability transition pore to stress-induced opening during compensated ventricular hypertrophy. Journal of Molecular and Cellular Cardiology *46*, 420–430.

Maucher, I.V., Rühl, M., Kretschmer, S.B.M., Hofmann, B., Kühn, B., Fettel, J., Vogel, A., Flügel, K.T., Manolikakes, G., Hellmuth, N., et al. (2017). Michael acceptor containing drugs are a novel class of 5-lipoxygenase inhibitor targeting the surface cysteines C416 and C418. Biochemical Pharmacology *125*, 55–74.

McArthur, K., Whitehead, L.W., Heddleston, J.M., Li, L., Padman, B.S., Oorschot, V., Geoghegan, N.D., Chappaz, S., Davidson, S., San Chin, H., et al. (2018). BAK/BAX macropores facilitate mitochondrial herniation and mtDNA efflux during apoptosis. Science *359*, eaao6047.

McKee, E.E., Ferguson, M., Bentley, A.T., and Marks, T.A. (2006). Inhibition of Mammalian Mitochondrial Protein Synthesis by Oxazolidinones. Aac *50*, 2042–2049.

McQuin, C., Goodman, A., Chernyshev, V., Kamentsky, L., Cimini, B.A., Karhohs, K.W., Doan, M., Ding, L., Rafelski, S.M., Thirstrup, D., et al. (2018). CellProfiler 3.0: Next-generation image processing for biology. PLoS Biol *16*, e2005970.

McWilliam, H., Li, W., Uludag, M., Squizzato, S., Park, Y.M., Buso, N., Cowley, A.P., and Lopez, R. (2013). Analysis Tool Web Services from the EMBL-EBI. Nucleic Acids Research *41*, W597–W600.

Melber, A., and Haynes, C.M. (2018). UPRmt regulation and output: a stress response mediated by mitochondrial-nuclear communication. Cell Res *28*, 281–295.

Menu, P., Mayor, A., Zhou, R., Tardivel, A., Ichijo, H., Mori, K., and Tschopp, J. (2012). ER stress activates the NLRP3 inflammasome via an UPR-independent pathway. Cell Death Dis *3*, e261.

Meunier, E., and Broz, P. (2017). Evolutionary Convergence and Divergence in NLR Function and Structure. Trends in Immunology *38*, 744–757.

Mewton, N., Croisille, P., Gahide, G., Rioufol, G., Bonnefoy, E., Sanchez, I., Cung, T.-T., Sportouch, C., Angoulvant, D., Finet, G., et al. (2010). Effect of Cyclosporine on Left Ventricular Remodeling After Reperfused Myocardial Infarction. Journal of the American College of Cardiology *55*, 1200–1205.

Méthot, P.-O., and Alizon, S. (2014). What is a pathogen? Toward a process view of host-parasite interactions. Virulence *5*, 775–785.

Miller, J.M., and Enemark, E.J. (2016). Fundamental Characteristics of AAA+ Protein Family Structure and Function. Archaea *2016*, 1–12.

Mills, E.L., Ryan, D.G., Prag, H.A., Dikovskaya, D., Menon, D., Zaslona, Z., Jedrychowski, M.P., Costa, A.S.H., Higgins, M., Hams, E., et al. (2018). Itaconate is an anti-inflammatory metabolite that activates Nrf2 via alkylation of KEAP1. Nature *556*, 113–117.

Minamikawa, T., Williams, D.A., Bowser, D.N., and Nagley, P. (1999). Mitochondrial Permeability Transition and Swelling Can Occur Reversibly without Inducing Cell Death in Intact Human Cells. Experimental Cell Research *246*, 26–37.

Misawa, T., Takahama, M., Kozaki, T., Lee, H., Zou, J., Saitoh, T., and Akira, S. (2013). Microtubule-driven spatial arrangement of mitochondria promotes activation of the NLRP3 inflammasome. Nat Immunol *14*, 454–460.

Mishra, N., Schwerdtner, L., Sams, K., Mondal, S., Ahmad, F., Schmidt, R.E., Coonrod, S.A., Thompson, P.R., Lerch, M.M., and Bossaller, L. (2019). Cutting Edge: Protein Arginine Deiminase 2 and 4 Regulate NLRP3 Inflammasome–Dependent IL-1β Maturation and ASC Speck Formation in Macrophages. The Journal of Immunology *203*, 795–800.

Miyata, N., Steffen, J., Johnson, M.E., Fargue, S., Danpure, C.J., and Koehler, C.M. (2014). Pharmacologic rescue of an enzyme-trafficking defect in primary hyperoxaluria 1. Proc Natl Acad Sci USA *111*, 14406–14411.

Mnatsakanyan, N., Llaguno, M.C., Yang, Y., Yan, Y., Weber, J., Sigworth, F.J., and Jonas, E.A. (2019). A mitochondrial megachannel resides in monomeric F1FO ATP synthase. Nat Comms *10*, 621.

Mogensen, T.H. (2009). Pathogen Recognition and Inflammatory Signaling in Innate Immune Defenses. Cmr *22*, 240–273.

Molofsky, A.B., Byrne, B.G., Whitfield, N.N., Madigan, C.A., Fuse, E.T., Tateda, K., and Swanson, M.S. (2006). Cytosolic recognition of flagellin by mouse macrophages restricts Legionella pneumophila infection. J Exp Med *203*, 1093–1104.

Monteleone, M., Stanley, A.C., Chen, K.W., Brown, D.L., Bezbradica, J.S., Pein, von, J.B., Holley, C.L., Boucher, D., Shakespear, M.R., Kapetanovic, R., et al. (2018). Interleukin-1β Maturation Triggers Its Relocation to the Plasma Membrane for Gasdermin-D-Dependent and -Independent Secretion. Cell Reports *24*, 1425–1433.

Moriyama, M., Nagai, M., Maruzuru, Y., Koshiba, T., Kawaguchi, Y., and Ichinohe, T. (2020). Influenza Virus-Induced Oxidized DNA Activates Inflammasomes. iScience *23*, 101270.

Mortimer, L., Moreau, F., MacDonald, J.A., and Chadee, K. (2016). NLRP3 inflammasome inhibition is disrupted in a group of auto-inflammatory disease CAPS mutations. Nat Immunol.

Mottis, A., Herzig, S., and Auwerx, J. (2019). Mitocellular communication: Shaping health and disease. Science *366*, 827–832.

Moullan, N., Mouchiroud, L., Wang, X., Ryu, D., Williams, E.G., Mottis, A., Jovaisaite, V., Frochaux, M.V., Quiros, P.M., Deplancke, B., et al. (2015). Tetracyclines Disturb Mitochondrial Function across Eukaryotic Models: A Call for Caution in Biomedical Research. Cell Reports *10*, 1681–1691.

Mukherjee, S., Kumar, R., Tsakem Lenou, E., Basrur, V., Kontoyiannis, D.L., Ioakeimidis, F., Mosialos, G., Theiss, A.L., Flavell, R.A., and Venuprasad, K. (2020). Deubiquitination of NLRP6 inflammasome by Cyld critically regulates intestinal inflammation. Nat Immunol *21*, 626–635.

Muñoz Sánchez, J., and Chánez Cárdenas, M.E. (2018). The use of cobalt chloride as a chemical hypoxia model. J Appl Toxicol *39*, 556–570.

Münch, C., and Harper, J.W. (2016). Mitochondrial unfolded protein response controls matrix pre-RNA processing and translation. Nature *534*, 710–713.

Muñoz-Planillo, R., Kuffa, P., Martínez-Colón, G., Smith, B.L., Rajendiran, T.M., and Núñez, G. (2013). K+ Efflux Is the Common Trigger of NLRP3 Inflammasome Activation by Bacterial Toxins and Particulate Matter. Immunity *38*, 1142–1153.

Murakami, T., Ockinger, J., Yu, J., Byles, V., McColl, A., Hofer, A.M., and Horng, T. (2012). Critical role for calcium mobilization in activation of the NLRP3 inflammasome. Proc Natl Acad Sci USA *109*, 11282–11287.

Murphy, K. (2016). Janeway's Immunobiology (9th edition. | New York, NY : Garland Science/Taylor & Francis: Garland Science).

Murphy, N., Grehan, B., and Lynch, M.A. (2013). Glial Uptake of Amyloid Beta Induces NLRP3 Inflammasome Formation via Cathepsin-Dependent Degradation of NLRP10. Neuromol Med *16*, 205–215.

Nacarelli, T., Azar, A., and Sell, C. (2014). Inhibition of mTOR Prevents ROS Production Initiated by Ethidium Bromide-Induced Mitochondrial DNA Depletion. Front. Endocrinol. *5*, 113.

Nair, D.P., Podgórski, M., Chatani, S., Gong, T., Xi, W., Fenoli, C.R., and Bowman, C.N. (2013). The Thiol-Michael Addition Click Reaction: A Powerful and Widely Used Tool in Materials Chemistry. Chem. Mater. *26*, 724–744.

Nakagawa, T., Shimizu, S., Watanabe, T., Yamaguchi, O., Otsu, K., Yamagata, H., Inohara, H., Kubo, T., and Tsujimoto, Y. (2005). Cyclophilin D-dependent mitochondrial permeability transition regulates some necrotic but not apoptotic cell death. Nature *434*, 652–658.

Nakahira, K., Haspel, J.A., Rathinam, V.A.K., Lee, S.-J., Dolinay, T., Lam, H.C., Englert, J.A., Rabinovitch, M., Cernadas, M., Kim, H.P., et al. (2010). Autophagy proteins regulate innate immune responses by inhibiting the release of mitochondrial DNA mediated by the NALP3 inflammasome. Nat Immunol *12*, 222–230.

Nakajima, S., Imamura, R., Yoshino, M., Sakurai, M., Tsuchiya, K., Sugihara, K., Asano, M., and Suda, T. (2018). Characterization of Innate and Adaptive Immune Responses in PYNOD-Deficient Mice. Ih *2*, 129–141.

Nakamura, Y., and Fukami, K. (2017). Regulation and physiological functions of mammalian phospholipase C. J. Biochem. mvw094.

NCBI Resource Coordinators, Agarwala, R., Barrett, T., Beck, J., Benson, D.A., Bollin, C., Bolton, E., Bourexis, D., Brister, J.R., Bryant, S.H., et al. (2017). Database resources of the National Center for Biotechnology Information. Nucleic Acids Research *46*, D8–D13.

Negash, A.A., Olson, R.M., Griffin, S., and Gale, M. (2019). Modulation of calcium signaling pathway by hepatitis C virus core protein stimulates NLRP3 inflammasome activation. PLoS Pathog *15*, e1007593.

Nour, A.M., Yeung, Y.-G., Santambrogio, L., Boyden, E.D., Stanley, E.R., and Brojatsch, J. (2009). Anthrax Lethal Toxin Triggers the Formation of a Membrane-Associated Inflammasome Complex in Murine Macrophages. Infect. Immun. *77*, 1262–1271.

Oliveira, I.V.P. de M., Deps, P.D., and Antunes, J.M.A. de P. (2019). Armadillos and leprosy: from infection to biological model. Rev. Inst. Med. Trop. S. Paulo *61*, 31.

Oltersdorf, T., Elmore, S.W., Shoemaker, A.R., Armstrong, R.C., Augeri, D.J., Belli, B.A., Bruncko, M., Deckwerth, T.L., Dinges, J., Hajduk, P.J., et al. (2005). An inhibitor of Bcl-2 family proteins induces regression of solid tumours. Nature *435*, 677–681.

Oltval, Z.N., Milliman, C.L., and Korsmeyer, S.J. (1993). Bcl-2 heterodimerizes in vivo with a conserved homolog, Bax, that accelerates programed cell death. Cell *74*, 609–619.

Oslowski, C.M., Hara, T., O'Sullivan-Murphy, B., Kanekura, K., Lu, S., Hara, M., Ishigaki, S., Zhu, L.J., Hayashi, E., Hui, S.T., et al. (2012). Thioredoxin-Interacting Protein Mediates ER Stress-Induced β Cell Death through Initiation of the Inflammasome. Cell Metabolism *16*, 265–273.

Paeshuyse, J., Kaul, A., De Clercq, E., Rosenwirth, B., Dumont, J.-M., Scalfaro, P., Bartenschlager, R., and Neyts, J. (2006). The non-immunosuppressive cyclosporin DEBIO-025 is a potent inhibitor of hepatitis C virus replicationin vitro. Hepatology *43*, 761–770.

Pakos Zebrucka, K., Koryga, I., Mnich, K., Ljujic, M., Samali, A., and Gorman, A.M. (2016). The integrated stress response. EMBO Rep *17*, 1374–1395.

Paludan, S.R., Pradeu, T., Masters, S.L., and Mogensen, T.H. (2020). Constitutive immune mechanisms: mediators of host defence and immune regulation. Nat Rev Immunol *454*, 428.

Pan, G., O'Rourke, K., and Dixit, V.M. (1998). Caspase-9, Bcl-X L, and Apaf-1 Form a Ternary Complex. Journal of Biological Chemistry *273*, 5841–5845.

Park, S., Juliana, C., Hong, S., Datta, P., Hwang, I., Fernandes-Alnemri, T., Yu, J.-W., and Alnemri, E.S. (2013). The Mitochondrial Antiviral Protein MAVS Associates with NLRP3 and Regulates Its Inflammasome Activity. The Journal of Immunology *191*, 4358–4366.

Park, Y.H., Wood, G., Kastner, D.L., and Chae, J.J. (2016). Pyrin inflammasome activation and RhoA signaling in the autoinflammatory diseases FMF and HIDS. Nat Immunol.

Pastorino, J.G., Simbula, G., Gilfor, E., Hoek, J.B., and Farber, J.L. (1994). Protoporphyrin IX, an endogenous ligand of the peripheral benzodiazepine receptor, potentiates induction of the mitochondrial permeability transition and the killing of cultured hepatocytes by rotenone. Journal of Biological Chemistry *269*, 31041–31046.

Pelegrín, P., and Surprenant, A. (2006). Pannexin-1 mediates large pore formation and interleukin-1β release by the ATP-gated P2X7 receptor. The EMBO Journal *25*, 5071–5082.

Peng, Y., Kim, J.-M., Park, H.-S., Yang, A., Islam, C., Lakatta, E.G., and Lin, L. (2016). AGE-RAGE signal generates a specific NF-κB RelA "barcode" that directs collagen I expression. Sci. Rep. *6*, 411.

Perregaux, D., and Gabel, C.A. (1994). Interleukin-1 beta maturation and release in response to ATP and nigericin. Evidence that potassium depletion mediated by these agents is a necessary and common feature of their activity. Journal of Biological Chemistry *269*, 15195–15203.

Perregaux, D., Barberia, J., Lanzetti, A.J., Geoghegan, K.F., Carty, T.J., and Gabel, C.A. (1992). IL-1 beta maturation: evidence that mature cytokine formation can be induced specifically by nigericin. The Journal of Immunology *149*, 1294–1303.

Peterson, L.W., and Artis, D. (2014). Intestinal epithelial cells: regulators of barrier function and immune homeostasis. Nat Rev Immunol *14*, 141–153.

Petrilli, V., Papin, S., Dostert, C., Mayor, A., Martinon, F., and Tschopp, J. (2007). Activation of the NALP3 inflammasome is triggered by low intracellular potassium concentration. Cell Death Differ *14*, 1583–1589.

Petronilli, V., Penzo, D., Scorrano, L., Bernardi, P., and Di Lisa, F. (2001). The Mitochondrial Permeability Transition, Release of Cytochrome cand Cell Death. Journal of Biological Chemistry *276*, 12030–12034.

Piot, C., Croisille, P., Staat, P., Thibault, H., Rioufol, G., Mewton, N., Elbelghiti, R., Cung, T.-T., Bonnefoy, E., Angoulvant, D., et al. (2008). Effect of Cyclosporine on Reperfusion Injury in Acute Myocardial Infarction. N Engl J Med *359*, 473–481.

Poltorak, A. (1998). Defective LPS Signaling in C3H/HeJ and C57BL/10ScCr Mice: Mutations in Tlr4 Gene. Science *282*, 2085–2088.

Ponnalagu, D., Hussain, A.T., Thanawala, R., Meka, J., Bednarczyk, P., Feng, Y., Szewczyk, A., GururajaRao, S., Bopassa, J.C., Khan, M., et al. (2019). Chloride channel blocker IAA-94 increases myocardial infarction by reducing calcium retention capacity of the cardiac mitochondria. Life Sciences *235*, 116841.

Poyet, J.-L., Srinivasula, S.M., Tnani, M., Razmara, M., Fernandes-Alnemri, T., and Alnemri, E.S. (2001). Identification of Ipaf, a Human Caspase-1-activating Protein Related to Apaf-1. Journal of Biological Chemistry *276*, 28309–28313.

Pradeu, T. (2020). Philosophy of immunology (Cambridge University Press).

Pressman, B.C. (1976). Biological Applications of Ionophores. Annu. Rev. Biochem. *45*, 501–530.

Prochnicki, T., Mangan, M.S., and Latz, E. (2016). Recent insights into the molecular mechanisms of the NLRP3 inflammasome activation. F1000Res *5*, 1469.

Proell, M., Riedl, S.J., Fritz, J.H., Rojas, A.M., and Schwarzenbacher, R. (2008). The Nod-Like Receptor (NLR) Family: A Tale of Similarities and Differences. PLoS ONE *3*, e2119.

Py, B.F., Kim, M.-S., Vakifahmetoglu-Norberg, H., and Yuan, J. (2013). Deubiquitination of NLRP3 by BRCC3 Critically Regulates Inflammasome Activity. Molecular Cell *49*, 331–338.

Qureshi, S.T., Larivière, L., Leveque, G., Clermont, S., Moore, K.J., Gros, P., and Malo, D. (1999). Endotoxin-tolerant Mice Have Mutations in Toll-like Receptor 4 (Tlr4). J Exp Med *189*, 615–625.

Rada, B., Park, J.J., Sil, P., Geiszt, M., and Leto, T.L. (2014). NLRP3 inflammasome activation and interleukin-1β release in macrophages require calcium but are independent of calcium-activated NADPH oxidases. Inflamm. Res. *63*, 821–830.

Raghavendra, P.B., Lee, E., and Parameswaran, N. (2013). Regulation of Macrophage Biology by Lithium: A New Look at an Old Drug. J Neuroimmune Pharmacol *9*, 277–284.

Raimundo, N., and Krisko, A. (2019). Editorial: Mitochondrial Communication in Physiology, Disease and Aging. Front. Cell Dev. Biol. *7*, 56.

Rajamäki, K., Lappalainen, J., Öörni, K., Välimäki, E., Matikainen, S., Kovanen, P.T., and Eklund, K.K. (2010). Cholesterol Crystals Activate the NLRP3 Inflammasome in Human Macrophages: A Novel Link between Cholesterol Metabolism and Inflammation. PLoS ONE *5*, e11765.

Randow, F., MacMicking, J.D., and James, L.C. (2013). Cellular Self-Defense: How Cell-Autonomous Immunity Protects Against Pathogens. Science *340*, 701–706.

Rao, A., Luo, C., and Hogan, P.G. (1997). TRANSCRIPTION FACTORS OF THE NFAT FAMILY:Regulation and Function. Annu. Rev. Immunol. *15*, 707–747.

Rapino, F., Robles, E.F., Richter-Larrea, J.A., Kallin, E.M., Martinez-Climent, J.A., and Graf, T. (2013). C/EBPα Induces Highly Efficient Macrophage Transdifferentiation of B Lymphoma and Leukemia Cell Lines and Impairs Their Tumorigenicity. Cell Reports *3*, 1153–1163.

Rashidi, M., Simpson, D.S., Hempel, A., Frank, D., Petrie, E., Vince, A., Feltham, R., Murphy, J., Chatfield, S.M., Salvesen, G.S., et al. (2019). The Pyroptotic Cell Death Effector Gasdermin D Is Activated by Gout-Associated Uric Acid Crystals but Is Dispensable for Cell Death and IL-1β Release. The Journal of Immunology *203*, 736–748.

Rathinam, V.A.K., Jiang, Z., Waggoner, S.N., Sharma, S., Cole, L.E., Waggoner, L., Vanaja, S.K., Monks, B.G., Ganesan, S., Latz, E., et al. (2010). The AIM2 inflammasome is essential for host defense against cytosolic bacteria and DNA viruses. Nat Immunol *11*, 395–402.

Rayamajhi, M., Zak, D.E., Chavarria-Smith, J., Vance, R.E., and Miao, E.A. (2013). Cutting Edge: Mouse NAIP1 Detects the Type III Secretion System Needle Protein. The Journal of Immunology *191*, 3986–3989.

Rehwinkel, J., and Gack, M.U. (2020). RIG-I-like receptors: their regulation and roles in RNA sensing. Nat Rev Immunol *20*, 537–551.

Rekuviene, E., Ivanoviene, L., Borutaite, V., and Morkuniene, R. (2017). Rotenone decreases ischemia-induced injury by inhibiting mitochondrial permeability transition in mature brains. Neuroscience Letters *653*, 45–50.

Ren, G., Zhang, X., Xiao, Y., Zhang, W., Wang, Y., Ma, W., Wang, X., Song, P., Lai, L., Chen, H., et al. (2019). ABRO1 promotes NLRP3 inflammasome activation through regulation of NLRP3 deubiquitination. The EMBO Journal *38*, e1293.

Reyna, D.E., Garner, T.P., Lopez, A., Kopp, F., Choudhary, G.S., Sridharan, A., Narayanagari, S.-R., Mitchell, K., Dong, B., Bartholdy, B.A., et al. (2017). Direct Activation of BAX by BTSA1 Overcomes Apoptosis Resistance in Acute Myeloid Leukemia. Cancer Cell *32*, 490–505.e10.

Richards, N., Schaner, P., Diaz, A., Stuckey, J., Shelden, E., Wadhwa, A., and Gumucio, D.L. (2001). Interaction between Pyrin and the Apoptotic Speck Protein (ASC) Modulates ASC-induced Apoptosis. Journal of Biological Chemistry *276*, 39320–39329.

Ridker, P.M., Everett, B.M., Thuren, T., MacFadyen, J.G., Chang, W.H., Ballantyne, C., Fonseca, F., Nicolau, J., Koenig, W., Anker, S.D., et al. (2017). Antiinflammatory Therapy with Canakinumab for Atherosclerotic Disease. N Engl J Med *377*, 1119–1131.

Riehl, A., Bauer, T., Brors, B., Busch, H., Mark, R., Németh, J., Gebhardt, C., Bierhaus, A., Nawroth, P., Eils, R., et al. (2010). Identification of the Rage-dependent gene regulatory network in a mouse model of skin inflammation. BMC Genomics *11*, 537.

Riganti, C., Doublier, S., Viarisio, D., Miraglia, E., Pescarmona, G., Ghigo, D., and Bosia, A. (2009). Artemisinin induces doxorubicin resistance in human colon cancer cells via calcium-dependent activation of HIF-1α and P-glycoprotein overexpression. British Journal of Pharmacology *156*, 1054–1066.

Riley, J.S., Quarato, G., Cloix, C., Lopez, J., O'Prey, J., Pearson, M., Chapman, J., Sesaki, H., Carlin, L.M., Passos, J.F., et al. (2018). Mitochondrial inner membrane permeabilisation enables mt DNArelease during apoptosis. The EMBO Journal *37*.

Robblee, M.M., Kim, C.C., Abate, J.P., Valdearcos, M., Sandlund, K.L.M., Shenoy, M.K., Volmer, R., Iwawaki, T., and Koliwad, S.K. (2016). Saturated Fatty Acids Engage an IRE1α-Dependent Pathway to Activate the NLRP3 Inflammasome in Myeloid Cells. Cell Reports *14*, 2611–2623.

Rogers, C., Erkes, D.A., Nardone, A., Aplin, A.E., Fernandes-Alnemri, T., and Alnemri, E.S. (2019). Gasdermin pores permeabilize mitochondria to augment caspase-3 activation during apoptosis and inflammasome activation. Nat Comms *10*, 621.

Rosenblum, M.D., Remedios, K.A., and Abbas, A.K. (2015). Mechanisms of human autoimmunity. J. Clin. Invest. *125*, 2228–2233.

Rossol, M., Pierer, M., Raulien, N., Quandt, D., Meusch, U., Rothe, K., Schubert, K., Schöneberg, T., Schaefer, M., Krügel, U., et al. (2012). Extracellular Ca2+ is a danger signal activating the NLRP3 inflammasome through G protein-coupled calcium sensing receptors. Nat Comms *3*, 1329.

Roy, N. (1997). The c-IAP-1 and c-IAP-2 proteins are direct inhibitors of specific caspases. The EMBO Journal *16*, 6914–6925.

Samir, P., Kesavardhana, S., Patmore, D.M., Gingras, S., Malireddi, R.K.S., Karki, R., Guy, C.S., Briard, B., Place, D.E., Bhattacharya, A., et al. (2019). DDX3X acts as a live-or-die checkpoint in stressed cells by regulating NLRP3 inflammasome. Nature *573*, 590–594.

Sandstrom, A., Mitchell, P.S., Goers, L., Mu, E.W., Lesser, C.F., and Vance, R.E. (2019). Functional degradation: A mechanism of NLRP1 inflammasome activation by diverse pathogen enzymes. Science *364*, eaau1330.

Sanman, L.E., Qian, Y., Eisele, N.A., Ng, T.M., van der Linden, W.A., Monack, D.M., Weerapana, E., Bogyo, M., and Cravatt, B.F. (2016). Disruption of glycolytic flux is a signal for inflammasome signaling and pyroptotic cell death. eLife *5*, e13663.

Sardão, V.A., Oliveira, P.J., Holy, J., Oliveira, C.R., and Wallace, K.B. (2008). Morphological alterations induced by doxorubicin on H9c2 myoblasts: nuclear, mitochondrial, and cytoskeletal targets. Cell Biol Toxicol *25*, 227–243.

Schinzel, A.C., Takeuchi, O., Huang, Z., Fisher, J.K., Zhou, Z., Rubens, J., Hetz, C., Danial, N.N., Moskowitz, M.A., and Korsmeyer, S.J. (2005). Cyclophilin D is a component of mitochondrial permeability transition and mediates neuronal cell death after focal cerebral ischemia. Proc Natl Acad Sci USA *102*, 12005–12010.

Schlee, M., and Hartmann, G. (2016). Discriminating self from non-self in nucleic acid sensing. Nat Rev Immunol *16*, 566–580.

Schmacke, N.A., Gaidt, M.M., Szymanska, I., O'Duill, F., Stafford, C.A., Chauhan, D., Fröhlich, A.L., Nagl, D., Pinci, F., Schmid-Burgk, J.L., et al. (2019). Priming enables a NEK7-independent route of NLRP3 activation. bioRxiv *9*, 799320.

Schmid-Burgk, J.L., Chauhan, D., Schmidt, T., Ebert, T.S., Reinhardt, J., Endl, E., and Hornung, V. (2016). A Genome-wide CRISPR (Clustered Regularly Interspaced Short Palindromic Repeats) Screen Identifies NEK7 as an Essential Component of NLRP3 Inflammasome Activation. Journal of Biological Chemistry *291*, 103–109.

Schneider, A. (2011). Mitochondrial tRNA Import and Its Consequences for Mitochondrial Translation. Annu. Rev. Biochem. *80*, 1033–1053.

Schubert, S., Heller, S., Löffler, B., Schäfer, I., Seibel, M., Villani, G., and Seibel, P. (2015). Generation of Rho Zero Cells: Visualization and Quantification of the mtDNA Depletion Process. Ijms *16*, 9850–9865.

Segal, A.W. (2005). HOW NEUTROPHILS KILL MICROBES. Annu. Rev. Immunol. *23*, 197–223.

Seidler, N.W., Jona, I., Vegh, M., and Martonosi, A. (1989). Cyclopiazonic acid is a specific inhibitor of the Ca2+-ATPase of sarcoplasmic reticulum. Journal of Biological Chemistry *264*, 17816–17823.

Shamas-Din, A., Kale, J., Leber, B., and Andrews, D.W. (2013). Mechanisms of Action of Bcl-2 Family Proteins. Cold Spring Harbor Perspectives in Biology *5*, a008714–a008714.

Shamas-Din, A., Brahmbhatt, H., Leber, B., and Andrews, D.W. (2011). BH3-only proteins: Orchestrators of apoptosis. Biochimica Et Biophysica Acta (BBA) - Molecular Cell Research *1813*, 508–520.

Sharma, R., Lahiri, R., Scollard, D.M., Pena, M., Williams, D.L., Adams, L.B., Figarola, J., and Truman, R.W. (2012). The armadillo: a model for the neuropathy of leprosy and potentially other neurodegenerative diseases. Disease Models & Mechanisms *6*, 19–24.

Shi, H., Murray, A., and Beutler, B. (2016). Reconstruction of the Mouse Inflammasome System in HEK293T Cells. Bio-Protocol *6*.

Shi, H., Wang, Y., Li, X., Zhan, X., Tang, M., Fina, M., Su, L., Pratt, D., Bu, C.H., Hildebrand, S., et al. (2015a). NLRP3 activation and mitosis are mutually exclusive events coordinated by NEK7, a new inflammasome component. Nat Immunol *17*, 250–258.

Shi, J., Zhao, Y., Wang, K., Shi, X., Wang, Y., Huang, H., Zhuang, Y., Cai, T., Wang, F., and Shao, F. (2015b). Cleavage of GSDMD by inflammatory caspases determines pyroptotic cell death. Nature *526*, 660–665.

Shi, J., Zhao, Y., Wang, Y., Gao, W., Ding, J., Li, P., Hu, L., and Shao, F. (2014). Inflammatory caspases are innate immune receptors for intracellular LPS. Nature.

Shimada, K., Crother, T.R., Karlin, J., Dagvadorj, J., Chiba, N., Chen, S., Ramanujan, V.K., Wolf, A.J., Vergnes, L., Ojcius, D.M., et al. (2012). Oxidized Mitochondrial DNA Activates the NLRP3 Inflammasome during Apoptosis. Immunity *36*, 401–414.

Shin, J.N., Fattah, E.A., Bhattacharya, A., Ko, S., and Eissa, N.T. (2013). Inflammasome Activation by Altered Proteostasis. Journal of Biological Chemistry *288*, 35886–35895.

Siegelin, M.D., Dohi, T., Raskett, C.M., Orlowski, G.M., Powers, C.M., Gilbert, C.A., Ross, A.H., Plescia, J., and Altieri, D.C. (2011). Exploiting the mitochondrial unfolded protein response for cancer therapy in mice and human cells. J. Clin. Invest. *121*, 1349–1360.

Sievers, F., Wilm, A., Dineen, D., Gibson, T.J., Karplus, K., Li, W., Lopez, R., McWilliam, H., Remmert, M., Söding, J., et al. (2011). Fast, scalable generation of high-quality protein multiple sequence alignments using Clustal Omega. Mol Syst Biol *7*, 539.

Sirois, C.M., Jin, T., Miller, A.L., Bertheloot, D., Nakamura, H., Horvath, G.L., Mian, A., Jiang, J., Schrum, J., Bossaller, L., et al. (2013). RAGE is a nucleic acid receptor that promotes inflammatory responses to DNA. J Exp Med *210*, 2447–2463.

Soberman, R.J., and Christmas, P. (2003). The organization and consequences of eicosanoid signaling. J. Clin. Invest. *111*, 1107–1113.

Sokolowska, M., Chen, L.-Y., Liu, Y., Martinez-Anton, A., Qi, H.-Y., Logun, C., Alsaaty, S., Park, Y.H., Kastner, D.L., Chae, J.J., et al. (2015). Prostaglandin E2 Inhibits NLRP3 Inflammasome Activation through EP4 Receptor and Intracellular Cyclic AMP in Human Macrophages. The Journal of Immunology *194*, 5472–5487.

Solle, M., Labasi, J., Perregaux, D.G., Stam, E., Petrushova, N., Koller, B.H., Griffiths, R.J., and Gabel, C.A. (2001). Altered Cytokine Production in Mice Lacking P2X 7Receptors. Journal of Biological Chemistry *276*, 125–132.

Song, N., Liu, Z.-S., Xue, W., Bai, Z.-F., Wang, Q.-Y., Dai, J., Liu, X., Huang, Y.-J., Cai, H., Zhan, X.-Y., et al. (2017). NLRP3 Phosphorylation Is an Essential Priming Event for Inflammasome Activation. Molecular Cell *68*, 185–197.e186.

Spadoni, I., Fornasa, G., and Rescigno, M. (2017). Organ-specific protection mediated by cooperation between vascular and epithelial barriers. Nat Rev Immunol *17*, 761–773.

Srinivasula, S.M., Poyet, J.-L., Razmara, M., Datta, P., Zhang, Z., and Alnemri, E.S. (2002). The PYRIN-CARD Protein ASC Is an Activating Adaptor for Caspase-1. Journal of Biological Chemistry *277*, 21119–21122.

Stutz, A., Horvath, G.L., Monks, B.G., and Latz, E. (2013). ASC Speck Formation as a Readout for Inflammasome Activation. In Mitochondrial DNA, (Totowa, NJ: Humana Press), pp. 91–101.

Stutz, A., Kolbe, C.-C., Stahl, R., Horvath, G.L., Franklin, B.S., van Ray, O., Brinkschulte, R., Geyer, M., Meissner, F., and Latz, E. (2017). NLRP3 inflammasome assembly is regulated by phosphorylation of the pyrin domain. J Exp Med jem.20160933.

Su, M.-Y., Kuo, C.-I., Chang, C.-F., and Chang, C.-I. (2013). Three-Dimensional Structure of Human NLRP10/PYNOD Pyrin Domain Reveals a Homotypic Interaction Site Distinct from Its Mouse Homologue. PLoS ONE *8*, e67843.

Subramanian, N., Natarajan, K., Clatworthy, M.R., Wang, Z., and Germain, R.N. (2013). The Adaptor MAVS Promotes NLRP3 Mitochondrial Localization and Inflammasome Activation. Cell *153*, 348–361.

Sun, L., Wu, J., Du, F., Chen, X., and Chen, Z.J. (2013). Cyclic GMP-AMP Synthase Is a Cytosolic DNA Sensor That Activates the Type I Interferon Pathway. Science *339*, 786–791.

Sutterwala, F.S., Ogura, Y., Szczepanik, M., Lara-Tejero, M., Lichtenberger, G.S., Grant, E.P., Bertin, J., Coyle, A.J., Galán, J.E., Askenase, P.W., et al. (2006). Critical Role for NALP3/CIAS1/Cryopyrin in Innate and Adaptive Immunity through Its Regulation of Caspase-1. Immunity *24*, 317–327.

Swanson, K.V., Deng, M., and Ting, J.P.-Y. (2019). The NLRP3 inflammasome: molecular activation and regulation to therapeutics. Nat Rev Immunol *19*, 477–489.

Swanson, K.V., Junkins, R.D., Kurkjian, C.J., Holley-Guthrie, E., Pendse, A.A., Morabiti, El, R., Petrucelli, A., Barber, G.N., Benedict, C.A., and Ting, J.P.-Y. (2017). A noncanonical function of cGAMP in inflammasome priming and activation. J Exp Med *214*, 3611–3626.

Szabo, I., and Zoratti, M. (1993). The mitochondrial permeability transition pore may comprise VDAC molecules. I. Binary structure and voltage dependence of the pore. FEBS Letters *330*, 201–205.

Szabo, I., De Pinto, V., and Zoratti, M. (1993). The mitochondrial permeability transition pore may comprise VDAC molecules. II. The electrophysiological properties of VDAC are compatible with those of the mitochondrial megachannel. FEBS Letters *330*, 206–210.

Takahashi, R., Deveraux, Q., Tamm, I., Welsh, K., Assa-Munt, N., Salvesen, G.S., and Reed, J.C. (1998). A Single BIR Domain of XIAP Sufficient for Inhibiting Caspases. Journal of Biological Chemistry *273*, 7787–7790.

Takeda, K., Kaisho, T., and Akira, S. (2003). Toll-like receptors. Annu. Rev. Immunol. *21*, 335–376.

Takeda, K., Takeuchi, O., and Akira, S. (2002). Recognition of lipopeptides by Toll-like receptors. Journal of Endotoxin Research *8*, 459–463.

Takeuchi, O., and Akira, S. (2010a). Pattern Recognition Receptors and Inflammation. Cell *140*, 805–820.

Takeuchi, O., and Akira, S. (2010b). Pattern Recognition Receptors and Inflammation. Cell *140*, 805–820.

Takeuchi, O., Sato, S., Horiuchi, T., Hoshino, K., Takeda, K., Dong, Z., Modlin, R.L., and Akira, S. (2002). Cutting Edge: Role of Toll-Like Receptor 1 in Mediating Immune Response to Microbial Lipoproteins. The Journal of Immunology *169*, 10–14.

Tang, T., Lang, X., Xu, C., Wang, X., Gong, T., Yang, Y., Cui, J., Bai, L., Wang, J., Jiang, W., et al. (2017). CLICs-dependent chloride efflux is an essential and proximal upstream event for NLRP3 inflammasome activation. Nat Comms *8*, 707.

Tapia-Abellán, A., Angosto-Bazarra, D., Martínez-Banaclocha, H., de Torre-Minguela, C., Cerón-Carrasco, J.P., Pérez-Sánchez, H., Arostegui, J.I., and Pelegrín, P. (2019). MCC950 closes the active conformation of NLRP3 to an inactive state. Nat Chem Biol *15*, 560–564.

Taylor, B., Adelaja, A., Liu, Y., Luecke, S., and Hoffmann, A. (2020). Identification and physiological significance of temporal NFκB signaling codewords deployed by macrophages to classify immune threats. *44*, 557.

Taylor, E.B., and Rutter, J. (2011). Mitochondrial quality control by the ubiquitin–proteasome system. Biochm. Soc. Trans. *39*, 1509–1513.

Tenthorey, J.L., Chavez, R.A., Thompson, T.W., Deets, K.A., Vance, R.E., and Rauch, I. (2020). NLRC4 inflammasome activation is NLRP3- and phosphorylation-independent during infection and does not protect from melanoma. J Exp Med *217*, 1045.

Thiele, D.L., and Lipsky, P.E. (1985). Regulation of cellular function by products of lysosomal enzyme activity: elimination of human natural killer cells by a dipeptide methyl ester generated from L-leucine methyl ester by monocytes or polymorphonuclear leukocytes. Proc Natl Acad Sci USA *82*, 2468–2472.

Thiele, D.L., and Lipsky, P.E. (1990). Mechanism of L-leucyl-L-leucine methyl ester-mediated killing of cytotoxic lymphocytes: dependence on a lysosomal thiol protease, dipeptidyl peptidase I, that is enriched in these cells. Proc Natl Acad Sci USA *87*, 83–87.

Tomasello, F., Messina, A., Lartigue, L., Schembri, L., Medina, C., Reina, S., Thoraval, D., Crouzet, M., Ichas, F., De Pinto, V., et al. (2009). Outer membrane VDAC1 controls permeability transition of the inner mitochondrial membrane in cellulo during stress-induced apoptosis. Cell Res *19*, 1363–1376.

Tsai, J.-Y. (2010). Effect of m-3M3FBS on Ca(superscript 2+) Movement in PC3 Human Prostate Cancer Cells. Chin. J. Physiol. *53*, 151–159.

Vacca, M., Böhme, J., Zambetti, L.P., Khameneh, H.J., Paleja, B.S., Laudisi, F., Ho, A.W.S., Neo, K., Leong, K.W.K., Marzuki, M., et al. (2017). NLRP10 Enhances CD4+ T-Cell-Mediated IFNγ Response via Regulation of Dendritic Cell-Derived IL-12 Release. Front. Immunol. *8*, 373.

van Meer, G., and de Kroon, A.I.P.M. (2010). Lipid map of the mammalian cell. Journal of Cell Science *124*, 5–8.

van Meer, G., Voelker, D.R., and Feigenson, G.W. (2008). Membrane lipids: where they are and how they behave. Nat Rev Mol Cell Biol *9*, 112–124.

Van Opdenbosch, N., Gurung, P., Vande Walle, L., Fossoul, A., Kanneganti, T.-D., and Lamkanfi, M. (2014). Activation of the NLRP1b inflammasome independently of ASC-mediated caspase-1 autoproteolysis and speck formation. Nat Comms *5*, 137.

Vande Walle, L., Stowe, I.B., Šácha, P., Lee, B.L., Demon, D., Fossoul, A., Van Hauwermeiren, F., Saavedra, P.H.V., Šimon, P., Šubrt, V., et al. (2019). MCC950/CRID3 potently targets the NACHT domain of wild-type NLRP3 but not disease-associated mutants for inflammasome inhibition. PLoS Biol *17*, e3000354.

Vince, J.E., De Nardo, D., Gao, W., Vince, A.J., Hall, C., McArthur, K., Simpson, D., Vijayaraj, S., Lindqvist, L.M., Bouillet, P., et al. (2018). The Mitochondrial Apoptotic Effectors BAX/BAK Activate Caspase-3 and -7 to Trigger NLRP3 Inflammasome and Caspase-8 Driven IL-1β Activation. Cell Reports *25*, 2339–2353.e4.

Vladimer, G.I., Weng, D., Paquette, S.W.M., Vanaja, S.K., Rathinam, V.A.K., Aune, M.H., Conlon, J.E., Burbage, J.J., Proulx, M.K., Liu, Q., et al. (2012). The NLRP12 Inflammasome Recognizes Yersinia pestis. Immunity *37*, 96–107.

Walev, I., Reske, K., Palmer, M., Valeva, A., and Bhakdi, S. (1995). Potassium-inhibited processing of IL-1 beta in human monocytes. The EMBO Journal *14*, 1607–1614.

Walliser, C., Wist, M., Hermkes, E., Zhou, Y., Schade, A., Haas, J., Deinzer, J., Désiré, L., Li, S.S.C., Stilgenbauer, S., et al. (2018). Functional characterization of phospholipase C-γ2 mutant protein causing both somatic ibrutinib resistance and a germline monogenic autoinflammatory disorder. Oncotarget *9*, 34357–34378.

Wang, D., Zhang, D.-F., Feng, J.-Q., Li, G.-D., Li, X.-A., Yu, X.-F., Long, H., Li, Y.-Y., and Yao, Y.-G. (2016). Common variants in the PARL and PINK1 genes increase the risk to leprosy in Han Chinese from South China. Sci. Rep. *6*, e5669.

Wang, Y., Hasegawa, M., Imamura, R., Kinoshita, T., Kondo, C., Konaka, K., and Suda, T. (2004). PYNOD, a novel Apaf-1/CED4-like protein is an inhibitor of ASC and caspase-1. International Immunology *16*, 777–786.

Wei, J., Gao, D.-F., Wang, H., Yan, R., Liu, Z.-Q., Yuan, Z.-Y., Liu, J., and Chen, M.-X. (2014). Impairment of Myocardial Mitochondria in Viral Myocardial Disease and Its Reflective Window in Peripheral Cells. PLoS ONE *9*, e116239.

West, A.P., Khoury-Hanold, W., Staron, M., Tal, M.C., Pineda, C.M., Lang, S.M., Bestwick, M., Duguay, B.A., Raimundo, N., MacDuff, D.A., et al. (2015). Mitochondrial DNA stress primes the antiviral innate immune response. Nature *520*, 553–557.

Westphal, D., Dewson, G., Czabotar, P.E., and Kluck, R.M. (2011). Molecular biology of Bax and Bak activation and action. Biochimica Et Biophysica Acta (BBA) - Molecular Cell Research *1813*, 521–531.

Wiedemann, N., and Pfanner, N. (2017). Mitochondrial Machineries for Protein Import and Assembly. Annu. Rev. Biochem. *86*, 685–714.

Wilson, K.P., Black, J.-A.F., Thomson, J.A., Kim, E.E., Griffith, J.P., Navia, M.A., Murcko, M.A., Chambers, S.P., Aldape, R.A., Raybuck, S.A., et al. (1994). Structure and mechanism of interleukin-lβ converting enzyme. Nature *370*, 270–275.

Wolf, A.J., Reyes, C.N., Liang, W., Becker, C., Shimada, K., Wheeler, M.L., Cho, H.C., Popescu, N.I., Coggeshall, K.M., Arditi, M., et al. (2016). Hexokinase Is an Innate Immune Receptor for the Detection of Bacterial Peptidoglycan. Cell *166*, 624–636.

Wolter, K.G., Hsu, Y.-T., Smith, C.L., Nechushtan, A., Xi, X.-G., and Youle, R.J. (1997). Movement of Bax from the Cytosol to Mitochondria during Apoptosis. J Cell Biol *139*, 1281–1292.

Xia, M., Zhang, Y., Jin, K., Lu, Z., Zeng, Z., and Xiong, W. (2019). Communication between mitochondria and other organelles: a brand-new perspective on mitochondria in cancer. Cell Biosci *9*, 685.

Xin, M., Li, R., Xie, M., Park, D., Owonikoko, T.K., Sica, G.L., Corsino, P.E., Zhou, J., Ding, C., White, M.A., et al. (2014). Small-molecule Bax agonists for cancer therapy. Nat Comms *5*, 727.

Yabal, M., Calleja, D.J., Simpson, D.S., and Lawlor, K.E. (2018). Stressing out the mitochondria: Mechanistic insights into NLRP3 inflammasome activation. Journal of Leukocyte Biology *105*, 377–399.

Yamaguchi, H., Bhalla, K., and Wang, H.-G. (2003). Bax plays a pivotal role in thapsigargin-induced apoptosis of human colon cancer HCT116 cells by controlling Smac/Diablo and Omi/HtrA2 release from mitochondria. Cancer Research *63*, 1483–1489.

Yan, Y., Jiang, W., Liu, L., Wang, X., Ding, C., Tian, Z., and Zhou, R. (2015). Dopamine Controls Systemic Inflammation through Inhibition of NLRP3 Inflammasome. Cell *160*, 62–73.

Yang, J. (1997). Prevention of Apoptosis by Bcl-2: Release of Cytochrome c from Mitochondria Blocked. Science *275*, 1129–1132.

Yang, J.H., Gross, R.L., Basinger, S.F., and Wu, S.M. (2001). Apoptotic cell death of cultured salamander photoreceptors induced by cccp: CsA-insensitive mitochondrial permeability transition. Journal of Cell Science *114*, 1655–1664.

Yang, J., Zhao, Y., Shi, J., and Shao, F. (2013). Human NAIP and mouse NAIP1 recognize bacterial type III secretion needle protein for inflammasome activation. Proc Natl Acad Sci USA *110*, 14408–14413.

Yao, Y., Chen, S., Cao, M., Fan, X., Yang, T., Huang, Y., Song, X., Li, Y., Ye, L., Shen, N., et al. (2017). Antigen-specific CD8+ T cell feedback activates NLRP3 inflammasome in antigen-presenting cells through perforin. Nat Comms *8*, 325.

Yates, A.D., Achuthan, P., Akanni, W., Allen, J., Allen, J., Alvarez-Jarreta, J., Amode, M.R., Armean, I.M., Azov, A.G., Bennett, R., et al. (2019). Ensembl 2020. Nucleic Acids Research *41*, D21.

Yeon, S.H., Yang, G., Lee, H.E., and Lee, J.Y. (2016). Oxidized phosphatidylcholine induces the activation of NLRP3 inflammasome in macrophages. Journal of Leukocyte Biology 1–11.

Yu, J., Nagasu, H., Murakami, T., Hoang, H., Broderick, L., Hoffman, H.M., and Horng, T. (2014). Inflammasome activation leads to Caspase-1–dependent mitochondrial damage and block of mitophagy. Proc Natl Acad Sci USA *111*, 15514–15519.

Zanoni, I., Tan, Y., Di Gioia, M., Broggi, A., Ruan, J., Shi, J., Donado, C.A., Shao, F., Wu, H., Springstead, J.R., et al. (2016). An endogenous caspase-11 ligand elicits interleukin-1 release from living dendritic cells. Science *352*, 1232–1236.

Zewinger, S., Reiser, J., Jankowski, V., Alansary, D., Hahm, E., Triem, S., Klug, M., Schunk, S.J., Schmit, D., Kramann, R., et al. (2019). Apolipoprotein C3 induces inflammation and organ damage by alternative inflammasome activation. Nat Immunol *21*, 30–41.

Zhang, J.Y., Kowal, D.M., Nawoschik, S.P., Dunlop, J., Pausch, M.H., and Peri, R. (2010). Development of an Improved IP 1Assay for the Characterization of 5-HT 2CReceptor Ligands. ASSAY and Drug Development Technologies *8*, 106–113.

Zhang, L.-N., Li, J.-Y., and Xu, W. (2012). A review of the role of Puma, Noxa and Bim in the tumorigenesis, therapy and drug resistance of chronic lymphocytic leukemia. Cancer Gene Ther *20*, 1–7.

Zhang, Y., Rong, H., Zhang, F.-X., Wu, K., Mu, L., Meng, J., Xiao, B., Zamponi, G.W., and Shi, Y. (2018). A Membrane Potential- and Calpain-Dependent Reversal of Caspase-1 Inhibition Regulates Canonical NLRP3 Inflammasome. Cell Reports *24*, 2356–2369.e5.

Zhang, Z., Meszaros, G., He, W.-T., Xu, Y., de Fatima Magliarelli, H., Mailly, L., Mihlan, M., Liu, Y., Puig Gámez, M., Goginashvili, A., et al. (2017). Protein kinase D at the Golgi controls NLRP3 inflammasome activation. J Exp Med *9*, jem.20162040.

Zhao, Y., Araki, S., Wu, J., Teramoto, T., Chang, Y.F., Nakano, M., Abdelfattah, A.S., Fujiwara, M., Ishihara, T., Nagai, T., et al. (2011a). An Expanded Palette of Genetically Encoded Ca2+ Indicators. Science *333*, 1888–1891.

Zhao, Y., Yang, J., Shi, J., Gong, Y.-N., Lu, Q., Xu, H., Liu, L., and Shao, F. (2011b). The NLRC4 inflammasome receptors for bacterial flagellin and type III secretion apparatus. Nature *477*, 596–600.

Zheng, Y., Shi, Y., Tian, C., Jiang, C., Jin, H., Chen, J., Almasan, A., Tang, H., and Chen, Q. (2003). Essential role of the voltage-dependent anion channel (VDAC) in mitochondrial permeability transition pore opening and cytochrome c release induced by arsenic trioxide. Oncogene *23*, 1239–1247.

Zhong, F., Liang, S., and Zhong, Z. (2019). Emerging Role of Mitochondrial DNA as a Major Driver of Inflammation and Disease Progression. Trends in Immunology *40*, 1120–1133.

Zhong, F.L., Mamaï, O., Sborgi, L., Boussofara, L., Hopkins, R., Robinson, K., Szeverényi, I., Takeichi, T., Balaji, R., Lau, A., et al. (2016). Germline NLRP1 Mutations Cause Skin Inflammatory and Cancer Susceptibility Syndromes via Inflammasome Activation. Cell *167*, 187–202.e17.

Zhong, Z., Liang, S., Sanchez-Lopez, E., He, F., Shalapour, S., Lin, X.-J., Wong, J., Ding, S., Seki, E., Schnabl, B., et al. (2018). New mitochondrial DNA synthesis enables NLRP3 inflammasome activation. Nature *560*, 198–203.

Zhou, Q., Wang, H., Schwartz, D.M., Stoffels, M., Park, Y.H., Zhang, Y., Yang, D., Demirkaya, E., Takeuchi, M., Tsai, W.L., et al. (2015). Loss-of-function mutations in TNFAIP3 leading to A20 haploinsufficiency cause an early-onset autoinflammatory disease. Nat. Genet. *48*, 67–73.

Zhou, R., Tardivel, A., Thorens, B., Choi, I., and Tschopp, J. (2009). Thioredoxin-interacting protein links oxidative stress to inflammasome activation. Nat Immunol *11*, 136–140.

Zhou, R., Yazdi, A.S., Menu, P., and Tschopp, J. (2010). A role for mitochondria in NLRP3 inflammasome activation. Nature *469*, 221–225.

Zhu, S., Ding, S., Wang, P., Wei, Z., Pan, W., Palm, N.W., Yang, Y., Yu, H., Li, H.-B., Wang, G., et al. (2017). Nlrp9b inflammasome restricts rotavirus infection in intestinal epithelial cells. Nature *546*, 667–670.

Zou, H., Henzel, W.J., Liu, X., Lutschg, A., and Wang, X. (1997). Apaf-1, a Human Protein Homologous to C. elegans CED-4, Participates in Cytochrome c–Dependent Activation of Caspase-3. Cell *90*, 405–413.

List of publications

1. Bzowska, M., Mężyk-Kopeć, R., **Prochnicki, T.**, Kulesza, M., Klaus, T., and Bereta, J. (2013). Antibody-based antiangiogenic and antilymphangiogenic therapies to prevent tumor growth and progression. Acta Biochim Pol *60*, 263–275. doi: 10.18388/ABP.2013_1982

2. He, J., Li, T., **Prochnicki, T.**, Horvath, G., Latz, E., and Takeoka, S. (2019). Membrane fusogenic lysine type lipid assemblies possess enhanced NLRP3 inflammasome activation potency. Biochemistry and Biophysics Reports *18*, 100623. doi: 10.1016/j.bbrep.2019.100623

3. Kleineidam, L., Chouraki, V., **Prochnicki, T.**, van der Lee, S.J., Madrid-Márquez, L., Wagner-Thelen, H., Karaca, I., Weinhold, L., Wolfsgruber, S., Boland, A., et al. (2020). PLCG2 protective variant p.P522R modulates tau pathology and disease progression in patients with mild cognitive impairment. Acta Neuropathol *139*, 1025–1044. doi: 10.1007/s00401-020-02138-6

4. Li, T., He, J., Horvath, G., **Prochnicki, T.**, Latz, E., and Takeoka, S. (2018). Lysine-containing cationic liposomes activate the NLRP3 inflammasome: Effect of a spacer between the head group and the hydrophobic moieties of the lipids. Nanomedicine: Nanotechnology, Biology and Medicine *14*, 279–288. doi: 10.1016/j.nano.2017.10.011

5. Li, T., Zehner, M., He, J., **Prochnicki, T.**, Horvath, G., Latz, E., Burgdorf, S., and Takeoka, S. (2019). NLRP3 inflammasome-activating arginine-based liposomes promote antigen presentations in dendritic cells. Int J Nanomedicine *14*, 3503–3516. doi: 10.2147/IJN.S202379

6. Mężyk-Kopeć, R., Wyroba, B., Stalińska, K., **Prochnicki, T.**, Wiatrowska, K., Kilarski, W.W., Swartz, M.A., and Bereta, J. (2015). ADAM17 Promotes Motility, Invasion, and Sprouting of Lymphatic Endothelial Cells. PLoS ONE *10*, e0132661. doi: 10.1371/journal.pone.0132661

7. Ostrowski, M., Porowinska, D., **Prochnicki, T.**, Prevost, M., Raynal, B., Baron, B., Sauguet, L., Corringer, P.-J., and Faure, G. (2016). Neurotoxic phospholipase A2 from rattlesnake as a new ligand and new regulator of prokaryotic receptor GLIC (proton-gated ion channel from G. violaceus). Toxicon *116*, 63–71. doi: 10.1016/j.toxicon.2016.02.002

8. **Prochnicki, T.**, and Latz, E. (2017). Inflammasomes on the Crossroads of Innate Immune Recognition and Metabolic Control. Cell Metabolism *26*, 71–93. doi: 10.1016/j.cmet.2017.06.018

9. **Prochnicki, T.**, Mangan, M.S., and Latz, E. (2016). Recent insights into the molecular mechanisms of the NLRP3 inflammasome activation. F1000Res *5*, 1469. doi: 10.12688/f1000research.8614.1

10. Rolfes, V., Ribeiro, L.S., Hawwari, I., Böttcher, L., Rosero, N., Maasewerd, S., Santos, M.L.S., **Prochnicki, T.**, Silva, C.M. de S., Wanderley, C.W. de S., et al. (2020). Platelets Fuel the Inflammasome Activation of Innate Immune Cells. Cell Reports *31*, 107615. doi: 10.1016/j.celrep.2020.107615